

QUESTION 110

QUESTION 110

QUESTION 110

SAFETY OF DAMS AND LEVEES FACING EXTREME HYDROLOGICAL EVENTS

1. Assessment of extreme events (e.g., flood, droughts, typhoons/hurricanes, glacial lake outburst floods) in the context of climate change, accounting for uncertainty.
2. Assessment for the safety of structures for extreme floods; management options (e.g., increasing dam height, spillway capacity, reservoir operation).
3. Flood forecasting, hydraulic management of multiple projects within river systems.
4. Reassessment of the flood data and mitigation e.g., fuse devices, overflow resistance, controlled breach formation, warning and evacuation, crisis and emergency management.

SÉCURITÉ DES BARRAGES ET DES DIGUES LORS DES ÉVÉNEMENTS MÉTÉOROLOGIQUES EXTRÊMES

1. Évaluation des événements extrêmes (crues, sécheresse, typhons/ouragans, vidange brutale de lac glaciaire) dans le contexte du changement climatique. Prise en compte de l'incertitude.
2. Évaluation de la sécurité des ouvrages pour les crues extrêmes ; gestion des options (augmentation de la hauteur du barrage, capacité de l'évacuateur, opération du réservoir).
3. Prévision des crues, gestion hydraulique de plusieurs retenues à l'intérieur de bassins hydrographiques.
4. Réévaluation des crues et des atténuations (dispositifs fusibles, résistance à la surverse, contrôle de la formation de la brèche, alerte et évacuation, gestion de crise et des urgences).

QUESTION 110

TABLE OF CONTENTS OF PAPERS

TABLE DES MATIÈRES DES RAPPORTS

R. 1	JUAN CARLOS DE CEA AZAÑEDO, DANIEL SANZ JIMÉNEZ, ENRIQUE MORENO CALLE, IGNACIO ESCUDER BUENO, ADRIÁN MORALES TORRES <i>(Spain)</i> Adaptation of 310 dams in Spain to extreme events and climate change through risk assessment	1
R. 2	M. HO TA KHANH, F. LAUGIER, J. VERMEULEN <i>(Vietnam)</i> PKW Spillways : An innovative, safe and economic solution from run-of-river dams in plains to large dams in mountains suitable for climate change challenges	16
R. 3	JAMES YANG, ANDERS FRISK, MATS BILLSTEIN, PETER MATTIASSON, LARS JOHNSSON <i>(Sweden)</i> Dam upgrade with Piano Key Weir for discharge of extreme floods.	30
R. 4	ENRIQUE CAMPOS, JUAN JOSÉ REBOLLO, JOSÉ MILLA, CARMEN BAENA, CARLOS GRANELL <i>(Spain)</i> Design of the new spillway for Regajo dam.	45
R. 5	ALEXANDRE JEAN PACHOUD, DANIEL VIVIROLI, ROGER FRAUCHIGER, EMMANUEL BROCARD, MILAINE CÔTÉ <i>(Switzerland)</i> New approach to estimate extreme floods for Swiss dams by means of continuous hydrometeorological simulations	58
R. 6	L. TARDIEUX, I. FENT, A. ARIGONI, B. M. QUIGLEY, A. JONNERET, P. SIPATELA, A. NKWEENDENDA, S. MHLANGA, MUNYARADZI C. MUNODAWAFA <i>(Switzerland)</i> Kariba dam plunge pool reshaping works for the safety of structures for extreme floods	80
R. 7	LE VAN NGHI, HOANG DUC VINH, DOAN THI MINH YEN, NGUYEN TIEN HAI <i>(Vietnam)</i> Piano Key Weir geometries adjustment for downstream hydraulic regime: lessons learned from case studies in Vietnam	100

R. 8	PETER HILL, ASHIQ RASHEED, YUE (ALBERT) SHEN, PHILLIP JORDAN, MICHEL RAYMOND (<i>Australia</i>) Regionalization of flood envelope curves to derive preliminary estimates of probable maximum floods	112
R. 9	CHIHAYA ONDA, KOUKI MORIMOTO, TETSUYA SUMI (<i>Japan</i>) Case study and analysis of surge wave and excessive flood in hydropower dams	127
R. 10	JULIEN VERMEULEN, THOMAS VIARD, MATTHIEU SECHER, DAMIEN PUYGRENIER, EMMANUEL PAQUET (<i>France</i>) Gestion des crues sur les grands bassins versants - prise en compte de la complexité hydrologique et hydraulique	145
R. 11	LOUIS SUCHIER, ALEXANDRE SIMON, EMMANUEL ROBBE, PHILIPPE KOLMAYER, FRÉDÉRIC LAUGIER, ALAIN FELZINES, RÉMI BERNARD (<i>France</i>) Characterization and feedback on the behavior of arch dams subjected to heatwaves and extreme cold	169
R. 12	THIBAUT MALLET, MARK CHEETHAM, PHILIPPE PELT, JEAN-JACQUES FRY, RÉMY TOURMENT, PIERRE BALAYN, MATHIEU NORMAND ET FABIENNE SCERRI, LAURENT POLLY, AKIM SALMI, ERIC VUILLERMET (<i>France</i>) Building a resilient system against flood in the Rhône delta	195
R. 13	NICOLAS AVISSE (<i>France</i>) A novel methodology for assessing extreme hydrological events in the context of climate change	220
R. 14	GAËTAN DAUTOIS, MATHIEU ROY, SAMUEL BALE, MARIE CUBAYNES, FRÉDÉRIC LAUGIER, ROMAIN TAJETTI, GUIREC PREVOT (<i>France</i>) Improvement of the safety of the French dams against floods	240
R. 15	PATRICK PINETTES, HANNA HADDAD, CHRISTOPHE PICAULT, STÉPHANE BONELLI, JEAN-ROBERTCOURIVAUD, THIBAUT MALLET (<i>France</i>) Two erosion tests to quantify resistance to erosion during overflow: the jet erosion test and the overflow test.	274
R. 16	ANDREA ABBATE, ANTONELLA FRIGERIO (<i>Italy</i>) Molare tragedy: the secondary dam collapse induced by a heavy rainfall event.	296

R. 17	CHENCEN (JANICE) ZHANG, ROBERT PHILLIP GREYLING, EDWIN LILLIE (<i>South Africa</i>) Case study – a dam raising options study for a dam in Southern Africa	317
R. 18	HENRY-JOHN WRIGHT (<i>South Africa</i>) Challenges experiences with upgrading a composite dam in South Africa - Tzaneen dam raising	331
R. 19	MUHAMMAD RIZA, HERRYAN KENDRA, AGUS JATIWIYONO (<i>Indonesia</i>) The effect of reservoir operation patterns on the material characteristics of old dams and their impact on dam safety	344
R. 20	ARJAN JOVANI, ERMAL KACURRI, ORLANDO MUCA, FAHRI MAHO (<i>Albania</i>) Assessment of the discharge capacities and safety of main structures in large dams of Drini river cascade.	370
R. 21	NIE-YUXIN, ZHANG RUI, LIN ZHIYAN, LIU-YUANGUANG, JIN JUNJIE, LI ZICHANG (<i>China</i>) Intelligent temperature control system for large concrete dam construction in hot and humid environments	382
R. 22	NING ZHOU, HONGEN LI, FANG WANG, ZHU ZHANG (<i>China</i>) Effects of spatial and temporal variation characteristics of extreme precipitation on dam safety in major river basins in China in recent 20 years	394
R. 23	MEI SHENGYAO, XU JIANJUN (<i>China</i>) A high-precision three-dimensional dam breach model considering breach evolution mechanisms	406
R. 24	YUELIN SUN, SHIFA XIA, JIAHONG ZHANG, PING SUN (<i>China</i>) Disaster assessment of the landslide surge caused by the deformation of the upstream reservoir bank of the dam.	417
R. 25	JINGCHUN LEI, KUNMING LU, GAOFENG ZHANG (<i>China</i>) Analysis of the impact of extreme events on dam disaster under climate change	433
R. 26	MATTHEW HALSO, DAVID F. VETSCH, FREDERIC M. EVERS, ROBERT M. BOES (<i>Switzerland</i>) Zoned embankment dam breaching due to overtopping: estimating outflow hydrographs through laboratory experiments and parametric numerical modeling	444

R. 27	JINSHENG JIA, CUIYING ZHENG, AILI LI (<i>China</i>) New progress of cemented material dams to meet the requirements on dam safety to resist overtopping in China	462
R. 28	HONGQIU HE, QIMING ZHONG, XUEMING WU, KAI CHENG, XUDONG CHEN, XIAOKANG CHEN (<i>China</i>) Machine learning method-based dam breach flood simulation	475
	General Report / <i>Rapport Général</i> Q. 110 ENRIQUE CIFRES (<i>Spain</i>), General Reporter / <i>Rapporteur</i> <i>Général</i>	487

PAPERS ON QUESTION 110

RAPPORTS SUR LA QUESTION 110



Taylor & Francis

Taylor & Francis Group

<http://taylorandfrancis.com>

COMMISSION INTERNATIONALE DES
GRANDS BARRAGES

VINGT-HUITIEME CONGRES DES
GRANDS BARRAGES
CHENGDU, MAI 2025

ADAPTATION OF 310 DAMS IN SPAIN TO EXTREME EVENTS AND CLIMATE CHANGE THROUGH RISK ASSESSMENT (*)

Juan Carlos DE CEA AZAÑEDO, Daniel SANZ JIMÉNEZ &
Enrique MORENO CALLE
General Water Directorate, Ministry of Ecological Transition, Madrid

Ignacio ESCUDER BUENO
Universitat Politècnica de València, Valencia
iPresas Risk Analysis, Valencia, Spain

Adrián MORALES TORRES
iPresas Risk Analysis, Valencia

SPAIN

SUMMARY

Spain faces significant vulnerability to the impacts of climate change, particularly in terms of water resource management and infrastructure resilience. In recognition of these challenges, the Ministry of *Ecological Transition* has launched a comprehensive risk-informed dam safety management system to assess the safety of dams across the country. This initiative is key to prioritizing investments and ensuring that Spain's dam infrastructure is properly adapted to the evolving risks posed by climate change. The system is being developed in close collaboration with various River Basin Authorities and involves the active participation of hundreds of professionals from diverse fields.

**Adaptation de 310 barrages espagnols vis-à-vis des événements extrêmes et du changement climatique en s'appuyant sur l'analyse de risques*

The assessment process is based on a comprehensive risk analysis that includes both semi-quantitative and quantitative phases. This integrated approach provides a detailed understanding of the vulnerabilities and strengths within the current infrastructure. By systematically analyzing each dam, the risk-informed management system identifies areas that require immediate intervention as well as those with potential long-term risks. The results of this thorough risk analysis will be essential in guiding the strategic allocation of resources, ensuring that investments are prioritized to enhance dam safety and resilience effectively.

In addition, the system is designed to address both current and future needs, considering the short, medium, and long-term impacts of climate change on dam safety. By strategically prioritizing investments based on these assessments, Spain can strengthen its infrastructure's resilience to extreme weather events, water scarcity, and other climate-related challenges. This proactive approach not only strengthens critical infrastructure, but also supports the broader national initiative to adapt to and mitigate the effects of climate change. Through this thorough assessment and prioritization process, Spain is taking significant steps to secure its water resources and protect its communities against the increasing threats posed by a changing climate.

RÉSUMÉ

L'Espagne est particulièrement vulnérable aux impacts du changement climatique, notamment en ce qui concerne la gestion des ressources en eau et la résilience des infrastructures. Face à ces défis, le Ministère de la Transition Écologique a lancé un système de gestion de la sécurité des barrages basé sur une analyse des risques, visant à évaluer la sécurité des barrages à travers tout le pays. Cette initiative est cruciale pour prioriser les investissements et garantir que les infrastructures de barrages en Espagne soient correctement adaptées aux risques évolutifs posés par le changement climatique. Le système est développé en étroite collaboration avec diverses autorités de bassins hydrographiques et implique la participation active de centaines de professionnels issus de différents domaines.

Le processus d'évaluation repose sur une analyse des risques complète qui inclut des phases semi-quantitatives et quantitatives. Cette approche intégrée permet de comprendre en détail les vulnérabilités et les points forts des infrastructures actuelles. En analysant systématiquement chaque barrage, le système de gestion axé sur les risques identifie les zones nécessitant une intervention immédiate ainsi que celles présentant des risques potentiels à long terme. Les résultats de cette analyse approfondie des risques seront essentiels pour orienter l'allocation stratégique des ressources, en veillant à ce que les investissements soient priorisés pour améliorer la sécurité et la résilience des barrages.

En outre, le système est conçu pour répondre aux besoins présents et futurs, en tenant compte des implications à court, moyen et long terme du changement climatique sur la sécurité des barrages. En priorisant les investissements sur la base de ces évaluations, l'Espagne pourra renforcer la capacité de ses infrastructures à résister aux événements météorologiques extrêmes, à la rareté de l'eau et à d'autres défis liés au climat. Cette approche proactive ne protège pas seulement les infrastructures critiques, mais elle contribue également à l'effort national plus large visant à atténuer les impacts du changement climatique. À travers ce processus d'évaluation et de priorisation complet, l'Espagne prend des mesures significatives pour sécuriser ses ressources en eau et protéger ses communautés contre les menaces croissantes posées par un climat en évolution.

1. INTRODUCTION

Dams are essential to Spain's development, with the country having the highest number of dams in Europe. These infrastructures are vital for ensuring water supply, supporting irrigation, and generating energy. However, the growing impacts of climate change, manifested through diminishing water resources and increased flooding, highlight the urgent need to adapt these structures. To address this challenge, the Ministry of Ecological Transition has launched an extensive risk-informed dam safety management system aimed at modernizing and strengthening dams to enhance their resilience against extreme hydrological events and climate change. This system is a collaborative initiative that spans multiple sectors, involving numerous companies and thousands of individuals, and is coordinated by the General Water Directorate and River Basin Authorities to ensure effective implementation and management.

The system is currently being implemented in several phases, starting with the development of a risk analysis methodology and an online platform. This methodology is actively being applied in a two-stage risk analysis of the 310 state-owned dams. The first stage focuses on 175 dams within four key River Basin Authorities: Guadalquivir, Júcar, Segura, and Ebro. The second stage covers the remaining dams, which are under the jurisdiction of the Duero, Tajo, Guadiana, Miño-Sil, and Cantábrico river basins, as well as the Mancomunidad de los Canales del Taibilla. Fig. 1 illustrates the progress of the system's implementation, highlighting the status of each stage. This visual representation provides a clear overview of how the methodology is being applied across various River Basin Authorities, and shows the progress made in the risk analysis of the state-owned dams.

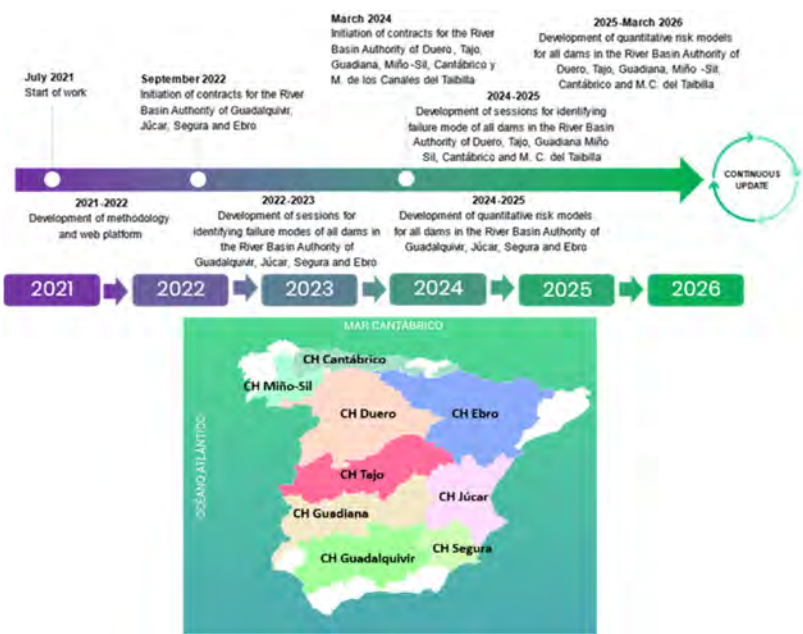


Fig. 1
General timeline for System Development.

This system represents a significant national effort to protect Spain's water resources and mitigate the risks posed by climate change, ensuring the country's long-term sustainability and resilience.

2. IMPACT OF CLIMATE CHANGE ON EXTREME HYDROLOGICAL
EVENTS IN SPAIN

In 2021, the Spanish Center for Studies and Experimentation in Public Works (CEDEX) conducted a study to assess the impacts of climate change on annual maximum precipitation in Spain using simulations from the EURO-CORDEX regional climate models. The study analyzed various precipitation variables (daily, hourly, convective, and cumulative) across different time periods and under two emission scenarios (RCP 4.5 and RCP 8.5).

The results reveal a widespread increase in maximum precipitation across Spain, particularly for short-duration events, indicating a rise in the intensity and

frequency of extreme events. These changes show considerable spatial variability, with more pronounced increases observed in specific regions and for certain return periods.

As a result, this study estimates the rates of change in precipitation quantiles as well as the changes in the temporal structure of precipitation. Specifically, it calculates the variation in the torrentiality factor for different return periods, various analysis horizons, and the two emission scenarios (RCP 4.5 and RCP 8.5) across the Spanish territory (discretized into 0.11° cells of about 12.5 km).

3. SEMI-QUANTITATIVE ANALYSIS

In the early stages of implementing the risk-informed safety management system, focus has been on identifying failure modes for each dam. This is achieved through a collaborative three-day workshop involving several engineers and technicians. The process includes a thorough review of available information, a technical visit to the dam, and a group assessment of the current condition of the dam. Failure modes are identified in two phases: an initial individual identification by the participants and a subsequent group phase where all failure modes are shared and discussed. The identified failure modes are then analyzed and classified, with proposed actions to reduce uncertainty and risk.

In September 2022, the session for the identification of failure modes of pilot dams was initiated by the Coordination, with the aim of training the companies contracted for the first four River Basin Authorities (Guadalquivir, Ebro, Júcar, and Segura). Since then, these companies have begun to apply the risk analysis methodology to each of the dams within their River Basin Authority. To date, these sessions have been completed for more than 150 dams, identifying more than 1900 failure modes. Over 50 specialists from consulting companies and over 90 technicians from the River Basin Authority have actively participated in these works, contributing their experience and knowledge to the process, as shown in.

Fig. 2. Additionally, work has begun to develop quantitative risk models for each dam, providing valuable risk results.

The preliminary outcomes of the semi-quantitative analysis are summarized in

Fig. 3, where each dot represents the sum of failure modes for each of the analyzed dams. Initial findings from the failure mode identification sessions have led to recommendations ranging from major rehabilitation works planned by the River Basin Authorities to minor maintenance measures or studies aimed at reducing uncertainty.



Fig. 2
Pictures of Failure Mode Identification Workshops

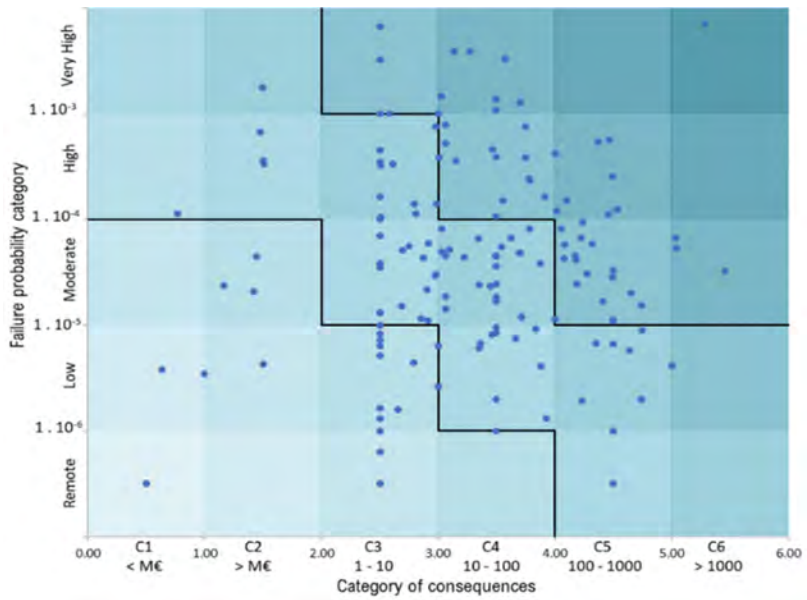


Fig. 3
Average semi-quantitative risk results of the analyzed dams.

4. QUANTITATIVE ANALYSIS AND IMPACT OF CLIMATE CHANGE

As mentioned above, the development of quantitative risk models for the Guadalquivir, Ebro, Júcar, and Segura River Basin Authorities is currently in progress. These models are essential for prioritizing critical actions and enhancing dam safety, particularly in the context of increasing climate-related risks. The quantitative risk analysis process is meticulously organized into four key phases: defining the risk model architecture, calculating the risks, assessing the results, and proposing risk reduction measures.

The foundation of this analysis is the risk model architecture, consisting of a structured network of nodes and connectors that integrate comprehensive information about the dam-reservoir system to enable accurate and detailed risk calculations (see Fig. 4). This architecture is constructed using influence diagrams and event trees—powerful analytical tools that estimate the probabilities and risks associated with various combinations of events that could potentially lead to dam failure.

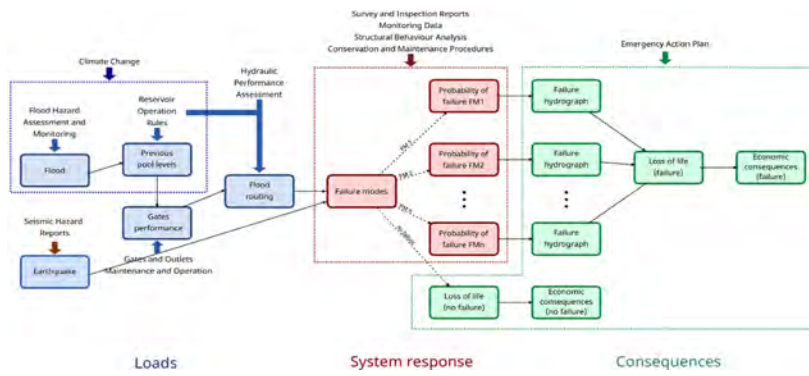


Fig. 4
Generic structure of a risk model.

Once the architecture is established, the next step is to input the relevant data into the model to perform risk calculations. This process involves integrating various probabilities with their respective consequences to generate a comprehensive quantitative risk assessment. A key aspect of this phase is the thorough analysis of climate change impacts, which are carefully evaluated to understand their influence on risk levels and how these risks may evolve over time.

The impact of climate change is particularly significant on two key nodes:

- **Flood Node:**
Flood estimates are recalculated to reflect changes in precipitation patterns, including both the rate of change in precipitation quantiles and the torrentiality factor, as determined by the CEDEX study.
- **Previous Pool Level (PPL) Node:**
Long-term simulations of water balance, which consider variation in water supply and demand, reveal changes in reservoir levels. These variations are incorporated into the risk model, modifying the probabilities associated with the PPL node, thereby enhancing the model's relevance in decision-making processes.

Moreover, the methodology incorporates the temporal variation in population at risk. This includes not only projected changes in population growth or decline, as forecasted by the National Institute of Statistics (INE), but also seasonal fluctuations in the population of tourist areas throughout the year. INE's experimental mobility statistics, derived from mobile phone data, provide valuable insights into both international and domestic tourism, including the origins and destinations of visitors. By incorporating these seasonal population dynamics into the risk model, the analysis becomes more robust and accurately reflects the dynamic nature of risk, particularly in areas with significant tourist activity.

The next stage is risk assessment, where the calculated risks are compared against international tolerability thresholds, such as those recommended by the USACE and USBR (United States), the Australian Committee on Large Dams (ANCOLD) and the Central Water Commission in India (CWC). This comparison is essential to determine whether the current conditions align with accepted safety standards or if corrective actions are needed. Incorporating climate change effects into this evaluation provides a dynamic and future understanding of how risks may evolve, particularly with regard to seasonal variations and the heightened exposure in tourist areas.

Fig. 5 presents the risk results from a pilot case, illustrating the temporal fluctuations in dam risk. This figure captures how risk levels evolve over time, driven by variations in key factors such as flood events, previous pool levels, and population dynamics. It includes recalibrated flood estimates based on altered precipitation patterns, reservoir levels fluctuations due to shifts in water supply and demand, and both seasonal and long-term variations in the population at risk. The seasonal population changes reflect annual fluctuations, especially in tourist areas, while long-term variations account for demographic trends over the years. By dynamically illustrating these interactions, Fig. 5 offers valuable insights into how these factors collectively influence overall dam safety across different periods, highlighting the importance of considering both immediate and evolving risks in dam management strategies.

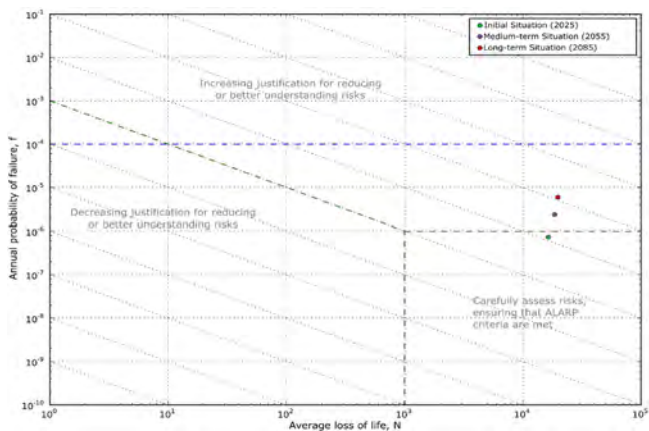


Fig. 5
Example of variation in risk over time in one of the dams.

Fig. 6 provides a comparison of long-term risk projections under two emission scenarios: RCP 4.5 and RCP 8.5. The RCP 4.5 scenario represents a moderate emissions pathway, while RCP 8.5 reflects a more severe emission trajectory. This figure demonstrates how the dam's risk profile may evolve over the long term under these contrasting emission scenarios.

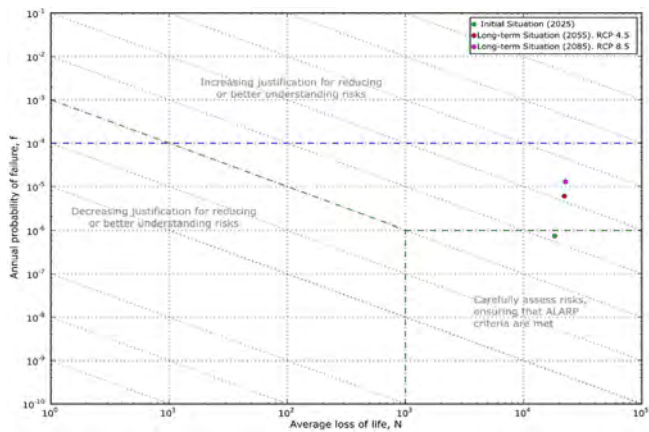


Fig. 6
Example of variation in risk depending on the emission scenario.

Together, these figures offer a comprehensive view of both short-term risk variations and long-term projections. They are fundamental to understanding how immediate and future climate scenarios affect dam safety, providing essential information for the development of robust risk management and mitigation strategies.

5. ACTION PRIORITIZATION AND DECISION MAKING

Once the risk assessment is completed for each one of the dams, these results will be used to prioritize risk reduction actions and to develop a National strategy to adapt Spanish dams to climate change. In order to combine the results of all the dams and prioritize risk reduction actions, the GARI online platform was developed.

The GARI (Management, Risk Analysis and Investment) platform, developed for the General Directorate of Water (DGA), is an indispensable tool for optimising the prioritisation of dam safety measures. This advanced system is designed to manage, analyze, and guide investments in dam infrastructure safety. The GARI platform integrates both semi-quantitative and quantitative risk assessments, allowing for a comprehensive evaluation of potential hazards. Using the iPresas GARI software, the platform carefully tracks the evolution of risks over time, enabling data-driven decision-making. This ensures that safety measures are prioritized based on their effectiveness and are implemented efficiently across multiple dams, significantly strengthening the strategic planning and resilience of Spain's dam infrastructure.

The prioritization process within the GARI platform unfolds in two main sequences of risk reduction actions:

1. **Semi-Quantitative Sequence:** This initial phase relies on the semi-quantitative classification of failure modes across all dams. By applying a matrix that evaluates the probability and potential consequences of each failure mode, critical areas requiring further investigation are identified. This approach prioritizes new studies and minor maintenance actions, particularly for high-priority failure modes, ensuring that resources are allocated to the most critical issues first.
2. **Quantitative Sequence:** The second phase leverages quantitative risk models to establish a prioritization criterion for proposed measures. The platform evaluates the risk reduction benefits and associated costs of each measure over its lifespan. Through an iterative process, the GARI software recalculates prioritization criteria, ensuring the selection of the most effective measures in sequence until all are addressed. This method guarantees an efficient and strategic implementation plan.

This two-sequences system to prioritize risk reduction actions is summarized in Fig. 7.

In the case of main risk reduction actions, the GARI platform aims to prioritize risk reduction measures to achieve the most rapid, effective, and equitable reduction in quantitative risk results. It uses risk indicators to quantify the efficiency and cost-effectiveness of each measure along time. The platform determines the optimal sequence for implementing these measures based on criteria such as immediate risk reduction, long-term benefits, or cost efficiency. By calculating indicators that consider costs and benefits over time, including replacement and maintenance costs (Fig. 8), the platform guides decision-making to focus on the most effective approach for each situation considering not only the current conditions but also the effect of climate change on risk.

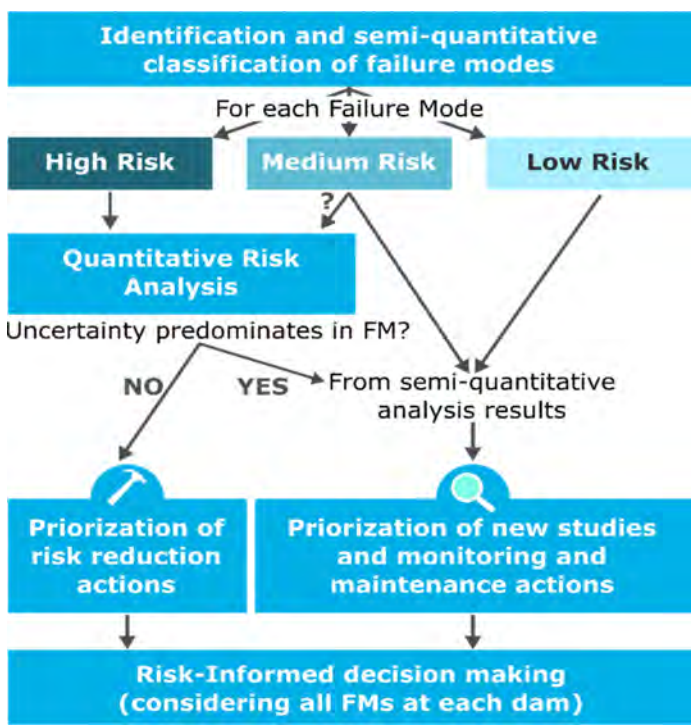


Fig. 7
Process to prioritize risk reduction actions.

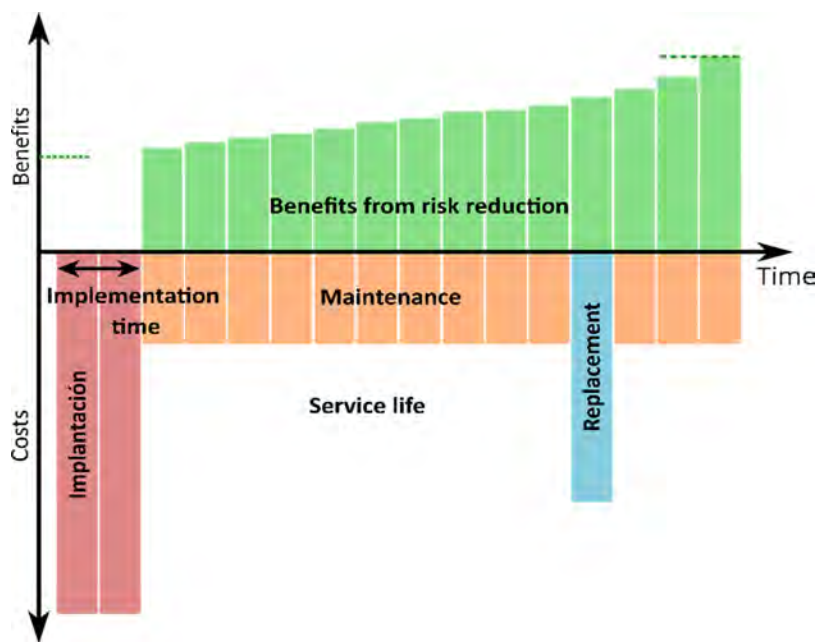


Fig. 8

Cost and benefits introduced for each risk reduction measure analyzed.

Furthermore, the GARI platform manages the temporal distribution of measure prioritization, considering variations in costs and benefits over time. Once a measure is selected, the timing for implementing subsequent measures depends on the annual budget available for safety measures. For example, if a measure chosen for 2022 costs €3.5 million and the annual budget is €1 million, the next measure will not be selected until the accumulated budget exceeds the cost of the following measure. This ensures measures are implemented efficiently within budget constraints.

Fig. 9 illustrates an example of the prioritization process for implementing 13 measures across 3 dams over time. This figure provides a clear visual representation of how these measures are scheduled and prioritized based on their risk reduction effectiveness and the available budget.

In addition, this platform can be used to prioritize risk reduction actions in each of the River Basis and at national level. In this sense, it is a very useful tool to support dam safety management at the different management levels.



Fig. 9

Results in GARI platform of Variation in risk over time and how it is reduced by effective implementation of measures.

In summary, the risk-informed dam safety management system optimally prioritizes safety measures through rigorous semi-quantitative and quantitative analyses. It effectively integrates budget constraints, evolving risk profiles, and temporal changes, ensuring that safety measures are implemented in a timely, efficient, and effective manner.

6. CONCLUSIONS

The development and implementation of Spain's risk-informed dam safety management system represents a significant advancement in adapting critical infrastructure to the challenges posed by climate change. As Spain, with its extensive network of dams, faces increasing risks from climate-induced alterations in precipitation and flooding patterns, this system offers a robust framework for enhancing the resilience of these vital structures.

The system's multi-phased approach, involving both semi-quantitative and quantitative risk analyses, ensures a comprehensive understanding of potential risks and their evolution over time. The integration of quantitative risk models allows for precise assessment and prioritization of risk reduction measures based on

detailed data. This method not only identifies immediate and critical areas needing attention but also adapts to long-term changes in climate conditions, ensuring that safety measures remain relevant and effective.

Semi-quantitative failure mode classification is a fundamental step in this process, categorizing potential problems based on their likelihood and potential impact. This classification informs the prioritization of new studies, monitoring enhancements, and maintenance actions, focusing on the most critical failure modes first. By addressing high-priority failure modes with significant consequences and high uncertainty, the system ensures that resources are allocated efficiently to mitigate the most pressing risks.

The methodology used further refines the prioritization process by calculating optimal implementation sequences for risk reduction measures. By considering both the benefits and costs of each measure over time, the platform generates a sequence that balances efficiency, effectiveness, and equity. This dynamic approach accommodates variations in costs, benefits, and budget constraints, facilitating the timely and effective implementation of safety measures.

The integration of climate change impacts into risk assessments and the strategic planning underlines the system's commitment to a forward-looking, adaptive management approach. The continuous evaluation and adjustment of risk management strategies ensure that dam safety is maintained in the face of evolving environmental conditions and increasing infrastructure demands.

In summary, Spain's comprehensive risk-informed dam safety management system is an example of a proactive and adaptive response to climate change. By leveraging advanced risk analysis methodologies and prioritization tools, the system not only addresses immediate safety concerns but also prepares for future challenges, ensuring the long-term sustainability and safety of dams.

REFERENCES

- [1] CEDEX, "Informe Técnico. Impacto del cambio climático en las precipitaciones máximas en España," 2021.
- [2] CWC, "Guidelines for Assessing and Managing Risks Associated with Dams", 2019.
- [3] SPANCOLD, "Análisis de riesgos aplicado a la gestión de seguridad de presas y embalses" Guía Técnica de explotación de presas y embalses. Vol 8, 2012.

- [4] USBR & USACE, "Best Practices in Dam and Levee Safety Risk Analysis" United States Bureau of Reclamation and United States Army Corps of Engineers, 2015.
- [5] FERC, "Engineering Guidelines Risk-Informed Decision Making" Federal Energy Regulatory Commission, 2015.
- [6] A. MORALES TORRES, A. SERRANO-LOMBILLO, I. ESCUDER BUENO & L. ALTAREJOS-GARCIA, "The suitability of risk reduction indicators to inform dam safety management", 2016.
- [7] FLUIXA-SANMARTÍN, J., ALTAREJOS-GARCÍA, L., MORALES-TORRES, A. & ESCUDER-BUENO, I. 2018. Review article: Climate change impacts on dam safety. *Nat. Hazards Earth Syst. Sci.*, vol. 18, no 9, p. 2471 2488.
- [8] FLUIXA-SANMARTIN, J., MORALES-TORRES, A., ESCUDER-BUENO, I. & PAREDES-ARQUIOLA, J. 2019. Quantification of climate change impact on dam failure risk under hydrological scenarios: a case study from a Spanish dam. *Nat. Hazards Earth Syst. Sci.*, vol. 19, no 10, p. 2117 2139.
- [9] FLUIXA-SANMARTIN, J., ESCUDER-BUENO, I., MORALES-TORRES, A. & CASTILLO-RODRÍGUEZ, J.T. 2020. Comprehensive decision-making approach for managing time dependent dam risks. *Reliab. Eng. Syst. Saf.*, vol. 203, p. 107100.

COMMISSION INTERNATIONALE DES
GRANDS BARRAGES

VINGT-HUITIEME CONGRES DES
GRANDS BARRAGES
CHENGDU, MAI 2025

**PKW SPILLWAYS: AN INNOVATIVE, SAFE AND ECONOMIC SOLUTION FROM
RUN-OF-RIVER DAMS IN PLAINS TO LARGE DAMS IN MOUNTAINS
SUITABLE FOR CLIMATE CHANGE CHALLENGES (*)**

Michel. HO TA KHANH
VNCOLD (Vietnam)

Frédéric LAUGIER & Jean VERMEULEN
EDF-CIH (France)

VIETNAM

SUMMARY

The paper describes two very different examples of Piano Key Weirs (PKW), highlighting the wide range of application and brought benefit: La Raviege dam PKW (40 m high concrete gravity dam, France) and the new Van Phong dam (Vietnam) equipped with 60 PKW units and 10 large radial gates.

RÉSUMÉ

L'article décrit deux exemples très différents de déversoirs à touches de piano (PKW), mettant en évidence le large éventail d'applications et les avantages apportés : le PKW du barrage de La Raviege (barrage-poids en béton de 40 m de haut, France) et le nouveau barrage de Van Phong (Viêt Nam) équipé de 60 unités PKW et de 10 grandes vannes radiales.

**Déversoirs à touches de piano : une solution innovante, sûre et économique pour les barrages au fil de l'eau dans les plaines et les grands barrages en montagne, adaptés aux défis du changement climatique*

1. INTRODUCTION

Piano Key Weirs (PKW), a special kind of labyrinth spillway, have been a quickly developing innovation during the past decade. In about 15 years since the first prototype was commissioned, more than 30 PKW were built all over the world in the 5 continents (Fig. 1).

The paper will focus on two very different examples of PKW, highlighting the wide range of application and brought benefit:

1. La Raviege dam PKW was commissioned in 2015 as part of a dam safety rehabilitation project.
2. The new Van Phong barrage was commissioned in 2014 (Vietnam). It is equipped with 60 PKW units and 10 large radial gates.

2. LA RAVIEGE DAM

2.1. GENERAL

La Raviege dam, operated by Electricité de France (EDF) is a gravity buttress dam 40m high (Fig. 2).



Fig. 2
La Raviege dam before the installation of the PKW

The release capacity of the two existing gated spillways, located in the centre of the dam, is $1000\text{m}^3/\text{s}$ under the reservoir Maximum Water Level (MWL). Recent update of the hydrology calculations of the dam catchment area revealed new extreme floods. The design flood peak discharge has been raised from $1000\text{m}^3/\text{s}$ to $1720\text{m}^3/\text{s}$ and a project aiming at increasing the dam safety has been studied.

Most of the solutions to face safely the new extreme floods combine the use of the reservoir storage capacity and an additional spillway on top of the dam. Following technical and economical studies including safety considerations, the new spillway has been designed as a free overflow one. Finally, the chosen solution consists of creating an additional structure on the left bank of the dam: this free surface spillway of the Piano Key Weir (PKW) type consists of 4 inlets, 5 outlets and 2 narrower closing inlets at each end. Considering that the existing gates will first operate, the new PKW will start to operate for major floods with return periods larger than 50 years.

The creation of the new PKW significantly improves the safety level of the dam:

- The PKW constitutes a new autonomous spillway whose failure rate is close to zero and the risks associated with the failure to open a gate will therefore be reduced thanks to this new PKW.
- With the consideration of a free space of 2 m above the PKW, the passage of floating debris during high flood will be improved.

2.2. MAIN FEATURES



Fig. 3
The hydraulic model



Fig. 4
La Raviège dam with the PKW

The PKW project combines the two existing radial gates and a new PKW spillway installed on the narrow crest of the dam. It can discharge $300\text{m}^3/\text{s}$. Beyond the 30% discharge increase, it significantly improves dam safety level especially in case of gate dysfunction and common mode.

A hydraulic model (Fig. 3), [1], was made for the detailed design phase to study several configurations. This model allowed the three following elements to be determined:

- Optimisation of the PKW flow rate by adapting its geometry,
- Definition of the stilling basin design to guide the flow to the chosen zone downstream,
- Checking the impact of the PKW's flow on the flow of the two gated spillways.

The PKW has a height of 4.22m, a global width of 25.82m and occupies the top of a little bit more than two blocks of the dam. Its crest is at the Full Supply Level (FSL). The weir developed length is 176.6m. The energy dissipation structure has been designed as a converging smooth channel with varied slopes and downstream deflectors (Fig. 4).

The final design of the flood control structures enables to maintain the FSL at its current elevation while releasing the updated design flood with a reservoir elevation 1.41 m above this normal level. In that case, peak discharge on the PKW is $300\text{m}^3/\text{s}$ and $1100\text{m}^3/\text{s}$ through the gates fully opened.

Huge works were necessary to build this new structure on the top of the existing dam: 1000m^3 of dam concrete were demolished, the new spillway was built as well as a new road bridge over the crest of the dam, and a stilling basin to protect the structure's downstream toe and guide the flow.

Treating the contact between the old and new layers of concrete and the continuity of the dam block joints in the PKW are two important issues in ensuring the safety, stability and watertightness of this new structure and therefore its durability.

During this work, safety issues related to the management of reservoirs and in particular the routing of floods were essential, so the deconstruction works during seasonal floods were carried out with great care.

The total cost of the project was 4800×10^3 USD (including the new bridge, the dam retrofitting and the downstream structures) but the cost of the PKW was only 1180×10^3 USD.

3. THE VAN PHONG BARRAGE

3.1. GENERAL

The Van Phong barrage, [4] & [5], is about 70km from Quy Nhon. The dam derives the water through a main canal for irrigation by gravity of 10 815ha in the plain near the ocean. The reservoir FSL is determined by the highest possible entrance canal level and the MWL must avoid large inundated zones upstream with probable huge resettlement issues.

Among the 3 alternatives examined (Fig. 5) in order to maximize the FSL and to make this scheme possible:

- Alternative 1: a barrage with 28 slide gates,
- Alternative 2: a barrage with 28 radial gates,
- Alternative 3: a combination of 60 PKW units on the Left Bank and Right Bank, and 10 radial gates (H= 3.5m, L= 15m) in the central part, this alternative was found as the most appropriated for the cost and the dam safety.

To note that a minimum of gates is necessary to lower the FSL if necessary and to evacuate the sediments. In the case of the Van Phong barrage, this minimum is found inferior to 10, but this last number was retained with caution.

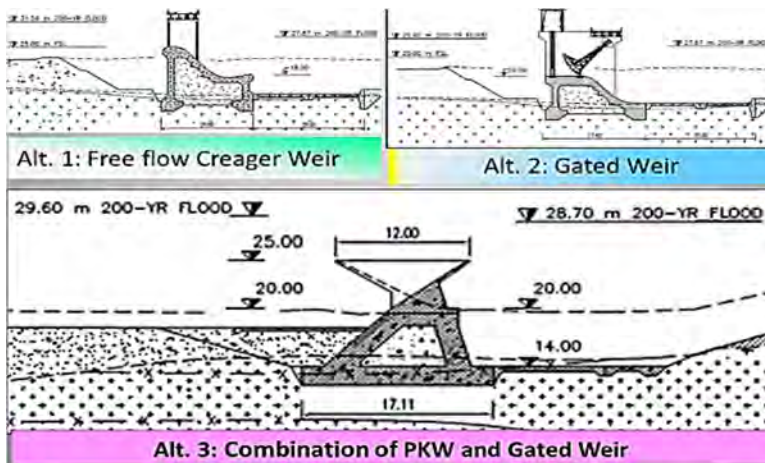


Fig. 5
Comparison of 3 Van Phong alternatives at the feasibility stage

Table 1
Comparison of Van Phong alternatives at the feasibility stage

NO	ITEMS	COST ESTIMATES IN 10 ³ USD		
		ALTERNATIVE 1 WITH 28 SLIDE GATES	ALTERNATIVE 2 WITH 28 RADIAL GATES	ALTERNATIVE 3 WITH 10 RADIAL GATES + PKW
1	Civil works	23 789	24 095	19 744
2	Mechanic & Electric- Electronic Equipment	10 169	8 460	3 085
3	Project Management	366	351	256
4	Consultancy Service	764	733	642
5	Others	492	472	561
6	Contingencies	3 558	3 411	2 394
7	Total	39 138	37 522	26 682

Table 1 shows a very significant investment cost saving for the Alternative 3, but this advantage is definitely greater if the operating and maintenance costs and the safety of functioning are taken into account in this comparison.

3.2. MAIN BARRAGE CHARACTERISTICS

The PKW were selected as part of the project design as they can spill a significant discharge for a low nappe depth, which fits the site constraint of low allowable upstream water level. This combination is also safer and cheaper than solutions with either all gates or flaps gates.

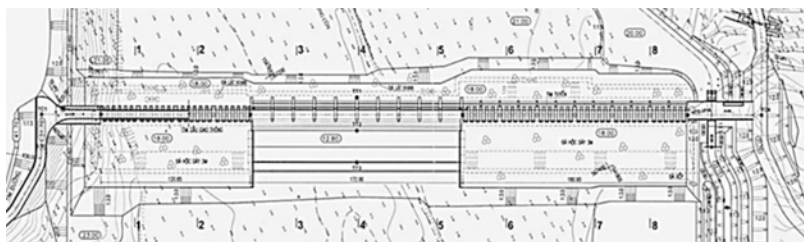


Fig. 6
Plan view of the Van Phong barrage

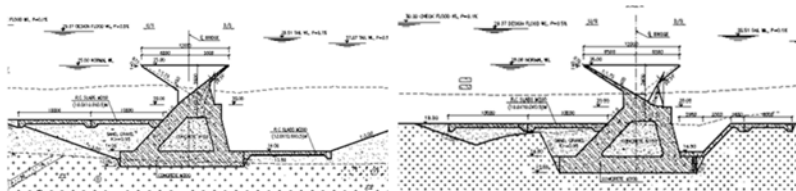


Fig. 7
Cross sections (inlet and outlet keys) of the PKW

The main characteristics of the Van Phong dam (Fig. 6 & Fig. 7) are:

- Total length of the dam: 474m, with a length of the PKW = (181m, on the R.B +121m, on the L.B) and length of the gates = 172m.
- Max height of the dam on foundation: 12m to 16m with 7m on the river bed.
- The dam, with 60 PKW units and 10 radial gates, was tested with a large scale hydraulic model (Fig. 8) in the SIWW Hydraulic Laboratory of Ho Chi Minh City with 3 models at different scales.
- The 1000-year flood event is 15 350m³/s and the maximum discharge of the PKW is 8700m³/s. For floods higher than the 100-year flood, the barrage is completely submerged.



Fig. 8
Hydraulic model tests for submerged flows

The Fig. 9 indicates the main dimensions of the Van Phong PKW units, according to the general notation for the PKW structures:

The Fig. 10 & Fig. 11 show the Van Phong barrage with the FSL and with a low overflow.

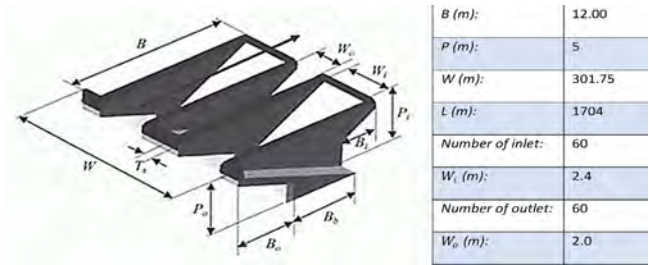


Fig. 9
Main dimensions of the Van Phong PKW units



Fig. 10
View of the Van Phong barrage with the FSL



Fig. 11
View of the Van Phong barrage during a low overflow

3.3. THE PEAK FLOOD ON THE 16TH OF DECEMBER 2016

During the peak flood ($3500\text{m}^3/\text{s}$), measured on a gauging station just upstream the dam on the 16th of December 2016, the max PKW discharge was $2630\text{m}^3/\text{s}$, the upstream level was 0.38m above the downstream level and 0.55m above the FSL at El. 25.00, very near the values measured on the hydraulic model and conform to the design (Fig. 12).

The water-surface profiles for the alternatives totally gated or with PKW are very similar upstream to downstream. This shows the very good hydraulic behaviour of the PKW for submerged flows and the efficiency of the PKW for evacuating the floods with a limited raising of the upstream water level (Fig. 13) [6].

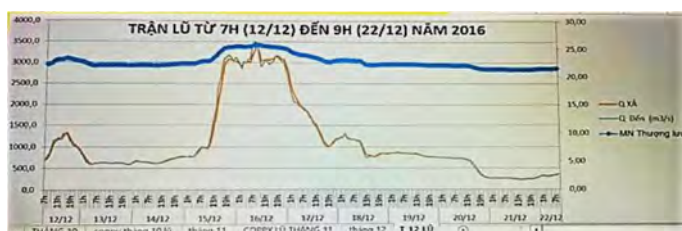


Fig. 12
Max discharge and Max Water Level



Fig. 13
Photos (U/S and D/S) of the 16th of December 2016 flood on the PKW

3.4. FLOATING DEBRIS

Water hyacinths (Fig. 14). used for artisanal baskets - arrived sometimes at the barrage, but they are automatically overflowed as soon as the reservoir level is higher than the FSL.



Fig. 14
Water hyacinths at the PKW

4. OBSERVATIONS ON THE ALTERNATIVE WITH (PKW+ GATES)

4.1. NECESSITY TO HAVE SOME RADIAL GATES

It's necessary to combine the PKWs with some radial gates in order to be able to lower the reservoir water level and to evacuate in operation a significant part of the sediments.

Lowering the water level H during high floods is often the main purpose of the project and it also justifies and optimizes the utilization of the PKW in place of a Creager weir as the ratio $\Delta Q/Q$ is higher for the low values of H , for a given PKW (Fig. 15).

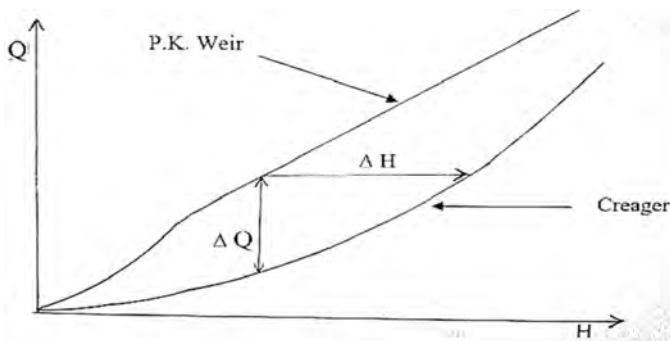


Fig. 15
The ratio $\Delta Q/Q$ is higher with the low values of H

4.2. PKW AND LABYRINTH WEIRS

The Fig. 17, with in abscissa the water head H and in ordinate the specific discharge q , shows that the PKW (type A) has a bit higher capacity than the two other alternatives.

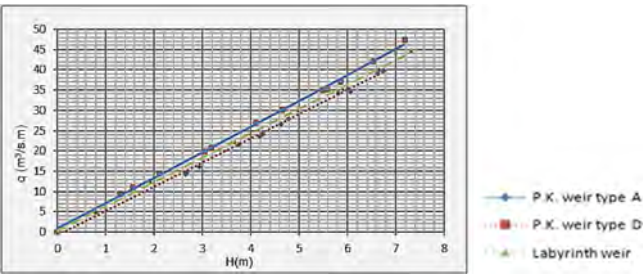


Fig. 16
Comparison of 3 alternatives

The choice between a PKW (type A), a rectangular PKW (type D) or a trapezoidal labyrinth at the Phu Phong barrage - a low dam downstream the Van Phong barrage (Fig 16) - depends essentially on the foundation conditions, the method of construction and the total cost of the three alternatives. It can be optimized only after a complete study of these three alternatives [4].



Fig. 17
The labyrinth weir on the Phu Phong barrage

5. CONCLUSION

A PKW solution has been designed at La Raviege dam to increase the dam safety towards extreme floods.

This example shows that with a PKW, a significant increase in the capacity of an existing spillway thanks to a new one placed on a short available length of the dam crest is possible. This solution has the advantage of being highly reliable, while requiring a minimum of the operating and the maintenance of the structure.

The feedback from other PKWs built at EDF facilities in France since 2006, [2] & [3], was used to build this new PKW. The methods, equipment and tools have improved and have been adapted to ensure the safety of the workers and faster execution.

The new solution of a combination of gates and PKW (or labyrinth weir) for a long barrage has many advantages of costs for investment and operation and safety during high floods [4].

The proposed hybrid solution of (PKW or labyrinth + Gates), compared with a traditional barrage, shows that the choice of a site, even with a broader stretch of the river, may be the best solution.

REFERENCES

- [1] ERPICUM, S., LAUGIER, F., NAGEL V. 2011. "PKW design optimization at Raviege dam". *International Workshop on Labyrinth and Piano Key weirs*, Liège, Belgium.
- [2] LAUGIER, F., VERMEULEN, J. – "Lessons learnt on Design and Construction of Labyrinth Piano Key Weir (PKW) Spillway for a large set of dams: Specific cases and research actions" - 2015 – *ICOLD 25th Congress – Stavanger – Q97* -
- [3] LAUGIER, F., VERMEULEN, J. & BLANCHER, B. "Overview of design and construction of 11 Piano Key Weirs spillways developed in France by EDF from 2003 to 2016 - *Labyrinth and Piano Key Weirs III – PKW 2017 – Erpicum et al. (Eds) © 2017 Taylor & Francis Group, London, ISBN 978-1-138-05010-5*"
- [4] HO TA KHANH, M., TRUONG CHI HIEN, PINCHARD, T., PRALONG, J., 2013. "Utilization of Piano Key weirs for low barrages". *International Workshop on Labyrinth and Piano Key weirs*, Paris, France

- [5] DINH SY QUAT, NGUYEN LUONG AM, NGUYEN MANH HUNG. 2017. Study, Design and Construction of the Van Phong Piano Key Weir. International Workshop on Labyrinth and Piano Key weirs, Qui Nhon, Vietnam. *Labyrinth and Piano Key Weirs III – PKW 2017 – Erpicum et al. (Eds)* © 2017 Taylor & Francis Group, London, ISBN 978-1-138-05010-5”.
- [6] HO TA KHANH, M., HAI NGUYEN THANH & THANG TANG DUC, “Research on Piano Key Weirs capacity for free and submerged flows”. International Workshop on Labyrinth and Piano Key weirs, Qui Nhon, Vietnam. *Labyrinth and Piano Key Weirs III – PKW 2017 – Erpicum et al. (Eds)* © 2017 Taylor & Francis Group, London, ISBN 978-1-138-05010-5”.

COMMISSION INTERNATIONALE DES
GRANDS BARRAGES

VINGT-HUITIEME CONGRES DES
GRANDS BARRAGES
CHENGDU, MAI 2025

**DAM UPGRADE WITH PIANO KEY WEIR FOR DISCHARGE OF EXTREME
FLOODS (*)**

James YANG
Ph. D. (Civ. Eng.), R&D Specialist
R&D Hydraulic Laboratory, Vattenfall AB
KTH Royal Institute of Technology

Anders FRISK
M. Sc. (Civ. Eng.), Senior Engineer
River Hydraulics and Environment, AFRY

Mats BILLSTEIN
Ph. D. (Civ. Eng.), R&D Hydro Manager
R&D Hydraulic Laboratory, Vattenfall AB
Luleå University of Technology

Peter MATTIASSON
M. Sc. (Civ. Eng.), Project Manager
Sydkraft Hydropower AB

Lars JOHANSSON
M. Sc. (Civ. Eng.), Dam Safety Engineer
Sydkraft Hydropower AB

SWEDEN

**Amélioration de la sécurité d'un barrage par l'ajout d'un déversoir à touches de piano pour l'évacuation des crues extrêmes*

SUMMARY

The Lillflyforsen dam suffers from aging and deterioration in its embankment dam and insufficient spillway discharge capacity. The former would require costly engineering measures to amend. Placed downstream of the dam, a piano key weir (PKW) is proposed to replace the embankment dam and to add additional discharge capacity. Model tests at two scales are performed to examine such issues as reservoir flow pattern, discharge capacity and energy dissipation. With partial excavation of the embankment dam and the cofferdam, decent approach flow conditions are attained at high flow discharges. The PKW and the gated spillway suffice to release the design flood of the dam, with satisfactory energy dissipation.

RÉSUMÉ

Le barrage de Lillflyforsen est impacté par le vieillissement et la détérioration de son barrage en remblai et une capacité de déversement insuffisante de l'évacuateur de crues. La modification du premier nécessiterait des mesures d'ingénierie coûteuses. Placé en aval du barrage, un déversoir à touche de piano (PKW) est proposé pour remplacer le barrage en remblai et ajouter une capacité de déversement supplémentaire. Des tests sur modèle à deux échelles sont effectués pour examiner des questions telles que le modèle d'écoulement du réservoir, la capacité de déversement et la dissipation d'énergie. Grâce à l'excavation partielle du barrage en remblai et du batardeau, des conditions d'écoulement d'approche raisonnables sont obtenues aux débits élevés. Le PKW et le déversoir à vannes suffisent à déverser la crue de projet du barrage, avec une dissipation énergétique satisfaisante.

1. INTRODUCTION

The Lillflyforsen hydropower scheme, commissioned in 1965, is situated on the Fjällsjö River in Mid Sweden. Fig. 1 shows its view from downstream. In addition to a power station, the facility is composed of a spillway, a 30 m gravity dam to its left, and an embankment dam to its right. The embankment has a max. structural height of ~10 m, and its crest is 5 m wide, 110 m long and 1.75 m above the full reservoir water level (FRWL). The three-opening spillway is equipped with upward-going tainter gates, with a total net width of 34 m. The leftmost and middle gates (denoted as A and B), each 12 m wide, are of the same make, with their sills 5.35 m under the FRWL. The rightmost gate (denoted as C) is 10 m wide, with its sill 2.65 m below the FRWL.



Fig. 1
The Lillflyforsen facility, downstream view
L'installation de Lillflyforsen, vue aval

In the light of the recommendations from the performed safety evaluations, dam upgrading is planned. The reason is threefold.

- The dam-safety evaluations show that the existing spillway is insufficient to accommodate the design flood as prescribed by the dam-safety guidelines, thus leading to the need for additional spillway capacity. The discharge from the three gates is $\sim 560 \text{ m}^3/\text{s}$ at the FRWL, which can be compared with the design flood within the interval $900\text{--}1000 \text{ m}^3/\text{s}$.
- Gate C suffers from deterioration, rendering it less reliable than gates A and B that are already refurbished, and is in need of rehabilitation to remain in operative conditions. Besides, its sill el. is only 2.65 m under the FRWL, giving rise to limited capacity ($\sim 60 \text{ m}^3/\text{s}$ at the FRWL).
- Geotechnical survey indicates that the embankment dam is in poor conditions due to aging, requiring substantial rebuilding measures to meet the structural safety standard.

2. UPGRADE ALTERNATIVE

A few options for the dam upgrade have been evaluated, including new spillway gates and rehabilitation of the embankment dam. Comparisons suggest that the most favourable and cost-effective upgrade alternative is the construction of a piano key weir (PKW) downstream of the embankment dam (Fig. 2). The PKW dam is assigned a L-shaped planform, connecting to the existing spillway section to its left and extending to the right riverbank via a short low buttress dam. The total PKW

length amounts to ~ 100 m. Its crest elevation is set the same as the FRWL. It is placed on a low concrete dam. Upon completion, the embankment dam is excavated to an elevation that does not unfavorably affect the approach flow.

As shown in Fig. 2, there exists remainder of a cofferdam in the reservoir from the dam construction period. In a bended planform, it runs from spillway opening C to the right riverbank, with a length ~ 220 m, a base width 13.0–16.0 m and a crest width 6.0–9.0 m. Its crest elevation is 3.0–4.0 m below the FRWL. In the existing situation, the cofferdam does not influence much the inflow to the spillway. Besides, due to the limited approach flow velocity, no obvious erosion of the cofferdam is observed.



Fig. 2

Layout of the rebuilding alternative, with a PKW downstream of the existing embankment, seen from downstream

Schéma de la proposition de reconstruction, avec un PKW en aval du remblai existant, vue depuis l'aval

To obtain satisfactory flow conditions of the PKW, hydraulic model tests are performed in two different sizes. At a 1:12 scale in a flume, two PKW models are first assessed, taking into account the discharge capacity and overflow patterns. With the selected PKW shape, an overall model, incorporating both the PKW and the existing spillway, is constructed at a 1:35 scale. The issues of concern include reservoir flow patterns, discharge capacity, and energy dissipation. As the embankment dam runs across the approach flow to the PKW, it must be excavated. It might also be necessary to lower the cofferdam to improve the flow pattern. To which elevation they should be removed needs to be evaluated.

3. PKW FLUME TESTS

Fig. 3 defines the major parameters of PKW with both up- and downstream overhangs, in which T_s = wall crest thickness, W_i , W_o = inlet and outlet key width, P_i ,

P_o = inlet and outlet key height, B_i , B_o = crest length of inlet and outlet key overhang (excluding T_s), B_b = weir base length, S_i , S_o = parapet wall height of inlet and outlet key, α_i , α_o = angle of the inlet and outlet key floor with the horizontal plane, and subscripts i and o denote the inlet and the outlet key, respectively. S_i and S_o may not necessarily be the same.

Two PKW options are examined in the flume (denoted as 1:12 flume model). Their prototype sizes listed in Table 1, with the weir height of each option being $P = 3.75$ m.

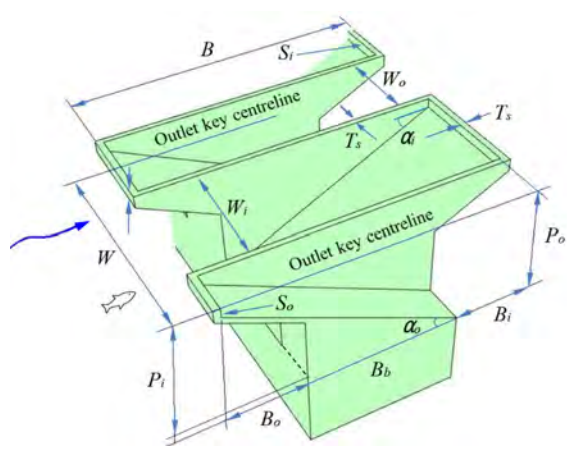


Fig. 3
Parameter definition of a PKW
Définition des paramètres d'un PKW

Table 1
Prototype dimensions of PKWs (length unit: m, angle unit: degree)

PARAMETER	W_i	W_o	T_s	B_i	B_b	B_o
Option 1	2.00	1.60	0.35	1.45	3.75	1.45
Option 2	1.80	1.40	0.35	1.45	3.75	2.45
PARAMETER	S_i	S_o	α_i	α_o	P_i	P_o
Option 1	0	0.50	31.6	30.0	3.20	3.50
Option 2	0	0.50	33.9	25.8	3.50	3.50

The tests are performed at the 1:12 scale, with three PKW units placed flush with the downstream end of a flume (Fig. 4). The flume length and width are 11.00

and 2.00 m. In the middle, a channel is set up, with a straight length of 4.50 m. Three weir units fit into the channel, whose width is individually adapted to each option. Owing to the long flume, satisfactory approach flow conditions are obtained. The models are 3D-printed. Each PKW model is 31.25 cm high ($P = 3.75$ m in prototype size), resting on a 0.20 m high base (2.40 m in prototype size). A calibrated magnetic flow meter ($\phi 200$ mm) records flow rates in the flume. Water stages are monitored at points M3 and M4 on the channel axis (3.00 and 4.00 m upstream of the PKW). The test rig description and surface finishing from 3D printing can be found in [1].

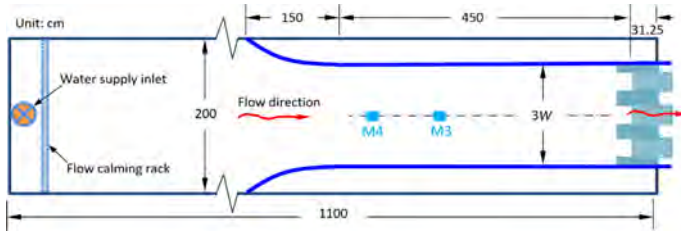


Fig. 4

Test layout of PKW in a flume, scale 1:12

Configuration d'essai du PKW dans un canal, échelle 1:12

The width of a single weir unit and the streamwise weir crest length (inclusive of the crest walls) are

$$W = W_i + W_o + 2T_s \quad (1)$$

$$B = B_i + B_o + B_b + 2T_s \quad (2)$$

The angle of each sloping key floor with the horizontal plane reads

$$\tan(\alpha_i) = (P_i - S_i) / (B_b + B_i) \quad (3)$$

$$\tan(\alpha_o) = (P_o - S_o) / (B_b + B_o) \quad (4)$$

Measured along the crest centreline, the developed crest length (referring to one single weir cycle) is

$$L = 2B + W_i + W_o \quad (5)$$

For option 1, $B = 7.35$ m, $W = 4.30$ m and $L = 18.30$ m; for option 2, $B = 8.35$ m, $W = 3.90$ m and $L = 19.90$ m. Fig. 5 displays, for option 2, the PKW in the flume and

the flow pattern at water head $H = 0.85$ m and the flow rate over one weir unit $Q = \sim 22$ m³/s. Fig. 6 compares the H - Q results between the two options.



Fig. 5

Flume test of option 2. (a) PKW mounted at the flume end; (b) Flow pattern at $H = 0.85$ m and $Q = \sim 22$ m³/s

Tests du canal de l'option 2. (a) PKW monté à l'extrémité du canal; (b) Modèle d'écoulement à $H = 0,85$ m et $Q = \sim 22$ m³/s

The results show that option 2 is more effective than option 1. At e.g., $H = 0.80$ m, their discharge $Q = 20.4$ and 17.3 m³/s, respectively. The augment in flow discharge is more obvious as H increases. Option 2 has somewhat smaller key widths, its streamwise crest (B) is however 1.00 m longer, leading to an 8.7% increase in developed crest length (L). Considering both the discharge capacity and the flow pattern at high heads, option 2 is chosen for further evaluation in the $1:35$ model. The submergence effect in the outlet keys is also an essential factor affecting the choice. It is observed that, at $H \approx 1.0$ m (perhaps the upper limiting water stage), the outflow is still free. Beyond this range, the performance is not relevant anymore for this practical application.

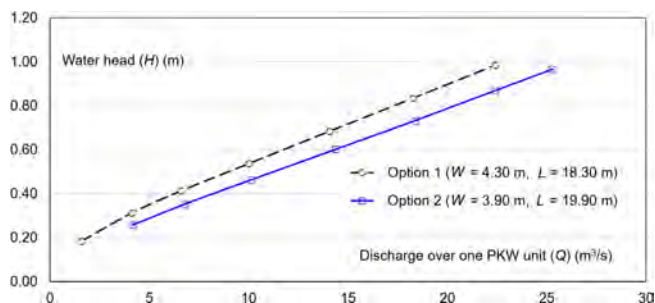


Fig. 6

Test results of discharge capacity of one weir unit (Q)

Résultats des tests de capacité de déversement d'une unité de déversoir (Q)

4. OVERALL FLOW BEHAVIOR

The 1:35 scale model includes a 150 m reservoir length and a 100 m river valley downstream and covers the whole river width (denoted as 1:35 floor model). To achieve high modelling accuracy, the reservoir bathymetry (echo-sounded), the river terrain downstream (laser-scanned), the PKW and the existing spillway (including piers and gates) are all manufactured with the machine milling technique. The surface finishing is smooth and uniform, which is essential taking into consideration the model dimensions. Fig. 7 shows the view of the model looking downstream. For the natural topography and the concrete structure, Styrofoam (density 300 kg/m^3) and Ureol material (density 700 kg/m^3) are used. A calibrated magnetic flow meter ($\phi 200 \text{ mm}$) measures flow rates into the model.



Fig. 7

Hydraulic model over the facility, scale 1:35
Maquette hydraulique de l'installation, échelle 1:35

4.1. PKW DISCHARGE CAPACITY

The PKW design involves 23 regular (identical) weirs, a half weir at each end, and an irregular weir in the corner. The upstream dihedral angle between the two straight segments is 108° . Counted along the wall crest centerline, their total developed crest length amounts to $L_{total} = \sim 488 \text{ m}$. As $L = 19.90 \text{ m}$ in option 2, the layout is equivalent to $L_{total}/L \approx 24.5$ regular weirs.

To compare the total discharge capacity of the $\sim 100 \text{ m}$ long PKW with the flume results, both the embankment dam and the cofferdam are levelled with the riverbed elevation in the model and the existing gates are all closed. Fig. 8 presents a comparison of flow capacity between the two models. The position for gauging the

water levels is ~ 35 m from the PKW on the right riverbank. The flow rate in the 1:12 flume model is converted to the prototype capacity in proportion to the total developed crest length. The 1:35 floor model results in a slightly lower capacity, and the difference between them gets somewhat larger as H increases.

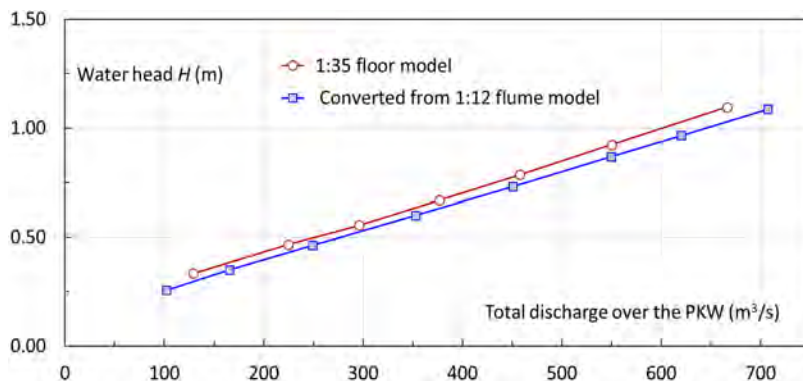


Fig. 8

Comparison of discharge capacity between the 1:12 and 1:35 models
Comparaison de la capacité de déversement entre les modèles 1:12 et 1:35

Besides manufacture and measurement errors, the reasons for the discrepancy are sought in the following aspects.

1. The PKW axis in the flume is at the right angle with the approach flow. With the L-shaped planform in the prototype, the axis of the left PKW portion (~ 33 m long) is at a 20° angle with the approach flow in the reservoir, which affects the capacity. However, no efforts are made to address this effect in the study.
2. The base beneath the PKW adopted in the flume experiments corresponds to a 2.4 m height, while the height in the prototype varies from 0.5 to ~ 7.0 m.
3. The reservoir being shallow, especially on the right riverbank, its bed roughness height is not small in relation to the flow depth, thus giving rise to head losses.
4. Erpicum et al. [2] evaluated the PKW flow discharges at three model scales (1:7, 1:15 and 1:25) and compared their results with the prototype data. They found that a minimum water head of $H = 3$ cm was required to avoid the scale effects caused by surface-tension and viscous forces. Similar results were found in [3]. However, in the 1:35 model, the maximum H value is below this limit, suggestive of certain scale effects in the experimental results.

These contributing factors presumably account for the flow difference between the two types of models.

4.2. REMOVAL OF EMBANKMENT AND COFFERDAM

When the construction of the PKW is accomplished, part of the embankment dam is removed. However, to excavate underwater is costly. There might not be a need to remove its whole height or length, instead only to an elevation that does not in an obvious way affect the discharge.

As shown in Fig. 9a, the lower part of the cofferdam follows roughly the flow direction. However, its upper part intersects the flow if the PKW is in operation. Besides, in relation to the water depth (6.0–9.0 m at the FRWL), its height is 3.0–4.0 m above the riverbed. Whether its whole height or only its upper part needs to be excavated has bearing on the costs. The underwater excavation is a trade-off between costs and flow conditions.

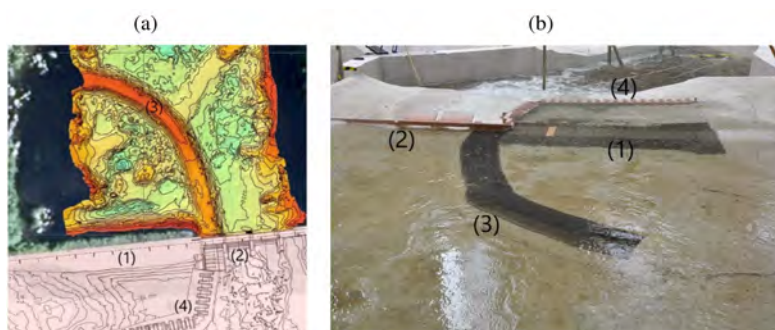


Fig. 9

Excavation of the embankment dam and the cofferdam

Excavation du barrage en remblai et du batardeau

- 1 embankment dam
- 2 existing spillway
- 3 cofferdam
- 4 piano key weir (PKW)

- 1 barrage en remblai*
- 2 déversoir existant*
- 3 batardeau*
- 4 déversoirs à touche de piano (PKW)*

For both the embankment dam and the cofferdam, flow patterns at a few excavation levels are examined at high flows. The tests show that, to obtain decent approach flow conditions and not to encroach much on the discharge capacity of the PKW, it is sufficient to lower the embankment dam to an elevation 3.0 m below the FRWL, extending ~72 m from the spillway. The adjacent 20 m, with shallow water even at high floods, is levelled with the surrounding riverbed.

Measurements also show that there is no need to excavate the cofferdam (Fig. 9b). Despite its large height in relation to the water depth, it does not affect the flow pattern and the approach flow in a measurable way. The flow velocity on the crests of the cofferdam and the remaining embankment measures below 1.5 m/s. However, there might be a risk of erosion in the embankment during high floods, resulting in deposition of fine sediment between it and the PKW. To mitigate this, the riprap in the dam slopes can be laid on the excavated crest, which also cuts costs as transport is avoided. To facilitate the excavation, the reservoir level should be lowered.

4.3. DISCHARGE CAPACITY AFTER EXCAVATION

With the existing cofferdam and the remaining height of the embankment dam, tests are made to determine the total discharge capacity of the facility. Due to its limited capacity and high costs for refurbishment, gate C will be removed, and the crest is elevated and re-shaped to form a free overflow weir, with a new sill elevation set at the FRWL. Its capacity is $\sim 10 \text{ m}^3/\text{s}$ at a 0.80 m water level above the FRWL. Thus, the design flood is jointly handled by the remaining two gates and the PKW.

Fig. 10 presents the relationship between reservoir water level and flow discharge. At the FRWL, there is no flow over the PKW and the weir in opening C; the discharge capacity of the two gates combined is $\sim 500 \text{ m}^3/\text{s}$. To release the design flood requires a temporary water-level rise in the reservoir. At a 0.80 m water level above the FRWL, the total capacity of the facility exceeds $1000 \text{ m}^3/\text{s}$. As discussed above, the PKW size in the 1:35 model causes certain scale effects on the discharge determination. However, from the safety point of view, the results are conservative and on the safe side.

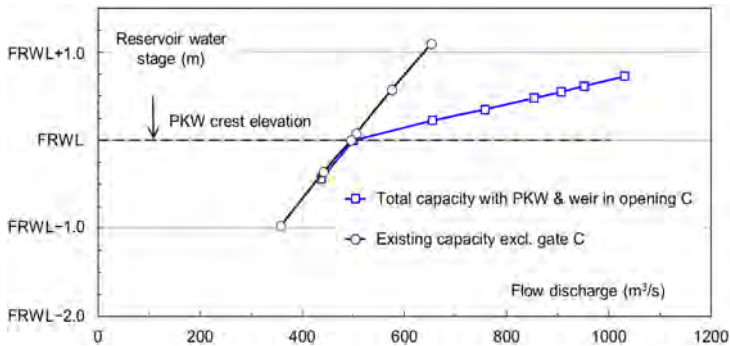


Fig. 10
Discharge capacity after excavation
Capacité de déchargement après excavation

4.4. FLOATING DEBRIS

In the event of large floods in Sweden, a significant number of trees may be eroded from the riverbanks and transported to the dam site. Their behavior at the PKW is an issue that affects the flood discharge reliability. The design and operation must consider how the trees will be handled and if there is need to install a debris boom at a proper location upstream. For a specific catchment, the tree origin, size, shape, etc. should be mapped. If trees accumulate in front of the PKW without passing over, the resulting reservoir water level increase should be estimated. Due to the roots and branches, to discharge and lift trees over the PKW requires seemingly a larger water head than to release ice floes.

4.5. ENERGY DISSIPATION

The energy dissipation is an issue of concern at high floods. The PKW involves the erosion risk from the falling jets at the impact location, where the receiving water depth depends on the layout downstream. This differs from a plunge-pool solution where the water depth is significant. At some EDF's PKWs, the jets fall directly on the downstream face of the concrete dams [4]. At a given discharge, the tailwater level is based on 1D numerical modelling and is regulated with a flap gate at the model end. With flows over the PKW and from the gated spillway, Fig. 11 shows the flow pattern downstream at discharge $\sim 1000 \text{ m}^3/\text{s}$.



Fig. 11

Energy dissipation of flows from the PKW and the existing spillway
Dissipation énergétique due aux débits du PKW et du déversoir existant

The flow from the left PKW portion (~33 m in length) interacts with the flow from the two gates, resulting in a standing wave at the interface. The flow from the gates is discharged directly on the bedrock, without formation of hydraulic jump. To the left the standing wave, the supercritical flow propagates some 90 m downstream, without being affected by the tailwater. At the design flood, the water depth along the toe of the PKW amounts to 1.5–3.5 m, providing, albeit limited, a cushion (not really a plunge pool) for the PKW flow jets.

It is observed that, except for the six rightmost PKW units, the jet falling from the downstream overhang impinges on the sloping concrete surface, both at low and high flows. The outflow from the outlet key leaves in the form of a concentrated jet, which has no direct contact with the concrete surface (except for at very low flows). It is envisaged that two or three horizontal steps can be installed in the lower part of the outlet key [4]. By so doing, the jet trajectory would be modified, with its impingement location moved somewhat downstream from the concrete-bedrock interface. This would also enhance the air entrainment into the flow, helping mitigate the impacts on the rock.

In the model, the free-falling jets are thin films of so-called black water, thus forming enclosed air cavities behind the jets. Judged from experiences from similar PKWs, air should be supplied to the air cavities to avoid jet fluctuations and vibration. As supported by both the theoretical analysis and prototype observations, air flow is not correctly simulated if the flow velocity in a model is below 6.5–7.0 m/s [5], which is the case in this project. The jets may break up and become (partially) aerated in the prototype. One can resort to CFD modeling to justify the issue. However, the CFD model must be validated before any predictions of jet behavior and air demand. For the proposed PKW, an air-supply pipe system will be designed to aerate the flow.

5. CONCLUSIONS

Due to the insufficient spillway discharge capacity and the aging deficiency in the embankment dam that is costly to remedy, a solution of piano key weir (PKW) is proposed to augment the spillway discharge at Lillflyforsen. It is constructed in a L-shaped planform downstream of the embankment dam. Upon the PKW completion, the embankment dam is partially removed.

With the purpose to obtain a favorable PKW configuration, flume tests at a scale of 1:12 are first performed. The models are 3D-printed. The configuration chosen for the upgrade design has a 3.90 m unit width and a 19.90 m developed crest length. The weir is 3.75 m in height, and it is built on a low concrete dam.

To evaluate the overall hydraulic behavior, a 1:35 floor model is built, incorporating both the PKW and the gated spillway. The rightmost spillway opening is modified to an overflow section. The whole model is manufactured with machine milling technique. Affected by several factors, the discharge capacity is somewhat lower than the upscaled result from the flume tests.

A height of 4.75 m below the embankment crest can be removed. To mitigate the risk of erosion, the riprap from the excavated dam slopes can be placed on it. There is no need to excavate the cofferdam, which does not in a measurable manner encroach on the flow discharge. The risk of rock erosion at the PKW toe is limited. Despite the uncertainty with respect to jet behaviors and air entrainment in the prototype, an air-supply system is designed.

As the upgrade design is not yet finalized, the PKW design and the excavation extent of the embankment dam may be subject to modifications. Nevertheless, the PKW at the Lillflyforsen dam will be the first of its kind to be constructed in Sweden. Its behaviors, both hydraulic and structural, need to be monitored upon completion. In the Nordic climate, related aspects that concern both design and operation of PKWs include ice formation, (design) ice loading, structural stability, downstream consequence at winter floods, discharge of floating debris inclusive of ice floes, etc. [6,7].

ACKNOWLEDGEMENTS

The hydraulic model studies were carried out at Vattenfall's Hydraulic Laboratory, Älvkarleby. Anna Helgesson, Pär Nilsen, Erik Skepparkrans, Anders Sjödin, Magnus Lagerkvist, Jennifer Persson, Patrik Lidberg and Pauline Beltrando, all at Vattenfall R&D, were acknowledged for part of the model tests, CAD drawings, 3D-printing, machine milling, construction oversight, model assembling, instrumentation and assistance with French translation. James Yang made the formal analysis of the experimental results and prepared the manuscript. All authors consented to the submitted version to ICOLD.

REFERENCES

- [1] YANG, J., LI, S.C., HELGESSON, A., SKEPPARKRANS, E., ANSELL, A. Geometric modification of piano key weirs to enhance hydraulic performance and discharge capacity. *Water*, 2023, 15(23), 4148.

- [2] ERPICUM, S., TULLIS, B.P., LODOMEZ, M., ARCHAMBEAU, P., DEWALS, B.J., PIROTON, M. Scale effects in physical piano key weirs models. *Journal of Hydraulic Research*, 2016, 54(6), 692–698.
- [3] PFISTER, M., BATTISACCO, E., DE CESARE, G., SCHLEISS, A.J. Scale effects related to the rating curve of cylindrically crested piano key weirs. In *Labyrinth and Piano Key Weirs II – PKW 2013*; Proc. 2nd Int. Workshop on Labyrinth and Piano Key Weirs, Paris, France, 20–22 Nov. 2013; CRC Press, London, UK, 2013.
- [4] LEITE RIBERIRO, M., BOILLAT, J.-L., SCHLEISS, A.J., LAUGIER, F. Coupled spillway devices and energy dissipation system at St-Marc Dam (France). In *Labyrinth and Piano Key Weirs – PKW 2011*; Proc. Int. Conf. on Labyrinth and Piano Key Weirs, Liège, Belgium, 9–11 Feb. 2011; CRC Press, London, UK, 2011.
- [5] YANG, J., LI, S., LIN, C. Plausible differences between the laboratory and prototype behaviors of spillway aerator flows. *Water*, 2022, 14(20), 3264.
- [6] YANG, J. *Labyrinth and piano key weirs in Nordic climate – the state of the practice* (in Swedish). Energiforsk report, 2024, Stockholm, Sweden.
- [7] YANG, J., NORDSTRÖM, E., LI, S.C., KOCAHAN, H. Labyrinth and Piano Key Weirs in Cold Climate – Experiences from Prototype Facilities and Laboratories. 92nd ICOLD Annual Meeting and International Symposium, 29 Sept–3 Oct. 2024, New Delhi, India.

COMMISSION INTERNATIONALE DES
GRANDS BARRAGES

VINGT-HUITIEME CONGRES DES
GRANDS BARRAGES
CHENGDU, MAI 2025

DESIGN OF THE NEW SPILLWAY FOR REGAJÓ DAM (*)

Enrique CAMPOS

M.Sc. Civil Engineer, Confederación Hidrográfica del Júcar

Juan José REBOLLO

M.Sc. Civil Engineer, Centro de estudios hidrográficos CEDEX

José MILLA

M.Sc. Civil Engineer, GRANELL Hydraulic Engineers

Carmen BAENA

Ph.D. Civil Engineer, GRANELL Hydraulic Engineers

Carlos GRANELL

M.Sc. Civil Engineer, GRANELL Hydraulic Engineers

SPAIN

SUMMARY

Regajo Dam, located in the municipality of Jérica (Castellón, Spain), is a safety class A gravity dam finished in 1962. It is currently operational, with its main uses being irrigation and flood attenuation. The dam has a height of 27.5 meters from its foundations and a length of 355 meters. Currently, Regajo Dam faces an issue of inadequate hydraulic discharge capacity, resulting in the absence of necessary safety margins prescribed by the 2021 Spanish Technical Safety Standards for a category A dam. The almost negligible flood attenuation capacity of

**Conception du nouvel évacuateur du barrage de Regajo*

the reservoir, combined with the dimensions of the spillway, cannot safely discharge the design floods (1,000 and 5,000 years). The proposed solution involves the following combination of actions: lowering the Full Supply Level (FSL), replacing the gates in the existing spillway, raising the crest, adding a parapet, and most importantly, constructing a new spillway on the left bank. This article details the conception process of the spillway, its optimization, and the validation of its design through numerical and physical models. The proposed typology for the new spillway consists of a free-flow weir aligned with the dam, discharging into a stilling basin (with a 7° turn), a discharge channel (with a second control section), and a flow restitution structure back to the riverbed.

RÉSUMÉ

Le barrage de Regajo, situé dans la municipalité de Jérica (Castellón), est un barrage-poids de catégorie A, achevé en 1962. Il est actuellement en exploitation et ses principales utilisations sont l'irrigation et l'écrêtement des crues. Le barrage à une hauteur de 27,5 mètres depuis ses fondations et une longueur de 355 mètres. Actuellement, le barrage de Regajo présente un problème de capacité d'évacuation insuffisante, ce qui entraîne l'absence des marges de sécurité nécessaires prescrites par les Normes Techniques de Sécurité Espagnoles de 2021 pour un barrage classé A. La capacité d'écrêtement presque nulle du réservoir, combinée aux dimensions de l'évacuateur, ne permet pas d'évacuer les crues de projet (1 000 et 5 000 ans) dans des conditions de sécurité adéquates.

La solution proposée consiste en la combinaison des actions suivantes : abaissement du niveau normal de retenue (RN), remplacement des vannes du déversoir existant, rehaussement de la crête, ajout d'un mur parapet, et surtout, construction d'un nouvel évacuateur sur la rive gauche. Cet article détaille le processus de conception de l'évacuateur, son optimisation et la validation de ses formes par des modèles numériques et physiques. La typologie projetée pour le nouvel évacuateur comprend un évacuateur en nappe libre aligné avec le barrage, déchargeant dans un bassin de dissipation (avec un virage de 7°), un canal de décharge (avec une deuxième section de contrôle) et une structure de restitution des débits au lit de la rivière.

1. INTRODUCTION

Regajo Dam has been in operation for over 60 years. The new requirements outlined in the 2021 Spanish Technical Safety Standards for Dams, along with new hydrological studies using more advanced methodologies and a greater amount of

data (compared to what was available when the dam was constructed), are leading to an increase in the discharge capacity of existing dams, such as the dam discussed in this report. Currently, the *“Project for compliance with Technical Safety Standards for Regajo Dam and Reservoir”* is being drafted in two phases, with the second phase focusing on actions related to the hydrological safety of the dam and the redesign of the flow restitution to the riverbed.

In these cases, it is essential to design the relevant works with minimal impact on the existing dam and the operation of its reservoir, while also paying attention to the aesthetics and the relationship of each structure with its surroundings.

2. DESCRIPTION OF THE EXISTING DAM

The dam has a maximum height of 27.5 meters above its foundations, and its primary discharge mechanism is the spillway, located over the dam's body in the central blocks. There are two bottom outlets (which discharge into the spillway channel) and two irrigation intakes, which also discharge into the spillway basin through the side bays.



Fig. 1
Regajo dam
Barrage de Regajo

The spillway is a frontal type, situated in the central area of the dam, and consists of three bays, each 10 meters wide and 4.03 meters high, separated by two central piers. The spillway sill is at elevation 401.53 m and has a Creager profile.

The spillway is controlled by three Taintor gates, each 3.50 m high, reaching the Full Supply Level (FSL) of 405.03 meters. The crest is located at elevation 406.53 m.

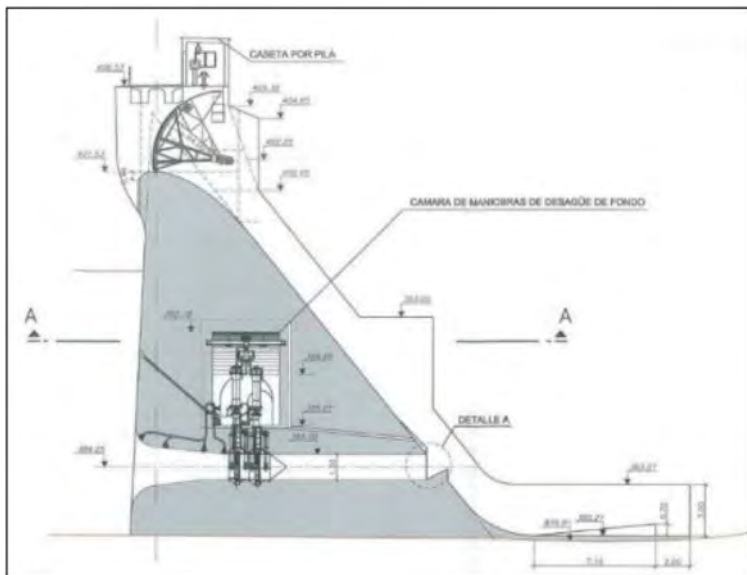


Fig. 2

Typical Section of Regajo Dam Through the Spillway and Drainage
Section type du barrage de Regajo au niveau du déversoir et de l'évacuation

It is important to note that the spillway was originally designed for a flood with a return period of 500 years, with a peak flow of 437.7 m³/s. Currently, there is a limitation of 2.54 meters in the gate openings, hence the flow discharged at the Full Supply Level (FSL) is 323 m³/s.

3. DESCRIPTION OF THE CURRENT ISSUES

In 2005, during the drafting of the dam's operating rules, a hydrological study was conducted, resulting in the following peak flood flows:

Table 1
Peak flows from the 2005 hydrological study

T	PEAK FLOWS (m ³ /s)
T500	1440,96
T1000	1884,41
T5000	2601,30
T10000	2924,50

These flows are much greater than those considered in the original project (the 500-year flow is more than three times greater), and the design flood to be considered should correspond to a 1,000-year return period. In the second safety review of the dam in 2021, the calculations indicated the elevations for the Design Flood Level (DFL): 408.28 and the Extreme Flood Level (EFL): 408.82, which would result in overflow over the crest, even for the 100-year return period flood. The studies of this review confirmed that the overflow would occur regardless of the seasonal freeboard adopted, given the minimal attenuation effect of the reservoir. Considering that the reservoir attenuates very little and that the peak flow of the new design flood is four times greater than that considered for the existing spillway design, it was anticipated that the magnitude of the works to be projected would be considerable.

4. DESCRIPTION OF THE PROJECTED WORKS

A new hydrological study has been completed in 2023, along with a study of solutions. The key conclusions were that, to increase hydraulic safety (with two objectives: ensuring that the Extreme Flood Level (EFL) does not exceed the new crest elevation, and that the EFL with wave action does not surpass the parapet), a combination of several factors were necessary: construction of a new spillway with a fixed crest on the left bank (about 132 meters of free spillway length), reduction of the Full Supply Level (FSL) (from 405.03 to 404.00 meters), and raising the crest elevation (from 406.53 to 407.50 meters), including a parapet if necessary. The crest elevation will be widened, and since the FSL is being modified, the existing gates will be replaced due to their current limitation in opening, as previously mentioned.

Below are the key aspects of the works to be carried out on the existing spillway and the geometry of the new spillway:

4.1. ACTIONS ON THE EXISTING SPILLWAY

The opening limitation of the current gates was a key issue to address. Therefore, it is planned to replace the gates with new ones that have a lower height, as the Full Supply Level (FSL) has been reduced by 0.97 meters, and without opening limitations. The spillway profile is to be maintained as its hydraulic shape is adequate, despite the new characteristic levels. The piers will need to be partially demolished to install the new gates but will be rebuilt with reinforced concrete and anchored to the existing structure.

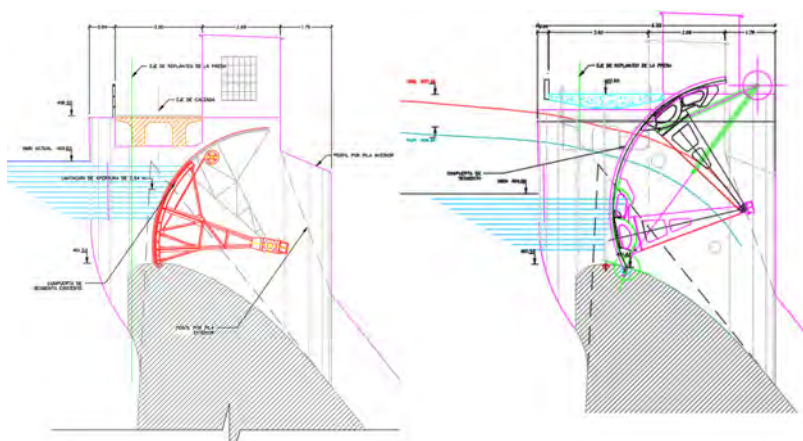


Fig. 3

Left: Existing spillway, Right: New arrangement
Gauche: Évacuateur existant, Droite: Nouvelle disposition

4.2. CONSTRUCTION OF A NEW SPILLWAY

On the left bank, Regajo Dam has a maximum height of about 13 meters above its foundations over a significant length. The replacement of this part of the dam with a spillway that will be fed directly from the reservoir is central to the chosen solution for increasing hydraulic capacity.

The flow discharged by this long spillway would be collected by a stilling basin designed to redirect the flow to the discharge channel, similar to how a stilling basin operates in a side-fed spillway. This discharge channel, open and in a canal form, reaches a cylindrical ski jump.

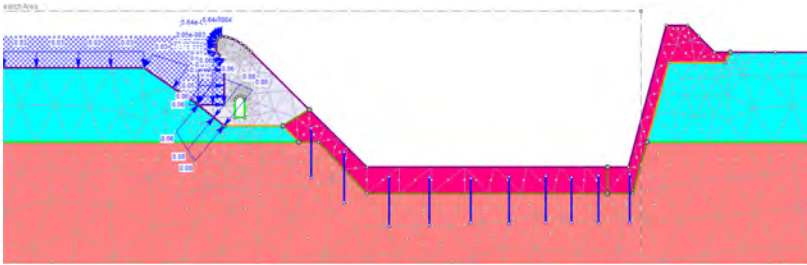


Fig. 5
Example of the Geo-Structural Model of the New Spillway
Exemple du modèle géotechnique du nouvel évacuateur

The discharge channel has a 4.2% slope, a length of approximately 106.7 meters, and an angle of 21.94° relative to the axis of the stilling basin. This gentle slope results in moderate flow velocities, around 13 m/s, during the 1,000-year flood event. The terminal structure is a cylindrical surface with a radius of 50.0 meters, starting at elevation 385.09 meters and with a spill edge at elevation 386.75 meters. This elevation is very close to the level reached in the riverbed in this area with the flow corresponding to the extreme flood. The riverbed in this restitution area is at elevation 379.0 meters. Below is a view of the new spillway projected on the left bank:

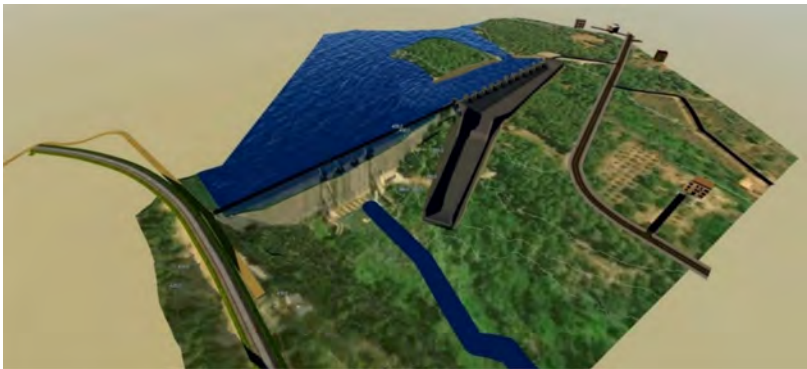


Fig. 6
Perspective of Regajo Dam with the New Spillway
Perspective du barrage de Regajo avec le nouvel évacuateur

Since there are various parameters to dimension, and the geometry of the new spillway influences the attenuation of the existing spillway, adjustments have been made until arriving at the final geometry of the project. This geometry meets the set conditions with optimal hydraulic performance for the Extreme Flood Level (EFL), as confirmed by CFD models. The attenuation and hydraulic capacity calculations also required an iterative process (along with calibrations) between conventional analytical calculations and CFD modeling.

5. OPTIMIZATION THROUGH NUMERICAL MODELING

The numerical model uses the software FLOW-3D®. The software employs the Finite Volume Method (FVM), which is specialized in solving complex geometries and free surface calculations. The accuracy of the results obtained by Granell Hydraulic Engineers using this software has been validated against numerous scaled physical models. In this case, the physical model was developed at a 1/60 scale in the Hydraulics Laboratory of CEDEX (Spain).

The model geometry includes the dam, the two spillways (with a roughness of 0.001 meters for the concrete elements), and the terrain (0.1 meters). The meshing has been configured using blocks or groups of parallelepiped cells. Each of these blocks is contained within the previous one, with cell sizes decreasing in a geometric progression with a ratio of $\frac{1}{2}$. The blocks with the smallest cell sizes are located where velocity gradients are highest, specifically in the areas of the spillway crests and channels. The general cell size is 0.5 meters, reducing to 0.25 meters and even 0.125 meters in the areas of greatest interest.

Although conventional calculations were initially performed to determine the capacity of each spillway, CFD results have allowed for verification of these calculations. It was confirmed that, for the existing spillway, there is no overflow of the side walls in the channel (thanks to a lateral widening of the bays at the end of the piers), the proper functioning of the current Creager profile under different operational conditions than those of the original design, and the performance of the current basin with the levels imposed in the riverbed.

Regarding the new spillway, due to its significant length, the CFD model has optimized the depth of the stilling basin along the longitudinal profile (from 5.5 meters at the left abutment to 13.7 meters at the start of the discharge channel). This ensures that the 11 bays operate uniformly and are not submerged, the flow direction change in the second control section, the functioning of the discharge channel (with a slope limited to 4.2%), and the restitution to the riverbed when both spillways are in operation. Even in the case of extreme flood conditions, the behavior in all bays is adequate. Additionally, it has been verified that the discharge flow from each bay is similar.

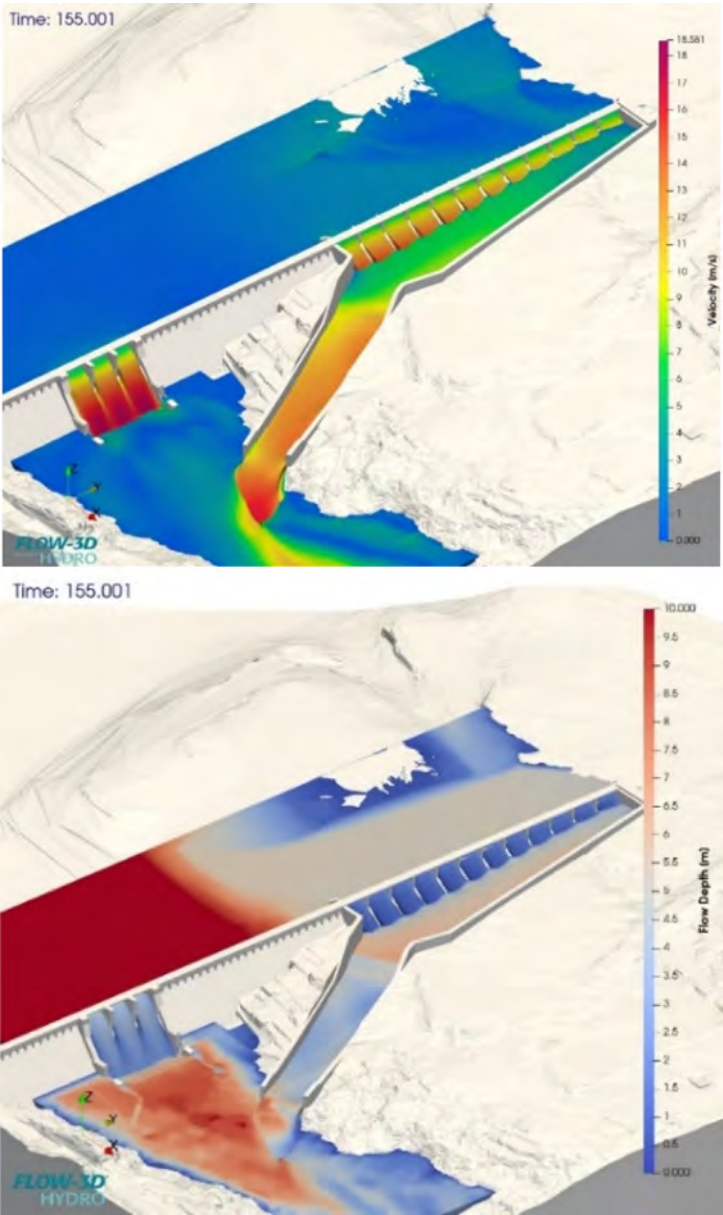


Fig. 7
Depths/Velocities from the CFD Model for T=1000 Years
Profondeurs/Vitesse du modèle CFD pour T=1000 ans



Fig. 8
Depths from the Reduced-Scale Model for T=1000 Years
Profondeurs du modèle réduit pour T=1000 ans

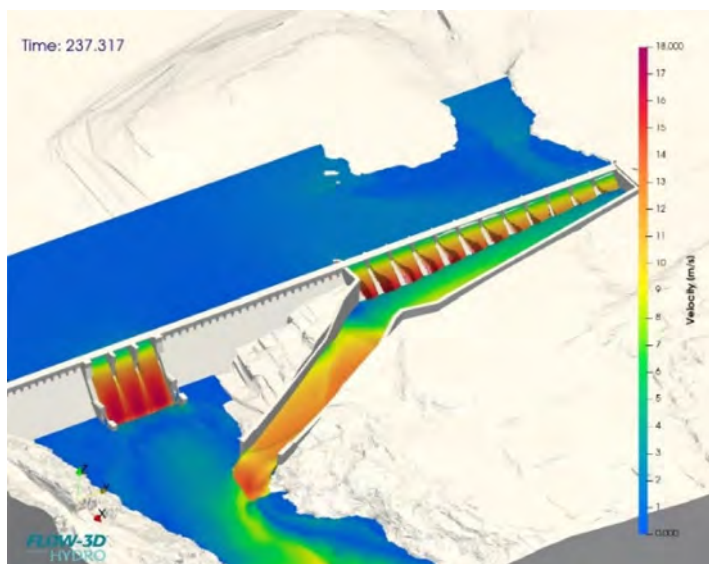


Fig. 9
Depths from the CFD Model for T=250 Years
Profondeur du modèle CFD pour T=250 ans

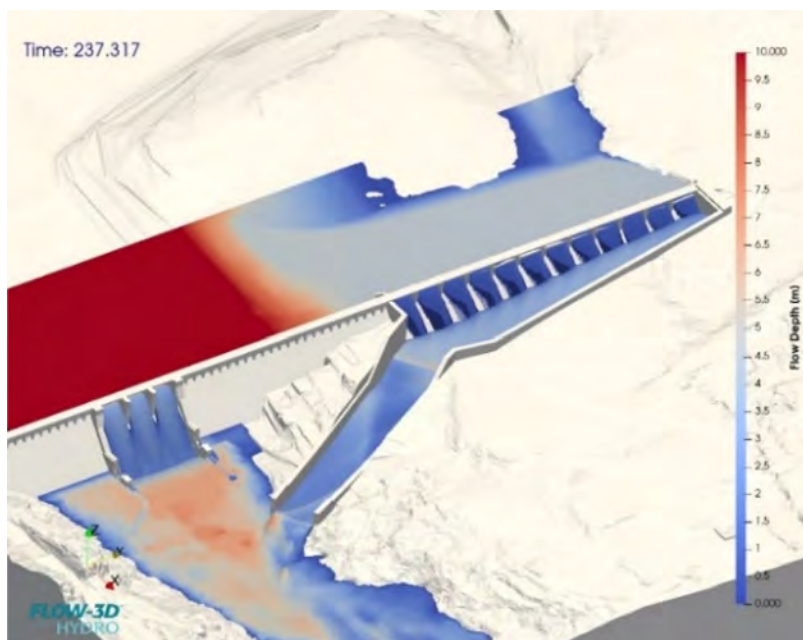


Fig. 10
Velocities from the CFD Model for T=250 Years
Vitesses du modèle CFD pour T=250 ans

Some aspects mentioned are very difficult to assess with conventional calculations, and until now, they have been addressed by allowing high safety margins. In the case of Regajo Dam, given the stringent hydraulic conditions, it was essential that the geometry tested in the physical model be as optimized as possible. This optimization required about 20 iterations, with various parameter combinations to evaluate.

After the stilling basin, a second control section of the spillway (for reduced flows) was situated with its crest at elevation 392 meters, preceding the channel that runs along the left bank.

This second control section has a dual purpose: to slow down the flow upstream in the stilling basin, ensuring that the flow direction change is adequately managed, and to smooth out the flow downstream, aiming to minimize, as much as possible, the presence of crosslines. Figure 6 shows this described operation during the discharge of the design flood peak. Below are attached some figures showing

depths (on the right) and velocities (on the left) to observe the operation of both spillways discharging the design flood together:

A reduced-scale physical model was constructed at CEDEX laboratory. Attached is a similar photograph of the depths from the physical model:

The results from this model have been used to confirm the results obtained through the numerical model and to make the minor geometric adjustments needed, as is customary when testing an already optimized geometry with CFD in a reduced-scale model.

It is interesting to compare them with the passage of a flood of a shorter return period (on the order of magnitude of the maximum flood supported by the dam, specifically in 1957, when it was partially constructed):

6. CONCLUSIONS

Given the severe problem of insufficient hydraulic capacity at Regajo Dam, it has been necessary to combine various measures to meet the Dam Safety Standards required by the regulations. The main measure is a new, long spillway located on the left bank, where the current dam has a very limited height.

Following the design process of the new spillway (with the objectives of minimizing impact on the dam and its operation, while also considering aesthetics and environmental integration), its optimization and shape validation were carried out using both a CFD numerical model and a reduced-scale physical model, resulting in an optimal geometry. The discharge to the riverbed has been planned 60 meters downstream from the current basin to avoid potential damage to the base of the dam.

Other measures were also necessary besides the new spillway: lowering the Full Supply Level (FSL), replacing the gates in the existing spillway, and raising the crest including the addition of a parapet.

COMMISSION INTERNATIONALE DES
GRANDS BARRAGES

VINGT-HUITIEME CONGRES DES
GRANDS BARRAGES
CHENGDU, MAI 2025

**NEW APPROACH TO ESTIMATE EXTREME FLOODS FOR SWISS DAMS BY
MEANS OF CONTINUOUS HYDROMETEOROLOGICAL SIMULATIONS (*)**

Alexandre Jean PACHOUD

Dam Safety Specialist, SWISS FEDERAL OFFICE OF ENERGY SFOE

Daniel VIVIROLI

Group Leader Mountain Hydrology, UNIVERSITY OF ZURICH

Roger FRAUCHIGER

Dam Safety Specialist, SWISS FEDERAL OFFICE OF ENERGY SFOE

Emmanuel BROCARD

Scientific Advisor, SWISS FEDERAL OFFICE FOR THE ENVIRONMENT FOEN

Milaine CÔTÉ

Dam Safety Commissioner, SWISS FEDERAL OFFICE OF ENERGY SFOE

SWITZERLAND

SUMMARY

In Switzerland, dam safety against floods must be evaluated for a design flood corresponding to a 1'000-year return period, and a safety check flood with a much larger return period. Estimating such extreme events is inherently subject to large uncertainties. The Swiss directive prescribes minimum methodological requirements, but the estimation remains a challenging task, particularly for small

**Nouvelle approche d'estimation des crues extrêmes pour les barrages suisses basée sur des simulations hydrométéorologiques continues*

ungauged alpine catchments. The Swiss authorities have deployed great efforts over the recent years to support the development of a comprehensive new approach to estimate extreme floods. It consists of very long continuous hydrometeorological simulations developed for the range of spatial scales relevant to Swiss dams and accounts for the main physical processes responsible for flood generation. The approach provides large ensembles of realistic extreme flood hydrographs, allowing for multivariate flood frequency analyses, and provides insight into the role of antecedent conditions. The future integration of this novel approach into the Swiss directive represents a paradigm shift with remaining challenges to be tackled from the regulatory perspective.

RÉSUMÉ

En Suisse, la sécurité des barrages en cas de crue doit être évaluée pour une crue de projet d'une période de retour de 1'000 ans et pour une crue de sécurité avec une période de retour bien plus élevée. L'estimation de tels événements est sujette à de grandes incertitudes. La directive suisse prescrit des exigences méthodologiques minimales, mais l'estimation reste une tâche difficile, en particulier pour les petits bassins versants alpins sans mesures. Les autorités suisses ont déployé des efforts importants ces dernières années pour soutenir le développement d'une nouvelle approche intégrale pour l'estimation des crues extrêmes. Elle repose sur la simulation hydrométéorologique continue à différentes échelles spatiales pertinentes pour les barrages suisses, et tient compte des principaux processus physiques en jeu pour la génération des crues. Cette approche produit de larges ensembles de crues extrêmes réalistes, permettant une analyse fréquentielle multivariée et l'étude du rôle des conditions antécédentes. La future intégration de cette nouvelle approche dans la directive suisse représente un changement de paradigme avec des défis importants à relever du point de vue de la régulation.

1. INTRODUCTION

Pursuant to the *Directive on the Safety of Water Retaining Facilities* in Switzerland [1] (referred to as the Swiss directive hereinafter), dam safety against floods should be evaluated for a design flood corresponding to a 1'000-year return period, and a safety check flood of a much lower probability of occurrence. Estimating such extraordinary and extreme events is inherently subject to large uncertainties, despite the availability of a comprehensive hydrometeorological measurement network covering Switzerland. While the Swiss directive [1] attempts to reduce uncertainties by prescribing minimum methodological requirements,

estimating extreme floods remains a challenging task, particularly for small ungauged alpine catchments [2].

Initially driven by the disaster of Fukushima (Japan) in 2011, the Swiss authorities have deployed great efforts over the recent years to support the development of a comprehensive new approach to provide a homogeneous hydrological basis for estimation of extreme floods. The approach consists of very long continuous hydrometeorological simulations in a model chain [3]–[4] and targets high return periods necessary to evaluate the safety of critical infrastructures against floods, including dams. Through a succession of projects, the approach has been extended to all of hydrological Switzerland.

In this paper, an overview of the Swiss dam portfolio is provided, and the current Swiss directive for dam safety against floods is briefly summarized. The main challenges with regards to estimation of extreme floods are outlined (Chapter 2). The proposed new approach by means of continuous, long-term simulations through a comprehensive hydrometeorological model chain is thereafter introduced (Chapter 3). Its established scientific foundations are emphasized with reference to relevant state-of-the-art techniques, and recent first applications are briefly presented. New opportunities and remaining challenges towards its possible integration in the Swiss directive for dam safety are discussed, before drawing conclusions (Chapter 4).

2. ESTIMATING FLOODS FOR SWISS DAMS

2.1. OVERVIEW OF THE SWISS DAM PORTFOLIO AND LEGAL FRAMEWORK

In Switzerland, the Swiss Federal Office of Energy (SFOE) is the federal authority responsible for supervising the safety of dams [5]. There are approximately 225 *large* dams under direct supervision and 200 *small* dams under indirect supervision of the SFOE. The distribution of the dams under direct supervision per dam types is shown in Fig. 1. Most of the large dams were built between the 1940s and 1970s, mostly for the purpose of generating hydroelectricity [2]. The legal framework for dam safety is set by the Federal Act on Water Retaining Facilities (WRFA[†]), further detailed into the Water Retaining Facilities Ordinance (WRFO[‡]), and where the Swiss dam safety concept[§] is detailed. In reference to the dam safety

[†]Swiss Confederation. Federal Act on Water Retaining Facilities (WRFA, SR 721.101) of 1 October 2010 (Status as of 1 July 2023).

[‡]Swiss Confederation. Water Retaining Facilities Ordinance (WRFO, SR 721.101.1) of 23 November 2022 (Status as of 1 January 2023).

[§]The Swiss dam safety concept is founded on three pillars [5]: (1) structural safety (including safety against floods); (2) surveillance and maintenance; and (3) emergency concept.

legislation, dams are classified into three classes, as function of the water storage height and capacity (see Fig. 2), implicitly approximating potential consequences in case of failure. In general, Class I and Class II dams are large dams under direct federal supervision, while Class III dams are mostly small dams under cantonal supervision with indirect federal supervision. The Swiss directive (in five parts from A to E) is further detailing the WRFO by establishing the recommendations relating to minimum safety requirements (depending on the dam class) and prescribing concepts and methods to address those requirements. The distribution of the Swiss dams under direct federal supervision through the classes is depicted in Fig. 2.

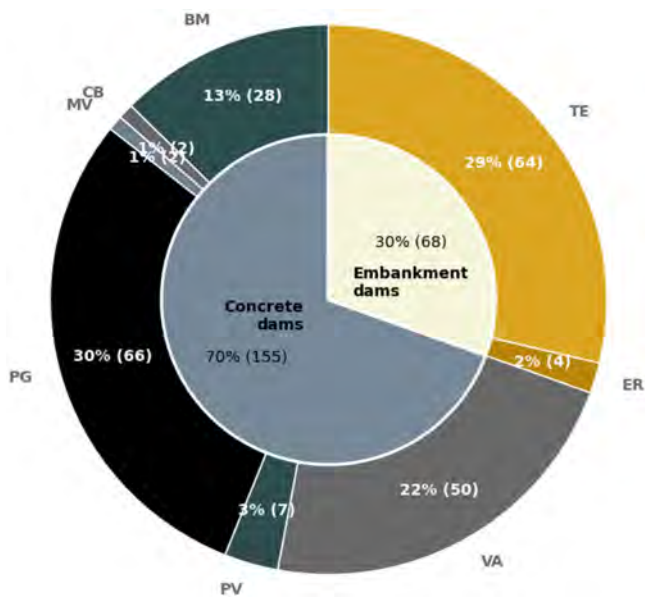


Fig. 1

Distribution of dams under direct federal supervision per dam type (BM: weir; CB: buttress dam; MV: multiple arch dam; PG: gravity dam; PV: gravity arch dam; VA: arch dam; ER: rockfill dam; TE: earth dam).

Répartition des barrages sous surveillance fédérale directe par types de barrages (BM : barrage mobile ; CB : contreforts ; MV : voûtes multiples ; PG : poids maçonnerie ou béton ; PV : poids-voûte ; VA : voûte ; ER : enrochement ; TE : terre).

2.2. CURRENT SWISS DIRECTIVE FOR DAM SAFETY AGAINST FLOOD

The minimum requirements with regards to dam flood safety in Switzerland are prescribed by the Part C2 of the Swiss directive [1]. Only the requirements in

terms of flood estimation are presented hereafter. The various safety requirements in terms of hydraulic verifications are not discussed.

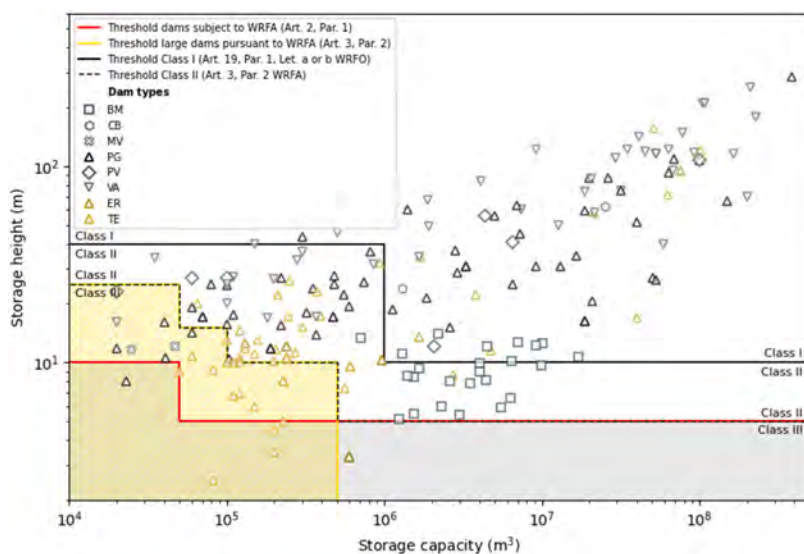


Fig. 2

Distribution of dams under direct federal supervision per dam class.

Répartition des barrages sous surveillance fédérale directe selon les classes.

Dams under direct federal supervision must be checked against a *design flood* (extraordinary situation) and a *safety check flood* (extreme situation). The design flood corresponds to the 1'000-year return period, whereas the safety check flood shall be of a *much larger return period*. For all dam classes, the design flood must be estimated based on the evaluation of two independent methods:

1. M1: statistical analysis of extremes based on inflow measurement series.
2. M2: statistical analysis of extremes based on precipitation measurement series, in combination with hydrological models to derive event hydrographs, such as the method of synthetic hydrographs (SG) or more complex precipitation-runoff models (NAM, from German).

The application of M1 may rely on the streamflow measurement network of the Swiss Federal Office for the Environment (FOEN) (more than 200 gauging stations in operation) and cantonal measurement networks (more than 400 gauging stations); see also Fig. 5 further below. In general, precipitation data for M2 may be

available from (i) the hydrometeorological measurement network of the Swiss Federal Office of Meteorology and Climatology (MeteoSwiss) (more than 300 stations automatically measuring precipitation with a time step of 10 min), partner networks as well as cantonal and private networks (refer also further to Fig. 4); (ii) precipitation measurements by dam operators; (iii) the Hydrological Atlas of Switzerland (HADES), latest version 2.0 from 2022 [6]–[7]. When using M2 with SG, the runoff coefficient must be assumed equal to 1 (the runoff volume flowing into the reservoir equals the precipitation volume) to be on the safe side regarding the model uncertainties. When M2 is envisaged with NAM, the model must be calibrated or verified, and the event antecedent conditions must be set to the least favourable conditions or determined from prevailing initial conditions associated to rare or extreme events. A sensitivity analysis should be conducted in the latter case. Those requirements may lead to a certain extent of conservatism [2], which is the essence of the Swiss directive to cover the uncertainties. For Class I dams, the safety check flood must be estimated by comparing the outcome of two approaches:

3. M3: multiplication of the design flood hydrograph by a factor of 1.5 for existing dams (for new or altered facilities, the event duration must also be multiplied by 1.5);
4. M4: use of a precipitation-runoff model (NAM) with Probable Maximum Precipitation (PMP) as input precipitation (also referred to as the PMP-PMF** method).

For dam classes II and III, M3 must be applied and M4 can be used optionally for comparison. For the implementation of M4, the CRUEx++ methodology [8] can be used, with the PMP maps for Switzerland developed in [9]. In case site-specific PMP studies are conducted, any deviation from the PMP maps should refer to precipitations with a yearly probability of occurrence of at least 10^{-4} , or lower.

2.3. PARTICULAR DIRECTIVES FOR THE AARE AND HIGH RHINE CATCHMENTS

The run-of-river dams (weirs, BM) of the High Rhine and the Aare rivers became subordinated under direct federal supervision with the enforcement of WRFA in 2010. Mostly of Class II, the features of these lower retaining height facilities were not sufficiently considered in the former Part C2 of the Swiss directive, from a technical point of view (other hazard scenarios) as well as from a legal point of view (along the border with Germany in the run of the High Rhine). The safety recommendations for the weirs on the High Rhine were thereof edited in cooperation with the German authorities and enforced in 2013 [10]. A similar document was later developed for the weirs on the Aare River and put into force in 2015, recently revised in 2024 [11]. In [10], the design flood is defined as the

**PMF standing for Probable Maximum Flood.

1'000-year return period flood. The safety check flood for this specific region was extrapolated by multiplying the design flood by a factor varying between 1.16 and 1.18. On the Aare, the revised document [11] incorporates the results from the EXAR project (see Chapter 3), based on continuous hydrometeorological simulations. The design flood is also defined as the 1'000-year return period flood, and the safety check flood corresponds to the return period of 10'000 years, accounting for bank overflow where applicable. The ratios between the design and safety check floods vary between 1.00 to 1.22. Both documents provide values for the design floods at the location of every weir in their scope. Alternatively, site-specific hydrological studies may be conducted by the operators, subject to the approval of the supervising authority.

2.4. CHALLENGES IN ESTIMATING EXTRAORDINARY AND EXTREME FLOODS

The estimation of floods with very high return periods is inherently subject to uncertainties. Despite the availability of a dense hydrometeorological measurement network in Switzerland, most of the Swiss dams were built in remote and elevated alpine catchments, with short or no direct natural inflow or precipitation measurements. Assessing the representativeness of the transfer of nearby hydrometeorological measurements, when possible, is prone to additional challenges on alpine environments, where abrupt topographical variations strongly influence local extremes or regional precipitation regimes. Catchment-specific characteristics (geological, hydrogeological, hydrological regime, glacier and snow cover, etc.) may also strongly influence the mechanisms that trigger (extreme) floods, further contributing to the estimation uncertainty. Fig. 3 depicts the distribution of the natural catchment areas for Swiss dams under direct federal supervision. More than 140 reservoirs are located at the outlet of a *small* catchment, with a surface of less than 1'000 km² (most below 300 km², and located in alpine catchments), while more than 30 facilities (mostly weirs) feature *large* catchments greater than 1'000 km², up to 35'000 km² (on the High Rhine, e.g., Birsfelden, Augst-Wyhlen or Rheinfelden dams).

In the application of M2, the HADES [6]–[7] data can be used as an alternative in case the station precipitation data are assessed as poorly reliable or not representative of a specific dam at the outlet of a small catchment. However, the HADES provides extreme point precipitation only, and extreme areal precipitation can therefore not be estimated directly from the HADES maps [7]. Nevertheless, areal reduction factors (also called depletion curves) presented in the former printed (older) version of HADES can be used to obtain information on areal extreme estimates [7]. When implementing M4 together with the CRUEX++ methodology, one shall bear in mind the application limits, i.e., the catchment area must be smaller

than 230 km² [8], while caution must be applied between 75 and 230 km². When envisaging NAM in the frame of M2 or M4, the determination of the antecedent conditions is also a major challenge, often subject to lack of consensus amongst stakeholders.

While engineering and scientific methodologies for flood estimation continue to evolve, a vast spectrum of data bases, methods and approaches are available to hydrologists and engineers. This heterogeneity, together with the fact that hydrological studies of some of the existing Swiss dams are ageing (some dating back to the original design analyses), make any attempt of evaluation and/or comparison a tedious task for the authorities [2]. Finally, the impacts of climate change must also be considered. In Switzerland, a clear trend of increase of heavy precipitation events is projected [12]. Climate change is also impacting other environmental features of catchments, likely to have direct impacts on the generation of extreme events. Addressing the entire spectrum of the uncertainties and challenges in the frame of regulation remains a challenge for any supervising authority [2]. Because of these considerations, regular updates of the dam hydrological studies are required, and the Swiss directive must be revised on a regular basis to follow the evolution of the state of the art.

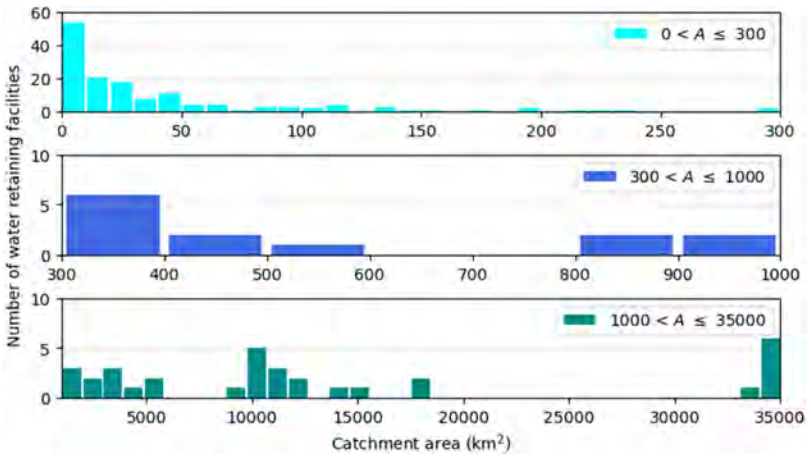


Fig. 3

Histograms showing the distribution of the catchment surface areas of Swiss dams under direct federal supervision.

Histogrammes montrant la répartition des surfaces de bassins versants des barrages suisses sous supervision fédérale directe.

3. NEW APPROACH: CONTINUOUS HYDROMETEOROLOGICAL SIMULATIONS

3.1. INTRODUCTION

Following the disaster of Fukushima (Japan) in 2011, the Swiss Confederation launched the project *Hazard information for extreme flood events on the rivers Aare and Rhine* (EXAR) [3]. The EXAR project was co-funded by FOEN, SFOE, MeteoSwiss, the Swiss Federal Nuclear Safety Inspectorate (ENSI) and the Swiss Federal Office for Civil Protection (FOCP). The objective of EXAR, achieved in 2021, was to establish a new homogeneous hydrological basis to evaluate the safety of critical infrastructures (including nuclear power plants and hydropower plants) against rare to extreme events, i.e., from 10^3 to more than 10^4 -year return period events. For its hydrometeorological part, the EXAR project explored the feasibility of the *continuous simulation* approach within the frame of a model chain combining weather generators, hydrological modelling and hydrological routing over 300'000 years [4]. The EXAR project was restricted to the Aare River basin ($\sim 17'700 \text{ km}^2$, including the Reuss and Limmat rivers) and provided results for 19 critical sites. After the successful completion of EXAR, FOEN and SFOE launched in 2020 the successor project *Extreme Floods in Switzerland* (EXCH), led by the University of Zurich, Switzerland, in collaboration with other research groups from France (Grenoble INP-UGA), Austria (University of Graz) and Switzerland (University of Bern). The EXCH project aims at extending the continuous simulation approach with the use of weather generators to all of hydrological Switzerland. From the perspective of dam safety, it is expected that EXCH will provide a new and comprehensive approach to estimate extraordinary floods (exceedance probability of the order of 10^{-3}), and to inform on extreme floods (exceedance probability below 10^{-4}). The methods, the expected results and the offered opportunities are briefly presented in the following sections. For more information, one may refer to the scientific references provided in this paper. For all figures not explicitly reproduced from another source, the map background come from the Federal Office of Topography swisstopo.

3.2. METHODS

While EXAR simulated extreme events at the outlet of *large* catchments (roughly greater than $1'000 \text{ km}^2$), EXCH required new scientific developments to cover smaller hydrological scales and needed to envisage the consideration of additional data. The project treats three different scales through specific developments, namely: (i) the *large* catchments ($\geq 1'000 \text{ km}^2$); (ii) the *small* catchments ($10\text{--}1'000 \text{ km}^2$); and (iii) the *very small* catchments ($1\text{--}10 \text{ km}^2$).

3.2.1. “Large” catchments ($\geq 1'000 \text{ km}^2$)

The adopted approach is largely based on the EXAR [4] set-up, extended to the Rhine, Rhone (including Doubs), Inn and Ticino river basins (see, e.g., Fig. 4, Fig. 5 and Fig. 9). The model chain relies on three components: (i) two independent weather generators^{††}: GWEX^{‡‡} [13] and SCAMP^{§§} [14]; (ii) the HBV hydrological model [15] implemented for a number of sub-catchments and taking as input the results from step 1; and (iii) the RS MINERVE model [16] to route the results from step 2 to every outlet of a large catchment considered.

GWEX is a multi-site stochastic weather generator for precipitation and temperature aiming at reproducing the statistical behaviour of weather events at various temporal and spatial resolutions, with a focus on extremes [13]. The parameters of the marginal distributions for the precipitation are determined based on an advanced regionalization method using a large dataset of observations in Switzerland and its neighbouring countries, see Fig. 4. The initially collected set consisted of more than 1'700 gauges with daily values, and more than 600 gauges with hourly values, finally reduced to a selection of approximately 1'100 and 500 gauges, respectively, based on length and quality requirements. GWEX is calibrated seasonally, and its distribution for precipitation is not only adequate to model extremes, but also the bulk of frequent weather characteristics, which is of particular interest to model realistic antecedent conditions. The alternative hybrid weather generator SCAMP is based on atmospheric and weather analogues [14] and is fully independent from GWEX. It generates series of synoptic weather using the ERA20C atmospheric reanalysis, yielding new and potentially unobserved trajectories. The generated series are further combined with a stochastic downscaling model based on atmospheric analogues to generate precipitation. The final aim of the weather generators is to produce 300'000 years of mean areal precipitation (MAP) and mean areal temperature (MAT) at the hourly time step, which will serve as inputs for the hydrological and routing modelling, producing 300'000 years of hourly discharges. The models' ability to adequately reproduce observations is successfully evaluated – with regional variations – through an ensemble of metrics (e.g., monthly mean precipitation, 1- and 3-day precipitation frequency, dry- and wet-spell lengths frequency, etc. [4]). The hydrological model parameters are regionalised. Calibration and evaluation are based on a selection of gauging stations from a broad collection of discharge observations, see Fig. 5. The hydrological routing model also relies on 2D hydraulic simulations where required to obtain realistic characterisation of bank overflow and floodplain retention. Moreover, a sensitivity analysis addressing weather generator and hydrological model is foreseen. Overall, the model chain can model explicitly the important physical processes in

^{††}The EXCH project also explored the feasibility of considering ensembles of reforecasts from the vast database of the European Center for Medium-Range Weather Forecasts (ECMWF). This is not presented here.

^{‡‡}Generator of Weather EXtremes.

^{§§}Sequential Construction of atmospheric Analogs for Multivariate weather Predictions.

relation to flood generation and routing, such as snow accumulation, snow melt, soil moisture storage, bank overflow, as well as lake and floodplain retention [4].

3.2.2. “Small” catchments (10–1'000 km²)

Producing continuous meteorological time series for the entire desired spatial range required major scientific developments in EXCH. A hybrid weather generator to generate MAP was developed, using a combination of GWEX [13] and a precipitation disaggregation model based on a Multiplicative Random Cascade (MRC) [17] to reach the sub-hourly time step. The parameters of this hybrid weather generator are estimated based on MAP observations extracted from CombiPrecip [18], a product of MeteoSwiss. It is a state-of-the-art, 1 km²-1 h resolution reanalysis of precipitation fields, based on an assimilation of radar data and precipitation gauge data. The parameters of the marginal distributions for GWEX are estimated based on all the non-zero precipitations, so that both extreme values and the entire range of precipitation statistics are reproduced (see also Subsection 3.2.3). While radar data reanalysis offers results at a spatial scale that can better capture local extreme events (e.g., thunderstorms), only 17 years of data were available at the start of EXCH, requiring some caution in the handling of extreme value statistics.

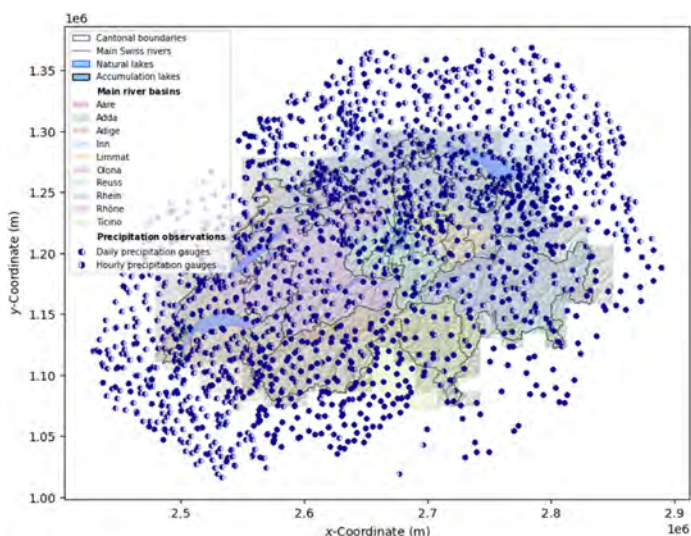


Fig. 4

Collected precipitation data in Switzerland and neighbouring countries.
Collection des données de précipitations en Suisse et dans les pays voisins.

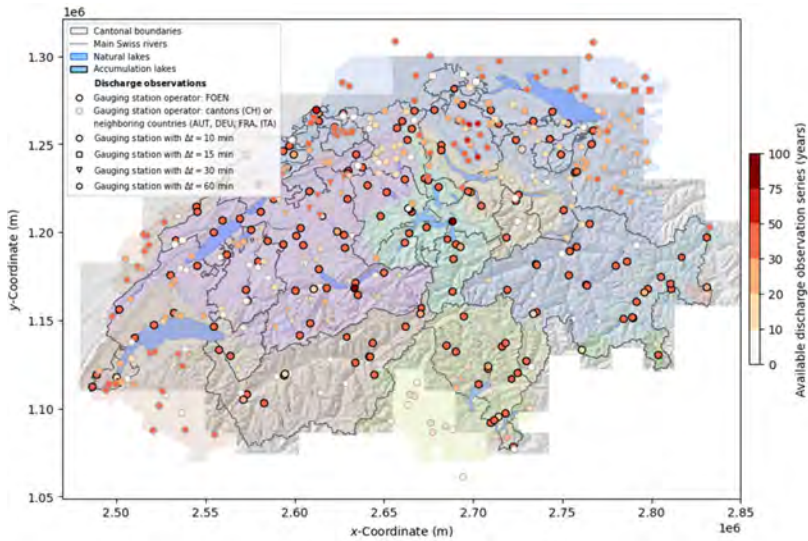


Fig. 5

Collected discharge data in Switzerland and neighbouring countries.

Collection des données de débits en Suisse et dans les pays voisins.

The hydrological simulations are performed with HBV [15]. Hydrological routing is not required due to the comparatively small size of the catchments and the lack of major natural lakes. Conversely to the *large* catchments, comparatively few undisturbed runoff measurement series are available at high-elevation sites (this is also illustrated with the example of the Ticino canton, see Fig. 8), meaning fewer catchments can be calibrated and used as a basis for regionalisation. Similarly to the *large* catchments, the model chain can model explicitly the important processes in relation to flood generation, and will produce 300'000 years of continuous discharge with a time step of 30 min.

3.2.3. “Very small” catchments (1–10 km²)

The spatial scale of *very small* catchments is not covered by the weather generators. For those catchments, Intensity-Duration-Area-Frequency (IDAF) curves are developed [19] that specifically account for the spatial extent of precipitation. To model the precipitation intensities, the extended generalised Pareto distribution (EGPD) is adopted, and the distribution parameters, linked to duration and area, are estimated via a data-driven approach based on all non-zero

precipitation observations extracted from CombiPrecip [18]. These models are also adopted for the marginal distributions of the precipitation intensities for GWEX in the *small* catchment module. The EXCH project will provide ID(A)F for the 1–72 h temporal range, for any catchment in Switzerland. Examples of results are provided in Fig. 6.

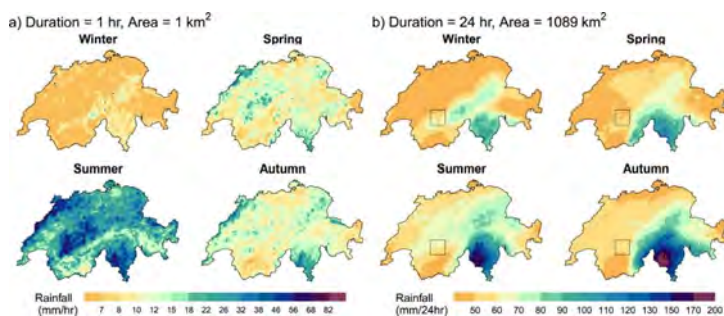


Fig. 6

Map of seasonal 20-year return period precipitation for two spatiotemporal scales: (a) $D = 1$ h, $A = 1$ km²; (b) $D = 24$ h, $A = 1'089$ km² (reproduced from [19]). The black-edge frame in panel (b) shows the extent of area used for data aggregation, i.e., 1'089 km².

Carte des précipitations saisonnières pour une période de retour de 20 ans pour deux échelles spatiotemporelles : (a) $D = 1$ h, $A = 1$ km²; (b) $D = 24$ h, $A = 1'089$ km² (reproduite de [19]). Le cadre noir au panel (b) représente l'étendue de la surface utilisée pour l'agrégation des données, i.e., 1'089 km².

On the right panel (b) of Fig. 6, rainfall intensities at each pixel of the map refer to the spatially aggregated data in the 1'089 km² square centred on that pixel. For example, one can observe that the Ticino region (southernmost canton of Switzerland) is subject to the highest values of high-return period precipitation [19]. For the 1–10 km² spatial scales, detailed hydrological simulations were out of scope. However, the ID(A)F models can serve as an input for further hydrological assessments.

3.3. OUTPUT FOR SWISS DAMS

The direct output in the scope of EXCH is presented in Fig. 7: (i) 25 dams and 36 FOEN gauging stations are covered by the *large* catchments module (i.e., 300'000 years of continuous discharge series, $\Delta t = 1$ h); (ii) 100+ dams are covered

by the *small* catchments module (i.e., 300'000 years of continuous discharge series, $\Delta t = 30$ min); and (iii) 40+ dams are covered by the *very small* catchments module.

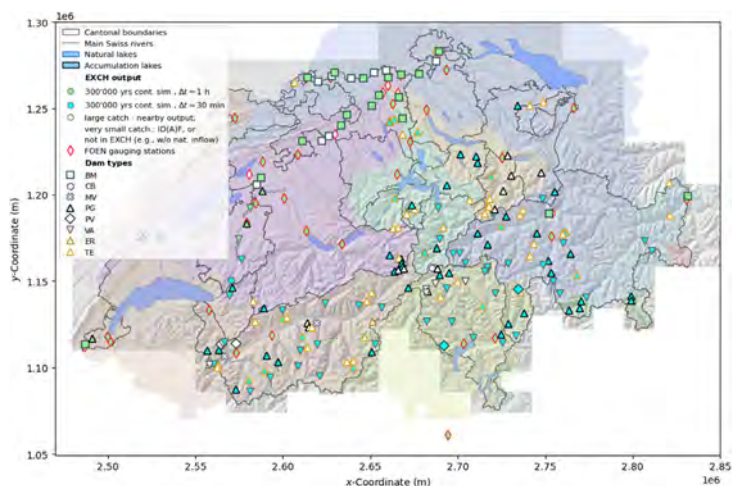


Fig. 7

Synthesis of the expected results from the EXCH project.

Synthèse des résultats attendus du projet EXCH.

In Fig. 7, some FOEN gauging stations at the outlet of large catchments may appear without direct results, but results can be transferred directly from a nearby dam. A closer look at the example of Ticino canton is provided in Fig. 8. For instance, on the Verzasca River, the Contra Dam (CON) is covered by the *small* catchments module. In the northwestern part of the canton, the catchment of Naret I and II dams (NAR) located at more than 2'000 masl (source of the Maggia River) is smaller than 10 km² and will therefore only be covered by the ID(A)F results. The Sambuco Dam (SAM) further downstream is at the outlet of a larger catchment and can be covered by the weather generator for the *small* catchments. In this region, the *large* catchments module will only cover gauging stations, namely the Maggia at Locarno-Solduno, and the Ticino at Bellinzona and Miorina.

3.4. EXAMPLE OF RESULTS

The methodological details and results of the EXAR project were published in 2021 and 2022 [3]–[4]. In the following, some selected results are reported to

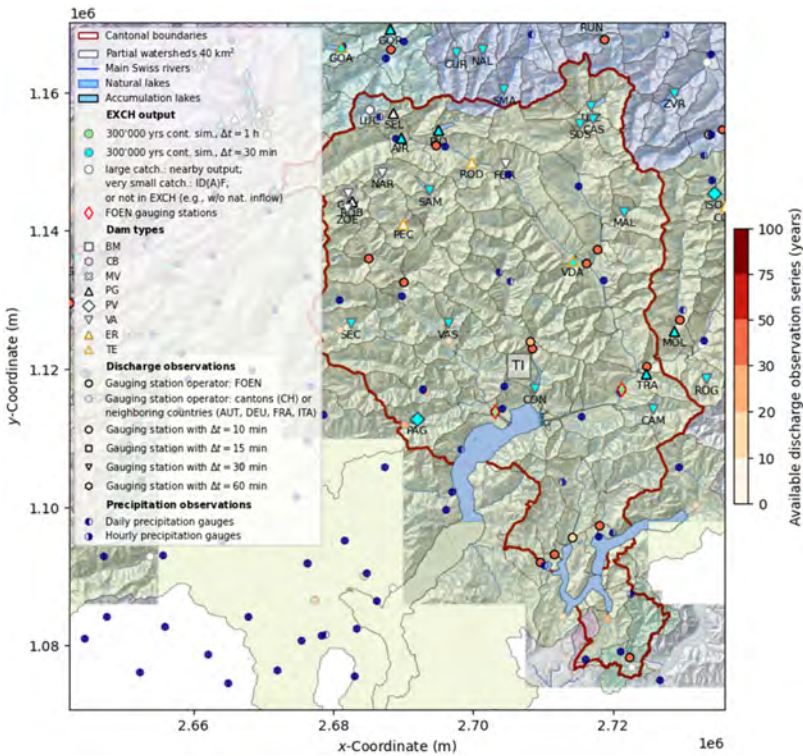


Fig. 8

Expected results from the EXCH project in the example of canton of Ticino.
Résultats attendus du projet EXCH pour l'exemple du canton du Tessin.

illustrate the performance and some of the opportunities offered by the continuous simulation approach. For the hydrological simulations (HBV) of the Aare River catchment, the basin was subdivided into some 80 sub-catchments (from 19 to 1'060 km²), for a total area of 17'700 km². The outputs from the HBV simulations were then combined with hydrological routing (RS MINERVE), providing results at 19 critical sites of interest, see Fig. 9.

As an example, the 72h-precipitation scenarios and hydrometeorological characteristics associated to the 10 largest simulated peak flows at the outlet of the Aare river basin (output node 8 in Fig. 9) are presented in Fig. 10 and Fig. 11, with results for each of the 80 sub-catchments. One can readily observe that different spatial conditions of precipitation as well as antecedent conditions may lead to

extreme events. Most of the simulated events have contributions from snowmelt runoff in a range of up to roughly 30% of total runoff.

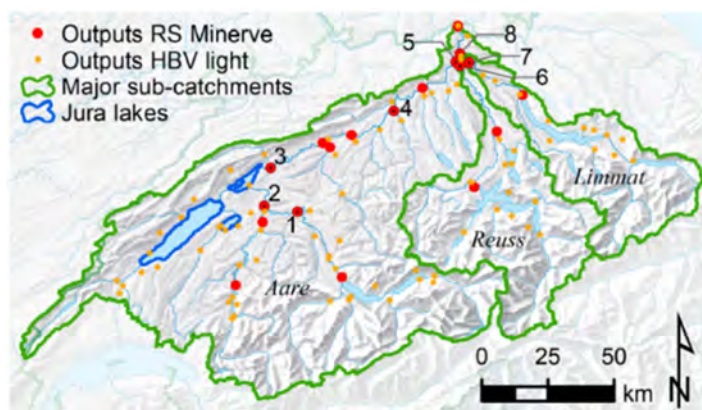


Fig. 9

Map of the Aare River basin presenting the location of the HBV model 80 output nodes (orange) and the RS MINERVE model 19 output nodes (red) (reproduced after [4]). The numbering of output nodes refers to sites discussed in [4]. Output node (8) is the Aare River at Stilli, close to its outlet.

Carte du bassin versant de l'Aar présentant la localisation des 83 points d'extraction des résultats du modèle HBV (orange) et les 19 points du modèle RS MINERVE (rouge) (reproduite de [4]). La numérotation des points d'extraction réfère aux sites discutés dans [4]. Le point d'extraction (8) est l'Aar à Stilli, proche de son exutoire.

While the ability of the continuous simulations to reproduce frequent and rare floods (i.e., up to roughly 100-year return period) can be satisfactorily assessed by comparing to extreme value statistics from observations, the available discharge records (ranging up to roughly 100 years in the best cases) do not allow for a statistical evaluation of the extreme floods [4]. However, the plausibility of the results can be evaluated against observed and reconstructed extreme floods in Switzerland [20], as well as empirical envelope curves derived from observed and reconstructed extreme floods in Switzerland [21], Europe [22] and the whole world [23]. This is presented in Fig. 12, where the Francou coefficient [24], allowing to compare flood magnitudes across catchments with different spatial scales, is also added. For more detailed conclusions, one may refer to [4]. From a global perspective, the results from EXAR for *large* catchments were judged plausible. The results were recently used to revise the directive for the weirs on the Aare River [11] (see Section 2.3).

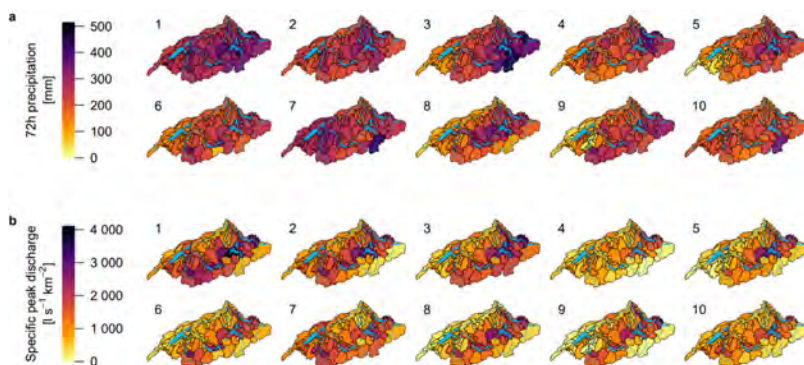


Fig. 10

Scenarios of maximum cumulative precipitation over 72h (a) and associated specific peak discharge (b) for the 10 largest peak flow events simulated at the outlet of the Aare catchment (reproduced after [4]).

Scénarios des précipitations cumulées maximum sur 72h (a) and les débit spécifiques associés (b) pour les 10 évènements simulés les plus importants en termes de débit de pointe à l'exutoire du bassin versant de l'Aar (reproduite de [4]).

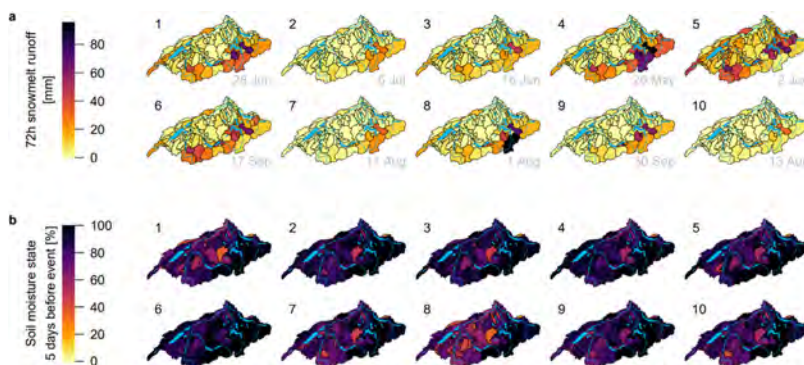


Fig. 11

Scenarios of snowmelt runoff (cumulated over the 72 hours preceding peak flow) (a) and soil moisture storage ratio (5 days preceding peak flow) for the 10 largest peak flow events simulated at the outlet of the Aare catchment (reproduced after [4]).

Scénarios de fonte des neiges (cumulée sur les 72 heures précédant le débit de pointe) (a) et de taux de saturation des sols (5 jours avant le débit de pointe) pour les 10 évènements simulés les plus importants en termes de débit de pointe à l'exutoire du bassin versant de l'Aar (reproduite de [4]).

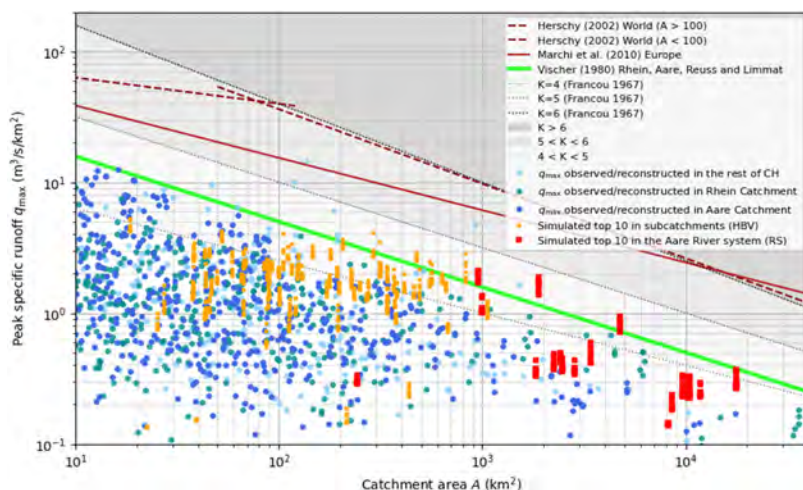


Fig. 12

The ten largest simulated peak specific runoff values with GWEX weather scenarios, compared to observed and reconstructed peak discharges and empirical flood envelope curves (modified and replotted after [4]).

Les dix plus grands débits spécifiques de pointe simulés avec les scénarios météo de GWEX, comparés aux débits de pointes observés et reconstruits ainsi qu'à des courbes empiriques enveloppes des plus grandes crues observées (modifiée et retracée d'après [4]).

3.5. NEW OPPORTUNITIES AND REMAINING CHALLENGES

National regulations worldwide often refer to T -return period events for dam design or safety check floods, without specifying which variables of the hydrograph shall be considered when determining its frequency. According to Brunner et al. (2016) [25], "*strictly, a T -year hydrograph does not exist*". Hydrological events are described by a set of correlated random variables (e.g., flood peak, volume and duration). When more than one of those variables are relevant to the dam design, multivariate frequency analyses must be conducted. If omitted, the analysis may not provide a complete assessment of the frequency of the design events [25]. The results of the continuous simulations allow for such analyses, by providing large ensembles of realistic rare to extreme event hydrographs, where the main physical processes leading to flood generation are considered. While only the peak discharge variable may typically be of importance for the flood safety evaluation of weirs, the flood volume and duration as well as the timing of the peak may play a significant role for storage reservoirs. Although the results of EXCH offer new opportunities towards better informed flood frequency analyses, from a regulatory

perspective, it raises the issue of an important change of paradigm regarding the definition of the design and safety check flood hydrographs. The integration of these results into the Swiss directive is yet to be defined. The precursory exercise was conducted with the results of EXAR [26], and will subsequently be extended to the results of EXCH in the next few years, with additional challenges. The results of the continuous simulations can also serve as a basis to systematically study the influence of the antecedent conditions to flood events [27], and may provide new insights leading to the rationalisation of the requirements when using other flood estimation approaches.

4. CONCLUSIONS

After the EXAR project, the EXCH project extends the approach of continuous simulation through a hydrometeorological model chain to all of hydrological Switzerland. Through regionalisation of the parameters of the weather generators, the project provides an unprecedented hydrological basis for flood safety evaluation in ungauged catchments, for every dam under federal supervision in Switzerland. It provides large and realistic ensembles of rare to extreme hydrometeorological events, accounting for the main physical processes responsible for flood generation. Quoting the ICOLD Bulletin 170 [28], this approach *“attempts to mimic “mother nature” in that the influence of all important stochastic inputs is explicitly considered [...]”*. It offers new opportunities such as better-informed flood frequency multivariate analyses, and the possibility of a systematic study of the role of antecedent conditions, although the model uncertainties remain an issue that imposes caution. The possible integration of this new approach into the Swiss directive as a comprehensive flood safety evaluation framework remains an important paradigm shift, with challenges to be tackled.

REFERENCES

- [1] Swiss Federal Office of Energy SFOE (ed.). Directive on the Safety of Water Retaining Facilities, Part C2: Flood safety and lowering the reservoir water level. Version 2.02, Bern, Switzerland, 2018.
- [2] SCHWAGER M.V., ASKARINEJAD A., FRIEDLI B., OBERENDER P.W., PACHOUD A.J., PFISTER L. Swiss dam safety regulation: Framework, recent changes and future perspectives. In *Role of Dams and Reservoirs in a Successful Energy Transition*, Boes R., Droz P., Leroy R. (eds.), CRC Press, London, 2023.

- [3] ANDRES N., STEEB N., BADOUX A., HEGG C. (eds.) Extremhochwasser an der Aare. Hauptbericht Projekt EXAR. Methodik und Resultate. WSL Berichte 104, 2021.
- [4] VIVIROLI D., SIKORSKA-SENONER A.E., EVIN G., STAUDINGER M., KAUZLARIC M., CHARDON J., FAVRE A.-C., HINGRAY B., NICOLET G., RAYNAUD D., SEIBERT J., WEINGARTNER R., WHEALTON C. Comprehensive space–time hydrometeorological simulations for estimating very rare floods at multiple sites in a large river basin. *Natural Hazards and Earth System Sciences* 22(9):2891–2920, 2022.
- [5] Swiss Federal Office of Energy SFOE (ed.). Directive on the Safety of Water Retaining Facilities, Part A: Introduction. Version 2.0, Bern, Switzerland, 2015.
- [6] Swiss Federal Office for the Environment FOEN. Hydrological Atlas of Switzerland (HADES), v2.0, Bern, Switzerland, 2022.
- [7] FREY C., FUKUTOME S. Explanations on B04 Extreme Point Precipitation, in the documentation of the Hydrological Atlas of Switzerland (HADES), Bern, Switzerland, 2022.
- [8] ZEIMETZ F. Development of a methodology for extreme flood estimations in alpine catchments for the verification of dam safety. Ph.D. Thesis No. 7307, École polytechnique fédérale de Lausanne EPFL, Switzerland, 2017.
- [9] HERTIG J.-A., FALLOT, J.-M. Cartes de précipitations extrêmes PMP pour la Suisse – Validation et utilisation des cartes PMP pour l'obtention de la PMF. Projet Cruex, Directives crues de l'OFEN. Version revue et augmentée, août 2009.
- [10] Swiss Federal Office of Energy SFOE (ed.). Sicherheitstechnische Anforderungen an den Bau und den Betrieb von Stauanlagen am Hochrhein. Switzerland, 2013.
- [11] Swiss Federal Office of Energy SFOE (ed.). Vollzugshilfe zur Stauanlagengesetzgebung betreffend den Bau und den Betrieb von Stauanlagen an der Aare unter direkter Bundesaufsicht. Switzerland, 2024.
- [12] CH2018. CH2018 – Climate scenarios for Switzerland, Technical Report. National Centre for Climate Services, Zurich, Switzerland, 2018.
- [13] EVIN G., FAVRE A.-C., HINGRAY B. Stochastic generation of multi-site daily precipitation focusing on extreme events. *Hydrology and Earth System Sciences* 22(1):655–672, 2018.
- [14] RAYNAUD D., HINGRAY B., EVIN G., FAVRE A.-C., CHARDON J. Assessment of meteorological extremes using a synoptic weather generator

- and a downscaling model based on analogues. *Hydrology and Earth System Sciences* 24(9):4339–4352, 2020.
- [15] SEIBERT J., VIS M.J.P. Teaching hydrological modeling with a user-friendly catchment-runoff-model software package. *Hydrology and Earth System Sciences* 16(9):3315–3325, 2012.
 - [16] GARCÍA HERNÁNDEZ J., FOEHN A., FLUIXÁ-SANMARTÍN J., ROQUIER B., BRAUCHLI T., PAREDES ARQUIOLA J., DE CESARE, G. RS MINERVE – Technical manual, v2.25. CREALP (ed.), Switzerland, 2020.
 - [17] MALOKU K., HINGRAY B., EVIN G. Accounting for precipitation asymmetry in a Multiplicative Random Cascades Disaggregation Model. *Hydrology and Earth System Sciences* 27(20):3643–3661, 2023.
 - [18] SIDERIS I.V., GABELLA M., SASSI M., GERMANN U. The CombiPrecip experience: development and operation of a real-time radar-raingauge combination scheme in Switzerland. In Proceedings of the 2014 International Weather Radar and Hydrology Symposium, Washington, DC, 7–9 April 2014.
 - [19] HARUNA A., BLANCHET J., FAVRE A.-C. Estimation of Intensity-Duration-Area-Frequency relationships based on the full range of non-zero precipitation from radar-reanalysis data. *Water Resources Research* 60(2): e2023WR035902, 2023.
 - [20] KIENZLER P., SCHERRER S. Verzeichnis grosser Hochwasserabflüsse in Schweizerischen Einzugsgebieten – Auswertung und graphische Aufbereitung. Bericht 17/229, Reinach, Switzerland, 2018.
 - [21] VISCHER D. Das höchstmögliche Hochwasser und der empirische Grenزابfluss. *Schweizer Ingenieur und Architekt* 98(40):981–984, 1980.
 - [22] MARCHI L., BORGA M., PRECISO E., GAUME E. Characterisation of selected extreme flash floods in Europe and implications for flood risk management. *Journal of Hydrology* 394(1-2):118–133, 2010.
 - [23] HERSCHY R.W. The world's maximum observed floods. *Flow Measurement and Instrumentation* 13(5-6):231–235, 2002.
 - [24] FRANCOU J., RODIER J.A. Essai de classification des crues maximales observées dans le monde. *Cah. O.R.S.T.O.M. sér. Hydrol.* IV(3):19–46, 1967.
 - [25] BRUNNER M.I., SEIBERT J., FAVRE A.-C. Bivariate return periods and their importance for flood peak and volume estimation. *WIREs Water* 3(6):819–833, 2016.

- [26] STAUDINGER M., FURRER R., VIVIROLI D. Hochwasserereignisse aus kontinuierlicher Langzeitsimulation zur Überprüfung der Sicherheit der Stauanlagen. Universität Zürich, Zürich, Switzerland, 2021.
- [27] STAUDINGER M., KAUZLARIC M., MAS A., EVIN G., HINGRAY B., VIVIROLI D. The role of antecedent conditions in translating precipitation events into extreme floods at catchment scale and in a large basin context. EGUsphere [preprint], 2024.
- [28] ICOLD (ed.) Flood evaluation and dam safety. ICOLD Bulletin 170, 2018.

COMMISSION INTERNATIONALE DES
GRANDS BARRAGES

VINGT-HUITIEME CONGRES DES
GRANDS BARRAGES
CHENGDU, MAI 2025

**KARIBA DAM PLUNGE POOL RESHAPING WORKS FOR THE SAFETY OF
STRUCTURES FOR EXTREME FLOODS (*)**

L. TARDIEUX, I. FENT, A. ARIGONI & B. M. QUIGLEY
Gruner Stucky SA, Renens, Switzerland

A. JONNERET
Norbert SA, Lausanne, Switzerland

P. SIPATELA, A. NKWEENDENDA, S. MHLANGA & Munyaradzi C.
MUNODAWAFA
Zambezi River Authority, Lusaka, Zambia

SWITZERLAND

SUMMARY

The Kariba Dam faced considerable spills of water, released through the six sluice spillways, which progressively scoured a deep and steep hole, deepening the plunge pool to a total depth of about 80 m. The presence of a geological fault, composed of weaker materials than the surrounding gneiss has caused differential erosion and backwards scour towards the dam, threatening its stability. Given the unprecedented scour depth and unique evolution of the pool, which posed a risk to the Kariba Dam foundations and its stability, various remedial studies and measures were implemented in order to investigate the situation and mitigate scour development. The final hydraulic shape of the plunge pool has been reached at the end of 2023 and protection works are ending in August 2024. During the works ongoing now, new engineering studies have been done in order to re-assess the scouring prediction

**Barrage de Kariba : reprofilage du bassin de dissipation pour assurer la sûreté des structures en cas de crues extrêmes*

and mitigate any future erosion. With the emptied pool, the detailed geological mapping became possible during the excavation works providing a better understanding of the geology and in particular of the fault characteristics. This new knowledge prompted an erodibility assessment of the upstream part of the plunge pool, updated to the actual geological conditions and a more refined examination of scouring under real conditions, directly downstream of the dam's foundations. The aim was to refine the fault protection project for optimal effectiveness. The site evaluations and the new additional analyses, resulted in adjustments of the on-site works, performed in relation to the erodibility and scour assessment based on the actual site conditions.

RÉSUMÉ

Le barrage de Kariba a été confronté à des déversements considérables d'eau, à travers ses six évacuateurs de crue, ce qui a progressivement creusé une fosse profonde, atteignant une profondeur totale d'environ 80 m. La présence d'une faille géologique composée de matériaux plus tendres que le gneiss environnant a provoqué une érosion différentielle et un affouillement vers l'arrière, menaçant la stabilité du barrage. Compte tenu de la profondeur d'érosion sans précédent et de l'évolution unique de la fosse, qui présentaient un risque pour les fondations du barrage et sa stabilité, diverses études et mesures correctives ont été mises en œuvre afin d'étudier la problématique et d'atténuer le développement futur de la fosse. Les travaux de reprofilage du bassin de dissipation se sont terminés fin 2023 conformément à la géométrie optimale définie par les études hydrauliques. La fin des travaux de protection de la faille est quant à elle prévue pour Aout 2024. Durant l'exécution du projet, de nouvelles études techniques ont été réalisées afin de réévaluer les prévisions d'érosion et de limiter tout risque éventuel d'affouillement futur. Avec le bassin vidé, un relevé géologique détaillé a été rendu possible lors des travaux d'excavation, permettant une meilleure compréhension de la géologie, notamment des caractéristiques des failles. Ces nouvelles connaissances ont donné lieu à une évaluation de l'érodabilité de la partie amont du bassin, actualisée selon les conditions géologiques rencontrées, et à un examen plus précis de du risque d'érosion en conditions réelles, directement à l'aval des fondations du barrage. Les nouvelles analyses complémentaires basées sur les données in-situ ont permis une mise à jour de l'évaluation de l'érodabilité et ont finalement conduit à des ajustements du design de la protection de la faille.

1. INTRODUCTION

During the first 20 years following the Dam construction, the heavy spillages of water, released through the six sluice spillways progressively scoured a deep and steep hole, deepening the Plunge Pool to a total depth of about 80 m below its original

level. The presence of a geological fault, composed of weaker materials than the surrounding gneiss has caused differential erosion and backwards scour towards the dam, threatening its foundations. Despite the additional quantity of water available for the dissipation of the jets, the Plunge Pool was not stabilized prior to the Kariba Dam Rehabilitation Works, due to flow recirculation induced by abrasive reverse currents.

Given the unprecedented scour depth and unique evolution of the Kariba Dam plunge pool, which posed a risk to the Kariba Dam foundations and its stability, various remedial studies and measures were implemented to investigate the Kariba Dam plunge pool situation and mitigate any potential future scour development. The first studies were performed by the EPFL University (Switzerland), where a physical model of the plunge pool was built and tested. Following the measurements done on the physical model, a comprehensive numerical model was developed to study the evolution of erosion, considering the new shape of the plunge pool and the characteristics of the rock, known at the time of the study.

With the plunge pool emptied, detailed geological mapping became possible during the excavation works providing a better understanding of the geology and in particular of the fault characteristics. This new knowledge prompted a review of erodibility of the upstream part of the Plunge Pool adapted to the actual geological conditions encountered and a more refined examination of scouring under real conditions, directly in front of the dam's foundations. The aim was to refine the fault concrete slab as protection of the fault for optimal effectiveness.

This article outlines the site evaluations conditions and the new analyses, bringing to works adjustments, performed in relation to the erodibility and scour assessment based on the actual site conditions. It also presents the challenges encountered during the Project implementation. This pertains particularly to the excavation and protection of vulnerable areas, with priority given to the protection of the dam's foundations above all else.

2. HISTORY OF THE PLUNGE POOL SCOURING AND RESHAPING

2.1. GENERAL CONTEXT

After 60 years of continuous operations, heavy spillages of flood water, particularly in the Dam early years, have progressively scoured an 80m deep hole in the plunge pool immediately downstream of the dam, corresponding approximately to two thirds of its total height.

The Kariba Dam spillway is composed of six submerged flood sluices in the central section of the dam with a combined discharge capacity of 9,400 m³/s.

As the spillway gates are located in the upper part of the dam wall with their sill approximately 30m below the dam crest, they operate under relatively low velocities, thus generating plunging jets that impact quite close to the dam foundations. Overtime, the abrasive currents from the jets created a backwards scours towards the dam foundations on the upstream rock face.

2.2. HYDROLOGY AND SCOUR DEVELOPMENT

As it can be seen from the Fig. 1, the scour development of the plunge pool rapidly evolved until 1981 where the plunge pool reached its deepest level at approximately 306 masl (cf.). From 1981 to 2011 the development of the plunge pool has been limited but not yet stabilized (cf.).

It is therefore possible to distinguish two periods from a hydrological standpoint:

- From 1962 to 1981 with frequent and multiple adjacent sluice gates operating for long and continuous periods with a cumulative volume of more than 511 km³ of flood water discharged through the gates and a volume of about 150'000 m³ of rock scoured. The figures below record the spillage episodes since the commissioning of the dam with the number of actual spillway gates operating in correlation with the scour development of the pool.
- From 1981 to 2011: with long periods without spillway operations: 17 years from 1981 to 1998 together with non-adjacent gate operations during spillage episodes

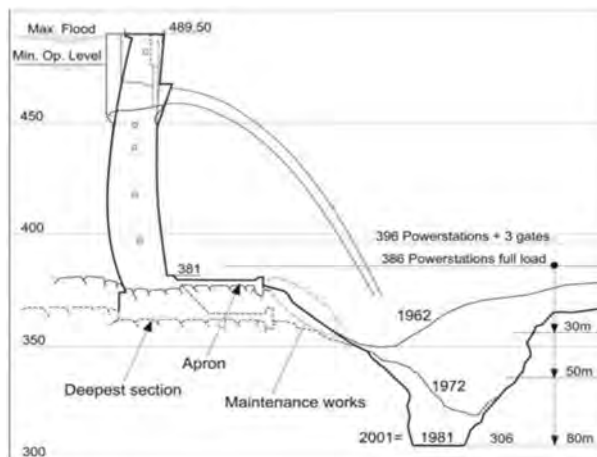


Fig. 1
Scour development – Evolution of Plunge Pool bathymetries

The slower evolution of the plunge pool development since 1981 is principally due to intentionally limited spillage episodes between 1979 and 2010. Indeed, the Zambezi River Authority purposefully undertook, since 1979, only partial spilling, with non-adjacent spillway gates in order to counter the high dynamic pressure fluctuations and to prevent the likelihood of further scour and erosion of the upstream plunge pool rock face.

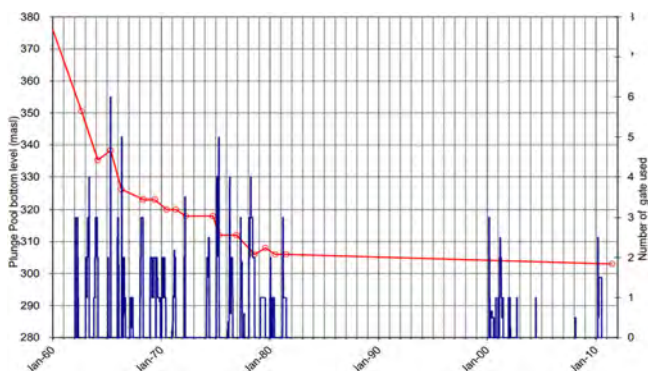


Fig. 2
Historical plunge pool development and gate opening from 1960 to 2011

Further, the fact that since 1981, despite the plunge pool having never been subjected to the full impact of the plunging jets of all gates spilling simultaneously under extreme floods and yet its scour development not being stabilized, motivated the need of further hydraulic modelling studies and future elaboration of the Kariba Dam Rehabilitation Project – Plunge Pool Reshaping.

The Plunge Pool Reshaping Project involved excavating the plunge pool to obtain the optimum shape as defined by the modelling studies presented thereafter.

3. PRELIMINARY ASSUMPTION AND SCOURING STUDIES

3.1. GEOLOGICAL CONTEXT AND ASSUMPTIONS

The Kariba Dam area geology consists of biotite gneiss, characterized by banding and foliation of quartzo-feldspathic and micaceous layers of the Precambrian era. The Gneiss is cut by granitic pegmatite dykes, generally oriented

perpendicular to the valley. On the upper part of the right bank of the existing dam, quartzites overlay uncomfortably the gneiss. The dominant geological feature of the site is a major fault running through the centre of the dam foundation, roughly parallel to the valley and inclined at approximately 60-70 degrees towards the left bank.

During the studies for the Tender design, as the plunge pool was covered by water, the geology was inferred from existing documentation dating from the construction period and from 4 additional boreholes drilled in 2012. It was predicted that the plunge pool would be excavated entirely within the biotite gneiss intersected by pegmatite dykes. The gneiss was expected to be a fairly massive and very strong rock. The fault zone was expected to be composed of highly fractured weak rocks with some clay infill. It was predicted that the fault contact with the surrounding gneiss could be locally open. Weak sub-horizontal biotite rich seams of poor quality were also expected.

3.2. SCOURING STUDIES BEFORE THE PROJECT

After realising that no theoretical formula, even the most elaborated ones, could anticipate the development of Kariba plunge pool, Zambezi River Authority (ZRA) contracted the "Laboratoire de Constructions Hydrauliques - EPFL (LCH)" and "AquaVision Engineering (AVE)" in May 2010 to perform the hydraulic model studies and define, in collaboration with Coyne et Bellier, the best technically suitable geometrical new setting for the plunge pool. Coyne et Bellier also acted on behalf of ZRA for the follow-up of the model.

EPFL And AVE have been working together coupling the physical model constructed at the Hydraulic Laboratory of the EPFL, with the numerical model developed by AVE on rigorous constitutive modelling methods that allow predicting numerically scouring problems with respect to the transient pressure in rock joints due to high-velocity jet impact: if stresses due to the hydrodynamic pressures at the tip of the joint exceed the fracture toughness of the rock, the rock will crack and the joint can grow further.

Several experiments were performed with the hydraulic model. The data of pressures and velocities measured during the experiments, were used to run the scouring model implemented by AVE, based on the preliminary studies and hypothesis about the rock characteristics. The model implemented and used by AVE is the Comprehensive Scour Model (CSM, Bollaert 2002 & 2004, [4] & [5]). The CSM estimates the ultimate depth of scour and the time evolution of scour in partially or totally fractured rock. The model is physically based and, at its origin, comprises a comprehensive assessment of the main physical processes that are responsible for rock break-up by turbulent flow impingement: (i) Comprehensive Fracture Mechanics (CFM) module; (ii) Dynamic Uplift (DI) module and (iii) Quasi-Steady Impulsion (QSI) module. The latter break-up mechanism is of particular

importance at Kariba Dam because governing potential regressive erosion towards the dam toe. The modules make use of the following parameters:

- the angle and location of the impacting turbulent jet;
- the diffusion of this jet through the local water depth;
- the velocity of this jet upon deviation at the pool bottom into a wall jet;
- the percentage of the flow that is deviated towards upstream;
- the velocity profile of the wall jet towards upstream;
- the rock foundation or plunge pool bottom protrusion that may deviate the currents and generate dynamic pressure fluctuations.

For those scour computations, each of the modules has been applied separately. The time evolution of scour formation is governed by the CFM module and then systematically applied to the other modules.

Using the geomechanical parameters available and assumed at that time (in 2015), before the works started and the dewatering of the Plunge Pool allowed the detailed study of the geology, AVE performed several runs of the model and the results in the case of 6 opened gates (which is the worst case scenario for turbulent effects) are shown in Fig. 3.

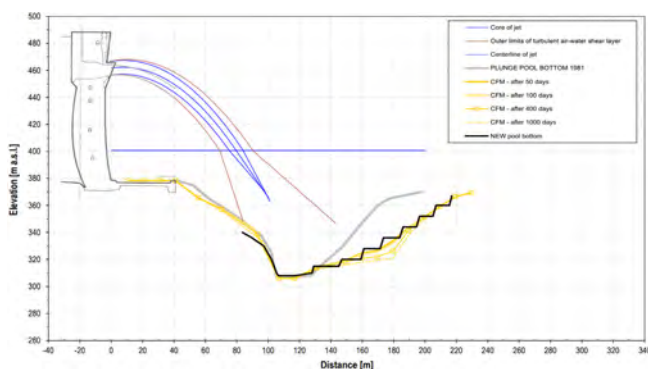


Fig. 3

Numerically computed scour predictions using the CFM method, for the second reshaped pool geometry n.2, at gate 6 (fault). Ref. to [5]

Referring to the EPFL final report they concluded that: "scour potential by block uplift remains quite significant in the deepest part of the pool. This, however, is based on the assumption that severe dynamic pressure fluctuations still exist in the deepest part of the pool, as well as stimulation to resonance of these fluctuations inside fissures. [...]. As such, the remaining scour potential as predicted by the numerical model is to be considered purely theoretical. In practice, remaining scour at gate 6 (over the

position of the fault) will be quasi negligible. Also, if the rock mass has to be fractured before being scoured, which is most plausible, even the numerically computed scour potential during the remaining lifetime of the dam remains very limited in space and intensity. [. . .] Along the side of the pool, at gate 6, moderate scour potential remains, but only loose material would be scoured. If the rock mass has to be fractured before being scoured, which is most plausible, the scour potential remains very limited in space and intensity. Hence, by applying a local concrete filling and/or bolting along the fault at this location, the pool may be considered as stable for the future."

4. PLUNGE POOL TENDER DESIGN

4.1. PLUNGE POOL EXCAVATION

In order to facilitate the stabilization of the Plunge Pool, control its future development and prevent further backwards scouring along the fault zone on the upstream side of the pool towards the dam foundations, several solutions were envisaged. The physical hydraulic modelling and numerical studies concluded that the optimal solution consisted in enlarging the plunge pool, mainly downstream but also on both banks' sides. This configuration should facilitate the evacuation of spillage flows towards downstream and prevent flow concentration and recirculation towards upstream.

The Reshaping works involved a significant volume of rock to be excavated, estimated to a final figure of 305'000 m³, by drill and blast method. These works are unprecedented and unusual owing to the magnitude of the 80m deep excavation below the Tail water level, at the foot of an existing dam in operation and the presence of critical structures such as the dam wall, the powerhouses, and the turbines.



Fig. 4

Tender Design of the Reshaping works and Fault Protection zone – Left: Cross section at the Dam axis – Right: 3D representation of the Reshaping works and concrete slab for fault protection

In order to allow the excavation works to proceed in dry conditions, the realization of a cofferdam composed of 8 Piers, anchored to the rock foundation by

post-stressed tendons and the dewatering of the stilling basin was required. The principal objective of the excavation and reshaping works was to increase the available water for energy dissipation and redirect the flow of flood waters downstream in order to ease the dynamic pressure fluctuations on the upstream side of the Plunge Pool which constitutes the driving factor for scour.

The reason for this particular attention to the upstream rock slope is the presence of a geological fault which is composed of weaker materials than the surrounding gneiss.



Fig. 5

View of the Plunge Pool Reshaping Works nearing completion – July 2024 –
Courtesy of Razel-Bec

4.2. FAULT PROTECTION TREATMENT OF THE UPSTREAM PLUNGE POOL SLOPE

The physical hydraulic model tests indicated reduced scouring potential on the upstream face of the plunge pool once the full excavation and reshaping of the plunge pool are complete. In the deepest part of the pool, only minor scour potential along part of the downstream rock slope remains.

The design of the optimum pool geometry was the sole mitigation measure against scour, i.e., without any additional need for structural measures such as rock bolt anchoring and placement of an abrasion-resistant high performance concrete slab. Nevertheless, the addition of a concrete treatment and consolidation grouting on the main geological fault along the upper rock slope was included in the mitigation measures, to ensure protection of the entire upstream fault zone and to secure the dam foundations in the event of future extreme floods.

- Casting of an abrasive-resistant reinforced concrete slab

- Installation of 40mm anchors, 10m long bars every 9m² to ensure stability of the slab against uplift pressure
- Consolidation grouting every 9m² of the fault zone to ensure watertight contact between the rock and the slab and to fill any voids or cavities

This concrete protection treatment, extended over the entire height of the upstream rock slope down to the deepest part of the scour hole, was also motivated by the Tender assumption that the fault zone in the Plunge Pool would require special treatment as it was foreseen to be an area with a high density of open joints and weak erodible breccia with erodible material.

It was very difficult to table a final design at the Tender stage without detailed information regarding the fault due to the fact that, being below the water level, it could not be inspected properly. Neither the exact geometry nor the geological and geomechanical properties of the fault were precisely known.

5. ACTUAL CONDITIONS ENCOUNTERED DURING EXCAVATION

5.1. GEOLOGICAL CONDITIONS OF THE PLUNGE POOL

The dewatering of the plunge pool and the following excavation works allowed detailed geological mapping of the rock faces to be carried out.

The mapping was complemented by an investigation of the fault that took place by means of laboratory testing on samples obtained from boreholes drilled through the fault. The permeability of the fault and its contact with the surrounding gneiss was investigated by Lugeon tests and by analysing the results of the contact grouting carried out in the upper part of the fault.

To complete the geological investigation, the colloidal concrete strength was also tested by UCS tests on 45 samples obtained by short boreholes cored through the concrete.

As expected, the plunge pool is mostly composed of strong to very strong biotite Gneiss with some inclusions of dark grey amphibolite, particularly on the Right Bank. The gneiss is intersected by pegmatite dykes (metric width) with an orientation mostly perpendicular but also parallel to the valley. The contact between the pegmatite dyke and the surrounding gneiss was always found to be tight. The discontinuities intersecting the rock mass were generally rough and wavy, their spacing was mostly wide to very wide, with an average of 2 m between joints and they were found to have locally a very high persistence (> 20 m).

The main subvertical joint set observed is broadly parallel to the valley and dips 70° towards the Left Bank, parallel to the main fault. The secondary set is

subvertical and perpendicular to the valley. In addition, sub horizontal joints are well developed, especially towards the top of the excavation. Their inclination differs notably on the Left and Right banks as they dip with an average angle of 20° towards the center of the valley.

The fault zone is mainly composed of Breccia which consists of angular clasts of rocks of various origins embedded in a silica-rich matrix containing alteration minerals (chlorite, iron oxide, sericite). The clasts range in size from a few centimeters to over 10 cm in diameter, and there is a general lack of structure (very few fractures were observed). The fault zone also contains some hydrothermally altered chlorite-rich gneiss, which can locally extend for a few meters on either side of the Breccia. However, the contact with the surrounding Gneiss was found to be tight and the fault appears to be fairly impermeable with very little seepage.

The strength of the Breccia matrix varies depending on the percentage of alteration minerals and the degree of recrystallization, which may account for varying levels of scouring within the fault. The fault's thickness changes with both depth and lateral position, generally widening towards the cofferdam. The fault's orientation aligns with Tender Design data, but its trace differs due to its intersection with the plunge pool, which is more eroded towards the Left Bank (Figure 6).

The rock conditions therefore generally confirmed the initial assessment of the gneiss's overall good quality. Contrary to the prevision, few horizontal altered biotite rich seams were found, and those had already been locally treated. However, variations in the intrinsic quality of the fault were observed, with the fault generally being much less fractured and stronger than anticipated in the Tender Documents. Nevertheless, the variation in strength of the fault material which was in most cases weaker than the surrounding gneiss led to the observed scouring. This erosion is particularly significant below elevation 330 masl where a cavity was found after dewatering.



Fig. 6
Trace of the main fault across the excavation

In order to assess the erodibility of the area where the fault treatment was envisaged at Tender Design, the rock mass was divided into 3 zones based on the geomechanical characteristics of the fault and of the surrounding Gneiss as shown in Fig. 7.



Fig. 7

Fault layout with zones of homogeneity in the area of the fault treatment

5.2. PRESENCE OF EXISTING COLLOIDAL CONCRETE REPAIR WORKS

During the Plunge Pool drawdown, some visible existing repair works had been performed on the upstream rock slope in the fault area and seemed to have held up well over the years (Fig. 8). Particularly, the fault in its upper part was covered by a colloidal concrete composed of cobbles and injected grout.

The analysis the historical data and archives indicated that some protection works were performed but the collected information was minimal and not detailed enough to know the number of repair works, extension within the fault, dates of execution or type of material used for the treatment. In order to collect more reliable information an investigation campaign was launched in 2023 to gather relevant data about the current state of the colloidal concrete, the fault material, and the contact between the two.

Although the contact was found to be tight and the fault zone to be impermeable, it was also discovered that the underwater repair works had purposefully been

implemented to protect the part where the breccia is the weakest. Indeed, the examination of the cores and the UCS tests revealed that, behind the existing colloidal concrete, the fault is mainly composed of chlorite rich breccia with very low mechanical characteristics. The characteristics of the colloidal concrete showed great dispersion, ranging from 7 MPa to 50 MPa, and weaker mechanical properties in the upper elevations which questioned its long-term behaviour and durability.

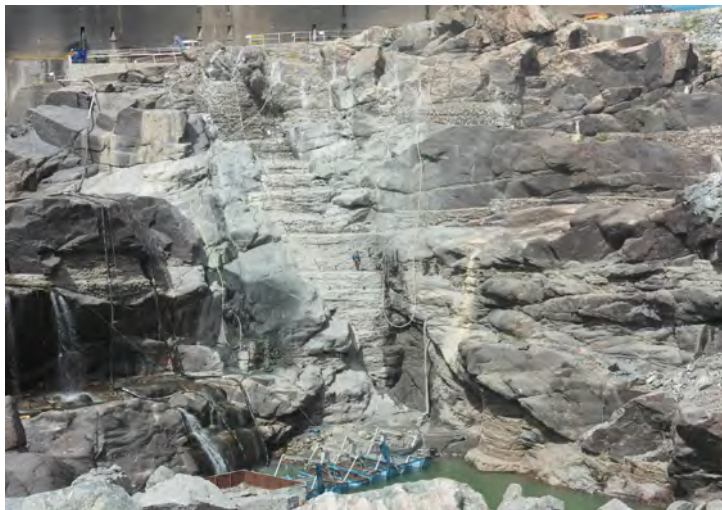


Fig. 8

Colloidal concrete repair works discovered during the Plunge Pool drawdown

6. ASSESSMENT OF THE ERODIBILITY OF THE FAULT AND SURROUNDING ROCK

The erodibility assessment was carried out following two different approaches:

- the Rational Method developed by G.W Annandale in 1995 for determining the erodibility of earth materials (soil and rock) and presented in the Journal of Hydraulic Research, Vol.33, No.4;
- the Fatigue Method applying the Paris-Erdogan law.

Both the approaches consider the energy/power produced by the jet impact when the 6 gates are fully opened and the geomechanical rock parameters which

are derived from information available at Tender stage complemented by the additional investigations and assessments carried out during excavation and dewatering of the plunge pool.

6.1. ERODIBILITY ASSESSMENT – ERODIBILITY INDEX

The headcut erodibility index, K_h , represents a measure of the resistance of the earth materials to erosion. The variables of the index K_h include key rock mass properties and geological parameters such as rock mass strength, block size, discontinuity shear strength, and shape of material units and their orientation relative to streamflow. The erodibility index is the scalar product of the below parameters. The index takes the general form:

$$K_h = M_s \times K_b \times K_d \times J_s$$

where: M_s is the Rock mass strength, K_b is the block size number, K_d is the discontinuity shear strength number and J_s is the relative ground structure number. The number, M_s , expresses the unconfined compressive strength of the rockmass. The number, K_b , refers to the mean block size of intact rock material (the cube root of the volume) as determined by the spacing of discontinuities within the rock. The number, K_d , represents the shear strength of a discontinuity in a rock mass, factoring in the roughness, aperture, and relative alteration of the joints. The number, J_s , accounts for the structures of the rockmass with respect to streamflow. It is a complex function that considers orientation and shape of individual blocks, as determined by the measurement of the spacing, dip angles, and dip directions of joint sets, with respect to direction of streamflow.

The assessment of the erodibility of the upstream slope of the plunge pool, was carried out considering the most dominant joint sets which are:

- The discontinuities parallel to the fault with a dip and dip direction of 67/320
- The joint sets corresponding to the pegmatite with a dip and dip direction of 78/230.

A number of 3 joint sets have been considered representative of the Right and Left Bank and only 1 joint set parallel to the fault has been considered for the Fault zone, for all the verifications. The direction of the stream has been assumed downstream to upstream, corresponding to the reverse abrasive currents.

Based on this analysis, only the chlorite rich Breccia shows a risk of erodibility. Due to its good quality and absence of closely spaced discontinuities, the gneiss on both the left and Right banks presents a low risk of erodibility.

Table 1
Erodibility assessment based on the Erodibility Index – Upstream slope

		Unit	Erodibility parameters - Upstream rock slope of the Plunge Pool			
			Gneiss adjacent to the fault		Fault	
			Gneiss Right Bank	Gneiss Left Bank	Chlorite rich matrix	Silica rich matrix
1	Rockmass strength	MPa	100	85	30	70
2	RQD Joint set number Jn Number of joint sets Block size Kb	%	90	90	20	60
		-	2,73	2,73	1,5	1,5
		-	3 sets	3 sets	1 set	1 set
			33,0	33,0	13,3	40,0
3	Joint roughness Jr Joint alteration Ja Friction angle Shear strength number Kd	-	1	1	1	1
		-	1	1	2	2
		-	-	-		
		-	1, 0	1, 0	0, 5	0, 5
4	Orientation Number Js	-	0,67	0,67	1	1
5	Erodibility Index Kh	-	2208,8	1877,5	200,0	1400,0
6	Stream Power Threshold	kW/m ²	322,3	285,3	53,2	228,9
7	Jet power - 6 gates open	kW/m ²	139	139	139	139
8	Erodibility assessment	-	Non Erodible	Non Erodible	Risk of Erodibility	Non Erodible

6.2. FATIGUE METHOD – PARIS-ERDOGAN LAW

The assessment methodology is composed of four-steps:

1. Defining the dynamic loading acting on the upstream face of the plunge pool, from experiments performed at LCH-EPFL (2017-2020),
2. Defining other input data
3. Applying the rainflow counting to the pressure data measurements,
4. Assessing crack propagation by fatigue under cyclic loading for different spillage durations, by applying the Paris-Erdogan law,
5. Carrying out the analysis for the current situation of the fault.

The third step, the Paris-Erdogan Law (fatigue), Mode I (tensile), is used to assess crack propagation during a single flood release event. The Paris–Erdogan equation is a crack growth equation that gives the rate of growth of a fatigue crack.

The stress intensity factor K characterizes the load around a crack tip and the rate of crack growth is experimentally shown to be a function of the range of stress intensity ΔK seen in a loading cycle.

The Paris-Erdogan equation is

$$da/dN = C(\Delta K)^m$$

where:

- a is the crack length and da/dN is the fatigue crack growth for a single load cycle N ,
- $\Delta K = K_{max} - K_{min}$ is the stress intensity range, calculated as the difference between the maximum and the minimum stress intensity for a cycle. It depends on the far field stress and the crack tip stress intensity,
- C is related to the characteristics of the rock mass,
- m is related to rock mass type and slope of the crack growth rate curve (for materials with low static fracture toughness the value can be up to 10).

Using the same hydrodynamic input data coming from experiments performed at the EPFL (as the shape of the pool is considered to be identical). The most critical scenarios are considered, and the selected test used for this erodibility assessment are the most relevant, with all orifices in operation and high reservoir levels, combined with low tailwater levels and partial dismantling of the downstream cofferdam.

The input data about rock mechanics are the one updated after last investigations: weak breccia (or chlorite rich breccia) protected by colloidal concrete (pessimistic case); colloidal concrete (pessimistic case – design characteristic value); silica rich breccia in the fault (realistic).

In order to apply the Paris-Erdogan equation, it is important to determine the coefficient C and the exponent m , as input data. Those parameters are taken from the Table III-7 in the article of Atkinson [3]. (Title of Table III-7: "Subcritical index n (Atkinson, 1984) and fatigue exponent m as a function of the type of rock. The environmental conditions correspond to water at 20-25°C").

The third step is to apply the rainflow counting method to the pressure data measurements. It is a method used to assess the statistics of dynamic pressure, in order to determine the number of fatigue cycles (loading and unloading of a part) present in a load-time history.

The fourth step is to assess the crack propagation under cyclic loading (fracture-mechanics methods) and it is done using the Paris-Erdogan law considering the failure mode I (tensile) for single-end cracks. The approach considers that there are no loose blocks at the pool surface but that the rock mass, the fault zone and the colloidal concrete are not flawless: these different materials may have

discontinuities that can be excited by dynamic loading. The discontinuities are here assumed to be of millimetric width, no filling and metric length (related with persistence), with variable initial length ranging from 1.0 m to 5.0 m.

Apart from geometry, the mechanical resistance of the solid surfaces is defined for:

- UCS values of 10 MPa (colloidal concrete, characteristic value), 30 MPa (weak breccia or chlorite rich breccia) and 60 MPa (Silica rich Breccia);
- Fatigue law parameter “m” ranging from 8.8 MPa.m^{1/2} (typical limestone) to 4.4 MPa.m^{1/2} (sandstone or limestone with a safety factor of 2) and 2 MPa.m^{1/2} (weak material), obtained from literature (e.g. Atkinson 1984 [11]);
- Fatigue law parameter “C” ranging from 2.7 E-7 to 1.1 E-8 MPa.m^{1/2} (from literature);
- Fatigue parameter $\Delta K_I/K_{Ic} = 0.9$, also labelled normalized stress intensity factor;
- Fatigue law parameter ΔK_I which is the difference between the maximum and minimum stress intensity factor at the tip of a growing crack [Kim & Mubeen, 1981]; for each pulse set, time-dependent crack propagation stop when ΔK_I is below a given threshold value (as per the plot below);
- Insitu minimum stresses defined at geostatic, i.e. gR.z, z being the distance to the initial riverbed level.

The onset from brittle to fatigue propagation is defined as $K_I = K_{Ic}$, $DK_I = 2$ and K_{Ic} was defined as function of UCS. Stress intensity at crack tip is function of only (a, Pmax), with Pmax the value measured in Laboratory at rock surface.

A summary of the most significant results is shown in Table 2. Generally, there is no relevant crack propagation for short duration spillage events. For the weaker conditions assessed, it is reached an incremental scour in the order of centimetres after 100 days of spillage, leading to metric-scale incremental scour after 1000 years of spillage.

The assessment of acting loading on the upstream surface of the plunge pool indicated that the remaining dynamic pressures are very low values, even in case of extreme spillage events (all orifices, maximum reservoir level, low tailwater level). For instance, maximum pressures at intermediate depth elevation (i.e. El. 346 m a.s.l.) are not more than even 1m of the static head at that location, minimum pressures dropping up to 6 meters.

Sensitivity analysis to key parameters shows that softer/harder surface conditions and shorter/longer initial crack length have impact but are not expected to play a significant role. The computed crack growth rates and lengths for 1 day, 10 days, 100 days and even 1000 days of consecutive spillage are very low. Given the assumptions of the model, it is wise not to overeat the absolute values and rather focus on the orders of magnitude.

In summary, the pool surface may undergo incremental scour (of millimetric/centimetric scale) after at least 100 days of spillage, which is more than one flood season, at intermediate elevations around El. 340, in weaker materials.

Table 2

Estimated time-dependent crack propagation under cyclic-loading for cumulated spillage time for different areas in the fault zone of the upstream face.

Cases	point	UCS	1 day	10 days	30 days	100 days		a	m	C
ID		MPa	[mm]	[m]	[m]	[m]	[m]	[m]	[Nmm ⁻³²]	[Nmm ⁻³²]
Silica rich Breccia	P3	60	0.00	0.00	0.00	0.00	0.00	1.0	8.8	1.10E-08
Silica rich Breccia	P3	60	0.00	0.00	0.00	0.00	0.00	1.0	8.8	2.70E-07
Chlorite rich breccia	P3	30	0.00	0.00	0.00	0.00	0.00	1.0	4.4	1.10E-08
Chlorite rich breccia	P3	30	0.00	0.00	0.00	0.00	0.00	1.0	4.4	2.70E-07
Chlorite rich breccia	P3	30	0.06	0.00	0.00	0.01	0.06	1.0	2	1.10E-08
Colloidal concrete	P3	10	0.00	0.00	0.00	0.00	0.00	1.0	4.4	2.70E-07
Colloidal concrete	P3	10	0.06	0.00	0.00	0.01	0.06	1.0	2	1.10E-08
Colloidal concrete	P3	10	1.49	0.01	0.04	0.15	1.49	1.0	2	2.70E-07

7. DESIGN CHANGES FOLLOWING THE NEW ERODIBILITY STUDIES

The actual conditions encountered during the successive phases of excavation and dewatering rendered possible the characterization of the fault in terms of geometry and composition. The trace of the fault, dipping towards the Left Bank, was found to be different from the Tender assumption which resulted in a realignment of the fault concrete protection works axis on the actual trace of the fault.

As shown by the erodibility studies, the fault composed of chlorite rich breccia is prone to future erosion whereas the silica rich breccia and the gneiss adjacent to the fault do not present a risk of future scour.

Decision was therefore made to only proceed with the protection of the chlorite rich breccia by means of a reinforced concrete slab anchored to the rock. Additionally, due to the lack of reliable data regarding the existing colloidal concrete,

a decision was made to apply the same treatment to the existing colcrete. Evidently, this choice was motivated by the investigation that identified the presence of the chlorite rich breccia behind the existing colloidal concrete.

All the concrete treatment initially foreseen as per Tender on the gneiss on the upstream face of the plunge pool (cf Fig. 4) was descoped. In the end, the fault treatment consumables for the concrete slab used on-site were significantly less than the bill of quantity allowance (Table 3).

Table 3
Fault treatment concrete slab consumables

Fault Treatment consumables	Contract BoQ		Used on site		% of the BoQ allowance consumed
	BoQ allowance	Unit	Total Quantity	Unit	
40mm anchor bars	4402	m	3150	m	71.60%
Consolidation holes	1479	m	1131	m	76.50%
Cement for Grouting	118	ton	17	ton	14.00%
Concrete C30	7171	m3	5017	m3	70.00%

The updated design applied to the final works was adapted to the actual in-situ geological conditions encountered on site during the excavation works (Fig. 9).



Fig. 9
Fault protection – Concrete slab – Upstream rock slope – July 2024

8. CONCLUSION

The close follow-up of the excavation of the plunge pool, complemented by new geological investigations, has revealed that the overall quality of the rock mass in the fault area is better than was expected at the Tender Design Stage. The new studies, based on the actual in-situ conditions, have shown a low risk of future scouring. Nevertheless, a residual risk remains, primarily linked to the presence of chlorite-rich breccia within the fault.

In the upper part of the plunge pool the sections of the fault consisting of weak breccia were covered with colloidal concrete, which appears in good condition due to ongoing maintenance over the years, but which nevertheless remains the weaker structural element of the fault area.

The Kariba Dam Rehabilitation Project aims to prevent regressive scour in the fault area and thus potential instability in the dam foundations. This objective implies that fault protection remains a critical part of the mitigation measures. Based on observations and studies, it was decided to reduce the scope of the initial project and limit the fault concrete slab protection works to the most sensitive areas, consisting of weaker breccia, which were identified based on in situ observations and geological mapping. The project was adapted to the actual location of the fault and the deep erosion found at the bottom of the plunge pool, focusing only on restoring hydraulically appropriate shapes.

REFERENCES

- [1] ANNANDALE G.W. Erodibility, *Journal of Hydraulic Research*, 33:4, 471–494. (1995)
- [2] ANNANDALE, G.W. *Scour Technology: Mechanics and engineering Practice*. McGraw-Hill. (2006)
- [3] ATKINSON, B. K.: Subcritical crack growth in geological materials. *J. Geophys. Res.* 89(B6), 4077–4114 (1984).
- [4] BOLLAERT, E., FALVEY, H.T., SCHLEISS, A. Assessment of turbulent jet impingement in plunge pools: the particular characteristics of a nearprototype physical model study, *Proceedings of Riverflow 2002*, Louvain-laNeuve, Belgique. (2002)
- [5] BOLLAERT, E.F.R. A comprehensive model to evaluate scour formation in plunge pools. *Int. Journal of Hydropower & Dams* 1, 94–101. (2004)

COMMISSION INTERNATIONALE DES
GRANDS BARRAGES

VINGT-HUITIEME CONGRES DES
GRANDS BARRAGES
CHENGDU, MAI 2025

**PIANO KEY WEIR GEOMETRIES ADJUSTMENT FOR DOWNSTREAM
HYDRAULIC REGIME: LESSONS LEARNED FROM CASE STUDIES IN
VIETNAM (*)**

Le VAN NGHI

*Vietnam National Committee on Large Dams and Water Resources Development
The National Key Laboratory of River and Coastal Engineering, Vietnam Academy
for Water Resources*

Hoang Duc VINH, Doan THI MINH YEN & Nguyen Tien HAI

*The National Key Laboratory of River and Coastal Engineering, Vietnam Academy
for Water Resources*

VIETNAM

SUMMARY

Piano Key Weirs (PKWs) are advanced spillway designs that significantly enhance the discharge capacity of dams, providing an efficient solution for flood-water management. However, the complexity of PKW structures presents considerable challenges in hydraulic optimization. This study investigates geometric modifications to PKWs, based on practical applications in Vietnam, to improve downstream hydraulic conditions and increase flood discharge capacity. Utilizing 3D physical hydraulic models at the Key Laboratory of River and Coastal Engineering (KLORCE), two projects were examined: the Da Si spillway, scaled at 1:16, and the Cao Ngoi spillway, scaled at 1:20. The Da Si project combined a PKW with an Ogee weir, directing discharge flow into a chute and energy dissipation basin. By refining the PKW design with a trapezoidal key at a 3-degree diagonal angle, flood drainage

**Ajustement de la géométrie de seuils à touches de piano pour tenir compte du régime hydraulique aval – deux études de cas au Vietnam*

capacity increased by 5-10%, while downstream flow became more uniform, reducing the unit flow difference on the chute by 1.5 to 6.2 times. The Cao Ngoi project employed a curved PKW with a central convergence angle, achieving a 9% to 12.7% increase in discharge capacity and improved energy dissipation by 4.5% to 8.2%. These modifications not only enhance hydraulic efficiency but also reduce construction costs and improve the overall stability of the projects, offering valuable insights for similar flood management infrastructure globally.

RÉSUMÉ

Les déversoirs à touches de piano (PKW) sont des déversoirs de conception avancée qui améliorent considérablement la capacité d'évacuation des crues des barrages, offrant ainsi une solution efficace pour la gestion des crues. Cependant, la complexité de conception pose des défis considérables en matière d'optimisation hydraulique. Cette étude examine les modifications géométriques apportées aux PKW de deux barrages au Vietnam, afin d'améliorer les conditions hydrauliques en aval et d'augmenter la capacité d'évacuation des crues. Deux projets ont été examinés à l'aide de modèles hydrauliques physiques en 3D au Key Laboratory of River and Coastal Engineering (KLORCE) : le déversoir de Da Si, à l'échelle 1:16, et le déversoir de Cao Ngoi, à l'échelle 1:20. Le projet Da Si combine un PKW avec un déversoir à seuil libre, dirigeant le débit dans un coursier et un bassin de dissipation d'énergie. En affinant la conception du PKW, la débitance a augmenté de 5 à 10 %, tandis que le débit en aval est devenu plus uniforme, réduisant la différence de débit unitaire sur le coursier. Le projet Cao Ngoi a utilisé un PKW incurvé, ce qui a permis d'augmenter la capacité d'évacuation de 9 à 12,7 % et d'améliorer la dissipation d'énergie de 4,5 à 8,2 %. Ces modifications permettent non seulement d'améliorer l'efficacité hydraulique, mais aussi de réduire les coûts de construction et d'améliorer la stabilité générale des projets, ce qui offre des indications précieuses pour des infrastructures similaires.

1. INTRODUCTION

The piano key weir (PKW) is an innovative structure engineered to efficiently discharge floodwaters from reservoirs, mitigating the geometric constraints associated with conventional labyrinth weirs [1], with its concept and design originally developed by Lempérière and Ouamane [2]. The importance of PKWs lies in their ability to safely pass large volumes of water over dams during flood events, reducing the risk of overtopping and structural failure [3]. Their application extends to both new dam constructions and retrofitting existing spillways, particularly in regions where space is limited or where increasing the capacity of a reservoir is critical.

The University of Liège's world register of Piano Key Weir prototypes, last updated on June 26, 2020, reveals that 75% of these weirs are installed atop dams, while only 19% are applied in-channel [4]. The top-dam-installation-PKWs are frequently integrated with free spillways, ogee weirs, chute, or roller-bucket systems. Given the higher discharge capacity of the PKW, it is essential to implement effective energy dissipation techniques, such as stilling basins or chutes, downstream of the weir to prevent scouring, and various configurations have been experimentally tested to identify the most efficient solution [1].

Many studies have been conducted over the years to examine the diverse factors affecting the efficiency and functionality of PKWs. Some studies recently focused on slight geometric alterations to standard rectangular PKWs, revealing variations in their flood discharge performance. For example, experimental study by Kumar et al (2020) demonstrated improved discharge efficiency in trapezoidal PKWs compared to rectangular designs with the same L/W ratio, with the trapezoidal weirs achieving a 2–15% increase in discharge coefficient [5]. Moreover, curved PKW designs have been evaluated, demonstrating an enhanced capacity for improving flood discharge efficiency. Mishra and Ahmad (2021) conducted experimental studies on PKWs featuring ogee-shaped outlet keys, revealing that, under water heads exceeding the design level, the discharge capacity of curvilinear PKWs increased by 5.2% compared to those with non-curved outlet keys [6]. E. Khanahmadi (2023) investigated curved Type-B PKWs with central convergence angles of 90° and 130° under varying head conditions, finding that, under low-head conditions, the discharge coefficients increased by 17.69% and 18.85%, respectively, compared to conventional weirs [7].

In Vietnam, the study, application and construction of PKWs have gained importance due to the country's need for effective flood management and dam safety. Researchers have conducted experimental and numerical studies, focusing on optimizing PKW designs for Vietnam's specific hydraulic and geographical conditions. Based on practical studies of PKW applications in Vietnam, the paper highlights two significant projects that focus on geometric modifications of PKWs to enhance flood discharge capacity and improve the downstream hydraulic regime. These PKW geometries adjustment not only boost hydraulic efficiency but also lead to reductions in construction volume and associated costs, thereby increasing the overall stability and economic feasibility of the project. The insights gained can serve as valuable lessons for similar projects globally, offering approaches for achieving both performance and cost-effectiveness in flood management infrastructure.

2. EXPERIMENTAL SETUP

The overall 3D physical models were conducted at the National Key Laboratory of River and Coastal Engineering (KLORCE), Vietnam Academy of Water Resources. The experimental setup provided a discharge flow of up to 300 l/s

through a system comprising an underground tank, elevated pressure tank, pumping stations, and circulation pipes. Inlet discharge was precisely regulated using rectangular thin-plate weir flumes with an accuracy of $\pm 1\%$. Water level profiles and flow depths were measured using nine fixed water level gauges along the structure, employing measuring needles, as well as mobile measurement points using Ni04, with a tolerance of less than 0.1 mm. Average velocity (V) and velocity fluctuations (σ_v) were recorded using electronic sensors, including E30, E40, and PEMS, all with an accuracy of $\pm 1\%$. The headworks were constructed from organic glass, maintaining an error margin of less than 0.1 mm. Additionally, cameras were installed at various locations for visual analysis.

The Da Si Spillway is engineered to manage floodwaters for the Da Si Reservoir in Lam Dong Province, Central Vietnam, which has a storage capacity of 21.77 million m^3 . The design discharge for a 100-year flood event is 96.8 m^3/s , while the 500-year flood event test discharge is 126.8 m^3/s . The spillway structure comprises an Ogee spillway, equipped with a gate at an elevation of +159.5 m, with a width of 5 m. This is flanked by two un-gated free spillways (Ogee) on either side, at an elevation of +162.5 m, each 5 m wide. Downstream of the spillway lies a 40 m long water chute with a 13.5% gradient, leading into an energy dissipation basin. The two 5m-wide free spillways on either side were subsequently replaced with two PKWs, each with a width of 3 meters. The PKW with a trapezoidal key design is an advanced form of the standard rectangular key piano weir. In this design, the side wall of the overflow key is angled at 3 degrees relative to the flow axis (Fig. 1).

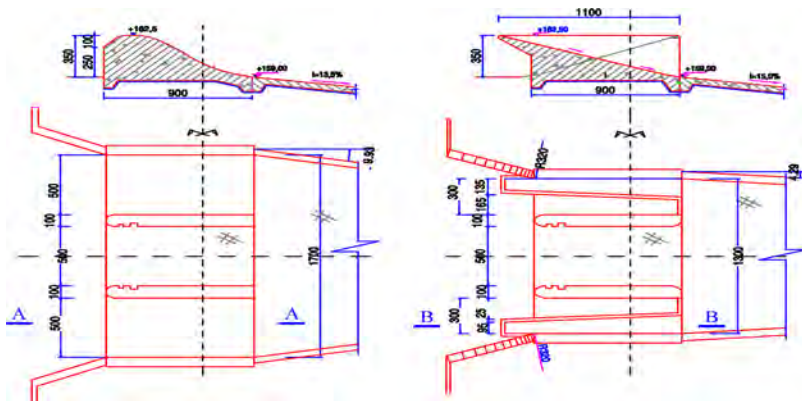


Fig. 1

The two 5-meter-wide free spillways on either side (left side) were subsequently replaced with two 3-meter-wide PKWs featuring a trapezoidal key design (right side)

The overall hydraulic model of Da Si spillway is designed in a scale of 1/16, with a total length of 32.0m, width of 8.76m, and height of 1.8m (Fig. 2).



Fig. 2
The overall hydraulic model of Da Si spillway

The Cao Ngoi Reservoir, with a capacity of 2.18 million m^3 , was constructed in Tuyen Quang Province, northern Vietnam. The PKW free-discharge spillway, 24 meters in width, is set at a threshold elevation of +130.5 meters. It is designed to handle a 100-year flood discharge of up to 229.0 m^3/s and has been tested for a 500-year discharge of 307.0 m^3/s , as well as discharges exceeding 500 years at 341.0 m^3/s . The PKW spillway is situated atop a 24-meter-high ogee spillway. The overall hydraulic model of Cao Ngoi spillway is designed in a scale of 1/20, with a total length of 18.0m, width of 7.5m, and height of 1.8m. In this project, the straight PKW was transformed into a curved PKW with a central convergence angle of 13.41° .

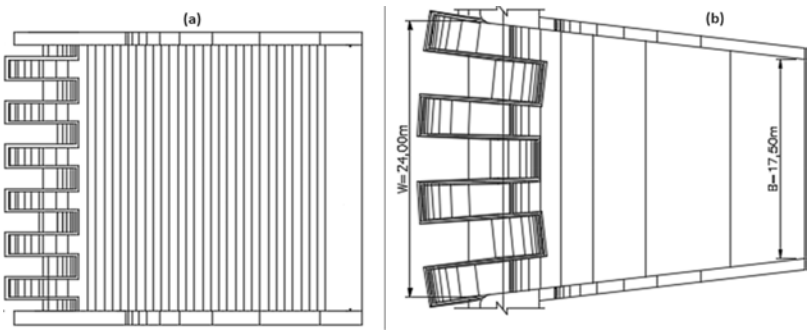


Fig. 3
Layout of the straight PKW (a) and curved PKW (b)

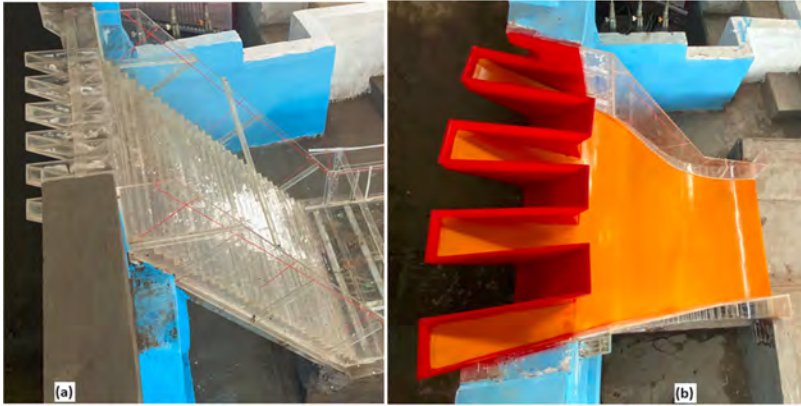


Fig. 4
The overall model of the straight PKW (a) and curved PKW (b)

Both models were tested under discharge levels corresponding to 50-year, 70-year, 100-year, 500-year, and 1,000-year flood frequencies.

3. RESULTS AND DISCUSSION

3.1. REPLACE OGEE SPILLWAYS WITH PKWs (DA SI PROJECT)

The experimental results obtained from the overall hydraulic model, scaled at a ratio of $\lambda = 16$, reveal significant differences in discharge capacity between the original Ogee spillway and the replacement PKW. Specifically, the discharge coefficient for the Ogee spillway was found to range between 0.39 and 0.44, while the PKW exhibited a substantially higher discharge coefficient of 1.34. When comparing the two structures under the condition of equal spillway widths, the PKW demonstrated a flood discharge capacity that is 3.03 times greater than that of the Ogee spillway.

To assess the hydraulic uniformity of the flow over both the spillway and the chute, we use the differential flow rate index (n).

$$n = \frac{q_1}{q_2}$$

where q_1 is unit discharge over side gate (Ogee/PKW); q_1 is unit discharge over middle gate (Ogee weir)

The experimental comparison between the Ogee spillway and the PKW highlights significant differences in unit discharge distribution behavior. For the Ogee spillway, the flow rate difference between the gated and free spillways ranges from 3.8 to 17.6 times, while the difference on the chute reaches values between 2.9 and 9.8 times. In contrast, the PKW shows a reduced flow rate difference between the gated and free spillways, ranging from 1.7 to 5.9 times, and a difference on the chute between 1.4 and 3.5 times. Consequently, replacing the Ogee spillway with a PKW results in a reduction of the flow rate difference by 2.0 to 8.0 times for the gated versus free spillway, and by 1.5 to 6.2 times on the chute. This reduction in flow rate differences fundamentally minimizes the interference phenomena on the chute, leading to more stable and efficient hydraulic performance Fig. 5.

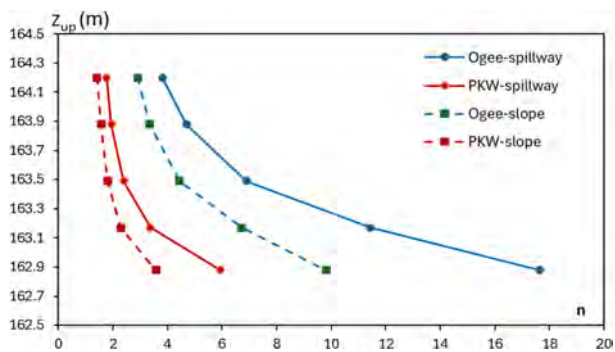


Fig. 5

Unit discharge difference on spillway and on chute. Z_{up} is water level on reservoir; n is differential flow rate index



Fig. 6

Flow through the Ogee spillway (left) and through the PKW (right)

The Ogee spillway exhibits a significant difference in flow rates across the chute, which causes the flow to diagonally shift towards the edges. This diagonal flow, moving from the center towards the sides, impacts the sidewalls of the chute, creating localized high-water levels and forming a water ridge that is redirected back onto the chute. This interaction generates a continuous pattern of diamond-shaped interference that persists along the length of the chute. In contrast, when a PKW is employed, the reduction in flow rate differences leads to a more uniform distribution of flow both after the spillway and along the chute. This uniformity significantly reduces collisions with the sidewalls, minimizes the water column rise along the sidewalls, and effectively eliminates the formation of diagonal waves and the associated diamond-shaped interference (Fig. 7).

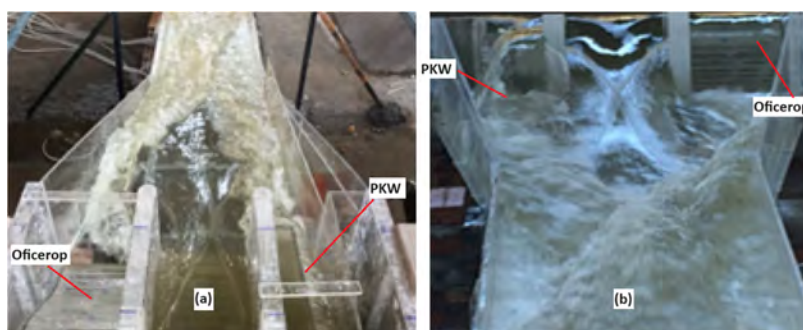


Fig. 7

Flow through the chute of Ogee and PKW. (a) upstream view; (b) downstream view

Moreover, the water level fluctuations across the cross-section of the PKW design are considerably less pronounced than those observed in the Ogee design. Specifically, the ratio of maximum to minimum flow depth (h_{max}/h_{min}) in the Ogee spillway ranges from 1.9 to 3.6 times, whereas in the PKW solution, this ratio is reduced to between 1.2 and 2.0 times. This more consistent water depth distribution across the spillway and chute enhances the hydraulic performance and stability of the PKW design, providing a more efficient solution for managing flow over the spillway.

3.2. REPLACE STRAIGHT PKW WITH CURVED PKW (CAO NGOI PROJECT)

Experimental results in 0 presented highlights the superior performance of the curved PKW design compared to the straight PKW in terms of both discharge coefficient (C_d) and flow rate (Q). Across all head levels, the curved PKW consistently

achieves higher discharge coefficients (C_{d2}) compared to the straight PKW (C_{d1}). The improvement in C_d ranges from 4% to 8%, indicating that the curved design enhances the efficiency of water flow over the weir, particularly at lower head levels. Furthermore, the flow rate (Q) for the curved PKW shows a significant increase over the straight PKW, with enhancements ranging from 9% to 15%. This substantial improvement in flow capacity is most pronounced at higher head levels, demonstrating the curved PKW's ability to manage larger volumes of water more effectively.

Table 1
Comparison of discharge coefficient (C_d) and flow rate (Q) between straight PKW and curved PKW

Z_{up} (m)	C_{d1}	C_{d2}	Q_1 (m ³ /s)	Q_2 (m ³ /s)	INCREASE (%)
132.56	1.155	1.203	327.83	369.42	12.69%
132.36	1.211	1.261	295.14	332.58	12.69%
131.88	1.409	1.497	217.66	250.34	15.01%
131.54	1.558	1.625	157.45	177.69	12.85%
131.46	1.592	1.654	143.43	161.25	12.42%
131.26	1.682	1.731	105.86	117.88	11.36%
131.11	1.748	1.786	79.36	87.82	10.66%
131.02	1.787	1.820	63.87	70.42	10.25%
130.96	1.814	1.843	53.71	59.08	9.99%
130.87	1.854	1.878	39.46	43.25	9.62%
130.74	1.909	1.925	21.71	23.69	9.12%

Note: C_{d1} , Q_1 represent of straight PKW; C_{d2} , Q_2 represent of curved PKW

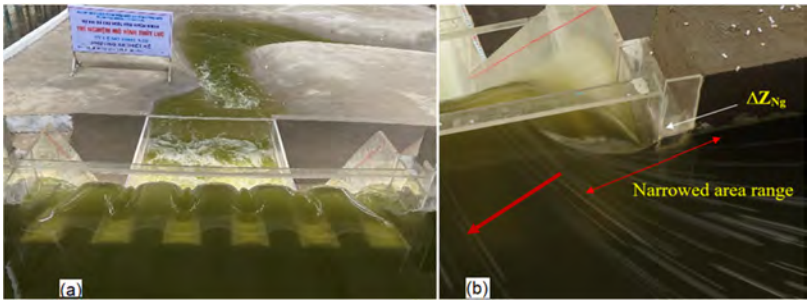


Fig. 8
Flow through the straight PKW is notably influenced by lateral constriction.

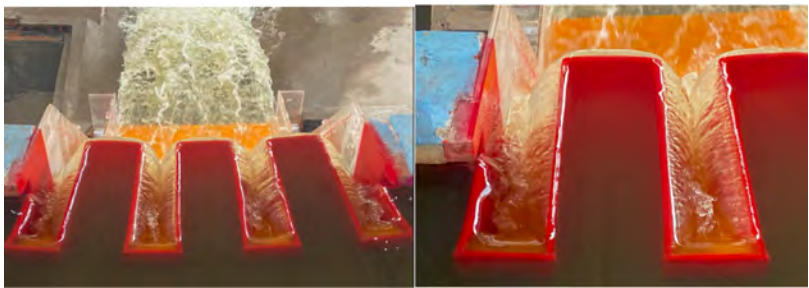


Fig. 9
Flow through the curved PKW

Flow through the straight PKW was significantly affected by lateral constriction, primarily caused by the obstruction from the lateral pillar and the positioning of the edge key as the water inlet. This lateral constriction can influence the flow dynamics, creating areas of restricted flow that extend up to 4.2 meters (Fig. 8). However, after modifying the design to a curved PKW, this lateral constriction phenomenon is effectively eliminated (Fig. 9). The curved design allows for a more uniform distribution of flow across the weir, removing the obstructions that previously hindered efficient water passage and improving the overall hydraulic performance of the structure.

Table 2
Energy efficiency through the project

Q(m ³ /s)	E0	E1	E2	% ΔE1	% ΔE2	% ΔE
341	26.5	8.1	7.3	69.3	72.6	4.74%
307	26.4	7.2	6.2	72.6	76.5	5.35%
229	25.8	6.3	4.4	76.7	83.0	8.21%

where: E0 is total energy at the cross-section before entering the spillway; E1, E2 are total energy at the cross-section right after the scour hole; ΔE is different energy at the two cross-sections; Number 1, 2 represents of straight PKW and curved PKW, respectively

The 0 shows the enhanced energy dissipation efficiency of the curved PKW compared to the straight PKW. The curved PKW consistently achieves higher energy dissipation efficiency than the straight PKW. Specifically, at a high discharge rate of 341 m³/s, the curved PKW improves energy dissipation by 4.74%. This

improvement becomes even more pronounced at lower discharge rates, with a 5.35% increase at 307 m³/s and an impressive 8.21% increase at 229 m³/s.

4. CONCLUSIONS

This study demonstrates that using PKW and geometric modifications can significantly enhance flood discharge capacity and improve downstream hydraulic conditions. In the Da Si project, implementing a trapezoidal PKW design increased flood discharge capacity by 5-10% and reduced flow differences on the chute by 1.5 to 6.2 times. Similarly, the curved PKW design in the Cao Ngoi project resulted in a 9% to 12.69% increase in discharge capacity and improved energy dissipation by 4.74% to 8.21%.

For future research, it is recommended to explore further geometric variations and their effects under different hydraulic conditions to refine PKW designs. Additionally, integrating computational fluid dynamics (CFD) simulations with physical models could provide deeper insights into flow behavior and design optimization.

The findings of this study have practical implications for designing and implementing PKWs in real-world scenarios. By adopting these optimized geometries, engineers can achieve more efficient flood management while minimizing construction costs, thereby ensuring safer and more cost-effective dam infrastructure.

REFERENCES

- [1] B. KUMAR, E. HASSAN, AND M. PANDEY, "Chapter 9 A Review on Parametric Studies of Piano," in *River Dynamics and Flood Hazards*, Springer Singapore, 2023, pp. 165–174.
- [2] F. LEMPÉRIÈRE AND A. OUAMANE, "The piano keys weir: a new cost-effective solution for spillways," *Int J Hydropower Dams*, pp. 10:144-149, 2003.
- [3] A. ABHASH AND K. K. PANDEY, "A review of Piano Key Weir as a superior alternative for dam rehabilitation," *ISH J. Hydraul. Eng.*, vol. 28, no. S1, pp. 541–551, 2022, doi:10.1080/09715010.2020.1767516.

- [4] L. BESSER AND M. OERTEL, "Tailwater Influence on Downstream Flow Conditions of Piano Key Weirs," *10th Int. Symp. Hydraul. Struct. Zurich, Switz. 17-19 June 2024*, 2024, doi:10.3929/ethz-b-000675978.
- [5] M. KUMAR, P. SIHAG, N. K. TIWARI, AND S. RANJAN, "Experimental study and modelling discharge coefficient of trapezoidal and rectangular piano key weirs," *Appl. Water Sci.*, vol. 10, no. 1, pp. 1–9, 2020, doi:10.1007/s13201-019-1104-8.
- [6] R. K. MISHRA AND Z. AHMAD, "Discharge Capacity of a Piano Key Weir with Curvilinear Keys," *8th Int. Jr. Res. Eng. Work. Hydraul. Struct. (IJREWHS 2021)*, 2021, [Online]. Available: <https://doi.org/10.26077/1e5d-bd83>
- [7] E. KHANAHMADI, A. A. DEGHANI, S. N. ALENABI, N. DEGHANI, AND E. BARRY, "Hydraulic of curved type-B piano key weirs characteristics under free flow conditions," *Model. Earth Syst. Environ.*, vol. 10, no. 1, pp. 313–330, 2024, doi:10.1007/s40808-023-01790-7.

COMMISSION INTERNATIONALE DES
GRANDS BARRAGES

VINGT-HUITIEME CONGRES DES
GRANDS BARRAGES
CHENGDU, MAI 2025

**REGIONALISATION OF FLOOD ENVELOPE CURVES TO DERIVE
PRELIMINARY ESTIMATES OF PROBABLE MAXIMUM FLOODS (*)**

Peter HILL
Principal Hydrologist, HARC

Ashiq RASHEED & Yue (Albert) SHEN
Senior Hydrologist, HARC

Phillip JORDAN & Michel RAYMOND
Principal Hydrologist, HARC

AUSTRALIA

SUMMARY

Several researchers have analysed databases of maximum floods recorded around the world to develop envelopes of recorded maximum floods. The application of these curves is generally constrained to low-latitude areas with greater moisture availability and is less applicable to other regions of the world.

This paper presents analyses of the maximum recorded floods, with consideration for the location of catchments and the atmospheric moisture availability associated with those locations. The maximum precipitable water from the ERA5 reanalysis data was used to explain the variation in maximum recorded floods across the world.

**Régionalisation des courbes-enveloppes de crues en vue de déduire des estimations préliminaires de crues maximales probables*

An empirical equation was developed to derive a preliminary estimate of Probable Maximum Flood (PMF) for any location and catchment, considering the variability in moisture availability across different parts of the world. The regional maximum flood envelope curves generated based on the equation in this study were compared with those from the previous studies documented in the literature. The initial benchmarking of the results demonstrates that the envelope curves are comparable to those from detailed regional studies.

The regional flood envelope curves can be used for conducting feasibility studies in data-sparse areas and for validating rainfall-based PMF estimates.

RÉSUMÉ

Plusieurs chercheurs ont analysé des bases de données de crues maximales enregistrées à travers le monde en vue de calculer des courbes-enveloppes de crues maximales enregistrées. L'application de ces courbes se limite généralement aux régions de basse latitude qui ont une plus grande disponibilité en humidité ; elle est moins utilisée dans les autres régions du monde.

Cet article présente des analyses de crues maximales enregistrées qui tiennent compte de la localisation des bassins versants et de la disponibilité en humidité atmosphérique qui leur est associée. Les maxima d'eau précipitable issus des données de réanalyse de la base ERA5 sont utilisés pour expliquer la variation entre les crues maximales enregistrées à travers le monde.

Une équation empirique est développée afin de déduire une estimation préliminaire de la crue maximale probable (CMP) pour toute localisation et tout bassin versant donnés, compte tenu de la variabilité de la disponibilité en humidité dans différentes régions du monde. Les courbes-enveloppes des crues maximales régionales générées à partir de l'équation dans cette étude sont comparées à celles d'études antérieures documentées dans la littérature. L'évaluation initiale des résultats montre que les courbes-enveloppes sont comparables à celles des études régionales détaillées.

Les courbes-enveloppes des crues régionales pourront servir à réaliser des études de faisabilité dans des zones à faible densité de données et à valider les estimations de CMP fondées sur les précipitations.

1. INTRODUCTION

The Probable Maximum Flood (PMF) is defined as the limiting value of flood that could reasonably be expected to occur. The PMF may be applicable for dams where it may not be possible to estimate a flood with an exceedance probability low enough to satisfy risk criteria, during the feasibility stage for a new dam with extreme consequences, and for assessing the cost-effectiveness of incremental risk reduction. The PMF was a common requirement for traditional standard-based flood capacity criteria for extreme consequence dams, and remains a common standard for extreme consequence dams in countries that have not adopted risk-informed approaches for dam safety standards.

Different approaches to extreme flood estimation include statistical analysis of flood data and transformation of rainfall using transfer functions or simulation models [1]. Envelope curves derived from statistical analysis of recorded maximum floods are a useful adjunct to the rainfall-based approaches for approximate estimates of the PMF.

The International Hydrological Programme of UNESCO compiled and published the World Catalogue of Large Floods in 1976 [2]. This was followed by the publication of the World Catalogue of Observed Floods in 1984 in partnership with the International Association of Hydrological Science (IAHS) [3] which documented 1400 world maximum floods from 95 countries.

Later, the catalogue was updated by UNESCO, IAHS and the WMO in 1999 with some revised values which provided a more reliable catalogue of world maximum observed floods [4].

Several researchers, notably Herschy [4] and the WMO [5], developed maximum flood envelope curves based on the global catalogue of world maximum observed floods. However, the largest floods used in these studies were predominantly recorded in tropical regions, which limits their relevance to other hydro-climatic regions.

Some studies produced maximum flood envelope curves for specific countries or regions based on the regional observed maximum floods. However, the outcomes from these studies are not directly transferable to any other part of the world, especially where there are no (or reliable) records of observed maximum floods available.

This paper presents a general approach to estimating regional maximum flood envelope curves that is applicable to any part of the world.

2. LITERATURE ON WORLD FLOOD ENVELOPE CURVES

Francou & Rodier [6] produced their seminal paper in 1967 which derived a coefficient, k that could be used to compare the magnitude (severity) of observed floods resulting from different catchment sizes. This conceptualisation has been used by numerous studies to estimate the maximum flood envelope. The Francou & Rodier coefficient k is expressed as shown in Eq 1.

$$k = 10 \left(1 - \frac{\log Q - 6}{\log A - 8} \right) \quad (1)$$

where k is the Francou & Rodier coefficient, Q is the largest flood in m^3/s and A is the catchment area in km^2 .

Rodier and Roche [3] initially used Francou & Rodier k to identify the more severe floods in their review of world maximum floods compiled by the UNESCO Division of Water Science in 1984. They identified 41 highest floods with k greater than 5.75 (for catchment area $> 100 \text{ km}^2$) and produced an envelope curve using linear regression (on a log scale) as shown in Eq 2. The regression line approximately coincided with Francou & Rodier coefficient, k of 6.

$$Q = 500A^{0.43} \quad \text{for } A > 100 \text{ km}^2 \quad (2)$$

The World Maximum Flood Catalogue was later updated in 1999 and 2003 with additional and revised data from 48 countries around the world (120 countries in total) through continuing cooperation between IAHS, UNESCO and WMO. A relationship was added for catchments smaller than 100 km^2 , as shown in Eq 3 [7]. Herschy [4] updated the catchment size threshold for these curves to 90 km^2 from 100 km^2 and derived the following equations for envelope curves.

$$\begin{aligned} Q &= 500A^{0.43} & \text{for } A > 100 \text{ km}^2 \\ Q &= 100A^{0.8} & \text{for } A \leq 100 \text{ km}^2 \end{aligned} \quad (3)$$

During the same period, ICOLD [8] updated the IHAS [3] world maximum observed flood catalogue with additional data. These additional observed maximum floods were also included in [4], although some differences were noted.

Based on a study conducted by Wang et al. [9], WMO presented a new set of flood envelope curves as given in Eq 4, using 51 world maximum floods sourced from different regions [5].

$$\begin{aligned} Q &= 1830A^{0.316} & \text{for } A > 300 \text{ km}^2 \\ Q &= 154A^{0.738} & \text{for } A \leq 300 \text{ km}^2 \end{aligned} \quad (4)$$

The application of the world envelope curves is generally constrained to low-latitude areas with higher moisture availability and therefore has limited applicability to other regions of the world. Hence, many studies have derived regional-specific maximum flood envelope curves, such as for Africa [10], Australia [11], China [12], Europe [7], [13], Greece [14], Malaysia [15], United Kingdom [16], United States [17], [18].

Despite the abundance of regional studies, a significant knowledge gap remains regarding the estimation of maximum flood envelopes in data-sparse regions and regions, in higher latitudes away from the tropics where moisture availability is less. Furthermore, insights into how the maximum flood estimates vary within a geographic region are limited as these curves do not account for flood-producing factors.

3. REGIONAL VARIATION IN MAXIMUM FLOODS

The generation of extreme floods for a given catchment size is influenced by a complex combination of hydro-meteorological and topographic factors. This study investigated a range of global data sets for their effectiveness in explaining the variability of recorded maximum floods.

3.1. DATABASE OF WORLD MAXIMA

Herschey [4] flood catalogue was used for this analysis as it was the most contemporary and comprehensive available catalogue of flood events. Given its pedigree and widespread use, the Francou & Rodier coefficient k (Eq 1) was used to standardise the recorded maximum floods around the world.

3.2. HYDROCLIMATIC VARIABLES

Probable Maximum Precipitation (PMP) is defined as the greatest depth of precipitation for a given duration meteorologically possible for a design watershed or a given storm area at a particular location at a particular time of year, with no allowance made for long-term climatic trends [5]. NRC [19] noted that one of the key inputs to the estimation PMP estimates is precipitable water. This study therefore explored whether variation in maximum precipitable water was a useful way to distinguish regional differences in world maxima floods.

Meteorological reanalysis uses numerical weather prediction models, forced with historical weather observations, to generate a global dataset that provides gridded outputs in both spatial and temporal dimensions. Several reanalysis datasets and derived products such as MEERA [20], ERA5 [21] and PXR [22] were considered in this study. ERA5 deterministic reanalysis developed by the European Centre for Medium-Range Weather Forecasts (ECMWF), was chosen due to its high spatial resolution (0.25° or ~ 31 km), high temporal resolution (1 hour) and open usage license. ERA5 has demonstrated good performance in representing rainfall depths [23] and applied in frequency distribution analysis of extreme rainfalls [22]. Extreme rainfall events and floods are correlated with the largest values of precipitable water in the atmosphere. Therefore, ERA5 is valuable for analysing atmospheric precipitable water, which plays a crucial role in driving extreme rainfalls, and hence floods.

Accordingly, hourly-gridded ($0.25^\circ \times 0.25^\circ$) precipitable water (also referred to as total column water vapour) was collected from the ERA5 reanalysis products for the period between 1950 and 2022. The daily mean values were calculated from the hourly data. For each grid cell, the maximum value from the time series was derived and presented in Fig. 1.

3.3. RELATIONSHIP BETWEEN FLOOD AND MAXIMUM PRECIPITABLE WATER

For each event in the Herschy [4] flood catalogue, the maximum precipitable water from 1950-2022 was estimated using ERA5 reanalysis data. The locations of the flood events were taken from the flood catalogue, and therefore the location reflects the location of the flood rather than the respective upstream catchment.

Fig 2 shows the Francou & Rodier k for each event plotted against the maximum recorded precipitable water at each location. As expected, it is evident that the largest k values are associated with higher values of precipitable water.

Previous studies have employed various methods to fit envelope curves to the maximum observed flood, ranging from linear regression analysis based on a selected small sample of the largest events to using an arbitrary curve that encompasses all available data points. In this study, a hybrid approach was adopted, incorporating both linear regression and subjective adjustments to the regression line to ensure conservative estimates.

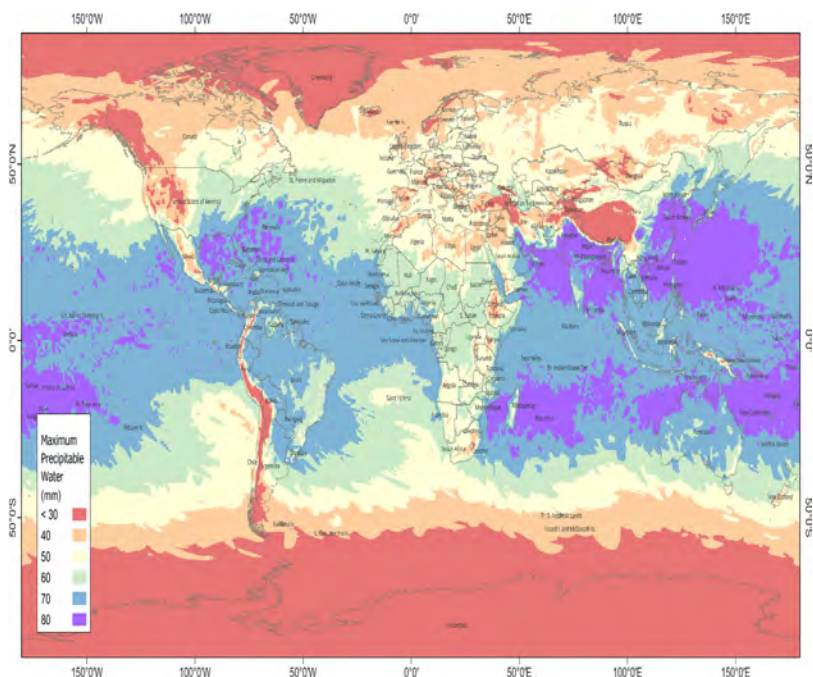


Fig. 1

Maximum daily precipitable water between 1950 and 2022 from ERA5 reanalysis data.

Maximums quotidiens d'eau précipitable entre 1950 et 2022 issus des données de réanalyse de la base ERA5.

Accordingly, a linear regression was initially fitted to the 60 largest floods (identified by the largest k values, shown as solid black dots in Fig 2). To provide more conservatism, the fitted regression line was moved upwards (with the same slope of the fitted regression line) so that only 10 maximum observed floods would exceed the enveloped curve as shown in Fig 2.

The majority of events in the Herschy [4] flood catalogue are associated with precipitable water values less than 30 kg/m^2 . It is unclear whether these regions of low precipitable water are under-represented in the catalogue or whether these regions are simply associated with much low flood peaks. Given this uncertainty, a conservative approach was adopted by extending the same relationship for values less than 30 (as indicated by the dotted line in Fig 2).

The developed relationship between the Francou & Rodier k and the maximum precipitable water was:

$$k = 0.0166 PW + 5.00 \quad (5)$$

where k is the Francou & Rodier coefficient and PW is the maximum precipitable water (in kg/m^2)

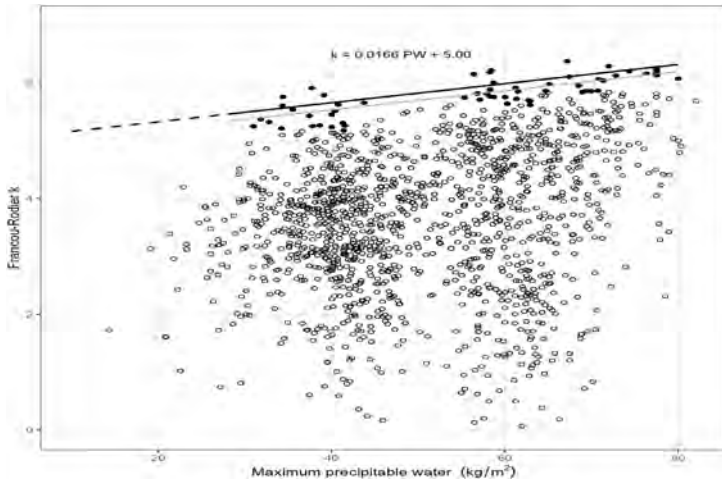


Fig. 2

Relationship between maximum precipitable water and Francou & Rodier k
Relation entre maximum d'eau précipitable et coefficient k de Francou-Rodier

4. MAXIMUM FLOOD ENVELOPES

The Francou & Rodier equation was modified to prepare a new set of maximum flood envelope curves based on the maximum precipitable water as shown in Eq 6 and Fig. 3.

$$Q = 10^6 \left\{ \frac{A}{10^8} \right\}^{1-0.1(0.0166 PW+5.00)} \quad (6)$$

where PW is the maximum precipitable water of the region, Q is the largest flood in m^3/s and A is the catchment area in km^2 .

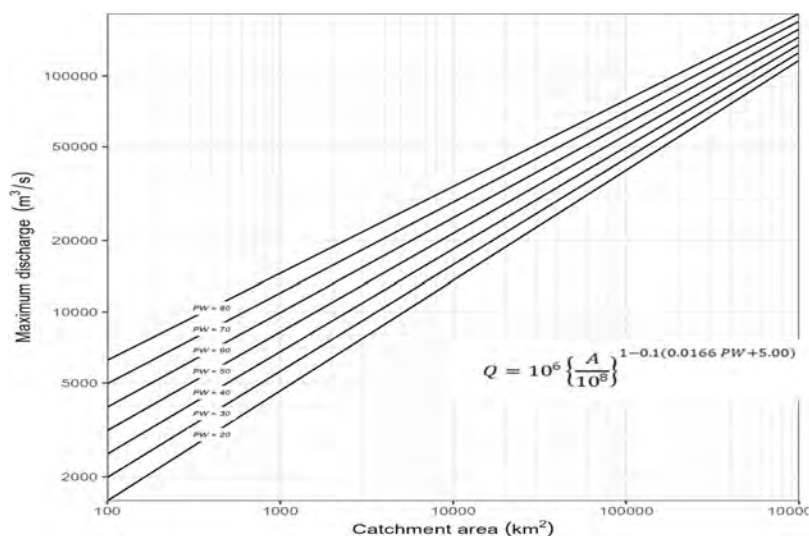


Fig. 3

Maximum flood envelope curves for different maximum precipitable water
Courbes-enveloppes des crues maximales pour différents maximums d'eau précipitable

The regional envelope curves can be generated from Eq 6 using the regional maximum precipitable water. Fig. 4 shows the observed maximum floods grouped based on the maximum precipitable water of the location of the observation against the flood envelope curves derived from Eq 6.

5. COMPARISON WITH REGIONAL STUDIES

The results from this study were compared to four previous regional studies in the USA [17], China [12], Europe and the UK [4] and Southern Africa [10], as presented in Fig 5.

The results for West Coast USA and China show a very close agreement with the regional studies. For Europe, the estimated envelope curve sits above Herschy [4] but is remarkably consistent with the three most severe recorded events. For Southern Africa, the envelope curve is positioned above that derived by Kovacs [10], potentially influenced by the selection of the representative maximum precipitable water for the region.

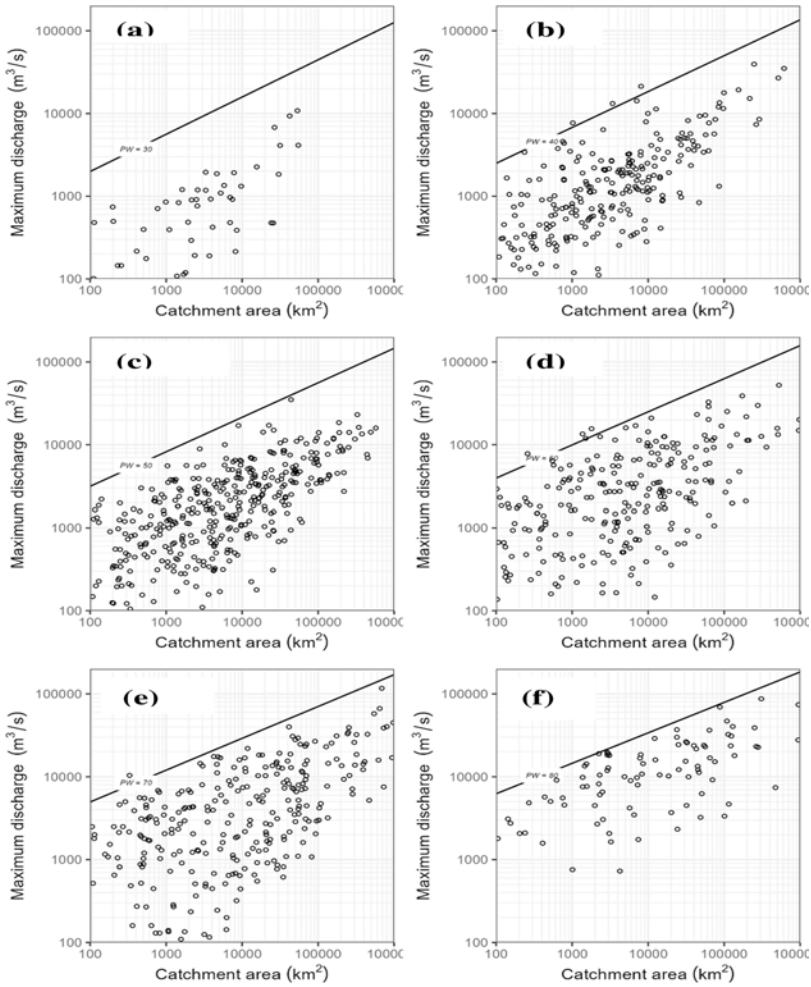


Fig. 4

Observed maximum floods grouped based on the maximum precipitable water of the location: (a) $PW < 30 \text{ kg/m}^2$, (b) $30 < PW \leq 40 \text{ kg/m}^2$, (c) $40 < PW \leq 50 \text{ kg/m}^2$, (d) $50 < PW \leq 60 \text{ kg/m}^2$, (e) $60 < PW \leq 70 \text{ kg/m}^2$ and (f) $70 < PW \leq 80 \text{ kg/m}^2$

Crues maximales observées regroupées en fonction du maximum d'eau précipitable du lieu [PW, precipitable water en kg/m^2]: (a) $PW < 30$, (b) $30 < PW \leq 40$, (c) $40 < PW \leq 50$, (d) $50 < PW \leq 60$, (e) $60 < PW \leq 70$ et (f) $70 < PW \leq 80$.

This initial benchmarking of the results demonstrates that the envelope curves are comparable to those from detailed regional studies.

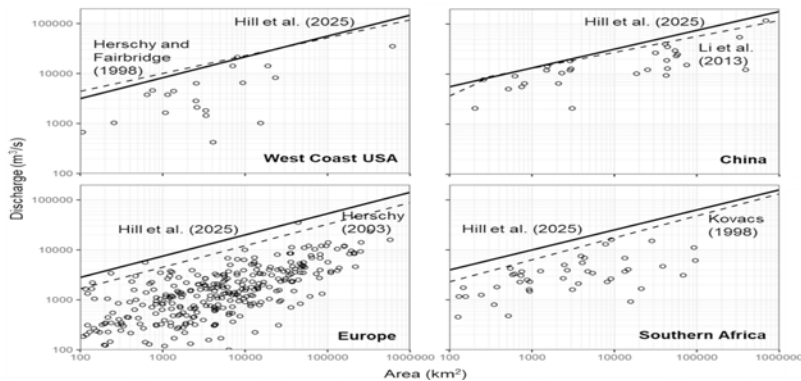


Fig. 5

Comparison of estimated flood envelope curve based upon maximum precipitable water with four regional studies. The floods from the Herschy database that were recorded in the respective regions are shown as open circles. The dotted line represents the flood envelope from the respective regional studies. The solid line shows the flood envelope from this study derived from the maximum precipitable water of the respective regions

6. APPLICATION OF APPROACH

The maximum flood can be estimated based on the catchment area and the maximum precipitable water at the location of interest. The maximum precipitable water can be estimated from Fig. 1 or from the detailed maps and grids available for download at www.harc.com.au

The preliminary estimate of the maximum flood can be derived using Eq 6 (as illustrated in Fig. 3). These estimates are valuable for feasibility studies in data-poor areas and for validating rainfall-based PMF estimates.

It should be noted that these estimates have been derived from recorded floods and do not account for future climate change. Adjustments for climate change are outside the scope of this paper. However, Wasko et al. [24] provided a comprehensive review of the climate change impacts on flood estimates.

7. LIMITATIONS AND RECOMMENDATIONS

This study has demonstrated the effectiveness of maximum precipitable water to explain some of the variability in recorded world maximum flood across different parts of the world. It is desirable to continue to enhance the data and the approach adopted in this study in the future. The key considerations include:

- (i) Other explanatory variables - Among the hydrometeorological parameters tested, precipitable water from ERA5 showed the most promise. However, other climate variables and parameters warrant further investigation.
- (ii) Representative estimates of precipitable water - For this initial analysis, the estimate of the maximum precipitable water was extracted at the reported location of the flood. For larger catchments, it would be more appropriate to define the catchment boundary and extract a representative estimate of precipitable water such as the average over the catchment or the value at the centroid of the catchment.
- (iii) Atmospheric Rivers - The estimate of maximum precipitable water was based on the location of the flood. However, in some mid-latitude, coastal regions of the world, atmospheric rivers can channel concentrated moisture, leading to extreme rainfall events. This phenomenon is notable along western North America and observed in some other regions of Australia and Western Europe. Atmospheric rivers are typically identified and characterised by integrated vapour transport (IVT) and this may be a useful predictor variable that could be explored. Further work is required to assess the suitability of this approach for regions affected by atmospheric rivers.
- (iv) Additional flood data - The existing maximum flood catalogues mainly focus on the largest global floods, but there is limited information about the largest observed floods in areas of lower precipitable water. Therefore, it would be desirable to collect more information on floods recorded in such regions.
- (v) Investigate precipitable water for specific events - This study has used maximum precipitable water to explain the spatial variability in recorded maximum floods. Given that the dates of the notable floods have been recorded, it would be possible to investigate the precipitable water for each event using the ERA5 data. This would help improve the relationship between precipitable water and flood magnitude.
- (vi) Climate Change - This study has assumed that the recorded maximum floods are stationary and the full catalogue of records can be analysed together without considering any adjustment for climate change. It would be desirable to analyse the data to investigate whether there is any evidence of recorded maximum floods increasing over time due to climate change.
- (vii) Comparison with local studies - As part of this study, comparisons were made with estimates available for specific countries or regions. This initial benchmarking indicated that the results are generally comparable. However, it would be beneficial to conduct further comparisons of the literature.

8. CONCLUSIONS

An equation has been developed to derive preliminary estimates of Probable Maximum Flood (PMF) for any location and catchment area globally. The advantage of this approach, compared to global general equations, is that it avoids bias in the flood estimates for areas outside the tropics. These estimates can be valuable for feasibility studies in data-sparse areas and for validating rainfall-based PMF estimates.

The initial benchmarking of the results demonstrates that the resulting envelope curves are comparable to those from detailed regional studies which provides confidence in the approach. However, the proposed envelope curves are not intended to replace the local/regional envelope curves, but to provide estimates where there is limited or no observed maximum flood information available and/or no detailed studies have been undertaken.

It should be noted that these estimates have been derived from recorded floods and do not account for future climate change.

A range of recommendations for future work has been identified to enhance the catalogue of recorded flood maxima and the approach.

REFERENCES

- [1] ICOLD, *Flood evaluation and dam safety*, Bulletin 170, 2018.
- [2] UNESCO, *Repertoire Mondial des très fortes crues. Etudes et rapports 'hydrologie* (Report of the world's very large floods), Paris: Les Presses de 1 'UNESCO, 1976.
- [3] J. RODIER AND J. ROCHE, *World Catalogue of Maximum Observed Floods*, IAHS Publ. no. 143, 1984.
- [4] HERSCHY, *World catalogue of maximum observed floods*, Wallingford: IAHS Press, IAHS, Publ. 284, 2003.
- [5] WMO, *Manual on estimation of probable maximum precipitation (PMP)*, Geneva: WMO no. 1045: World Meteorological Organization, 2009.
- [6] F. J AND J. RODIER, *Essai de classification des crues maximales observées dans le monde*, ORSTOM Bondy, France: série Hydrologie I V (3), 19—46, 1967.

- [7] HERSHEY, *The world's maximum observed floods, The Extremes of the Extremes: Extrorcdiary Floods*, Reykjavik, Iceland: IA1IS Publ. no. 271. 2001, p335–360, 2001.
- [8] ICOLD, *Dams and Floods – Guidelines and cases histories, Bulletin 125*. 2003, 2003.
- [9] G. WANG, J. WANG AND B. LI, *Known maximum flood in the world and its envelope curve formula*. Yellow River, Yellow River, 2006, 28(2): 1–5, 2006.
- [10] P. KOVACS, *Regional maximum flood peaks in Southern Africa. Technical Report TR 137*, South Africa: Pretoria: Department of Water Affairs, 1988.
- [11] H. RHODES AND T. MALLEN, *Proposed Technique to Validate and Constrain Extreme Flood Estimates*, ANCOLD conference preceding 2018, p214–228, 2018.
- [12] C. W. G. LI AND L. R, *Maximum observed floods in China*, Hydrological Sciences Journal, 58:3, 728–735, DOI:10.1080/02626667.2013.772299, 2013.
- [13] ICOLD, *Report on Dams and Floods in Europe. Role of Dams in Flood Mitigation, European working group on Dams and Floods*, 2010.
- [14] Mimikou, *Envelope curves for extreme flood events in northwestern and western Greece, Amsterdam, The Netherlands: Journal of Hydrology*, 67 (1984) 55–66 Elsevier Science Publishers B.V., 1983.
- [15] J. ABDULLA, S. M. NUR, A. M. SITI AND Y. J. PIERRE, *Envelope curves for the specific discharge of extreme floods in Malaysia*, Journal of Hydro-environment Research, Volume 25 , Pages 1–11, ISSN 1570-6443, 2019.
- [16] J. HINKS AND A. MURPHY, *Is there a place for regional coefficients in the UK*, Dams and Reservoirs 25(1): 24–27, 2015.
- [17] R. W. HERSHEY AND R. FAIRBRIDGE, *Encyclopedia of Hydrology and Water Resources*, Kluwer, Dordrecht, The Netherlands, 1998.
- [18] J. E. COSTA, *A comparison of the largest rainfall-runoff floods in the United States with those of the Peoples Republic of China and the world*, *J. Hydrol.* 96. 101–111, 1987.
- [19] NRC, *Modernizing Probable Maximum Precipitation Estimation*, Washington, DC: National Academies of Sciences, Engineering, and Medicine. The National Academies Press. <https://doi.org/10.17226/27460>, 2024.
- [20] GMAO, 2015, *Global Modeling and Assimilation Office, version 5.12.4*, Greenbelt, MD, USA: Goddard Space Flight Center Distributed Active Archive

Center (GSFC DAAC), https://gmao.gsfc.nasa.gov/reanalysis/MERRA-2/citing_MERRA-2/.

- [21] H. HERSBACH, B. BELL, P. BERRISFORD, S. HIRAHARA, A. HORÁNYI, J. MUÑOZ-SABATER, J. NICOLAS, C. PEUBEY, R. RADU AND D. SCHEPERS, *The ERA5 global reanalysis*, *Quarterly Journal of the Royal Meteorological Society*, 146(730), 1999–2049, 2020.
- [22] L. G. COURTY, R. L. WILBY, J. K. HILLIER AND L. J. SLATER, *Intensity-duration-frequency curves at the global scale*, *Environmental Research Letters*, 14(8), 084045, 2019.
- [23] H. E. BECK, M. PAN, T. ROY, G. P. WEEDON, F. PAPPENBERGER, A. I. J. M. VAN DIJK, G. J. HUFFMAN, R. F. ADLER AND E. F. WOOD, *Daily evaluation of 26 precipitation datasets using Stage-IV gauge-radar data for the CONUS*, *Hydrology and Earth System Sciences*, 23(1), 207–224., 2019.
- [24] C. WASKO, S. WESTRA, R. NATHAN, A. PEPLER, T. RAUPACH, A. DOWDY, F. JOHNSON, M. HO, M. K. D. JAKOB, J. EVANS, G. VILLARINI AND H. FOWLER, *A systematic review of climate change science relevant to Australian design flood estimation*, *Hydrol. Earth Syst. Sci. Discuss. Preprint* hess-2023–232, 2023.

COMMISSION INTERNATIONALE DES
GRANDS BARRAGES

VINGT-HUITIEME CONGRES DES
GRANDS BARRAGES
CHENGDU, MAI 2025

CASE STUDY AND ANALYSIS OF SURGE WAVE AND EXCESSIVE FLOOD IN HYDROPOWER DAMS (*)

Chihaya ONDA
*Dr Eng., Dam Upgrading Office, CIVIL & Architectural Engineering Dept.
ELECTRIC POWER DEVELOPMENT COMPANY*

Kouki MORIMOTO
*West Regional Headquarters, Hydropower Dept.
ELECTRIC POWER DEVELOPMENT COMPANY*

Tetsuya SUMI
*Professor, Disaster Prevention Research Institute
KYOTO UNIVERSITY*

JAPAN

SUMMARY

This paper investigates the impact of extreme hydrological events on hydro-power dams, examining the surge wave phenomena, excessive sedimentation, and flood flows exceeding design capacities. The occurrence of these events has become more frequent due to climate change, necessitating revised and innovative approaches to dam safety and management.

The study outlines the evolution of design flood flow standards in Japan, highlighting that many existing dams, constructed based on past standards, may not be equipped to handle current and future hydrological challenges. It presents

**Étude de cas et analyse de l'onde de choc et de l'inondation excessive concernant les barrages hydroélectriques*

detailed case studies of three dams: Hiranabe, Horoka, and Setoishi, each experiencing unique issues such as debris flow-induced surge waves, sedimentation from heavy rainfall, and flood flows significantly beyond their design capacity.

For Hiranabe Dam, a landslide triggered by a typhoon caused a surge wave, resulting in overflow. Numerical analysis was used to investigate the debris flow and surge wave behavior, leading to the implementation of measures to improve the watertightness of flood spillway gate control devices.

Horoka Dam faced sedimentation challenges from heavy rainfall, leading to the cessation of power generation. A sediment bypass tunnel was selected as a permanent countermeasure, expected to increase the dam's discharge capacity, and manage sediment more effectively.

Setoishi Dam experienced a flood flow 1.7 times its design capacity, highlighting the need for improved flood spillway gate control systems, downstream warning devices, and sediment management strategies to ensure continuous operation and safety.

The paper emphasizes the importance of considering both flow and sedimentation measures in dam management to address the increasing risks posed by climate change. It suggests that understanding the specific characteristics and vulnerabilities of each dam is crucial in developing targeted safety measures. Moreover, it advocates for the use of numerical analysis to predict future challenges and select appropriate sedimentation measures, contributing to the sustainable management of dams.

In conclusion, the study underscores the need for integrated and forward-thinking strategies in hydropower dam management, incorporating both structural and operational measures to enhance resilience against extreme hydrological phenomena.

RÉSUMÉ

Cette recherche examine l'impact des événements hydrologiques extrêmes sur les barrages hydroélectriques, en se concentrant sur les phénomènes de vagues de choc, la sédimentation excessive et les flux d'inondation dépassant les capacités de conception. L'augmentation de la fréquence de ces événements, due au changement climatique, nécessite une révision et des approches innovantes pour la sécurité et la gestion des barrages.

L'étude détaille l'évolution des normes de flux d'inondation de conception au Japon, soulignant que de nombreux barrages existants, construits selon les normes

passées, pourraient ne pas être équipés pour faire face aux défis hydrologiques actuels et futurs. Elle présente des études de cas détaillées de trois barrages : Hiranabe, Horoka et Setoishi, chacun confronté à des problèmes uniques tels qu'une vague de débris induite par un glissement de terrain, une sédimentation due à de fortes pluies et des flux d'inondation dépassant largement leur capacité de conception.

Pour le barrage de Hiranabe, un glissement de terrain déclenché par un typhon a causé une vague entraînant un débordement. Une analyse numérique a été utilisée pour étudier le comportement des coulées de débris et des vagues de choc, conduisant à la mise en œuvre de mesures pour améliorer l'étanchéité des dispositifs de contrôle des vannes de décharge.

Le barrage de Horoka a été confronté à des défis de sédimentation dus à de fortes pluies, entraînant l'arrêt de la production d'énergie. Un tunnel de déviation des sédiments a été choisi comme contre-mesure permanente, avec l'espoir d'augmenter la capacité de décharge du barrage et de gérer plus efficacement les sédiments.

Le barrage de Setoishi a subi un débit de crue d'inondation 1,7 fois supérieur à sa capacité de conception, soulignant la nécessité d'améliorer les systèmes de contrôle des vannes de déversement, les dispositifs d'alerte en aval et les stratégies de gestion des sédiments pour assurer une opération continue et la sécurité.

Le document souligne l'importance de prendre en compte à la fois les mesures de flux et de sédimentation dans la gestion des barrages pour faire face aux risques croissants posés par le changement climatique. Il suggère que comprendre les caractéristiques spécifiques et les vulnérabilités de chaque barrage est crucial pour développer des mesures de sécurité ciblées. De plus, il prône l'utilisation d'analyses numériques pour prévoir les défis futurs et sélectionner les mesures de sédimentation appropriées, contribuant à la gestion durable des barrages.

En conclusion, l'étude met en évidence la nécessité de stratégies intégrées et prospectives dans la gestion des barrages hydroélectriques, incorporant à la fois des mesures structurelles et opérationnelles pour renforcer la résilience face aux phénomènes hydrologiques extrêmes.

1. INTRODUCTION

In recent years, there has been an increase in extreme flood events, and it is predicted that the frequency of such events will continue to rise due to global warming. The Ministry of Land, Infrastructure, Transport and Tourism (MLIT) is currently revising its plans to accommodate for the increase in river flow resulting

from the increased rainfall brought about by climate change, under a scenario that assumes a 2-degree Celsius rise in temperature [1].

The role of dams, as outlined in the Dam Upgrading Vision [2], has evolved to not only ensure safety, but also to be used wisely and sustainably. Among these, measures to improve the safety of dams, such as enhancing their discharge capacity to increase safety during floods, are being implemented domestically. Furthermore, there are also instances of efforts towards sustainable dam management, such as permanent sediment controls including sluicing and bypass tunnels.

This paper will analyze cases of dams impacted by phenomena such as a surge wave causing damage to a hydropower dam, extreme rainfall leading to a dam reservoir becoming completely filled with sediment, and a dam experiencing a flow rate 1.7 times its designed flood volume due to extreme rainfall, resulting in the loss of its main power supply. Countermeasures for these incidents will be summarized.

2. ON THE DESIGN FLOOD FLOW OF DAMS AT THE TIME OF DESIGN AND PRESENT

The concept of design flood flow for dams in Japan has evolved as follows [3].

2.1. PAST STANDARDS

In 1957, two types of flood flows were defined: the planned flood flow and the extraordinary flood flow. The planned flood flow for concrete dams was set based on a flow that occurs once in one hundred years, and for rockfill dams, once in two hundred years, and it had to be no less than the maximum historical flood flow. On the other hand, the extraordinary flood flow was considered to be about 20% higher than the planned flood flow and was used to check the safety of dams in emergencies.

2.2. CURRENT CONCEPT

In 1976, the concept of dam design flood flow was introduced. This is the maximum flood event assumed in the design of a dam, regarded as the maximum flood flow that could potentially occur at the dam site. The dam design flood flow is determined by the largest of the following: the flood flow with a 200-year return period, the flood flow determined from the envelope of the maximum specific discharge per region, and the maximum flow at the dam site to date. However, for fill dams, this was further increased by 20%. The dam design flood flow is essentially

the maximum possible flow, akin to an L2 seismic motion or maximum possible earthquake. Although this should apply regardless of dam type, fill dams are considered to have lesser durability against floods, which is why a larger flow is assumed for them compared to concrete dams.

From the above evolution, dams constructed before 1976 may have smaller target flows. However, after experiencing the threat of natural disasters from the Great East Japan Earthquake in 2011, the safety of fill dams for hydropower against extreme rainfall has been evaluated by a working group under the Ministry of Economy, Trade and Industry, which is the primary regulatory authority for electricity [4]. According to their documents, for fill dams dedicated to power generation with a height of 15m or more, an investigation was conducted to estimate the flood flow occurring once in two hundred years and whether an overtopping event of the dam embankment could occur. Out of 42 power-generation-specific fill dams examined, 36 dams had a 200-year probability flow smaller than the design flood flow, 3 dams had a 200-year probability flow larger than their flood handling capacity, and the remaining 3 dams had a 200-year probability flow larger than their flood handling capacity but were confirmed to be able to handle floods through the use of storage capacity, shown in Fig. 1. It was concluded that all dams were within their flood handling capacity, but further examination and organization, including regional impact analysis, are necessary.

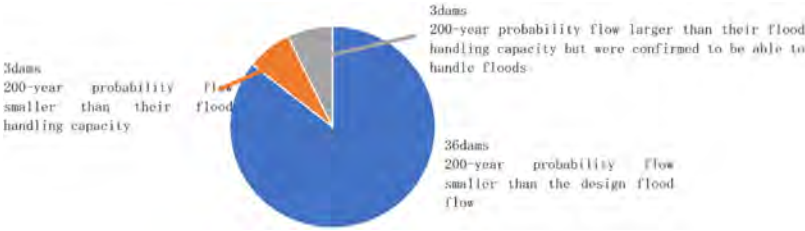


Fig. 1

Survey result of hydropower dams against extreme rainfall
Résultats de l'enquête sur la résistance des barrages hydroélectriques aux précipitations extrêmes

For all 44 dams (both rockfill and concrete) over 15m in height managed by ELECTRIC POWER DEVELOPMENT COMPANY (J-POWER), an investigation into their flood handling capacity showed that over 90% of the dams had a flood handling capacity greater than the 200-year probability flow, and the dams where the 200-year probability flow was greater were all concrete dams. Qualitatively, considering the initial design concept, it can be understood that rockfill dams have higher resistance to flood flows than concrete dams.

3. SPECIFIC CASES OF EXTREME HYDROLOGICAL PHENOMENA AND DISCUSSION

3.1. HIRANABE DAM

The specification of Hiranabe Dam is shown in Table 1 and its location is shown in Fig. 2. In July 2011, accompanied by Typhoon No. 6, the cumulative rainfall exceeded 1,000 mm, leading to a landslide upstream of Hiranabe Dam, which resulted in over 300,000 m³ of debris flow into the reservoir, creating a surge wave [5]. This caused an overflow phenomenon at the dam. The situation was visually confirmed by the dam's gate operator and through ITV cameras; the overflow wave reached about 2m above the dam crest, and the overflow lasted for a dozen seconds (Fig. 4).

Table 1
Specifications of Hiranabe Dam

Catchment Area	233km ²	Dam	Type	Gravity
Design flood	2,500m ³ /s		Height	38.0m
Power plant	Name: Nagayama		Crest length	124.0m
	Max. output: 37MW	Reservoir	Initial capacity	4.24Mm ³
			Sediment volume (2023)	2.39Mm ³



Fig. 2
Location of dams
Localisation des barrages

The landslide occurred on a steep slope with a 30 to 45-degree angle, roughly rugged, spanning about 100m in width, with a vertical difference of about 160m, a horizontal distance of 210m, and a depth of 22m (Fig. 3). The volume of soil produced by the collapse was about 190,000 m³, with an additional 170,000 m³ from riverbank erosion by the debris flow and about 40,000 m³ of sediment deposition within the river, making the total sediment deposition near the confluence (in the reservoir) about 320,000 m³. Since there was no precedent for dam overflow caused by a debris flow, the situation of the landslide and the accompanying debris flow was investigated, and the behavior of the surge wave in the reservoir due to the debris flow was reproduced through numerical analysis.



Fig. 3
Photo of collapsed area
Photo de la zone effondrée



Fig. 4
Left: Image of overflowing dam, right: Photo of Hiranabe Dam
Gauche : Image d'un barrage débordant, droite : Photo du barrage de Hiranabe

The analysis method applied was a two-layer flow analysis considering the debris flow and the stored water as independent fluids, with a terrain model extending 3.5km east-west and 2.5km north-south, mapped on a 10m grid. Assuming a total sediment volume of 360,000 m³ from the collapse and riverbank erosion, the collapse stop time was set at one hundred seconds in the calculation, which could roughly reproduce the overflow height at the dam and the sediment deposition shape within the reservoir. The analysis results, including the velocity distribution of the debris flow and the propagation condition of the surge wave in the reservoir, are shown in Fig. 5, respectively. The results show that the dam overtopped only once, approximately 130 seconds after the start of the slope failure, and that the duration of the overflow was 16 seconds. The flooding of the spillway gate's control equipment caused by the overflow, lasting a dozen seconds at a height of 2m above the dam crest, led to its malfunction. As recovery measures for the malfunctioning spillway gate, shade panels were installed to suppress temperature rise inside the equipment, ventilation ports were sealed, and emphasis was placed on ensuring the watertightness of the equipment.

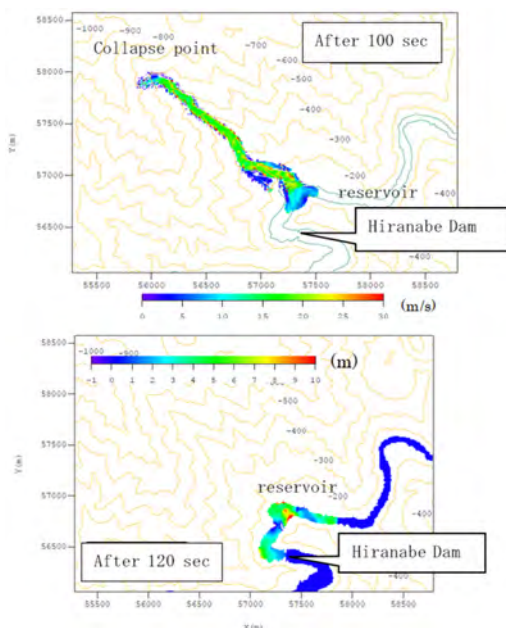


Fig. 5

Upper: Distribution of velocity of debris flow (analysis result) Lower: Propagation Height of surge waves in the dam reservoir (just before overflow) (analysis result)
 En haut : Distribution de la vitesse de la coulée de débris (résultat de l'analyse) En bas : Hauteur de propagation des ondes de choc dans le réservoir du barrage (juste avant le débordement) (résultat de l'analyse)

Regarding the sediment deposition shape in the dam reservoir, although there was a significant amount of sediment influx due to the flood and debris flow, the shape of the deposited sediment approached equilibrium because the spillway gate was kept in free flow after the flood. Comparing the riverbed before and after the overflow, and the most recent riverbed, it is found that the post-overflow and the most recent riverbed shapes are similar, indicating that this surge wave has become a good opportunity to plan for future riverbed shapes (Fig. 6).

Despite the overflow occurrence, there was no abnormality in the dam embankment, and power generation was resumed two months after the recovery of the flood spillway gate control equipment.

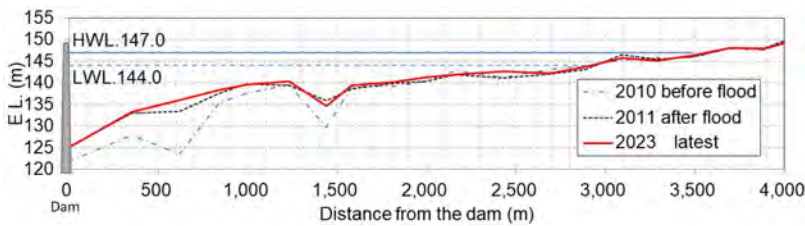


Fig. 6

Change of the mean riverbed level at Hiranabe Dam reservoir
Changement du niveau moyen du lit de la rivière au réservoir du barrage de Hiranabe

3.2. HOROKA DAM

The specification of Horoka Dam is shown in Table 2 and its location is shown in Fig. 2. Since its operation began in 1965, Horoka reservoir has experienced progressive sedimentation, and dredging has been carried out to ensure the storage capacity for power generation.

Table 2
Specifications of Horoka Dam

Catchment Area	69.1km ²	Dam	Type	Rockfill
Design flood	300m ³ /s		Height	32.0m
Power plant	Name: Horoka		Crest length	135.5m
	Max. output: 10MW	Reservoir	Initial capacity	0.49Mm ³
			Sediment volume (2023)	0.40Mm ³

In 2016, the reservoir was filled with sediment due to heavy rainfall caused by three typhoons hitting Hokkaido directly, resulting in the intake being buried and the cessation of power generation. The inflow rate during this heavy rainfall reached $316 \text{ m}^3/\text{s}$, which was 1.9 times the previous maximum inflow rate of $166 \text{ m}^3/\text{s}$ and 1.1 times the dam's design flood flow. Estimating the inflow sediment volume since 1992 using the LQ formula suggests that approximately $300,000 \text{ m}^3$ of sediment entered the reservoir, with an estimated $80,000 \text{ m}^3$ of deposition. The riverbed shape before and after the flood, and the current situation, is as shown in Fig. 7.

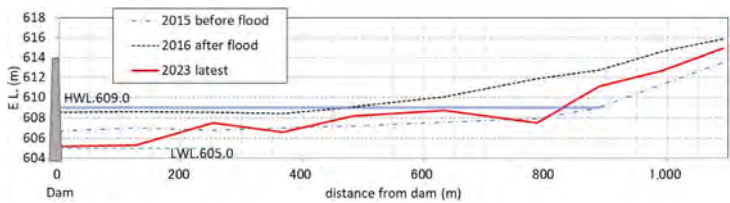


Fig. 7

Change of the mean riverbed level at Horoka Dam reservoir
Variation du niveau moyen du lit de la rivière au réservoir du barrage d'Horoka

Removing the sediment from the reservoir and around the intake took time, requiring 20 months until power generation could be resumed.

As a permanent sediment countermeasure, after comparing dredging, spill-way modification, and other options, it was decided to adopt a sediment bypass tunnel (Fig. 8). The specifications of the bypass tunnel are a length of 272 meters, a tunnel shape with 4.5m channel width and Canopy type, and a flow rate of $120 \text{ m}^3/\text{s}$, with construction started in 2023 (Fig. 9) [6].

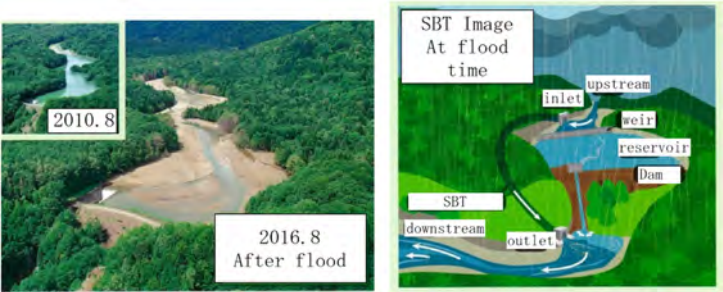


Fig. 8

Left: Photo of Horoka reservoir before and after flooding Right: Image of Sediment Bypass Tunnel (SBT)
Gauche : Photo du réservoir d'Horoka avant et après l'inondation A droite : Image du tunnel de dérivation des sédiments (SBT)

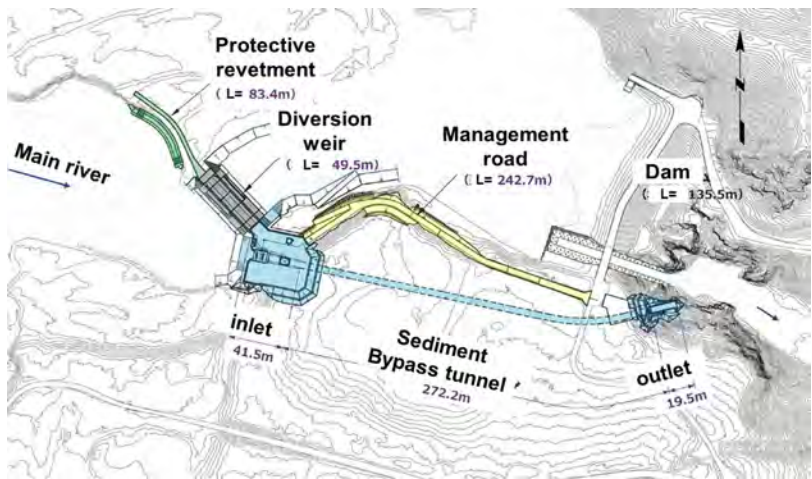


Fig. 9
Plan view of SBT
Vue en plan du SBT

3.3. SETOISHI DAM

The specification of Setoishi Dam is shown in Table 3 and its location is shown in Fig. 2, and a photograph of it under normal conditions is shown in Fig. 10. The Setoishi Dam is in the middle reaches of the main river (approximately 29 km from the mouth) and has been operating as a power generation-exclusive dam since September 1958, with 66 years having passed. For about the last decade, to mitigate flood damage due to sedimentation, power generation has been halted during the winter, the flood spillway gates have been fully opened to lower the reservoir, and sediment removal from the reservoir has been carried out. Additionally, during the flood season, when floods are anticipated, sediment flushing with lowering the reservoir water level has been implemented.

Table 3
Specifications of Setoishi Dam

Catchment Area	1629.3km ²	Dam	Type	Gravity
Design flood	6,000m ³ /s		Height	26.5m
Power plant	Name: Setoishi		Crest length	139.35m
	Max. output: 20MW	Reservoir	Initial capacity	9.93Mm ³
			Sediment volume (2023)	0.38Mm ³



Fig. 10
Photo of Setoishi Dam under normal condition
Photo du barrage de Setoishi en conditions normales

In July 2020, due to the influence of a stationary front and a linear precipitation zone, the dam, designed for a flood flow of 6,000 m³/s, was hit by a flow of about 10,000 m³/s, equivalent to 1.7 times the design flood flow. Compared to the maximum flood in July 1982, the rate of increase in inflow from 2,000 m³/s to the maximum within an hour changed from 600 m³/s to 1,500 m³/s, a 2.5-fold increase [7]. Fig. 11 shows a photograph of the outflow and Fig. 12 shows a graph of rainfall, water level, and flow rate. In Fig. 12, water levels above 51.0 m are estimated values because they are outside the range of water level measurements, and inflows and outflows above 6,000 m³/sec are estimated values because they are outside the range of the flow calculation formula (estimated values are indicated by dashed lines). Additionally, the gate operator stationed at the dam management office on the upper left bank upstream of the dam evacuated to higher ground through land around the dam that was submerged up to knee-level after fully opening the flood gates. The damage affected the dam access bridge, the backup power source for the flood gates, downstream warning systems, intake and discharge ports, and power generation equipment within the power plant, requiring 1 year and 10 months for recovery.



Fig. 11
Photo at the flood peak; Left: from left bank, right: Satellite photo
Photo au pic de la crue ; à gauche : depuis la rive gauche, à droite : Photo satellite

Comparing the riverbed shape before and after the flood and the latest shape, as shown in Fig. 13, the sediment within the reservoir was moving due to the scouring force of the natural river with the flood spillway gates fully opened from the peak of the heavy rain until the resumption of power generation. After the resumption of power generation, the water level at the time of the flood has been treated as the free-flow water level, and measures based on sediment passage have been implemented, resulting in a reduction of sediment within the reservoir. Additionally, its effectiveness has been confirmed through one-dimensional riverbed fluctuation calculations. Fig. 14 shows the image of sluicing.

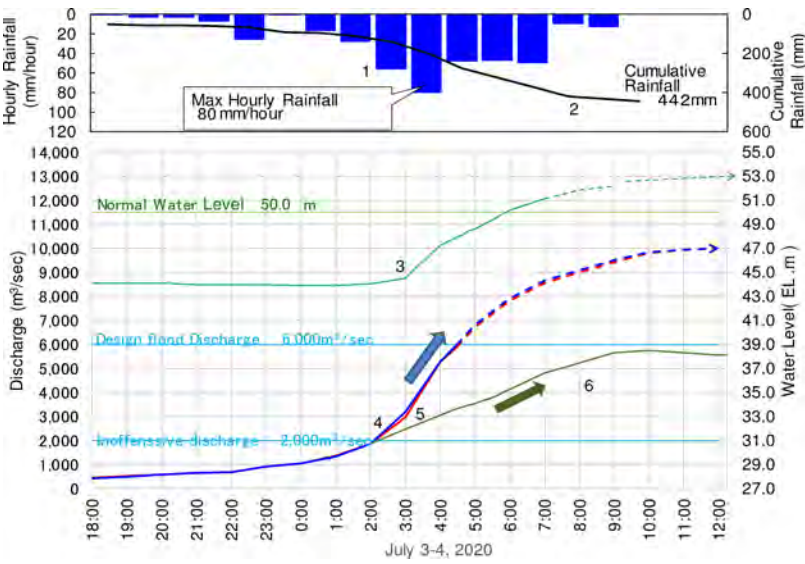


Fig. 12
Hyetograph and hydrograph at runoff
Hyétogramme et hydrogramme à l'écoulement

- | | |
|-------------------------------|-------------------------------|
| 1 Hourly rainfall (bar) | 1 Pluies horaires (barres) |
| 2 Cumulative rainfalls (line) | 2 Pluies cumulées (ligne) |
| 3 Water level | 3 Niveau d'eau |
| 4 Inflow (blue line) | 4 Débit entrant (ligne bleue) |
| 5 Outflow (red line) | 5 Débit sortant (ligne rouge) |
| 6 Previous maximum flow | 6 Débit maximal précédent |

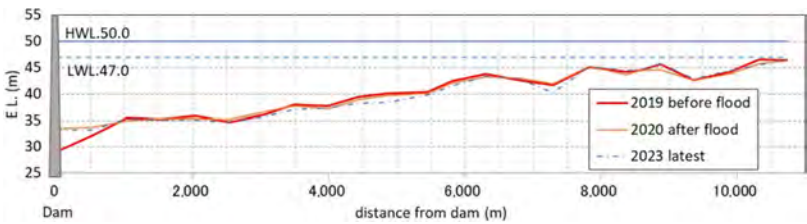


Fig. 13
Change of the mean riverbed level at Setoishi Dam reservoir
Changement du niveau moyen du lit de la rivière au réservoir du barrage de Setoishi

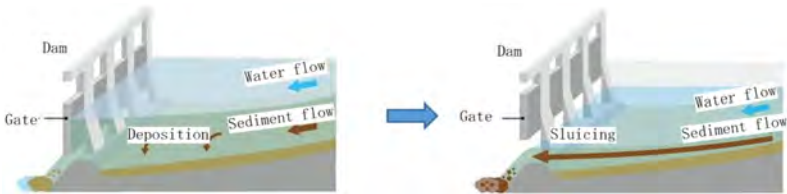


Fig. 14
Image of sluicing at Setoishi Dam
Image de l'éclusage au barrage de Setoishi

4. EVALUATION OF EXTREME HYDROLOGICAL PHENOMENA

4.1. HYDROLOGICAL PHENOMENA

In the case of all three dams, unforeseen hydrological events occurred, forcing the cessation of power generation.

For Hiranabe Dam, since it is difficult for dam managers to implement slope stability measures that would prevent the inflow of sediment, such as debris flow, the strategy was to minimize damage in the event of a surge wave by focusing on ensuring the watertightness of dam control equipment. Additionally, given the nature of surge waves - not causing prolonged submersion but rather waves lasting a dozen seconds - measures were considered with this short duration in mind. For dams with similar topography, it is necessary to consider measures that can minimize the impact of surge waves.

Considering the Horoka Dam became filled with sediment, measures are needed to prevent the intake from being buried even if a large amount of sediment

enters, preventing the dam from becoming fully silted. After comparing based on economic efficiency, a sediment bypass tunnel was chosen as the measure. Furthermore, this sediment bypass tunnel is expected to serve as a secondary measure for future increases in flow by effectively increasing the dam's discharge capacity. While the spillway's discharge capacity is more than twice the design flood flow, and a certain margin is preserved due to it being a fill dam, this also contributes to risk reduction for future increases.

Setoishi Dam not only experienced flows 1.7 times the design flood flow but also saw the rate of flow increase per hour doubling compared to past events. Additionally, the impact of significantly inaccurate weather forecasts highlighted the need for remote operation and an operational system. Considering the possibility of roads to the site being impassable due to flooding was also necessary. This necessitates measures for continuously operable flood spillway gate control equipment, downstream warning devices, flood prevention devices at the power plant entrance to continue power generation, and measures to prevent sediment deposition at the intake and outlet. The dam body itself, being a gravity concrete dam, has been confirmed safe even with flow passing through roads on both banks at 1.7 times the design flood flow.

All three dams experienced flows significantly exceeding their planned target flows. The cause includes the brief period available for planning at the time of construction, necessitating plans under then-current conditions, and the anticipation of a further approximate 1.2 times increase in flow due to future climate change [1], underscoring the importance of further preparedness.

4.2. SEDIMENT COUNTERMEASURES

The occurrence of extreme hydrological events has provided a good opportunity to consider permanent measures for the riverbed shapes of the three dams.

For Hiranabe Dam, as shown in Fig. 6, the riverbed formed after the debris flow approximates the current riverbed. Approximately 8% of the reservoir capacity worth of debris flow descended, and the subsequent operation of fully opening the flood spillway caused significant changes in the riverbed shape. However, no changes in the riverbed shape were observed during subsequent discharges of similar magnitude, suggesting that an equilibrium riverbed may have been formed due to the debris flow.

For Horoka Dam, due to its free overflow spillway design, it is highly possible that this discharge of the design flood scale has formed a riverbed shape starting from high water level at the dam site. With an annual average sediment deposition of about 20,000 m³, such discharges could quickly fill the dam with sediment, indicating the necessity for sedimentation measures anticipating such events.

Setoishi Dam, having received a massive influx of sediment during a discharge 1.7 times the design flood flow, resulted in most of the sediment passing through due to the fully opened flood spillway. By lowering the sluicing water level more than before after the 2020 discharge, the amount of sediment has further decreased.

Regarding sedimentation measures, previous studies have shown that the applicability of methods at a specific dam site can be derived from the reservoir turnover rate (annual average inflow volume / total storage capacity) and the reservoir's life (total storage capacity / annual average sediment inflow). As shown in Fig. 15, the sedimentation measures implemented for the three dams are generally consistent with the methods derived from the figure. For Hiranabe Dam and Setoishi Dam, measures primarily focusing on sediment passage, including during discharges, have been implemented. Additionally, it seems possible to respond without significant facility modifications due to the relationship between the dam and the spillway location. On the other hand, as Horoka Dam is a gateless dam, it does not align with the measures shown in Fig. 15, leading to the selection of a bypass tunnel as the optimal measure after conducting predictive simulations using two-dimensional planar riverbed fluctuation calculations.

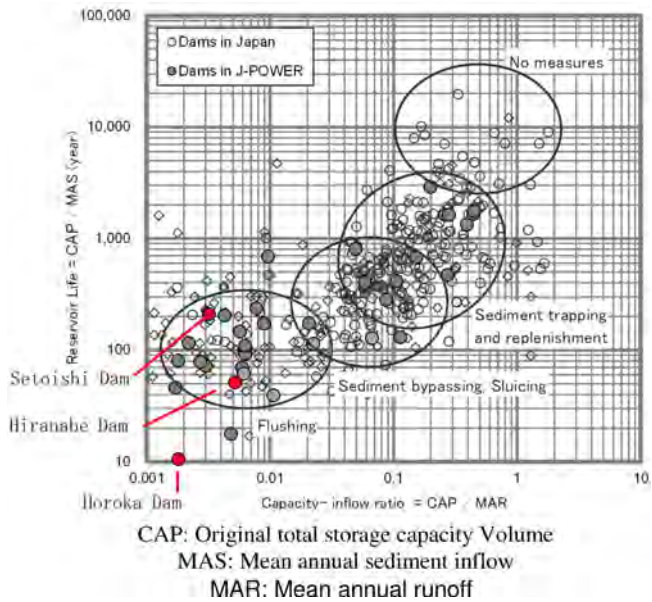


Fig. 15
Representative sediment management options in Japan [8]
Options représentatives de gestion des sédiments au Japon [8]

For all dams, it seems important to understand the impact on the downstream river through monitoring and other means in advancing further sediment passage.

Furthermore, from the perspective of dam managers, in the event of flows exceeding planning, soft measures such as horizontal development of cases, risk communication, and efforts in Disaster Information Gathering (DIG) are considered important. These efforts are being continued.

5. CONCLUSIONS

The conclusions of this study are as follows. In this paper, we discussed power generation dams that have experienced exceedance floods and confirmed that it is necessary to implement not only flow measures but also sedimentation measures simultaneously to manage dams safely and sustainably.

- (1) Due to the effects of climate change, flows exceeding the design flood volume are predicted, making dam safety measures tailored to the characteristics of each dam important.
- (2) For dams where surge waves may occur, measures for structures at the dam crest, such as watertight measures for the flood spillway gate control devices, are necessary.
- (3) For fill dams experiencing exceedance floods, it is essential to ensure sufficient discharge capacity. Sediment bypass tunnels installed as sedimentation measures may also contribute to improving discharge capacity.
- (4) For power generation concrete dams affected by exceedance floods, while there may not be issues with the dam body's safety, measures for flood spillway gate control devices, flood prevention at power plants, and sediment measures for intakes and discharge ports are often necessary.
- (5) Sedimentation measures for dam reservoirs during exceedance floods are crucial, and when selecting measures, narrowing down from Fig. 15, and considering the future sediment management's appropriateness through numerical analysis in advance can be effective. This leads to the realization of sustainable dam management.

REFERENCES

- [1] TECHNICAL REVIEW COMMITTEE ON FLOOD CONTROL PLANNING. CONSIDERING CLIMATE CHANGE. Recommendations on the Approach to Flood Control Planning Considering Climate Change. 2021. (In Japanese)

- [2] MINISTRY OF LAND, INFRASTRUCTURE, TRANSPORT AND TOURISM, RIVER BUREAU. DAM Upgrading Vision. 2017. (In Japanese)
- [3] MATSUMOTO, N. Development of earthfill and rockfill dam engineering in Japan. *Journal of Japan Society of Civil Engineers, Series F*, vol.65(4), 394–413. (In Japanese)
- [4] WORKING GROUP ON MEASURES FOR ELECTRICAL FACILITIES AGAINST NATURAL DISASTERS, ETC. F Interim Report of Advisory Committee for Industrial Structure, Subcommittee on Safety, Electricity Safety Subcommittee. 2014. (In Japanese)
- [5] HATANO, T., NAKAYAMA, Y., SAITO, F. Overflow Phenomena at Hiranabe Dam Due to Debris Flow Influx. *Journal of Electric power civil engineering*, (362), 44–47.2012. (In Japanese)
- [6] HAGIWARA, Y., ARIZONO, H. Design of the Sand Bypass Tunnel Facilities for the Horoka Power Station Horoka Regulation Pond. *Journal of Electric power civil engineering*, (426), 47–51.2012. (In Japanese)
- [7] Electric Power Development Co., Ltd. Current Status of the Setoishi Dam. https://www.jpower.co.jp/bs/renewable_energy/hydro/seto/ (In Japanese)
- [8] ONDA C., OKUMURA H., ASAH T. Analysis of sedimentation counter-measures in hydropower dams considering properties of reservoir sedimentation. *ICOLD, 26th Congress, Vienna, Q100-R30*.

COMMISSION INTERNATIONALE DES
GRANDS BARRAGES

VINGT-HUITIEME CONGRES DES
GRANDS BARRAGES
CHENGDU, MAI 2025

GESTION DES CRUES SUR LES GRANDS BASSINS VERSANTS - PRISE EN COMPTE DE LA COMPLEXITÉ HYDROLOGIQUE ET HYDRAULIQUE (*)

Julien VERMEULEN, Thomas VIARD, Matthieu SECHER &
Damien PUYGRENIER
EDF-CIH

Emmanuel PAQUET
EDF-DTG

FRANCE

SUMMARY

This article describes a set of tools to improve the consideration of hydrological risk both short term (forecasts) and long term (extreme floods) for a safe and optimized management of a valley with one or more dams.

For the knowledge of extreme floods, it is necessary to correctly determine the floods knowing the hydrology and hydraulics of a watershed.

- The **SHADEX** probabilistic method is based on a semi-continuous rain-flow simulation process, based on the estimation of precipitation probabilities and the MORDOR hydrological model developed at EDF. The simulation process calculates a wide range of simulated rainfall events on each hydrological situation, generating a comprehensive set of crossings between precipitation and soil saturation risks. The **SHADEX-SD** method makes it possible to divide the large catchments into several more homogeneous sub-catchments, while ensuring the meteorological homogeneity of the scenarios over the entire zone.

**Flood management in large watersheds – consideration of hydrological and hydraulic complexity*

- The **SHYDONHY** method is then used to construct synthetic hydrographs for each simulated event, based on donor hydrographs selected based on spatial proximity, size and runoff production criteria.
- **Melyor** and **AutoMaT**: Most of the current methods for determining extreme hydrological risk have limits for the representativeness of the risk on the large French watersheds. Indeed, they do not take into account the hydroclimatic heterogeneity of different tributaries and the presence of hydraulic influences (presence of large dams or containment systems). The AutoMaT and Melyor tools presented in this article use the simulation of a large number of hydrological scenarios (several hundred thousand) obtained with the SCHADEX-SD and SHYDONHY methods using hydraulic models to overcome these limits. Indeed, adding hydraulic simulation in the chain of determination of extreme hazards makes it possible to represent major influences such as dams and flood plains and to provide coordinated hydrology on the different tributaries. The simulations are based on five elementary bricks to (i) group hydrographs, (ii) model the behaviour of reservoirs, (iii) simulate spillways or gate in case of flood routing (iv) apply the flood control defined on the dams and (v) model the diffusion and propagation of hydrographs from upstream to downstream.

In operational use, extreme floods are rare, it is appropriate to put in place an operational process that allows the management of water bodies to better anticipate current floods by considering economic and safety constraints.

- The **Linear Trajectory** makes it possible to significantly improve the flood management of large reservoirs from a proportional-integral regulation freeing from the knowledge of the incoming flow (approach based on the coast and the recent evolution of the coast).
- **FREGATE** is a decision support tool, based on 14-day probabilistic flow forecasts propagated in rivers and transformed into score forecasts, allowing from a target matrix (probability of flooding as a function of inflow and time of year) to optimize the day-to-day management of a valley (economic and organizational gains) by limiting the risk of passing into standby situation or flood situation, testing different scenarios of turbinated flows at each dam.

The Ain River is used here as an example of application of these different tools.

RÉSUMÉ

Le présent article décrit un ensemble d'outils permettant d'améliorer la prise en compte du risque hydrologique aussi bien court terme (prévisions) que long terme (crues extrêmes) pour une gestion sûre et optimisée d'une vallée avec un ou plusieurs barrages.

- Melxor et AutoMaT : La plupart des méthodes actuelles de détermination du risque hydrologique extrême présentent des limites pour la représentativité du risque sur les grands bassins versants français. En effet, elles ne tiennent pas compte de l'hétérogénéité hydroclimatique de différents affluents et de la présence d'influences hydrauliques (présence de grands barrages ou de systèmes d'endiguement). Les outils AutoMaT et Melxor présentés dans cet article utilisent la simulation d'un grand nombre de scénarii hydrologiques (plusieurs centaines de milliers) obtenus avec les méthodes SCHADEX-SD et SHYDONHY à l'aide de modèles hydrauliques pour dépasser ces limites. En effet, ajouter de la simulation hydraulique dans la chaîne de détermination des aléas extrêmes permet de représenter les grandes influences comme les barrages et les plaines d'inondations et de fournir des hydrologies coordonnées sur les différents affluents.
- FREGATE et Trajectoire Linéaire : les crues extrêmes étant rares, il est opportun de mettre en place un processus opérationnel qui permette une gestion des plans d'eau permettant de mieux anticiper les crues courantes en prenant en compte les contraintes économiques et de sûreté. La Trajectoire Linéaire permet d'améliorer significativement la gestion des crues des grands réservoirs à partir d'une régulation proportionnelle-intégrale s'affranchissant de la connaissance du débit entrant (approche basée sur la cote et l'évolution récente de la cote). FREGATE est un outil d'aide à la décision basé sur de nombreux scénarios de prévision de débits à 14 jours permettant à partir d'une matrice cible (probabilité de passer en état de crue en fonction du débit entrant et de la période de l'année) d'optimiser la gestion quotidienne d'une vallée (gains économiques et organisationnels).

La rivière Ain est utilisée ici comme exemple d'application de ces différents outils.

1. INTRODUCTION

La présence de barrages sur de grands bassins versants et la vérification de la capacité à assurer la sécurité de ces aménagements tout en n'aggravant pas les conséquences naturelles en cas de crues (courante ou extrême) est aujourd'hui un sujet prioritaire dans un contexte de changement climatique.

Les études hydrologiques de nombreux bassins versants sont régulièrement mises à jour, mais l'application des méthodes historiques purement hydrologiques se heurte à certaines limites dans le cadre de grands bassins versants (Ain, Durance, Isère ...) :

- Le bassin versant présente une variabilité hydrologique élevée ne permettant pas la mise en œuvre d'une méthode globalisée ;

- Les effets hydrauliques de laminage des grandes plaines inondables et de propagation des crues ainsi que de possible concomitance des confluences ne sont pas explicitement modélisés dans les méthodes hydrologiques classiques ;
- La présence de barrages avec des capacités volumiques notables a une influence majeure sur les crues, jusqu'aux extrêmes.

De même, en exploitation, les évolutions méthodologiques en hydrologie et en hydraulique n'étaient pas toutes intégrées dans la gestion en temps réel (et si possible avec une anticipation notable) lors des situations de crues. C'est pourquoi EDF a développé récemment des méthodes et des outils permettant d'intégrer non seulement l'hydrologie, mais aussi l'hydraulique naturelle (écoulements en rivière) ou influencée (gestion des barrages).

Afin d'être cohérents dans les différentes approches, ce changement de paradigme combinant étroitement l'hydrologie et l'hydraulique s'applique aussi bien à la détermination des crues extrêmes lors d'études de sûreté des barrages que dans une utilisation plus opérationnelle de détermination du risque de passage en crue en temps réel et de gestion anticipée des retenues.

Le présent rapport détaille les méthodes et les outils mis en place dans ce cadre.

2. EVALUATION DES CRUES EXTREMES

2.1. CONTEXTE

La méthode hydrologique de référence à EDF pour l'évaluation des crues extrêmes est la méthode SCHADEX, valable pour des bassins versants de quelques km² à quelques milliers de km² de fonctionnement hydroclimatique homogène et non perturbé par des barrages ou systèmes d'endiguement complexifiant le fonctionnement du bassin.

Pour certains bassins, il a été nécessaire de développer de nouvelles méthodes pour l'estimation des crues extrêmes afin de dépasser les limites de la méthode SCHADEX, parfois trop « spatialisée ». Cette partie présente quelques développements permettant aujourd'hui de traiter ces questions :

- SCHADEX-SD (une version semi-distribuée) génère des centaines de milliers de scénarios hydrologiques au pas de temps journalier, tenant compte de la variabilité spatiale des processus générateurs de crues au sein d'un bassin versant ;

- SHYDONHY construit les hydrogrammes horaires à partir d'hydrogrammes journaliers sur les différents cours d'eau du bassin versant afin d'alimenter la modélisation hydraulique ;
- Melxor simule l'acheminement de ces ensembles d'hydrogrammes à travers un ou plusieurs réservoirs écrêtant les crues ;
- AutoMaT traite les mêmes séries d'hydrogrammes à travers un modèle hydraulique 1D d'écoulement à surface libre (Mascaret), intégrant la modélisation des plaines inondables (casiers), de retenues peu capacitives et de la diffusion d'ondes de crue dans une vallée.

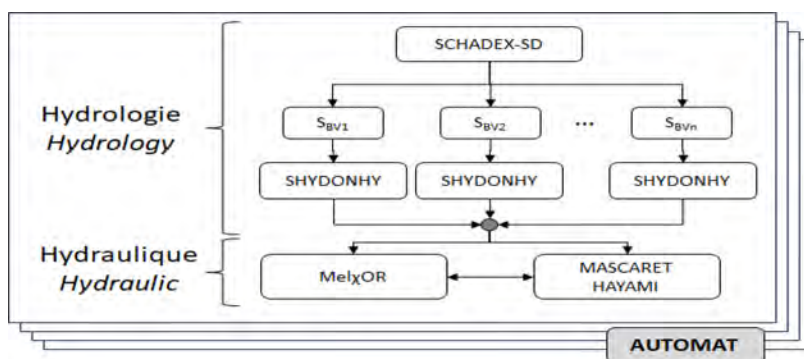


Fig. 1
Principe d'évaluation des crues extrêmes
Extreme flood assessment principle

2.2. MODELISATION HYDROLOGIQUE DES CRUES

2.2.1. Méthode SCHADEX – Estimation exhaustive des crues extrêmes

La méthode probabiliste SCHADEX a fait l'objet de nombreuses publications [[1]]. Cette méthode est basée sur un processus semi-continu de simulation pluie-débit. La méthode a été développée autour de deux modèles : la distribution MEWP (Multi-Exponential Weather Pattern) pour l'estimation des probabilités de précipitations et le modèle hydrologique MORDOR [[2]] développé à EDF. Le processus de simulation permet de calculer une distribution estimée des volumes de crue au pas de temps de l'étude, ainsi qu'une distribution des pics de crue basée sur un rapport pic-volume calculé à partir des hydrogrammes observés des crues significatives. Un large éventail d'événements pluvieux est simulé sur chaque état hydrologique, générant un ensemble exhaustif de croisements entre les précipitations et les risques de saturation du sol.

2.2.2. Méthode SCHADEX-SD – Approche semi-distribuée

Le modèle hydrologique MORDOR, utilisé dans le cadre de SCHADEX, est un modèle global, ce qui implique que les processus hydrologiques, par exemple les précipitations et la saturation du sol, sont supposés être homogènes sur l'ensemble du bassin versant modélisé. Les processus nivologiques sont néanmoins représentés en fonction de l'altitude. Cette homogénéité est discutable pour les grands bassins versants (de plusieurs milliers de kilomètres carrés), ou dans les zones de climatologie très contrastée.

Pour éviter un modèle entièrement distribué, une solution intermédiaire est appliquée ici, fournissant une meilleure représentation de la diversité hydro-climatique du bassin versant étudié, tout en conservant en même temps le cadre de simulation de SCHADEX. Le bassin versant est divisé en plusieurs sous-bassins plus homogènes, comprenant également tous les bassins versants en amont des réservoirs importants. Les modèles pluie-débit sont paramétrés individuellement pour chaque sous-bassin versant, en utilisant les données de débit locales pour l'étalonnage si elles sont disponibles. Une première simulation SCHADEX est effectuée à l'échelle globale (c'est-à-dire pour l'ensemble du bassin versant), ce qui permet d'attribuer une probabilité à chaque événement simulé, principalement sur la base de la pluviométrie surfacique globale tirée pour l'événement. Ensuite, les précipitations de chaque événement sont distribuées dans les différents sous-bassins versants en utilisant les modèles spatiaux calculés grâce à la réanalyse des précipitations SPAZM [[3]], en utilisant des situations comparables sur une période longue (en termes de saison et d'intensité). Les événements pluvieux simulés sont ainsi désagregés sur le domaine de manière réaliste, garantissant que, pour les crues simulées, les contributions de chaque sous-bassin versant sont pertinentes. Les séquences de débit journalier correspondantes sont ensuite calculées à l'aide des modèles hydrologiques à l'exutoire de chaque sous-bassin versant.

2.2.3. SHYDONHY - Génération d'hydrogrammes de crue

La méthode SHYDONHY [[4]], utilisée pour construire des hydrogrammes synthétiques pour chaque événement simulé, est basée sur 1300 stations de jaugeage en France et en Suisse, couvrant une large gamme de taille et de climatologie. Pour chaque station, une moyenne de deux crues par an sont sélectionnées par une méthode de pic sur seuil, fournissant une base de données étendue d'environ 69 000 hydrogrammes au total. Pour un bassin versant donné, certaines "stations donatrices" sont sélectionnées selon des critères de proximité dans l'espace, de taille et de production de ruissellement. Ces stations fournissent des centaines d'hydrogrammes qui peuvent compléter ceux enregistrés localement ou les remplacer si aucun hydrogramme n'est disponible. Pour une séquence de débit journalier donnée (simulée grâce à SCHADEX-SD), un hydrogramme synthétique pertinent est généré en combinant les hydrogrammes appropriés de ce sous-ensemble.

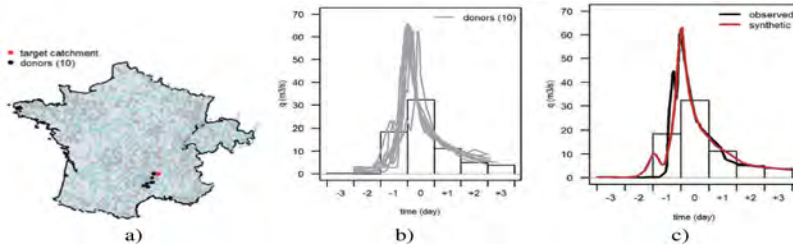


Fig. 2

Exemple de génération d'un hydrogramme synthétique
Example of generation of a synthetic hydrograph

- | | |
|--|---|
| (a) Emplacement des centroïdes des bassins versants cibles et donateurs; | (a) Location of centroids of target and donor watersheds; |
| (b) séquence journalière simulée et hydrogrammes candidats des donateurs | (b) simulated daily sequence and donor candidate hydrographs; |
| (c) hydrogrammes synthétiques et observés. | (c) synthetic and observed hydrographs |

2.3. MODELISATION HYDRAULIQUE DES CRUES

2.3.1. Melxor : propagation hydraulique dans les rivières et par les réservoirs

L'outil Melxor [[5]] a été développé pour modéliser l'écroulement d'un grand nombre de crues à travers un ou plusieurs barrages. Pour représenter une vallée, l'outil Melxor prend en compte cinq briques élémentaires (classes) :

- La classe **Crue** est utilisée pour regrouper les hydrogrammes générés par SHYDONHY dans le système.
- La classe **Réservoir** modélise le comportement du réservoir pendant les crues en résolvant les équations différentielles du premier ordre (1) où V est le volume du réservoir, y est le niveau du réservoir, Q_E et Q_S sont les débits en amont et en aval et t est le temps.

$$\frac{\partial V(y(t), t)}{\partial t} = Q_E(t) - Q_S(y(t), t) \quad (1)$$

- La classe **Evacuateur de crue** (EVC) simule un déversoir ou une vanne, afin (i) d'estimer le débit maximal en aval pour chaque déversoir pour un niveau donné dans le réservoir, (ii) d'estimer si ce débit peut être contrôlé (vanne) ou non (déversoir) et (iii) de calculer la vitesse d'ouverture des vannes.
- La classe **Régulation** modélise la gestion des crues des barrages en calculant le débit réel en aval pour chaque pas de temps. Deux approches sont

mis en œuvre : (i) la régulation simplifiée, où l'ouverture de la vanne est instantanée, peut être modulée à chaque pas de temps et le gradient de débit en aval n'est pas limité, et (ii) la régulation complexe simule la méthode de gestion des crues par "trajectoire linéaire" décrite ci-dessous, inspirée de l'automatique et d'une loi proportionnelle-intégrale. Contrairement à l'approche simplifiée, la vitesse d'ouverture des vannes, les périodes d'observation et les périodes d'ouverture des vannes sont prises en compte.

- La classe **Hayami** modélise la diffusion et la propagation des hydrogrammes dans le lit mineur d'une rivière entre deux barrages. Elle est basée sur les équations de Hayami [[6]] permettant de s'affranchir de la bathymétrie.

Un modèle Melxor est construit à partir d'objets et de relations entre eux. La figure suivante montre l'exemple d'un modèle de deux barrages avec propagation Hayami entre eux. Deux vannes et un déversoir de crête sont utilisés pour la gestion des crues sur chaque barrage.

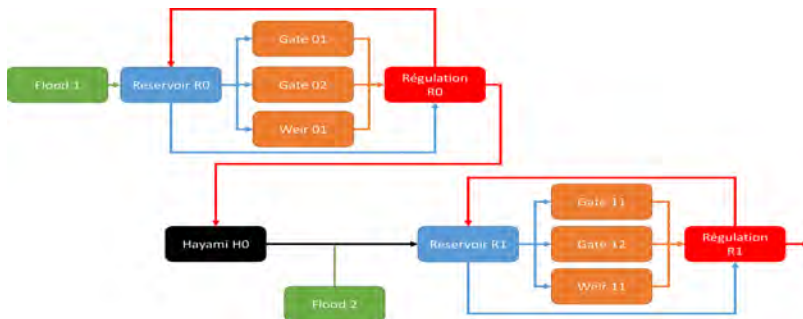


Fig. 3

Melxor – Exemple (modèle avec deux barrages et propagation de Hayami)
Melxor – Example (model with two dams and Hayami propagation)

Peu de paramètres sont nécessaires pour générer un Melxor (hydrogrammes, courbes de capacité, abaques des EVC ...). Il est à noter la possibilité, pour le niveau initial, de choisir entre une retenue à niveau normal, le niveau d'eau historique ou une gestion saisonnière.

2.3.2. AutoMaT - modélisation des plaines inondables

AutoMaT, pour Automatic Mascaret Treatment, est une Automatisation de simulation massive 1D à casiers. Mascaret est un logiciel open source de modélisation hydraulique (www.opentelemac.org) dédié aux écoulements

unidimensionnels à surface libre, basé sur les équations de Saint Venant. Mascaret inclut, avec son noyau instable sous-critique, un module de stockage de crue en plaine afin de représenter un modèle quasi-2D.

AutoMaT fonctionne en deux étapes. Dans un premier temps, pour simuler un scénario hydrologique, AutoMaT affecte les hydrogrammes générés par SHYDONHY à la rivière et à tous ses affluents et lance deux simulations Mascaret : une simulation d'écoulement permanent pour générer des conditions initiales (niveaux d'eau et vitesses) avec la première valeur de l'hydrogramme et une seconde, transitoire, simulant toute la crue.

Dans un second temps, pour effectuer de très nombreuses simulations, AutoMaT assure la parallélisation massive des simulations sur un cluster et la gestion des erreurs entraînant des plantages Mascaret (en testant de petites variations du débit initial, un ajustement du pas de temps ou de la discrétisation verticale des sections transversales).

Le modèle AutoMaT ne nécessite pas plus de données que celles nécessaires à la construction du modèle Mascaret de la rivière et des scénarios hydrologiques.

3. GESTION OPERATIONNELLE DES CRUES

3.1.1 Contexte

L'évaluation des crues extrêmes est une étape indispensable au dimensionnement des aménagements et à la compréhension de leur fonctionnement en crue. Pour autant, les crues extrêmes étant rares, il est nécessaire de mettre en place un processus opérationnel qui permette aussi de gérer les crues courantes et si possible de les anticiper.

Depuis les années 2010, de nombreuses évolutions ont vu le jour dans le domaine de la gestion des crues des grandes retenues d'EDF, notamment : (i) une nouvelle méthode de gestion des crues appelée Trajectoire Linéaire, (ii) l'émergence des prévisions probabilistes des apports aux barrages, (iii) la capacité à prévoir le passage à l'état de crue grâce aux éléments ci-dessus, et (iv) l'échange en temps réel entre les parties prenantes (optimiseur, exploitant, prévisionnistes, etc.) sur la base d'éléments objectifs.

EDF a développé un outil nommé FREGATE intégrant les évolutions ci-dessus et qui permet de mieux préparer la gestion opérationnelle des réservoirs à l'approche de situation de crues.

3.1.2. Objectifs visés

Les barrages sont généralement soumis à la définition des états de fonctionnement selon la réglementation du pays et les pratiques habituelles appliquées par les gestionnaires. On peut en général distinguer (i) les conditions normales d'exploitation, (ii) l'état de veille, nécessitant une mobilisation de l'opérateur et certains contrôles à effectuer et (iii) l'état de crue qui nécessite des manœuvres pour évacuer des débits.

La gestion des barrages lors d'une crue, plus précisément le passage d'un état d'exploitation normal à un état d'exploitation en crue, soulève généralement des questions.

La fréquence des passages en état de crue¹ dans les grands réservoirs est généralement faible, souvent moins d'une fois tous les 10 ans. L'objectif est généralement d'éviter les crues et les déversements autant que possible, pour chaque événement hydrologique. Cette stratégie, que l'on peut qualifier de "stratégie zéro crue", vise à minimiser les risques immédiats en aval et à éviter les pertes d'eau en cas de crue. Cependant, elle peut avoir des effets indirects préjudiciables comme (i) un maintien des compétences et de l'équipement non garanti, en raison de la rareté des événements, (ii) des impacts potentiels en aval tels que les conditions morphodynamiques et environnementales, mais aussi la connaissance des crues par les avalisants et (iii) un impact sur la gestion de la performance énergétique, lié à une gestion prudente des retenues à cote basse.

Par ailleurs, la gestion actuelle des retenues repose parfois sur des approximations comme (i) l'anticipation des crues basée uniquement sur le volume disponible et non pas sur la dynamique des crues et (ii) une gestion basée sur un unique scénario de prévision sans intégration de l'incertitude future inhérente aux modèles. C'est pourquoi il est nécessaire de privilégier les prévisions hydrologiques probabilistes dans l'anticipation des crues.

3.1.3. Mise en œuvre de nouveaux concepts dans un outil opérationnel

Un outil d'aide à la décision existe à EDF pour intégrer les évolutions mentionnées ci-dessus. Il est conçu comme une plateforme de travail partagée efficace et intuitive. Il est disponible pour une utilisation opérationnelle industrielle afin de fournir en temps réel (i) la gestion optimale de cote des réservoirs à l'approche de crues possibles et (ii) l'objectivation des décisions visant à éviter ou assumer les passages en état de veille et en état de crue (par exemple, gestion des quarts de travail).

¹Les crues au sens "apports hydrologiques" du terme sont fréquentes, c'est bien l'impossibilité de la stocker intégralement sans avoir à utiliser les évacuateurs de crue (« état de crue ») qui est rare.

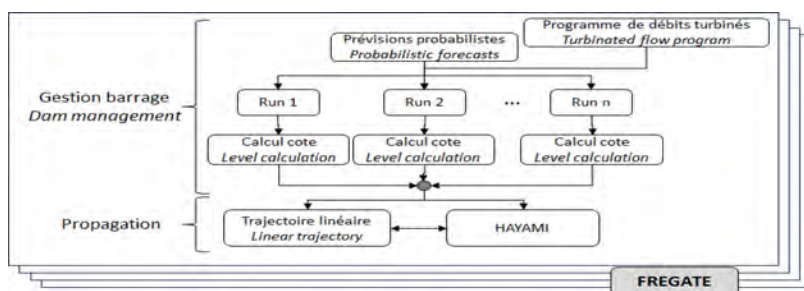


Fig. 4

Principe de gestion des crues en opérationnel et outil d'aide à la décision d'EDF
Flood management principle in operation and EDF decision support tool

Les différents principes intégrés dans l'outil sont détaillés ci-dessous.

Trajectoire linéaire

Afin d'améliorer significativement la gestion des crues dans les grands réservoirs, une méthode appelée "Trajectoire Linéaire" a été développée [[7]].

Cette méthode se base sur les améliorations suivantes : (i) simplification et objectivation des études visant à paramétrer les lois, (ii) meilleure stabilité et robustesse des lois en termes de perturbations dues aux crues et (iii) justification générique du paramétrage, grâce à la résolution globale de l'algorithme en l'absence de valeurs du débit entrant, qui peut être incertain ou manquant dans des conditions de crue [[8]].

L'équation de la trajectoire linéaire et de la gestion des débits sortants peut être résumée par la formule suivante, décrivant une régulation proportionnelle-intégrale :

$$\Delta Q_s = \frac{KS}{T} (\Delta y - \Delta y_p)$$

Où :

- ΔQ_s : variation du débit sortant à appliquer (m³/s)
- K : gain de la régulation
- S : surface de la retenue (m²)
- T : pas de temps de manœuvre (min)

- Δy : variation de cote de la retenue (m)
- Δy_p : valeur de la trajectoire pilote (m)

La trajectoire pilote est définie par la relation suivante :

$$\Delta y_p = p(y - y_c)$$

Avec :

- p : pente (cm/m)
- y_c : cote de consigne (m)

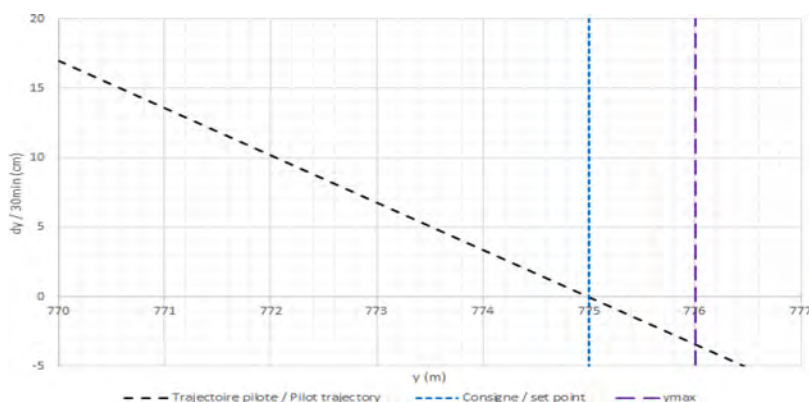


Fig. 5
Exemple de trajectoire pilote dans le plan $(y, \Delta y)$
Example of pilot trajectory in the plane $(y, \Delta y)$

L'outil EDF intègre la méthode de la "trajectoire linéaire" afin de détecter des changements d'état (en préparation de l'état de veille ou de crue). Il reste possible d'utiliser l'outil avec d'autres types de régulations que celle de la trajectoire linéaire.

Prévisions des apports hydrologiques

L'anticipation et la préparation des réservoirs avant les crues sont basées sur des prévisions hydrologiques probabilistes des apports et des programmes de débits turbinés. Les prévisions probabilistes utilisées pour l'anticipation reflètent les incertitudes liées aux différents scénarios météorologiques modélisés [[9]].

Ainsi, un scénario de prévision unique ne représente qu'un avenir possible, souvent faux, sans aucune notion d'incertitude. L'utilisation d'une prévision déterministe induit par conséquent des biais importants dans la stratégie suivie (cf. *infra*).

Jusqu'à présent, la richesse des prévisions probabilistes était rarement exploitée : les utilisateurs finaux des prévisions probabilistes avaient rapidement réduit l'information disponible à une seule trajectoire (la moyenne, les quantiles 10%/50%/90%), perdant ainsi la richesse de l'information contenue dans les prévisions, en particulier pour la prévision des crues [[10]].

L'outil EDF permet de valoriser l'ensemble de la prévision, jusqu'à la fin de tous les calculs : évolution des cotes de la retenue, passage en état de veille ou de crue... En effet, les calculs statistiques qui traduisent des trajectoires probabilistes complexes en indicateurs intelligibles ne sont pas réalisés très en amont mais au plus près de l'utilisation finale.

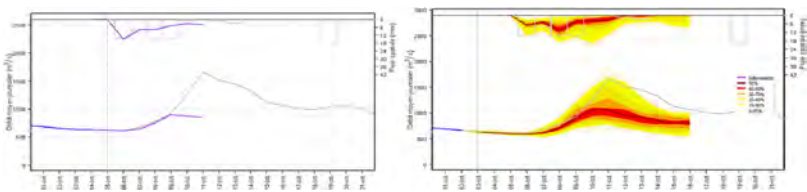


Fig. 6
Exemple de prévision déterministe (à gauche) et probabiliste (à droite)
Example of deterministic (left) and probabilistic (right) forecasting

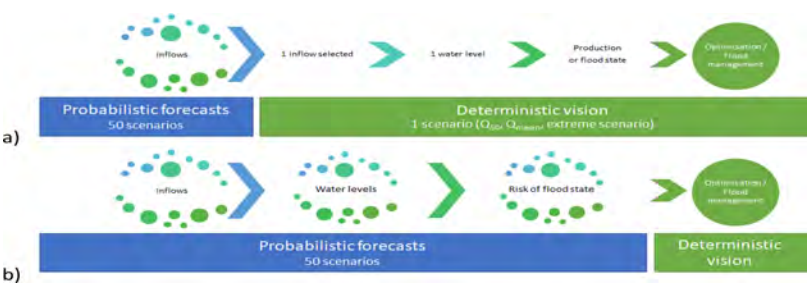


Fig. 7
Vision actuelle (a) et future (b) d'utilisation des prévisions probabilistes à EDF
Current (a) and future (b) vision of using probabilistic forecasts at EDF

Probabilité d'atteindre un état de veille/de crue

Pour chaque prévision de débit entrant disponible, la simulation des programmes de production permet d'identifier les éventuels franchissements de seuil des passages en état de veille et/ou de crue et d'établir une probabilité de changement d'état, par comparaison avec des courbes d'état préétablies.

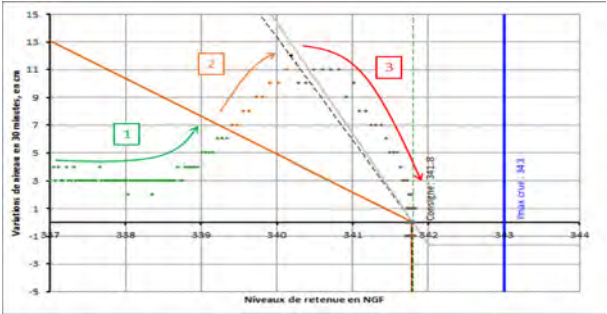


Fig. 8

Principe d'interception d'un scénario avec les courbes de changement d'état
Principle of interception of a scenario with situation change curves

- | | |
|-------------------------|----------------------|
| 1. Exploitation normale | 1. Normal operation |
| 2. Etat de veille | 2. Standby situation |
| 3. Etat de crue | 3. Flood situation |

Il est alors possible de comparer cette probabilité de changement d'état obtenue avec la probabilité cible pour la période d'anticipation (cf. *infra*).

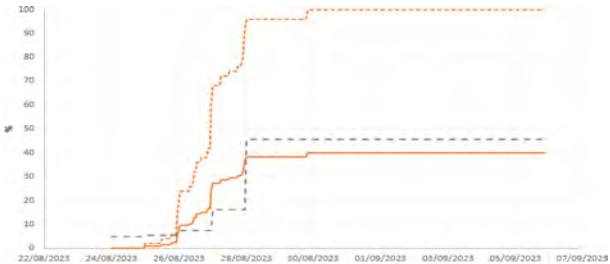


Fig. 9

Probabilité de passage en état de veille
Probability of going into standby situation

- | | |
|---|--|
| Gris : probabilité cible | Grey: target probability |
| Orange pointillé : probabilité dans une situation initiale de débits turbinés | Dashed orange: probability in an initial situation of turbinated flows |
| Orange plein : probabilité dans une situation modifiée de débits turbinés | Full orange: probability in a modified situation of turbinated flow |

L'outil EDF permettant l'ajustement des prévisions de débit turbinés modifie l'évolution des volumes stockés, et donc les évolutions attendues des niveaux d'eau, des stratégies alternatives peuvent être discutées entre les utilisateurs autorisés (optimiseur, opérateurs), pour converger vers une stratégie partagée (et optimisée) et contrôler ou limiter le risque de passage en état de veille ou de crue.



Fig. 10
Changements d'état actuels (a) et futurs (b)
Current (a) and future (b) situation changes

- | | |
|---|---|
| 1. Exploitation normale | 1. Normal operation |
| 2. Anticipation « empirique » / 2'. | 2. « empirical » anticipation / 2'. Opti- |
| Anticipation optimisée / 2''. Crue évitée | mized anticipation / 2''. Flood avoided |
| 3. Etat de veille / 3'. Etat de veille | 3. Standby situation / 3'. Optimized |
| optimisé | standby situation |
| 4. Etat de crue / 4'. Etat de crue | 4. Flood situation / 4'. Optimized flood |
| optimisé | situation |
| 5. Sortie de crue | 5. Flood situation exit |

Dans le premier cas, l'état de crue peut être évité en plaçant les débits turbinés plus tôt.

Dans le second cas, on suppose qu'il y a des états de crues, avec des états de veille/crue plus courts et une meilleure préparation de ces épisodes.

L'outil EDF permet ainsi de réduire considérablement les coûts, notamment dans les cas suivants : (i) prévention des crues en limitant le creusement des niveaux d'eau des réservoirs (perte économique), (ii) meilleure anticipation des débits sortants afin d'alerter éventuellement les agences extérieures, (iii) anticipation des périodes de débits turbinés afin d'éviter les périodes de faible valeur de l'eau (les week-ends par exemple), (iv) retardement, dans une certaine mesure, d'une crue pour des raisons d'optimisation économique et/ou pour permettre aux équipes d'opérer à des moments plus appropriés (jour/nuît, semaine/week-end), et (v) meilleure gestion de la fin de la crue pour retrouver un niveau d'eau optimal dans le réservoir [[11]].

Matrice cible

Le passage à l'état de veille ou à l'état de crue, entraînant la mobilisation d'une équipe d'astreinte sur le barrage, et une gestion locale de la crue, est parfois

dicté par des critères simplistes, eux-mêmes rarement partagés entre les parties prenantes (optimiseur et exploitant en particulier)².

La gestion d'un réservoir avec un risque nul de passer à l'état de crue (principe de "zéro crue") peut être une stratégie très sous-optimisée car elle nécessite de maintenir les réservoirs à un niveau d'eau très bas en suivant un principe de précaution potentiellement exagéré. En revanche, il n'est évidemment pas souhaitable d'augmenter trop fortement ce risque, pour la sécurité des personnes en amont et en aval.

L'objectif est donc de définir un "risque acceptable" de passer en état de veille ou de crue. Une analyse dite « matrice cible » doit permettre de définir a priori ce risque acceptable en fonction du débit entrant et de la période de l'année et servir de référence objectivée pour aider à prendre les bonnes décisions en temps réel, avant l'état de crue. Elle prend en compte différents critères partagés par les différents acteurs de la gestion du barrage (exploitant, optimisateur, etc.). En tout état de cause, cette matrice cible propose un guide pour la phase d'anticipation uniquement : une fois l'état de crue atteint, la sûreté des barrages est garantie uniquement par les consignes de crues en vigueur.

L'outil EDF applique la matrice cible sur les prévisions de débits entrants pour établir une probabilité cible de passage en état de veille ou de crue pour les jours à venir.

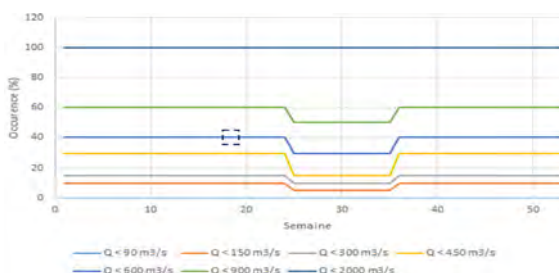


Fig. 11
Exemple de matrice cible
Example of target matrix

Ici, durant la semaine 10 (cadre tirets bleus), la probabilité cible pour un débit inférieur à 600 m³/s est de 40%

Here, in week 10 (framed by blue dashes), the target probability for flow below 600 m³/s is 40%

²En France, à EDF, on trouve généralement les indications suivantes dans les Consignes Générales d'Exploitation des Crues : "L'état de veille doit être déclaré si au moins une des conditions est remplie [...] : décision du directeur d'exploitation lorsque les informations hydrologiques et météorologiques indiquent qu'un événement de crue est prévisible".

La matrice cible se base généralement sur des valeurs caractéristiques des débits entrants connues de l'exploitant : débits des turbines, débits de crue ...

Ces matrices constituent donc la base de référence pour l'établissement d'une stratégie d'anticipation, basée sur des critères documentés, objectifs et partagés par tous les protagonistes. Elles peuvent servir de référence et de base de discussion pour la prise de décision en temps réel, tout en restant non prescriptives. Elles permettent également de mettre en place des alarmes (liées aux risques de changement d'état) pour aider à optimiser la gestion du site lorsque c'est pertinent.

Intégration de plusieurs barrages dans une vallée

La gestion hydroélectrique d'un bassin versant est généralement basée sur le potentiel hydraulique de la vallée, sur tout le linéaire de son cours d'eau. Dans ce cas, la gestion doit être "intégrée" afin de répondre aux objectifs d'optimisation et de gestion des crues dans l'ensemble de la vallée.

L'outil EDF permet la configuration des barrages en cascade en modélisant la propagation hydraulique des débits entre chaque barrage et les éventuels affluents. Il permet la visualisation des conséquences de la gestion proposée sur l'ensemble de la chaîne amont-aval, tout en permettant d'examiner les changements de gestion possibles pour chaque structure et de prévoir leurs impacts au niveau de la vallée.

4. APPLICATION AU BASSIN VERSANT DE L'AIN

4.1. CONTEXTE

L'Ain est une rivière française qui prend sa source en Bourgogne-Franche-Comté, à 681 mètres d'altitude, et se jette dans le Rhône un peu en amont de Lyon, après avoir parcouru 189,9 km pour une superficie de bassin de 3 765 km².



Fig. 12
Situation de la vallée de l'Ain en France
Location of the Ain Valley in France

L'Ain a de nombreux affluents dont certains notables, comme (i) la Bienne et l'Oignin en rive gauche et (ii) la Valouse en rive droite.

EDF exploite six barrages dans le bassin versant pour la production d'électricité : Vouglans, Saut Mortier, Coiselet, Moux (sur l'Oignin), Cize-Bolozon et Allement. Le barrage de Vouglans, en amont de la chaîne, influence notablement le comportement hydrologique de l'Ain, en particulier lors des crues.

Des études ont été réalisées pour (i) confirmer les débits des crues extrêmes aux différents aménagements, en prenant en compte l'hydrologie de chaque affluent, la propagation hydraulique des cours d'eau et la gestion des barrages en crue, notamment la capacité d'écroulement du barrage de Vouglans et (ii) suivre en temps réel le risque de crue sur les aménagements en fonction de prévisions de débits sur les différents affluents.

4.2. CONNAISSANCE DES CRUES EXTREMES

Les outils Melxor et AutoMaT ont été utilisés pour déterminer les valeurs de crues extrêmes à chaque aménagement de l'Ain.

L'étude s'est ainsi basée sur les étapes suivantes :

Réalisation d'une étude hydrologique où le bassin de l'Ain a été « découpé » entre l'Ain en amont de Vouglans et 4 sous-bassins versants contributeurs (affluents et bassins versants intermédiaires) pour tenir compte des « coupures hydrauliques » que représentent les barrages de Vouglans, Coiselet et Cize-Bolozon en amont du barrage de l'Allement. Une simulation **SCHADEX-SD** des crues, suivie d'une génération d'hydrogrammes par **SHYDONHY**, est réalisée, fournissant ainsi un ensemble d'environ 200 000 scénarios hydrologiques. Chaque scénario correspond à un ensemble de 5 hydrogrammes, un pour chaque sous-ensemble de bassins versants, couvrant une large gamme d'intensités et de dynamiques de crues (période d'observés historiques : 1950-2021)

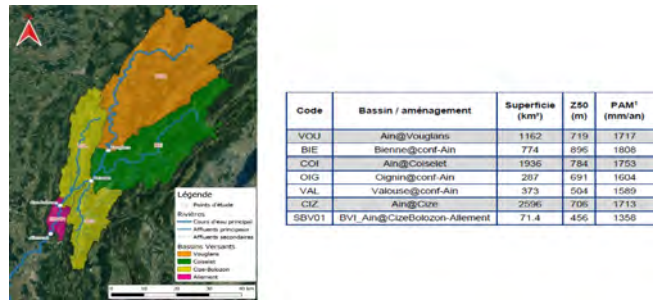


Fig. 13

Localisation et description des sous-bassins contributeurs et des 3 barrages
Location map and description of contributing sub-basins and 3 dams

- Simulation du barrage amont (Voglans) avec **Melxor** pour intégrer l'effet du laminage sur les crues (Fig. 14)
- Réalisation d'un modèle **MASCARET** basé sur une topographie et une bathymétrie récentes et le calage de crues historiques (cote et dynamique de crue) de l'aval immédiat du barrage de Saut-Mortier au barrage de l'Allement (Fig. 15).
- La validité du modèle a été vérifiée sur des crues et événements observés. Sa robustesse a également été vérifiée pour toutes les gammes de débits, et notamment les crues extrêmes. Les simulations ont été réalisées avec AutoMaT sur l'ensemble des 200 000 hydrogrammes en chaque point d'injection du modèle hydraulique tout en intégrant le laminage potentiel de Voglans par l'outil Melxor.

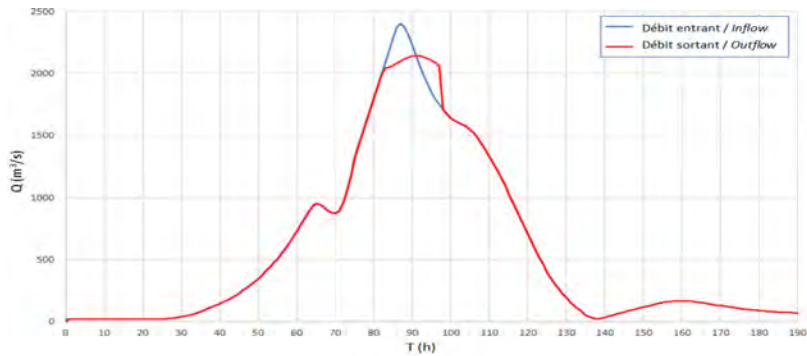


Fig. 14

Simulation de Voglans – Effet du laminage sur le débit sortant
Voglans dam simulation – Effect of flood routing

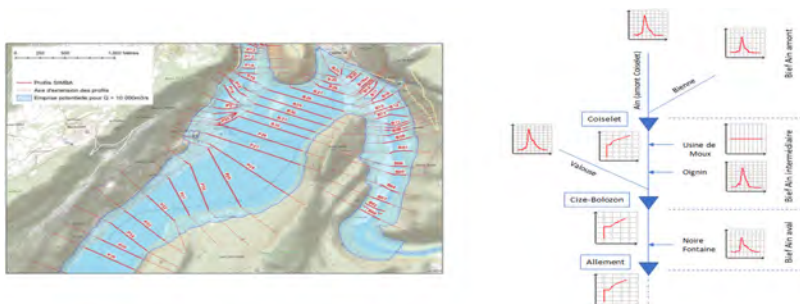


Fig. 15

Modélisation hydraulique 1D de l'Ain
1D hydraulic modelling of the Ain River

4.3. RESULTATS

Les résultats ont permis de montrer les influences de la spatialisation de l'hydrologie pour un grand bassin versant, de la propagation hydraulique (concomitance des crues sur les affluents) et du laminage des grandes retenues.

Par ailleurs, l'étude AutoMaT permet de mieux connaître les phénomènes générateurs des crues. On peut notamment noter que, pour une période de retour donnée, les crues extrêmes peuvent être générées de différentes manières et ne sont pas systématiquement issues de crues concomitantes sur l'Ain et ses affluents.

	$Q_{1\,000}$ (m ³ /s) AutoMaT vs globale GRADEX	$Q_{10\,000}$ (m ³ /s) AutoMaT vs GRADEX
Vouglans	+7%	-1%
Coiselet	+2%	-6%
Cize Bolozon	-8%	-12%
Allement	-12%	-15%

Fig. 16

Comparaison des résultats entre l'étude AutoMaT et l'étude précédente réalisée avec la méthode GRADEX. On note un gain croissant de l'amont vers l'aval
Comparison of results between the AutoMaT study and the previous GRADEX study. There is an increasing gain from upstream to downstream

En effet, on peut voir sur la Fig. 17 que pour une période de retour donnée, un grand nombre de crues sont concomitantes (droite où le débit de pointe à Coiselet est égal à la somme du débit de pointe venant de Vouglans et de la Bienne) et aussi un certain nombre de crues non concomitantes (somme des débits de pointe de Vouglans et de la Bienne supérieure au débit de pointe à Coiselet).

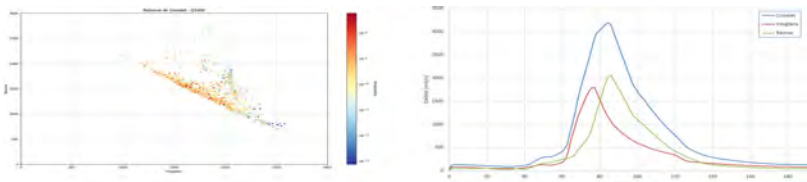


Fig. 17

Répartition des contributions Ain/Bienne pour une Q_{1000} à Coiselet et exemple de scénario Q_{1000} à Coiselet
Distribution of Ain/Bienne rivers contributions for a Q_{1000} at Coiselet and example of scenario Q_{1000} at Coiselet

Enfin, AutoMaT a permis de démontrer le gain sur le débit de pointe lié à l'écêtement par Vouglans (Fig. 18), pour des crues de période de retour élevée. En effet, en supposant la retenue initialement à RN et l'attente de la saturation des EVC avant un écêtement de la crue, les débits de pointe supérieurs à un temps de retour 4 000 ans sont écêtés (débit sortant inférieur au débit entrant), influençant le risque crue extrême pour les barrages plus en aval.

Dans le cas de la vallée de l'Ain, l'outil a été principalement utilisé pour étudier la concomitance des crues des différents affluents et l'impact de l'écêtement des crues par l'ouvrage de tête. Il est à noter que les outils Melxor et AutoMaT ont aussi été utilisés sur d'autres vallées pour dimensionner par exemple un creux saisonnier, gérer une vallée pour limiter les déversements d'un ouvrage en attente de travaux ou encore tenir compte de grands systèmes d'endiguement créés pour protéger de grandes villes des inondations.

4.4. SURVEILLANCE DES CRUES EN TEMPS REEL

En parallèle de cette connaissance des crues extrêmes, l'outil FREGATE a été déployé sur la vallée de l'Ain pour anticiper la connaissance des crues et leur gestion. L'outil intègre :

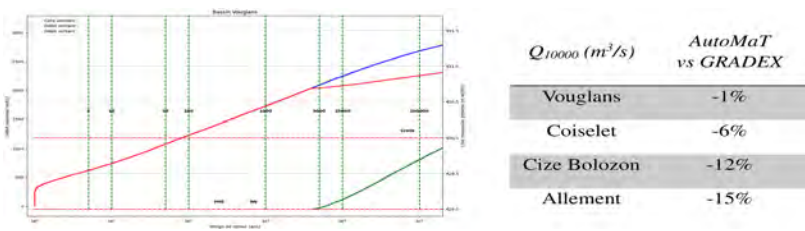


Fig. 18
Simulation de Vouglans – Effet du laminage sur les périodes de retour.
Vouglans dam simulation – Effect of flood routing on return periods

- La connaissance des prévisions probabilistes à 14 jours sur Vouglans, les apports naturels entre Vouglans et Coiselet, entre Coiselet et Cize-Bolozon et entre Cize-Bolozon et Allement, ainsi que les prévisions de programmes turbinés à chaque aménagement (Fig. 19),
- La connaissance des courbes de passage en état de veille et de crue, afin de déterminer le risque lors de chaque prévision en fonction d'une courbe cible (Fig. 20).

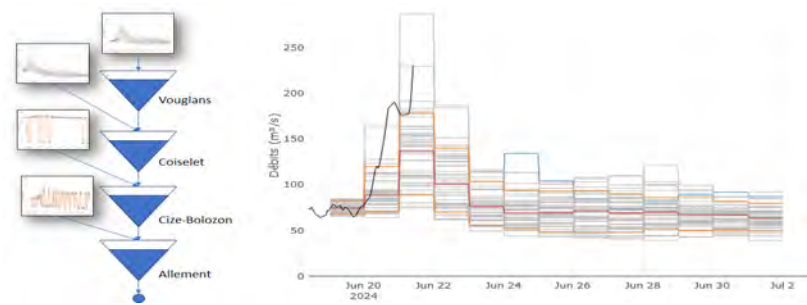


Fig. 19
Simulation de l'Ain – schéma de principe et prévision probabiliste à Vouglans
Ain river simulation – schematic diagram and probabilistic forecast at Vouglans dam



Fig. 20
Simulation de Vouglans – Risque de passage en état de veille à partir du 26 mai –
action sur les débits turbinés à prévoir?
*Simulation of Vouglans dam – Risk of switching to standby situation from 26 May –
action on the turbinated flows to be expected?*

5. CONCLUSION ET PERSPECTIVES

Concernant l'évaluation de la sécurité des barrages dans des bassins versants vastes et complexes, les méthodes et outils présentés ouvrent une nouvelle perspective technique. Ils permettent une modélisation étendue des réservoirs, des rivières et des plaines inondables et tiennent compte de la gestion des réservoirs en amont. Cette modélisation hydraulique est alimentée par une simulation stochastique sophistiquée des précipitations et du ruissellement qui fournit un ensemble

complet d'évènements hydrologiques, décrivant la gamme complète des amplitudes de crue et des contributions des sous-bassins versants.

Globalement, l'évaluation de la sécurité des barrages est réalisée sur une base beaucoup plus solide et complète qu'en utilisant un nombre limité d'hydrogrammes ou de scénarios de référence et prend en compte davantage d'effets hydrauliques (laminage par les retenues et les systèmes d'endiguement, décalages temporels des affluents, diffusion de l'onde ...) intervenant lors de la propagation dans la vallée.

Concernant l'utilisation opérationnelle de ces informations, plusieurs nouveaux concepts ont été développés pour le temps réel : nouvelles prévisions, nouvelle gestion des crues, objectivation des risques de crue... Il était donc opportun de les implémenter dans un outil opérationnel mettant en évidence leur potentiel pour la prise de décision en temps réel.

Les objectifs de l'outil sont d'améliorer la stratégie de gestion opérationnelle (niveau de la retenue vs risque de passer en état de veille/crue) pour les réservoirs à différents horizons de temps, en début et en fin de crue, voire en cas d'indisponibilité des organes évacuateurs de crues ou de chantiers.

La simplification des échanges entre acteurs (optimiseur, exploitants, prévisionnistes) permet de coordonner les actions d'anticipation, de prendre des décisions plus rapidement et plus sereinement avant de s'engager dans la gestion de la crue.

L'ensemble de ces outils (FREGATE, Melxor, AutoMaT) permet ainsi de couvrir l'ensemble du risque hydrologique, depuis l'estimation des évènements extrêmes influencés par la réalité du terrain jusqu'à la prévision en temps réel, de manière robuste et adaptée aux besoins de l'exploitant.

RÉFÉRENCES

- [1] PAQUET E. ET AL. (2013). The SCHADEX method: A semi-continuous rainfall-runoff simulation for extreme flood estimation. *Journal of Hydrology*, 495, 23–37
- [2] GARAVAGLIA F. ET AL.. (2017). Impact of model structure on flow simulation and hydrological realism: from a lumped to a semi-distributed approach. *Hydrology and Earth System Sciences*, 21(8), 3937–3952

- [3] GOTTARDI F. ET AL. (2012). Statistical reanalysis of precipitation fields based on ground network data and weather patterns: Application over French mountains. *Journal of Hydrology*, 432, 154–167.
- [4] PAQUET E. (2019) Synthetic hydrograph generation by hydrological donors, *Hydrological Sciences Journal*, 64:5, 570–586.
- [5] LASSUS C. ET AL. (2017). Outil d'estimation de la distribution complète des cotes de retenue atteintes en crue pour un barrage capacitif. In Colloque "Hydraulique des barrages et des digues". Chambéry : CFBR-SHF - 29,30 novembre 2017, 103–114.
- [6] HAYAMI S. (1951). On the Propagation of Flood Waves. Bulletins - Disaster prevention research institute, *Kyoto University*, 1: 1–16.
- [7] ANTUNES-VALLEREY M. (2016), "Sûreté en crue des grands barrages d'EDF : retour d'expérience et nouveaux développements ", CFBR 2016, DOI: 10.24346/cfbr_colloque2016_d05.
- [8] ANTUNES-VALLEREY M. ET AL. (2019), "Dam safety during floods : Taking care of site condition?", HYDRO 2019 Porto
- [9] MOULIN L. ET AL. (2018), "Prévision hydrométéorologique opérationnelle à EDF-DTG Progrès récents et états des lieux en 2018", SHF 2018
- [10] BERTHET L. ET AL. (2018), "Cohérence des prévisions et place de l'expertise : les nouveaux défis pour la prévision des crues", SHF 2018
- [11] PUYGRENIER D. ET AL. (2023), "Innovative methods to anticipate flood management at "Electricité de France" dams", HYDRO 2023 Edinburg

COMMISSION INTERNATIONALE DES
GRANDS BARRAGES

VINGT-HUITIEME CONGRES DES
GRANDS BARRAGES
CHENGDU, MAI 2025

**CHARACTERIZATION AND FEEDBACK ON THE BEHAVIOR OF ARCH DAMS
SUBJECTED TO HEATWAVES AND EXTREME COLD (*)**

Louis SUCHIER
Structural Design Engineer, EDF

Alexandre SIMON
Dam Monitoring Expert, EDF

Emmanuel ROBBE
Expert in dam Behavior and Monitoring, EDF

Philippe KOLMAYER
Dam Expert, EDF

Frédéric LAUGIER
Safety Expert, EDF

Alain FELZINES
Head of Monitoring of Hydraulic Structures, EDF

Rémi BERNARD
Civil Engineering Project Manager, EDF

FRANCE

* *Caractérisation et retour d'expérience du comportement des barrages-voûtes soumis aux canicules et aux grands froids*

SUMMARY

In 2018, the French Committee of Dams and Reservoirs recommendations for justifying the behavior of arch dams proposed the consideration of “increased” thermal loads for the analysis of the behavior of structures presenting vulnerability to thermal conditions.

Indeed, the behavior of arch dams, particularly when the arch is thin, is generally strongly influenced by thermal loads. In summer, concrete expansion causes the arch to move upstream, which in some cases can lead to cracks opening up in the downstream face parallel to the abutments and/or to the instability of gravity abutments. In winter, the arch moves downstream, increasing the opening of the dam-foundation interface at the upstream toe of the arches affected by this mechanism.

This article presents EDF's robust methodology for taking account of exceptional meteorological events in the justification of arch dam behavior, applicable in countries where seasonal temperature variations are consistent.

This methodology has been developed to characterize the increase in thermal loading of an arch dam using the HSTT method. It meets French regulatory requirements for assessing the behavior of arch dams, which recommend more detailed study of certain dams presenting vulnerability to thermal conditions. Although the method can only be applied to operating dams that have been operating for many years, and requires reliable, qualified measurements of air temperature and dam crest displacement, it also has many positive aspects. First, its uniformity means that all structures can be treated under equal conditions. Simple to implement, it limits the need for assumptions concerning the thermal properties of materials and the choice of climatic scenarios. Finally, it is based on the monitoring data representative of the dam's actual behavior.

The inclusion of 10-year thermal loads has generally had only a limited impact on the justification of the behavior of structures under thermal loading. In most cases, their modelling did not reveal any sensitivities that had not already been highlighted with average seasonal loads. 10-year thermal loads therefore appear more like sensitivity studies regarding a potential failure mechanism. Nevertheless, in certain cases, additional calculations with more advanced modelling have sometimes been undertaken to justify a potential failure mode.

These conclusions, drawn from numerical models, are consistent with observations relayed by detailed monitoring of structures during exceptional climatic events, such as the 2022 heatwave in France. Enhanced monitoring of certain arch dams particularly vulnerable to thermal conditions during this heatwave episode is a prudent approach proposed by engineering. This allowed to collect monitoring measurements in atypical situations, which will help to better calibrate dam behavior

models. Feedback from this monitoring also highlights some difficulties in carrying out measurements, which can however be anticipated. In the end, the close monitoring in summer 2022 confirmed the good behavior of the thermally sensitive arch dams, thanks to the perfect reversibility of the phenomena monitored.

RÉSUMÉ

En 2018, les recommandations du CFBR pour la justification du comportement des barrages-voûtes ont proposé la prise en considération de chargements thermiques dits « majorés » pour l'analyse du comportement des ouvrages présentant une vulnérabilité aux conditions thermiques.

En effet, le comportement des barrages-voûtes – d'autant plus que la voûte est mince – est généralement fortement influencé par les sollicitations thermiques. En été, l'expansion du béton génère un déplacement de la voûte vers l'amont, ce qui peut conduire dans certains cas à l'ouverture de fissures sur le parement aval parallèlement aux appuis et/ou à l'instabilité de culées-poids. En hiver, la voûte se déplace vers l'aval, augmentant l'ouverture de l'interface barrage-fondation au niveau du pied amont des voûtes concernées par ce mécanisme.

Cet article présente une méthodologie robuste d'EDF concernant la prise en compte des événements météorologiques exceptionnels, pour la justification du comportement des barrages-voûtes, applicable dans des pays présentant des variations saisonnières de températures.

Cette méthodologie a été développée pour caractériser l'augmentation du chargement thermique d'un barrage-voûte en utilisant la méthode HSTT. Celle-ci répond aux exigences réglementaires françaises pour l'évaluation du comportement des barrages-voûtes, qui recommandent d'étudier plus finement certains barrages présentant une vulnérabilité aux conditions thermiques. Bien que la méthode ne s'applique qu'aux barrages en exploitation existants depuis de nombreuses années, qu'elle exige des mesures fiables et qualifiées de la température de l'air et du déplacement de la crête du barrage, celle-ci possède également de nombreux aspects positifs. Son uniformité tout d'abord, permet de traiter l'ensemble des ouvrages dans des conditions égales. Simple à mettre en œuvre, elle limite l'exigence des hypothèses relatives aux propriétés thermiques des matériaux et au choix de scénarios climatiques. Enfin, elle s'appuie sur des données d'auscultation représentatives du comportement réel du barrage.

La prise en compte de chargements thermiques décennaux n'a eu en général qu'un impact limité vis-à-vis de la justification du comportement des ouvrages sous chargement thermique. Dans la majorité des cas, leur modélisation ne fait pas apparaître de sensibilités qui n'avaient pas déjà été mises en évidence avec les

chargements saisonniers moyens. Les chargements thermiques décennaux apparaissent donc davantage comme des études de sensibilité vis-à-vis d'un mécanisme de défaillance potentiel. Néanmoins, dans certains cas, des calculs complémentaires avec une modélisation plus poussée ont parfois été engagés pour justifier un mode de défaillance potentiel.

Ces conclusions, issues de modèles numériques, sont cohérentes avec les observations relayées par l'auscultation fine des ouvrages lors d'événements climatiques exceptionnels, tels que la canicule 2022 en France. La surveillance rapprochée de certaines voûtes particulièrement vulnérables aux conditions thermiques à l'occasion de cet épisode caniculaire est une approche prudente proposée par l'ingénierie. Cette surveillance rapprochée a permis de collecter des mesures d'auscultation dans des situations atypiques qui aideront à mieux caler les modèles de comportement de barrages. Le Retour d'Expérience de cette surveillance met également en évidence quelques difficultés de réalisation de mesures, qui peuvent toutefois être anticipées. Au final, la surveillance rapprochée à l'été 2022 a permis de confirmer le bon comportement des voûtes sensibles thermiquement grâce à une parfaite réversibilité des phénomènes surveillés.

1. INTRODUCTION

In 2018, the French Committee of Large Dams guidelines for the assessment of the behavior of arch dams [1] proposed the consideration of "increased" thermal loads for the analysis of the behavior of structures presenting vulnerability to thermal conditions.

Indeed, the behavior of arch dams, particularly when the arch is thin, is generally strongly influenced by thermal loads. In summer, concrete expansion causes the arch to move upstream, which in some cases can lead to cracks opening up in the downstream face parallel to the abutments and/or to the instability of gravity abutments. In winter, the arch moves downstream, increasing the opening of the dam-foundation interface at the upstream toe of the arches affected by this mechanism.

The aim of this paper is to present the way in which exceptional climatic events are dealt with - through monitoring, modelling and post-event analysis - at EDF. Since such climatic events are likely to increase in intensity, frequency and duration, capitalizing on them is crucial to improving the efficiency of the various players involved in similar situations in the future.

Firstly, the methodology used to model increased thermal loads is described, considering here a 10-year return time. An initial assessment of the application of this methodology, in terms of increments generated on certain characteristic

variables and potential changes in behavior, within EDF's arch dams, is presented. Secondly, the specific monitoring implemented during the heatwave episode of summer 2022 in France, characterized by high temperatures and a historically low reservoir filling level due to insufficient precipitation, is detailed.

2. CHARACTERIZATION OF 10-YEAR THERMAL LOADS

Classically, the resistance of arch dams to failure mechanisms is assessed for various loads, including summer and winter thermal loads. At EDF, these thermal loads are adjusted based on monitoring data, and in particular the seasonal component of an HST or HSTT analysis. In order to assess increased thermal loads during heatwave or extreme cold, we need to define a methodology for estimating such loads.

2.1. STATISTICAL PROCESSING OF MONITORING DATA AND METHODOLOGY

Establishing the methodology requires the statistical processing of two types of data:

- Reliable air temperature series with at least 50 years of average daily temperature measurements. Each dam is associated with one of the reference stations distributed throughout France, according to its geographical location.
- Arch dam monitoring data, in particular radial displacements at a point on the crest - and if possible, at crown - with at least 10 years of reliable data.

2.1.1. *Monitoring data and HSTT model*

The characterization of increased thermal loads is complex, as it depends on the inertia of the structure. While a thin arch dam will react quickly to a short but intense cold spell, the behavior of a thicker structure will depend on the temperature of the preceding weeks or months.

The Hydrostatic Seasonal Temporal Thermal (HSTT) model was developed by EDF [2] following the 2003 heat wave in France, in order to take into account the average seasonal thermal effect as well as the actual daily average air temperature. This statistical model, calibrated using multiple linear regression, highlights:

- The irreversible effect of time t :

$$g_1(t) = b_1 t \quad [1]$$

- The reversible hydrostatic effect related to reservoir level h , normal reservoir level NWL and empty reservoir level WL_{empty} :

$$g_2(Z) = b_2 Z + b_3 Z^2 + b_4 Z^3 + b_5 Z^4 \quad [2]$$

where $Z = (NWL - h) / (NWL - WL_{empty})$

- The thermal effect related to the temperature distribution in the structure, with:
 - A first sinusoidal seasonal term representing the annual change in temperature from one year to the next, linked to a seasonal variable S varying from 0° on 1st January to 360° on 31st December.

$$g_{3a}(S) = a_6 \cos(S) + a_7 \sin(S) + a_8 \cos(2S) + a_9 \sin(2S) \quad [3]$$

- A second term for temperature deviations from this seasonal average.

$$g_{3b}(t) = K \Delta \Theta_R(t) \quad [4]$$

where $\Delta \Theta_R(t)$ is the delayed temperature deviation from the mean seasonal temperature, calculated from the following formula involving the characteristic time T_0 of thermal diffusion inside the dam, and $\Delta \Theta(t)$ is the instantaneous temperature deviation from the mean seasonal temperature:

$$\Delta \Theta_R(t + dt) = \Delta \Theta(t + dt)(1 - e^{-dt/T_0} \{XET_0\}) + \Delta \Theta_R(t)e^{-dt/T_0} \quad [5]$$

This last component, $g_{3b}(t)$, can be used to quantify the intensity and duration of an exceptional event. This component is the product of two quantities from the HSTT model:

- K , calculated using multiple linear regression. It quantifies the sensitivity of the phenomenon to temperature deviations from the mean. In the case of displacement, K is expressed in $\text{mm}/^\circ\text{C}$.
- The second term $\Delta \theta_R$ results from a treatment of instantaneous temperature deviations from the seasonal mean temperature. Thanks to a numerical parameter, T_0 , derived from the HSTT model, this term considers both the duration and intensity of cold or hot periods, and accounts for the thermal inertia of the phenomenon.

The parameter T_0 is thus representative of the structure's inertia for the phenomenon under consideration. While a low T_0 indicates short response times for thin structures, a high T_0 will be more often encountered for thicker structures. This parameter is expressed in days, and Eq. [5] calculates the so-called "delayed temperature deviations" corresponding to the parameter $\Delta \theta_R$ used previously, considering heat propagation in a wall of a certain thickness as a function of T_0 .

2.1.2. *Gumbel's law for assessing probability of occurrence*

The probability of occurrence of a critical event can be determined using Gumbel's law, which is a special case of the generalized extremum law. This is a very satisfactory approximation when analysing a sample of independent random variables all following the same law. This law can be used to determine the probability of occurrence of an event related to temperature: this makes it possible to associate a statistical probability with an event in a list of events sorted in ascending order.

From the maxima identified over a fixed period, we associate an empirical frequency F given by Hazen's formula (Eq. [6]) (i = rank of maxima in the sorted list, n = number of years over which the statistic is calculated). We then calculate the Gumbel statistic G (Eq. [7]).

$$F[i] = (i - 0.5)/n \quad [6]$$

$$G[i] = -\ln(-\ln(F[i])) \quad [7]$$

2.1.3. *Methodology*

To assess a peak radial displacement increment due to temperature deviations from the seasonal normal, it is necessary to know the K and T_0 parameters of the HSTT model of the phenomenon being monitored. Arch dams are instrumented with pendulums that provide sufficient data to perform a reliable HSTT analysis over a significant period, thereby obtaining the K and T_0 parameters.

The increase in thermal loading is therefore expressed as a displacement increment D_{10} for a return period of ten years. This displacement is calculated at the point studied, at crest level, if possible at crown, since this is the point that "most integrates" the arch dam's behavior. The displacement increment can be calculated in winter ($D_{10,winter}$) and/or summer ($D_{10,summer}$). Once this displacement increment has been quantified, the finite element analyses are calibrated to obtain thermal loads reaching the displacement increment D_{10} .

2.2. APPLICATION OF THE METHODOLOGY

2.2.1. *Steps in the methodology for arch dams inspected by a crest pendulum*

Fig. 1 describes the method used to define the 10-year thermal loading of arch dams investigated by a crest pendulum. The methodology consists of the following two sequential steps:

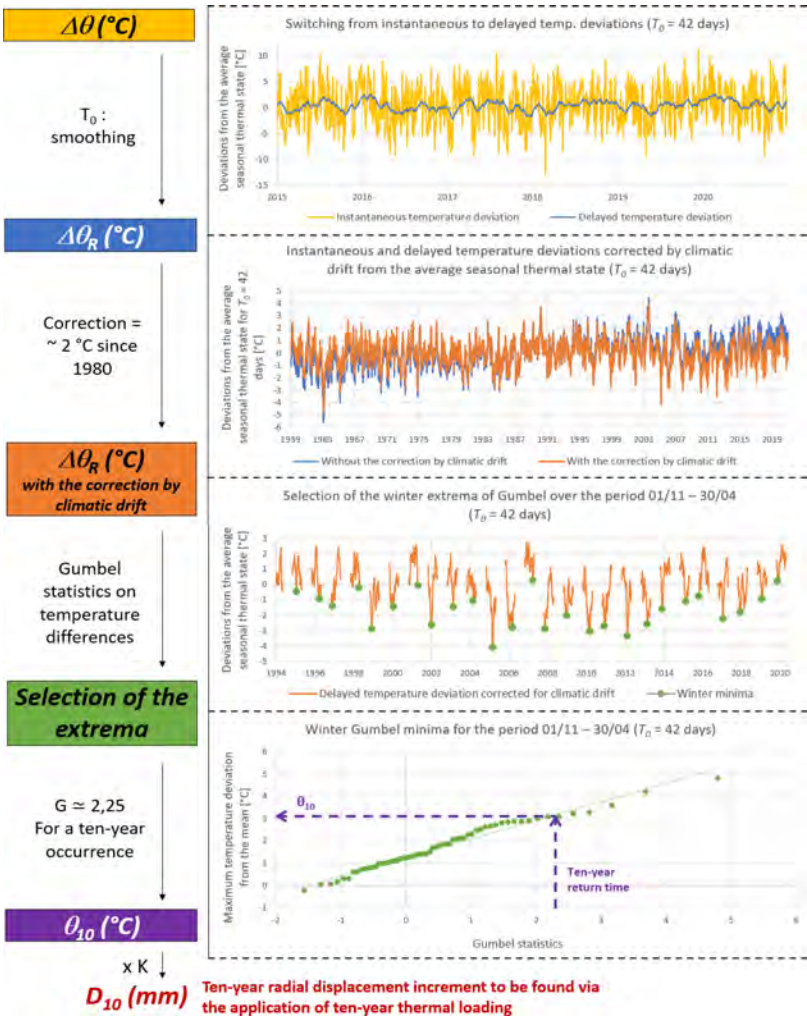


Fig. 1

Methodology for obtaining the radial displacement increment D_{10} for arch dams monitored by one or more pendulums at the crest.

Méthodologie pour l'obtention de l'incrément de déplacement radial D_{10} pour les barrages-voûtes auscultés par un ou plusieurs pendules en crête.

- The determination of a temperature increment θ_{10} from a Gumbel statistic on the delayed temperature deviation $\Delta\theta_R$.
- The estimation of the increased displacement increment, D_{10} , at the point studied at the crest from a simple multiplication between the coefficient K of the associated phenomenon and the value θ_{10} .

The difference between the instantaneous temperature and the seasonal mean temperature provides the instantaneous temperature deviation. The successive steps in determining the 10-year temperature difference θ_{10} are summarized below.

1. Passage from instantaneous temperature deviation to delayed temperature deviations $\Delta\theta_R$ using Eq. [5].
2. Correction by the climatic drift due to climate change (around 2°C between 1980 and 2020 in France) to prevent this drift from distorting deviations from the mean (which would lead, for example, to numerous summer major events over the recent period). A forthcoming publication by the authors will demonstrate that the effect of climatic drift on dam behavior is of second order to the major events presented here.
3. Determining the maximum annual delayed temperature difference. Depending on the event under consideration (heatwave or extreme cold), the maximum annual delayed temperature deviation is chosen: from 1st November to 30th April for a winter event, or from 1st May to 30th October for a summer event.
4. Use of Gumbel statistics (§ 2.1.2) to determine the temperature associated with the different occurrences.

2.2.2. *Determination of the peak radial displacement increment D_{10} for arch dams monitored by one or more crest pendulums*

From the parameter K calculated by the HSTT model and the 10-year temperature difference θ_{10} , the 10-year radial displacement increment D_{10} at the point studied on the crest is obtained by the formula:

$$D_{10} = K \times \theta_{10} \quad [8]$$

This method was applied to 31 EDF arch dams monitored by a crest pendulum. Each arch is identified in Fig. 2 by a number, which is retained in the following. For most structures, the D_{10} to be added to simulate a 10-year thermal load represents between 10 and 40% of the seasonal amplitude (obtained from annual temperature variations). This ratio is highly dependent on the value of T_0 : the thicker the dam (on the right in Fig. 2), the greater the T_0 and the less sensitive it is to rapid temperature variations (and therefore to deviations from the mean season). On the other hand, the thinner the arch (on the left in Fig. 2), the more likely it is to react significantly to a rapid or intense heat or cold wave.

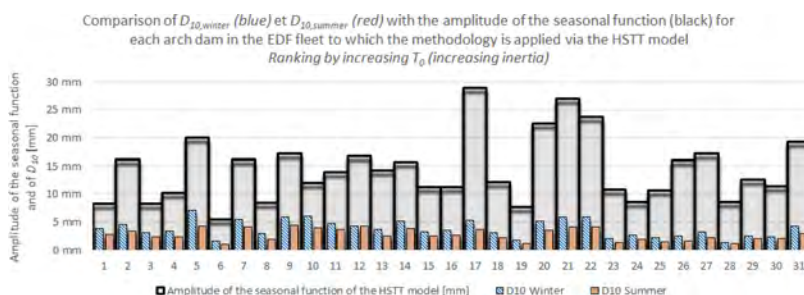


Fig. 2

Comparison of $D_{10,winter}$ and $D_{10,summer}$ in relation to the magnitude of the seasonal effect for each arch dam, ranked by increasing T_0 , i.e. increasing inertia.

Comparaison de $D_{10,hiver}$ et $D_{10,été}$ par rapport à l'ampleur de l'effet saisonnier pour chaque barrage-voûte, classé par T_0 croissant, c'est-à-dire par inertie croissante.

2.2.3. Numerical simulation of 10-year thermal loading

To simulate the increase in thermal loading using finite element analysis, transient calculations must be carried out to simulate first the seasonal thermal loading and then the increase.

Analyses involving seasonal thermal loading are generally carried out using the mean seasonal air temperature on the crest and downstream face of the dam. Specific boundary conditions are also chosen for the upstream face of the dam, considering the influence of the reservoir. The numerical model (properties, assumptions) is generally calibrated to match the seasonal displacements observed at various monitored points on the dam (including the crest).

Next, the aim is to calibrate the temperature assumptions to achieve the targeted 10-year radial displacement increment D_{10} on the crest.¹

2.2.4. The case of arch dams monitored by topographic measurements at the crest

Some arch dams monitored with topographic measurements can be treated using the established methodology, provided that the resulting HSTT analyses are statistically relevant. For the others, a simplified methodology has been developed

¹Please note: the numerical temperature increment used to find the maximum radial displacement increment is different from the θ_{10} calculated using the Gumbel statistic and is related only to the chosen phenomenon. This numerical increment corresponds more closely to a "boundary conditions" type temperature at the concrete surface.

based on multiple studies leading to the conclusion illustrated in Fig. 2, namely a dependence of the radial displacement increment D_{10} on the T_0 . For these dams, the T_0 is determined numerically using the finite element model, by applying a temperature increment to the dam, which makes it possible to determine a numerical equivalent of the T_0 usually obtained statistically using the HSTT model.

Arch dam/Season	Winter	Summer
Thin ($T_0 < 20$ days)	$(40 - T_0) \% \cdot A_s$	$(30 - 0.8 \cdot T_0) \% \cdot A_s$
Thick ($T_0 > 20$ days)	$20 \% \cdot A_s$	$15 \% \cdot A_s$

Fig. 3

Simplified 10-year scenario for arch dams that cannot be subjected to a statistically relevant HSTT analysis.

Scénario décennal simplifié pour les voûtes ne pouvant pas faire l'objet d'une analyse HSTT statistiquement pertinente.

The D_{10} is then defined as a percentage of the seasonal amplitude (A_s) of the phenomenon under consideration, by the following relationships (Fig. 3):

Comparisons carried out using both methods on arch dams inspected by pendulums have demonstrated the good reliability of this simplified method, and the low influence of the slight deviations in D_{10} that can result from it, which are always less than a millimetre.

3. FEEDBACK FROM THE FIRST NUMERICAL STUDIES

The behavioural studies carried out at EDF aim to analyse the preponderance of one or more potential failure modes for a structure, and to assess the structure's behavior in relation to these modes. Among these, three can be influenced by thermal loading: sliding along an abutment, shear failure at the foot of central blocks and exceeding admissible compressive or tensile stresses in concrete.

In summer, the upstream displacement of the arch, caused by the expansion of the concrete, tends to put more stress on the arch abutments, while in winter, the downstream displacement of the arch puts more stress on the central blocks, which can also lead to an opening of the dam-foundation contact.

The methodology described above is systematically applied to arch dams where at least one of the potential failure modes is strongly influenced by summer

and/or winter thermal loading, and where the behavioural analysis shows that the structure has a reduced margin for the mode in question. First, an example of the methodology's application to an EDF structure is presented, followed by a summary of studies carried out on a set of arch dams, enabling the sensitivity of these structures to be assessed. Finally, the value of this type of sensitivity study is discussed.

3.1. EXAMPLE OF A 10-YEAR THERMAL LOAD ON AN ARCH DAM

The study carried out under normal thermal conditions on arch dam no. 4 (Fig. 2) highlighted the thermal sensitivity of the structure, both in summer, regarding the shear stress under one of the bank blocks, and in winter, regarding the tensile stresses obtained in the middle of the downstream face, which caused horizontal cracking when the structure was young. This structure is affected by a concrete swelling pathology, which is considered in the results presented. The downstream view of the dam is shown in Fig. 4 below.

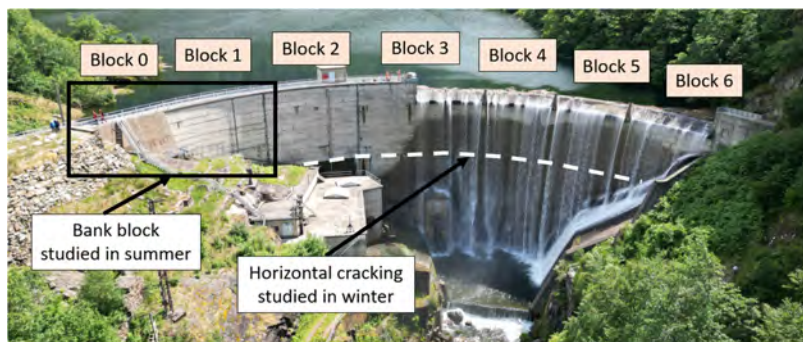


Fig. 4
Downstream view of the dam.
Vue aval du barrage.

Winter loading leads to the development of a tensile zone at the foot of the central blocks, with tensile stresses of around 4 to 5 MPa in 10-year winter, which, given their orientation and calculated values, should not generate significant cracking. At the level of horizontal cracking of the downstream face, the maximum tensile stresses, initially 2.0 MPa at NWL, are increased to 3.9 MPa at NWL + Winter and to 5.5 MPa at NWL + 10-year Winter (Fig. 5). For a better understanding of the impact of the 10-year thermal scenario on this cracking, it is not modelled by non-linearity, which results in high tensile stresses in excess of 5 MPa, lower today due to crack opening.

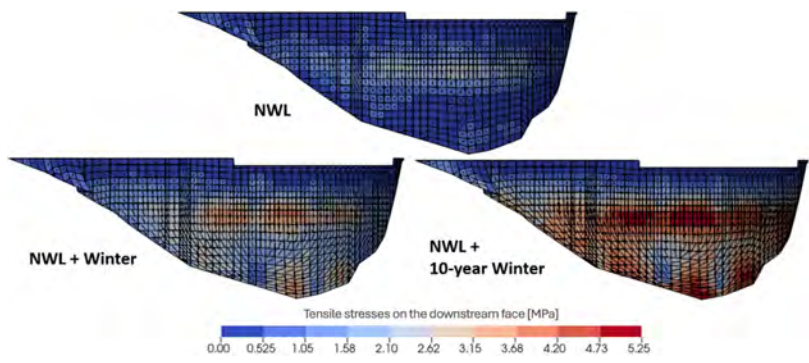


Fig. 5

Tensile stresses on the downstream face at NWL, NWL + Winter and NWL + 10-year Winter.

Contraintes de tractions sur le parement aval à RN, RN + Hiver et RN + Hiver décennal.

The 10-year winter also results in a larger opening at the downstream foot of the structure's block joints. While this is estimated by the model at around 0.5 mm at NWL + Winter, it rises to 1.3 mm at NWL + 10-year Winter, which is characterized by a visible increase in leakage.

In summer, as the dam moves upstream, tensile stresses may tend to increase downstream. In the case of this dam, this translates into an opening of the joint at the dam-foundation contact on the downstream face, from 2.8 mm at NWL + Summer to 3.9 mm at NWL + 10-year Summer at the downstream foot of the bank block (Block 0) studied, as shown in Fig. 6.

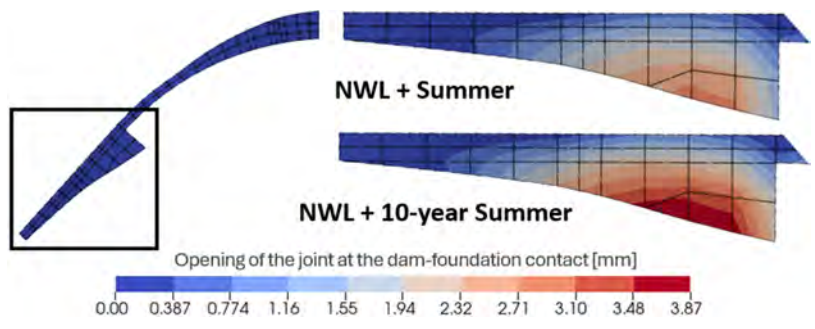


Fig. 6

Opening of the joint at the dam-foundation contact on the downstream face at NWL + Summer and NWL + 10-year Summer.

Ouverture du joint au contact à RN + Été et RN + Été décennal.

Finally, the two 10-year scenarios have the effect of increasing the shear resistances that need to be mobilised at the dam-foundation interface, respectively for the bank blocks in summer and the central blocks in winter. Here, the increment between an average season and a 10-year event is on average slightly lower than that between the situation at NWL and NWL + Average season. Fig. 7 illustrates this phenomenon:

- The cohesion mobilised under the bank blocks increases by 50 to 200 kPa during the 10-year summer, without however exceeding a threshold of 300 kPa under block 0 during the 10-year summer, as provided by on site geological reconnaissance. Maximum cohesion reaches 350 kPa under block 1.
- Similarly, during 10-year winter, mobilised cohesion at the foot of the central blocks increases by around 50 to 150 kPa, reaching a maximum of 430 kPa.
- The cohesions obtained remain within acceptable ranges for arch dams of this type (according to [5]). As a result, these 10-year thermal loads did not give rise to any additional calculations.

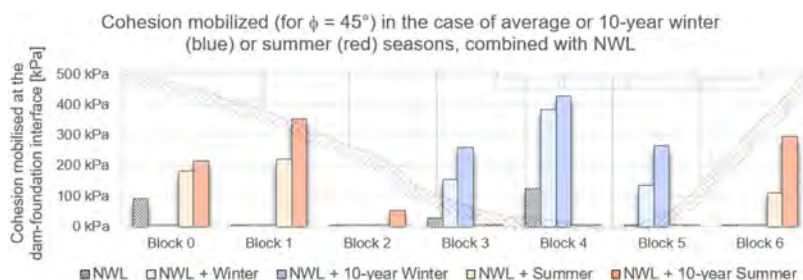


Fig. 7

Cohesions mobilised during average seasons and 10-year thermal loads.

Cohésions mobilisées lors de saisons moyennes et de chargements thermiques décennaux.

3.2. SUMMARY OF STUDIES CARRIED OUT ON FIFTEEN ARCH DAMS

Following on from the previous results obtained on a single structure, the following paragraphs summarize the results obtained on fifteen arch dams, grouped according to failure mode. For each failure mode “indicator” studied, Figs. 8 to 11 compare the absolute values excluding thermal effect, the increment generated by seasonal loading, and the increment generated by increasing seasonal loading to 10-year thermal loading.

3.2.1. Sliding along an abutment

This mechanism, which is accentuated by summer thermal stresses, is assessed by analysing the shear strength parameters (angle of friction ϕ and cohesion mobilised) required to prevent sliding. For ease of comparison, the angle of friction is arbitrarily set at 45° , so that only mobilised cohesion is compared.

Fig. 8 shows the mobilised cohesion at NWL + 10-year Summer (black) and the increments at the dam-foundation interface for seasonal (orange) and 10-year summer (red) thermal loading. The various arch dams studied are ranked by increasing T_0 (i.e. by increasing inertia). The average cohesion increment on the edge blocks between an average summer and a 10-year period generally varies between 100 and 300 kPa, with a range of 0 to 400 kPa. These results are difficult to predict, and only modelling can quantify the influence of each load.

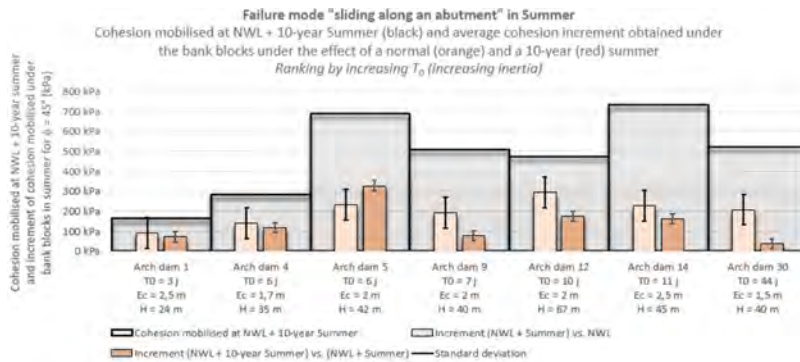


Fig. 8

Failure mode by sliding along an abutment in summer. Cohesion mobilised at NWL + 10-year Summer, and average cohesion increment obtained under the effect of an average summer compared to a thermally neutral situation, and under the effect of a 10-year summer compared to an average summer.

Mode de défaillance par glissement le long d'un appui en été. Cohésion mobilisée à RN + Été décennal, et incrément de cohésion moyen obtenu sous l'effet d'un été moyen par rapport à une situation neutre thermiquement, et sous l'effet d'un été décennal par rapport à un été moyen.

Among these examples, arch dam no. 5, for which the average cohesion mobilised on the banks was only 130 kPa at NWL, sees this cohesion rise to 360 kPa at NWL + Summer and 690 kPa at NWL + 10-year Summer. This doubling of the cohesion generated by the 10-year summer was reflected in the behavioural

study by additional calculations involving the implementation of an elastoplastic model to study the potential adaptation of the abutment. Similarly, for arch dam no. 9, the high mobilised cohesion values obtained led us to calculate these cohesions on the scale of a whole abutment, rather than a single block. Lastly, for arch dam no. 2, not shown on this graph, a reinforcement of an abutment, carried out in 2019, was considered to justify a high mobilised cohesion value under it.

3.2.2. *Shear failure at the foot of the central blocks*

This mechanism, accentuated by winter conditions, is assessed by analysing two parameters. Firstly, as for sliding along an abutment, by estimating the shear resistance parameters (angle of friction and cohesion) required to prevent any sliding. Secondly, regarding the opening of the dam-foundation contact at the upstream toe. With regard to shear, Fig. 9 highlights the following points:

- The effect of winter at the foot of the central blocks seems slightly less marked than in summer on the banks, with an average increment of 0 to 250 kPa, for a range of 0 to 350 kPa.
- The greater the T_0 , and therefore the lower the inertia, the greater the increment due to a 10-year situation compared with a thermally neutral situation, which argues in favour of a greater sensitivity of the arch dam. Moreover, the thicker the arch dam, the smaller the increments analysed appear to be.
- These 8 studies highlighting the effect of a 10-year winter on mobilised cohesion at the foot of the central blocks did not, unlike the 10-year summer, generate any additional modelling.

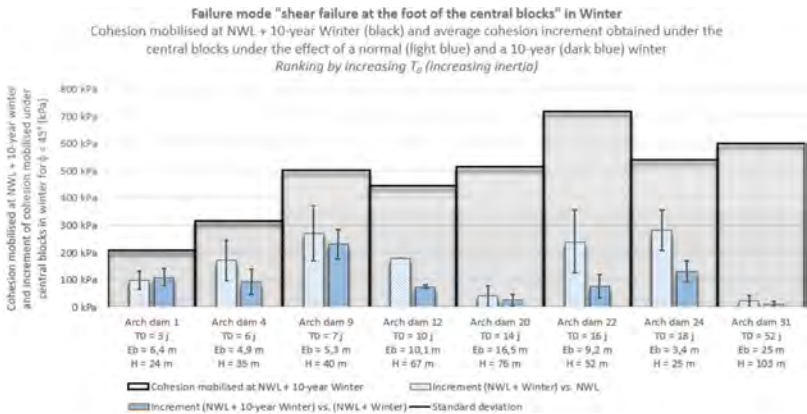


Fig. 9

Failure mode due to shear failure at the foot of the central blocks in winter. Cohesion mobilised at NWL + 10-year Winter, and average cohesion increment obtained under seasonal and 10-year winter loading.

Mode de défaillance par non-reprise des efforts en pied des plots centraux en hiver. Cohésion mobilisée à RN + Hiver décennal, et incrément de cohésion moyen obtenu sous l'effet d'un chargement hivernal saisonnier et décennal.

Almost all the studies are non-linear, with the integration of joint elements at the dam-foundation contact, allowing us to model the opening of the interface and the propagation of associated uplifts. Fig. 10 shows the opening increments of the dam-foundation contact for seasonal (light blue) and 10-year (dark blue) loading, compared with the opening at NWL + 10-year Winter (black).

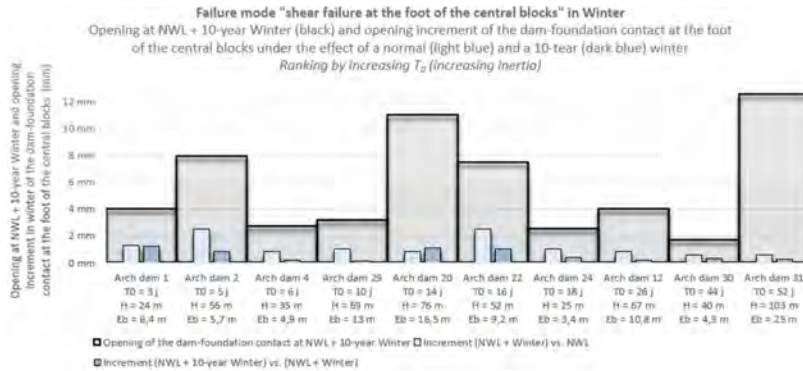


Fig. 10

Opening at NWL + 10-year Winter and opening increment of the dam-foundation contact under seasonal and 10-year winter loading.

Ouverture à RN + Hiver décennal et incrément d'ouverture du contact barrage-fondation sous l'effet d'un chargement hivernal saisonnier et décennal.

The increments between one winter and a 10-year winter are of the order of a few tenths of a millimetre, reaching 1.2 mm at the most. They represent an increment sometimes similar to, but often less than, that due to the average winter compared with a thermally neutral situation. It appears that the higher and thicker the arch dam at the foot, the smaller the increment due to winter thermal loading (10-year or otherwise) in proportion to that already present at NWL. However, these increments are relatively small and difficult to interpret, as there are few devices for measuring the opening at the foot of arch dams, apart from those where the opening is significant enough to compare these values.

3.2.3. Exceeding permissible stresses

Compressive stress increments in summer are concentrated most of the time near the banks on the upstream face. For arch dams calculated in a 10-year situation (Fig. 11), the overall increments due to a 10-year summer compared with an

average summer (in red) are on average around 1.2 MPa, i.e. around half the 2.6 MPa average increment between a seasonal summer and a thermally neutral situation (in orange). However, these values need to be put into perspective, as they show wide disparities and give no indication of the absolute stress level in the structure. Compressive stress levels remain well below the permissible stresses for arch dam concretes, whose compressive strength generally exceeds 25 MPa. Moreover, the effect on stresses thus appears to be less than the increase in mobilised cohesion presented above.

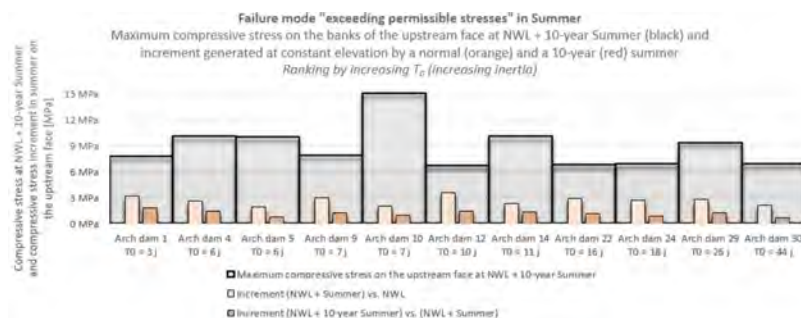


Fig. 11

Maximum compressive stress on the upstream face at NWL + 10-year Summer, and compressive stress increment on the upstream face generated at constant reservoir level by a normal and 10-year summer.

Contrainte de compression maximale sur le parement amont à RN + Été décennal, et incrément de contrainte de compression sur le parement amont engendré à cote constante par un été normal et décennal.

3.3. DISCUSSION OF THE BENEFITS OF INCREASED THERMAL LOADING MODELLING

In view of the elements highlighted in this chapter, the modelling of 10-year thermal loads highlights the following elements for the different failure mechanisms considered:

- Justifying the potential mode of failure by sliding along an abutment under the effect of increased summer loading sometimes required additional calculations and modelling, given the increments of shear characteristics required for certain structures.
- Regarding shear failure mechanism at the foot of the central blocks, the modelling, particularly in winter, did not reveal any sensitivities that had not already been highlighted with average seasonal loads. Nevertheless, it should be remembered that historically it is these situations that have led to

- significant uplift propagation near the downstream foot under certain arch dams, leading in some cases to reinforcement work [6].
- About exceeding permissible stresses, despite a wide disparity in the results for the arch dams studied, the compression increments under increased thermal loads are far from leading to the required criteria being exceeded.

Thus, the modelling of increased thermal loads appears to be more of a sensitivity study. However, such modelling is particularly useful during periods of heat-wave or extreme cold, in order to “anticipate” the potential behavior of the dam and identify areas requiring special monitoring, as was the case during the summer of 2022, presented in the following chapter.

4. FEEDBACK ON THE SUMMER HEATWAVE OF 2022

4.1. CHARACTERIZATION OF THE 2022 HEAT WAVE IN FRANCE

A heatwave like the one in the summer of 2022 can be revealed by various indicators: Météo France has identified 45 heatwaves since 1947, characterized by their duration (in days) and maximum intensity (in °C) (Fig. 12). The July 2022 episode began on July 12 and lasted 14 days. It ranks 5th by duration (since 1947) and 3rd by intensity, behind 2003 and 2019. In terms of severity (a Météo France indicator that combines duration and intensity), the July 2022 episode ranks 6th. The 2003 heatwave remains the benchmark heatwave in mainland France.

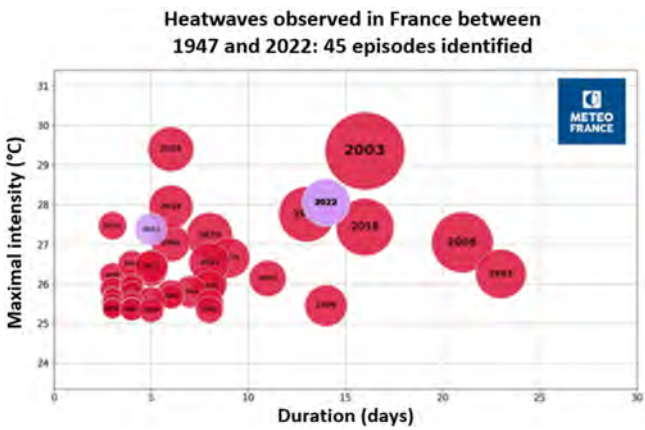


Fig. 12
Comparison by Météo France of episodes classified as heatwaves since 1947.
Comparaison par Météo France des épisodes classés caniculaires depuis 1947.

The 2022 heatwave is also characterized by limited water supply. Météo France reports that precipitation has been very low since 1st July 2022 over almost all of France. July 2022 could be one of the least-watered July months since 1959.

The consequence of limited water inflow is a lower summer water level than usual on some structures, such as the one below.

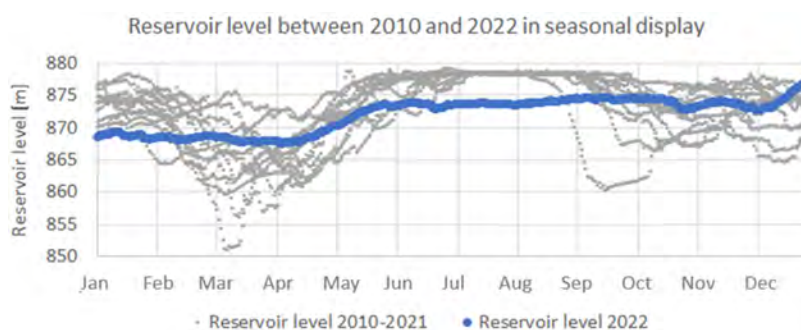


Fig. 13

2010 to 2022 reservoir rating example in seasonal display – The 2022 reservoir rating is shown in blue (lower than usual in summer) and the 2011 to 2021 reservoir ratings are shown in grey for comparison.

Exemple de cote de retenue de 2010 à 2022 en affichage saisonnier – la cote de retenue 2022 est en bleu (cote plus basse que d'habitude en été) et les cotes de retenue 2011 à 2021 sont indiquées en gris pour comparaison.

4.2. COMMENTS ON MONITORING MEASUREMENTS

From mid-July onwards, concomitant with but a few days later than the onset of the heatwave, some arch dams experienced historic upstream displacements. Fig. 14 shows a time series example of an upstream-downstream displacement in the crown of the arch dam.

The July 2022 values clearly exceed the latest historical values, with an additional upstream positioning of 2.6 mm in 2022 compared with the last historical value in 2007. The HSTT model estimates the seasonal mean increment due to the 2022 heatwave at 1.6 mm (compared with 2.0 mm in 2003), the absolute upstream displacement also being strongly influenced by a lower reservoir level than in previous summers.

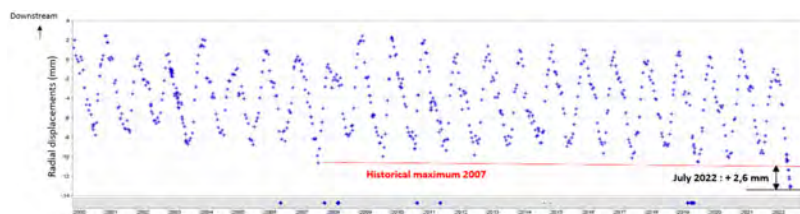


Fig. 14

Example of an upstream-downstream displacement time series in crown. Values are raw data, i.e. uncorrected (de-influenced) for the reversible effects of reservoir level and air temperature.

Exemple de série chronologique de déplacement amont-aval en clé. Les valeurs sont des données brutes, c'est-à-dire non corrigées (désinfluencées) des effets réversibles de la cote de retenue et de la température de l'air.

4.3. MEASUREMENT DIFFICULTIES

During the heatwave, feedback from the field (from operators and engineers) revealed that some sites were experiencing difficulties or impossibility in carrying out measurements using pendulums, due to functional problems. Indeed, some of the pendulum wires were very close to the limits of their free range, and in some cases were even at an abutment. In Fig. 15, it can be seen that, as the structure moves upstream, the pendulum wire almost touches the reading table, making it impossible to carry out the measurement. It is therefore necessary to move the measuring table. The limitation to the movement of the pendulum wire may come from the measuring table, the remote pendulum frame (if present) or the casing or borehole in which the wire is located. When the wire touches the pendulum table, the table can be shifted. However, when the wire touches the casing, it is generally not possible to intervene quickly, as the solutions to be implemented are more complex (creating a new borehole, moving the anchor head, etc.).



Fig. 15

As the structure moves upstream, the pendulum wire almost touches the reading table, making it impossible to take the measurement.

Sous l'effet du déplacement de l'ouvrage vers l'amont, le fil de pendule touche ici quasiment la table de lecture, ce qui ne permet plus la réalisation de la mesure.

4.4. ENHANCED SURVEILLANCE

Based on the analyses of the mechanical behavior of concrete dams and in particular arch dams (finite element modelling), the results of which are summarized in § 3, certain structures whose mechanical behavior might, as a precaution, require special attention in the event of higher summer temperatures, were studied.

4.4.1. *Enhanced monitoring*

Initially, the following criteria were selected for structures that might require close monitoring:

- Structures with concrete swelling pathology leading to significant irreversible upstream displacement.
- Structures whose behavioural analysis reveals significant tensile stresses in the downstream face in summer (higher than about 3 MPa).
- Structures with cracks in the downstream face, parallel to the abutments and potentially reactivated or accentuated in the event of increased thermal loading.
- Structures supported by one or more bank abutments whose stability in summer is close to limit criteria.

This analysis focused mainly on arch dams, as other types of dams are less sensitive to the stresses caused by thermal expansion of concrete. Finally, around twenty of the 80 arch dams and multi-arch dam dams in the EDF fleet were concerned by an enhanced monitoring.

4.4.2. *Prioritisation*

Secondly, it also appeared necessary to prioritise these structures in order to distribute the close monitoring actions chronologically. This prioritisation was based on the following 3 criteria:

- Presence (or not) of a monitoring device for the most prevalent failure mechanism in the summer period (based on the most recent behavioural analysis) that can be measured quickly.
- Reservoir elevation during the period under consideration (a low elevation combines two unfavourable effects: the lower hydrostatic load positions the structure further upstream, and a greater surface area of the upstream face is exposed to the air, accentuating the effect of hot thermal conditions).
- Pre-existing disorders and pathologies (foot cracks, swelling).

Various types of enhanced monitoring recommendations were proposed by mutual agreement between engineering and operations:

- Recommendation type A: Carry out topographic measurements during the heatwave phase to determine the specific behavior of certain arch dams. The results of a digital twin named SITCOM (SimulaTion du COMportement des barrages) are used to simulate the raw data over a few days, knowing the evolution of the reservoir level and air temperature.
- Type B recommendation: Weekly clock measurements.
- Recommendation type C: Targeted visual inspection by a specialist: detailed inspection of specific areas, in particular by monitoring or searching for cracks on the downstream face in areas assessed as potentially in tension by the FEA.

Structures subject to close monitoring recommendations were examined every week, and enhanced monitoring was adjusted according to weather conditions and monitoring progress (monitoring measurements and/or visual inspections).

4.5. ASSESSMENT OF STRUCTURE BEHAVIOR

The heatwave ended at the end of August.

An initial assessment at the beginning of September showed that most of the dams experienced perfectly reversible phenomena, reflecting their good behavior following the heatwave. Only a few dams, with high thermal inertia or low impoundment levels, were still being closely monitored at the beginning of September to ensure that they were behaving properly. By the end of September 2022, no dams were still under close surveillance.

23 arch dams in upstream positions exceeded their measurement history (observed or simulated) this summer, with generally two types of situations observed:

- Arch dams with swelling pathology (and which tend to exceed the maximum upstream position every summer).
- Arch dams with an exceptionally low reservoir in 2022.

It is worth highlighting the good behavior of all the park's structures, for which no significant damage or irreversible behavior has been identified.

4.6. COMPARISON OF THE 10-YEAR LOAD CASE (D_{10}) AND THE EFFECTS OF DIFFERENT HEATWAVES

In order to compare the effect of different periods of heatwave and extreme cold, it is possible to track the thermal effect calculated with the HSTT model based on seasonal effects (identical each year) cumulated with seasonal deviations. Fig. 16 shows the effects of the 2003 heatwave and the 2012 period of intense cold on an example of crown radial displacement. The structure studied has historically experienced colder periods than 2012, but that the 2003 heatwave was the most severe.

Fig. 16 also shows the position of the D_{10} summer and winter 10-year increments, the calculation methodology for which was described at the start of this article. Analysis of the curve confirms the 10-year nature of thermal loading, since the D_{10} value is reached approximately once every 10 years for heatwaves and less than once every 10 years for extreme cold. In our methodology, D_{10} is cumulated at the maximum (resp. minimum) of the seasonal function, which is not systematically the case in actual climatic events.

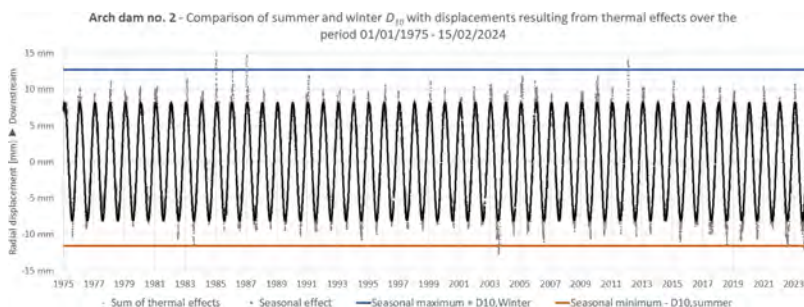


Fig. 16

Time series of thermal displacements and positioning of D_{10} (radial displacement increments) in summer and winter from 1975 to 2024.

Série chronologique des déplacements d'origine thermique et positionnement des D_{10} (incréments de déplacement radiaux) été et hiver de 1975 à 2024.

5. CONCLUSION

This article presents the methodology developed by EDF to take account of exceptional meteorological events, for the justification of arch dam behavior, applicable in countries with seasonal temperature variations.

This methodology has been developed to characterize the increase in thermal loading of an arch dam using the HSTT method. It meets the French guidelines proposal, which recommend more detailed study of certain dams presenting vulnerability to thermal conditions. Although the method only applies to operating dams that have been in existence for many years, and requires reliable, qualified measurements of air temperature and dam crest displacement, it also has many positive aspects. First and foremost, its uniformity means that all structures can be treated under equal conditions. Simple to implement, it limits the need for assumptions concerning the thermal properties of materials and the choice of climatic scenarios. Finally, it is based on monitoring data that are representative of actual dam behavior.

The inclusion of 10-year thermal loads has generally had only a limited impact on the assessment of structures under thermal loading. In most cases, their modelling did not reveal any sensitivities that had not already been highlighted with average seasonal loads. 10-year thermal loads therefore appear more like sensitivity studies regarding a potential failure mechanism. Nevertheless, in certain cases, additional calculations with more advanced modelling have sometimes been undertaken to justify a potential failure mode.

These conclusions, drawn from numerical models, are consistent with observations relayed by detailed monitoring of structures during exceptional climatic events, such as the 2022 heatwave in France. Enhanced monitoring of certain arch dams particularly vulnerable to thermal conditions during this heatwave episode is a prudent approach proposed by engineering. This allowed to collect monitoring measurements in atypical situations, which will help to better calibrate dam behavior models. Feedback from this monitoring also highlights some difficulties in carrying out measurements, which can however be anticipated. In the end, the enhanced monitoring in summer 2022 confirmed the good behavior of the thermally sensitive arch dams, thanks to the perfect reversibility of the phenomena monitored.

REFERENCES

- [1] CFBR, *Recommandations provisoires pour la justification du comportement des barrages-voûtes – Octobre 2018*.
- [2] PENOT & FABRE & DAUMAS, 2009. Analyse et modélisation du comportement des ouvrages de génie-civil par la prise en compte des températures de l'air: méthode HST Thermique. *Q91-R60, Commission internationale des grands barrages, Brasilia*, 2009.
- [3] E. ROBBE, L. SUCHIER, A. SIMON, T. GUILLOTEAU. Characterization of arch dam's behavior during increased thermal load such as heat or cold wave – *12st ICOLD European Club Symposium – Interlaken 5-8 September 2023*.
- [4] E. ROBBE, L. SUCHIER, A. SIMON, T. GUILLOTEAU. Characterization of arch dam's behavior during increased thermal load such as heat or cold wave – *Symposium "Management for Safe Dams" – 91st Annual ICOLD Meeting – Gothenburg 13-14 June 2023*.
- [5] E. ROBBE, D. ANDRIAN, N. ULRICH, C. JOUY. Cisaillement à l'interface béton-rocher des barrages voûtes: retour d'expérience de voûtes existantes – *27ème congrès des grands barrages. Marseille, Juin 2022*.
- [6] E. ROBBE, F. MOREL, Laouzas dam: behavior of an arch dam in a wide valley and foundation stability improvement, *2021 USSD annual conf.*

COMMISSION INTERNATIONALE DES
GRANDS BARRAGES

VINGT-HUITIEME CONGRES DES
GRANDS BARRAGES
CHENGDU, Mai 2025

BUILDING A RESILIENT SYSTEM AGAINST FLOOD IN THE RHÔNE DELTA (*)

Thibaut MALLET

General manager of SYMADREM, Arles

Mark CHEETHAM

Expert SNCF RESEAU, Directions techniques Réseau, Paris

Philippe PELT

Project manager SYSTRA, Marseille

Jean-Jacques FRY

Consultant, retired from EDF Hydro, Le Bourget du Lac

Rémy TOURMENT

Expert INRAE, Aix-en-Provence

Pierre BALAYN

Project manager CNR ingénierie, Lyon

Mathieu NORMAND & Fabienne SCERRI

Project managers EGIS, Montpellier

Laurent POLLY

Project manager Suez Consulting, Aix-en-Provence

Akim SALMI

Project manager ISL ingénierie, Montpellier

Eric VUILLERMET

Project manager BRL ingénierie, Nîmes

FRANCE

*Construction d'un système résilient de protection contre les crues dans le delta du Rhône

SUMMARY

The 100-year flood of December 2003 caused 4 breaches in the levees of the large Rhône delta, resulting in the release of 217 million m³ into the protected area, flooding more than 12,000 persons and generating 700 million euros in damage. It revealed the need for a coherent and mutually supportive flood prevention policy for the whole Rhône watershed, which led to the implementation of an inter-regional project under the aegis of the State and the regions, known as the “Plan Rhône”. The €450 million flood protection program carried out under SYMADREM's management is one of the main components of this plan.

Rather than raising the levees, which until now has been the response of the public authorities after each flooding, the following principles have been adopted:

- Accept flooding for rare floods (100-year floods upstream of Arles and 50-year floods downstream of Arles);
- Consider breach formation as unacceptable up to the 1000-year flood.

This involves securing the entire levee system up to the 1000-year flood, implementing spillways on levees and draining the volumes of water spills to the sea.

Between 2003 and 2023, 73 km of river levees were secured (out of 227 km), including the construction of 10 km of levees resistant to overflow (local name to make acceptable the notion of “spillways”) between Beaucaire and Arles, for a total of €220 million out of the €450 million needed to secure the entire protection system. Major works (€70 million) to make the railway embankment between Tarascon and Arles hydraulically transparent have also been carried out by the SNCF train company to allow floods to pass through.

This report reviews the key elements of these 20 years of consultations, studies and works. The first chapter is devoted to the historical context: the construction, after the catastrophic floods of 1840 and 1856, of levees described as unsinkable, and the main accidentology findings based on the 114 breaches and breaches in progress recorded since 1840. The second chapter briefly recalls the course and outcome of the 100-year flood of December 2003, the highest flood since 1856, before detailing the response provided by the “Plan Rhône”: a paradigm shift based on the acceptance of flooding and the development of a risk culture. In particular, this chapter highlights the significant shift from the random, unpredictable and very high risk of flooding due to breaching to the certain, predictable and very low risk of flooding due to overflow without breaching. The third and fourth chapters deal respectively with the hydraulic design of the front line protection system and the management of the volumes spilled once the Rhône has overtopped the levees resistant to overflow: second line levees, hydraulic transparency of a railway embankment and embanked canals.

The fifth chapter is devoted to the definition of the system's danger level and the ensuing lessons learned (adapting the design of levees located upstream of the system). The sixth chapter deals with the choices made for the design and sizing of urban structures (quays, masonry levees) and those built outside towns (embankment levees not reinforced against overtopping and levees resistant to overflow). The conclusion describes the benefits of the works, up to its current progress and concludes with the interactive digital mapping that has been set up to create a real memory and culture of risk throughout the delta.

RÉSUMÉ

La crue « centennale » de décembre 2003, qui a occasionné 4 brèches dans les digues du grand delta du Rhône provoquant le déversement de 217 millions de m³ dans la zone protégée, l'inondation de plus 12 000 personnes et générant 700 millions d'euros de dommage, a révélé la nécessité d'une politique de prévention des inondations cohérente et solidaire sur l'ensemble du bassin rhodanien. Elle s'est traduite par la mise en œuvre d'un projet interrégional sous l'égide de l'État et des régions : le plan Rhône. Le programme de sécurisation mené sous maîtrise d'ouvrage du SYMADREM, d'un montant de 450 millions d'euros, est l'une des principales composantes du volet inondations de ce plan.

Plutôt que de rehausser les digues, ce qui avait été, jusque-là, la réponse apportée par les pouvoirs publics après chaque inondation, les principes suivants ont été retenus :

- Accepter les inondations pour les crues rares (crue centennale en amont d'Arles et cinquantennale en aval d'Arles) ;
- Considérer la formation de brèche comme inacceptable jusqu'à la crue millénale.

Ce choix passe par une sécurisation complète des systèmes d'endiguement jusqu'à la crue millénale, la réalisation de digues résistantes à la surverse et la gestion et le ressuyage des volumes d'eaux déversées.

De 2003 à 2023, 73 km de digues fluviales ont été sécurisées (sur 227 km) avec la réalisation notamment de 10 km de digues résistantes entre Beaucaire et Arles, pour un montant total de 220 millions d'euros sur les 450 millions nécessaires à la sécurisation globale du système de protection. D'importants travaux (70 millions d'euros) de mise en transparence hydraulique du remblai ferroviaire entre Tarascon et Arles ont également été réalisés par la SNCF pour permettre le transit des crues débordantes.

Le présent rapport revient sur les éléments essentiels de ces 20 années de concertation, d'études et de travaux. Le premier chapitre est consacré au contexte historique : la construction, après les inondations catastrophiques de 1840 et 1856, de digues qualifiées d'insubmersibles ainsi que les principaux enseignements de l'accidentologie basées sur les 114 départs de brèches et de brèches recensées depuis 1840. Le second chapitre rappelle rapidement le déroulement et le bilan de la crue centennale de décembre 2003, la plus forte crue depuis 1856 avant de détailler la réponse apportée par le plan Rhône : un changement de paradigme fondé sur l'acceptation des inondations et le développement d'une culture du risque. Ce chapitre pointe notamment le passage sensible d'un risque aléatoire, imprévisible et très fort d'inondation par brèche au risque certain, prévisible et très faible d'inondation par surverse sans brèche. Les troisièmes et quatrièmes chapitres évoquent respectivement la conception hydraulique du système de protection de 1er rang et la gestion des volumes déversés une fois les digues résistantes à la surverse franchies par le Rhône : digues de 2^{ème} rang, transparence hydraulique d'un remblai ferroviaire et de canaux en remblai. Le cinquième chapitre est consacrée à la définition de la cote de danger du système et l'enseignement qui a suivi (adaptation de la conception des digues situés en amont du système). Le sixième chapitre traite des choix opérés pour la conception et le dimensionnement des ouvrages urbains (quais, digues maçonnées) et ceux réalisés hors des villes (digue en terre non renforcées au déversement et digue résistante à la surverse). La conclusion décrit les bénéfices apportés par les travaux en fonction de l'état d'avancement des travaux pour conclure sur la cartographie numérique interactive mise en place pour faire émerger une véritable mémoire et culture du risque à l'échelle du delta.

1. INTRODUCTION

The Rhône delta, located downstream of the Rhône watershed, covers an area of 1500 km², where 100 000 people permanently live (X3 during the summer season). The territory is protected by three river levee systems (225 km) and a coastal levee system (50km), managed by the Syndicat Mixte Interrégional d'Aménagement des Dignes du Delta du Rhône et de la Mer (SYMADREM), a public institution created in 1999 following the floods of 1993/1994 and the failure of the associations of riparian owners who had been managing the structures since the middle of the 19th century.

These structures were designed as levees systems after the catastrophic floods of 1840 and 1856 (return periods estimated at 300 and 200 years respectively) in place of other even older structures, some of which date back to the 12th century. Due to their construction technique (compaction with 15 kg manual tamping devices, not taking into account the optimum water content concept discovered in 1933 by Ralph Proctor and the "onion" effect due to successive raising phases), the Rhône levees are highly vulnerable to failures by internal erosion, although described, by civil engineers, at the

time they were built, as “non submersible levees”. 114 breaches and breaches in progress have been identified since 1840 [14]. The main cause is internal erosion and more precisely concentrated leak erosion through badger burrowing [13] or along crossing pipes (80% and 20 % of cases respectively).

The probability of a breach in 19th century levees, confirmed by historical floods is more than 50% once the Rhône flow reaches 9,500 m³/s and passes 100% for a 10,500 m³/s flow rate [15] (all flows are given at the Beaucaire/Tarascon reference station upstream of the large delta). Hydrological data actualized in 2018 [1] are shown in table 1.



Fig. 1
successive stages of elevation of Rhône Delta levees since the 12th century to 2003 (left) and a badger burrow (right) (©SYMADREM)
Stades successifs d'élévation des digues du delta du Rhône depuis le XII^e siècle jusqu'en 2003 (à gauche) et terrier de blaireau (à droite) (©SYMADREM)

Table 1
Peak flow for the Rhône at Beaucaire/Tarascon and return period [1]

RETURN PERIOD (IN YEARS)	PEAK DISCHARGE (m ³ /s)			
	FOR HYDROLOGICAL YEAR (NOV. TO OCT.)		FOR CIVIL YEAR (JAN. TO DEC.)	
	GUMBEL	GEV*	GUMBEL	GEV
1	4 030	4 020	4 060	4 090
5	7 730	7 710	7 840	7 640
10	8 910	8 770	9 030	8 670
50	11 480	10 920	11 660	10 770
100	12 570	11 770	12 770	11 600
500	15 090	13 580	15 340	13 390
1000	16 170	14 310	16 440	14 110
5000	18 680	15 880	19 000	15 670

* GEV (Generalized Extreme Value) hydrological data used by SYMADREM

Eight major Rhône floodings have taken place on the territory since 1840, leading each time to the spilling of several hundreds of millions of cubic meters in the protected area and creating several hundreds of millions of euros in damages.

2. PARADIGM SHIFT FOLLOWING THE DECEMBER 2003 FLOOD

2.1. THE DECEMBER 2003 FLOOD AND THE RESPONSE: THE PLAN RHÔNE

The “centennial” flood of the 3rd and 4th December 2003 ($11,500 \text{ m}^3/\text{s} \pm 5 \%$), which caused 4 breaches in the protective structures of the large Rhône delta, resulting in the spillage of 227 million m^3 , the flooding of more than 12,000 persons and generating 700 million euros in damages, revealed the need for a coherent and mutually supportive flood prevention policy throughout the Rhône watershed: The Plan Rhône [7]. The SYMADREM has included the flood elements of this plan in a safety program for the levees from the Vallabrègues dam to the sea [11].

Rather than raising the levees, which had been the response of public authorities after each flooding, the following principles were adopted:

- Not heightening the levees to avoid transferring inevitable water spills upstream, downstream or on to the opposite bank;
- Accepting overflow for rare floods (flow over $11,500 \text{ m}^3/\text{s}$ upstream Arles and over $10,500 \text{ m}^3/\text{s}$ downstream Arles), qualified as protection floods, with an equal amount of water spilled on each riverbank (this last choice was political);
- Considering breach formation as unacceptable below a flow rate of $14,160 \text{ m}^3/\text{s}$ (exceptional flood with a return period around 1,000 years), qualified as safety flood.

This choice involves:

- Securing the entire levees system to avoid any breach up to the safety flood;
- Implementation of spillways on levees to resist overflows above the protection floods;
- Implementation of structures for drainage of the protected area to halve the duration of flooding.

An environmental strategy, based on the avoidance of environmental issues and the ecological enhancement of the river banks, has been put in place to accompany these works [19]. Climate change (possible increase in flood frequency and certain rise in sea level [11]) has been considered in design scenarios.



Fig. 2

Flooding of the Rhône delta in December 2003 (© Spot image, SDIS13 and J. Roche)
Inondation du delta du Rhône en décembre 2003 (© Spot image, SDIS13 et J. Roche)

2.2. CONSULTATION, CONFRONTATION AND ACCEPTATION

Many concertation meetings were required to make acceptable the change from managing a very high risk of unpredictable breach towards a very low risk of certain and predictable overflow without breach. They were organized with the support of the State services and locally relayed by SYMADREM.

2.2.1. *First public meetings: the gap between the information sent to the public and the information understood by the public*

The hydraulic design of the system was mainly dictated by the morphology of the river as it flows through Arles, the main town in the Rhône delta (population of 52,000) located just downstream of the Rhône diffuence. This location is characterised by an “abrupt” narrowing of the active (unprotected) major bed, from a width of 2 km to zero km, and of the minor bed, from a width of 400 metres to 150 metres. This narrowing is characterised by a steep hydraulic gradient (0.2%) over 300 metres, compared with 0.03% upstream and 0.01% downstream. Flow velocity exceeds 4 m/s, with a head loss of around 1 metre for the important flood events. This bottleneck constitutes a “control section”, which limits the flow capable of passing through Arles during major floods and increases the risk of overtopping with breaches upstream of Arles.

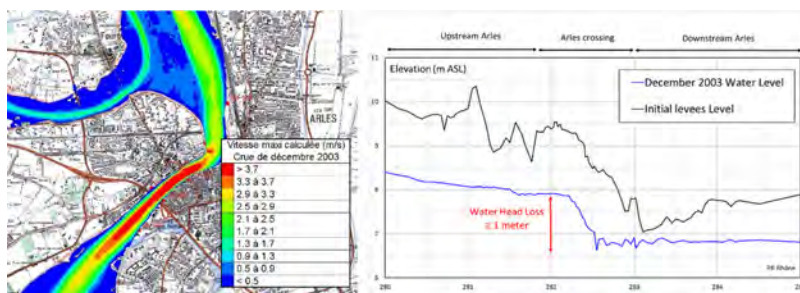


Fig. 3

Flow velocity in 2003 (left) and headloss (right) crossing Arles

Vitesse d'écoulement en 2003 (à gauche) et perte de charge (à droite) dans la traversée d'Arles

During the initial public meetings, the message from the public authorities was as follows: *"The capacity of the river through Arles is 11,900 m³/s. The Rhône's exceptional flood of 14,160 m³/s cannot flow through Arles without overtopping. It is therefore necessary to build overflowing levees to organise overflow upstream of Arles in order to limit the flow through Arles"*.

"Saving the town of Arles by flooding the countryside" was the initial message understood by the people living on the cultivated floodplains between Beaucaire/Tarascon and Arles. Many demonstrations were organised to oppose this "sacrifice" of the rural population for the benefit of the urban population. The creation of a flood canal to bypass Arles, in consultation with the local population, even had to be studied and appraised by the State [5]. But this solution was finally abandoned, given its low hydraulic efficiency and the fact that it did not obviate the need to renovate the "unsinkable" 19th-century levees.



Fig. 4

Demonstrations against the project (©La Provence, SYMADREM)

Manifestations contre le projet (©La Provence, SYMADREM)

2.2.2. Communication focused around the negative consequences of inaction and the benefits of action

While the term “spillway” was never used in the public meetings, as it was considered misleading, the term “overflowing levee” was also considered inappropriate, after several public meetings as it was equated with voluntary flooding. SYMADREM decided to replace the initial information with a new one: « *The bottleneck at Arles, which cannot be modified even by creating a bypass canal, causes the river level to rise upstream of Arles, resulting in overtopping with levee breaching in agricultural areas. As these structures are not designed to resist overtopping, they need to be reinforced to prevent breaches during overflow floods. Inaction means living with breaches during floods. Building levees resisting to overflow means accepting rare flooding with lower water levels that can be managed by stakeholders involved in crisis management* ».

It was also decided to change the term “overflow levees” to “levees resistant to overflow”, which is more appropriate to the functionality of the new system and more acceptable to the public.

SYMADREM also built its communication strategy by comparing the risk associated with inaction (remaining in the initial state with breaches during floods) to the risk of overtopping without breaches. Figures and photos such as the following were presented and explained at the meetings.

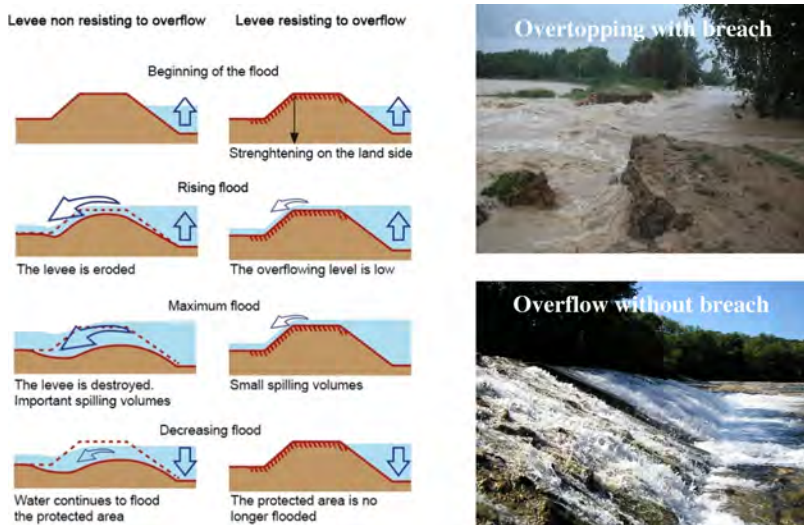


Fig. 5

Comparison between overtopping with breach and spillway flow without levee breaching (© SYMADREM and Aimargues)

Comparaison entre la surverse avec brèche et sans brèche (© SYMADREM et Aimargues)

Visualisation of inundation mapping with and without breaches allowed the public to compare the initial state with the projected state.

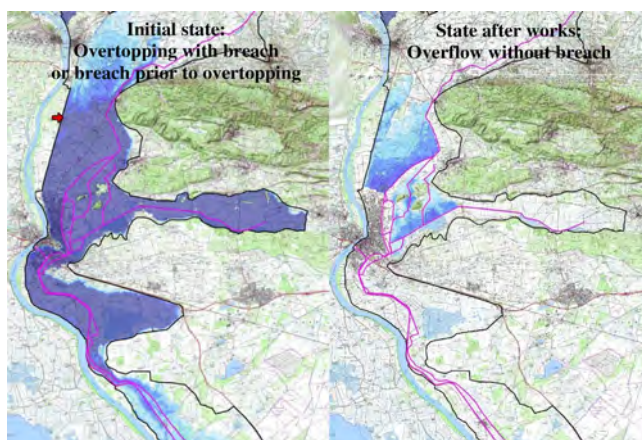


Fig. 6

Inundation mapping with and without breaches for the left bank levees system
(modelling EGIS)

*Cartographie des inondations avec et sans brèches dans le système d'endiguement
rive gauche (modélisation EGIS)*

The choice of words, the in-depth study of alternative scenarios requested by the public, the use of hydraulic modelling to compare the risk associated with breaches in the event of inaction and the risk associated with overflow without a breach in the event of action, all helped to convince virtually the entire population.

3. HYDRAULIC DESIGN OF LEVEES SYSTEM

3.1. TYPOLOGY OF LEVEES AND CHOICE OF LEVELS OF PROTECTION, OF SAFETY AND OF DANGER

The safety program for the levees includes:

- 25 km of levees resistant to overflow set at protection level, as defined below,
- 202 km of so-called “millennial” levees, not designed to resist to overflow, set 50 cm above the safety level as defined below,

- close protection levees, also called second line levees, in densely populated areas.

The hydraulic design of the system [12] has been based on three levels defined as follows:

- **The protection level** (level of first spills) corresponds, on the Rhône between Beaucaire and Arles, to the water level reached for a flood with a peak flow estimated at $11,500 \text{ m}^3/\text{s} \pm 5\%$ (\cong 100-year flood). Downstream of Arles, this elevation corresponds to the water level reached for a flood with an estimated peak discharge of $10,500 \text{ m}^3/\text{s}$ (\cong 50-year flood).
- **The safety level** corresponds to the water level reached by the exceptional flood of the Rhône, whose peak flow is estimated at $14,160 \text{ m}^3/\text{s}$ (\cong 1,000-year flood). At this level, levees must have a sufficient safety margin to ensure that the probability of breach is very low (since 2017, French regulations have required a breach probability of less than or equal to 5%, but SYMADREM's choices have led to a conditional breach probability for the safety flood of significantly less than 1% [15]).
- **The danger level** corresponds to the level of the crest of the so-called "millennial" levees, i.e. 50 cm above the safety level. This is the level above which the structure is likely to suffer major damage that could quickly lead to failure (high probability of breach).

A 50 cm freeboard, corresponding to the difference between the safety and the danger levels, has been adopted. It takes into account the hydrological and hydraulic uncertainties of the system, estimated at 30 cm, the uncertainty linked to digital modelling, the absolute accuracy of which is estimated at 20 cm, and the 35 cm uncertainty linked to the effect of wind-generated waves (waves of 20 to 30 cm observed locally during the December 2003 flood, but strongly attenuated by the riparian vegetation adjacent to levees) [12].

3.2. BUILDING OF THE HYDRAULIC MODEL, CALIBRATION AND SENSITIVITY ANALYSIS

CNR_{ingénierie} was commissioned to carry out a study to hydraulic design the structures between Beaucaire and Arles. The used model includes the river bed between levees from downstream of the Vallabrègues dam to the sea, except downstream of the Grand Rhône. It is a 2D model (TELEMAC code developed by EDF) with a 315,000 elements mesh. It was built from a digital terrain model (topographic survey using helicopter-borne LIDAR with an x,y,z accuracy of around 3 cm) and very accurate bathymetry. The model was calibrated against the December 2003 flood on the basis of 9 CNR water level gauges and the available high-water marks, and is estimated to have an absolute accuracy of 10 cm in the minor bed, 20 cm through Arles and 30 cm in the major bed, i.e. the order of accuracy of the measurements [12]. In addition, a sensitivity analysis on the calculated levels was

carried out on the following parameters: calibration flow, roughness coefficients in the minor bed and variation in bathymetry between 2002 and 2007. It demonstrated the hydraulic consistency of the modelling and validated the use of the model to compare different flood scenarios.

3.3. SETTING THE RHÔNE LEVEES AND SENSITIVITY ANALYSIS

The various stages of the calibration were as follows:

- Identification of low points across the towns of Arles, Beaucaire and Tarascon (masonry structures),
- Determination of the maximum water level acceptable through Arles for the exceptional flood, corresponding to the lowest point (danger elevation) minus the 50 cm freeboard,
- Adjustment of levees resistant to overflow so as to:
 - Prevent any overflow upstream Arles up to the protection level,
 - Above this level, ensure equal distribution of overflow volumes between the two banks of the Rhône (political choice),
 - Limit the level through Arles for the safety flood to the maximum acceptable level (safety level of the structure),
 - Guarantee the absence of impacts on water levels upstream and downstream spillways up to the safety flood.

These objectives involved :

- Setting the structures located upstream and downstream of the levees resisting to overflow to a so-called millennial flood level in order to avoid any risk of bypassing during overflowing floods,
- Checking that the freeboard at the masonry structures (quays) through Arles, Beaucaire and Tarascon, whose elevation could not be modified, was sufficient.

The calibration focused on three parameters: the layout, the length of the overflow and the protection level (centimetre variation around the predetermined protection objective). A sensitivity analysis was also carried out on the following parameters: discharge coefficient, influence of sea level, flood gradient. It helped to determine the freeboard value.

The design of the spillway lengths was the subject of several tests. In the end, the decisive criterion for sizing the lengths was the absence of any significant hydraulic impact upstream and downstream, which led to the choice of five km of levees resistant to overflow on each bank.

3.4. CHOICE OF DISCHARGE COEFFICIENT FOR LATERAL OVERFLOW AND SENSITIVITY TO LEVELS

The assessment of lateral overflow (perpendicular to the main flow of the river) and the associated discharge coefficient was a particularly sensitive stage in the hydraulic design of the levees resisting to overflow. On the basis of existing literature [6] and its own experience with physical models, CNR_{ingénierie} used a discharge coefficient of 0.25 and 0.27 for overflowing water levels of 20 and 30 cm respectively (which is consistent with Dominguez formula).

A sensitivity analysis was carried out for the safety flood with a discharge coefficient of respectively [0.21; 0.27; 0.33] (variation of $\pm 20\%$ around the “nominal” value). The impact of underestimating or overestimating the lateral threshold flow coefficient by 20% is reflected respectively in:

- a rise or a fall in the calculated level, averaging between 1 and 3 cm over the whole of the sector affected,
- a decrease or increase in flow rates and volumes discharged of around 10% for the exceptional flood scenario.

The system is therefore not very sensitive to the discharge coefficient considered, which can be explained by the presence of the “control section” found in Arles’ narrowing. The diagram below provides a simplified illustration of the “self-regulation” of spill flows/calculated levels following a deterioration in the flow rate of the spill sections. The adjacent figure illustrates the principle of altimeter setting for the new levees.

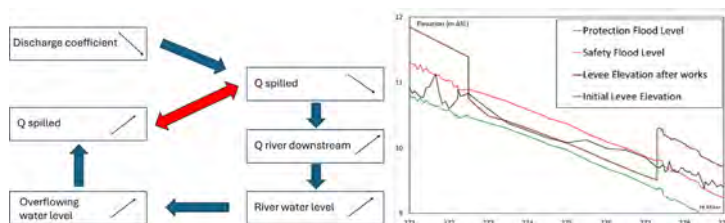


Fig. 7

Self-regulation of overflow (left) and principles of altimeter setting between old and new levees (right)

Autorégulation des déversements (à gauche) et principes du calage altimétrique entre les anciennes et les nouvelles digues (à droite)

CNR_{ingénierie}'s conclusion on the calibration of the sections resistant to overflow is that it is robust and not very sensitive to the considered flow coefficient and therefore ultimately to the engineer's assumptions. The difference in levels between

the sections resistant to overflow and the sections not designed to resist to overflow is 80 cm (30 cm of overtopping water between the protection and safety floods and 50 cm of freeboard). Similar calibration on the Petit Rhône and the Grand Rhône have been carried out by EGIS and CNR_{ingénierie} respectively.

For the safety flood (1,000-year flood), the overflowing discharge and spilled volumes are for each bank 1,000 m³/s and 100 millions m³ ± 20 % respectively.

The following diagram shows the layout of the levees resisting to overflow. Those upstream of Arles were carried out between 2016 and 2021 and those downstream of Arles are planned in the next ten years.

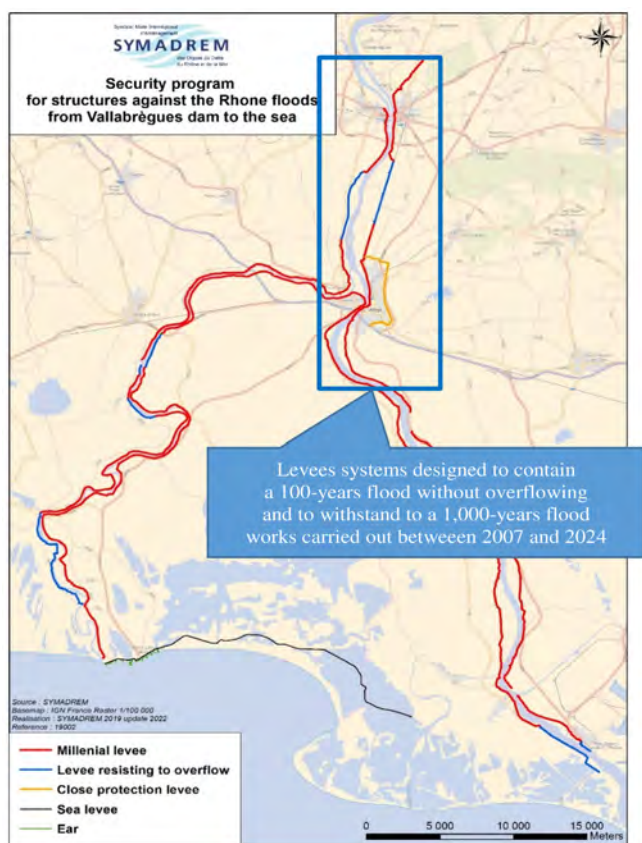


Fig. 8

Safety program in the Rhône delta (carried out and planned works)
Programme de sécurisation dans le delta du Rhône (travaux réalisés et prévus)

4. MANAGEMENT OF OVERFLOWS

4.1. MEASURES TO SPEED UP FLOOD DRAINAGE

The roof-shaped configuration of the Rhône prevents floodwaters from returning to the riverbed when it recedes. This water is then gradually drained back to the sea by a network of agricultural drainage channels. In this configuration, the time it takes for flooded land to dry out depends very much on the topography of the natural terrain and sea level. While the overall securing of the levees systems greatly reduces the volumes of water spilled and helps to significantly reduce the risk in the protected zone, measures designed to speed up flood drainage were deemed necessary to help making acceptable the principle and location of levees resistant to overflow. The aim was to halve inundation time compared to a secure system without additional drainage structures. To achieve this objective, 5 of the 11 existing pumping stations on the right bank of the Rhône were reinforced and a new station was created, increasing the pumping capacity from 45 to 74 m³/s.

On the island of Camargue, drainage is provided by 6 pumping stations with a total drainage capacity of 30 m³/s and by three gravity structures with a drainage capacity of between 20 and 35 m³/s depending on sea level. It has been decided (works planned in 2025/2026) to further reinforce this system by adding another station with a capacity of 8 m³/s, doubling the main gravity structure and rehabilitating the other structures, thereby enabling the drainage capacity to be increased from 50-65 m³/s to 73-93 m³/s depending on the sea level. The left bank was characterised by a cascading system, due to the presence of embanked canals that obstructed the flow in the event of the Rhône overflowing. This system showed its limitations in December 2003, holding back the water and worsening the floods in the city of Arles. It was therefore decided to create a second line levee as close as possible to the city centre; to make the Alpines irrigation canal hydraulically transparent over a distance of 300 m by siphoning off the canal and to create two siphons (2 x 20 m³/s) under the Vigueirat canal to help the transit of overflow water from upstream to downstream and thus halve the inundation duration (Fig 8).



Fig. 9

Flood waters from the Rhône blocked by the Vigueirat embankment canal (Dec. 2003) and creation of a siphon in 2022 (© Arles & SYMADREM)
Inondation du Rhône bloquée par le canal en remblai du Vigueirat (déc. 2003) et création d'un siphon en 2022 (© Arles & SYMADREM)

4.2. HYDRAULIC TRANSPARENCY OF THE RAILWAY EMBANKMENT BETWEEN TARASCON AND ARLES

On the left bank of the Rhône [4], flood protection had been provided by a railway embankment since 1844. As part of the Plan Rhône and after a study of different solutions [4], it was decided to create a new 9km levee, separated from the railway embankment by 15 metres, including a 5km section resistant to overflow, and to make the railway embankment hydraulically transparent up to the safety flood. The works to ensure hydraulic transparency involved installing ten reinforced concrete bridge structures 20 m wide by 4 m high in the railway embankment, spaced 500 m apart, designed to allow the total transit of 1,000 m³/s for the safety flood. The hydraulic design of these frames led to a specific study requiring, firstly, the construction of a 3D model and, secondly, of a 2D model [9]. The hydraulic uncertainties associated with the lateral overflow on the levee and the capable flows between the new levee and the railway embankment led SNCF to design the structures for 2,000 m³/s flow rate, assuming a homogeneous overflowing water level of 30 cm over 5 km. These bridge structures, each weighing 1,700 tonnes, were then pushed into the railway embankment in four operations of duration between 44h30 and 55h00, planned two years in advance, which involved cutting the railway line, dismantling the rails, clearing the embankment, pushing the structures (in less than 10 minutes!), backfilling and re-constructing the rails.



Fig. 10

Pushing concrete bridge structures (©SNCF RESEAU, SYMADREM)
Ripage des ouvrages de transparence hydraulique en béton (©SNCF RESEAU, SYMADREM)

The figure below describes how the left bank system operates during flooding.

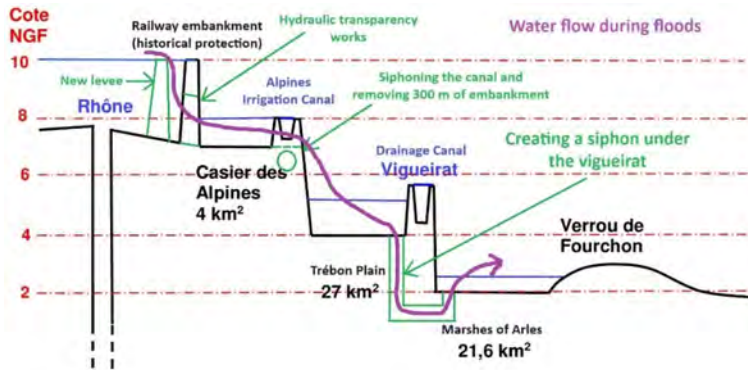


Fig. 11

Management of the spilled water on the left bank side
Gestion des eaux déversées en rive gauche

5. SYSTEM BEHAVIOUR FOR THE DANGER FLOOD AND ADAPTATION OF UPSTREAM LEVEES

Flood scenarios significantly higher than the safety flood (up to 24,000 m³/s!) have been modelled to qualify the discharge of the danger flood (the flood reaching the crest of the millennial levee). The flood control caused by the overflows between Beaucaire and Arles tends to limit the downstream water levels. On the opposite, the extra flow upstream the delta elevates the water level upstream of sections resisting to overflow. This leads possible overtopping of masonry and embankment levees upstream of the system for a discharge of 15,500 m³/s (return period over 3,000 years). Overtopping then occurs upstream of urban area before the protected area is pre-filled by spilling on levees resisting to overflow. There is therefore a risk of overflow failure, threatening the non-evacuated population.

To reduce this risk, the design of the structures was adapted to withstand a 10cm head of overflowing water. The gravel initially planned for the downstream shoulder has been replaced by small boulders (100-300 mm) on the slope and by 300/1000 kg boulders at the foot of the embankment. The operating track at the crest of the embankment, which is normally made of untreated gravel, was made of cemented gravel and given a two-layer bituminous coating.

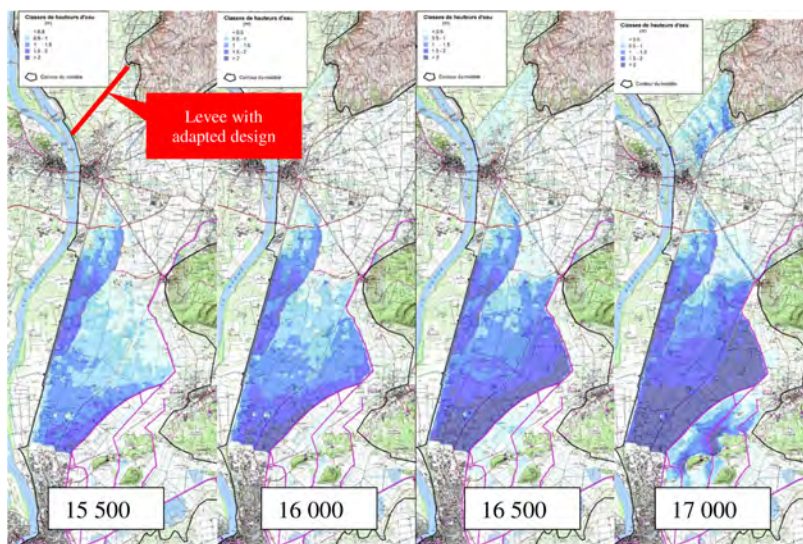


Fig. 12

Inundation mapping for discharges over safety flood (modeling EGIS)
*Cartographie des inondations pour les débits supérieurs à la crue de sécurité
(modélisation EGIS)*



Fig. 13

Drainage materials replaced by boulders to resist to overflow over danger level
(©SYMADREM)

*Matériaux de drainage remplacés par des blocs rocheux pour résister au
dérèglement au-dessus du niveau de danger*

6. MULTIPLE BARRIERS DESIGN AND WORKS PRINCIPLES

Considering its scale (more than 450 million €), the safety program has been divided into several operations, with works prioritized regarding the following requirements: human activities nearby the levees; consequences of a breach on the protected area; ownership or not of the land; regulatory procedure linked with the works; initial state of the constructions confirmed by the historical feedback or by the risks analysis; financial programming. These criteria led SYMADREM to prioritize actions in front of the urban areas and then from upstream to downstream of the delta.

The complete renovation of the protection system and the construction of safe and sustainable levees, has been based on a risk assessment and the restoring of following safety functions [15]: impermeability; resistance; filtration; drainage; stability; protection; spillway (resistance to overflow); surveillance and environment.

Impermeability is the first safety barrier in a flood defence structure. Different types of intervention were carried out. For the masonry levees, the waterproofing consisted of fully taking over the masonry by plugging the cracks [8][20], or by carrying out a new siding in shotcrete on the siding already concreted [8]. The embankment constructions [16][3] have been systematically dismantled, to break the multiple layers effect created by 800 years of successive crest raisings, and rebuilt according to current guidelines. The compactness minimum level required was 95% SPD on 100 % of control measures and the moisture content, before compaction, between 0 and 3% above the optimal moisture content (OMC) with a tolerance of 20 % of measurements between 0 and 1 % below OMC. These two parameters ensure optimal resistance to internal erosion [2]. Several construction steps are required:

- Clay filled cut off, which allows the treatment of the foundation surface layer;
- Aeration or humidification of the material to bring it to the right moisture content;
- Reduction of clods with pulvimixer to homogenise the material moisture content;
- 30 cm layer compaction by a vibrating roller with padfoot;
- Compaction control with a gamma densimeter and dynamic penetrometer.

The control plan [3] was developed as follows:

- 1 identification + sedimentology + organic matters every 2500 m³;
- 1 SPD test every 2500 m³;
- 1 moisture content carried out in a heat chamber every 200 m³;
- 1 gamma-densimeter measurement every 200 m³;
- 1 panda every 40 linear metres on 1 m depth to check homogeneity.

The filtration and drainage of the embankment and its foundation allow, in case of impermeability failure, to ensure the water flow without internal erosion. They constitute, therefore, a second safety barrier, which will increase very noticeably the levee safety level. These functions have been ensured by a filter geotextile encompassing a gravel layer (solution adopted between Beaucaire and Arles [3]) or by a geocomposite (solution adopted downstream Arles [19]). For the masonry levees, this can be achieved by a drilling of the facing, on the landward side, to improve the ability of drain possible seepages and to dissipate pore pressures within the embankment [8]. An optical fibre [10] has been installed, on an experimental basis, in the protected landward side drain of the Beaucaire / Fourques and Tarascon / Arles levees, on a linear of 22 km of levees. It will make it possible to detect very small temperature variations, an early indication of possible infiltrations in the levee during flood. This device will allow the early detection of upgradeable latent leaks; identification of potential failure warning signs in the whole filter-drain system and precisely locate the position of the leak on the monitored sections.

Stability and protection: The filter is stabilized to avoid its uplift by an embankment shoulder on the landward side, in the event of internal pressure. Slopes are softened. Furthermore, a protection against burrowing animals has been implemented to avoid the creation of new burrows (Note that 80% of the breaches by internal erosion, observed since 1993, were initiated in badger burrows [13] [14]).



Fig. 14

Components of the millennial Levee (left) and levee resisting to overflow (right) protected side (©SYMADREM)

Composants de la digue millénaire (à gauche) et de la digue résistante à la surverse (à droite) côté protégé

For the levees resisting to overflow, the landward side has been reinforced with concreted 200 to 400 kg riprap so as to resist to high flow velocities, in case of overflow. The surface of the riprap has been deliberately left rough to allow better dissipation of energy during overflow. Upstream and downstream of the spillways, the levees are set 50 cm above the millennial flood level to avoid a risk of

circumvention in case of overflowing (construction steps beside). A concrete beam, to precisely fix the overflow level and to avoid infiltration into concreted riprap, has been realized on the levee crest.



Fig. 15

Concreting of 200 to 400 kg riprap (left) and concrete beam to determine the overflow level (right) (©SYMADREM)
Bétonnage des enrochements 200/400 kg (à gauche) et poutre en béton pour caler le niveau de débordement (à droite) (©SYMADREM)

The concrete riprap has been covered with topsoil to blend in better with the landscape. Hydraulic structures crossing levees have been designed and constructed with similar principles.



Fig. 16

Levee to resisting to overflow (©SYMADREM)
Digue résistante à la surverse (©SYMADREM)

7. CONCLUSION

Between 2003 and 2023, 73 km of river levees (out of 227 km) have been secured, including the construction of 10 km of levees resisting to overflow, for a

total cost of 220 million euros out of the 450 million required to secure the entire protection system. 190 million euros are programmed downstream of Arles over the next five years. The benefits associated with the project have been the subject of a socio-economic analysis [18]. The figures below show the changes over time and as a function of the discharge of the Rhône river, in the four main indicators used in this analysis: the number of people guaranteed to be protected (a criterion defined by the regulations) ; expected flooded population ; expected damages and expected spilled water volumes.

It can be seen that expected spilled water volumes have only slightly decreased despite the works. Historically located upstream of the delta; they are now concentrated downstream of the delta. On the other hand, the number of people with guaranteed protection has risen sharply. They are now 70,000 for the 100-year flood of the Rhône, compared with less than 20,000, 20 years ago. Expected number of flooded people and expected damage have significantly decreased.

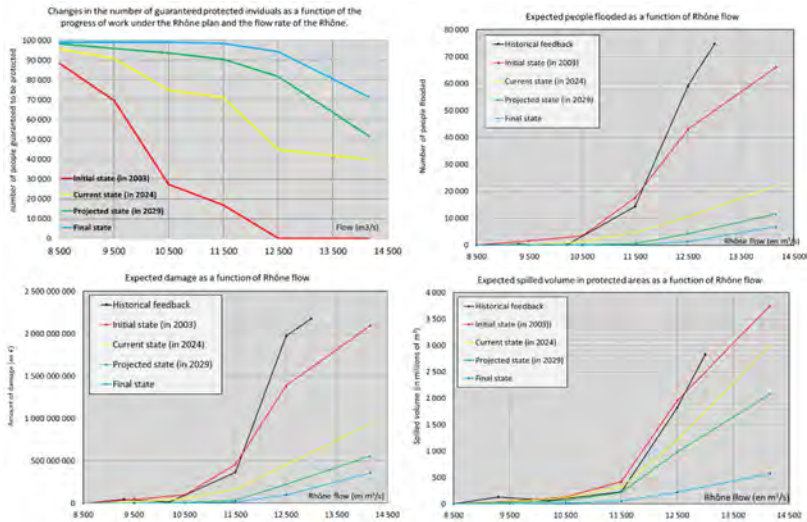


Fig. 17
Main criteria of the socio-economic analysis [18]
Principaux critères de l'analyse socio-économique [18]

To keep alive the memory of past floodings and to give residents a better understanding of their exposure to the current risk, thereby encouraging the development of a vivid risk culture throughout the region, SYMADREM [17] has decided

to make the results of the risk assessment available to the public in simplified, interactive map form. This digital tool, based on highly accurate data and maps, enables every resident of the delta protected by the Rhône levees to immediately view and compare the results according to the criteria selected by the Internet user. It's an ergonomic and educational (though still highly technical) approach, providing information at the scale of a single home:

- water depths reached by the Rhône during past floods;
- the level of dry-foot protection "guaranteed" by SYMADREM, expressed in terms of Rhône flow;
- beyond this level of protection, the probable height of flooding as a function of the Rhône flow.

This application can be accessed from the SYMADREM website at the following address: <https://cartographie.symadrem.fr/>

REFERENCES

- [1] BILLY P. & AL., 2018. *Actualisation de l'hydrologie des crues du Rhône et révisions méthodologiques, 3ème conférence internationale I.S. Rivers 2018, 4-8 juin 2018, Lyon*
- [2] BOUTONNIER L. & AL., 2019. *Conception et construction des ouvrages en sols fins – presse des ponts, 2019.*
- [3] CHAUSSÉE D. & AL., 2019, *Travaux de sécurisation de la digue du Rhône entre Beaucaire et Fourques : retour d'expérience sur le suivi géotechnique d'exécution, sa supervision et son contrôle – 3ème colloque national – Dignes2019 - 20-21 mars 2019 – Aix-en-Provence*
- [4] CHEETHAM M. & AL, 2015. Building a resilient system of defence against flooding from the Rhône. *Proceedings of the Institution of Civil Engineers-Water Management*, vol. 168, n° 2, p. 74–84
- [5] DEGOUTTE G. & SARRALDE R., 2008. *Expertise du schéma de protection contre les crues du secteur de Tarascon-Arles – partie technique – rapport 005602-01 CGEDD.*
- [6] DEGOUTTE G. & TOURMENT R., 2021 – *Spillways on river levees – édition Quae.*
- [7] DREAL RHÔNE-ALPES, 2009. *Schéma de gestion des inondations des inondations du Rhône aval pour une stratégie de gestion des crues du Rhône à l'aval de Viviers.*

- [8] GILBERT & AL., 2019, Réhabilitation de la protection contre les inondations de Tarascon - un panel d'ouvrages variés : la digue de la Montagnette, le château Royal de Provence aux pieds dans le fleuve et un ancien quai – 3^{ème} colloque national – Dignes2019 - 20-21 mars 2019 – Aix-en-Provence
- [9] GIRARD & AL., 2013, *Modélisation hydraulique de la mise en transparence du remblai ferroviaire entre Tarascon et Arles - Dignes maritimes et fluviales de protection contre les submersions 2ème Colloque national*, Aix-en-Provence, 12-14 juin 2013
- [10] GUIDOUX ET AL., 2019, Conception et installation d'un système de surveillance innovant pour des digues de protection contre les crues du Rhône, 3^{ème} colloque national – Dignes2019 - 20-21 mars 2019 – Aix-en-Provence
- [11] MALLET T., 2012. Programme de sécurisation des ouvrages de protection contre les crues du Rhône du barrage de Vallabrègues à la Mer, SYMADREM. www.symadrem.fr
- [12] MALLET ET AL., 2013, *Sécurisation des digues du Rhône entre Beaucaire et Arles : conception hydraulique du système et des digues résistantes à la surverse - Dignes maritimes et fluviales de protection contre les submersions*, 2ème Colloque national, Aix-en-Provence, 12-14 juin 2013
- [13] MALLET T., OUTALMIT K. & FRY J.J. (2014) Probability of failure of an embankment by internal erosion using the Hole Erosion Test. *ICOLD BALI International Symposium*.
- [14] MALLET & AL., 2019, Accidentologie des digues du delta du Rhône de 1840 à nos jours. *Dignes maritimes et fluviales de protection contre les inondations – 3ème colloque national – Dignes2019 - 20-21 mars 2019 – Aix-en-Provence*
- [15] MALLET T. & AL. (2018). *Etude de dangers du système d'endiguement rive gauche du delta du Rhône – ICOLD Vienna Congress*.
- [16] MALLET & AL, 2019, *Dignes du Rhône du Symadrem : retour d'expérience de quatre chantiers réalisés entre 1998 et 2018 et évolution de la conception et du cahier des charges des terrassements - Revue Française de géotechnique*. 2019, 160, 2 © CFMS-CFGI-CFMR-CFG, 2020
- [17] MALLET T. 2024, *Interactive digital mapping of the Rhône Delta flood risk, from hazard studies to the development of a risk culture*. Symposium "Dams for People, Water and Environment and Development" - 92nd ICOLD Annual Meeting – New Delhi, India 2024
- [18] MALLET T. & MATEO F., 2024. *Analyse multicritères (AMC) inondation dans le grand delta du Rhône : mise en place d'une méthode probabiliste d'évaluation des enjeux impactés et des dommages*. ACB 4ème colloque national – Dignes2024 - 27-29 mars 2024 – Aix-en-Provence

- [19] NORMAND & AL., 2019, *Recul stratégique des ouvrages de protection contre les inondations au service de la préservation et valorisation des milieux aquatiques - Confortement de la digue sud d'Arles* – 3ème colloque national – Dignes2019 - 20-21 mars 2019 – Aix-en-Provence
- [20] PROST & AL., 2019, *Travaux de confortement des quais du Rhône en traversée d'Arles* – 3ème colloque national – Dignes2019 - 20-21 mars 2019 – Aix-en-Provence

COMMISSION INTERNATIONALE DES
GRANDS BARRAGES

VINGT-HUITIEME CONGRES DES
GRANDS BARRAGES
CHENGDU, MAI 2025

A NOVEL METHODOLOGY FOR ASSESSING EXTREME HYDROLOGICAL EVENTS IN THE CONTEXT OF CLIMATE CHANGE (*)

Nicolas AVISSE
Water Resources & Climate Vulnerability Expert, TRACTEBEL

FRANCE

SUMMARY

Flood safety is a key issue when designing a dam or reviewing its design, even more today in the context of climate change. Most methods typical used in the historical context to assess floods are either based on historical precipitation or rivers flows, and require a stationary climate to be applied. These conditions make them inadequate for climate vulnerability studies.

Other approaches have been proposed to provide storm and flood estimates considering climate change (e.g., the Clausius-Clapeyron empirical method for storm rainfall, a statistical fit on flows simulated with a hydrological model for extreme floods). However, detailed reviews have proven these methods unfit for most catchments. The Clausius-Clapeyron method, in particular, lacks a robust scientific basis for local applications: work conducted over Europe and presented in this paper has shown no correlation between projected changes in temperature and local changes in high extreme precipitation.

The combination of stochastic weather generation, a practical multi-hydrological model ensemble and dynamic weighting of calibrated flow time-series is proposed in this paper as an alternative solution for producing extreme flood

**Une méthodologie innovante pour évaluer les événements hydrologiques extrêmes dans le contexte du changement climatique*

estimates in the context of climate change. If the combination of stochastic weather generation and conceptual hydrological modeling has been proposed to provide extreme flood values in historical climate conditions, applying such combination in a climate change context leads to significant challenges due to the intrinsic limitations of conceptual hydrological models. Building a multi-hydrological model ensemble with a novel calibration process based on dynamic weighting of the outputs provides a new perspective as it enables to overcome these limitations.

The results presented in this paper for the Rio Madeira catchment in Brazil are quite promising. The proposed methodology significantly improves the performance of hydrological modeling in contrasted climate conditions. Further work is now being conducted to go deeper in the analysis and confirm the improved robustness of combining dynamically weighted time-series and multi-hydrological model ensemble, and for several catchments with different characteristics.

RÉSUMÉ

La sécurité contre les crues est une question clé lors de la conception d'un barrage ou de la révision de sa conception, encore plus dans le contexte du changement climatique. La plupart des méthodes typiquement utilisées sont basées sur les précipitations historiques ou les débits des cours d'eau, et nécessitent un climat stationnaire pour être appliquées. Ces conditions les rendent inadéquates pour les études de vulnérabilité au changement climatique.

D'autres approches ont été proposées pour fournir des estimations en tenant compte du changement climatique ; par exemple, la méthode empirique de Clausius-Clapeyron pour les averses, ou un ajustement statistique sur les débits simulés avec un modèle hydrologique pour les inondations extrêmes. Toutefois, des études sur projets ont montré que ces méthodes n'étaient pas adaptées à l'échelle de la plupart des bassins versants. La méthode de Clausius-Clapeyron, en particulier, manque d'une base scientifique solide pour les applications locales : des travaux menés sur l'Europe et présentés dans cet article n'ont montré aucune corrélation entre les changements projetés de température et les changements de précipitations extrêmes locaux.

La combinaison d'un générateur stochastique de données météorologiques, d'un ensemble multi-modèles hydrologiques et d'une pondération dynamique des sorties de modèles calibrés est proposée dans cet article comme solution alternative pour évaluer les crues extrêmes dans le contexte du changement climatique. Si la combinaison d'un générateur stochastique de pluies et d'un modèle hydrologique conceptuel a déjà été proposée pour fournir des valeurs de crues extrêmes dans des conditions climatiques historiques, l'application d'une telle combinaison dans un contexte de changement climatique pose des défis non-négligeables du fait

des limites intrinsèques des modèles hydrologiques conceptuels. La construction d'un ensemble multi-modèles hydrologiques associé à un processus de calage basé sur la pondération dynamique des sorties offre une nouvelle perspective car elle permet de surmonter ces limites.

Des résultats très prometteurs sont présentés dans cet article pour le bassin versant du Rio Madeira (Brésil). L'approche proposée améliore considérablement les performances de la modélisation hydrologique dans des conditions climatiques contrastées. Des travaux complémentaires sont actuellement menés pour approfondir l'analyse et confirmer l'amélioration de la robustesse de la méthodologie proposée pour l'ensemble multi-modèles, et pour plusieurs bassins versants présentant des caractéristiques différentes.

1. INTRODUCTION

Climate change is becoming increasingly tangible and even a source of social concern for a growing number of people today [1][2]. Temperature has increased globally for at least 40 years [3] and now reaches an unprecedented rate of +0.26°C/decade [4]. The link between this rising temperature and the occurrence of hydro-climatic extremes is now acknowledged (Fig. 1) – the Intergovernmental Panel on Climate Change (IPCC) states with *high confidence* the fact that a warmer climate will have implications on floods and droughts, both in terms of intensity and frequency [3].

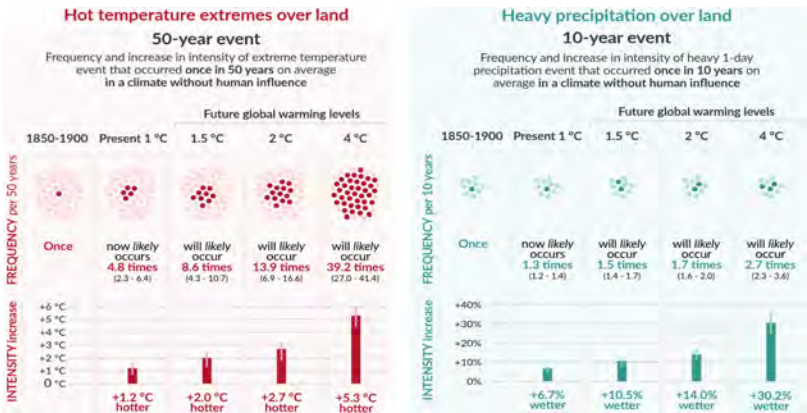


Fig. 1

Projected changes in hot temperature extremes and heavy precipitation with each increment of global warming [3]

Changements projetés de températures extrêmes chaudes et d'averses intenses pour chaque degré de réchauffement global supplémentaire [3]

Regarding extreme precipitation, the change would be towards more intense and more frequent events globally [5]. However, beyond such qualitative statement, assessing in more details the impact of projected climate changes on precipitation and river flow extremes is still a challenge for the scientific community.

Herein below, “extreme events” refer to high intensity hydro-climatic events with return periods exceeding 1,000 years. These events are indeed among the most difficult to assess and the ones that pose the highest safety risks to dams and reservoirs in the context of climate change [6][7].

As an attempt to provide estimates of the potential impact of climate change on hydrological extremes, a set of precipitation-based flood assessment methods that are currently used have been recommended for dams and reservoirs [6], including *(i)* extreme precipitation frequency analysis combined with a rainfall-runoff transformation, *(ii)* flood frequency analysis based on simulated flows from a hydrological model calibrated with historical climate conditions or *(iii)* stochastic weather generator also combined to a hydrological model calibrated with historical climate conditions.

The use of the Clausius-Clapeyron empirical approach for assessing changes in extreme precipitation has also been widely used recently [6] due to its simple formulation.

While all these methods cover various approaches (empirical, statistical and stochastic), they have significant limitations that are sometimes ignored or not comprehensively presented. Methods and tools that perform well with historical and stationary conditions may not always be valid with climate change. This additional uncertainty on the performance of the available approaches is a critical issue for water resources planners and operators who have always planned and designed based on “known unknowns” [2], i.e. considering a set of threats and uncertainties for which the intensity and frequency could be evaluated.

When recognizing the difficulty to qualify and quantify the source, nature and type of uncertainty [8] associated to climate change, some have called for changing the approach to spend more resources on identifying the potential risks than on tools and methods to assess the future [9]. Bottom-up and robustness-based approaches have been designed as a solution for Decision making under deep uncertainty (DMDU): e.g., low regret strategies [9], real options [10], decision scaling [11], adaptation pathways [12] or Climate risk informed decision analysis (CRIDA, [2]).

However, DMDU flexible strategies still have limitations to be addressed [13]. Without a comprehensive view on the potential futures, some errors and uncertainties may be involuntarily ignored and lead to significant errors in the results.

The present paper aims at proposing a more comprehensive methodology to estimate the impact of climate change on hydrological extremes and to assess the uncertainty of the results that are eventually provided.

A review of the current methods' limitations in the context of climate change is presented in Section 2 with the objective to serve as a basis for the development of a novel alternative methodology. Such innovative approach is described in Section 3 with an illustrative case study. Conclusions are eventually provided in Section 4.

2. REVIEW OF CURRENT APPROCHES

The following sections provide a review of two main approaches: (i) the Clausius-Clapeyron empirical relationship, as it is an approach often mentioned as a reference for flood analyses in a climate change context, and (ii) the combination of stochastic generation of rainfall and hydrological modeling. The latter approach, and particularly the French reference methods SCHADEX [14] and SHYPRE [15], has been evaluated as more reliable in general for operational hydrology applications [16] compared to others such as the Soil Conservation Service (SCS) unit hydrograph [17] or Gradex [18] hydro-probabilistic methods, with the limitation that they require a significant amount of input data.

2.1. THE CLAUSIUS-CLAPEYRON EMPIRICAL RELATIONSHIP

The Clausius-Clapeyron (CC) equation governs the theoretical relationship between the water-holding capacity of the atmosphere and its temperature: for each 1K increase in the air temperature, the air water-holding capacity would increase by ~7%. Assuming that precipitation during extreme rainfall events is constrained by the water already available in the atmosphere, the Clausius-Clapeyron equation could be applied to estimate the intensity of such events.

The 7%/1K scaling (hereafter referred to as CC scaling) has been validated for Europe as a whole [19], but irregularities have been found for other parts of the world, particularly in the tropics [20][21]. Moreover, even in Europe, when looking at a local scale, the change in the precipitation extremes with temperature has not been found to be as clear as the CC scaling (e.g., hook shape observed by Drobinsky [22] for the French Mediterranean region).

To clarify whether the CC scaling or another one could be used for applications at a dam catchment scale, a protocol has been designed:

- ERA5 Reanalysis daily precipitation and temperature data have been collected from the Copernicus platform for the European region. This global dataset produced by the European Center for Medium-Range Weather Forecast (ECMWF) provides climate data at a 0.5° spatial resolution for 1950-present;
- The two ERA5 datasets have been separated in two 30-year periods following recommendations from the World Meteorological Organization [23]: 1950-1979 and 1985-2014;
- A first analysis has been conducted by deriving for each 0.5° -grid cell the change in mean temperature between the two periods. Obtained values have then been taken as a basis for the calculation of the CC scaling at a local scale;
- As a second complementary analysis to evaluate the extreme precipitation scaling, the change in the 99.9th percentile of daily precipitation between the two periods has been calculated for each ERA5 0.5° -grid cell. This percentile has been chosen as a first step to compare the results with those of the literature (e.g., [19]). It is indeed considered as “extreme” in most of the literature on CC scaling validation even though it represents an event that would occur once every ~ 3 years – a regular storm rainfall event when applied to dam safety studies.

The difference between the change in the 99.9th percentile and the change in mean temperature can be observed on Fig. 2.

No correlation can be seen between the Clausius-Clapeyron relationship and the observed changes in extreme precipitation at a local scale. Two complementary tests have then been conducted to go deeper in the analysis: (i) a spatial aggregation has been tested to assess whether the two maps of Fig. 2 would be similar starting from a certain number of cells aggregated. (ii) A Gumbel fit has also been applied to the 30 annual maxima of daily precipitation for each historical period to remove a potential bias induced by the choice of the percentile: the change in precipitation extremes has then been calculated as the change in the increase rate of the fit. However, results remain the same in both cases with the absence of any correlation.

It must be stressed that, in the case of this European case-study, the issue is not so much the impossibility to evaluate the observed changes in precipitation using temperature. More importantly, the issue is about not being able to quantify the error / uncertainty of using the CC scaling approach for providing useful information to decision makers.

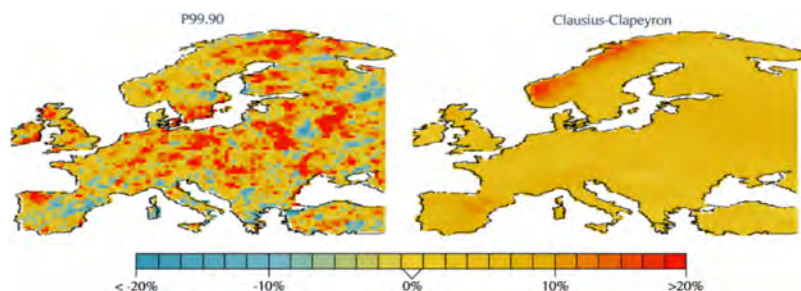


Fig. 2

Comparison between the relative scaling of daily precipitation's 99.9th percentile and Clausius-Clapeyron scaling over Europe (1985-2014 vs. 1950-1979)

Comparaison sur l'Europe entre le changement relatif du 99,9^{ème} centile des précipitations journalières et le changement relatif d'après la relation de Clausius-Clapeyron (1985-2014 vs. 1950-1979)

2.2. COMBINATION OF STOCHASTIC GENERATION OF RAINFALL AND HYDROLOGICAL MODELING

2.2.1. Stochastic generation of rainfall

Precipitation data is the start of any flood analysis in a climate change context. The distribution of precipitation, and a potential change of it, is accounted by the reference climate models [24], at least at a catchment scale large enough to circumvent the impossibility for actual climate models to reproduce convection [25]. Consequently, the stochastic generation of rainfall based on climate projections is considered to make sense and to be reliable in the present paper.

2.2.2. Hydrological modeling

Conceptual (parsimonious) hydrological models are commonly used in operational hydrology due to their easiness to be implemented and to the frequent lack of observed *in situ* data in many parts of the world. While these models have proved to perform well in stationary hydro-climatic conditions, studies have shown their limitations when applied in contrasting climate conditions and their potential underestimation of the hydrological and safety risks [26][27][28][7].

The source of the hydrological modeling uncertainty is twofold: some uncertainty is due to the search of an optimal parameter set that is robust to climate changes [29], and there is uncertainty caused by the dependence of the optimal parameter set to the climate conditions. The former has been evaluated to be lower than the latter [30].

The fact that these models' structure and parameters may not be transferable over different climate conditions led previous studies to advocate for testing hydrological models before using them [31][32]. The common approach for testing the performance of a hydrological model in a changing climate has been introduced by Klemes [33] with the differential split-sample test (DSST). This test consists of calibrating and validating a model in different climate conditions to measure its robustness in a changing climate. A generalized split-sample test (GSST) has also been implemented by Coron *et al.* [31] with the objective to provide a more robust analysis of the transposability of model parameters between catchments and climate conditions: their analysis corroborated previous findings on the lack of robustness of conceptual models under a changing climate and on the fact that transferring model parameters could actually increase the uncertainty for practical applications.

As a solution, some have tried to implement a dynamic parametrization of hydrological models and obtained contrasted results [34][35]. Moreover, even when a successful correlation is found between covariates and the parameter set, it seems that such correlation is catchment and model specific [36] and that it cannot be easily replicated.

Regarding the impact of the choice of the hydrological model on the climate impact assessment, studies have compared the results of different models to assess their sensitivity to projected climate changes [31]. Seiller *et al.* [37] went further by evaluating the added value of using an ensemble of 20 hydrological models for simulating flows in contrasted climate conditions: they found that no model surpasses the performance of the multi-model ensemble. Similar to the use of an ensemble of climate models (such as CMIP6 or CORDEX), the idea behind the use of an ensemble of hydrological models is that a single model has its own sensitivity to specific variables that may lead to simulations errors, but that combining several models with different structures and design strategies may compensate each other and provide better results than any unique calibrated hydrological model [38]. The results provided by Thibault *et al.* [39] with the use of Seiller *et al.*'s [37] 20 models over 31 catchments also corroborate this finding (see Fig. 3).

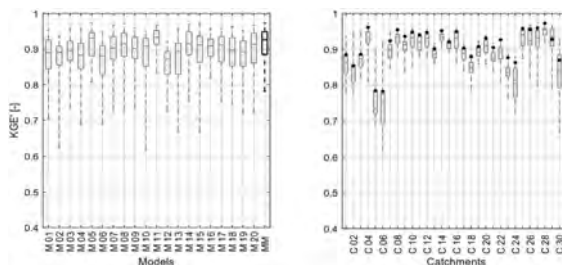


Fig. 3

Performance of 20 hydrological models and a multi-model (MM) ensemble over 31 catchments. The performance of the MM is shown with the black dots in the right panel [39]

Performance de 20 modèles hydrologiques et de l'ensemble multi-modèles (MM) sur 31 bassins versants. La performance du MM peut être visualisée avec les points noirs sur la figure de droite [39]

2.3. COMMENT ON THE CHAIN OF UNCERTAINTY

In addition to the uncertainty of individual climate and hydrological models, statistical downscaling methods have sometimes been implemented to bias-correct climate projections. Indeed, CMIP6 Global circulation models (GCM), and sometimes Regional circulation models (RCM), have a coarse spatial resolution compared to most catchments – GCM grid cells typically cover between 10,000 km² and 450,000 km².

For operational hydrology studies, the uncertainty analysis has often stopped after considering the climate models and bias-correcting them. The hydrological model calibration and multi-model simulation issues presented in Section 2.2.2 are a step forward pursuing the uncertainty review, and a step forward providing more relevant results for the decision makers in the end.

However, using DSST/GSST and building a multi-model ensemble can be much more time-consuming. And even then, the hydrological modeling issue is not the final step if one wants to address all uncertainties: a number of uncertainties have been highlighted for each step of the modeling chain from climate drivers to risk metrics in the context of climate change [9] – one could also add the uncertainty on the source data that are used at the beginning of any hydro-climatic study. This is sometimes referred to as a “cascade of uncertainty” (see Fig. 4).

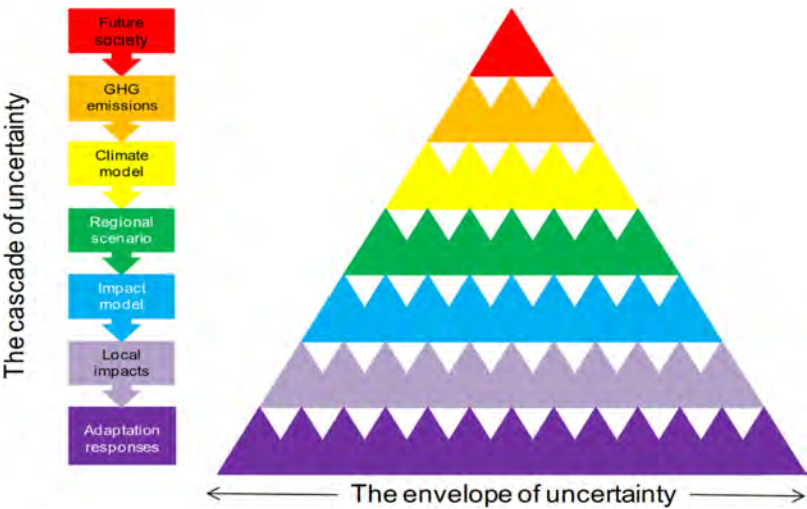


Fig. 4

Cascade of uncertainty in the context of climate change [9]
Cascade d'incertitudes dans le contexte du changement climatique [9]

Two conclusions should be drawn from this figure and the review above. First, as results and uncertainties are propagated from each modeling chain to the next (SSP → RCP → GCM → RCM → statistical downscaling → hydrological model → model parameterization → impact model → adaptation response → economic analysis ...), it is essential to consider the largest set of climate / hydrological / impact / response projections as possible to avoid presenting results that may seem accurate with not many possibilities, but that would miss possible futures. A distribution of the uncertainty (i.e. variability of results across all models) over each modeling chain has for instance been analyzed by Lemaître-Basset [40] for the Hérault River catchment in the French Mediterranean region. Their results for the highest flows, which are presented in Fig. 5, show a larger uncertainty with RCP and GCM, but the uncertainty with hydrological model selection and calibration significantly increases for average and lowest flows.

Second, if not many uncertainty aspects can be considered when conducting a study, the uncertainty of the results should be highlighted, and the results should be interpreted carefully and more qualitatively than quantitatively. It is better to provide results with a high uncertainty range than a single value that would lead stakeholders to take the wrong decisions. Climate change being deeply uncertain by its nature, the first adaptation measures are by any means often related to the implementation of a monitoring, evaluation and reporting plan to prepare for most adequate adaptation solutions for the future. Such conclusions also follow the DMDU recommendations mentioned in Section 1.

Based on the review of the current methods and of their limitations for an application in climate vulnerability studies, a practical alternative methodology is proposed in the next section.

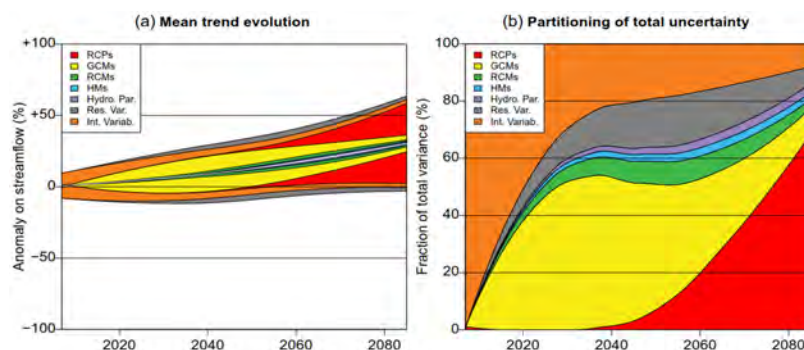


Fig. 5

Projected change and uncertainty distribution for the annual 5th percentile of highest daily flows in the Hérault River [40]

Changements et distribution de l'incertitude projetés pour le 5^{ème} centile annuel des débits journaliers les plus élevés de l'Hérault [40]

3. PROPOSED ALTERNATIVE METHODOLOGY

Based on the above results, a methodology combining (i) stochastic generation of climate parameters, (ii) an ensemble of hydrological models and (iii) dynamic weighting of simulated flows produced with models calibrated in contrasted climate conditions is proposed.

The stochastic generation of climate parameters not being a main issue for assessing extreme hydrological events (see Section 2.2.1), it has not been investigated in detail. The focus is put on the hydrological modeling in the present section.

Regarding the ensemble of several hydrological models, the HOOPLA toolbox [39] has been implemented and slightly updated to enable GSST and run faster for practical applications. HOOPLA includes the 20 hydrological models originally considered by Seiller *et al.* [37], 3 potential evaporation assessment methods and 1 snow accounting routine. 2 probabilistic sequential data assimilation techniques (Sequential Importance Resampling method and Ensemble Kalman Filter) are also available. The calibration can be performed with a Dynamic Dimensioned Search (DDS) algorithm for optimizing among 17 criteria including the modified Kling-Gupta efficiency (KGE'), Root-mean-square error (RMSE), Nash-Sutcliffe efficiency (NSE) or NSE on log values of flows.

Besides the stochastic weather generator and the HOOPLA toolbox, the main improvement of existing tools that is proposed in the present paper concerns the calibration of hydrological models and the production of time-series that can match the reference time-series in contrasted climate conditions. As an example, to illustrate the process, the Rio Madeira catchment at Abuna (Brazil) has been considered as a case study. This catchment covers an area of 921,000 km², mostly over Bolivia (Fig. 6). Flows are available at a daily time step for 1976-2014 from the GRDC database. Over this period, there has been some deforestation in a negligible part of the catchment. There is no significant impact from other anthropogenic activities upstream.

WFDE5 (bias-adjusted ERA5 Reanalysis) precipitation and temperature data have been collected over the catchment for the same period of availability of flow data. Temperature has been converted into potential evaporation using the formula by Oudin [41]. A GSST analysis of the GR4J hydrological model [42] has then been performed considering the ratio of precipitation (P) over potential evaporation (PE) as a climate index. The test has been conducted considering ten 3-hydrological year (i.e. October Y-1 to September Y) periods with indices from 1.05 to 1.32. The choice of a period of 3 years is based on previous research [30][43] that concluded that considering longer periods for calibration would not produce more robust simulation results.



Fig. 6
Map of the Rio Madeira catchment at Abuna (Brazil)
[Carte du bassin versant du Rio Madeira à Abuna (Brésil)]

As a start for the proposed alternative methodology, the analysis focuses on the Bias. Further analyses are currently being conducted for other performance indicators with other objectives.

The evolution of the Bias is presented in Fig. 7 for 10 simulations of 4 GR4J models calibrated over 4 periods with climate indices of 1.05, 1.12, 1.15 and 1.32 represented in light blue to dark blue. The 10 simulations of the GR4J model calibrated over the full period 1976-2014 ($P/PE=1.15$) are also presented in black in the figure.

It is interesting to note that the rate of the Bias increase with the climate indicator P/PE is almost the same for each calibrated model, which means that the ratio of flow averages for two different periods remains stable no matter the calibration period. The rate of the Bias and the Bias are also the same if the calibration has been performed over the whole period or over a 3-year period with the same index P/PE . These results are consistent with the ones of previous studies (e.g., [44]).

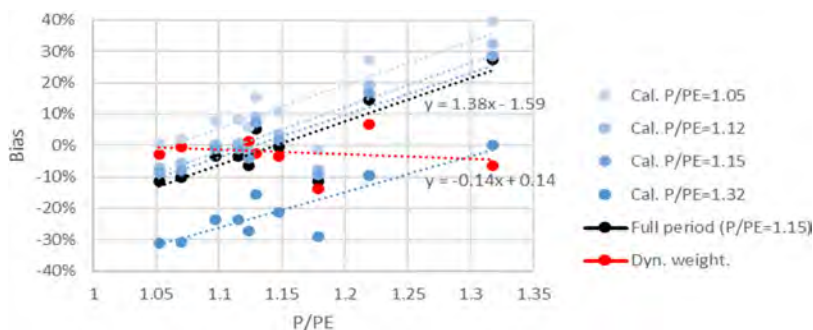


Fig. 7

Evolution of the Bias with P/PE for a GSST analysis over 10 different periods
Evolution du biais avec PIPE dans une analyse GSST sur 10 périodes différentes

Beyond the similar trend that can be observed, some differences can also be visualized with specific P/PE values (e.g., around 1.18 where the bias is higher in absolute value with all the calibrated models) and with similar P/PE values (black line and blue lines next to it). This may be due to the selection of the optimal parameter set, but further analysis will be required to conclude on the matter. By any means, the focus should be put on the trend instead of specific values when interpreting the figure: the objective is to improve the general functioning of a hydrological model in a changing climate.

A more concerning issue is the fact that the simulation errors in terms of average flows can be very significant for climate conditions different from the ones of the calibration period: the Bias varies between -15% and +25% in this case study for a model that has been calibrated over the whole period of data availability. This result is an illustration of the limitations identified in previous studies (Section 2.2.2). It also suggests that if a GR4J hydrological model were used to simulate flows in a future where P/PE would reach 1.35 compared to 1.15 now, the Bias of simulated flows would be quite significant (+30%). Similar results (not presented here) have been found with other hydrological models of HOOPLA: considering several hydrological models may not be sufficient to correct the error of models taken individually.

An interesting result of this analysis that would compensate the error, though, is that because the Bias seems to only depend on the indicator P/PE, it is possible to correct the average of flows *a posteriori* if one is only interested by the mean.

To go further in the analysis and correct not only the average flows but also each day's simulated flows in climate conditions different from the ones of the

calibration period, a dynamic weighting of simulated flows has been implemented. While most past studies have focused on finding relationships to dynamically define the parameters of the conceptual models, a similar analysis has been conducted for the output of the model. The idea is to compute streamflows using Eq. [1], where Q refers to the weighted discharge, α to the dynamic weight, \bar{Q} to the discharge simulated with the model calibrated over the wettest period of time and \bar{Q} to the discharge simulated over the driest period of time.

$$Q(t) = \alpha \bar{Q}(t) + (1 - \alpha) \bar{Q}(t) \quad (1)$$

α can then be defined as in Eq. [2] with D_{wet} the difference between the climate index of the wettest 3-year period and the climate index for the 365 days preceding t , and D_{dry} the difference between the climate index for the 365 days preceding t and the climate index of the 3-year driest period of time.

$$\alpha = D_{wet} / (D_{wet} - D_{dry}) \quad (2)$$

The Bias for the dynamically weighted time series is presented in red in Fig. 7. It can be seen that the Bias as per this combined dataset is closer to zero on average over all the climate indices.

Other performance indices (coefficient of determination R^2 , Bias, modified Kling-Gupta efficiency KGE' and Nash-Sutcliffe efficiency NSE) are represented in Fig. 8 for the comparison between the observed flows for the whole period and the models calibrated over different 3-year periods (blue), and the dynamically weighted flows (red). It is important to remember that considering these other indices for assessing a calibration / validation performance serves different objectives:

- R^2 characterizes the correlation between observed and simulated flows;
- The Bias measures the difference in average flows. It is useful if one is only interested in the mean, but it doesn't provide information for all daily flows;
- The KGE' is recommended for assessing the performance regarding all kinds of flows. Its calculation is based on the Bias, coefficients of variation and R^2 ;
- The NSE is an index that characterizes the performance for the highest flows;
- The NSE on log values (NSE ln) characterizes the performance for the lowest flows.

The results of Fig. 8 indicate that the dynamical weighting does not only correct for the Bias but also provides the best performance regarding the other indices. The very good performance of KGE' and NSE is particularly promising as it means that the combined series would provide the best estimates for the highest flow values such as flood events.

It must be stressed that these results are not dependent on GR4J. Similar results (not shown in the present paper) have been found for other hydrological models available in HOOPLA.

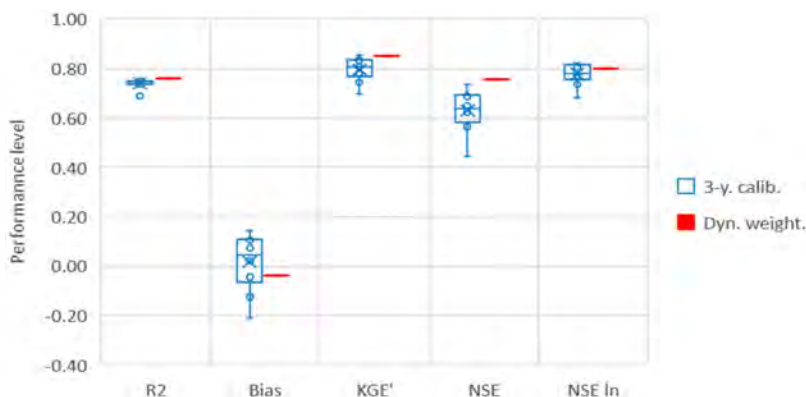


Fig. 8

Comparison of the performance between all 3-year calibrated models and the dynamically weighted combination

Comparaison de la performance entre les modèles calés sur des périodes de 3 ans et la combinaison pondérée dynamiquement

Further work is currently being conducted to go deeper into the analysis and to verify the systematic performance of a dynamically combined time-series for the ensemble of hydrological models, and for several catchments with different characteristics.

4. CONCLUSIONS

This paper reviewed current methods' limitations for assessing the impact of climate change on hydrological extremes. Two main approaches have been analyzed: the Clausius-Clapeyron empirical relationship and the use of hydrological models to be combined to stochastically generated climate datasets.

Results suggest that the use of the Clausius-Clapeyron relationship should be avoided when other methods can be implemented. Indeed, this empirical method lacks a robust scientific basis for local applications: work conducted over Europe has shown no correlation between projected changes in temperature and changes in extreme precipitation.

The combination of hydrological modeling and stochastic weather generation is generally considered the most reliable approach. The literature review and case

study analysis in this paper have focused on the hydrological modeling aspects. Results indicate that: (i) hydrological models should be tested before any use in a climate change context to avoid any large bias when assessing future river flows, (ii) integrating or mentioning the limitations and unknown uncertainties when providing future (extreme flows) is of paramount importance as there is also deep uncertainty for the steps of the modeling chain following climate models.

As a methodology to better account for hydrological modeling uncertainty, the combination of stochastic weather generation, a practical multi-hydrological model ensemble and dynamic weighting of calibrated flow time-series has been proposed in the present paper. Results are quite promising, as a method to significantly improve the performance of hydrological modeling in contrasted climate conditions has been implemented. The HOOPLA modular framework has also been revisited to be able to work with the dynamic weighting.

Further work is now being conducted to go deeper in the analysis and confirm the improved robustness of combining dynamically weighted time-series and multi-hydrological model ensemble, and for several catchments with different characteristics.

REFERENCES

- [1] World Economic Forum (2022): *Global Risks Report 2022*. Cologne/Geneva, Switzerland: World Economic Forum, retrieved from <https://wef.ch/risks22>
- [2] MENDOZA, G., MATTHEWS, J. H., STAKHIV, E., KUCHARSKI, J., & GILROY, K. (2019): *Climate Risk Informed Decision Analysis*. Paris: UNESCO, retrieved from <https://www.unesco.org/>
- [3] IPCC (2023): *Summary for Policymakers. In: Climate Change 2023: Synthesis Report. Contribution of Working Groups I, II and III to the Sixth Assessment Report of the Intergovernmental Panel on Climate Change* [Core Writing Team, H. Lee and J. Romero (eds.)]. IPCC, Geneva, 1–34. <https://doi.org/10.59327/IPCC/AR6-9789291691647.001>
- [4] FORSTER ET AL. (2024): Indicators of Global Climate Change 2023: annual update of key indicators of the state of the climate system and human influence. *Earth Syst. Sci. Data*, 16: 2625–2658. <https://doi.org/10.5194/essd-16-2625-2024>
- [5] MYHRE, G., ALTERSKJÆR, K., STJERN, C.W. ET AL. (2019): Frequency of extreme precipitation increases extensively with event rareness under global warming. *Sci. Rep.*, 9: 16063. <https://doi.org/10.1038/s41598-019-52277-4>

- [6] IHA. (2019): *Hydropower Sector Climate Resilience Guide*. London, United Kingdom, retrieved from <https://www.hydropower.org/>
- [7] FLUIXÁ-SANMARTÍN, J., ALTAREJOS-GARCÍA, L., MORALES-TORRES, A., AND ESCUDER-BUENO, I. (2018): Review article: Climate change impacts on dam safety, *Nat. Hazards Earth Syst. Sci.*, 18: 2471–2488. <https://doi.org/10.5194/nhess-18-2471-2018>
- [8] VAN DER KEUR, P., HENRIKSEN, H.J., REFSGAARD, J.C. ET AL. (2008): Identification of Major Sources of Uncertainty in Current IWRM Practice. Illustrated for the Rhine Basin. *Wat. Resour. Manage.* 22: 1677–1708. <https://doi.org/10.1007/s11269-008-9248-6>
- [9] WILBY, R.L. AND DESSAI, S. (2010): Robust adaptation to climate change. *Weather*, 65: 180–185. <https://doi.org/10.1002/wea.543>
- [10] HALLEGATTE, S., SHAH, A., LEMPERT, R., BROWN C., AND GILL, S. (2023): Investment Decision Making under Deep Uncertainty - Application to Climate Change. *Policy Research Working Papers*. <https://doi.org/10.1596/1813-9450-6193>
- [11] BROWN, C., GHILE, Y., LAVERTY, M., AND LI, K. (2012): Decision scaling: Linking bottom-up vulnerability analysis with climate projections in the water sector, *Wat. Resour. Res.*, 48, W09537. <https://doi.org/10.1029/2011WR011212>
- [12] HAASNOOT, M., MIDDELKOOP, H., OFFERMANS, A. ET AL. (2012): Exploring pathways for sustainable water management in river deltas in a changing environment. *Climatic Change* 115: 795–819. <https://doi.org/10.1007/s10584-012-0444-2>
- [13] KWAKKEL, J. H. (2020): Is real options analysis fit for purpose in supporting climate adaptation planning and decision-making? *Climate Change*, 11 (3). <https://doi.org/10.1002/wcc.638>
- [14] PAQUET, E., GARAVAGLIA, F., GARÇON, R., GAILHARD, J. (2013): The SCHADEX method: a semi-continuous rainfall-runoff simulation for extreme flood estimation. *Journal of Hydrology*. 495: 23–27. <https://doi.org/10.1016/j.jhydrol.2013.04.045>
- [15] CERNESSON, F., LAVABRE, J., AND MASSON, J.M. (1996) : Stochastic model for generating hourly hyetographs. *Atmospheric Research*. 42 (1–4). [https://doi.org/10.1016/0169-8095\(95\)00060-7](https://doi.org/10.1016/0169-8095(95)00060-7)
- [16] LANG, M., ARNAUD, P., CARREAU, J., DEAUX, N., DEZILEAU, L., ET AL. (2014): Résultats du projet ExtraFlo (ANR 2009-2013) sur l'estimation des pluies et crues extrêmes. *La Houille Blanche - Revue internationale de l'eau*, EDP Sciences, 2: 5–13. <https://doi.org/10.1051/lhb/2014010>

- [17] VEN TE CHOW, Hydrology and its development (1964). In: *Handbook of Applied Hydrology*, ed. by. V. T. Chow, McGraw-Hill, New York, 1–22. [https://doi.org/10.1016/0022-1694\(81\)90058-5](https://doi.org/10.1016/0022-1694(81)90058-5)
- [18] GUILLOT, P., AND DUBAND, D. (1967): La méthode du Gradex pour le calcul de la probabilité des crues à partir des pluies. *IASH*, 84, retrieved from <https://unesdoc.unesco.org/>
- [19] FISCHER, E.M., KNUTTI, R. (2016). Observed Heavy Precipitation Increase Confirms Theory and Early Models. *Nat. Clim. Change*, 6: 986–991. <https://doi.org/10.1038/nclimate3110>
- [20] O'GORMAN, P.A., SCHNEIDER, T. (2009): The physical basis for increases in precipitation extremes in simulations of 21st-century climate change. *PNAS*, 106 (35): 14773–14777, <https://doi.org/10.1073/pnas.0907610106>
- [21] ROCA, R. (2019): Estimation of extreme daily precipitation thermodynamic scaling using gridded satellite precipitation products over tropical land. *Environ. Res. Lett.*, 14, 095009. <https://doi.org/10.1088/1748-9326/ab35c6>
- [22] DROBINSKI, P., ALONZO, B., BASTIN, S., SILVA, N.D., AND MULLER, C. (2016): Scaling of precipitation extremes with temperature in the French Mediterranean region: What explains the hook shape?, *J. Geophys. Res. Atmos.*, 121: 3100–3119. <https://doi.org/10.1002/2015JD023497>
- [23] WMO. (2017). *WMO Guidelines on the Calculation of Climate Normals*. Geneva: World Meteorological Organization, retrieved from <https://library.wmo.int/idurl/4/55797>
- [24] THACKERAY, C. W., DEANGELIS, A. M., HALL, A., SWAIN, D. L., AND QU, X. (2018): On the connection between global hydrologic sensitivity and regional wet extremes. *Geophys. Res. Lett.*, 45: 11343–11351. <https://doi.org/10.1029/2018GL079698>
- [25] ZHANG, X., ZWIERS, F., LI, G. ET AL. (2017): Complexity in estimating past and future extreme short-duration rainfall. *Nature Geosci.*, 10: 255–259. <https://doi.org/10.1038/ngeo2911>
- [26] SAFT, M., PEEL, M.C., WESTERN, A.W., PERRAUD, J.-M., AND ZHANG, L. (2016): Bias in streamflow projections due to climate-induced shifts in catchment response, *Geophys. Res. Lett.*, 43: 1574–1581, <https://doi.org/10.1002/2015GL067326>
- [27] BRULEBOIS, E., UBERTOSI, M., CASTEL, T., RICHARD, Y., SAUVAGE, S., ET AL. (2018): Robustness and performance of semi-distributed (SWAT) and global (GR4J) hydrological models throughout an observed climatic shift over contrasted French watersheds. *Open Water Journal*, 5 (1): 41–56, retrieved from <https://byu.edu/>

- [28] MCINERNEY, D., THYER, M., KAVETSKI, D., WESTRA, S., MAIER, H.R., SHANAFIELD, M., CROKE, B., GUPTA, H., BENNETT, B., LEONARD, M. (2024): Neglecting hydrological errors can severely impact predictions of water resource system performance, *Journal of Hydrology*, 634. <https://doi.org/10.1016/j.jhydrol.2024.130853>
- [29] FOWLER, K.J.A., PEEL, M.C., WESTERN, A.W., ZHANG, L., AND PETERSON, T.J. (2016): Simulating runoff under changing climatic conditions: Revisiting an apparent deficiency of conceptual rainfall-runoff models, *Wat. Resour. Res.*, 52: 1820–1846, <https://doi.org/10.1002/2015WR018068>
- [30] BRIGODE, P., OUDIN, L., AND PERRIN, C. (2013): Hydrological model parameter instability: A source of additional uncertainty in estimating the hydrological impacts of climate change. *Journal of Hydrology*, 476: 410–425. <https://doi.org/10.1016/j.jhydrol.2012.11.012>
- [31] CORON, L., ANDRÉASSIAN, V., PERRIN, C., LERAT, J., VAZE, J., BOURQUI, M., AND HENDRICKX, F. (2012): Crash testing hydrological models in contrasted climate conditions: An experiment on 216 Australian catchments. *Wat. Resour. Res.*, 48, W05552. <https://doi.org/10.1029/2011WR011721>
- [32] THIREL, G., ANDRÉASSIAN, V., & PERRIN, C. (2015): On the need to test hydrological models under changing conditions, *Hydrological Sciences Journal*, 60: 1165–1173, <https://doi.org/10.1080/02626667.2015.1050027>
- [33] KLEMES, V. (1986): Operational testing of hydrological simulation models, *Hydrological Sciences Journal*, 31 (1), 13–24, <https://doi.org/10.1080/02626668609491024>
- [34] WESTRA, S., THYER, M., LEONARD, M., KAVETSKI, D., AND LAMBERT, M., (2014): A strategy for diagnosing and interpreting hydrological model nonstationarity. *Wat. Resour. Res.*, 50: 5090–5113, <https://doi.org/10.1002/2013WR014719>
- [35] PAN, Z., LIU, P., GAO, S., XIA, J., CHEN, J., AND CHENG, L. (2019): Improving hydrological projection performance under contrasting climatic conditions using spatial coherence through a hierarchical Bayesian regression framework, *Hydrol. Earth Syst. Sci.*, 23: 3405–3421. <https://doi.org/10.5194/hess-23-3405-2019>
- [36] LESPINAS, F., LUDWIG, W., AND HEUSSNER, S. (2014): Hydrological and climatic uncertainties associated with modeling the impact of climate change on water resources of small Mediterranean coastal rivers. *Journal of Hydrology*, 511: 403–422. <https://doi.org/10.1016/j.jhydrol.2014.01.033>
- [37] SEILLER, G., ANCTIL, F., AND PERRIN, C. (2012): Multimodel evaluation of twenty lumped hydrological models under contrasted climate conditions,

- Hydrol. Earth Syst. Sci.*, 16: 1171–1189. <https://doi.org/10.5194/hess-16-1171-2012>
- [38] AJAMI, N.K., DUAN, Q., GAO, X., AND SOROOSHIAN, S., (2006): Multimodel Combination Techniques for Analysis of Hydrological Simulations: Application to Distributed Model Intercomparison Project Results. *J. Hydrometeor.*, 7: 755–768, <https://doi.org/10.1175/JHM519.1>
- [39] THIBOULT, A., SEILLER, G., PONCELET, C., AND ANCTIL, F. (2020): The HOOPLA toolbox: a HydroIOlogical Prediction LABoratory to explore ensemble rainfall-runoff modeling, *Hydrol. Earth Syst. Sci. Discuss.* [preprint]. <https://doi.org/10.5194/hess-2020-6>
- [40] LEMAITRE-BASSET, T., COLLET, L., THIREL, G., PARAJKA, J., EVIN, G., AND HINGRAY B. (2021): Climate change impact and uncertainty analysis on hydrological extremes in a French Mediterranean catchment, *Hydrological Sciences Journal*, 66:5, 888–903, <https://doi.org/10.1080/02626667.2021.1895437>
- [41] OUDIN, L., HERVIEU, F., MICHEL, C., PERRIN, C., ANDRÉASSIAN, V., ANCTIL, F., AND LOUMAGNE, C. (2005): Which potential evapotranspiration input for a lumped rainfall–runoff model?: Part 2—Towards a simple and efficient potential evapotranspiration model for rainfall–runoff modelling. *Journal of Hydrology*, 303: 290–306. <https://doi.org/10.1016/j.jhydrol.2004.08.026>
- [42] MOUELHI, S., MICHEL, C., PERRIN, C., & ANDRÉASSIAN, V. (2006): Stepwise development of a two-parameter monthly water balance model. *Journal of Hydrology*, 318: 200–214. <https://doi.org/10.1016/j.jhydrol.2005.06.014>
- [43] ANCTIL, F., PERRIN, C., ANDRÉASSIAN, V. (2004): Impact of the length of observed records on the performance of ANN and of conceptual parsimonious rainfall-runoff forecasting models. *Env. Model. & Softw.*, 19 (4): 357–368. [https://doi.org/10.1016/S1364-8152\(03\)00135-X](https://doi.org/10.1016/S1364-8152(03)00135-X)
- [44] CORON, L., ANDRÉASSIAN, V., PERRIN, C., BOURQUI, M., AND HENDRICKX, F. (2014): On the lack of robustness of hydrologic models regarding water balance simulation: a diagnostic approach applied to three models of increasing complexity on 20 mountainous catchments, *Hydrol. Earth Syst. Sci.*, 18: 727–746. <https://doi.org/10.5194/hess-18-727-2014>

COMMISSION INTERNATIONALE DES
GRANDS BARRAGES

VINGT-HUITIEME CONGRES DES
GRANDS BARRAGES
CHENGDU, MAI 2025

IMPROVEMENT OF THE SAFETY OF THE FRENCH DAMS AGAINST FLOODS (*)

Gaëtan DAUTOIS & Mathieu ROY
ARTELIA

Samuel BALE, Marie CUBAYNES, Frédéric LAUGIER & Romain TAJETTI
EDF-CIH

Guirec PREVOT
PoNSOH DGPR

FRANCE

SUMMARY

French dams stakeholders have always considered the issues of dam safety during floods. Taking into account flood hazard has been a continuous improvement process through past decades. Nowadays flood risks requirements are clarified within a formal regulation and technical framework. This regulation requires dams to be compliant before 2030 or 2035 according to dam class. The three examples highlighted in this article (La Raviege dam, La Laye dam and Pinet Dam) show that it could be necessary sometimes to use innovative solutions and include more and more multi-fields approaches. Moreover, the achievement of these works should be considered as a step to improve dam safety during floods which remains a continuous process. Further challenges will be faced within the background of climate change. However, current flood design criteria represent an efficient line of defense and a significant step in terms of dam safety which will give time to dam stakeholders to face forthcoming challenges.

*Amélioration de la sûreté des barrages français vis-à-vis des crues

RÉSUMÉ

Les acteurs de la profession des barrages en France ont toujours intégré l'importance de la sécurité en crue des ouvrages. La prise en compte de ce risque et sa formalisation ont été progressive et ont abouti aujourd'hui à un cadre unifié sur l'ensemble du territoire d'objectifs inscrits dans une réglementation. Cette réglementation vise à un respect de standard à l'horizon 2030 et 2035 en fonction de la classe de l'ouvrage. Les trois exemples cités dans cet article (les barrages de La Raviège, La Laye et Pinet) illustrent qu'il faut parfois utiliser des techniques innovantes et de plus en plus multi-métiers. De plus, l'achèvement de ces travaux doit être considéré comme une étape dans l'amélioration de la sureté des barrages en crue, qui reste un processus continu. De nouveaux défis nous attendent dans le contexte de changement climatique global et nous poussera à se questionner de nouveau sur la sécurité de nos ouvrages. Néanmoins, les périodes de retours des crues visées par la réglementation constituent un rempart efficace et nous permettent de prendre le temps de la réflexion pour relever ce nouveau défi.

1. CONTEXT

Dam safety stakeholders in France (dam owners, engineers, government) have always been concerned by safe passage of floods for dams. The context of dam safety with regards to flood has significantly evolved for the last 30 years.

1.1. FROM LOCAL VARIOUS PRACTICE TO UNIQUE REGULATORY CONTEXT

Dam safety policy towards floods was build step-by-step in different stages.

- (i) Firstly, early French large dams were designed without any established or shared rules. They were designed according to rules, principles, methodologies and practices belonging to dam owner or their Engineer. In addition to dam safety goals for floods, methodologies used to assess floods were also different. So were hydraulic calculation assumptions and main design principles. Other projects could be reviewed and took advantages of lessons learnt by past floods. It was sometimes stated that some design criteria were optimistic and design principles non conservative [1].
- (ii) Later, the creation of big dam owners, the creation of FrenchCOLD, ICOLD and their technical publications [2][3][4][5][6], the actions of French Authorities [7] contributed to a general improvement and awareness of stakeholders regarding dam safety issues. Primary design principles and methodologies were accordingly shared within the dam stakeholders. They led to

technical proposals which were sometimes applied for dams, either on a voluntary basis by dam owners and/or under the pressure of the French Authorities.

- (iii) More recently, in France, the improvement process of flood dam safety was probably made possible thanks to systematic dam safety periodic assessments concerning the whole French large dam portfolio (around 650 dams). Since 2007, the French regulation requires the implementation of periodic Safety Review Risk Assessment (SaRRA). SaRRA led to a review or an update of hydrological studies and dam stability analysis. These studies provided the opportunity to detect more critical dams towards flood hazard. They helped dam owner and Authorities to take informed decisions with regard to dam safety towards floods. Compared to traditional deterministic approaches, SaRRA functional systemic analysis includes organizational and hydromechanical issues which are two key factors to ensure safe passage of floods.
- (iv) A few years later, FrenchCOLD guidelines for spillway in 2013 [9] and dam safety governmental decree in 2018 [11] provided a common base in terms of methodologies and safety prescriptions to ensure French dam safety.

The present paper shows in the following paragraphs different projects corresponding to different aforementioned time background: La Raviège dam case study corresponds to period (ii) while La Laye dam corresponds to periods (ii) and (iii). Pinet dam case study is interesting as it was rehabilitated several times in the past following lessons learnt after floods (1980 flood on Tarn river) (i) and (ii), and more recently following periodic risk assessment SaRRA (iii) and compliance to recent French regulation requirements (iv). Several ICOLD articles issued for past congresses exemplified dam rehabilitation corresponding to phase (i). Dam rehabilitation projects corresponding to phase (iv) are mainly on a study stage in 2025. According to regulation requirements, they should be completed before 2030 or 2035 according to the class dam.

1.2. GOALS, METHODOLOGIES AND SPECIFIC ISSUES

French regulation [11] and FrenchCOLD guidelines [9] show requirements based on return periods for “rare” floods (see table hereafter). International practices are quite varied in terms of flood requirements as shown in FrenchCOLD 2021 issue [10]. Some countries have requirements in terms of “extreme” or “safety” floods, some other in terms of “rare” floods like France, sometimes in terms of both “rare” and “extreme”. There is no normalized naming worldwide for these flood situations (check flood, safety flood, project flood, extreme flood, exceptional flood etc..).

In France, the reservoir level corresponding to the passage of “rare” flood shall keep reasonable safety margins for the dam. These margins are assessed through structural analysis referring, when possible, to safety factors proposed in FrenchCOLD guidelines [9]. French Regulation requirements are different for existing or new dams. This point is not common among other practices abroad.

Table 1
French legal requirement for floods for existing dams – Flood return period for a “rare” situation including reasonable safety margins

DAM CLASS	CONCRETE DAM	EARTHING DAM
A ($H > 20$ m and $V > 14$ hm ³)	1,000	10,000
B ($H > 10$ m and $V > 4$ hm ³)	1,000	3,000 1,500 for channelled dam

Many types of solutions exist to improve safe passage of flood as shown in following case studies.

- First type: The addition of new spillway or the modification of an existing spillway. La Raviege, and La Laye case studies illustrate the addition of an additional freeflow spillway. Pinet Dam case study exemplifies a spillway modification (profiling of piers) which increases the discharge coefficient. La Raviege case study also includes a modification of both existing gates through an over-opening of gates which matches with an increase of the maximum water level (available air freeboard) following refined dam structural analysis. This maximum water level increase also increases the discharge capacity of existing gates.
- Second type: Taking advantage of the reservoir peaking effect by increasing the maximum water level. It requires to optimize the dam safety margins (generally through refined structural analysis) or to reinforce the dam, sometimes by simple and cheap (improvement of water-proofing and/or drainage – for instance geomembrane...) or by more expensive structural solutions (by means of tendons, or modification of dam profile).
- The three case studies provide example of such increase of the allowable maximum water level, permitted by structural analysis or flood routing calculation.
- Third type: Non-structural solutions by rehabilitation, modification of hydromechanical equipment, organization and operating methods can be applied to improve dam safety during floods as it was often recommended by dam Risk Analysis SaRRA. La Raviege and La Laye dam illustrate this last option.

2. LA RAVIEGE DAM

2.1. CONTEXT

La Raviège dam and reservoir are in the Tarn department in France. Built on the Agout river from 1954 and filled between May 1957 and March 1958, La Raviège dam is a hollow-gravity type concrete dam. The RD n°52 secondary road runs along the crest, linking the 2 banks of the Agout river. The dam is at the top of the Agout valley and is one of the group of EDF power stations in the Agout and Arn valleys, consisting of 9 structures and 7 plants.

The main characteristics of the reservoir and of the dam are:

- Normal Water Level (NWL): 662.00
- Maximum Water Level before works (MWL): 663.00
- Total volume of reservoir at NWL: 44.73 hm³
- Surface area at NWL: 438.59 ha
- Length of reservoir: 12.7 km at NWL
- Type: Straight, hollow-gravity, concrete dam
- Length of the crest: 227 m
- Height above foundations / natural terrain : 40 m / 37 m



Fig. 1
La Raviège Dam before the works
Le barrage de La Raviège avant travaux

2.2. FLOOD ISSUE

2.2.1. *Determining the rare flood risk*

The hydrological study carried out by EDF-DTG in 2007 using the SCHADEX method reassesses the 1,000-year flood at about 1,700 m³/s, i.e. a 70% increase

relative to the initial value. This flood is calculated at the dam for the whole of the upstream catchment of 369 km², i.e. a specific flow for the 1000-year flood of 4.65 m³/s/km².

2.2.2. *Consequences on the safety during flood for LA RAVIEGE Dam*

La Ravière dam was originally designed to be capable of channeling 1000 m³/s through two gated spillways (radial gates). Updating the studies of rare floods assessed the peak value of the 1,000-year flood at 1700 m³/s and leads to reaching the MWL (Maximum Water Level) for a 200-year flood. The lack of discharge capacity is not 1,700-1,000 = 700 m³/s, thanks to a significant peaking effect provided by the large reservoir area.

2.3. CHOSEN SOLUTION IN THE CONSTRAINED CONTEXT OF AN OPERATING DAM

2.3.1. *Constraints*

Geometry is a strong constraint: indeed, the dam crest is more than 200 meters long. But the hydroelectric powerplant is at the right bank foot of the dam and the two original gates are in the middle of the dam. The only available space is the left bank of the dam, where is the emergency generator implanted.

2.3.2. *Margins research*

The Maximum Water Level before works (MWL) was 663.00. In order to highlight stability margins and raise the maximum acceptable retention level, soil and concrete investigations were proceeded in 2009 to clarify main geomechanical and geotechnical characteristics: compressive strength, tensile strength, density (average of 21 tests), cohesion ... These extensive investigations (18 test cores including large diameters boreholes) led to less conservative values than the ones usually considered for dam stability analysis (especially for the concrete / foundation interface).

Table 2
Main geomechanical characteristics for stability analysis

CHARACTERISTICS	INSIDE THE DAM'S CONCRETE	CONCRETE/FOUNDATION INTERFACE
Cohesion	1 MPa	0.44 MPa
Compressive strength	36 MPa	36 MPa
tensile strength	1 MPa	0.1 MPa

Based on these results, a dam stability analysis was led taking into account the 3D geometry. It was then possible to increase MWL to 663.50 (+50 cm).

The constraint of geometry, the span of the bridge to be built above the new PKWeir spillway and the number of dam blocks affected rapidly led to opting for the narrowest spillway possible. The detailed design study allowed the new structure to be optimized. The PKWeir solution was put forward by EDF-CIH after a techno-economic analysis and approved by the Owner (EDF-UPSO). Several PKWeirs were studied at the preliminary design stage to optimize the total width and the increase in the MWL thanks to a 3D scale model made at Liege University, by trying different geometries.

2.3.3. Description of the chosen solution

After studying many types of solutions, the chosen solution is a combination of several of them:

- The rise of the Maximum Water Level (MWL) by 50 cm, considering the results of the stability study without reinforcement of the structure. This will have a double benefit by improving at the same time for passing the 1,700 m³/s flood:
 - The discharge capacity of existing gates : 1,100 m³/s for both gates
 - The peaking effect of the large reservoir area : 300 m³/s.
- The construction of a new PKW spillway [13] : Piano Key Weir (PKW) free surface spillway consists of 4 inlets, 5 outlets and 2 inlets with a narrower closure at each end. The total width of the structure is 23.5 m. Two enclosure walls are built to guide the water and close the dam's upper gallery. The PK-Weir covers all of block n°4 and 2/3 of block n°5. The left bank enclosure wall is on block n°3 (cf. Fig. 5). The enclosure walls also play the role of support for the road bridge. The structure is about 5 m high.

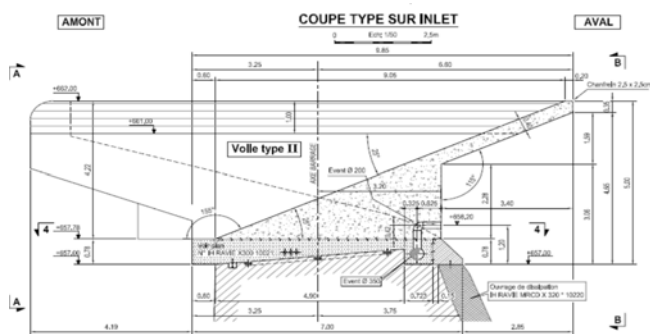


Fig. 2
Cross-section of the PKWeir
Coupe de l'évacuateur PKWeir

- The creation of a water transfer and dissipation structures for the PKW : concrete protection slab anchored on the dam's downstream facing, a flipbucket set on the rock and a guide wall on the left bank to guide the flow.
- The modification of the gates to open wider in relation to the higher MWL (keeping the freeboard, passage of debris ...).
- The crest road which was raised by 90 cm in order to respect the freeboard for the passage of the 1,000-year flood.

Finally, this solution allows the evacuation of 300 m³/s at the PK-Weir and 1,100 m³/s for all the structure's spillways at the new MWL (raised 50 cm). In addition, the reservoir peaking effect allows to pass the 1,700 m³/s peak flood.

2.3.4. *Execution of works*

The construction of this spillway meant demolishing a volume of about 1,000 m³ of dam concrete, then building the spillway and a road bridge so that the secondary road going over the crest of the dam could be put back into service. Then the water transfer and dissipation structures (dam downstream face protection slab and flip bucket) are built. The construction of the PKWeir was carried out as follows based on a two years schedule: Season 1 – Upstream works / Season 2 – Downstream works.

- Package 1: creation of the PKWeir: January - September 2014

Sawing of the entire volume to be demolished then micro-blasting in six phases with specific blasting patterns to encourage the debris to fall downstream: 1,000 m³ of demolition in total.

Construction of the apron: the preparation of the interface is important with, in particular, the construction of a drainage system connected to the existing vertical drains, the passage of the ducts for the I&C package, the treatment of the connection of the copper strips with waterstop, reinforcement and anchors, the passage of the inlets' aeration system and the concreting of the apron in three phases so as to respect the block joints of the existing dam (in total 90 m³ to 135 kg/m³ of steel).



Fig. 3

- a) Demolition of dam crest, b) PKW under construction
a) Démolition de la crête du barrage, b) PKWeir en construction

Putting the upstream and downstream platforms in place, anchored in the apron and sized, amongst other things, for the weight of the formworks and to hold them during concreting.

Construction of the vertical walls, prefabricating the reinforcement at the downstream toe of the structure (10 walls in total of 16 m³ to 180 kg/m³ of steel).

Construction of the inlet and outlet ramps with reinforcement on site using connectors and starter bars to ensure the connection with the walls (in total 5 outlet slabs and 6 inlet slabs of 20 to 25 m³ to 50 kg/m³ of steel).

- Package 2: creating a road bridge and connections: July to December 2014

The second package of this civil engineering contract consisted of creating a road bridge spanning 25 m over the PKWeir. The decision was made to build a mixed bridge with a welded reconstituted beam to minimize the apron's thickness and thereby have the least impact possible on the secondary road which was raised 90 cm in order to respect the freeboard for the passage of the 1,000-year flood. This increase meant the road had to be altered along a 90 m portion in order to respect the requirements and constraints imposed by the Tarn department Regional Council (radius of curvature, gradients, etc.).



Fig. 4

- a) Upstream and b) downstream during bridge construction
a) amont et b) aval durant la construction du pont

- Package 3: creating the stilling basin: March to September 2015

The stilling basin guides the water discharged by the PKWeir. It is made up of a slab anchored on the dam's downstream facing, a bucket set on the rock and a guide wall on the left bank to guide the flow. Three inspection galleries offer access to the spaces in the buttresses that are still there under the new structure. Joints have been created in this new structure so as to respect the existing blocks of the gravity dam and their movements.

The structure's design has been defined using the scale model that was made at the study phase. The 3D view below presents this new structure.

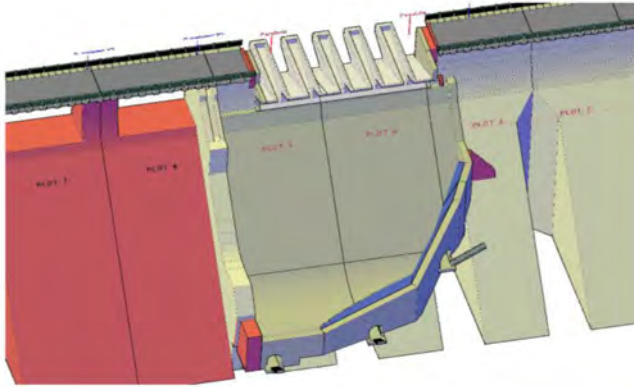


Fig. 5
Downstream 3D view of the project
Vue 3D du projet depuis l'aval

- Prefabricated brackets anchored in the structure's buttresses (20 prefabricated brackets anchored in the buttresses to support the 50cm thick stilling slab).
- Earthworks at the structure's downstream toe to reach healthy rock.
- Excavation preparation: creating a drainage system and collection point as the low point of the excavation is below the dam's downstream level.
- Putting in the apron - Putting in the bucket and the three galleries giving access to the underside of the slab.
- Putting in the slab anchored to the downstream facing and connected to the PKWeir and creating joints coherent with the dam block joints.
- Building the guide walls.



Fig. 6
a) Protection slab, b) flip bucket
a) protection du parement, b) Cuillère de dissipation

In total, the volume of reinforced concrete used was around 2,500 m³. Treating the contact between the old and new layers of concrete and the continuity of the dam block joints in the PKWeir are two important elements in ensuring the stability and water-tightness of this new structure and therefore its durability.

The cost of the works was 4,4 M€2015. An average of 10 to 12 workers were on the site during 10 months (~32,000 hours) with a winter break.



Fig. 7
a), b) Achievement of works
a), b) travaux de La Raviège terminés

2.3.5. Safety during the project study and the works

During the study phase, after knowing about the new hydrology, EDF changed the way of operating the reservoir to ensure the safety during flood [12] by using the two hollow jet valves during flood. And by lowering level to 2 meters below the Normal Water Level during the flood period (September to December). These conditions allowed to justify the stability of the dam until a 1,000 years flood during works under for an extreme calculation situation.

During the works, many measures were taken for safety, especially:

- The deconstruction phase, in particular during the mining phase, with the sawing of the demolished part before blasting and 3 recording devices placed in the dam to measure the vibrations.
- During the works, safety issues linked to water movements and floods were paramount. A risks assessment with flood attenuation calculations allowed to define some organizational and technical measures.

2.3.6. Dam safety after works

The creation of the new PKWeir considerably improves the dam's safety level: indeed, the creation of an additional PKW spillway at La Raviège dam made it

possible to justify with margin the stability of the dam at the 1,000-year flood after updating the hydrological studies. But other safety advantages could be noticed:

- The PKWeir constitutes a new independent spillway whose reliability rate is close to 100%. The risks associated with a gate's failure to open will therefore be reduced thanks to the new PKWeir. The dam is able to pass a minor flood in case of common mode without any available gates.
- PKW surface spillway needs no human actions contrary to the gates. If the access of the dam is difficult, this spillway allows to pass water before the employees arriving to operate the gates.
- With the inclusion of a freeboard of 2 m above the nappe of the PKW, this opening will also improve the passage of debris during flood.
- The stability study justifies the Failure Danger Water Level up to 665.20, corresponding to a flood up to 10,000-year flood with the operated gates.

3. LA LAYE DAM

3.1. CONTEXT

3.1.1. *Short presentation of the dam*

The La Laye dam is a 30-meter-high earthfill dam with clayish core located next to the city of Forcalquier in the South-East of France. It was constructed between 1962 and 1964 to supply water for irrigation (85% of the volume of the reservoir) and for drinking water. The dam is owned by the SIIRF (French public agency) and operated by the Société du Canal de Provence (SCP). A typical cross-section of the dam in its 2023 configuration is shown here below.

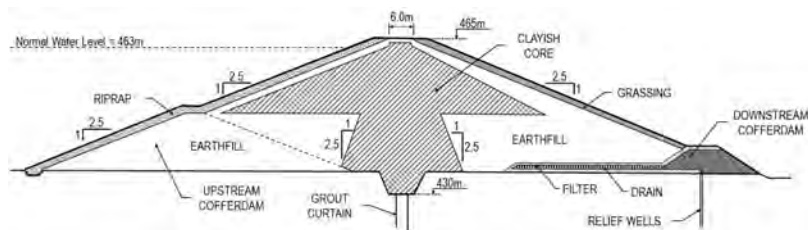


Fig. 8
Typical cross-section of La Laye dam
Coupe type du barrage de la Laye



Fig. 9

Upstream (left) and downstream (right) faces of La Laye dam
Parement amont (gauche) et aval (droite) du barrage de la Laye

3.1.2. Current spillway capacity

The spillway capacity is currently mainly ensured by a morning glory spillway located in the reservoir on the left bank. The sill of the morning glory is set at the elevation 460 m asl. It is supplemented by a steel cylindric gate (diameter 7.5 m, height 3 m), which purpose is to regulate the reservoir water level at the Full Supply Level of 463 m asl. The opening of the cylindric gate is thus automatically controlled to maintain the reservoir at the FSL.

The spillway discharge capacity can be increased using the bottom outlet, which is controlled by a 2.4 x 3.6 m roller gate located at the bottom of the intake tower, a few meters upstream the morning glory.

Both morning glory and bottom outlet discharge in the same horse-shoe shape tunnel (diameter 5.20m) which crosses the dam on the left abutment. The total discharge capacity is limited by the dimensions of the tunnel. When both gates are fully open, the maximum discharge capacity is about 400 m³/s which was the design requirement considered at the construction of the dam. The tunnel then releases the flows to the downstream river through a concrete bucket provided with concrete blocks.

Owing to the regulation capacity of the cylindrical gate on the morning glory and of the roller gate of the bottom outlet, the Maximum Water Level (MWL) was initially considered equal to the Full Supply Level (FSL): MWL = FSL = 463 m asl.

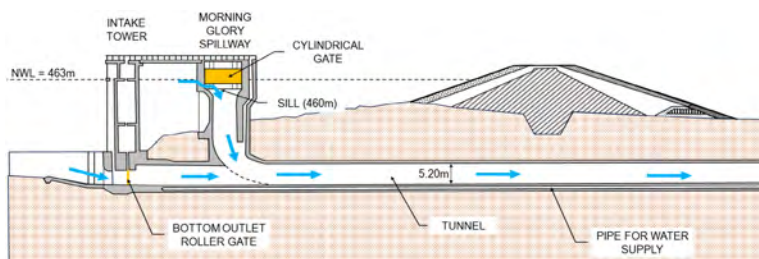


Fig. 10
Cross-section in the hydraulic structures
Coupe dans les organes hydrauliques

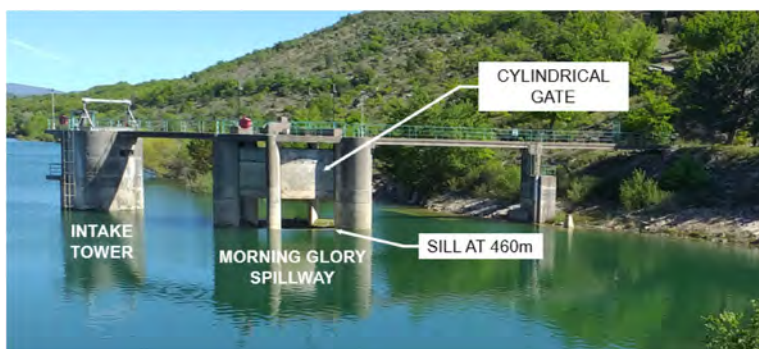


Fig. 11
Pictures of the hydraulic structures
Photos des organes hydrauliques

3.2. FLOOD ISSUE

The hydrological behaviour of the catchment area is significantly influenced by the presence of karsts. Based on the SCHADEX method, the hydrological study performed by ARTELIA in 2019 advantageously considers a progressive saturation of the karsts for the most frequent floods and a probabilistic distribution of the rain-fall. The methodology and results of this study were validated by comparison with a real flood event which occurred in Decembre 2019, after the completion of the study.

The main output of the hydrological study is the peak discharge of the “rare” flood (leading to Maximum Water Level) which is the 10,000-years flood (Q_{10000}) for an embankment dam higher than 20m according to French regulations.

The peak discharge of this Q_{10000} has been assessed at $603 \text{ m}^3/\text{s}$. A safety factor of 15% corresponding to the confidence interval has been additionally considered, leading to a final design value of $694 \text{ m}^3/\text{s}$. This value is 75% higher than the existing spillway capacity ($400 \text{ m}^3/\text{s}$ when morning glory and bottom outlet work simultaneously). The spillway capacity must therefore be increased to fulfil the safety requirements and the construction of an additional spillway is found to be necessary.

Pending the creation of an additional spillway the operating level has been lowered to the elevation 460 m asl by a prefectural decree in July 2015, leading to a significant loss in the storage capacity of the reservoir.

3.3. CHOSEN SOLUTION IN THE CONSTRAINED CONTEXT OF AN OPERATING DAM

3.3.1. *Constraints*

In a region of dry climate where the water resource is at stake, the first constraint is to restore the Full Supply Level at the elevation 463 m asl.

The second main constraint is related to the space available to implement a large hydraulic structure. Although some previous studies mention the possibility of founding an additional spillway on the downstream face of the dam, this option was discarded for reliability and safety reasons. The right abutment of the dam is also discarded because it is steep and not accessible by any existing road. Eventually, the best option is considered to be the left bank, even though it is already occupied by the existing hydraulic structures.

3.3.2. *Research of margins*

The previously mentioned constraints encouraged ARTELIA's experts to minimize the dimensions of the new spillway, which is thus designed to release the remaining discharge over the capacity of the existing structures ($694 - 400 \approx 300 \text{ m}^3/\text{s}$).

In addition, it is considered acceptable to increase the Maximum Water Level on condition that the stability of the dam is duly checked and that the top of the impervious core is raised accordingly.

3.3.3. *Description of the chosen solution*

The chosen solution to increase the spillway capacity is to create an additional free-surface lateral spillway on the left abutment of the dam. This structure is divided

in several parts which are shortly described here after, from upstream to downstream:

- A labyrinth weir. The sill is set at the elevation of the Full Supply Level (463 m asl). The structure comprises 3 labyrinth cycles, for a total length of 30 meters. The dimensions of the weir are optimized to the available space between the crest of the dam and the existing morning glory. Since the weir cannot be placed on the dam, a lateral inlet has been designed.
- A collecting basin. This structure aims to collect and steady the flows coming from the labyrinth weir and redirect them towards the spillway chute downstream. The shape of the basin has been optimized to minimize the excavation works and ensure the best hydraulic performance (checked on a physical scale model)
- A spillway chute. In order to minimize the excavation works, the chute has been divided in an upstream part with low slope (0.5%) and a downstream part with steep slope (60%). An elbow is implemented between both parts in order to direct the flows in the downstream river. The downstream part is provided with concrete steps in order to dissipate a part of the energy.
- A concrete stilling basin. This structure aims to dissipate the flow energy in a controlled manner before releasing the discharge to the river. The retained design is a USBR type IV, with dissipation blocks.

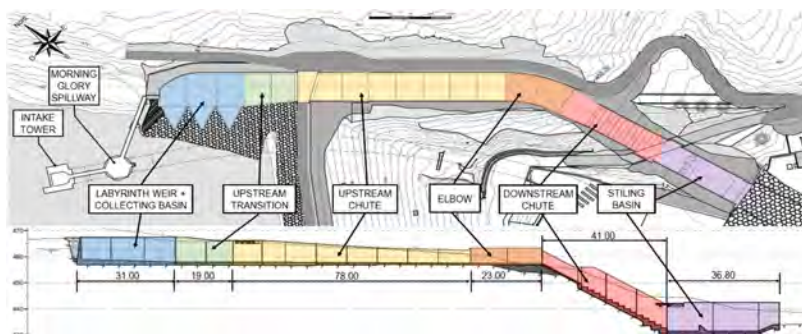


Fig. 12

Plane view and longitudinal section of the additional spillway

Vue en plan et coupe longitudinale de l'évacuateur de crues complémentaire

In addition to the lateral spillway, the clay core of the dam has to be raised higher than the new Maximum Water Level. The design simply consists in a trench filled with clay material and anchored by 1 meter in the existing core. The minimum requirements in terms of transition material leads to raise the crest of the dam by

1.1 meter. The freeboard against the waves is provided by riprap placed in the continuity of the upstream face protection.

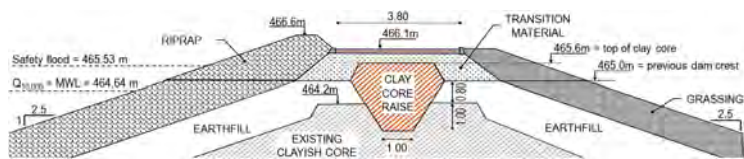


Fig. 13
Cross-section of the additional clay core at dam crest
Coupe de la recharge de la réhausse du noyau argileux en crête

The hydraulic design of the spillway has been first drafted using empirical formulas, then developed on a 3D numerical model, and finally confirmed and optimized on a scale physical model performed in ARTELIA hydraulic laboratory.

This latter model allowed to test all the relevant situations.



Fig. 14
Physical scale model
Modèle physique hydraulique

3.3.4. Execution of the works

The execution of the works started in December 2023. The commissioning is currently planned in July 2025. The overall budget of the works is about 8 M€.



Fig. 15
Excavation and concrete works
Travaux de terrassement et bétonnage

3.3.5. Safety during the project study and the works

As mentioned before, the capacity of the existing spillway is about 400 m³/s, which corresponds to a 1,000-years flood approx. To maintain the same safety level during the works, the following measures have been implemented:

- Lower the operating water level to 455 m asl during the works at the vicinity of the crest of the dam and to 459 m asl during the rest of the works. This allows limiting the water level to 461.4 m asl approx. in the case of a Q₁₀₀₀ flood. The regulation of the reservoir level is carried out by a new valve implemented on the water supply pipe, downstream the dam.
- Maintain a minimum closure of the reservoir at the elevation 461.5 m asl (higher than the maximum Q₁₀₀₀ flood level). This measure is implemented owing to an appropriate work schedule and to the construction of a temporary cofferdam during the works upstream the dam crest.

The planning of the works has been defined in order to minimize the impact of the limitation of the water level on the usual operation of the dam. Thus, the works upstream the dam crest are planned in Summer and Fall, when the reservoir level is usually the lowest.

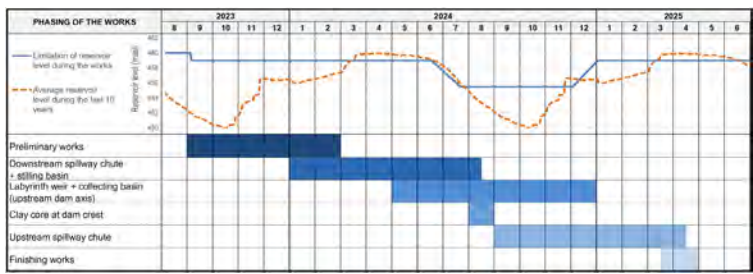


Fig. 16
Limit and usual water level
Cote de réservoir usuelle et limite

3.3.6. Dam safety after the works

The construction of the lateral spillway will significantly increase the safety level. The dam will thus be safe against:

- The “rare” flood, (10,000-years flood as per French regulations, with a discharge of 700 m³/s), which is the design flood considered in the study, corresponding to a Maximum Water Level of 464.64 m asl.
- The “safety” flood, which has been defined as Q_{10,000} + 20%, for a total discharge of 830 m³/s. The stability of the dam and the flow conditions have been

checked accordingly to ensure acceptable safety factor against sliding, guarantee sufficient freeboard at the dam crest and in the spillway chute, and avoid excessive damage at the stilling basin outlet.

In addition to the previously described civil works, the restoration of the cylindrical gate of the morning glory shall also be planned in the medium term to increase the reliability of the flood management (see below).

3.3.7. Flood management

After the works, the flood discharge capacity is ensured by the lateral spillway, the morning glory and the bottom outlet. Two from the three structures are provided with gates which shall be operated following specific rules.

The flood operating rules shall be such that they ensure (i) the best safety level, (ii) a smooth release of the flood discharge in the downstream river, (iii) the operation of the lateral spillway for the most frequent floods, (iv) the discharge under free-surface flow conditions in the tunnel as long as possible, and (v) simple and robust instructions for the operator. These rules are outlined here below.

Up to the elevation 463.90 m asl, the free surface lateral spillway is the only operated structure. This aims to put this newly created structure to the test and check that the behavior is satisfactory. The corresponding discharge is approx. 110 m³/s, which is equivalent to the peak discharge of a 50-year flood.

The morning glory is the second structure to be operated. The control level of the cylindrical gate is set at the elevation 463.90 m asl. The gate will thus open automatically owing to the automaton to maintain this water level in the reservoir. When the opening of the gate reaches 230 cm, the discharge through the tunnel is approx. 275 m³/s. According to 3D numerical hydraulic calculations, the tunnel is under free-surface flow conditions ensuring low head losses and limiting pressure loads on the concrete faces. The total discharge (also considering the lateral spillway) is approx. 385 m³/s, corresponding to a 1,000-year flood.

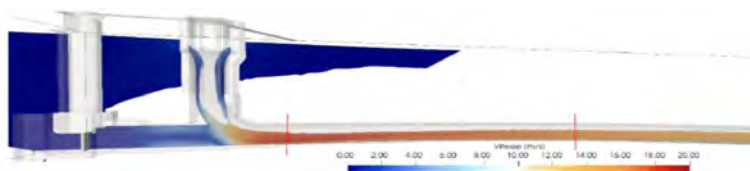


Fig. 17

3D hydraulic model. Bottom outlet is closed. Regulation by cylindrical gate on the morning glory

Modèle hydraulique numérique 3D. Vidange de fond fermée. Régulation par la vanne cylindrique de l'évacuateur de crues tulipe

The bottom outlet is operated for higher discharges (i.e., for return periods higher than 1,000 years). The roller gate is manually open in 4 stages: 25%, 50%, 75% and 100%. The opening shall be slow enough to allow the cylindrical gate of the morning glory to regulate the water level at the elevation 463.90 m asl and thus avoid suddenly releasing a much greater discharge in the downstream river.

The regulation of the reservoir water level at the elevation 463.90 m asl is possible as long as the maximum discharge capacity of the tunnel is not reached. When both cylindrical and roller gate are open at 100%, the discharge through the tunnel is limited to approx. 400 m³/s. At the elevation 463.90 m asl, the total discharge is therefore approx. 510 m³/s (also considering the lateral spillway), which is higher than the discharge of a 3,000-year flood.

For even higher discharges (return periods up to 10,000 years), the incremental discharge will flow through the surface lateral spillway. The reservoir water level will thus increase accordingly and reach the Maximum Water Level of 464.64 m asl.

4. PINET DAM

4.1. CONTEXT

4.1.1. *Short presentation of the dam*

The Pinet dam is situated in the Aveyron department in southern central France. It is a concrete gravity dam approximately 40m high that blocks the river Tam approximately 30km downstream of the town of Millau and is used for hydro-power production via 5 Francis turbines installed in a powerhouse 400m downstream. The dam and powerhouse are operated and maintained by EDF. A public road crosses the river above the dam's crest.



Fig. 18
Pinet dam viewed from downstream
Barrage de Pinet vu depuis l'aval

Facts and figures:

- End of construction: 1929
- Max height above foundation: 40.0m (from normal reservoir level)
- Max thickness at foundation level: 39 m
- Upstream face inclination: 0.05
- Downstream face inclination: 0.70
- Length at crest: 177m
- Normal reservoir level: 320.0m
- Initial design flood reservoir level: 321.0 m
- Drainage system:
 - Foundation: 42 vertical drains and 15 inclined drains under the abutments
 - Foundation: Sub-horizontal drains from the downstream toe
 - Dam body drainage system: 32 vertical drains
- Flood gates:
 - 3 bottom hinged flap gates installed between 1987 et 1991.
 - 40.26 m wide by 6.20 m high.
 - Discharge capacity: 4400 m³/s at the initial design flood reservoir level.
- Foundation rock: Gneiss and Amphibolite

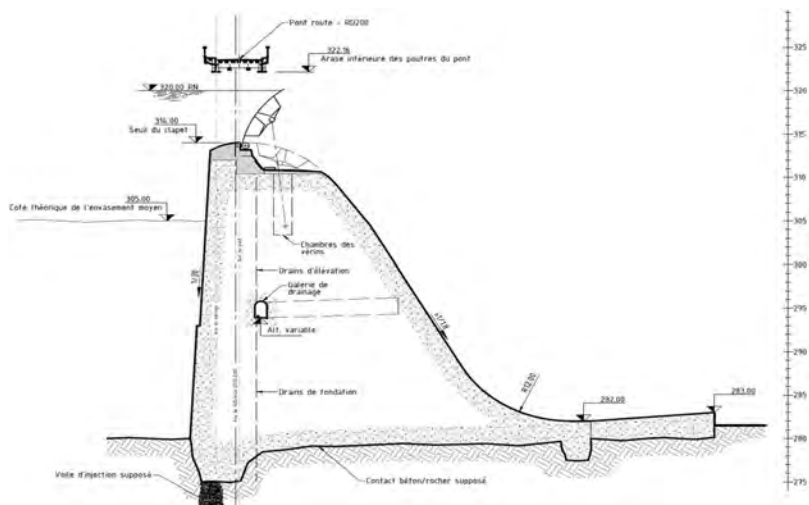


Fig. 19
Cross-section of Pinet dam
Coupe du barrage de Pinet

4.1.2. Flood design and history

The river Tarn catchment (2623 km², 1370m altitude difference at Pinet) is situated in the Cevennes mountains of central southern France. The area is well-known for its frequent heavy rain event associated with flash flooding, caused by the meeting of cold air from Atlantic depressions meeting warm humid air from the Mediterranean Sea above the mountain ranges that border the Mediterranean coast.



Fig. 20
Pinet dam - 1982 flood
Barrage de Pinet – crue de 1982]

The design flood considered for the construction of the dam was 3,500 m³/s, which was an estimation of the maximum historical flood on the river (1875). Initially, the dam was equipped with 18 small (6,5m wide by 5,15m high) radial gates along the entire width of the crest. In November 1982, a severe flood (about 2,800 m³/s) carrying a large amount of floating debris caused the reservoir level to rise to close to the design flood level, despite the flow being well below the initial design flow.



Fig. 21
Pinet dam – bottom-hinged flap gates and new road bridge
Barrage de Pinet – Faces aval des clapets fermés et nouveau pont-route

It was determined that the presence of the floating debris had caused a large reduction in the discharge capacity of the radial gates, but also that a hydrological study was required in order to determine the 1,000-year flood (discharge capacity demanded by French safety requirements for this type and size of dam and reservoir) using modern statistical methods.

The study was published in 1985 and concluded that the 1,000-year flood flow was $4,400 \text{ m}^3/\text{s}$. To ensure the safe discharge of this new design flood, including floating debris, the original radial gates were removed and replaced by much larger flap gates with a lower sill. The road bridge was also replaced at a slightly higher level in order to increase the air draft.

This new configuration of the crest of the dam allowed for a discharge of $4,400 \text{ m}^3/\text{s}$ while retaining the reservoir flood level at 321 m, correspond to a water head of 7 m over the opened flap gate.

In 2010 however, the safety review risk assessment (SaRRA) of the dam determined that the 1985 hydrological study was no longer valid, and a new study using modern statistical analyses more suited to the extreme weather events specific to the zone was recommended.

4.2. REVISION OF THE HYROLOGICAL STUDY — INCREASED SAFETY FLOOD

A new study of the rare and extreme floods on the river Tarn was therefore undertaken using the SCHADEX method [14]. The results of this study, which also considered the influence of the karst topography of the catchment (effective catchment area modified as compared to the surface topography by sink streams etc.), were published in 2018 and concluded in a revised 1,000-year flood of $6,900 \text{ m}^3/\text{s}$. It corresponds to a very important increase of about 70% ($+2,500 \text{ m}^3/\text{s}$).



Fig. 22
Pinet dam during a flood
Barrage de Pinet durant une crue

Therefore the dam is not capable any more to pass the new project flood with the existing MWL which will significantly increase of about 2.6 m.

An addendum to the SaRRA was therefore produced, specifically considering this very significant revision of the safety flood, and hydraulic and structural studies were undertaken in order to consider the eventual modifications needed to ensure the safe discharge of this revised flow rate.

4.3. CHOSEN SOLUTION IN THE CONSTRAINED CONTEXT OF AN OPERATING DAM

4.3.1. *Geometry, operating constraints and costs*

The peaking effect of the reservoir is minor considering the reservoir area and the flood peak. Keeping the same MWL would mean to create a new spillway with a discharge capacity of 2,500 m³/s. The available space is quite limited on the crest. It would require to build a very large and very high gate or to replace existing flap gates by rather higher ones.

These solutions are very expensive. So it was decided at early design stages to explore the possibility to globally keep the same existing spillway (with minor modifications) and to explore the dam stability margins.

4.3.2. *Optimization of the solution and Structural analysis*

In order to highlight stability margins and raise the maximum acceptable retention level, a finite element model was implemented. The initial objective was to try to characterize an arch effect in the dam. Indeed, although it is rectilinear, an arch (called active arch) is likely to develop in the structure if it is devoid of joints between blocks (which is the case of Pinet in the lower part), thick enough and not too slender. The finite element model allows this effect to be quantified.

If a weak arch effect could be characterized in the dam by the model under normal conditions, the model showed that this effect completely disappears with the application of winter thermal loading on the arch due to the contraction of the concrete.

Despite this absence of an arch effect, the stability conditions of the dam evaluated by the finite element model still appeared slightly more favorable than those obtained via a classic approach by 2D analytical model.

To try to understand the origin of this favorable result, a finite element model, two-dimensional this time, was subsequently carried out.

This model contains joint elements arranged at the contact and on the concrete restarts which allow the introduction of uplift pressures and the opening of these interfaces if the tensile strength of the concrete is surpassed. In a manner analogous to an analytical calculation, stability conditions are analyzed on horizontal sections located in the body of the structure and in contact with the foundation. At the contact, due to the presence of a shear key (concrete cut-off), two modes of rupture were analyzed: detachment around the perimeter of the concrete cut-off and cracking between the concrete cut-off and the main body of the dam.

It turned out that it is not the three-dimensional effects that explain the more favorable results of the finite element model, but the consideration of the deformability of the materials.

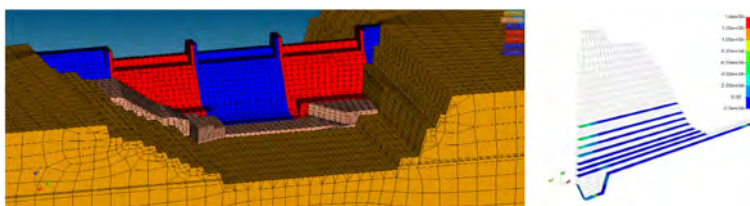


Fig. 23
3D and 2D models
Modèles 2D et 3D

Indeed, analytical models assume a linear distribution of stresses which would be the shape obtained if the dam materials were infinitely rigid. A finite element calculation, conducted for control purposes, with very high deformation modulus, thus obtains the same results as the analytical model.

In Figure 24, the blue curve represents the stress distribution calculated by the finite element model along a concreting restart, assuming a very high deformation modulus ($>>100$ GPa). The tensile strength (100kPa) is exceeded on the upstream face, leading to cracking over the first 7 meters (horizontal part of the curve) then the profile is linear.

However, when the deformability of the materials is considered, the stress distribution is not linear, this distribution is amplified by the deformations especially near the faces (stress concentration phenomenon). The orange curve in Figure 24 represents the distribution obtained by assuming a realistic concrete deformation

modulus (20 GPa). The stability conditions are more favorable with this assumption since the tensile strength is no longer exceeded at the upstream face.

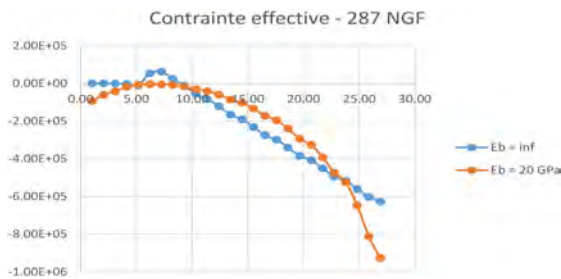


Fig. 24
Stress distribution obtained along a section of the dam depending on whether the materials are very rigid (in blue) or deformable (in orange)
Distribution des efforts le long d'une section du barrage en fonction de la déformabilité du matériau

To understand why this phenomenon is favorable to the stability of gravity dams, it is necessary to apply the loads successively. The blue curve in the Figure 25 represents the normal stress at the contact under self-weight only. The compressions (noted negatively on the graph) are significantly increased upstream due to the stress concentration compared to what would have been obtained with a linear distribution.

However, gravity is the dominant load of gravity dams, the addition of the hydrostatic load (in yellow), therefore does not completely erase this initial stress increment upstream. This allows the tensile stress at the upstream face to remain below the tensile strength of the concrete, assumed to be 100 kPa for this section, initiating a crack that then develops progressively by introducing uplift pressures.

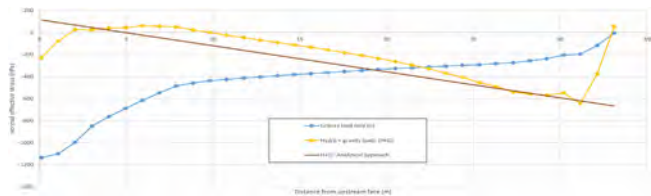


Fig. 25
Stress distribution obtained along the contact section of the dam depending for different load cases.
Distribution des efforts le long de la section du contact en fonction des différents cas de charge étudiés

This approach, with the assumptions stated above, shows that the French regulation's stability criteria are respected for all calculation sections and for the two modes of failure envisaged at the contact with the foundation.

Sensitivity studies on the hydrostatic load were also carried out to evaluate the residual safety margins. These studies show that the stability criteria are satisfied up to a reservoir level of 324.50 m in a flood situation, which is 1.7 m above the maximum level justifiable via the classical approach.

4.3.3. *Other optimisations*

Given the revision of the safety flood, a physical hydraulic model (Liège University, Belgium) was used to analyse several aspects pertaining to the capacity of the dam and its flood gates to accommodate the flow:

- Water surface profile over the crest of the dam, with particular attention to the air draft under the bridge, given the risk of floating debris.
- Hydrodynamic pressures on the open flap gate for reservoir levels > design head for the sill form.
- Reservoir level for rare floods including the new safety flood of 6,886 m³/s.
- Form of the hydraulic jump at the foot of the dam, as pertaining to the erosion risk.

The impact and the solutions to the first two items are presented after.

Water surface profile: In order to prevent a reduction in discharge capacity and any damage to the road bridge, particularly considering the floating debris risk, the water surface profile was given specific attention. Given the wide gates and large draft over the crest of the dam, a minimal air draft under the bridge (approx. 30cm) was considered sufficient to allow the safe discharge of the 1,000-year flood and any floating debris. This criterion was examined using the physical hydraulic model. The results showed that the criterion was met in the center of each opening. However, close to the piers the water surface was above the lower beams of the bridge due to the contraction of the flow.

In order to obtain the required air draft at all points along the bridge, different modifications to the pier noses were tested. Several different forms were tested, but all involved moving the nose of the pier, and therefore the water level rise due to the contraction effect, upstream of the sill crest. It was determined that a circular profile provided the best compromise between improving the discharge rate (a few %) and optimization of the water surface profile.

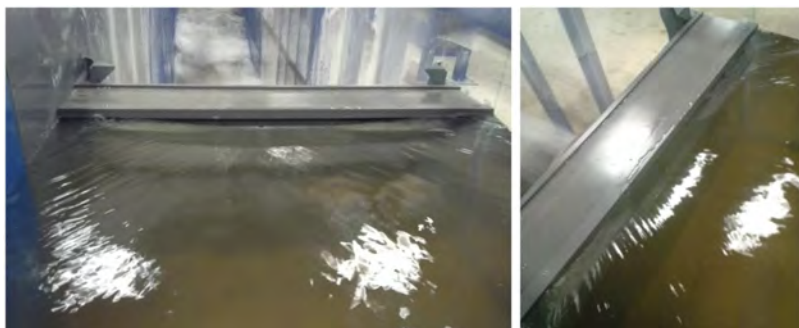


Fig. 26

Pinet dam – water surface profile for the new safety flood ($6,886 \text{ m}^3/\text{s}$) without pier modification

Barrage de Pinet – ligne d'eau pour la nouvelle crue de dimensionnement ($6886 \text{ m}^3/\text{s}$) sans modification des piles



Fig. 27

Selection of some pier nose shapes tested on the physical hydraulic model.

Sélection de plusieurs types de formes de piles testées dans le modèle hydraulique

Flap gate modifications: Since the reservoir level for the revised safety flood is significantly higher than the design head used to define the geometry of the flap gate (which forms the sill crest in its open position), it was feared that the hydrodynamic pressures on the gate could become negative. This could have led to the partial closure of the gates, but more importantly oscillations due to instabilities and ultimately the failure of the gate. Pressure measures were therefore taken at regular intervals along the sill profile on the physical model.

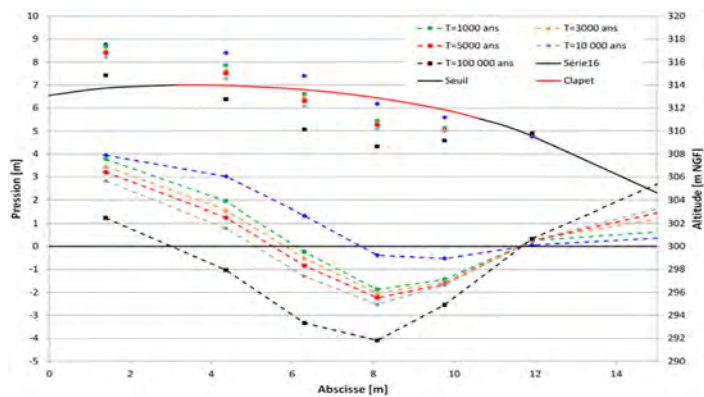


Fig. 28

Physical hydraulic model results – pressure measurements on the sill
Résultats du modèle physique hydraulique – mesures des pressions sur le seuil

As shown by the graph above, this was indeed the case, with the theoretical resulting uplift force being superior to the self-weight of the gate. In order to adress this problem, different solutions were considered, primarily the addition of automatic mechanical retention systems or the blockage of the gates via modifications to the hydraulic jacks that open and close the gates. The chosen solution however was somewhat more innovative. Rather than blocking the gates, it was decided to raise thier open position slightly, effectively changing the sill geometry to make it closer to that defined by a design head corresponding to the reservoir level for the revised 1000-year flood.



Fig. 29

Cross section showing the modified open position of the flap gates.
Coupe montrant la position modifiée du clapet en position ouverte

This design was checked using a numerical CFD model to confirm that the hydrodynamic pressures were modified to acceptable values and that the associated reduction in discharge rate remained acceptable.

4.3.4. Description of the chosen solution

At the issue of the different design and optimisation phases, the works required to permit the safe passage of the revised safety flood are summarized below:

- Modification of the upstream pier noses in order to optimise the air draft below the bridge. It also slightly improves the spillway discharge capacity by improving the contraction effect by piers.
- Modification to the open position of the flap gates in order to remove the risk of negative pressures for the new reservoir level $>$ sill design head.
- Protection from overtopping at the dam abutments.
- Raising of essential mechanical and control systems above the safety flood reservoir level.
- Flood protection of the drainage gallery.
- Reconstruction and extension of concrete protection to the banks downstream of the dam.

Further to the physical hydraulic model, the form of the pier noses was further studied using numerical CFD software. The structure itself, made from structural steel beams and plates in order to allow rapid installation with minimum disruption to dam operation and to the public road.

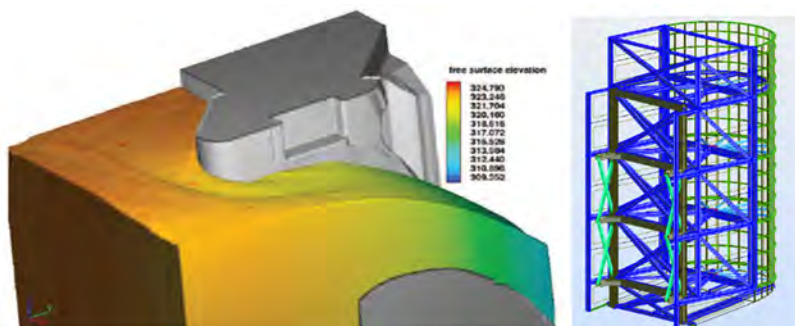


Fig. 30
Pier nose modifications – CFD analysis and structural design
Modification des nez de piles – Design de la structure

The new gate position was obtained simply by raising the existing stoppers situated on the concrete crest of the dam below the gates.

4.3.5. Execution of the works

The cost of the works was 1.9 M€₂₀₂₃. An average of 10 to 12 workers were on the site during 7 months.

Some quantities and rough estimate:

- Downstream consolidation: 500 m³ of concrete, 1600 anchorages, 8 tons of steel.
- Pier noses: 4 units (14 à 17 t/unit).
- Walls to avoid bypassing flood: 46 meters.



Fig. 31
a), b), c) Pier nose construction
Construction des nez de piles



Fig. 32
Achievement of works
Travaux terminus

4.3.6. *Dam safety during the works*

Dam safety during works was not a critical issue. Existing spillways remained fully operational during works and could be operated in case of floods. As always for this type of works, a flood warning system was put in place so that the site construction could be warned in advance and properly evacuated and adapted in case of flood. There was no construction critical phase (demolition ...) during works whereby the dam safety would be lowered. The dam safety level was kept at the same level during works.

4.3.7. *Dam safety after the works*

After the works, the dam is compliant with the French regulation requirements. It is capable of passing a 1,000-years flood with fair safety margins. The dam failure danger water level is reached for a flood above 3,000-years return period. Consequences analysis show that a dam break during such an extreme flood would expose less than 100 people within the inundation area in addition to the already inundated area. This was deemed to be acceptable by the dam owner.

5. CONCLUSION

French dams stakeholders have always considered the issues of dam safety during floods. Taking into account flood hazard has been a continuous improvement process through past decades. Nowadays flood risks requirements are clarified within a formal regulation [11] and technical framework. This regulation requires dams to be compliant before 2030 or 2035 according to dam class. Therefore, it is probable that there will be many flood passage improvements projects in France within the coming years. According to the examples highlighted in this article, they will sometimes be based on innovative solutions and will include more and more multi-fields approaches. Moreover, the achievement of these works should be considered as a step to improve dam safety during floods which remains a continuous process. Further challenges will be faced within the background of climate change. However, current flood design criteria represent an efficient line of defense and a significant step in terms of dam safety which will give time to dam stakeholders to face forthcoming challenges.

REFERENCES

- [1] BILLORÉ J. *ET AL.* (1982). – Révision des bases d'établissement du projet. Exemples de barrages en France. ICOLD 14e Congrès. Rio de Janeiro, Q52R75.
- [2] Commission Internationale des Grands Barrages (CIGB) – Choix de la crue de projet – Méthodes actuelles – Bulletin 82 – 1992;
- [3] BISTER D., LEMPÉRIÈRE F., LE DELLIOU P., MARCHESINI P. – *Évaluation et amélioration de la sécurité vis-à-vis des crues* – 18ème congrès de la CIGB, Q.68, R.41 – 1994 ;
- [4] Comité Français des Grands Barrages (CFGB) – Les crues de projet des barrages : méthode du Gradex – 18ème congrès de la CIGB – Bulletin n°2 du Comité Français des Grands Barrages – 1994;
- [5] BISTER D., coordinateur – Recommandations pratiques pour améliorer la sécurité des barrages en crue. *Practical guidelines for improvement of dam safety during floods* – CFGB, *Revue Barrages et Réservoirs* n°8 – 1998;
- [6] Comité Français des Grands Barrages (CFGB) – Barrages et Réservoirs n°8 – Recommandations pratiques pour améliorer la sécurité des barrages en crue – 1998
- [7] Bureau d'Étude Technique et de Contrôle des Grands Barrages (BETCGB) - Ministère de l'Économie, des Finances et de l'Industrie – Guide pour le contrôle des barrages en exploitation – 2002
- [8] République Française - Arrêté du 12 juin 2008 définissant le plan de l'étude de dangers des barrages et en précisant le contenu
- [9] Comité Français des Barrages et Réservoirs (CFBR) – Recommandations pour le dimensionnement des évacuateurs de crue (<https://www.barragescfbr.eu/Recommandations.html>) – 2013;
- [10] Comité Français des Barrages et Réservoirs (CFBR) – Sûreté des évacuateurs de crues de barrages : Enquête sur les projets d'évacuateurs de crues postérieurs à la publication des recommandations CFBR 2013 et enseignements – Comparaison aux pratiques internationales – Accidentologie récente des évacuateurs de crues – mai 2021;
- [11] République Française - Arrêté du 6 août 2018 fixant des prescriptions techniques relatives à la sécurité des barrages

- [12] CUBAYNES M. *ET AL.* Safety issues of La Raviège dam during the construction of a new spillway. *Proceedings of CFBR 2016 conference*. https://www.barrages-cfbr.eu/IMG/pdf/colloque2016_surete.pdf
- [13] CUBAYNES M. *ET AL.* Construction of a Piano Key Weir spillway at La Ravière dam. In Erpicum *et al.* (Eds) *Labyrinth and Piano Key Weirs – PKW 2017*, CRC Press, London.
- [14] PAQUET *ET AL.* Schadex method for rare and extreme flood estimation: overview, applications and perspectives, *24th ICOLD Congress*, Jun 2012, Kyoto, Japan.

COMMISSION INTERNATIONALE DES
GRANDS BARRAGES

VINGT-HUITIEME CONGRES DES
GRANDS BARRAGES
CHENGDU, Mai 2025

TWO EROSION TESTS TO QUANTIFY RESISTANCE TO EROSION DURING OVERFLOW: THE JET EROSION TEST AND THE OVERFLOW TEST (*)

Patrick PINETTES
geophyConsult, Jacou

Hanna HADDAD & Christophe PICAULT
CNR-CESAME, Lyon

Stéphane BONELLI
INRAE-RECOVER, Aix-en-Provence

Jean-Robert COURIVAUD
EDF Hydro, La Motte Servolex

Thibaut MALLET
SYMADREM, Arles

FRANCE

SUMMARY

This report presents two erosion tests for quantifying the resistance to external erosion of a dam or dike embankment during overflow: the JET erosion test and the overflow test. Three experimental devices are currently used in France. The first is the Jet Erosion Test initially developed at the Agricultural Research Service (ARS, USA), and currently used by GeophyConsult (France) and INRAE (France). The second experimental apparatus concerns an overflow device on embankment at the CNR-SESAME hydraulic laboratory (France). The third concerns an overflow field

**Deux essais d'érosion permettant de quantifier la résistance à l'érosion de surverse : l'essai d'érosion par jet et l'essai de surverse*

device developed by INRAE (France). This set of devices has been used in France for operational needs (e.g. design and hazard studies) and for research (e.g. development of new techniques such as the use of treated soils).

RÉSUMÉ

Ce rapport présente deux essais d'érosion pour quantifier la résistance à l'érosion externe du talus d'un barrage ou d'une digue lors d'une surverse : le JET erosion test et l'essai de surverse. Trois dispositifs expérimentaux sont utilisés en France. Le premier est le Jet Erosion Test initialement développé à l'Agricultural Research Service (ARS, USA), et actuellement utilisé en France par geophyConsult et l'INRAE. Le second dispositif expérimental concerne un dispositif de surverse sur remblai au laboratoire hydraulique CNR-SESAME (France). Le troisième concerne un dispositif de terrain de surverse développé par l'INRAE (France). Cet ensemble de dispositifs est utilisé en France pour des besoins opérationnels (par exemple, conception et études de dangers) et pour la recherche (par exemple, développement de nouvelles techniques telles que l'utilisation de sols traités).

1. INTRODUCTION

Overflow accounts for almost half of all dam and embankment dike failures. It is therefore essential to have a reliable estimate of the resistance to external erosion of a dam or dike embankment to mitigate the potential risks associated with overflow. In addition, climate projections indicate a downward trend in average flow, but a variable, even upward trend in extreme flows on several rivers in France. It is therefore important to be able to assess the possibility of a limited overflow with no consequences for the embankment. Numerous laboratory tests in hydraulic flumes have been carried out to quantify the resistance of surface protections to free-surface flow (riprap, grass, etc.). The results of these tests are most often compiled in abacuses that are widely used for design or verification (e.g. [1]). Where abacuses are not available, surface protection can be tested in the laboratory in large hydraulic flumes (e.g. [2]).

The situation is more complex when it comes to the embankment's soil resistance to external erosion. The first reason is that this resistance is extremely variable depending on soil type, and for a given soil depending on its water status and density. This resistance is known to vary over several orders of magnitude. In practice, no equipment is presently capable of testing all soils against external erosion, either in terms of accuracy (for very weak soils) or erosion capacity (for very strong soils).

The second reason why quantifying embankment's soil resistance to external erosion is not an easy task is because earthen dam and dike embankments soils are

compacted during construction. The resistance to erosion of soils is highly dependent on the type of compaction, as well as on the compaction water content and density. In addition, compaction is always made in layers, giving the embankment a distinctive structure. This is impossible to reproduce in a hydraulic flume in the laboratory.

The third reason is because the granulometry of the considered soils can be extremely variable, as it depends on the type of soil. This granulometry can vary by several orders of magnitude. No equipment is therefore presently able to test all soils against external erosion, unless the characteristic size of the hydraulics has the same order of magnitude as the D_{max} of the tested soil.

These last two specific features need to be taken into account when carrying out and interpreting erosion tests, with regard to the following two points: i) the size of the test (small scale or scale one); ii) the type of soil specimen (intact in place, intact brought to the laboratory or remoulded).

A final point is that the fundamental processes involved in external erosion are not yet totally understood. These processes differ according to soil type and granulometry. In the case of sand, the active phenomenon is surface erosion. In the case of clay soils, surface erosion, scouring and head-cut erosion are coupled. For soils with large and spread-out grain sizes, these processes are currently unknown. It is therefore essential to have several types of equipment, at several scales, in the laboratory (under controlled conditions) and in situ, in order to integrate these different external erosion processes.

This report presents two erosion tests to quantify resistance to erosion during overflow: the JET erosion test and the Overflow test. Three experimental devices are currently used in France. The first is the Jet Erosion Test initially developed by Hanson and Temple [4] at the Agricultural Research Service (ARS, USA), and currently used by geophyConsult (France) and INRAE (France). To our knowledge, this is the only device that can be used for both laboratory and field tests. The second setup is an overflow test on an embankment at CNR-CESAME hydraulic laboratory (France). The third one is an overflow field device developed by INRAE (France).

These two erosion tests are mentioned in the reference document in France dealing with the risk of internal and external erosion for dams and dikes [3]. Note that other devices exist [4], for example, the Erosion Function Apparatus EFA initially developed by J.L. Briaud at Texas A&M University.

2. THE JET EROSION TEST AT THE LABORATORY AND IN SITU

2.1. INTRODUCTION

The Jet Erosion Test (JET) is a device used to quantify the resistance to external erosion of cohesive soils. It involves impacting the soil with a submerged

jet, and measuring the erosion depth as a function of time (Fig. 1). It can be used in the laboratory or in the field. The JET was originally developed and tested by Hanson in the 1990s and has become one of the most widely used instruments for quantifying the erodibility of cohesive soils, particularly for stream restoration, bridge scour, and dam failure analyses [4]. Significant research has been conducted on the JET Erosion test, including its design, operation, measurement types, and interpretation. An ASTM standard (D5852) was developed for the first version of the JET in 2007, which used a 13 mm nozzle. The most widely used device uses a 6 mm nozzle to erode soil in a 30 cm diameter immersion tank, with provisions for testing on both horizontal and sloping surfaces (e.g., on a slope).

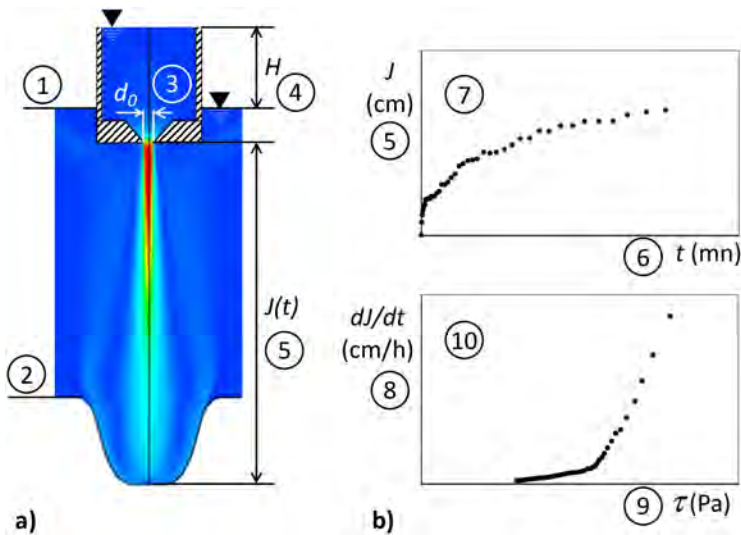


Fig. 1

a) Schematic of circular submerged impinging jet (JET's numerical modeling is taken from [6]), b) Typical results curves

a) Principe du jet impactant immergé (la modélisation numérique du JET est issue de [6]), b) Courbes typiques de résultat

- | | |
|---------------------------------|---|
| 1 Water surface | 1 Surface de l'eau |
| 2 Soil surface | 2 Surface du sol |
| 3 Nozzle diameter d_0 | 3 Diamètre de la buse d_0 |
| 4 Differential head H | 4 Pression différentielle H |
| 5 Scour depth J | 5 Profondeur d'affouillement J |
| 6 Time t | 6 Temps t |
| 7 JET Scour depth curve | 7 Courbe d'affouillement du JET |
| 8 Erosion rate dJ/dt | 8 Vitesse d'érosion dJ/dt |
| 9 Hydraulic shear stress τ | 9 Contrainte de cisaillement hydraulique τ |
| 10 JET Erosion law | 10 Loi d'érosion du JET |

2.2. THE DIFFERENT TYPES OF JET APPARATUS

Fig. 2 shows two examples of field equipment similar to the USDA device. Carrying out an in-situ JET test requires stripping approximately one square meter of soil. This stripping can be done with a hand shovel if it is only a matter of removing 20 or 30 cm of the topsoil (Fig. 2a). It is preferable to do it with a mechanical shovel if a deeper layer needs to be reached or a larger surface area needs to be stripped (Fig. 2b). The ground may be sloping (as in the case of a dike embankment Fig. 2b).

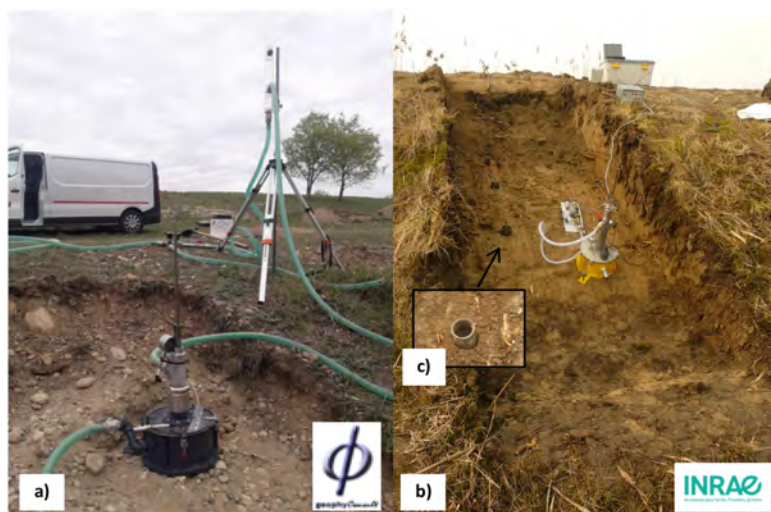


Fig. 2

View of the JET devices on field: a) Jet geophyConsult, b) Jet INRAE. The two Jets were installed on the downstream slope of a dike after stripping; c) Cutting kit installed in the ground to take an intact soil sample.

Vue des dispositifs JET sur le terrain: Jet geophyconsult, b) Jet INRAE. Les deux Jet ont été installé sur le talus aval d'une digue après décapage ; c) Trousse coupante installée dans le sol pour prélèvement d'un échantillon intact.

Fig. 3 shows two examples of lab equipment similar to the USDA device. Two types of samples can be tested in the laboratory: intact samples and remoulded samples. The intact soil sample is taken in situ after preliminary stripping with a cutting kit of similar dimensions to the CBR mold ($D=152$ mm and $H=177$ mm approximately). This sample is immediately placed in a hermetically sealed double plastic bag, then brought back to the laboratory and stored in a room not exposed to sunlight. At the time of the test, the sample is placed in the free surface tank of the

JET. The interest of intact samples is to have the erosion resistance values corresponding to the site.

The remoulded soil is skimmed to 5 mm. It is then mixed with water to the desired water content. The soil is then stored for 24 to 48 hours (depending on the nature of the soil and its fines content) in an airtight bag to ensure good uniformity of the water content. Reconstitution can be carried out using a Proctor tamper or by manual compaction. Generally, the dry density and water content values are set either in relation to the characteristics of the in-situ soil or according to the W_{OPN} and γ_{dOPN} values, obtained at the optimum Proctor Normal, from the Proctor test. In this case, the Proctor mould is placed in the free surface tank of the JET. The size of the test specimen is $D=80$ mm and $H=150$ to 200 mm. Fig. 4 shows an example of a sample in a Proctor mold before and after Jet testing. The interest of reworked samples is to be able to study the influence of a parameter (e.g. water content or density) on resistance to erosion.



Fig. 3
View of the JET devices at the laboratory
Vue des dispositifs JET au laboratoire



Fig. 4
Example of soil sample in a Proctor mold before and after Jet test
Exemple d'échantillon de sol dans un moule Proctor avant et après essai Jet

The duration of the erosion phase of a test depends on its resistance: it ranges from 10 minutes to 1 hour (approximately). In practice, 3 tests can be carried out per half-day (approximately). The quantity of water for a test is approximately 1.5 to 3 m³/h, depending on the duration of the test, and for the standard 6 mm nozzle.

2.3. WHY CARRYING OUT JET TESTS?

During an overflow, water flows down the downstream face of the structure, most often forming a “staircase” composed of a succession of mini-waterfalls. This process is called “head-cut erosion”. This external erosion of the embankment can lead to the opening of a breach. The JET test was designed to study this situation.

A JET test allows the quantification of two erosion parameters: the critical stress τ_c which provides the erosion threshold, and the erosion coefficient k_d which controls the erosion kinetics. The erosion law is $dJ/dt=k_d (\tau - \tau_c)$ when $\tau > \tau_c$ (see Fig. 1 for notations).

The Jet test is usually used in one of the following cases: i) to position the erosion parameters of the tested soil compared to other already tested soils ; ii) to study the influence of a geotechnical quantity on the erosion parameters (e.g. water content or density); iii) to estimate the probability of initiation of erosion during an overflow; iv) to allow a calculation of the opening of a breach with a software which takes the erosion parameters (τ_c, k_d) as input data (e.g. Windam or HR-Breach [4]).

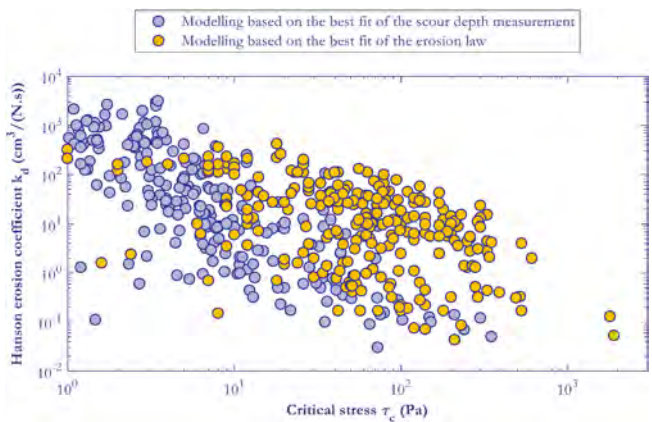


Fig. 5

The point cloud made up of the 550 JET tests carried out by geophyConsult
Le nuage de points constitué des 550 essais JET réalisés par geophyConsult

After each test, it is essential to position the new results on the cloud of all the results of the previous tests. Fig. 5 shows the point cloud made up of the 550 JET tests carried out by geophyConsult. This cloud shows a trend: the higher the critical stress τ_c , the smaller the erosion coefficient k_d (i.e. the slower the erosion). More details regarding the orders of magnitude of the erosion parameters are given in [7], as well as the influence of important geotechnical quantities on them (e.g. water content and density).

3. OVERFLOW TESTS CONDUCTED IN CNR-CESAME LABORATORY

The OVERCOME research project (Overflowing EROsion of COarse Material Embankments) was initiated in 2018 to improve our understanding of the physical erosion processes during overflow of coarse material embankments. As part of the OVERCOME project, a series of large-scale laboratory overflowing tests are conducted in CNR-CESAME lab. Overtopping tests in the laboratory are tools among others that allow (i) the observation of the erosion processes during overtopping and (ii) to acquire input data for numerical models. Therefore, the objectives of these tests are to better understand and model coarse soil embankment overflowing erosion and breach processes. This section presents the general framework and methodology adopted for two laboratory tests conducted in July 2023 and in January 2024 and some preliminary results.

3.1. DESIGN AND CONSTRUCTION OF THE EMBANKMENTS

The material used for the construction of the different embankments was typical gravel and sand from the Rhone River previously used to build embankments along the river. The soil had the following characteristics: $d_{10}=0.1$ mm, $d_{50}=11$ mm and $d_{90}=41$ mm. The construction of each dike was similar to operations on real embankments: sand and gravel were placed in layers (of approximately 30 cm) using a mechanical shovel and each layer was compacted (using a vibrating plate) to obtain a targeted density.

The constructed dikes in the lab had all the same geometry: 8.5 m long, 4 m large and 2.4 m high (Fig. 6). A notch was dug at the center of the crest of the dike to stay far from the boundary conditions (lateral walls) and to allow the observation of the lateral evolution of the erosion during the breach. To avoid excessive seepage through the embankment during the overflow erosion test, the upstream face was sealed by applying a layer of approximately 3 cm of Kaolinite.

The two tests slightly differed in terms of water content and density. The first test's humid density was about 2.05 as the objective was to target the low density measured in-situ on the downstream shoulder of an embankment on the Rhône River (Montfaucon embankment). The second test's humid density was about 2.15 as the objective was to represent the compacted sand and gravel in the core of the in-situ embankments.

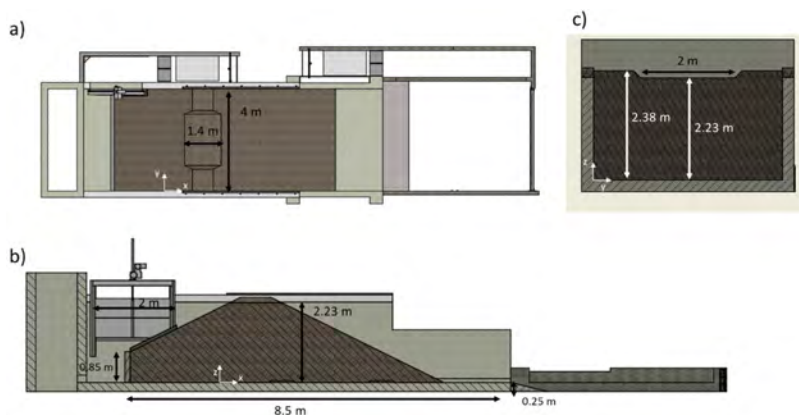


Fig. 6
Geometry of the embankments
Géométrie des remblais

3.2. TEST PROCEDURE AND MONITORING

The specificity of the tests was to simulate overflowing over the embankment with a constant water level above the notch as long as possible before the breach or the collapse of the dike. Therefore, to control the upstream water level, an over-supply discharge was used and combined to a lateral upstream weir to evacuate over-supply and control the water level in the upstream reservoir. The test procedures were the following:

- The upstream reservoir was gently and slowly filled making sure the Kaolinite layer was not removed.
- To initiate overflowing, the discharge was increased and the lateral upstream weir was adjusted to keep a constant upstream water level of 5 cm above the notch during the erosion process.
- When the breach was significant and an equilibrium slope was obtained or if the embankment collapsed, inflow was stopped.

Even though there are small differences in the monitoring between the two tests, during each test, three main physical variables were monitored: flowrates, water levels and embankment topography (Fig. 7). Each of these variables was monitored at different locations and/or by employing different technologies to avoid data loss and to compare the different devices. Flowrates were monitored at 3 locations: inflow was measured using an electromagnetic flowmeter on the upstream water pipe, overflow and over-supply were measured using gauging weirs placed downstream of the infrastructure. Water levels were measured using ultrasonic sensors placed at key places along the embankment (upstream, over the notch, over the downstream face of the dike and downstream of the dike). In addition to water level measurements above the dike, interstitial pressure probes were used to monitor eventual seepage through the dike during the filling phase. Photogrammetry measurements were performed to obtain real time topography of the embankment. This was done using 6 synchronized reflex cameras and attached to an aerial structure above the dike. In addition to the photogrammetry that allowed to obtain spatial topography data (between 0.5 m upstream of the notch to 3.5 m downstream of the notch), elevation probes were implemented over the notch (and on the downstream face of the dike for the second test) to measure local topography.

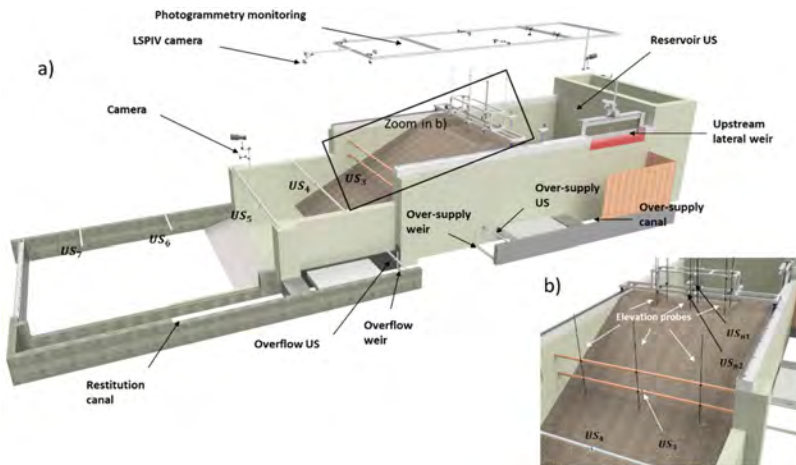


Fig. 7

Scheme of the embankment and its instrumentation for the second test
Schéma du remblai et de son instrumentation pour le deuxième essai

3.3. OBSERVATIONS

Both tests led to similar observation with four successive phases (Fig. 8): (1) filling of the upstream reservoir, (2) overflow with surface erosion, (3) headcut erosion and (4) breach.

For the first test, a small seepage (10-20 L/s) was observed during the reservoir filling. More kaolinite was applied for the second test and allowed to completely seal the upstream face of the dike. Overtopping was considered as the reference time t_0 as soon as water reached the notch. For both tests, the surface erosion phase on the downstream face of the dike began just after overtopping. It lasted approx. 1 min for both tests.

The headcut erosion phase was longer: it lasted 2 min for the first test and 7 min for the second one. The headcut process was characterized by the formation of multiple steps of erosion on the downstream face of the dike (corresponding at the beginning to the consolidation layers during the construction of the dike). During the process, these steps combined and formed larger and deeper ones. For both tests, regressive erosion was observed as the erosion began on the downstream face of the dike and propagated upstream through the notch. The overflow discharges during the headcut erosion phase were between 50 and 100 L/s depending on the maneuvers (upstream discharge and lateral weir).

When the erosion reached the upstream edge of the notch, the breach of the embankment took place. This phase was characterized by a rapid vertical erosion combined with an increase of inflow and drop of water level in the reservoir. The peak overflow discharge measured for both tests was about 290 L/s and was limited by the laboratory facility. For both tests, the erosion was asymmetrical and the embankment ended up collapsing at the end (left side of the dike for the first one and right side for the second one).

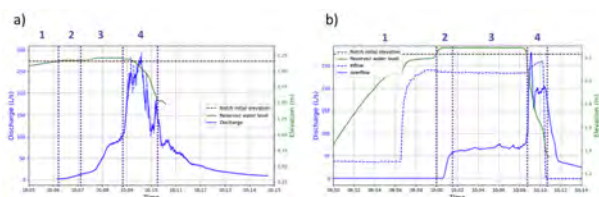


Fig. 8

Failure hydrograph and upstream water level during a) the first test and b) the second test.

Hydrogramme de rupture et niveau d'eau amont lors a) du premier essai et b) du deuxième essai

- | | |
|--|---------------------------------------|
| 1 Filling of the reservoir | 1 Remplissage du réservoir |
| 2 Surface erosion on the downstream face | 2 Erosion de surface du parement aval |
| 3 Headcut erosion on the downstream face | 3 Head-cut érosion du parement aval |
| 4 Breach formation | 4 Formation de la brèche |

One criterion for assessing the dike's resistance to overflow is the duration of the process between the onset of overflow and collapse. This duration doubled between test 1 and test 2 which was composed of more dense material. Furthermore, the duration of the surface erosion phase and of the breach phase remain the same between both tests, but the headcut erosion phase was more than 4 times longer for the second test (Fig. 8). The photogrammetry analysis allowed to obtain the real-time shape of the embankment during the process. It revealed that the topography evolution during the headcut phase was significantly different between the two tests (Fig. 9). During the first test, multiple steps formed and propagated upstream. On the contrary, during the second test, a single high step (approx. 80 cm high) was rapidly obtained and transferred upstream. Fig. 10 shows two pictures taken during the breach for the first and second test. In conclusion, the acquired dataset highlighted that the density and the moisture of the soil (main differences between the tests) seem to be key variables in the resistance and erosion behavior of the embankment.

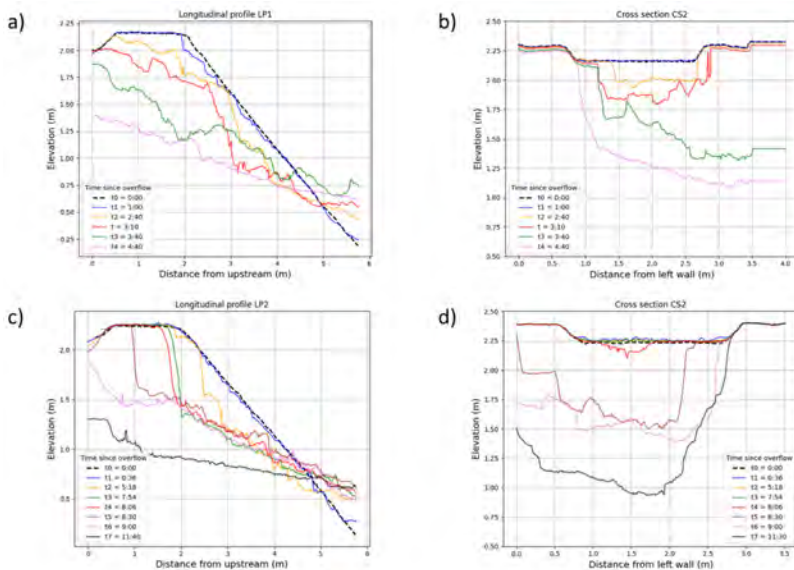


Fig. 9

Longitudinal (a,c) and lateral (b,d) profiles of the topography of the dike for the first (a,b) and second (c,d) test

Profils longitudinaux (a, c) et latéraux (b, d) de la topographie de la digue pour le premier (a, b) et le deuxième (c, d) essai

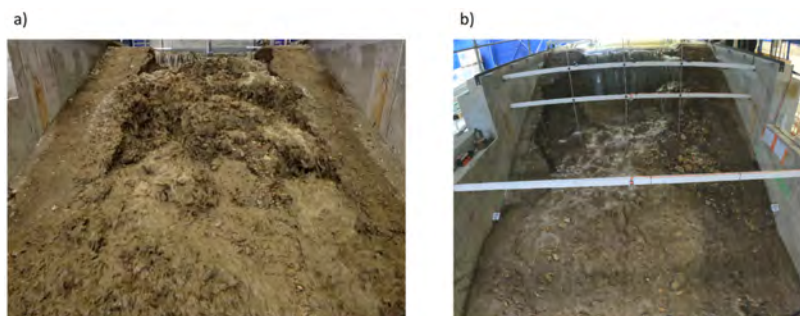


Fig. 10

Pictures taken during the breach for the first and second test
Photos prises lors de la brèche pour le premier et le deuxième test

4. THE INRAE OVERFLOW FIELD DEVICE

4.1. INTRODUCTION

In 2015, INRAE developed an on-site overflow device to account for all the physical phenomena that are not represented on the small scale (effects of layer compaction, large granulometry, etc.). The principle of the test is to create a flow in a hydraulic channel located on the dike, reproducing overflow hydraulics. The procedure followed is based on ASTM-D6460 standard. Channels are 60 cm to 1 m wide, with side walls smooth enough to ensure that wall friction is negligible compared with ground friction. The choice of width depends on site and test conditions. The flow is carried out in stages. The flow rate is constant over each stage. The unit discharge can reach 0.5 m³/s.m. The duration of each stage is around 20 to 30 minutes. The sequence can reproduce the rate of rise in flood. The measurements carried out during these flow stages are the inlet flow rate, flow velocities and flow heights along the channel. Between each flow stage, there is a no-flow period lasting 30 minutes, during which measurements are taken on ground position along the channel (topography) in order to deduce soil erosion. In particular, the on-site overflow device has shown that lime treatment gives treated soil remarkable resistance to overflow [8]. Two examples of results are presented here.

4.2. OVERFLOW TESTS ON THE SALIN DE GIRAUD EMBANKMENTS

Three tests were performed in May 2018 on three SYMADREM embankments near Salin de Giraud (France). The embankments are 2.00 m high (slope 5H/2V).

Slopes are covered with a layer of topsoil between 30 and 40 cm thick. Three hydraulic channels were built (1 m wide and 14.00 m long, Fig. 11). Two of them are presented: i) channel 1 built on untreated soil; ii) channel 2 built on lime treated soil. Fig. 12 shows an overview of the experimental set-up. The initial flow rate was $q=60$ l/s/m, corresponding to a water depth at crest $h_0=11$ cm. This flow was gradually increased to $q=400$ l/s/m, corresponding to a water depth at crest $h_0=38$ cm. The total duration of flow was 8.50 hours for the sequence of 10 stages (Fig. 13).

Fig. 14 shows the velocity profiles at the last stage ($h_0=38$ cm), as well as the final soil position for untreated soil (a) and lime-treated soil (b). The maximum velocity reached is 5 m/s on the lime-treated soil, which has not been eroded (the difference between initial and final soil profiles on Fig. 14b corresponds to topsoil). Analysis of the bottom position measured after each of the 10 stages (Fig. 15) shows that: i) the topsoil was eroded in the first stage ($h_0=11$ cm), ii) embankment soil erosion was mainly initiated at the slope toe for $h_0=42$ cm. It spread to the entire slope, leading to a 1.50 m deep erosion pit. The eroded embankment after 8.5 hours of flow is shown in Fig. 16.

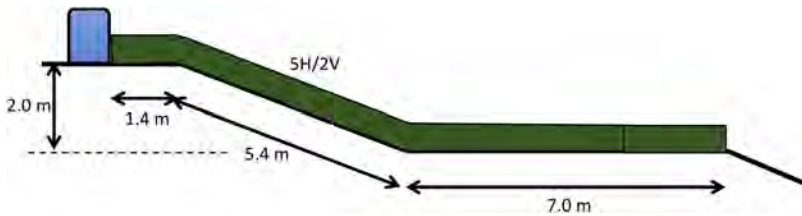


Fig. 11

Cross-section of the Salin de Giraud embankments and hydraulic channels
Coupe-type des remblais de Salin de Giraud et des canaux hydrauliques

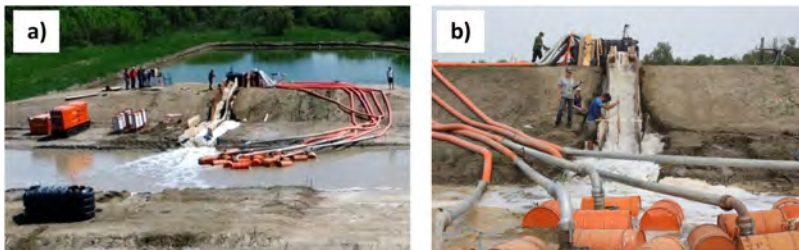


Fig. 12

Salin de Giraud: a) Channel 1 on untreated soil; b) Channel 2 on treated soil
Salin de Giraud : a) Canal 1 sur sol non traité ; b) canal 2 sur sol traité

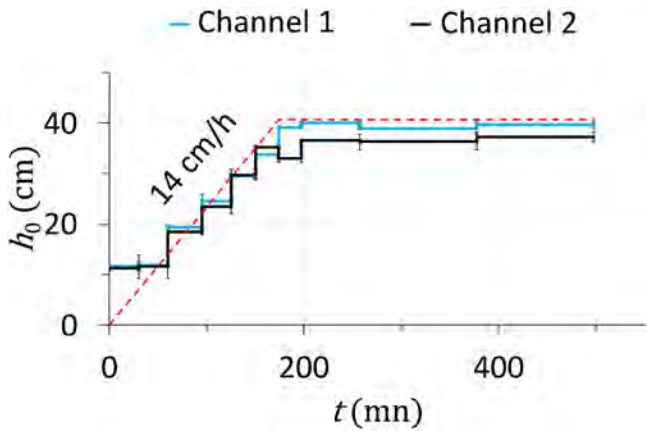


Fig. 13
Salin de Giraud: Crest water height h_0 for channels 1 and 2
Salin de Giraud - Hauteur d'eau en crête h_0 pour les canaux 1 et 2

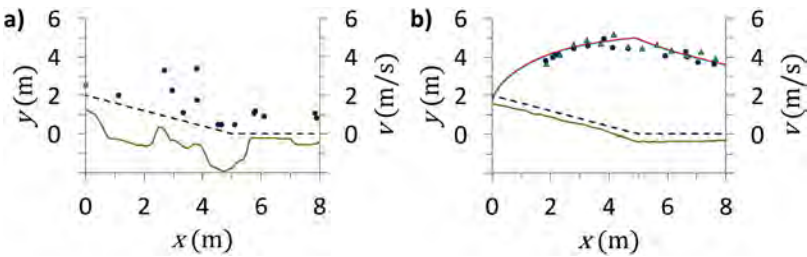


Fig. 14
Salin de Giraud: Measured flow velocities v (symbols), initial (dotted line) and final (solid line) ground positions; a) Channel 1 on untreated soil; b) Channel 2 on treated soil
Salin de Giraud : Vitesse d'écoulement mesurées (symboles), position initiale (trait pointillé) et finale (trait continu) du sol ; a) canal 1 sur sol non traité ; b) canal 2 sur sol traité

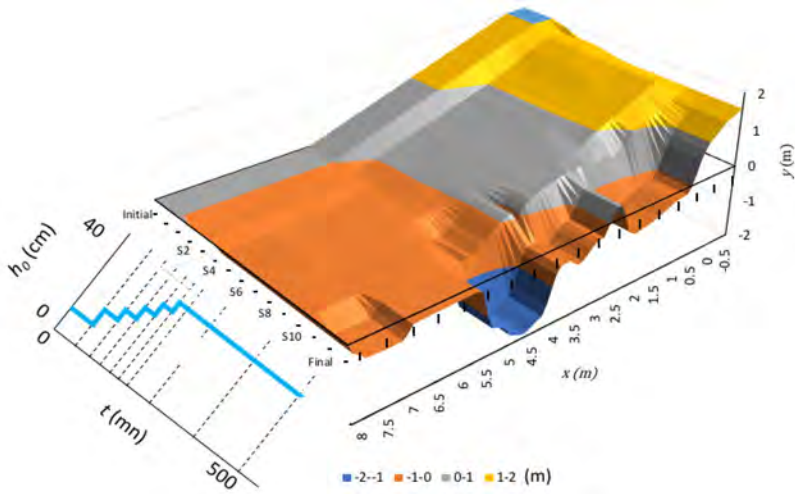


Fig. 15

Salin de Giraud - Channel 1: Bottom position measured after each stage
 Salin de Giraud - Canal 1 : Position du fond mesurée après chaque palier



Fig. 16

Salin de Giraud - Channel 1: a) eroded embankment after 8.5 hours of flow
 Salin de Giraud - Canal 1 : remblai érodé après 8h30 d'écoulement

4.3. OVERFLOW TESTS ON THE MONTFAUCON DIKE

As part of the OVERCOME project, two tests were performed in May 2022 on a CNR dike near Montfaucon (France). The dike is 6.20 m high. It consists of compacted silt (slope 4H/1V), 3.50 m thick at the top. In the downstream section, there is a layer of sandy gravel (0-30 mm, with larger boulders of 10-20 cm), about 1 m thick and 20 m long. In the lower section, the soil is an in-situ silt 2.70 m thick (slope 2H/1V). A 2.70 m-thick gravel embankment (0-30 mm) is placed at the foot of the dike (slope 3H/1V). The crest of this shoulder forms a 6.00 m wide berm, which includes a 3.00 m wide roadway (compact gravel). The rest of the berm is covered with deposited silt (approx. 3 m wide). Both slopes are covered with natural grass, about 3 cm high at the time of testing. The first layer of the foundation consists of alluvial gravel. The top of this layer corresponds to the level of the back channel.

Two hydraulic channels were built (Fig. 17): i) channel 1 built on intact soil (1 m wide and 25.00 m long) to apply the flow to the grass cover and gravel fill; ii) channel 2 built on soil stripped to a depth of 20 to 25 cm (0.6 m wide and 20 m long) to apply the flow to the soil making up the dike, in particular the compacted silt and sandy gravel. For channel 1, the initial flow rate was $q=12.8$ l/s/m, corresponding to a water depth at crest $h_o=3.7$ cm. This flow was gradually increased to $q=128$ l/s/m, corresponding to a water depth at crest $h_o=17.3$ cm. The total duration of flow was 6 hours for the sequence of 12 stages (Fig. 18a). For channel 2, the initial flow rate was $q=24$ l/s/m, corresponding to a water depth at crest $h_o=5.7$ cm. This flow rate was gradually increased to $q=142$ l/s/m, corresponding to a crest water depth $h_o=18.5$ cm. The total flow duration for the 9 stages was 4.5 hours (Fig. 18b).

Fig. 19 shows the twelve flow velocity profiles measured on the grass slope, the berm and the gravel slope. Fig. 19 also shows the hydraulic shear stress at the bottom, calculated under unsettled conditions from the flow velocity and height profiles. The maximum velocity on the grass slope is 4.2 m/s, corresponding to a maximum stress of 120 Pa. On the 0-30 mm gravel slope, the orders of magnitude of the Pilarczyk critical velocity and the Shields critical stress for 30 mm diameter grains are positioned. Fig. 20 shows, for channel 1, a flow corresponding to a crest water height of 18 cm, and the soil after 6h of flow on which no significant erosion was observed.

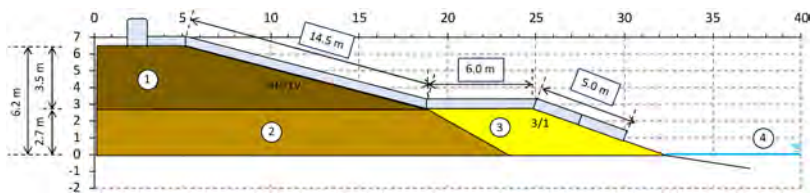


Fig. 17

Cross-section of the Montfaucon dike and hydraulic channel

Coupe-type de la digue de Montfaucon et canal hydraulique

1 Compacted silt

2 Silt in place

3 Gravel (0-30 mm)

4 Back channel

1 Limon compacté

2 Limon en place

3 Gravier (0-30 mm)

4 Contre-canal

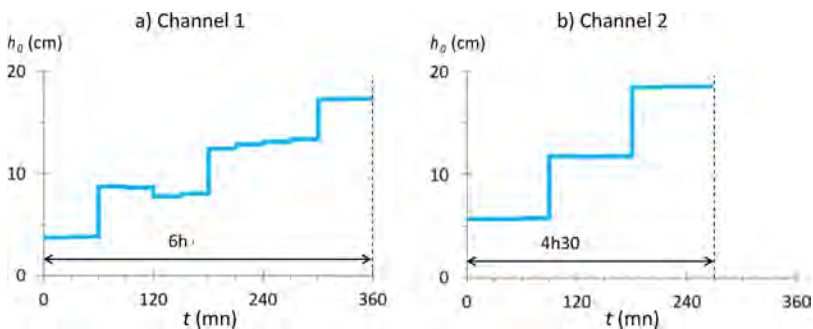


Fig. 18

Montfaucon - Crest water height h_0 for Channel 1 (a) and Channel 2 (b)

Montfaucon - Hauteur d'eau en crête h_0 pour le canal 1 (a) et le canal 2 (b)

No significant erosion of the grassy slope was observed (Fig. 21). Fig. 21a shows the gravel embankment after 6 hours of flow, where 3 to 4 m³ of soil were eroded. Analysis of the bottom position measured after each of the 12 stages (Fig. 21b) shows erosion developed in two stages. Initiation occurred at stage 8 for $h_0=13$ cm by surface erosion, corresponding to a flow velocity of 1.5 to 2 m/s. The 2nd erosion phase was a scouring at stage 11 for $h_0=17$ cm. Average velocity of erosion of the gravel was 30 cm/h, while maximum velocity of erosion was 160 cm/h.

Fig. 22a shows the eroded slope of channel 2 after 4.5 hours of flow, where 9 m³ of soil were eroded. The bottom position measured after each stage shows a

complex erosion process, including the formation and regression of a step (final step height ≈ 1.40 m, Fig. 22b). The erosion revealed a layer of sandy gravel, which eroded at a flow velocity of 2 m/s from the first flow. Surface erosion of compacted silt was initiated at a velocity of 3 m/s, but the bulk of the departure took place in the form of clods because of gravity, after erosion of the sandy gravel below.

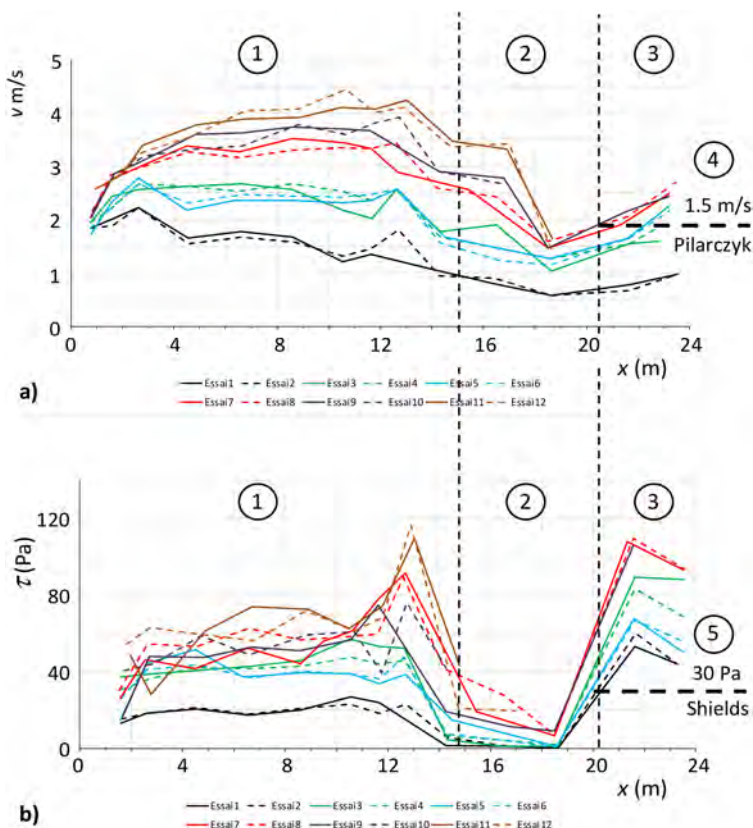


Fig.19

Montfaucon - Channel 1: a) Flow velocity, b) Hydraulic bottom stress

Montfaucon - Canal 1 : a) Vitesse d'écoulement, b) Contrainte hydraulique

1 Slope (grass)

2 Berm

3 Slope (gravel 0-30 mm)

4 Pylarczyk critical velocity

5 Shield stress

1 Talus (enherbement)

2 Risberme

3 Talus (gravier 0-30 mm)

4 Vitesse critique de Pylarczyk

5 Contrainte critique de Shields

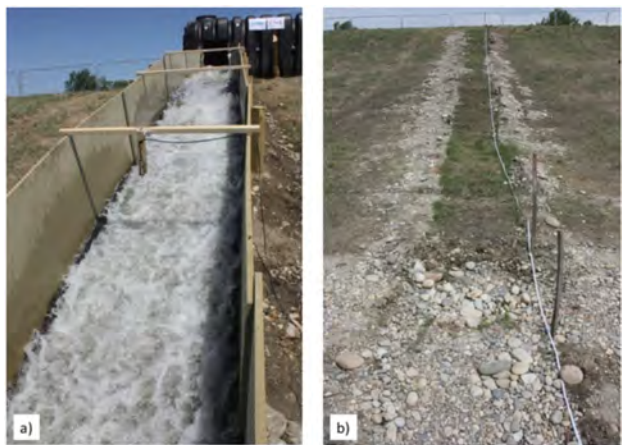


Fig. 20

Montfaucon - Channel 1: a) Flow for a crest water height $h_0=18$ cm; b) No significant grass erosion after 6 h of flow.

Montfaucon - Canal 1 : a) Ecoulement pour une hauteur d'eau en crête $h_0=18$ cm ;
b) Pas d'érosion significative de la couverture enherbée après 6 h d'écoulement.

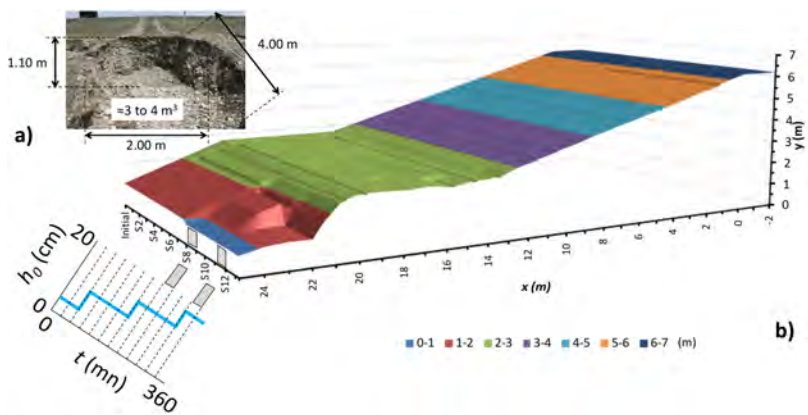


Fig. 21

Montfaucon - Channel 1: a) Photo of the gravel embankment after 6 hours of flow, b) Bottom position measured after each stage

Montfaucon - Canal 1 : a) Photo du remblai en gravier après 6 heures d'écoulement, b) Position du fond mesurée après chaque palier

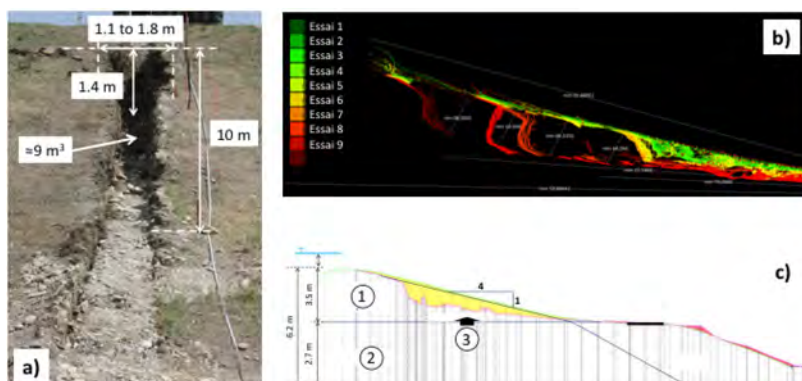


Fig. 22

Montfaucon - Channel 2: a) eroded slope after 4.5 hours of flow, b) Bottom position measured after each stage, c) Cross-section after erosion

Montfaucon - Canal 2 : a) talus érodé après 4h30 heures d'écoulement, b) Position du fond mesurée après chaque palier, c) Coupe-type après érosion

1 Compacted silt
2 Silt in place
3 Sandy gravel

1 Limon compacté
2 Limon en place
3 Gravier sableux

REFERENCES

- [1] HEWLETT H.W.M., BOORMAN L.A., BRAMLEY M.E. (1987). Design of Reinforced Grass Waterways. *CIRIA Report 116, Construction Industry Research and Information Association, London, England*, 116 p.
- [2] COX A., THORNTON C., ABT S. (2014). Articulated concrete block stability assessment for embankment-overtopping conditions. *Journal of Hydraulic Engineering*, 140(5), 06014007.
- [3] CFBR. *Recommandations pour la justification de la tenue à l'érosion des barrages et des digues en remblai* (to be published).
- [4] RECLAMATION-USACE (2019) *Best practices in dam and levee safety risk analysis*.
- [5] FOX G.A. ET AL. (2022). *Perspective: Lessons Learned, Challenges, and Opportunities in Quantifying Cohesive Soil Erodibility with the Jet Erosion test (JET)*, *Journal of the ASABE*, Vol. 65(2): 197–207.

- [6] BONELLI S. (2012) *Erosion of Geomaterials*, (Ed), John Wiley & Sons, 372 p.
- [7] BONELLI S. (2013) *Erosion in Geomechanics Applied to Dams and Levees*, (Ed), Wiley–ISTE, 388 p.
- [8] NERINCX N., BONELLI S., MERCIER F., CORNACCHIOLI F., FRY J.-J., HERRIER G., RICHARD J.-M., PUIATTI D., TACKER P. (2018), *DigueElite overflow resistant lime treated soils for dikes and earthdams*, *26th International Congress on Large Dam*, Vienna, Austria, 4-6 July.

COMMISSION INTERNATIONALE DES
GRANDS BARRAGES

VINGT-HUITIEME CONGRES DES
GRANDS BARRAGES
CHENGDU, MAI 2025

MOLARE TRAGEDY: THE SECONDARY DAM COLLAPSE INDUCED BY A HEAVY RAINFALL EVENT (*)

Andrea ABBATE & Antonella FRIGERIO
Ricerca sul Sistema Energetico – RSE S.p.A

ITALY

SUMMARY

On 13 August 1935, an intense cloudburst caused a sudden rise in the level of Lake Ortiglieto, in the province of Genoa. The main spillway became clogged with mud and debris and the secondary discharges were not sufficient to prevent the overtopping of the two dams: the main dam of Molare, 47 m high, and the secondary dam of Sella Zerbino, 14 m high, the latter not foreseen in the original project. The overflowing water eroded the fractured and poor-quality rocks of the Zerbino saddle and caused the sudden collapse of the secondary dam in the early afternoon. Approximately 20-25 million cubic metres poured into the valley below, reaching the town of Ovada within half an hour and killing over 100 people. It was clear that the geological characterisation of the Zerbino saddle was not carried out properly. However, it was the underestimation of the discharge system (spillways and syphons) compared to the hydrological characteristics of the Orba watershed that led to the overfilling of the Molare basin during the 1935 event. In previous literature investigations, uncertainties still persist regarding the magnitude of the rainfall event and the subsequent hydrological response of the Orba basin that triggered the sharp water level increase. Therefore, in this study, a reanalysis of that event based on numerical modelling has been conducted and compared with recent heavy rainfall episodes that occurred in the investigated area in 1977, 2014 and 2019. The results have shown that the 1935 event was intense but not extreme and that quick

**La tragédie de Molare : la deuxième rupture de barrage causé par de fortes précipitations*

rainfall-runoff hydrological response, with peak discharge around 2000 m³/s is predictable for that area. The analysis has confirmed that the catastrophic scenario could be avoided primarily with a better design of the dam's outflow structures (increasing the maximum discharge) and later with an accurate design and construction of the secondary dam taking into account the local geological characteristics.

RÉSUMÉ

Le 13 août 1935, de fortes précipitations ont provoqué une élévation soudaine du niveau du lac d'Ortiglieto, dans la province de Gênes. Le déversoir principal s'est obstrué avec de la boue et des débris et les décharges secondaires n'ont pas été suffisantes pour empêcher le débordement des deux barrages : le barrage principal de Molare, d'une hauteur de 47 m, et le barrage secondaire de Sella Zerbino, d'une hauteur de 14 m, ce dernier n'ayant pas été prévu dans le projet initial. Les eaux débordantes ont érodé les roches fracturées et de mauvaise qualité de la selle de Zerbino et ont provoqué la rupture soudain du barrage secondaire en début d'après-midi. Environ 20 à 25 millions de mètres cubes se sont déversés dans la vallée en contrebas, atteignant la ville d'Ovada en l'espace d'une demi-heure et tuant plus de 100 personnes. Il est clair que la caractérisation géologique de la selle de Zerbino n'a pas été effectuée correctement. Cependant, c'est la sous-estimation du système d'évacuation (déversoirs et siphons) par rapport aux caractéristiques hydrologiques du bassin versant de l'Orba qui a conduit au débordement du bassin du Molare lors de l'événement de 1935. Dans les études précédentes, des incertitudes persistent quant à l'ampleur des précipitations et à la réponse hydrologique ultérieure du bassin de l'Orba qui a déclenché la forte augmentation du niveau de l'eau. Par conséquent, dans cette étude, une réanalyse de cet événement basé sur la modélisation numérique a été réalisée et comparée aux récents épisodes de fortes précipitations qui se sont produits dans la zone étudiée en 1977, 2014 et 2019. Les résultats ont montré que l'événement de 1935 était intense mais pas extrême et qu'une réponse hydrologique rapide des précipitations et du ruissellement, avec un débit de pointe d'environ 2000 m³/s, est prévisible pour cette zone. L'analyse a confirmé que le scénario catastrophique pouvait être évité principalement grâce à une meilleure conception des structures d'évacuation du barrages (en augmentant le débit maximal) et, aussi, grâce à une conception et une construction précise du barrage secondaire tenant compte des caractéristiques géologiques locales.

1. INTRODUCTION

A dam break represents one of the most catastrophic risks related to the presence of a dam within a river basin [1] [2]. Dam breaks can cause extensive

damage, injuries and fatalities, but fortunately, this type of scenario is nowadays remote, especially in those countries where infrastructure monitoring, structural maintenance and retrofitting have improved the safety of dams [3]. However, a residual risk may exist when external forces severely hit the infrastructures, such as earthquakes and floods. The latter may cause significant damages to infrastructures if not properly managed or when outflow systems are poorly designed [4]. Italy has experienced several disasters in the past related to poor design or lack of adequate control systems [1]. Among others, the Molare disaster that happened in August 1935 was primarily triggered by a flash flood generated by an intense rainstorm that hit the upper part of the Orba basin, across the Piedmont and Ligurian regions [5]. As reported by chronicles and literature survey [6], the poor design of the outflow structures caused an initial reservoir overfilling that undermined the stability of the Sella Zerbino secondary dam of Lake Ortiglieto. The secondary dam was also poorly designed due to the final tweaking of the executive project and the inadequate geological and geotechnical survey of the rock substrate and dam foundation prior to construction [7]. The collapse of the secondary dam caused catastrophic damages, injuries and fatalities along the downstream Orba Valley and in the proximity of Molare and Ovada towns [3].

The Molare disaster was subjected to legal proceedings [8] and several studies have been published to analyse the possible causes of the disaster [6], [7], [3]. The investigations highlighted the difficulties and uncertainties encountered in estimating the real magnitude of the 1935 rainfall event and in reconstructing the Orba basin hydrological response. The latter has caused a rapid and uncontrolled Ortiglieto reservoir overfilling which triggered the subsequent Sella Zerbino secondary dam collapse [6] [3]. Bearing in mind these issues and considering that such type of disaster may occur again in the future due to the influence of ongoing climate change on the increase in extreme precipitations [9], a reanalysis of the Molare disaster is proposed to better understand what happened on that occasion. The analysis compares the historical data gathered from a literature survey with a numerical modelling reconstruction of the 1935 event: the hydrological rainfall-runoff evaluation and the Ortiglieto reservoir water balance are here presented. The instrument and the methodology adopted for the analysis are reported in the Materials and Methods section, the results are described in a dedicated paragraph and the main findings are commented on in the Discussion and Conclusion sections.

2. MATERIALS AND METHODS

Firstly, the analysis was carried out by gathering data about the dam design characteristics and the August 1935 event that triggered the Molare disaster [8]. Fig. 1 reports the location of the dam and the characteristics of Lake Ortiglieto formed by the Molare (principal) and Sella Zerbino (secondary) dams.

In January 1925 the Molare plant came into operation. The Molare dam was an arch-gravity structure (radius of about 200 m), 47 m high, with a maximum reservoir height of 322 m asl, and a dam crest height of 324.7 m asl. The discharge system consisted of 12 reinforced concrete surface siphons with a total flow rate of $500 \text{ m}^3/\text{s}$, equipped with an automatic trigger (Heyn system) and having a rectangular cross-section of $2 \times 3 \text{ m}$. The automatic syphons trigger took place in groups of 3 when the level exceeded 322 m asl. A side channel spillway was located on the right bank (capacity of $150 \text{ m}^3/\text{s}$) while the bottom outlet consisted of an iron pipe (diameter 1.80 m) positioned in the centre of the dam at an altitude of 280 m asl and equipped with a butterfly valve (capacity of $55 \text{ m}^3/\text{s}$). Furthermore, a mid-level outlet was located at an altitude of 280 m asl and equipped with a bell valve (capacity of $150 \text{ m}^3/\text{s}$). The maximum outflow rate was evaluated to be $855 \text{ m}^3/\text{s}$. The Sella Zerbino secondary dam was a gravity structure, 14 m high, with a maximum crest length of 110 m. This dam was designed and built in a very hasty manner, without adequate geological investigations that would have revealed the poor quality of the foundation materials [4] [5].



Fig. 1

Orba basin location in Piedmont region (Italy), map of Lake Ortiglieto in 1935 and pictures of the principal (Molare) and secondary (Sella Zerbino) dams, modified from [8].

Localisation du bassin de l'Orba dans la région du Piémont (Italie), carte du lac d'Ortiglieto en 1935 et photos des barrages principal (Molare) et secondaire (Sella Zerbino), d'après [8].

According to [5], in the Orba Basin, 364 mm of rain fell in less than 8 hours in August 1935. In other places of the basin the following data were recorded: 453 mm in 8 hours in Pianpaludo Locality (municipality of Tiglieto, upper Orba valley); 377 mm in Masone (upper Stura valley, contiguous to the Orba Valley); 390 mm in Belforte (Stura valley, just upstream of Ovada); 554 mm (182 mm in 2 hours) in Lavagnina Locality (Piota Valley). The event brought precipitation equal to almost 30% of the annual average in less than 24 hours, namely $15 \text{ m}^3/\text{s}$ per km^2 of the catchment area of the Orba Torrent, whose extension is about 140 km^2 . The outflow rate at the dam crest, nearby Bric Zerbino (i.e. 5 km upstream of Molare town), was between $1800 - 2000 \text{ m}^3/\text{s}$ with peaks of $2200 - 2300 \text{ m}^3/\text{s}$. According to a literature survey documented in [5], statistically, an event of such "magnitude" has a return time of about 1000 years. Nonetheless, other studies [10] have reduced such evaluation to 200-300 years, raising the question about the effective exceptionality of this event.

2.1. MODELS ADOPTED IN THE ANALYSIS

In this study, a reanalysis was conducted to investigate the triggering factor that caused the Molare disaster. The attention was pointed to rainfall-runoff reconstruction of the heavy rainfall that occurred in August 1935. According to [3] [6], uncertainties in runoff estimates represent the major challenge since the peak flow that occurred during that day was rather difficult to quantify through classical expeditious hydrological models. In this analysis, the CRHyME spatially distributed numerical model was adopted to analyse the 1935 event. CRHyME model (Climatic Rainfall Hydrogeological Model Experiment) [11] [12] is an open-source routine developed to address geo-hydrological processes occurring at a basin scale. Among them, the discharge routing represents an essential feature of the model that is carried out using the kinematic model [13]. The kinematic model has already been tested in basins located in mountain areas, it is rather fast, and it is retained sufficiently accurate where the slope gradient is of the order of 1% [14]. The kinematic approach is conventionally adopted in those contexts where lamination made by rivers is considered negligible, i.e. where valleys are supposed to carry the flood hydrograph downstream without modifying their shape [13]. Therefore, the CRHyME model was considered suitable for the hydrological reconstruction of the inflow hydrograph for Lake Ortiglieto.

The hydrological analysis cannot be designed if rainfall fields are not accurately described [15]. In this light, several studies have been conducted in the past years through the Orba Valley to collect data on the total cumulated rainfall that occurred during the 1935 event [3] [6]. A "hypothetical" reconstruction of the hyetograph was retrieved by examining the old studies carried out during the legal process following the disaster [6]. To feed the CRHyME model, the total daily quantities of 12 rain gauge stations across the Orba Basin have been extracted from

the SCIA archive (Sistema nazionale per la raccolta, elaborazione e diffusione di dati climatici, powered by ISPRA) [16]. These values have been temporarily down-scaled considering the synthetic hourly-based hyetograph proposed by [6]. To address the magnitude of the event and its return period, an analysis has been carried out using the IDF (Intensity Duration Frequency) curves for precipitation and the peak discharge recurrence statistics [17] [13], the latter evaluated by the ARPA (Agenzia Regionale Protezione Ambientale) Piedmont Environmental Agency [18], the PAI (Piano di Assetto Idrogeologico) Project (conducted by AdBPo Agency) [19] [20] [16] and the VAPI (Valutazione Piene Italiane) Project (conducted at national level) [21]. Similarly, the discharge statistics have been elaborated considering the PAI and VAPI projects. The evaluation of the return period of the event was necessary to establish the 1935 event exceptionality with respect to the 1000-years reference return period, conventionally adopted for the design discharge for dam construction [22].

The outcomes of the CRHyME simulations have been then taken into account for the reconstruction of the hydraulic behaviour of the Ortiglieto reservoir before the Sella Zerbino dam collapse. Attention was paid to simulating the increase in the reservoir level by simply implementing a reservoir volume V (in m^3) continuity equation. Then the activation of the outflow structures (spillway and syphon) has been simulated taking into account the back analysis studies and the related hydraulic formula [23] [3] [13]. Eq. 1 describes the reservoir water storage balance where q_{in} (in m^3/s) is the hydrological inflow discharge coming from the upstream Orba basin while q_{out} (in m^3/s) is the total outflow discharge from the outflow structures of the dam:

$$\frac{dV}{dt} = q_{in} - q_{out} \quad (1)$$

In Eq. 2, the water level h_{water} (in m) and the volume V_M (in Mm^3) relation retrieved from Lake Ortiglieto geometry is presented:

$$h_{water} = 294.2 * V_M^{0.0313} \quad (2)$$

Eq. 3 evaluates the Δh_{water} necessary for activating the 12 syphons (Eq. 4) and the lateral spillway (Eq. 5) with $L_{spillway} = 20$ m after reaching the maximum regulation height of 322 m asl:

$$\Delta h_{water} = (h_{water} - 322) \quad (3)$$

$$q_{out, spillway} = 0.385 * L_{spillway} * \Delta h_{water} * (2 * 9.81 * \Delta h_{water})^{0.5} \quad (4)$$

$$q_{out, syphons} = 12 * (10.40 * \ln(\Delta h_{water}) + 23.3) \quad (5)$$

The Molare reservoir reached full capacity about an hour before the collapse [6], and the water started to spill spontaneously above the crest of the two dams

after reaching the maximum height of 324.7 m asl. This additional discharge has been considered in the reservoir balance: the additional discharge Δh_{water_2} was evaluated as in Eq. 6 and $q_{out\ MOLARE}$ was estimated with Eq. 7 considering $L_{spillway\ MOLARE} = 145.5\text{ m} + 108.0\text{ m}$ that are respectively the crest linear development of the principal and secondary dams.

$$\Delta h_{water_2} = (h_{water} - 324.7) \quad (6)$$

$$q_{out\ MOLARE} = 0.385 * L_{spillway\ MOLARE} * \Delta h_{water_2} * (2 * 9.81 * \Delta h_{water_2})^{0.5} \quad (7)$$

2.2. THE REANALYSIS STUDY WORKFLOW

The workflow followed to carry out the back analysis of the Molare disaster is here presented. The results of each analysis step are reported in the next Result section.

1. Meteorological data reconstruction: based on data from 12 rain gauge stations located across the Orba Basin;
 - (a) Rainfall data magnitude estimation: the return period (TR) has been evaluated from local rainfall statistics (ARPA Piedmont, PAI and VAPI Projects)
2. Event-based hydrological simulation with CRHyME numerical model:
 - (a) Calibration and Validation of the model based on more than 13 years of simulation (from 01/09/2009 to 31/12/2022);
 - (b) Reconstruction of the event occurred in August 1935;
 - (c) Comparison of this event with others characterized by similar magnitude occurred in October 1977, 2014, and 2019.
3. Event-based hydraulic simulation considering the reservoir and outflow dynamic occurred in August 1935 and the equations listed in section 2.1.

3. RESULTS

3.1. RAINFALL MAGNITUDE ACROSS THE ORBA BASIN

The SCIA dataset contains the historical rainfall data for the entire Italian territory with a temporal resolution of 1 day [16]. The actual rainfall duration and temporal distribution of the 1935 event were reconstructed with past chronicles reporting that the August event lasted 8-10 hours [6]. The analysis of the rainfall volumes was carried out for 12 stations located across the Orba Basin and a typical average value between 350-400 mm was evaluated as representative of the 1935

event. In Fig. 2, the hourly rainfall distribution was downscaled from the daily dataset using the reconstructed hyetograph information. As can be noted, the Rossiglione, Lavagnina and Pianpaludo rain gauges were those stations that registered the highest rainfall intensities. The rainfall magnitude was evaluated using the IDF curves and reported in Table 1. The ARPA Piedmont IDF curves relative to the Lavagnina rain gauge station, the PAI Project IDF curves averaged across the entire Orba Basin, and the VAPI Project coefficients were considered for the rainfall statistics. As can be appreciated from Table 1, the event return period has significant variability with respect to the considered statistics. The PAI Project gives a return period in the order of 2000 years while ARPA Piedmont and VAPI Project converge to a lower value, around 200 years. This variability can be explained by looking at the local coefficients that were applied in the GEV (Generalized Extreme Value) rainfall statistics for the return period (TR) evaluation [21]. In the VAPI report, these coefficients are mapped for the north-western Italy area, and, within the Orba basin, they exhibit a significant gradient that made it difficult to homogenize the rainfall statistics. According to [21] [15], the fact may be related to the presence of a robust orographic effect that can significantly perturb the temporal and spatial distribution of the rainfall in that area, especially during the late-summer and autumn period where historically the highest cumulates and intensity have been recorded [24]. In this regard, a return period of the 1935 rainfall of around 200-300 years is deemed to be representative, which makes this event undoubtedly intense but not so as exceptional as expected or as described in past chronicles.

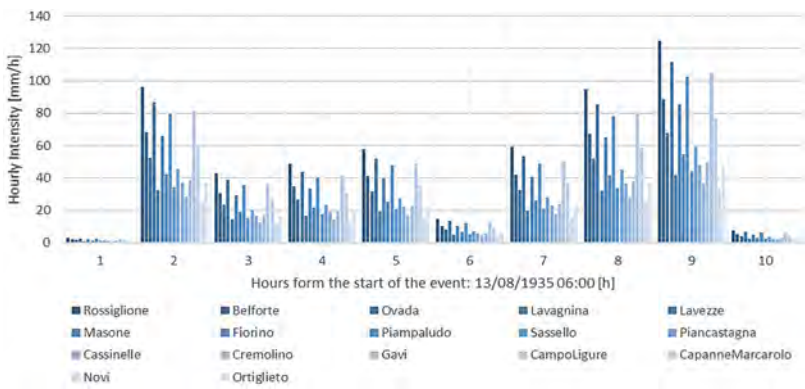


Fig. 2

13 August 1935 event: the rainfall distribution across the Orba basin.
L'événement du 13 août 1935 : la répartition des précipitations dans le bassin de l'Orba.

Table 1
Rainfall statistics of the 1935 event considering IDF curves from ARPA Piedmont, PAI and VAPI Projects.

Statistiques pluviométriques de l'événement de 1935 en tenant compte des courbes IDF des projets ARPA Piedmont, PAI et VAPI.

EVENT YEAR	TOTAL MEAN RAINFALL [MM]	EVENT MEAN DURATION [H]	EVENT RETURN PERIOD [YR] IDF ARPA PIEMONTE	EVENT RETURN PERIOD [YR] PAI PROJECT	EVENT RETURN PERIOD [YR] VAPI PROJECT
1935	370	10	200-500	~2000	100-200

3.2. HYDROLOGICAL RECONSTRUCTION ACROSS THE ORBA BASIN

3.2.1. Model calibration

The hydrological analysis was conducted by applying the numerical model CRHyME. The model was already tested in several mountain basins across the Italian territory [11] but was never performed in the Orba basin, characterized by such an amount of rainfall in a short time. To realistically reproduce the 1935 event on an hourly basis, the model was trained through a spin-up period of ~13 years between 09/09/2009 and 31/12/2022. This period was chosen due to the availability in [25] of rainfalls and discharge series for the whole investigated basin, which permits verification of whether the rainfall-runoff dynamic was reconstructed consistently with reality. For this purpose, 12 rain gauge stations were considered (settled in the proximity of the historical gauges that recorded the 1935 event) and 2 hydrometric stations (Ortiglieto and Basaluzzo) were considered for measuring the discharges. The Ortiglieto station is in the proximity of the small basin formed by the new dam built in 1940, after the disaster, 450 m upstream from Sella Zerbino, and the Basaluzzo station is situated at the Orba basin outlet.

Even if the CRHyME model can address several geo-hydrological processes (sediment transport, erosion etc.), in this analysis, attention was paid only to the hydrological outflow reconstruction. In the map in Fig. 1 the rain gauge location (blue), the runoff monitoring stations (green) and the 2 hydrometers of Ortiglieto and Basaluzzo (red) are represented within the Orba basin. In Table 2 the performance of the model at the check section of Ortiglieto and Basaluzzo are reported. The indexes NSE (Nash Sutcliffe Efficiency), RMSE (Root Mean Square Error) and PBIAS (Percent Bias) were considered for assessing the performance of the model training period [14] [11]. Regarding the volume, the model has performed rather conservatively in both sections, giving a value of NSE around 0.8-0.9. In terms of discharge, the model performances are sensible lower, especially for the station of Basaluzzo where a significant lamination of the peak discharges is expected due to the reduction of the valley slopes and the increase of the section width in the downstream part of the Orba River [20]. Applying the kinematic approach, the model

performance obtained in the proximity of the Molare dam at the Ortiglieto hydro-metric station was deemed satisfactory for conducting the event-based simulation of the 1935 event.

Table 2
Model CRHyME calibration scores using NSE, RMSE and PBIAS indexes.
Modèle CRHyME : résultats d'étalonnage à l'aide des indices NSE, RMSE et PBIAS.

ERRORS	NSE	RMSE	PBIAS
Discharge Ortiglieto	0.143	7.797	9.450
Volume Ortiglieto	0.975	–	3.307
Discharge Basaluzzo	0.388	26.550	–17.505
Volume Basaluzzo	0.808	–	–22.026

3.2.2. *Model validation*

Since the CRHyME model was trained on daily-based data, a validation on a sub-hourly event was conducted, taking into account the Orba flood that happened on 7-8 October 2024 [25]. The CRHyME model was fed by hourly-based rainfall data from 01/09/2024 up to 10/10/2024 and the computed discharges were compared with those measured by ARPA Piedmont. Since only the water levels (not the discharges) were available for that event, the stage-discharge relations were reconstructed from the historical data and then applied to retrieve the river discharge from the stage measurements. As can be appreciated from Fig. 3, the discharges computed by CRHyME range between the possible variability of the retrieved stage-discharge relations (dashed lines represent the stage-discharge relations obtained from reference curves: the green evaluated by ARPA Piedmont and the red obtained by stage-discharge regression from past data series). Through this validation test, the Orba Basin showed a typical torrential rainfall-runoff behaviour, characterized by a rapid flood generation with high peak discharges and with a rather short memory of the antecedent soil moisture conditions (the influence of which is smoothed in a few weeks). This evidence has been confirmed by other authors [3] [24] who have studied the basin in the past and found a correlation with the typical heavy rainfall statistically expected in the area across the Apennines ridge [21].

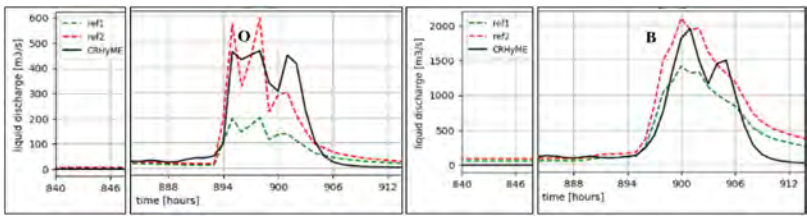


Fig. 3

Validation of the CRHyME model computations using a recent event at Ortiglieto and Basaluzzo sections. The modelled peak discharge (black) is approximately between the red and green lines describing the possible variability of stage-discharge relations.

Validation des calculs du modèle CRHyME à l'aide d'un événement récent dans les sections d'Ortiglieto et de Basaluzzo. Le pic de décharge modélisé (noir) est approximativement entre les lignes rouge et verte décrivant la variabilité possible des relations stade-décharge.

3.2.3. Model verification for the 1935 event

After CRHyME calibration and validation, the reconstruction of the 1935 event was carried out. Fig. 4 reports the resulting hydrograph recorded in Ortiglieto station.

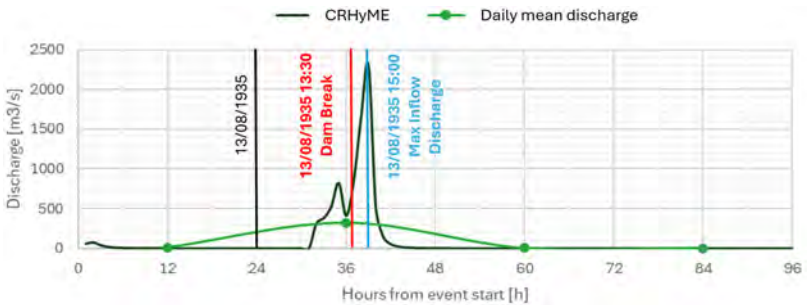


Fig. 4

Verification of the CRHyME model simulating the 1935 event. The maximum discharge is around 2300 m³/s which is in accordance with the literature surveys. The green line represents the daily mean discharge that reached a maximum of 300 m³/s.

Vérification du modèle CRHyME simulant l'événement de 1935. Le débit maximal est d'environ 2300 m³/s, ce qui est conforme aux études bibliographiques. La ligne verte représente le débit moyen quotidien qui atteint un maximum de 300 m³/s.

As can be appreciated, the peak discharge computed by CRHyME reaches a value of 2300 m³/s for Ortiglieto. These data are in accordance with the literature surveys and the empirical estimates obtained using a simplified hydrological model [5] [3]. Looking at the graph, a sharp rise in the discharge can be appreciated at the beginning of the event which is representative of a fast hydrological response of the Orba basin, which was already encountered during the validation phase of the model.

3.3. HYDRAULIC RECONSTRUCTION OF ORTIGLIETO RESERVOIR WATER BALANCE

The next step of the analysis focused on the Ortiglieto water reservoir balance during the event, a few hours before the Sella Zerbino secondary dam collapse. Eq. 1 was applied by taking the CRHyME outputs as the inflow hydrograph of the reservoir and by reproducing the outflow using the hydraulic design characteristics of the syphons and spillways of the Molare dam. However, to convert the reservoir volume into water level, the stage-volume curve of Lake Ortiglieto was reconstructed according to information available in the literature [3] [6]. The evolution of the water level as a function of the inflow discharge from the upstream Orba basin is reported in Fig. 5. The first graph on the left shows the discharge provided by the literature study documented in [3] [6] while the second graph considers the inflow discharge simulated by CRHyME. The shape of the inflow hydrographs is very similar but the peak value of CRHyME is lower (2300 m³/s) than that of the literature study (3000 m³/s).

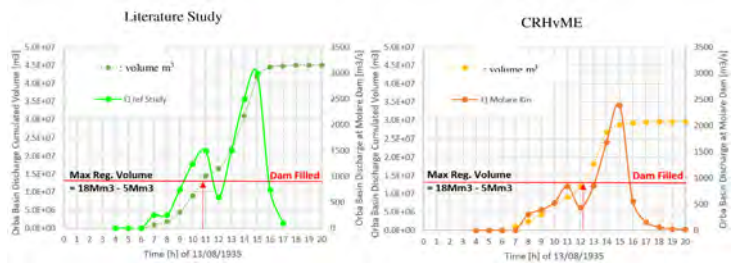


Fig. 5

Molare dam disaster: hydrological reconstruction provided respectively by the literature study in [3] [6] and by the CRHyME numerical simulation.

Catastrophe du barrage de Molare : reconstruction hydrologique fournie respectivement par l'étude de la littérature dans [3] [6] et par la simulation numérique CRHyME.

In Fig. 6, the first graph shows a significant anticipation in time of the estimated water level (orange) with respect to the reference measured level (green). The volume computed at the instant of dam collapse is around 38 Mm³ which is significantly higher

than the maximum regulation volume of 18 Mm³. On the other hand, the CRHyME simulation appears to be better, providing an estimated reservoir water level evolution (orange) rather in accordance with the reference one (green). In this case, the maximum volume reached before the collapse is around 28 Mm³, which is similar to the literature hypothesis reported in [4] [5]. In both cases, the maximum regulation height of 322 m asl (corresponding to 18 Mm³) volume was reached between 10:30 and 12:00 a. m. on 13 August 1935, very close to 11:00 a.m. reported in the historical chronicle.

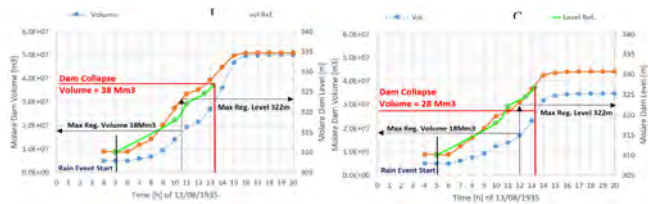


Fig. 6

Molare dam disaster: Ortiglieto reservoir balance reconstruction provided by the literature study in [3] [6] and by the CRHyME numerical simulation.
Catastrophe du barrage de Molare : Reconstruction de l'équilibre du réservoir d'Ortiglieto fournie par l'étude de la littérature [3] [6] et par la simulation numérique CRHyME.

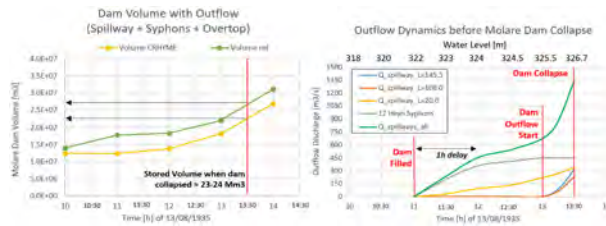


Fig. 7

Outflow dynamic of Ortiglieto reservoir a few hours before the Sella Zerbino secondary dam collapse. The 1-hour delay in starting the outflow was caused by inefficient activation of the Heyn system of the 12 syphons.
Dynamique du débit du réservoir d'Ortiglieto quelques heures avant l'effondrement du barrage secondaire de Sella Zerbino. Le retard d'une heure dans le début de l'écoulement a été causé par l'activation inefficace du système Heyn à 12 siphons.

However, the last part of the water level reconstruction (after reaching 322 m asl) is affected by additional uncertainty due to the activation of the outflow systems of the Molare principal dam that were designed to drain a maximum discharge of 855 m³/s [5]. As can be noted, this value significantly underestimated the maximum discharge of 2000-2500 m³/s reached during the 1935 event. Fig. 7 (left) represents

the reduction of the water volume stored by the Ortiglieto reservoir before the dam break due to the activation of the outflow systems. Thus, the maximum total volume computed with CRHyME must be reduced from 28 Mm³ to 23-24 Mm³. Fig. 7 (right) shows the temporal evolution of the dam's discharges. The activation system of the 12 syphons proved to be significantly inadequate (according to the analysis conducted by [23]) causing a delay in the reservoir regulation (and water level stabilization): a reasonable efficiency (> 0.8, Fig. 7) in relation to the maximum designed discharge was only reached one hour after the maximum regulation level was exceeded. Before the dam overtopping began, the total discharge was about 650 m³/s, sensibly below the 855 m³/s because the bottom outlet was not functioning, being completely occluded [4]. When the overtopping of the two dams began, the outflow reached a value of around 1350 m³/s, which was in any case sensibly below the incoming discharge peak of 2300 m³/s (Fig. 4). The hydraulic analysis, based on the design data of the outflow systems, has confirmed that it was inadequate to deplete such an amount of water volume incoming from the upstream basins.

3.4. COMPARISON WITH RECENT EVENTS

The 1935 event was considered exceptional by [5] [8] [10]. Therefore, a comparison with other similar events that occurred more recently within the Orba basin was conducted. In Table 3 the event of 1935 is analysed together with those of October 1977 [26], October 2014 [18] and October 2019 [27]. These events occurred in the autumn season, historically the wettest period in the Orba Basin. These events have caused significant geo-hydrological issues throughout the basin and have in common not only the amount of rainfall that fell on the area but also the short duration, generally less than a day. In this regard, 2019 is much more similar to 1935 in terms of rainfall parameters. As can be appreciated from Table 3, the return period estimate is affected by significant uncertainties and differences depending on the rainfall statistics considered. Nevertheless, the ARPA Piedmont and VAPI Project seem to converge in their final results, which show a similarity in magnitude between the 1935 and 2019 events.

Table 3
Comparison of the rainfall statistics related to different rainfall events (1977, 2014 and 2019), that occurred in the Orba Basin.

Comparaison des statistiques pluviométriques relatives à différents événements pluviométriques (1977, 2014 et 2019) survenus dans le bassin de l'Orba.

EVENT YEAR	TOTAL MEAN RAINFALL [MM]	EVENT MEAN DURATION [H]	EVENT RETURN PERIOD [YR] ARPA	EVENT RETURN PERIOD [YR] PAI	EVENT RETURN PERIOD [YR] VAPI
1935	370	10	200-500	~2000	100-200
1977	361	24	~50	~200	~20
2014	213	24	~10	<2	~3
2019	326	11	100-200	~500	~ 100

Using the precipitation data from the three-added events, the hydrological simulation was again conducted with CRHyME keeping the same calibration parameters as for the 1935 event. In Fig. 8 (left, top graph) the hydrograph recorded at the Ortiglieto dam section was compared with the four investigated events while the total volumes are reported in Fig. 8 (left, bottom graph). The peak discharge of 1935 and 1977 are the highest with a maximum value between 2000-3000 m³/s. In terms of volume, as anticipated before from rainfall analysis, the 1935 and 2019 events have shown similar values confirming the hypothesis of similarity between the two rainfall events. The 2014 event is the weakest of those considered, with a peak discharge sensibly lower than the others. In Fig. 8 (right) the statistics on the return period (TR) of the four peak discharges have been reported considering the available statistics from PAI and VAPI projects. These two statistics seem to converge in identifying the return period of the analysed peak discharges.

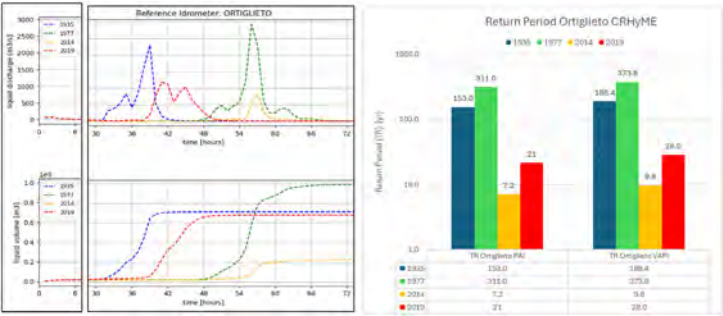


Fig. 8

Hydrographs provided by CRHyME for the 4 investigated events (left) and return period evaluations of the peak discharge (right).
Hydrogrammes fournis par CRHyME pour les 4 événements étudiés (à gauche) et évaluations de la période de retour du débit de pointe (à droite).

In the last step of the comparison, the iso-frequency hypothesis between rainfall intensities and peak discharges magnitude were verified. According to the literature [17] [13], this hypothesis is generally accepted for flash flood events but, in some cases, it may be not completely fulfilled since it assumes a uniform spatial distribution of the rainfall amounts over the investigated watershed. Looking at Table 4, for the 1935 and 2014 events, this hypothesis is considered valid since the rainfall-discharge return period statistics are comparable. On the other hand, for 1977 and 2019 the two statistics are not similar. A possible explanation for this can be sought in the inhomogeneity of precipitation amounts and duration that, probably, for 1977 and 2019 were rather scattered within the Orba basin portion upstream of the Ortiglieto section. For 1977, the duration of 24 hours seems slightly overestimated, but no additional references have been found in the investigated literature [26]. Considering the daily maximum values recorded in Piancastagna (432 mm) as the most representative

station of the upstream western part of the Orba Basin, the return period spans across ~200 years for the ARPA Piedmont IDF curves, ~500 years for the PAI project, ~50 years for the VAPI project), with a mean value of 250 years that is similar to the return period of the modelled discharge. For 2019, the iso-frequency hypothesis is addressed by the VAPI project while the others yield a sensible overestimation of the magnitude. Looking at the rainfall data series from [25], the average duration of the event was slightly longer (around 15 – 20 hours) in the upstream portion of the Orba Basin. After applying the correction, the mean rainfall returns period results in 25 years which is closer to that computed for the discharge.

The high spatial and temporal variability of precipitation (which is also found in the rainfall statistic coefficients) represents a crucial point that may undermine the rainfall-runoff iso-frequency hypothesis. The corrected results (shown in Table 4) are now more in accordance with the return period of the discharges. They confirm the existence of an iso-frequency between rainfalls and runoff at least for not large mountain basins where the hypothesis of kinematic runoff routing is retained sufficiently accurate.

Table 4

Comparison of the rainfall statistics between different rainfall events (1977, 2014 and 2019) occurred in the upstream portion of Orba Basin close to the Ortiglieto section. The (*) events have been corrected considering the possible local variability of precipitation.

Comparaison des statistiques pluviométriques entre différents événements pluviométriques (1977, 2014 et 2019) survenus dans la partie amont du bassin de l'Orba, à proximité de la section Ortiglieto. Les événements () ont été corrigés en tenant compte de la possible variabilité locale des précipitations.*

EVENT YEAR	TOTAL MEAN RAINFALL [MM]	EVENT MEAN DURATION [H]	RAINFALL RETURN PERIOD [YR] ARPA	RAINFALL RETURN PERIOD [YR] PAI	RAINFALL RETURN PERIOD [YR] VAPI	DISCHARGE RETURN PERIOD [YR] PAI	DISCHARGE RETURN PERIOD [YR] VAPI
1935	291	10	~200	~500	~50	153	188
1977	355	24	~50-100	~20-50	~10-20	311	374
2014	117	24	< 2	~2	<2	7.2	9.8
2019	241	11	~100	~100	~20	21	28
1977*	432*	24	~200	~500	~50	311	374
2019*	241	15*	~20-50	~50	~10	21	28

4. DISCUSSION

The study here conducted has shown a reanalysis of the meteorological, hydrological, and hydraulic triggering causes of the Sella Zerbino secondary dam collapse in August 1935. The literature review has addressed the event as extreme

but uncertainties about its real magnitude were found. In this work, a comprehensive evaluation of the rainfall-induced catastrophe was carried out to clarify any doubts. The CRHyME software was adopted to simulate the rainfall-runoff dynamics of the Orba basin and to reconstruct the water balance of the Ortiglieto reservoir. The main outcome of the study has revealed that the 1935 event was not so exceptional when considering both rainfalls and discharge amounts. Bearing in mind the uncertainties encountered in the rainfall and discharge statistics study, the event was characterized by a return period in the range of ~ 200 years. This value is significantly lower than the expected dam design return period, generally addressed for 1000-year flood magnitude. The results are in agreement with a previous study conducted by [10] for the Lavagnina rain gauge station where in 1935 event the highest rainfall amounts in the Orba basin were recorded. Since the 1935 event was defined as non-exceptional by the analysis presented here, this flood was compared with more intense ones reported in the literature and historical chronicles that occurred in 1977, 2014 and 2019 during the autumn seasons. The analysis has shown that a high peak discharge is a characteristic of the Orba basin's rapid response to rainfall-runoff and that is not infrequent to reach these values during the most intense floods. According to [14], this behaviour is typical of the Apennine area where rainfall-runoff transformation is strongly perturbed by the orographic effects [21] [15]. The rainfall and discharge statistics gathered from the VAPI project show a high spatial gradient of the extreme values parameters that address the significant variability of the hydrological cycle in these areas. The meteorological and hydrological analyses were theoretically conducted to understand what happened within the Ortiglieto reservoir a few hours before the collapse. Considering the previous studies that addressed this problem, the main uncertainties were related to the lake inflow discharge evaluation. Since the analysis conducted with the CRHyME model has helped to reduce the rainfall-runoff uncertainties through a numerical approach, the reservoir dynamics were restudied and compared with the reference ones. The inflow discharge reconstruction operated using CRHyME results as input data has performed rather well, addressing correctly the reservoir water level evolution. This simulation also correctly evaluated the time when the maximum regulation altitude (322 m) was reached (around 11:00 a.m. on 13 August 1935). After that, a correction of the reservoir balance was performed considering the outflows of the lateral spillway and the 12 syphons. According to previous studies [23], the syphons activation system did not function properly, causing a significant delay (about 1 hour) before reaching the design efficiency, as was simulated in Fig. 7. From a hydraulic viewpoint, this fact was crucial for the rapid overfilling of the reservoir and the subsequent collapse of the Sella Zerbino secondary dam. In our opinion, the discharge systems were significantly underestimated with respect to the possible peak discharge coming from the upstream basin. On that occasion, as was also reported in the literature and verified in this analysis, the maximum outflow discharge of $855 \text{ m}^3/\text{s}$ was not sufficient to manage such natural peak flows. Even if the collapse had not happened, the reservoir overfilling would have caused uncontrolled downstream discharge from the two dams, especially during the incoming hydrograph peak of about $2000\text{-}2500 \text{ m}^3/\text{s}$, which was theoretically reached at 15:00 on 13 August 1935 according to numerical simulation (Fig. 4). As a result, we can conclude that the

primary cause of the Molare disaster was the poor design and management of the reservoir hydraulic structures.

This reanalysis study was possible thanks to the availability of data coming from historical chronicles and previous analyses that addressed different aspects of that disaster. Our work was carried out to provide a comprehensive and analytical framework of that event, addressing the importance of numerical-based analysis. The results obtained were evaluated from the CRHyME model that has been already tested for simulating geo-hydrological issues (floods and landslides) at a basin scale [14]. Using such numerical models on some occasions may add further complexity to the analysis but, in this case, the calibration and validation phase helped not only to improve the model performance but also to better understand the rainfall-runoff peculiarities of an area that is one of the wettest in Italy [24]. The Orba basin shows a behaviour that is typical of torrential rivers where rapid flash floods may occur in a rather short time [28]. Nonetheless, all the analyses have shown how delicate it is to study such types of rivers, characterized by such sharp variations in peak discharge. The Molare disaster happened in a context where human-induced climate change was absent, but nowadays this represents an effect that should not be neglected [9]. Recently, in the surrounding area of the Orba basin, severe floods have hit towns and cities (Piedmont in 1994 and 2000 and Genoa in 2011) [29] and their strength was reported to be rather anomalous with respect to historical recordings. Moreover, the highest rainfall rates and amounts recorded in Italy were measured in these areas (for example, Rossiglione station on 4 October 2021 recorded 883,8 mm in 24 hours) [25]. Since in the future, the climate models project an increase in rainfall severity across the Mediterranean Sea area [9], the studied areas would be subjected (with high confidence) to possible severe floods triggered by extreme rainfall events amplified by orographic effects [15] and the proximity of the warm sea [30]. In this context, the analysis conducted describes a possible approach to the problem by highlighting the hypothetical undesirable effects that may cause a dam collapse and the importance of considering the hydrological peculiarities of the area that could be significantly altered in the future by the effects of climate change.

5. CONCLUSION

The Molare disaster was determined by twofold causes that consequently triggered the Sella Zerbino secondary dam collapse: the wrong design of the dam discharge systems that caused the reservoir overfilling and the poor quality of the foundation materials of the secondary dam (not studied here). The first aspect was analysed exploring the meteorological, hydrological and hydraulic characteristics of the heavy rainfall event that in August 1935 triggered the dam-break. The magnitude of the rainfall was expressed through the evaluation of the return period, which was established around 200 years. The 1935 event was therefore classified as non-

exceptional and for this reason, it was compared with similar rainfall-discharge magnitude events that occurred in 1977, 2014 and 2019. These results were also confirmed by the frequency analysis of the peak discharges, reproduced through the CRHyME hydrological model, confirming the validity of the iso-frequency hypothesis between rainfalls and discharges for flash flood events.

After the CRHyME model calibration and validation, which has shown a good reproduction of the past Orba basin hydrology, the code was applied for reconstructing the hydrograph from the 1935 rainfall series. The resulting hydrograph was considered for simulating the Ortiglieto reservoir dynamics (i.e. water level evolution) that were reproduced coherently with the reference data available in the literature. The ongoing climate change may modify the intensity of the precipitation, increasing the frequency of the extreme events that may undermine in the future the functionality of dams that in the worst cases may evolve similarly to the Molare disaster. The reanalysis proposed has shown a possible analytical framework to address such complex problems related to the safety of dams against intense rainfall-induced floods.

REFERENCES

- [1] F. LUINO, G. TOSATTI E V. BONARIA, «Dam failures in the 20th century: nearly 1000 avoidable victims in Italy alone,» *Journal of Environmental Science and Engineering*, vol. 3, p. 19–31, 2014.
- [2] R. ALBANO, L. MANCUSI, J. ADAMOWSKI, A. CANTISANI E A. SOLE, «A GIS Tool for Mapping Dam-Break Flood Hazards in Italy,» *ISPRS International Journal of Geo-Information*, vol. 8, p. 250, 2019.
- [3] G. PETACCIA E L. NATALE, «1935 Sella Zerbino dam-break case revisited: A new hydrologic and hydraulic analysis,» *Journal of Hydraulic Engineering*, vol. 146, p. 05020005, 2020.
- [4] V. BONARIA E G. TOSATTI, «13th August 1935: A catastrophic dam failure in the Orba valley (Piedmont, Italy),» *Italian journal of engineering geology and environment*, p. 383–391, 2013.
- [5] V. BONARIA E G. TOSATTI, «Il disastro di Molare del 1935 in Valle Orba (AL): un Vajont dimenticato,» *GEOLOGIA DELL'AMBIENTE*, vol. 1, p. 29–34, 2011.
- [6] G. PETACCIA E L. NATALE, «Design flood estimation: Lessons learnt from Sella Zerbino Dam-break,» *Italian journal of engineering geology and environment*, p. 437–443, 2013.

- [7] G. PETACCIA, C. MILAZZO, L. NATALE E C. G. LAI, «The collapse of the Sella Zerbino gravity dam,» *Engineering geology*, vol. 211, p. 39–49, 2016.
- [8] V. BONARIA, «13 agosto 1935: Il Disastro di Molare,» 1 11 2024. [Online]. Available: <http://www.molare.net/>.
- [9] P. FAGGIAN, «Future Precipitation Scenarios over Italy,» *Water*, vol. 13, 2021.
- [10] O. BAIETTO, A. LIBERTINO E M. VOLPATO, «Ricostruzione del periodo di ritorno del nubifragio di Molare del 13 Agosto 1935,» Politecnico di Torino, Torino, 2012.
- [11] A. ABBATE, L. MANCUSI, F. APADULA, A. FRIGERIO, M. PAPINI E L. LONGONI, «CRHyME (Climatic Rainfall Hydrogeological Modelling Experiment): a new model for geo-hydrological hazard assessment at the basin scale,» *Natural Hazards and Earth System Sciences*, vol. 24, p. 501–537, 2024.
- [12] F. FUSCO, A. ABBATE, D. CALCATERRA, P. DE VITA, L. GUERRIERO, L. LONGONI E M. PAPINI, «Susceptibility mapping of shallow landslides inducing debris flows: a comparison of physics-based approaches,» *Italian journal of engineering geology and environment*, p. 63–71, 2023.
- [13] V. T. CHOW, D. MAIDMENT E L. MAYES, *Applied hydrology*, New York: McGraw-Hill, 1988.
- [14] A. ABBATE, Hydrogeological hazards evaluation under climate change scenarios : an application of the CRHyME model (Climatic Rainfall Hydrogeological Modelling Experiment), Milano: Politecnico di Milano, 2022.
- [15] A. ABBATE, M. PAPINI E L. LONGONI, «Orographic Precipitation Extremes: An Application of LUME (Linear Upslope Model Extension) over the Alps and Apennines in Italy,» *Water*, vol. 14, p. 2218, 2022.
- [16] ISPRA, «SCIA - Dati ed Indicatori,» 1 11 2024. [Online]. Available: <https://scia.isprambiente.it/>.
- [17] A. ABBATE, M. PAPINI E L. LONGONI, «Analysis of meteorological parameters triggering rainfall-induced landslide: a review of 70 years in Valtellina,» *Nat. Hazards Earth Syst. Sci.*, vol. 21, n. 7, pp. 2041–2058, 2021.
- [18] ARPA Piemonte Dipartimento Sistemi Previsionali, «ANALISI EVENTO 9-13 OTTOBRE 2014,» ARPA Piemonte, Torino, 2014.
- [19] M. FURIA, M. MOLINARI e A. Da Corte, «STUDIO IDRAULICO PER LA DEFINIZIONE DELLE AREE A PERICOLOSITA' IDRAULICA NEL VERSANTE PADANO DELLA PROVINCIA DI SAVONA BACINI DEL

- TORRENTE ERRO, ORBA, OLBICELLA E MIOGLIA,» PROVINCIA DI SAVONA, Savona, 2005.
- [20] Autorità di Bacino del Fiume Po e Regione Piemonte, «SCHEMA DI PROGETTO DI VARIANTE AL PAL: Torrente Orba Da Silvano d'Orba alla confluenza nel fiume Bormida,» Autorità di Bacino del Fiume Po, Alessandria, 2015.
- [21] C. DE MICHELE E R. ROSSO, «Rapporto sulla Valutazione delle Piene in Italia Nord Occidentale,» CNR, Milano, 2001.
- [22] ITCOLD, «La gestione dell'interrimento dei serbatoi artificiali italiani,» ITCOLD, Roma, 2009.
- [23] L. NATALE E G. PETACCIA, «Verifica sperimentale dello scarico a sifone della diga di Bric Zerbino,» *Proc. XXXII Convegno Nazionale di idraulica e Costruzioni Idrauliche, Brescia, Italy*, 2012.
- [24] A. MANDARINO, F. LUINO E F. FACCINI, «Flood-induced ground effects and flood-water dynamics for hydro-geomorphic hazard assessment: the 21–22 October 2019 extreme flood along the lower Orba River (Alessandria, NW Italy),» *Journal of Maps*, vol. 17, p. 136–151, 2021.
- [25] ARPA Piemonte, «ARPA Piemonte Richieste Dati,» 1 11 2024. [Online]. Available: <https://www.arpa.piemonte.it/ricerca/dati>.
- [26] M. ENRICO FERRARIO E A. MARINO, «Evento Alluvionale del 6-7 Ottobre 1977,» UNI-MET, 1977.
- [27] L. MERCALLI, «NUBIFRAGI DEL 21 OTTOBRE 2019 NELL'ALESSANDRINO,» Nimbus, Moncalieri (TO), 2019.
- [28] V. FERRO, *La sistemazione dei bacini idrografici*, McGraw-Hill, 2006.
- [29] CNR, «Popolazione a Rischio da Frana e da Inondazione in Italia - Report,» 1 11 2024. [Online]. Available: <https://polaris.irpi.cnr.it/>.
- [30] D. SPANO, V. MEREU, V. BACCIU, M. SERENA, A. TRABUCCO, M. ADINOLFI, B. GIULIANA, F. BOSELLO, M. BREIL, G. COPPINI, A. HRST ESSENFELDER, G. GALLUCCIO, T. LOVATO, S. MARZI, S. MASINA, P. MERCOGLIANO, J. MYSIAK, S. NOCE, J. PAL E M. ZAVATTARELLI, *Analisi del Rischio. I cambiamenti climatici in Italia*, 2020.

COMMISSION INTERNATIONALE DES
GRANDS BARRAGES

VINGT-HUITIEME CONGRES DES
GRANDS BARRAGES
CHENGDU, MAI 2025

CASE STUDY – A DAM RAISING OPTIONS STUDY FOR A DAM IN SOUTHERN AFRICA (*)

Chencen (Janice) ZHANG
Senior Civil Engineer, KNIGHT PIESOLD

Robert Phillip GREYLING
Technical Director, KNIGHT PIESOLD

Edwin LILLIE
Section Manager, KNIGHT PIESOLD

SOUTH AFRICA

SUMMARY

This Dam in Southern Africa provides approximately 20 million cubic meters of live storage that is utilised to supply flow to several downstream hydropower stations as part of a cascading system. The Owner observed that during rainy seasons significant excess runoff volume exists which is currently spilled as the dam reservoir is unable to store the extra volume. The Dam was originally designed to be raised by 5 m from its current Full Supply Level (FSL) in the future to increase the dam storage capacity.

This paper will discuss various dam raising options (downstream embankment raising and parapet wall) and spillway modifications (ogee, radial gates, radial gates combined with rubber dam and labyrinth) designs that were proposed for the raising of the dam. Preliminary cost estimates and a multi-criteria analysis were used to identify the most favourable option.

**Etude de cas – options de surélévation d'un barrage en Afrique australe*

RÉSUMÉ

Ce barrage en Afrique australe fournit environ 20 millions de mètres cubes de stockage actif qui est utilisé pour alimenter plusieurs centrales hydroélectriques en aval dans le cadre d'un système en cascade. Le propriétaire a observé que pendant la saison des pluies, il existe un volume de ruissellement excédentaire important qui est actuellement déversé car le réservoir du barrage est incapable de stocker le volume supplémentaire. Le barrage a été initialement conçu pour être surélevé de 5 m par rapport à son niveau de remplissage actuel afin d'augmenter la capacité de stockage du barrage.

Ce rapport discute de diverses options de surélévation du barrage (surélévation du remblai en aval et mur de parapet) et des modifications du déversoir (seuil libre, vannes radiales, vannes radiales combinées avec une digue en caoutchouc et un labyrinthe) qui ont été proposées pour le rehaussement du barrage. Des estimations de coûts préliminaires et une analyse multicritère ont été utilisées pour identifier l'option la plus favorable.

1. BACKGROUND

The existing, 47 m high, embankment dam is a zoned, clay-core rockfill dam with a side channel spillway. The dam provides approximately 20 million cubic meters of live storage that is utilised to supply flow to several downstream hydro-power stations as part of a cascading system. In recent years, the Owner observed that the existing live storage capacity is only just adequate to provide for the peak annual generation requirements and during the rainy season there is excess runoff to the dam which is unable to store the extra volume. Sometimes the excess inflows are used to extend the power generation periods at one of the power stations, during standard and off-peak periods, but a significant quantity of the inflow spills from the uncontrolled side channel spillway in a time when the system is full. As such the value of spilled water is not being realised.

When the dam was initially designed, the structure was proportioned to allow a potential future 5 m raise to be developed in the future. If the dam is raised by 5 m, storage capacity will be increased by approximately 40%. This extra capacity would give the Owner more control of the releases made to the downstream cascading hydropower schemes and potentially increase the peak energy generation throughout the year.

The Owner requested that the viability of various spillway and dam-raising options be investigated at a preliminary level, and the findings of the study are discussed in the following sections of this paper.

2. ENGINEERING DESIGN FOR THE DAM RAISING

The Options Study considered a maximum raise of 5 m above the existing full supply level (FSL). This will require changes to the spillway and the main dam wall. A raised FSL will also increase the upstream flood inundation extents.

As per the SANCOLD Guideline on Safety in Relation to Floods [1] due to its height being greater than 30 m, making it a large dam and having a significant hazard potential rating the Dam is classified as a Category III dam. The SANCOLD guideline recommends that for Category III dams the 1:200-year flood be adopted for the Recommended Design Flood (RDF) and the Regional Maximum Flood (RMF)+ Δ should be adopted for the Safety Evaluation Flood (SEF).

A flood hydrology study (not discussed in this paper) was carried out for the Dam and the findings in accordance with the SANCOLD guidelines, recommended that the raised spillway be sized for an RDF value of 2 062 m³/s (1 in 200-year flood) plus freeboard allowance, and to accommodate a SEF of 3 948 m³/s (RMF + Δ) with negligible freeboard.

From a technical viability perspective, the raising requirements have been assessed independently for the spillway and dam wall but have favoured least impact alternatives to the existing sensitive appurtenant structures, specifically regarding maintaining accessibility to the existing roadway bridge and the embankment crest and minimising modification to the intake and outlet works of the dam.

3. SPILLWAY RAISING OPTIONS

The current spillway for the dam comprises a 220 m long uncontrolled ogee crested weir, which spills into a trapezoidal side channel trough and discharge chute. It is important to note that the topographic conditions upstream of the existing ogee crest have been inferred from the drawings but are otherwise unknown and will need to be investigated as part of a geological and geotechnical investigation in future phases. The spillway designs applied for these options assume that competent rock foundations will be apparent at the spillway.

Four spillway configurations were considered as follows:

3.1. OPTION 1: OGEE SPILLWAY

Option 1 considers an ogee shaped crest to the raised FSL. The new ogee crest profile was designed according to USBR standards based on the updated flood peaks from the hydrology study. It will be constructed with a reinforced concrete skin and a doweled mass concrete infill.

The raised ogee crest will be constructed upstream of the existing ogee crest. The existing ogee crest will be demolished by 1 meter to act as a passive support and form a projecting sill to dissipate energy from the water flowing over the raised ogee crest (to mitigate scour in the existing spillway trough), as presented in Fig. 1 below. An approximate bulk concrete volume of 13 100 m³ is estimated for this option.

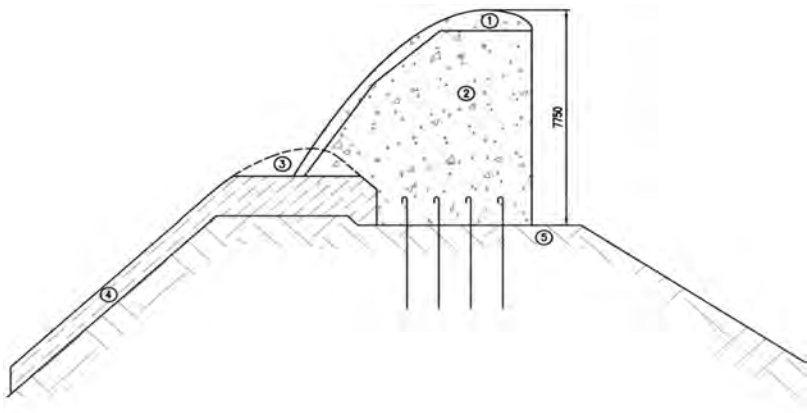


Fig. 1
Typical Cross Section of an Ogee Crest Raise
Coupe transversale typique d'une élévation d'Ogee Crest

- | | |
|--|---|
| 1. New ogee crest skin - reinforced concrete | 1. Nouvelle crête en béton armé |
| 2. Mass concrete | 2. Béton de masse |
| 3. Existing ogee crest to be removed | 3. Crête déversante existante à supprimer |
| 4. Existing spillway overflow slab | 4. Dalle aval existante |
| 5. Assumed competent foundation | 5. Fondation présumée résistante |

In combination with the 5 m raised ogee crest, the embankment non-overspill crest (NOC) level must be raised by 4.5 m from the existing NOC level to achieve a 2 m freeboard under the 1:200-year flood Recommended Design Flood (RDF) and to fully pass the Safety Evaluation Flood (SEF), namely, the extreme flood, with negligible freeboard.

3.2. OPTION 2: RADIAL GATED SPILLWAY

Option 2 considered the construction of 16 number off, 10 m wide by 8 m high radial gates installed along the existing spillway alignment. The existing spillway ogee crest will be demolished by 1 meter to form part of the radial gate sill, as presented illustratively in Fig. 2 below. The radial gate sill will be extended upstream to accommodate the hydromechanical works and to avoid impact on flow downstream into the side channel trough. The radial gate structure will include reinforced concrete piers with a crane and stoplog slots to allow for maintenance activity. An approximate total reinforced concrete volume of 25 200 m³ is required for this option, excluding the hydromechanical equipment requirements.

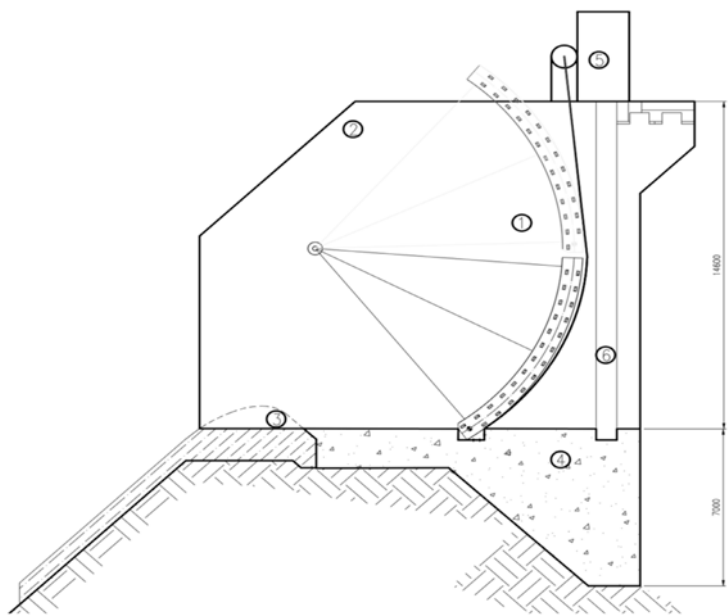


Fig. 2
Typical Cross section of the Radial Gate
Coupe transversale typique de la porte radiale

- | | |
|--------------------------------------|------------------------------|
| 1. Radial gate | 1. Vanne segment |
| 2. Radial gate structure | 2. Structure de la vanne |
| 3. Existing ogee crest to be removed | 3. Seuil existan à supprimer |
| 4. Mass concrete | 4. Béton de masse |
| 5. Crane and Hoist | 5. Grue et palan |
| 6. Stop log slot | 6. Emplacement du batardeau |

In combination with the radial gates, a raised NOC requirement for this option is only 1.8 m above the existing NOC level, requiring the least impact/modification to raise the existing embankment dam. However, the cost of the radial gates is high and will require regular maintenance to ensure reliability.

3.3. OPTION 3: RADIAL GATES AND RUBBER DAM SPILLWAY

Option 3 is a combination of radial gates and a rubber dam. 9 number of 10 m wide by 8 m high radial gates as per option 2, and a 90 m long, 3 m high rubber dam that is fitted on a raised concrete sill as presented below in Fig. 3.

An approximate total concrete volume of 15 700 m³ is required, excluding the hydromechanical equipment.

The motivation of this option is to reduce the comparatively high cost of a complete radial gated spillway solution, by reducing the number of radial gates to accommodate only the 1:200-year design flood requirements, supplemented by a collapsible rubber dam in the event of a SEF arriving.

In this case, the main embankment NOC would need to be raised by 2.4 m, which is similarly attractive considering the reduced impact on the main dam wall embankment.

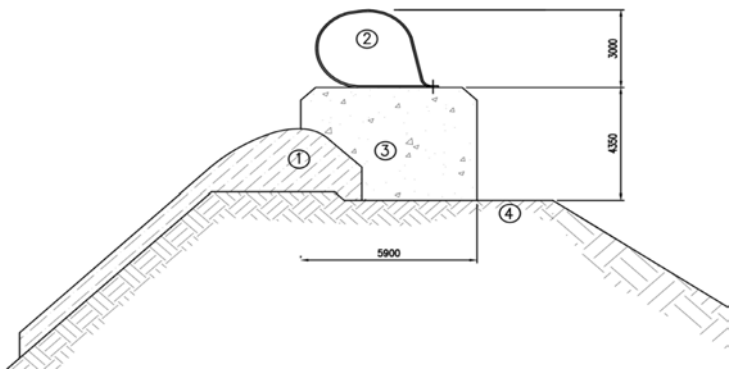


Fig. 3
Typical Cross Section of the Rubber Dam
Coupe transversale typique du boudin gonflable

- | | |
|---------------------------------|----------------------------------|
| 1. Existing ogee crest | 1. Crête du seuil existant |
| 2. Rubber dam | 2. Boudin en caoutchouc |
| 3. Mass concrete | 3. Béton de masse |
| 4. Assumed competent foundation | 4. Fondation présumée résistante |

3.4. OPTION 4: LABYRINTH SPILLWAY

The fourth option considered included the provision of a conventional labyrinth spillway, configured with 16 cycles that span the entire length of the existing spillway and provide an effective crest length of approximately 408 m.

The proposed labyrinth will be constructed at a sill level which is one meter lower than the current Ogee crest level, requiring a 6 m high bay wall/approach depth to the half-round crest to raised FSL. The typical cross-section of the labyrinth spillway is presented Fig. 4. An approximate total concrete volume of 7 500 m³ will be required.

In this case, a raised NOC requirement is 3.8 m above the existing NOC level. Compared to Option 1, the benefit of the labyrinth spillway is apparent, re-equipping the dam with an uncontrolled, low-maintenance spillway but having lesser upstream impact due to its greater discharge capacity. Owing to uncertainty in the topography upstream of the existing spillway heel, a piano key weir (PKW) configuration was not evaluated in this study. The labyrinth spillway could be accommodated within the constraints of the existing spillway and although a piano key configuration would result in a reduced height of the embankment parapet wall, its construction is considered more complex and typically more expensive.

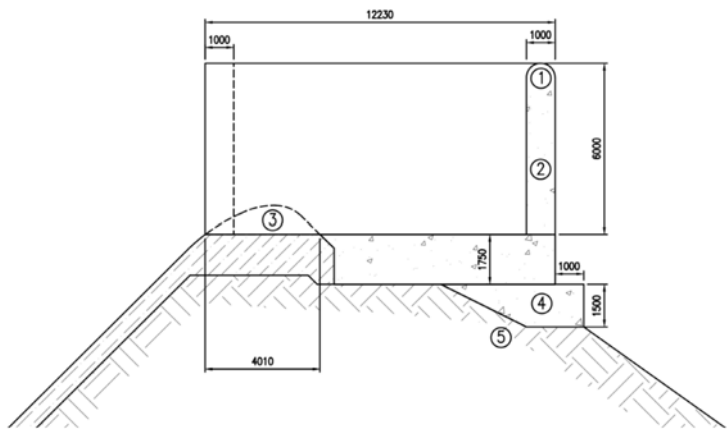


Fig. 4
Typical Cross Section of the Labyrinth Spillway
Coupe transversale typique du déversoir du labyrinthe

- | | |
|--------------------------------------|----------------------------------|
| 1. Labyrinth crest | 1. Crête du labyrinthe |
| 2. Béton armé | 2. Reinforced concrete |
| 3. Existing ogee crest to be removed | 3. Seuil existant à supprimer |
| 4. Mass concrete | 4. Béton de masse |
| 5. Assumed competent foundation | 5. Fondation présumée résistante |

4. SPILLWAY OPTIONS EVALUATION

A 2-dimensional (2D) hydraulic analysis (not discussed in this paper) was performed to evaluate the hydraulic characteristics of the existing side channel spillway trough and chute section, to determine whether the spillway trough capacity is adequate to safely pass the routed design floods with the spillway crest raise options, without submerging the existing bridge crossing and/ or drowning the spillway approach as this will affect the spillway discharge capacity. The analysis shows that capacity modifications are not required for the side channel spillway trough and chute sections. The current bridge deck soffit maintains appropriate freeboard and the spillway trough capacity is adequate. The raised spillway crests will not be drowned during the spillway operation.

5. DAM WALL RAISING OPTIONS

The zoned, clay-core rockfill dam wall was inferred to have been designed to allow for a future 5 m raise, but no drawings are available to indicate the proposed raised configuration.

When considering the dam wall raising options it was also important to note that the crest of the dam wall serves as a public access road and a spillway bridge crossing is connected to the left bank to cross over the spillway. This access must be maintained. Two dam wall-raising options were evaluated:

5.1. WALL RAISING SCENARIO A

Raising the dam using a downstream construction method on the existing slope of the embankment, as presented by the shaded areas in Fig. 5. This option comprises an extension of the current embankment zones at the equivalent slope geometry. This is the safest option, which maintains the existing design basis and can be implemented without significant dealing with water during construction-related aspects. The clay core and transition zones are similarly extended above the raised FSL to affect a full cut-off.

However, as Fig. 5 indicates, a downstream raise method impacts the culvert access shaft, which must extend to the new berm height, the outlet tower may need to be modified as a kicker wall and most significantly, the alignment of the existing public access road will be offset higher and further downstream. This will impact the approach toward the bridge crossing on the side channel spillway.

The crest width, downstream slope and profile will be maintained and an approximate total fill volume of 360 000 m³ will be required. In addition, the inclusion of a short parapet near the bridge crossing will be required to facilitate access and prevent a complete redesign of the bridge crossing.

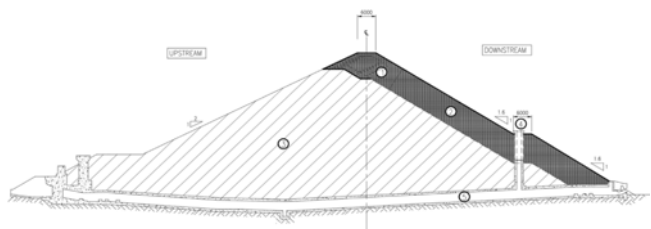


Fig. 5
Typical Section of the Downstream Raise Dam Wall
Section typique du mur du barrage surélevé en aval

- | | |
|----------------------------------|-------------------------------------|
| 1. Material zones | 1. Zones matérielles |
| 2. Proposed downstream raise | 2. Augmentation en aval proposée |
| 3. Existing embankment wall | 3. Mur de remblai existant |
| 4. Culvert Access Shaft Extended | 4. Puits d'accès au ponceau allongé |
| 5. Conduit | 5. Conduite |

5.2. WALL RAISING SCENARIO B

Construction of a parapet wall along the upstream side of the crest as presented in raising the embankment using a parapet wall method will require no significant changes being made to the current embankment, aside from the bulk excavations to the proposed parapet wall foundation level (and associated dealing with water considerations) and then backfilling and reinstating the access road to the current NOC level.

Several design precedents for a parapet wall raise exist, which is often the cheapest method to affect an embankment raise. In this case, it is proposed that the parapet wall be founded to the existing clay core cut off level, which may require stabilisation of surface layer works (to be determined in geological and geotechnical investigations to still be undertaken).

The proposed parapet wall includes both a shear key and secondary cut-off key as the base level will be 1 m lower than the proposed full supply level (FSL). It is preferable to find the parapet wall at a higher level than FSL, but this would result in a net reduction of the available crest width that doubles as the permanent access road.

The design height required and net roadway crest width of the parapet wall for the different spillway options are tabulated below in Table 1.

Raising the dam with an uncontrolled ogee spillway (Option 1) will require the highest parapet wall of 5.7 m. A labyrinth spillway (Option 4) has the second highest parapet wall requirement at 4.8 m, while the radial gate option will require a parapet wall that is only 3 m high. The crest width reduction for the ogee spillway is 0.7 m from the current width of 6 m, resulting in a total crest width of 5.3 m (excluding) the distance required to install an Armco barrier.

The labyrinth spillway option with a parapet wall will reduce the embankment crest width to 5.8 m compared to 6 m for a radial gated and rubber dam option.

Founding the parapet on the clay core of the embankment assumes favorable, well-compacted, and consolidated conditions exist. The need for foundation improvement/cement stabilising methods could be employed along the parapet base to improve founding conditions which will be evaluated as part of the geological and geotechnical investigations.

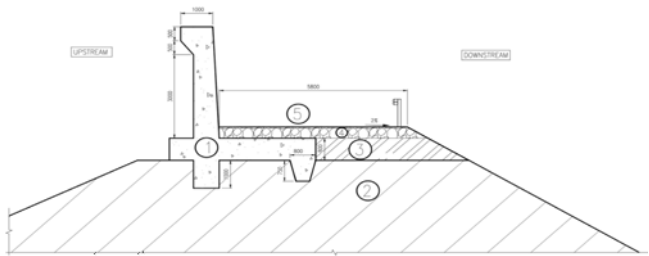


Fig. 6
Typical Section of the Parapet Wall on the Current Wall
Coupe type du mur de parapet sur le mur actuel

- | | |
|-------------------------------------|---------------------------------|
| 1. Reinforced concrete parapet wall | 1. Mur de parapet en béton armé |
| 2. Existing embankment wall | 2. Mur de remblai existant |
| 3. Subbase | 3. Sous-base |
| 4. Gravel Capping | 4. Coiffage de gravier |
| 5. Road | 5. Route |

Table 1
Parapet Parameters for the Different Spillway Raising Options

OPTIONS	HEIGHT OF PARAPET WALL (M)	CREST WIDTH (M)	CHANGE IN CREST WIDTH (M)
Current Crest	-	6.0	0.0
1 – Ogee Spillway	5.7	5.3	0.7
2 – Radial Gates	3.0	6.0	0.0
3 – Radial Gate and Rubber Dam	3.6	6.0	0.0
4 – Labyrinth Spillway	4.8	5.8	0.2

6. COST ESTIMATES

A preliminary Bill of Quantities (BoQ) for the different options was compiled using South African National Standards (SANS)[1–4] and the quantities were taken from the design drawings. Construction rates were estimated based on database data of recently completed projects.

Option 1a and 1b were included to evaluate the cost difference of the downstream embankment and the parapet wall, the Ogee spillway was selected as it required the biggest parapet wall structure.

A percentage summary of the costs is presented in Table 2 below. Option 4-the Labyrinth spillway has the lowest cost estimate followed by Option 1b – the Ogee with the parapet wall.

Compared to a parapet wall raise, the downstream construction raise cost is approximately 4 times higher. The parapet wall option to raise the embankment is therefore more favourable in terms of cost.

Table 2
Percentage Summary of the Cost of the Different Options

	OGEE AND EMBANKMENT RAISE	OGEE AND PARAPET WALL	RADIAL GATE	RADIAL GATE AND RUBBER DAM	LABYRINTH SPILLWAY
	OPTION 1A	OPTION 1B	OPTION 2	OPTION 3	OPTION 4
Percentage from lowest	132%	4%	239%	159%	0%

7. MULTI-CRITERIA ANALYSIS (MCA)

As there are multiple parameters which influence the selection of the most favourable design option for the Dam wall raising, a weighted Multi-Criteria Analyses (MCA) was used to rank the suitability of the different options so that the most favourable option could be recommended.

The criteria selected were weighted according to their relative importance. If the weighting of the criteria changes, so may the optimum solution.

The criteria selected for the MCA and their weightings for the different dam wall raising options were as follows:

- Cost of Implementation (30%)
- Time of Completion (30%)

- Risk to the Safety of the Dam (20%)
- Ease of Construction (15%)
- Environmental Impact (5%)

Each criterion was rated against a five-tier rating system and the results of the MCA for the different spillway options are summarised in Table 3.

It presents that Option 4 – (Labyrinth Spillway) is the most favourable with a final score of 81.25%, while Option 1b –(Ogee crest with the parapet wall) as second most favourable and a feasible alternative with a score of 77.25%, Option 2 – (Radial Gates) is the least favourable option with a score of 38.38%.

Table 3
Results of Multi-Criteria Analysis

OPTIONS	FINAL SCORE
Weighting (%)	100
Option 1a – Ogee Crest (Embankment)	50.88
Option 1b – Ogee Crest (Parapet)	77.25
Option 2 – Radial Gates	38.38
Option 3 – Radial Gates and Rubber Dam	44.38
Option 4 – Labyrinth Spillway	81.25

8. CONCLUSION

Based on the findings of the study, the following conclusions are drawn:

- The various spillway options evaluated for the dam are all considered viable to raise the FSL and attain an additional 5 m of storage capacity. By raising the FSL by 5 m the storage will increase by 40%. This increase will give the Owner more control of releases made to the cascading system.
- Flood peaks for the RDF and SEF are revised and impacts of inundation of the up- and downstream (reservoir and flood lines) must be considered in future studies.
- Based on 2-dimensional hydrodynamic modelling, the existing side channel spillway trough and chute sections do not require capacity modification to pass the design floods despite the spillway crest raise. The current bridge deck soffit maintains appropriate freeboard and the spillway trough capacity is adequate. The raised spillway crest will not be drowned during the spillway operation.
- Although the bridge will not be impacted by the water surface level, the erodibility of the rock mass in the chute and downstream area will need to be carefully investigated due to the high velocities computed to assess scour risk. This will be investigated in further project stages.

- The most favourable option as presented by the MCA is Option 4, namely, *the Labyrinth Spillway*. It offers the most economically attractive option and provides an uncontrolled, low-maintenance spillway with lesser upstream impact due to its greater overall discharge capacity.
- Owing to uncertainty in the topography upstream of the existing spillway heel, a piano key weir configuration was not evaluated in this study. The labyrinth spillway could be accommodated within the constraints of the existing spillway and although a piano key configuration would result in a reduced height of the embankment parapet wall, its construction is considered more complex and typically more expensive. This can, however, be considered in the next phase when detailed topographic and geotechnical information is available.
- Application of a reinforced concrete parapet wall is the cheapest method to affect the embankment raise and still maintain the roadway alignment and accessibility along the existing crest level to access the bridge. While several prototypes exist, the parapet wall founding conditions must be investigated and proved suitable. This will be revealed through the geological and geotechnical investigations in the next phase. Cement stabilising methods could be used along the parapet base to improve founding conditions if required.
- When designing new dams, take into account the potential for future increases in height and plan accordingly. This allows for more resilient and adaptable dam structures that can meet future demands and changes in climate.
- When carrying out a raising option assessment it is important to:
 - Maintain as much of the existing infrastructure as possible, by trying to increase the discharge capacity of the raised spillway to lower the total freeboard requirement thus reducing the NOC level.
 - Consider the environmental impacts of the raising options and the construction process.
 - The raising options should be cost-effective.

ACKNOWLEDGEMENT

The authors wish to express their gratitude to all other present and past members of Knight Piésold who contributed in some way or another to the development of the above-mentioned paper. The opinions expressed are those of the authors and do not necessarily reflect the views of the Client or the Company.

REFERENCES

- [1] SABS, Standardized Specification for Civil Engineering Construction – C: Site Clearance, 1980.

- [2] SABS, Standardized Specification for Civil Engineering Construction – DE: Small Earth Dams, 1984.
- [3] SABS, Standardized Specification for Civil Engineering Construction – G: Concrete Structural, 1982.
- [4] SABS, Standardized Specification for Civil Engineering Construction – H: Structural Steelwork, 1990.
- [5] SANCOLD. Guidelines on Safety in Relation to Floods. South African Committee on Large Dams Report No 4. December 1991.
- [6] USBR, Design of Small Dams, 1987.

COMMISSION INTERNATIONALE DES
GRANDS BARRAGES

VINGT-HUITIEME CONGRES DES
GRANDS BARRAGES
CHENGDU, MAI 2025

CHALLENGES EXPERIENCES WITH UPGRADING A COMPOSITE DAM IN SOUTH AFRICA - TZANEEN DAM RAISING (*)

Henry-John WRIGHT
Director, ARQ DAMS (PTY) LTD

SOUTH AFRICA

SUMMARY

Tzaneen Dam, completed in 1977, comprises a concrete gravity spillway section flanked with zoned earthfill embankments. The existing spillway is an uncontrolled ogee, with a crest length of 90.47 m, while the total dam crest length is 1 140 m. The concrete section indicates a height of 51 m above riverbed level, while the embankment, incorporating an inclined clay core, is approximately 40 m in height.

The raising of Tzaneen Dam forms part of a regional project to increase the assurance of yield and to enhance the water resources of the Groot Letaba River in serving the needs of the Mopani District of eastern Limpopo Province.

The final design of the dam raising will involve the raising of the Full Supply Level (FSL) by 3 m to increase the gross storage of the dam from 157.3 million m³ to 194.7 million m³. The FSL raising is achieved with a raising of the non-overspill crests of the earthfill embankments and the concrete tongue walls by 1.7 m. Changes to the existing dam include the demolition of the ogee crest, construction of a reinforced concrete labyrinth spillway, raising of the concrete tongue wall sections, raising the embankment, raising the inlet works and revision of the energy dissipation measures at the toe of the dam to form a facility more suited to the discharge pattern of a labyrinth weir spillway.

*Amélioration d'un barrage composite en Afrique Du Sud - élevage du barrage de Tzaneen

This paper discusses the challenges w.r.t. dam height increase, demolition requirements, the spillway capacity increase and energy dissipation measures design, and changes during construction to ensure a safe structure with an increased lifespan.

RÉSUMÉ

Le barrage de Tzaneen, achevé en 1977, comprend une section de déversoir gravitaire en béton flanquée de remblais de terre zonés. Le déversoir existant est un seuil libre non contrôlé, avec une longueur de crête de 90.47 m, tandis que la longueur totale de crête du barrage est de 1 140 m. La section en béton a une hauteur de 51 m au-dessus du niveau du lit de la rivière, tandis que le remblai, intégrant un noyau d'argile incliné, mesure environ 40 m de hauteur.

Le rehaussement du barrage de Tzaneen fait partie d'un projet régional visant à accroître l'assurance du rendement et à améliorer les ressources en eau de la rivière Groot Letaba pour répondre aux besoins du district de Mopani, dans l'est de la province du Limpopo.

La conception finale du rehaussement du barrage implique l'élévation du niveau d'approvisionnement total (FSL) de 3 m pour augmenter le stockage brut du barrage de 157.3 millions de m³ à 194.7 millions de m³. Le rehaussement du FSL est réalisé par un rehaussement des crêtes anti-débordement des remblais en terre et des murs en béton de 1.7 m. Les modifications apportées au barrage existant comprennent la démolition de la crête en seuil libre, la construction d'un déversoir à labyrinthe en béton armé, le rehaussement des sections de paroi de béton, le rehaussement du remblai, le rehaussement des ouvrages d'entrée et la révision des mesures de dissipation d'énergie au pied du barrage. pour former une installation plus adaptée au schéma de déversement d'un déversoir à labyrinthe.

Ce rapport traite des défis liés à la l'augmentation de la hauteur du barrage, les exigences de démolition, l'augmentation de la capacité du déversoir et la conception des mesures de dissipation d'énergie, ainsi que les changements pendant la construction pour garantir une structure sûre avec une durée de vie accrue.

1. INTRODUCTION

Raising an existing dam poses significant challenges, many of which do not exist when designing a new dam. These challenges range from the availability of accurate as-built information, non-compliance with current design criteria, as well as

challenges continuing with operation during implementation. It also, in many cases, involves changes in design once construction starts to facilitate hidden challenges only becoming evident during construction.

This paper highlights the challenges experienced during the design and the early part of the construction of the raising of Tzaneen Dam.

2. TZANEEN DAM

2.1. PROJECT BACKGROUND

The construction of Tzaneen Dam was completed in 1977. The dam is owned and operated by the Department of Water and Sanitation (DWS). The dam is located in the town of Tzaneen, in the Limpopo Province in the north of South Africa. The dam comprises a concrete gravity spillway section flanked with zoned earthfill embankments with a total crest length of 1 140 m. The existing spillway is an uncontrolled ogee with a crest length of 90.47 m. Energy dissipation is provided at the toe of the spillway section by a slotted roller bucket. The concrete section has a height of 51 m above the riverbed level, while the maximum embankment height is 40 m. The dam is owned by the Department of Water and Sanitation (DWS). The dam functions primarily as a storage of water for irrigation and domestic use [1].

2.2. RAISING DETAILS

The raising of Tzaneen Dam forms part of the Groot Letaba River Water Development Project (GLeWaP) to increase the assurance of yield and to enhance the water resources of the Groot Letaba River in serving the needs of the Mopani District of eastern Limpopo Province. A 3 m raising (heightening) of the full supply level will increase the gross storage of the dam from 157.3 million m³ to 194.7 million m³.

Changes to the existing dam to achieve the required increase in capacity can be defined as [2]:

- Demolition of approximately 4.1 m of concrete from the top of the existing ogee spillway crest;
- The construction of a reinforced concrete labyrinth on the lowered gravity section raising the full supply level by 3 m;
- Raising of the concrete NOC tongue wall sections by 1.7 m;
- Changing the layout of the inlet works control house to ensure impermeability for an additional 3 m water depth;

- Raising the embankment NOC by 1.7 m;
- Placement of additional earthfill material downstream of the existing embankment to increase the stability/strengthen the embankment portions of the dam; and
- Revision of the energy dissipation measures at the toe of the dam to form a facility more suited to the discharge pattern of a labyrinth spillway.

The opportunity was also used to address dam safety concerns at the same time.

3. RAISING DESIGN

3.1. DESIGN CRITERIA

Primarily, the design had to satisfy the requirements of the South African Dam Safety legislative environment [3]. Secondary, the existing SANCOLD guidelines for flood peaks [4] and freeboard [5] were used to define the relevant criteria for floods and criteria. Thereafter, international best practice (including standards and methods) was applied to the various aspects of dam design, including technical bulletins of the International Commission on Large Dams (ICOLD) and the various and numerous engineering guidelines, manuals and technical letters of the United States Army Corps of Engineers (USACE).

As the dam is classified as a large dam with a high hazard potential (Category 3 in the South Africa dam safety regulatory environment – the highest category), the following criteria were used with regard to the recommended flood peaks used in the design:

- Based on the SANCOLD Guidelines on Safety in Relation to Floods, the spillway design for Tzaneen Dam Raising should be capable of discharging a Recommended Design Flood (RDF) equal to the 200-year flood with adequate “dry” freeboard for wave action and without any damage to the dam. This flood peak was determined from the results of the statistical analysis of observed flood peaks in the catchment of the dam.
- In addition, the spillway should also accommodate an extreme flood, the so-called Safety Evaluation Flood, based on the Regional Maximum Flood (RMF) concept with a zero “dry” freeboard, accepting damage to the dam but not catastrophic failure. For this design, two extreme flood conditions were considered, one with the RMF-peak ($K = 5.2$) but with a 2tc (time of concentration) rainfall event, and another with a RMF-peak with a k value one increment higher ($K = 5.4$) with a 1tc rainfall event.

3.2. SPILLWAY AND ENERGY DISSIPATION DESIGN

3.2.1. *Spillway demolition considerations*

Optimisation of the spillway configuration developed iteratively, commencing with an existing model comprising a hybrid labyrinth/PKW structure. One of the specific objectives of the original hybrid labyrinth/PKW arrangement was to enable the dam raising with a reduced requirement for demolition of the spillway crest level, compared to the requirements of a more traditional labyrinth. The objective of a reduced demolition height is related directly to reduced requirements for water level control during construction and, consequently, a reduced impact on the water users.

The hybrid labyrinth/PKW originally considered in earlier studies indicated that an ogee crest level demolition of only 2.8 m would be required. A review of the configurations confirmed that removing an additional 2.3 m in the form of a wedge at the upstream part of each cycle would also be required.

In the environmental regulatory and legislative framework in South Africa, concrete has been classified as a hazardous material that requires careful management when demolishing existing structures. This includes the removal of the concrete and transport to an approved waste disposal facility. Before this environmental requirement, typically, the demolished spillway concrete was disposed of upstream into the dam reservoir at other similar raising projects in South Africa.

3.2.2. *Model study*

A physical hydraulic model was used to design the new raised spillway, optimising the crest configuration and confirming the discharge capacity. The study also included investigations into energy dissipation measures required due to a revised spillway configuration.

A 1:44 scale model of the proposed spillway layout was constructed and tested at the DWS Hydraulic Laboratory in Pretoria West, consisting of the concrete gravity structure as a base and providing an ability to vary the configuration of the crest and energy dissipation structures. The principal aims of the model study were to:

1. Determine the optimum spillway configuration based on enhanced flow capacities of labyrinth or Piano Key (PK) weirs and confirm its final stage-discharge curve. This optimisation needed to include minimising the extent of any demolition of the existing spillway crest to maintain maximum storage capacity during raising construction.
2. Observe the flow regime over the modified spillway and investigate appropriate measures to address the altered flow regime and energy dissipation requirements at the toe of the dam.

The model was accordingly used as a design tool to develop an appropriate spillway configuration, both concerning the control structure itself, the effect it has on the existing spillway side walls and the energy dissipation measures required at the toe of the structure.

The following conclusions were drawn from the model study and used for the final design:

- A hybrid control structure consisting of four cycles of a 6.1 m deep labyrinth flanked by conventional ogee portions on either side was the most efficient crest design.
- Retention of the existing slotted roller bucket energy dissipation structure at the toe of the dam but, including an additional erosion protection slab.
- The optimised spillway requires limited demolition of the existing spillway to maximise the storage during construction.
- The flow nappe at the routed Recommended Design Flood (RDF) and Safety Evaluation Flood (SEF) was recorded and was used to size the sidewall.
- Irregular flow patterns consisting of flow concentrations and diffusions were observed downstream of the dam, as is generally expected with labyrinth spillways. As a result of these flow concentrations, high positive and negative pressures are induced at the toe, requiring protection against scour.
- While an impact slab to manage the varying pressures is viable, optimisation of the new spillway structure allows for the retention of the existing slotted roller bucket, augmented with a simple erosion protection slab.
- Scour measurements downstream of the roller bucket indicated that scour is not expected for flows up to the RDF but that it will occur for higher flows and scour protection in the form of an extension of the concrete at the toe of the roller bucket is required. While, in terms of SANCOLD guidelines, a certain amount of damage can be allowed for flows in excess of the RDF, the condition of the rock downstream of the dam is unknown. It was accordingly considered prudent to make provision for this scour protection, pending a more detailed evaluation of the rock conditions once the tailpond can be dewatered, specifically in light of scour that has already been identified.

3.2.3. *Energy dissipation provisions*

The raised spillway inherently dissipates hydraulic energy with the crossflows generated over the spillway. Initially, the raising was to be done with a PKW, which would project the water further downstream than the chosen Labyrinth Ogee hybrid design, and associated energy dissipation would have been accommodated by an impact slab at the spillway toe.

An impact slab proved viable but required additional scour protection for a limited distance downstream. It was decided to retain the existing energy dissipation provisions, i.e. a slotted roller bucket, as part of the hydraulic model testing. Due to

the flow concentrations created by the labyrinth, the existing slotted roller bucket would operate at varying flow intensities simultaneously. The existing slotted roller bucket was accordingly augmented with a simple erosion protection slab. Additionally, the existing slotted roller bucket still functions as originally designed, and while most of the energy is dissipated at low flows, energy dissipation is less efficient for higher flows. The scour protection is based on the original impact slab design and consists of a concrete slab with a 1 m minimum thickness and extends 15 m downstream of the existing Slotted Roller Bucket toe with a cut-off into competent rock.

3.3. EMBANKMENT RAISING

Following detailed materials investigations and analyses, the Tzaneen Dam embankment did not indicate the same level of stability that preceding Dam Safety Inspections have suggested. The reliability indices for the reservoir at FSL and the Reservoir Empty scenarios are considered poor to be below average according to [6]. The situation presented a significant dam safety concern, which had to be addressed through suitable strengthening in the embankment raising proposals. Initially, only a local crest raising was envisaged, with no changes to the downstream slope. Having established the need for strengthening the downstream embankment, however, a revised raising arrangement was developed, incorporating a raised crest and a strengthened downstream embankment shell, with a flatter slope (2.6H: 1V as opposed to the original 2H: 1V). The proposed raising of the Tzaneen Dam embankments will consequently comprise an extension of the inclined clay core, supported on the upstream side by a reinforced concrete retaining wall and on the downstream side by additional fill, with a final crest width of 6 m.

The wrap-around contact between the embankment and concrete sections also required strengthening. The construction sequence was analysed, and it proved that the slope would be stable during the temporary conditions. Additionally, the long-term stability was analysed. The final design selected was based on the concept of placing an additional weight at the toe of the embankment to stabilise the slip circle mechanism. The extra weight was added in the form of reinforced soil. Terramesh was used to stabilise the new fill at a steep slope. Terramesh is a soil reinforcement product comprising 1 m x 1 m x 3 m gabions filled with rockfill and anchored with tails/grids. To facilitate the construction of this solution, it was necessary to undercut the toe of the existing embankment at certain positions.

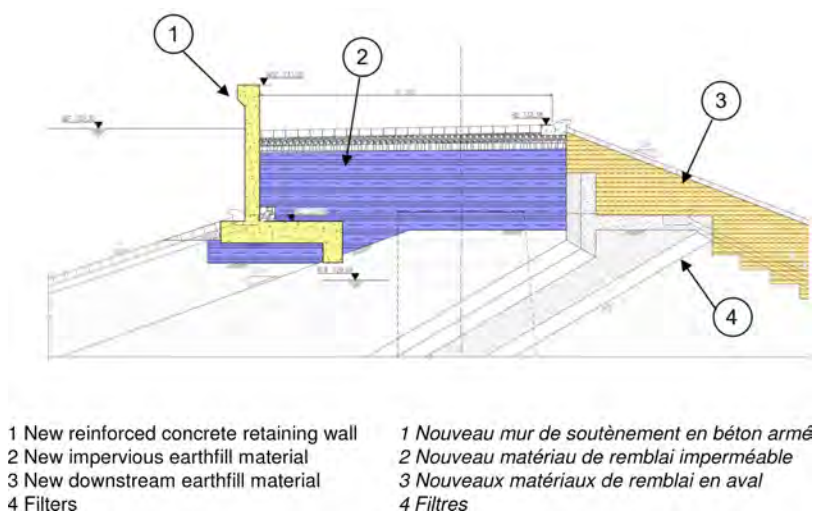


Fig. 1
Embankment raising detail
Détail de rehaussement du remblai

3.4. OPERATION DURING CONSTRUCTION

It is a requirement to ensure that the dam remains operational during construction to supply the existing water users. The works envisaged under the raising will entail seasonal water management using pipeline diversion facilities. Where these are insufficient, flood flows will be discharged over the demolished crest of the dam. The dam will be kept at a water level of 2 m below the demolished crest level. Reliance will be made on absorbing inflows in the volume of the dam at this lower level and the top of the demolished spillway crest.

4. DESIGN CHANGES DURING CONSTRUCTION

Dewatering of the downstream area of the dam was not undertaken during the design stage, nor was an underwater survey of the area undertaken.

Once the river diversion works were in place, dewatering, clearing and excavation immediately downstream of the spillway during early 2024 revealed a quite

different situation compared to the design drawings. A concrete slab was discovered, varying in thickness between approximately 1.5 and 3.25 m and extending approximately 45 m downstream of the slotted roller bucket. The concrete slab is stepped, with the majority of the slab 1.8 m below the base of the roller bucket. This situation implies a greater depth of tailwater immediately downstream of the roller bucket than initially thought, in conjunction with the presence of some concrete erosion protection. Fig. 2 shows the arrangement encountered.

Establishing the indicated difference, the design of the roller bucket extension had to be revised. The presence of the existing concrete slab and the greater depth of tailwater reduced the size of the new components, and it was possible to reduce the planned extensive drilling and grouting of new dowel bars in this area. A reduction in the scope of this work was beneficial in increasing the chance of some recovery on the programme.



Fig. 2

Downstream area after dewatering showing presence of concrete slab
Zone aval après assèchement montrant la présence d'une dalle en béton

Dewatering the stilling basin at Tzaneen Dam also revealed some significant unexpected damage to the roller bucket reinforced concrete teeth, as shown in Fig. 3. While some of the apparent damage was evidently incurred in excavating the gravel and boulders deposited in the stilling basin, it is clear that a significant amount of erosion had already occurred, exposing and undermining steel reinforcement in many places.

Additionally, the extent of gravel and sand covering the stilling basin was quite a surprise, as was the presence of large rocks and boulders. It would seem that

these rocks and boulders have probably entered the stilling basin from downstream of the dam or the old river channel, and they may be responsible for the apparent condition of the roller bucket concrete teeth. This eventuality would require some retrogressive eddying of currents during spillway discharge, and the expectation would be that there would be high-velocity water flow uniquely in a downstream direction at this location. In this case, the damage to the splitter teeth would have been caused by water and possibly some re-circulated gravel. It could also have been that quality issues were experienced with this particular concrete during the original construction. Rehabilitation of these splitters was considered in conjunction with revisions to the stilling basin.



Fig. 3
Damage to Existing Slotted Roller Bucket
Dommages au godet à rouleaux à fentes existant

Taking into consideration the poor condition of the roller bucket teeth and the presence of the concrete protection slab, the design was adapted. Removal of the damaged teeth was required as a minimum, as repair thereof would be more complex and time-consuming, hence the proposal to remove them. A saw-cut joint will be made at the contact with the dam wall. The portion to be removed is shown in Fig. 4.

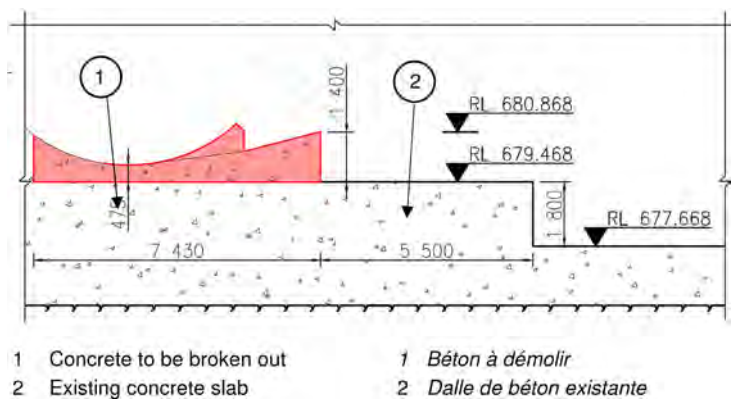


Fig. 4
Demolition/removal Extent
Etendue des zones à démolir

Once removed, a new reinforced concrete stilling basin with splitter teeth, similar to the previous roller bucket, will be constructed. The same splitter and opening ratios as previously present were selected. The overall length of the energy dissipation structure is shorter than the original design, but this is considered adequate due to the presence of the concrete protection slab. Fig. 5. shows the arrangement.

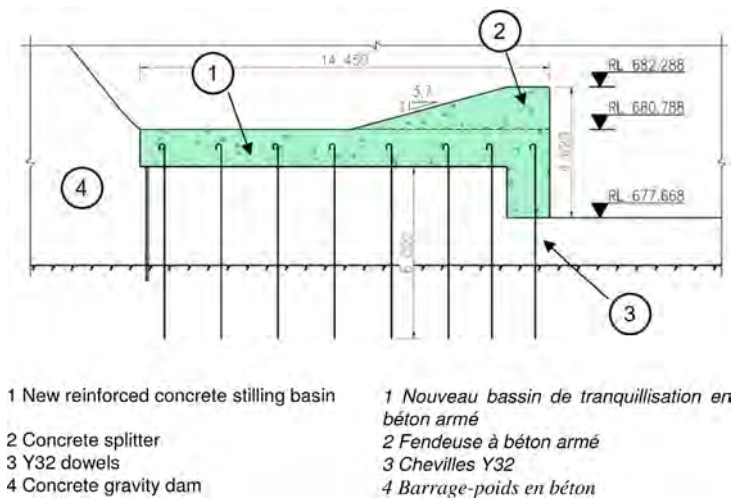


Fig. 5
New energy dissipation arrangement
Nouvel agencement de dissipation d'énergie

5. CONCLUDING REMARKS

Raising an existing dam poses significant challenges, including challenges continuing with operation during implementation. It also involves changes in design once construction starts, as hidden challenges only become evident during construction.

While each project is unique, the paper discussed the unique challenges encountered during the Tzaneen Dam Raising. For future raising projects, the following can be considered:

- Understand the owner's operation requirements and incorporate them into the works design.
- The aid of a hydraulic model study during the design phase is necessary to ensure an optimised solution. The cost of such a study usually is tiny in relation to the overall scheme cost.
- The impact of demolition requirements, if applicable, including the environmental requirements pertaining to concrete demolition, must be considered during the design and construction stages.
- Consider upfront works such as underwater surveys or dewatering of a plunge pool to assist with the design optimisation, rather than adapting the design at a later stage.

ACKNOWLEDGEMENTS

The authors wish to express their gratitude to all other present and past members of ARQ who contributed in some way or another to the development of the above-mentioned paper. The opinions expressed are those of the authors and do not necessarily reflect the views of the Department of Water and Sanitation (DWS). The authors wish to acknowledge the permission of DWS to publish this paper and SANCOLD for the review.

REFERENCES

- [1] Department of Water Affairs. DWA. 2010. Groot Letaba River Water Development Project. Technical Study Module: Preliminary Design of the Raising of Tzaneen Dam. Volume 7. Report No. P WMA 02/B810/00/0608/7.
- [2] ARQ. 2023. Tzaneen Dam Raising – Raising Design Report.

- [3] Department of Water Affairs. 2012. Regulations Regarding Safety of Dams. Government Notice No R.139. 24 February 2012. Pretoria. (Government Gazette No 35062).
- [4] SANCOLD. Guidelines on Safety in Relation to Floods. South African Committee on Large Dams Report No 4. December 1991.
- [5] SANCOLD. 2011. Guidelines on Freeboard for Dams. Volumes I and II. WRC Report No 1759/2/11. South Africa.
- [6] PHOON KK. 2008. *Reliability-Based Design in Geotechnical Engineering Computations and Applications*. CRC Press. London.

COMMISSION INTERNATIONALE DES
GRANDS BARRAGES

VINGT-HUITIEME CONGRES DES
GRANDS BARRAGES
CHENGDU, MAI 2025

THE EFFECT OF RESERVOIR OPERATION PATTERNS ON THE MATERIAL CHARACTERISTICS OF OLD DAMS AND THEIR IMPACT ON DAM SAFETY (*)

Muhammad RIZA

*Department of Civil Engineering, Faculty of Civil and Environmental Engineering,
Institut Teknologi Bandung, Member of Indonesia Dam Safety Commission*

Herryan KENDRA

*President Director, PT. Aditya Engineering Consultant, Member of Indonesia Dam
Safety Commission*

Agus JATIWIYONO

Member of Indonesia Dam Safety Commission

INDONESIA

SUMMARY

Reservoir operation patterns significantly influence the material characteristics of aging dams (≥ 50 years old), particularly embankment dams constructed from residual soil. Degradation of the embankment material quality resulting from alterations in reservoir operation patterns directly impacts dam safety. This study observed the effects of changes in the reservoir operation patterns on the physical and mechanical properties of tropical residual materials in several aging dams in Indonesia. Fluctuations in reservoir water levels and rainfall rates contribute to the degradation of dam material quality, subsequently affecting dam safety. The findings of this study highlight the importance of regular monitoring and assessment of dam material quality to ensure dam safety, particularly in tropical regions, where climatic and environmental variations can accelerate the deterioration of dam

**L'effet des modes d'exploitation des réservoirs sur les caractéristiques des matériaux des anciens barrages et leur impact sur la sécurité des barrages*

material quality. By integrating geotechnical and hydrological evaluations, this study aimed to provide a comprehensive framework for enhancing the management and safety of aging dams in tropical environments.

RÉSUMÉ

Les modes d'exploitation des réservoirs influencent considérablement les caractéristiques des matériaux des barrages vieillissants (≥ 50 ans), en particulier les barrages en remblai construits à partir d'un sol résiduel. La dégradation de la qualité des matériaux de remblai résultant des modifications des modes d'exploitation des réservoirs a un impact direct sur la sécurité des barrages. Cette étude a observé les effets des changements dans les modes d'exploitation des réservoirs sur les propriétés physiques et mécaniques des matériaux résiduels tropicaux dans plusieurs barrages vieillissants en Indonésie. Les fluctuations des niveaux d'eau des réservoirs et des taux de précipitations contribuent à la dégradation de la qualité des matériaux des barrages, ce qui affecte ensuite la sécurité des barrages. Les résultats de cette étude soulignent l'importance d'une surveillance et d'une évaluation régulières de la qualité des matériaux des barrages pour garantir leur sécurité, en particulier dans les régions tropicales, où les variations climatiques et environnementales peuvent accélérer la détérioration de la qualité des matériaux des barrages. En intégrant les évaluations géotechniques et hydrologiques, cette étude vise à fournir un cadre complet pour améliorer la gestion et la sécurité des barrages vieillissants dans les environnements tropicaux.

1. INTRODUCTION

The safety of old dams is a significant concern in the technical assessment of dam safety in Indonesia, particularly because of the substantial number of dams exceeding 50 years of age. According to data from the Indonesian National Committee for Large Dams (KNIBB) as of 2024, Indonesia has 10 dams that are over 100 years old (with the oldest being the Butak Dam at 122 years), and 34 dams ranging from 50 to 99 years of age. From the 44 dams, 38 were classified as earthfill dams.

According to Indonesian statistical data for 2024, Indonesia is situated in a tropical region (24,50' 00"N - 23.50' 00"S) with a mean temperature of 27.58°C (19.9°C minimum and 35.7°C maximum), and average annual precipitation of 2194.6 mm/year (331.1 mm/year minimum and 5313.7 mm/year maximum, with peak rainfall occurring in December and January). The average number of precipitation days in Indonesia is approximately 188 days, with a mean daily sunshine

duration of 6.3 hours and average relative humidity of 80% (40% minimum and 100% maximum). Furthermore, Indonesia is characterized by a predominance of volcanic activity, resulting in a diverse distribution of tropical residual soils exhibiting varying degrees of weathering and mineral composition.

Residual soil is formed by chemical weathering and remains in the location where it is formed (not transported). Over time, residual soil undergoes aging, changes in cementation, stress history, structure (fissure/fracture), and composition (mineral content). Consequently, the characteristics of the residual soil materials are significantly influenced by climatic and environmental changes.

The dams constructed during the Dutch Colonial era were predominantly off-stream dams with limited storage capacity, resulting in reservoir operation patterns that primarily function as a supply source during the dry season. As these reservoirs exceed their intended lifespan (≥ 50 years), their storage capacity diminishes owing to sedimentation. This reduction in capacity leads to fluctuations in water levels as a consequence of excess water release.

Over time, alterations in climate, environment, and reservoir operation patterns are likely to induce degradation of the dam material quality, which may impact dam safety. However, this phenomenon remains insufficiently researched, particularly in Indonesia. Therefore, to elucidate the relationship between reservoir operation patterns and the characteristics of dam material, specifically tropical residual soil, several old dams in the Bengawan Solo watershed, including Plumbon, Mulur, Botok, Brambang, Belimbing, Gembong, and Gebyar Dams, were utilized as case studies. The influence of fluctuations in reservoir water level and rainfall resulting in the degradation of dam material quality was analyzed to determine their effect on dam safety. This study aimed to develop effective management strategies to ensure the safety and functionality of dams over time. By integrating geotechnical and hydrological evaluations, this research endeavors to provide a comprehensive framework for improving the management and safety of old dams in tropical regions.

2. DAM AND LOCATION OF STUDY CHARACTERISTICS

2.1. LOCATION OF STUDY

The Plumbon, Mulur, Botok, Brambang, Belimbing, Gembong, and Gebyar dams, which serve as the study sites for this research, are situated within the Bengawan Solo watershed. The Bengawan Solo watershed represents the largest drainage basin in the Bengawan Solo Water System (WS), including the Upper Bengawan Solo Subwatershed ($\pm 6,072 \text{ km}^2$), Madiun River Subwatershed ($\pm 3,755 \text{ km}^2$), and Lower Bengawan Solo Subwatershed ($\pm 6,273 \text{ km}^2$). The Upper

Bengawan Solo and Madiun River subwatersheds drain water from the tapered mountain slopes of Mount Merapi (2914 m), Mount Merbabu (3,142 m), and Mount Lawu (3265 m). Consequently, the tributaries transport substantial quantities of sedimentary material resulting from erosion of these slopes, leading to significant sedimentation in the Bengawan Solo River.

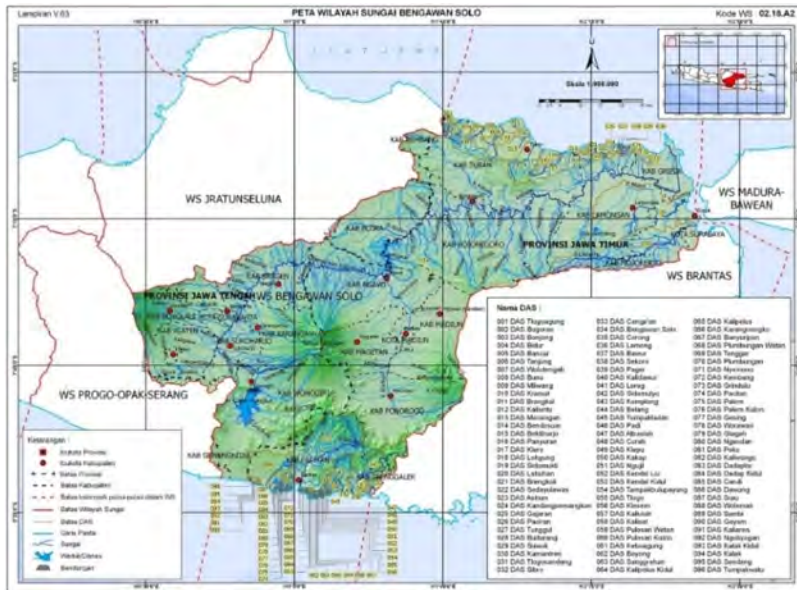


Fig. 1
Location map of the Bengawan Solo river basin

The Bengawan Solo River, with an average annual precipitation of 2100 mm/year, is a significant water resource for management and development programs, serving various purposes, including domestic consumption, clean water for residential and industrial use, irrigation, and other applications. However, the Bengawan Solo River Basin frequently experiences aridity during the dry season, whereas in the rainy season, several districts are vulnerable to flooding, resulting in substantial property damage and loss of human life.

The development of water resource infrastructure in this study area began in the 18th century under the Dutch colonial government, which initiated the construction of the Solo Vallei Werken Canal and Bengawan Solo Sudetan from Plangwot-Sedayu Lawas. However, these projects were discontinued because of

Table 1
List of dams in the BBWS Bengawan Solo working area until 2024

NO	UPB ZONE	DAM	REGISTER NO.	CONSTRUCTION FINISHED	RESERVOIR AGE	HEIGHT (M)	RESERVOIR TYPE
1	I	Nawangan	1019760048	1976	48	25.00	Earthfill
2		Ngancar	1019460036	1946	78	25.40	Rockfill with core
3		Plumbon	1019280019	1928	96	28.80	Earthfill
4		Song Putri	1019840076	1984	40	32.00	Rockfill w/ upright core
5		Pidekso		2022	2	48.00	Random material w/ core
6	II	Kedung Uling	1019170006	1917	107	14.00	Earthfill
7		Krisak	1019430035	1943	81	20.00	Earthfill
8		Mulur*)	1019260016	1926	98	7.44	Earthfill
9		Parang Joho	1019800058	1980	44	25.00	Earthfill Non Homogen
10		Rawa Jombor	1020070231	1920 / 2007	17	4.40	Earthfill
11		Cengklik	1019310022	1931	93	14.50	Earthfill
12		Delingan	1019230011	1923	101	27.00	Earthfill
13		Ketro	1019840072	1984	40	15.00	Masonry composite & Earthfill
14		Lalung	1019400031	1940	84	12.14	Earthfill
15	III	Blimbing*)	1019220218	1922	102	4.77	Earthfill
16		Botok*)	1019420034	1942	82	10	Earthfill
17		Brambang*)	1019400219	1940	84	4.5	Earthfill
18		Gebyar*)	1019550038	1955	69	17.00	Earthfill
19		Gembong*)	1019540238	1954	70	3.96	Earthfill
20		Gondang ²⁾	1020190248	2019	5	71.00	Zonal w/ upright core
21		Kembangan*)	1019400030	1940	84	10.00	earthfill homogen
22	V	Bendo		2021	3	74.00	Zonal w/ upright core
23		Gonggang	1020110198	2011	13	60.00	Material Random w/ upright core
24		Telaga Pasir*)	1019310023	1931	93	15.00	earthfill, rockfill
25		Tukul		2018	6	74.30	Zonal, upright core
26		Dawuhan	1019620041	1962	62	14.00	Earthfill
27	VI	Notopuro*)	1019410033	1941	83	12.00	Earthfill
28		Kedung Brubus	1020080186	2008	16	20.00	Earthfill
29		Saradan	1019350028	1935	89	9.00	Earthfill
30	VII	Kedung Bendo	1019480037	1948	76	17.50	Rockfill dam with upstream face concrete membrane
31		Pondok	1019950121	1955	69	32.00	Rockfill w/ upright core
32		Sangiran	1020000165	2000	24	28.00	Rockfill w/ upright core

(Continued)

Table 1
Continued

NO	UPB ZONE	DAM	REGISTER NO.	CONSTRUCTION FINISHED	RESERVOIR AGE	HEIGHT (M)	RESERVOIR TYPE
33	VIII	Gondang	1020190248	1986	38	27	Earthfill
34		Gongseng		2021	3	12.00	Earthfill Homogen
35		Pacal	1019330025	1933	91	35	Rockfill with concrete membran
36		Prijetan	1019160004	1916	108	23	Earthfill

*)Offstream

2.2. TOPOGRAPHY & GEOLOGICAL CONDITIONS

The topographic characteristics of the Bengawan Solo River Basin are predominantly flat, with a significant portion situated in lowland areas, particularly in the Lower Bengawan Solo sub-watershed (DAS Bengawan Solo). The gradient of the Bengawan Solo riverbed exhibits variability ranging from gentle to steep. The geomorphological zones within the Bengawan Solo River Basin are categorized into six distinct zones that extend in an east-west orientation parallel to the coastline of Java Island. These zones alternately formed depressed and uplifted areas as a result of tectonic activity, as illustrated in the table and map below.

Table 2
Geomorphological zone
(source : CDMP Study, 2001)

ZONE	CONDITION	ELEVATION
Zone Semarang-Rembang	Lowland and single volcano	0 m - 100 m (low area) more than 500 m (top of volcano)
Zone Rembang	Hilly area	Less than 400 m
Zone Randublatung	Lowland area	Less than 100 m
Zone Kendeng	Hilly terrain	100 m - 300 m (Pandan mountain approaching 500 m)
Zone Solo	Lowlands and single volcano	50 m - 100 m (Low area) more than 2.500 m sea level (top of mountain)
Mountains in the South	Mountainous	100 m - 1.300 m

According to Van Bemelen (1949), the geological formations found in the Bengawan Solo watershed are predominantly composed of Merapi–Merbabu and Lawu volcanic complexes. The predominant rock types are conglomerate pumice, breccia, tuff, quartz-containing andesite, and volcanic rock. The Bengawan Solo Watershed originates in a tertiary mountain range that extends along the southern coast of Java. This mountainous region consists of parent rock formations and limestone formed during the Miocene. The upper and middle Solo valleys are surrounded

Table 3
Division of Geological and Geomorphological Zones
(Source : CDMP Study, 2001)

ZONE	GEOMORPHOLOGY	TERTIARY GEOLOGY			QUARTERN GEOLOGY	
		OLIGOCENE	MIOCENE	PLIOCENE	PLIESTOCENE	HOLOCENE
Semarang-Rembang	Lowlands	-			-	Aluvial
	Single volcano	-			Volcano eruption	
Rembang	Hilly area	Sedimentation material (calcareous and saline)		Limestone	*	
Randublatung	Lowlands	-			Caused by sedimentation	Aluvial
Kendeng	Hilly terrain	-	Sedimentation material (calcareous and saline)		*	
Solo	Lowlands	-			Caused by sedimentation (including from a volcano)	Aluvial
	Single volcano	-			Volcano eruption	
Mountains in the South	Mountainous	Sedimentation and Eruption		Limestone	*	
Geologic time (million years ago)		-	26	12	2	0.01

- : spreads

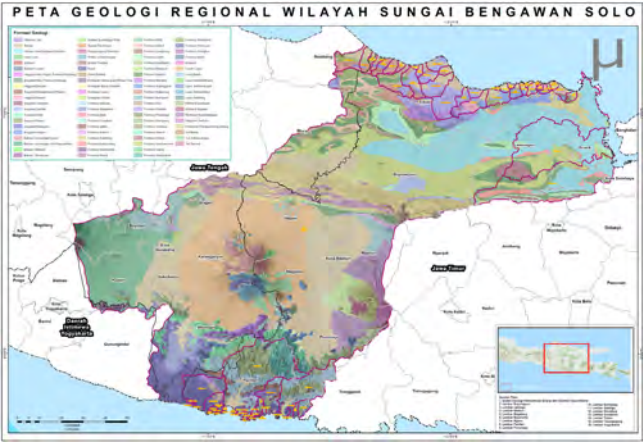


Fig. 4
Geological map of Bengawan Solo River Basin

2.3. TECHNICAL DATA OF DAM

The technical specifications of the dams in the BBWS Bengawan Solo operational area utilized as case study comprise Plumbon, Mulur, Botok, Brambang, Belimbing, Gembong, and Gebyar Dams, which are off-stream dams exceeding 50 years. The comprehensive technical specifications of these dams are as follows:

Table 4
Technical data on dams at the study location at BBWS Bengawan Solo
(Source : Analysis result by PT Aditya EC, 2024)

NO	ITEM	BENDUNGAN PLUMBON	BENDUNGAN MULUR	BENDUNGAN BOTOK	BENDUNGAN BRAMBANG	BENDUNGAN BLIMBING	BENDUNGAN GEBYAR	BENDUNGAN GEMBONG
1	No Registrasi Bendungan:	1019280019	1019260016	1019420034	1019400219	1019220218	1019550038	1019540238
2	Nama Bendungan:	Plumbon	Mulur	Bendungan Botok	Brambang	Blimbing	Gebyar	Gembong
3	Lokasi Bendungan:	Desa Baran Mundu Kec. Eromoko, Kab. Wonogiri Prov. Jawa Tengah	Desa Mulur, Kec. Bendosari Kab. Sukoharjo	Ds. Mojodoyong, Kec. Kedawung, Kab. Sragen Prov. Jawa Tengah	Desa Brambang, Kec. Kedawung, Kab. Sragen	Desa Blimbing, Kec. Sambirejo, Kab. Sragen, Jawa Lengah	Desa Sambirejo, Kec. Sambirejo, Kab. Sragen, Jawa Lengah	Desa Gembong, Kec. Karangmalang, Kab. Sragen
4	Pemilik:	Kementerian PUPR Direktorat Jenderal SDA	Kementerian PUPR Direktorat Jenderal SDA	Kementerian PUPR Direktorat Jenderal SDA	Kementerian PUPR Direktorat Jenderal SDA	Kementerian PUPR Direktorat Jenderal SDA	Kementerian PUPR Direktorat Jenderal SDA	Kementerian PUPR Direktorat Jenderal SDA
5	Pengelola:	Balai Besar Wilayah Sungai Bengawan Solo	Balai Besar Wilayah Sungai Bengawan Solo	Balai Besar Wilayah Sungai Bengawan Solo	Balai Besar Wilayah Sungai Bengawan Solo	Balai Besar Wilayah Sungai Bengawan Solo	Balai Besar Wilayah Sungai Bengawan Solo	Balai Besar Wilayah Sungai Bengawan Solo
6	Selesai Konstruksi:	1928	1926	1942	1940	1922	1955	1954
7	Nama Sungai Utama:	Kali Baran	Kali Jlantah	Kali Melikan (Suplesi dari bendung jetis)	Kali Sragen	Kali Kenantan	Kali Gebyar	Saluran Irigasi Embung Lerban
8	Tipe Sumber Air:	Instream	Offstream	Offstream	Offstream	Offstream	Offstream	Offstream
9	Sumber Air:	Hilir Bendung Desa Baran	Bendung Pepen	Bendung Jetis	Bendung Krikilan	Bendung Gempol	Bendung Gebyar	Bendung Sidowayah
10	Luas Daerah Tangkapan Air:	DTA Bendung: 240.39 Ha, DTA Waduk: 144.17 Ha	DTA Bendung: 5812.24 Ha, DTA Waduk: 300.99 Ha	DTA Bendung: 3515.80 Ha, DTA Waduk: 25.61 Ha	DTA Bendung: 282.76 Ha, DTA Waduk: 4.18 Ha	DTA Bendung: 820.69 Ha, DTA Waduk: 1.09 Ha	DTA Bendung: 518.74 Ha, DTA Waduk: 13.37 Ha	DTA Bendung: 571.89 Ha, DTA Waduk: 0.93 Ha
11	Elevasi Muka Air:							
	Elevasi Muka Air Banjir /FWL (m):	+205.61	111.5	+ 183.41	171.53	+190.18	+328.5	+120.9
	Elevasi Muka Air Normal/ NWL (m):	+204.00	+110.56	+182.96	+171.20	+189.70	+325.50	+120.84
	Elevasi Muka Air Minimum/ LWL (m):	+200.00	+106.00	+178.00	+167.00	+186.5	+314.00	+118.00

(Continued)

Table 4
Continued

NO	ITEM	BENDUNGAN PLUMBON	BENDUNGAN MULUR	BENDUNGAN BOTOK	BENDUNGAN BRAMBANG	BENDUNGAN BLIMBING	BENDUNGAN GEBYAR	BENDUNGAN GEMBONG
12	Luas Genangan Air Waduk:							
	Pada Muka Air Banjir (m2):	146,318.85	1,123,000.00	153,500.00	41,900.00	11,100.00	102,200.00	10,300.00
	Pada Muka Air Normal (m2):	123,964.20	1,013,995.02	139,972.55	41,753.58	10,874.64	98,875.53	9,257.05
	Pada Muka Air Minimum (m2):	52,295.38	100,158.78	14,053.77	11,228.62	35.07	1,544.23	867.04
13	Volume Genangan Waduk:							
	Pada Muka Air Banjir (m3):	543,623.87	4,201,143.66	540,788.90	168,049.09	32,223.83	670,841.57	29,742.52
	Pada Muka Air Normal (m3):	379,340.00	3,096,113.23	474,747.09	147,132.05	25,092.90	620,562.58	21,383.77
	Pada Muka Air Minimum (m3):	37,605.17	25,039.69	3,513.44	2,807.16	8.77	388.56	216.76
14	Kedalaman Waduk MAN (m):	5.50	5.06	5.46	4.70	3.70	12.00	3.34
15	Tipe bendungan:	Urugan Tanah Homogen	Urugan Tanah Homogen	Urugan tanah homogen	Urugan tanah homogen	Urugan tanah homogen	Urugan Lanah Homogen	Urugan Lanah Homogen
17	Elevasi Puncak (m):	+206.13	+ 112.50	+284.30	+172.5	+190.5	+327.60	+121.29
18	Lebar Puncak (m):	5	5	4	0.6	3	4	8
19	Panjang Puncak (m):	539	2,010	738	856	433	465	382
20	Tinggi Bendungan:							
	Tinggi di Atas Galian (m):	22.38	7.44	14.64	5.12	4.77	19.80	3.96
21	Manfaat:							
	Irigasi (ha):	392	51	2,488	989	295	1531	148
	Air Baku (liter/detik):							
	Listrik/PLTA (MW):							
	Manfaat Lain:							

3. RESERVOIR OPERATIONS PATTERNS

The reservoir operation pattern is implemented through the regulation of water release via gates and other complementary structures, including release facilities, such as bottom outlets or emergency exits, to meet water demands. In the Bengawan Solo River Basin, several dams are classified as old infrastructure (≥ 50 years) constructed during the Dutch colonial period to irrigate rice and sugarcane crops. Most of these dams are off-stream reservoirs, with their primary water source originating from weirs or irrigation channels that function as water suppliers during periods of low precipitation and recharge during the rainy season.

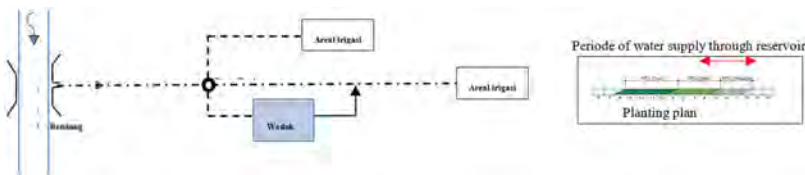


Fig. 5
Illustration of Offstream reservoir

Saat At present, the allocation of water for irrigation of paddy fields is predominantly determined by requests from water-user farmer associations (P3A), as stipulated in the water allocation or global cropping plan (RTTG). However, over time, the reservoir volume deviated from the conditions present at the time of construction. This resulted in reservoir water levels being significantly below the lowest permissible threshold, with some locations experiencing complete depletion. Reservoir depletion can persist for several months ($\pm 3-4$ months), with replenishment occurring only during the rainy season. These extreme water-level fluctuations substantially impact the dam's condition, particularly in earthfill dams constructed from residual soil. The actual water delivery frequently deviates from the Annual Reservoir Operation Plan (RTOW), which is based on the Reservoir Operation Pattern (POW). This deviation is attributed to the unregulated release of water. This situation is evidenced by the balance of inflow and outflow in the planned RTOW graph, significantly exceeding the lower normal operating line. This condition substantially affects the offstream reservoirs that depend on the capacity of the intake gates and the balance at the DTA of the weir.

4. DAM MATERIAL CHARACTERISTICS

4.1. STRATIFICATION OF DAM MATERIAL

The seven dams at the study site were predominantly homogeneous earthfill dams. In the 2024 investigation, the standard penetration test (SPT) procedures were conducted exclusively on the dam foundation stratum, excluding the dam body. Existing N_{SPT} values were derived from previous studies. Additionally, the Brambang, Blimbing, Gembong, and Gebyar dams were subjected to only Cone Penetration Test (CPT) procedures. The comprehensive results of the dam body material stratification, based on the characteristics of the N_{SPT} and q_c values, are presented in the table and figure below.

Table 5
Characteristic of N_{SPT} and q_c values of Dam Material
(source : Engineering report of PT. Aditya EC, 2024)

NO	DAM	DEPTH (M)	SOIL TYPE	CHARAC. N_{SPT}	CHARAC. Q_c (KG/CM ²)
1	Plumbon	2.00 – 24.00 12.00 – 24.00	Calcareous Silty clay (Marl)	5 - > 60 ^{*)} 5 - 24	8 - 150
2	Mulur	6.00 – 8.00	Silty clay	7 - 15	9 - 150
3	Botok	8.00 – 10.00	Sandy clayey silt	3 - 4	10 - 150
4	Brambang	0.00 – 5.60	Sandy Silty Clay	-	7 - 150
5	Blimbing	0.00 – 4.20	Sandy Silty Clay	-	12 - 50
6	Gembong	0.00 – 5.80	Sandy Silty Clay	-	10 - 150
7	Gebyar	0.00 – 12.40	Sandy clayey silt	2 - 17 ^{*)}	14 - 150

*) study of Plumbon dam, 2016

Based on the N_{SPT} value profile, it is evident that the material layers of the Plumbon, Mulur, Botok, and Gebyar dams exhibited heterogeneous densities. Certain depths demonstrated very soft-to-soft N_{SPT} values. This layer is hypothesized to accumulate water during the rainy season and consequently weaken over time. According to the q_c value, Blimbing, Gembong, and Gebyar Dams still exhibit relatively adequate densities with q_c values ≥ 12 kg/cm². It is noteworthy that the SPT and CPT tests in this study were conducted during the dry season, when almost all dams are in dry conditions with exceptionally low soil moisture content. This results in denser soil conditions than those during the rainy season. Therefore, to ascertain the stratification condition of the dam body material under fully saturated conditions, it is advisable to conduct tests during the rainy season.

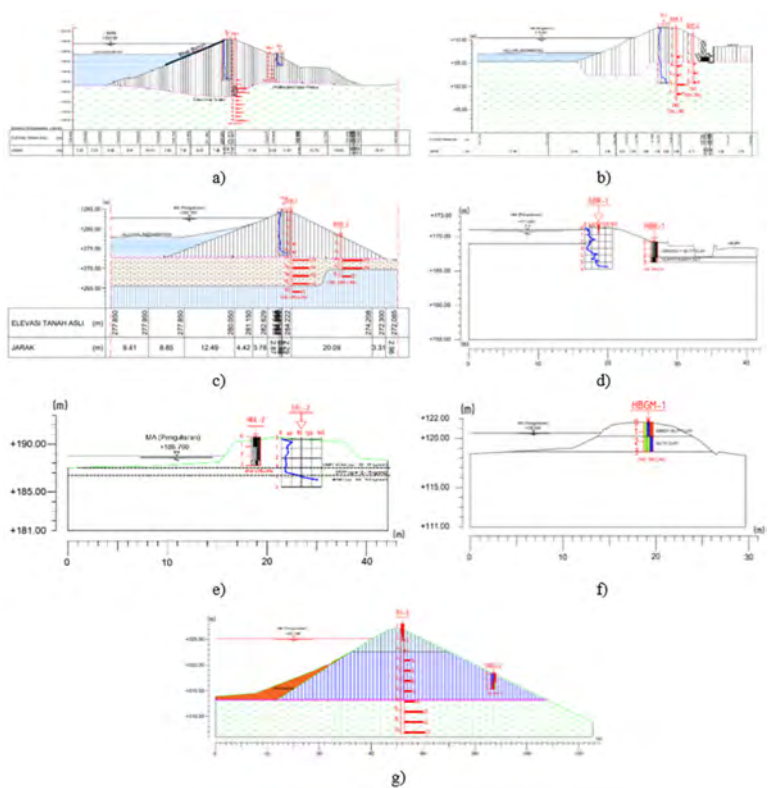


Fig. 6
Material stratification profile of dam body a) Plumbon, b) Mulur, c) Botok, d) Brambang, e) Belimbing, f) Gembong, g) Gebyar

4.2. CHARACTERISTICS OF INSITU PERMEABILITY

The permeability characteristics of the dam body material describe its capacity to transmit water. This property is determined through in situ permeability testing using the falling head method, which yields the permeability coefficient parameter k at various depth intervals. The results of in situ permeability testing conducted on the seven dams are presented in the table below.

Based on the characteristic profile of the in situ permeability values, it was determined that certain segments of the dam exhibit inhomogeneous permeability

coefficient values that exceed those typical of silty clay to clayey silt materials ($k_{sat} \leq 1 \times 10^{-6}$ cm/s). In the case of the Plumbon dam, the crest demonstrated a permeability coefficient in the range of 10^{-3} to 10^{-4} cm/s. Some areas with permeability coefficients of 10^{-6} cm/s at the Plumbon Dam consist of materials that have been displaced by landslides.

Table 6
Characterisation of insitu permeability values of dam material
(source : Engineering Report of PT. Aditya EC, 2024)

NO	DAM	INSITU PERMEABILITY K_{SAT} (CM/S)
1	Plumbon	$1,52 \times 10^{-3}$ - $4,26 \times 10^{-6}$
2	Mulur	$1,71 \times 10^{-3}$ - $9,33 \times 10^{-6}$
3	Botok	$3,40 \times 10^{-5}$ - $8,26 \times 10^{-6}$
4	Brambang	$1,31 \times 10^{-3}$ - $2,26 \times 10^{-5}$
5	Blimbing	$2,52 \times 10^{-5}$ - $5,33 \times 10^{-6}$
6	Gembong	$1,33 \times 10^{-5}$ - $5,23 \times 10^{-6}$
7	Gebyar	$1,82 \times 10^{-5}$ - $8,87 \times 10^{-5}$

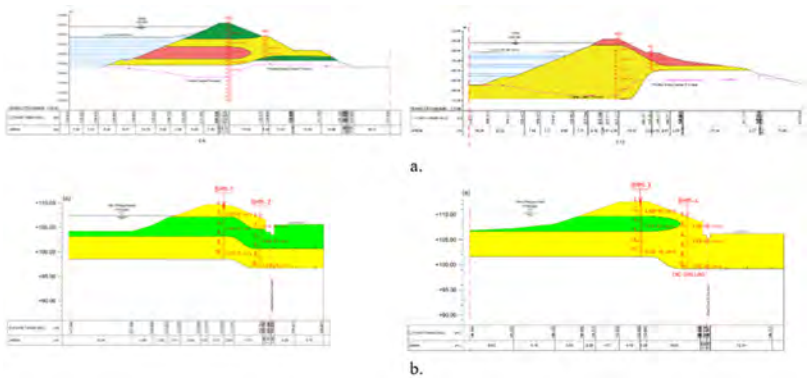


Fig. 7

At the Mulur dam, the crest retains material with a permeability coefficient of 10^{-5} cm/s. However, at a depth of approximately 2 m from the surface, the permeability coefficient increased to 10^{-3} cm/s. A similar pattern was observed in Brambang Dam. In contrast, the Botok, Belimbing, Gembong, and Gebyar dams maintained permeability coefficient values of $k \leq 10^{-5}$ cm/s. The permeability coefficient profile is closely associated with the potential for seepage and formation of perched water within the dam body. This phenomenon may result in material weakening and a gradual decrease in the shear strength of the dam body material, particularly in residual materials that continue to weather owing to climate change and fluctuations in the phreatic line within the dam structure.

4.3. CHARACTERISTICS OF INDEX PROPERTIES

It is important to note that all tests at these seven dams were conducted during the dry season (September-October), which is characterized by approximately 4-5 months without rainfall and empty or dry reservoir water levels. Sampling at the Plumbon, Mulur, and Botok Dam locations was performed through machine drilling, accompanied by standard penetration tests (SPT) and in situ permeability testing (falling head method). At the Brambang, Belimbing, Gembong, and Gebyar dams, hand drilling was employed, complemented by in-situ permeability testing. The results of the properties index characteristics of the 7 dams indicate a relatively high initial void ratio value ($e \geq 1.0$), with only the Brambang dam exhibiting an initial void ratio value below 0.5 ($e \leq 0.5$). The void ratio is associated with the porosity value (n), which is indirectly related to the hydraulic conductivity of the material, as described by the permeability coefficient parameter k . The degree of saturation of the dam material is below 100%, suggesting that the dam body material is in an unsaturated condition with the lowest water content ranging from 20% to 30%. Some samples demonstrating the degree of saturation values approaching 100% with a water content above 40% are hypothesized to be influenced by residual water from in situ permeability testing and drilling. Furthermore, the specific gravity (G_s) values remain within normal ranges for compacted clay materials, ranging from 16 to 18 kN/m³ and 2.5 - 2.7 respectively.

Table 7
Index properties of dam material characteristics
Source : Laboratory test by PT. Aditya EC & PT. BSG, 2024

No.	Dam	Material Type	Water Content	Specific Gravity	Void Ratio	Unit Weight	Deg. Of Saturation
			w (%)	G _s	e	g (kN/m ³)	Sr (%)
1	Plumbon	Sandy Clayey Silt, Clayey Sandy Silt, Silty Clay	31,13 - 46,76	2,58 - 2,69	0,96 - 1,37	16,20 - 17,8	77,32 - 93,93
2	Mulur	Sandy Silty Clay, Sandy Clayey Silt	28,58 - 56,31	2,52 - 2,67	0,81 - 1,46	16,00 - 18,70	79,00 - 97,40
3	Botok	Sandy Silty Clay, Sandy	42,74 - 47,12	2,57 - 2,65	1,11 - 1,34	16,60 - 17,40	92,85 - 99,11

(Continued)

Table 7
Continued

No.	Dam	Material Type	Water Content	Specific Gravity	Void Ratio	Unit Weight	Deg. Of Saturation
			w (%)	Gs	e	g (kN/m ³)	Sr (%)
		Clayey Silt					
4	Brambang	Sandy Silty Clay, Gravelly Sandy Silt	27.66 - 35.58	2.5 - 2.53	0.45 - 1.06	16.6 - 18,00	84,73 - 94,20
5	Belimbing	Sandy Silty Clay	25.69 - 35.33	2.58 - 2.64	1.25 - 1.26	14.7 - 15.50	53,94 - 72,77
6	Gembong	Sandy Silty Clay, Clayey Sandy Silt	20.75 - 43.15	2.53 - 2.72	1.02 - 1.28	15.90 - 17.50	52,96 - 98,26
7	Gebyar	Sandy Clayey Silt	41.51 - 51.65	2.46 - 2.68	1.10 - 1.54	16,00 - 16.60	89,88 - 93,08

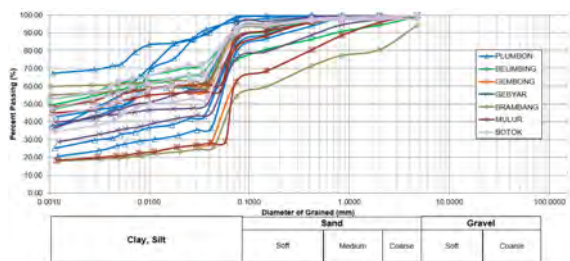
4.4. CHARACTERISTICS OF GRAIN SIZE DISTRIBUTION (GSD) AND CONSISTENCY LIMIT

The grain size distribution (GSD) was determined using the wet sieve method in accordance with ASTM D2217. The consistency limits were determined through Atterberg limit testing, as specified in ASTM D4318-17. For the Atterberg limit test, the sample was not initially dried but immediately provided with de-aired water to achieve the water content at which the minimum number of blows required for the test was attained. Prior to assessing the consistency limit, soil samples that had been combined with a predetermined water content were subjected to a 24-hour curing period to ensure a uniform water content distribution. This methodology aligns with several previous investigations on tropical residual soils.

Table 8
Grain size distribution (GSD) characteristic and consistency limit of Dam material
Source : Laboratory test by PT. Aditya EC & PT. BSG, 2024

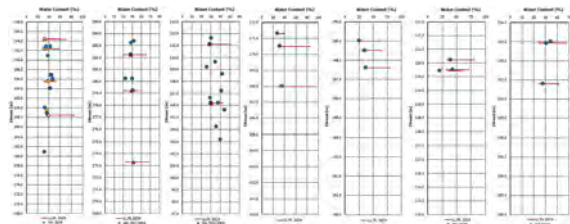
NO	DAM	MATERIAL TYPE	USCS CLASS.	GRAIN SIZE DISTRIBUTION (GSD)				CONSISTENCY LIMITS		
				GRAVEL	SAND	SILT	CLAY	LL	PL	PI
				(%)	(%)	(%)	(%)	(%)	(%)	(%)
1	Plumbon	Sandy Clayey Silt to Silty Clay, and Clayey Sandy Silt	CH, MH	0,00 - 2,87	1,55 - 27,29	37,49 - 56,47	23,04 - 60,43	48,96 - 84,87	33,56 - 47,27	10,40 - 48,95
2	Mulur	Sandy Silty Clay to Sandy Clayey Silt	CH, MH	0,04 - 3,41	9,57 - 22,38	32,97 - 42,63	35,59 - 56,87	41,61- 50,33	28,79 - 30,78	12,82 - 19,55
3	Botok	Sandy Silty Clay, Sandy Clayey Silt	CH, MH	0,48 - 2,26	5,45 - 7, 71	35,90 - 53,26	37,45 - 56,40	58,13 - 72,38	30,32- 37, 15	20,98 - 38,53
4	Brambang	Sandy Silty Clay and Gravelly Sandy Silt	CH, ML	0.79 - 19.52	7.16 - 26.25	31.7 - 35.34	18.88 - 60.35	38.69 - 86.7	26.26 - 34.52	12.42 - 56.8
5	Belimbing	Sandy Silty Clay	CH	0.65 - 5.75	6.76 - 19.34	26.01 - 38.16	48.90 - 56.16	61.32 - 78.32	30.21 - 34.84	31.11 - 43.49
6	Gembong	Sandy Silty Clay and Clayey Sandy Silt	CH, MH	0.92 - 4.01	11.98 - 33.36	34.6 - 42.92	19.71 - 51.78	57.18 - 79.66	32.66 - 36.73	20.45 - 44.31
7	Gebyar	Sandy Clayey Silt	MH	0.16 - 2.41	5.06 - 22.11	43.13 - 51.72	32.34 - 42.59	56.19 - 70.83	36.73 - 37.57	19.46 - 33.26

Based on the study results at seven offstream dam sites in Bengawan Solo WS, the dam body material is predominantly composed of sandy silt clay to sandy clay silt with high plasticity, classified as CH to MH according to the Unified Soil Classification Society (USCS). Some dams, such as Plumbon and Gembong, have dam material mixed with clayey sandy silt material, whereas the Brambang dam contains gravel. The grain size distribution (GSD) curves of the 7 dam locations reveal a gap graded material in the grain diameter range of 0.04 mm to 0.1 mm, which is characteristic of material that has undergone weathering. At the Plumbon Dam location, there is material that differs from the original composition owing to landslide-induced alterations. Regarding the consistency limits of the dam body material, the lowest water content condition, reaching $\pm 20\text{-}30\%$ in the dry season, indicated that the dam material was below the plastic limit (PL). This resulted in the formation of fine to large fissures during the dry season, particularly in materials with high plasticity ($LL \geq 50$). During the rainy season, these fissures are closed as rainwater infiltrates through them. In highly plastic materials with swelling potential, fissures close as rainwater infiltrates through the fissures.



Source : Laboratory test by PT. Aditya EC & PT. BSG, 2024

Fig. 8
GSD curve characteristics of Plumbon, Mulur, Botok, Brambang, Belimbing, Gembong, and Gebyar Dam materials



Source : Laboratory test by PT. Aditya EC & PT. BSG, 2024

Fig. 9
Graph of natural moisture content against consistency limits of dam material a) Plumbon, b) Mulur, c) Botok, d) Brambang, e) Belimbing, f) Gembong, dan g) Gebyar in dry season

4.6. CHARACTERISTICS OF COMPRESSIBILITY

Based on the results of oedometer testing (ASTM D2435-11) with a sample diameter of 63.5 mm and a height of 20 mm, it was determined that the dam body material falls within the category of materials exhibiting low compressibility ($0.05 < C_c/1 + e_0 < 0.1$). Furthermore, the preconsolidation pressure/yield stress value indicates that the dam body material is classified as slightly overconsolidated ($0 < \sigma'_m < 100$ kPa) to heavily overconsolidated ($\sigma'_m > 400$ kPa). This classification is consistent with that of typical compacted embankment materials. However, to ensure the absence of creep potential in the dam body material, further creep testing is necessary.

Table 9
Compressibility characteristic of dam material
Source : Laboratory test by PT. Aditya EC & PT. BSG, 2024

NO	DAM	COEF. COMPRESSION	COEF. CONSOLIDATION	COEF. RE-COMPRESSION	YIELD STRESS	INITIAL VOID RATIO	
		C_c	C_v	C_r	P'_c (kPa)	e_0	
1	Plumbon	0,33 – 0,61	0,0001 – 0,0023	0,03 – 0,15	27 – 240	3,12 – 7,84	0,04 – 0,10
2	Mulur	0,28 – 0,53	0,0002 – 0,0026	0,01 – 0,08	79 – 550	2,88 – 5,36	0,06 – 0,08
3	Botok	0,41 – 0,54	0,0003 – 0,0023	0,03 – 0,12	120 – 240	4,31 – 5,59	0,06 – 0,10
4	Brambang	0,4 – 0,52	0,0002 – 0,0013	0,04 – 0,06	230 – 260	2,23 – 2,39	0,12 – 0,15
5	Blimbing	0,35 – 0,44	0,0007 – 0,0015	0,01 – 0,09	34 – 270	3,1 – 4,00	0,07 – 0,11
6	Gembong	0,45 – 0,71	0,0007 – 0,0021	0,07 – 0,09	145 – 310	3,18 – 4,32	0,09 – 0,13
7	Gebyar	0,37 – 0,74	0,0033 – 0,0043	0,04 – 0,09	120 – 410	4,56 – 5,23	0,06 – 0,13

4.7. CHARACTERISTICS OF SWELLING PRESSURE AND METHYLENE BLUE VALUE (MBV)

Based on the results of swelling pressure testing (ASTM D4546-14) and Methylene Blue values (MBV) from all locations, it was determined that the Brambang and Gembong dam body materials exhibited medium swelling (200–400 kPa) to very high swelling (≥ 700 kPa). In contrast, the Plumbon, Mulur, Blimbing, and Gebyar dams fall into the low (< 200 kPa) to medium swelling category. Furthermore, the MBV values across all locations indicated high to very high swelling criteria. Given these conditions, it can be concluded that all seven dams in BBWS Bengawan Solo exhibit significant sensitivity to changes in weather, moisture content, and drying-wetting processes resulting from fluctuations in reservoir water levels. Additionally, MBV testing is recommended as an efficient method for the early detection of swelling potential, owing to its relatively short testing duration. Complementary findings, during the swelling tests conducted at seven dam sites in Bengawan Solo WS, the swelling pressure attained a constant load of 50 kPa after a period of 4–18 days.

Table 10
Swelling & MBV Characteristics of Dam material
Source : Laboratory test by PT. Aditya EC & PT. BSG, 2024

NO	DAM	SWELLING PRESS. (KPA)	INDEX SWELL	SWELLING CRITERIA	MBV	SWELLING CRITERIA BASED ON MBV
1	Plumbon	220 - 240	1.91 - 2.22	Medium	22.5 – 28.51	Very High
2	Mulur	150 - 230	0.65 – 0.79	Low - Medium	15	Very High
3	Botok	Un-test	Un-test	Un-test	14.21	High
4	Brambang	250 - 800	3.00 - 12.66	Medium to Very high	22.5	Very High
5	Blimbing	170 - 240	0.77 - 2.25	Low to Medium	13.99 - 15	High to very high
6	Gembong	460 - 550	4.91 – 6.22	High	13.5 - 24.29	High to Very High
7	Gebyar	80	0.26	Low	10.3	High

4.8. CHARACTERISTICS OF SHEAR STRENGTH

Based on the results of the undrained triaxial consolidated testing (ASTM D4767-11/20), it was determined that the undrained shear strength parameter value (c_u) ranges from 6.22 - 18.85 kPa (stiff to very stiff consistency) for the Mulur, Botok, Brambang Blimbing, Gembong, and Gebyar dams. The plumbon Dam exhibits an undrained shear strength of 28.59 - 32.85 kPa (hard consistency). Several dam materials exhibited effective cohesion (c') values approaching 0 kPa, indicating that the cementation bonds resulting from iron-oxide interactions were leached. The effective angle of friction (ϕ') ranged from 21.8 °to 38.2°. It is noteworthy that the sampling was conducted during the dry season, resulting in very stiff samples despite undergoing a saturation process for 2–4 days to achieve a B Skempton value ≥ 0.95 .

Table 11
Shear strength Characteristics of dam materials
Source : Laboratory test by PT. Aditya EC & PT. BSG, 2024

NO	DAM	TOT. STRESS PARAMETER		EFF. STRESS PARAMETER	
		c_u (kPa)	f_u (°)	c' (kPa)	ϕ' (°)
1	Plumbon	28.59 – 32.85	13.8 - 19.7	12.9 - 15.1	30.1 - 35
2	Mulur	8.03 – 14.5	18.6 – 19.6	0.23 – 4.78	30.4 – 35.6
3	Botok	9.03 - 10.32	16 – 17.2	1.3 – 6.31	26.8 – 30.8
4	Brambang	6.22 - 14.34	17.6 - 23.4	5.13 – 5.64	24.5 - 38.2
5	Blimbing	18.85	15.9	1.82	39.4
6	Gembong	9.13 - 10.04	14.6 – 26.7	7.46 - 8.53	21.8 – 35.3
7	Gebyar	7.22 – 8.58	15.1 - 28.7	5.53 – 6.45	26.1 - 35.3

5. RESULT AND DISCUSSION

5.1. EFFECT OF CHANGES IN RESERVOIR OPERATION PATTERNS ON STORAGE CAPACITY

Considering that the offstream reservoir operation pattern differs from the instream reservoir operation pattern, in the preparation phase of the Reservoir operation pattern, it is essential to assess the condition of the withdrawal building balance as the primary structure in the following manner:

1. Evaluation of the Catchment Area of the Weir to Determine if the Upstream Section Contains Other Infrastructure (Dams / Irrigation Areas, etc.)
2. Evaluasi of the water balance of the suplesi dam on the area to be irrigated, including the reduction of water demand upstream of the suplesi dam.
3. Evaluasi of the maximum capacity of the conveyance channel from the intake of the Suplesi Weir
4. Based on the cropping pattern determined in the RTTG, a water balance analysis is conducted
5. The result of the water balance analysis will indicate the succes of the cropping pattern as evidenced by the IP (%) achievement.
6. If the achievement in one cropping cycle does not meet 100% and beyond, the reservoir functions as a supply to optimize IP
7. Under these conditions, the reservoir water level will be maintained according to the capacity of the supply channel from the intake of the weir; reservoir filling will be conducted during the rainy season (excess river discharge) and released according to the capacity of the channel from the intake to the reservoir inlet

The figure below illustrates an example of a combination of water balance and operation patterns of offstream reservoirs and documentation of one of the offstream dams (Botok reservoir). In the RTOW Plan, it is evident that the Low Water Level occurs from July to October (for 4 months), while the line (——) representing realization shows a decrease in the reservoir water level on January 1 and 2.

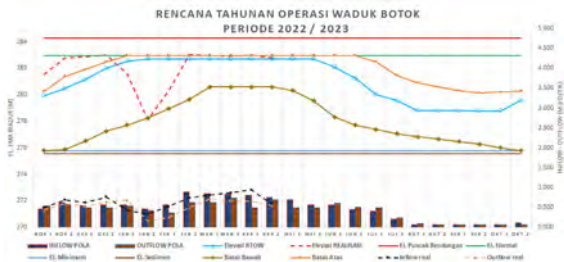


Fig. 11
Graphic of annual plan of reservoir operation for the period 2022-2023 at Botok reservoir

5.2. EFFECT OF RESERVOIR WATER LEVEL FLUCTUATION ON DAM SAFETY

Significant fluctuations in reservoir water levels, particularly rapid drawdowns owing to flooding or operational requirements, substantially impact dam safety. Consequently, based on the existing material properties of the dam, rapid drawdown conditions were modeled with a drawdown rate of 0.5 m/day. The analysis was conducted exclusively on dams with upstream slopes lacking concrete protection, such as the Mulur and Gebyar Dams. The results of this analysis are as follows.

Table 12
Safety factor value of dam against reservoir water level fluctuations

NO	DAM	STEADY STATE CONDITION	RAPID DRAWDOWN
1	Plumbon*	12.29	Uneffected
2	Mulur	1.56	1.14
3	Botok*	1.32	Uneffected
4	Brambang*	2.81	Uneffected
5	Blimbing*	3.24	Uneffected
6	Gembong*	3.30	Uneffected
7	Gebyar	2.24	1.40

*)upstream slope covered by concrete

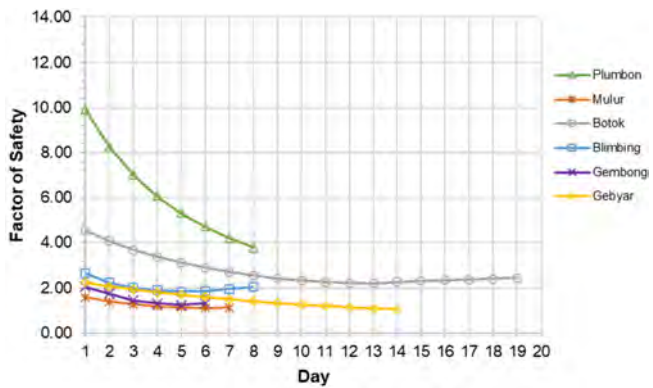


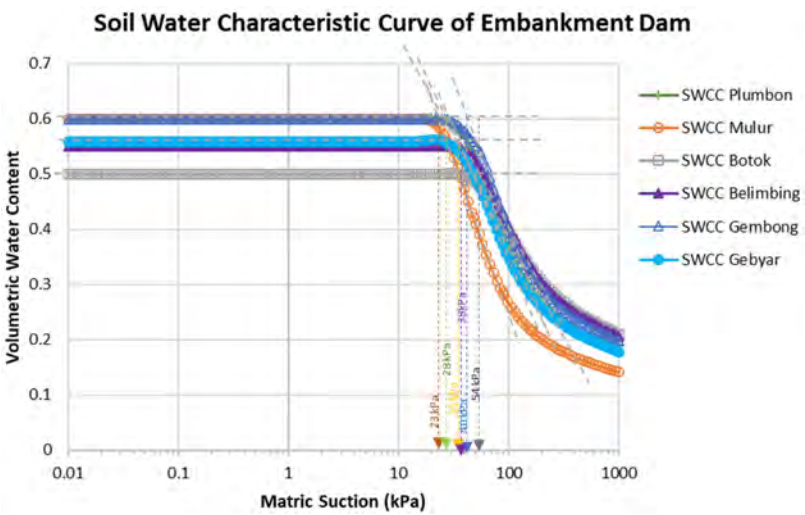
Fig. 12
Graphic of reservoir water level fluctuations against safety factor value (drawdown rate 0.5 m/days)

5.3. EFFECT OF RAINFALL ON DAM SAFETY

The effect of rainfall was analyzed on the downstream slopes. The results of the rainfall analysis for dam safety are presented below.

Table 13
Safety factor of dam against rainfall rate

NO	DAM	RAINFALL RATE (MM/DAY)	FOS FOR RAINFALL CONDITION		FOS FOR NORMAL CONDITION	
			UPSTREAM	DOWNSTREAM	UPSTREAM	DOWNSTREAM
1	Plumbon	56	3.80	1.81	3.91	2.16
2	Mulur	139	1.41	1.26	1.69	1.36
3	Botok	158	3.24	1.13	3.58	1.38
4	Brambang	238.8				
5	Blimbing	147.5	2.47	1.43	2.76	1.55
6	Gembong	140	1.66	1.30	1.58	2.31
7	Gebyar	177	2.04	1.10	2.13	1.33



6. CONCLUSION

This study was conducted to determine the effects of reservoir operation patterns on the characteristics of old dam materials and their impact on dam safety. The investigation encompassed seven offshore dams in the Bengawan Solo River area. The findings of this study are as follows:

1. The dam body material consists of volcanic residual soil, which exhibits expansive. This material demonstrates high sensitivity to changes in weather, moisture content, and drying-wetting process resulting from fluctuationw in reservoir water levels.
2. For offstream dams in the Bengawan Solo river basin, the annual operation plan frequently deviates from the actual reservoir operation pattern. Consequently, it is necessary to restrict the reservoir operation pattern to the minimum operational level relative to the annual operation plan. This measure was implemented to mitigate significant changes in water levels in the drying-wetting cycle owing to weather changes and fluctuation in reservoir water levels. However, this operating pattern control is only applicable to dams whose upstream slopes are not covered with concrete, such as the Mulur and Gebyar dams.
3. The sudden drop in the reservoir water lever/rapid drawdown reduces the safety factor of the upstream slope at the Mulur and Gebyar Dams.
4. Consideration of the effects of rainfall decreased the safety factor of the downstream slope
5. Further studies are recommended to determine the characteristics of the dam body material during the rainy season and to conduct creep test of the dam body material.

ACKNOWLEDGMENTS

The authors extend their gratitude to BBWS Bengawan Solo, the entire UPB Bengawan Solo, PT Aditya Engineering Consultant, the Head of the Dam Engineering Centre, and the Indonesian National Committee for Large Dams (INACOLD) for their contributions and assistance in this research.

COMMISSION INTERNATIONALE DES
GRANDS BARRAGES

VINGT-HUITIEME CONGRES DES
GRANDS BARRAGES
CHENGDU, Mai 2025

**RE-ASSESSMENT ON THE DISCHARGE CAPACITIES AND SAFETY OF
STRUCTURES IN LARGE DAMS OF DRINI RIVER CASCADE (*)**

Arjan JOVANI & Ermal KACURRI
ALBCOLD

Orlando MUCA
KESH sha

Fahri MAHO
EBS shpk

ALBANIA

SUMMARY

This report provides a description on the assessment for the safety of structures in large dams of Drini river cascade in Albania including the current monitoring and management of the dams and reservoirs, efforts to improve operations, and measures planned for the future to increase energy potential and dams safety.

The height and types of dams, conditions of operation, the water volumes of reservoirs created by dams, the multiply purpose of their operation, the installed power capacities and the dynamic of exploitation of Hydro power plants make this river cascade to be unique cascade in Europe.

The design of this cascade started 60 years ago. Till now, there are constructed 9 large dams (Dams of HPP Fierza is the biggest dams in Albania) and 8 HPPs with total power capacity of 1520 MW and average energy production of 5 000

**Vérification de la capacité des évacuateurs de crues et de la sûreté des grands barrages en cascade sur la rivière Drini*

GWH per year. KESH operates three hydropower plants in the Drin River cascade which produces approximately 70% of the electricity of the country.

Dam of HPP Fierza dam that is the first dam in upper part of this cascade, it is the highest dam in Albania. It is a rock-fill dam with a clay core, measuring 166.5 m in height and 380 m in length at the crest. The reservoir created by this dam is the biggest reservoir in Albania with designed maximum volume of 2.7 billion m³. On the left side of the dam are all the facilities for the hydro power plant, while on the right side are the water spillway systems with a total capacity of 2670 m³/s.

Dam of HPP Koman is a concrete faced rock-fill dam with height 115.5 m and with a actual maximum discharge capacity of 3,600 m³/s.

Drini River Cascade is a reservoir operation and flood routing model, which has been specifically tailored for the performance of flood routing and reservoir operation studies in this cascade. Based on the hydrological modeling of the Drin River Basin and applying the existing KESH operation rules (they are approved at 1988) for the three HPPs, flood routing and reservoir operation studies were carried out. The existing rainfall data base was extended for the operation period from 1980 till 2015. An extensive analysis was performed for rainfall events of different durations. Considering PMPs of different durations, temperature and snow cover analysis, PMFs of 1-day to 7-day events were generated by means of the PANTA RHEI rainfall-runoff model.

The results show that, in order to render the Drin River Cascade safe for the event of a PMF:

- Dam of HPP Fierza requires additional spillway capacities of some 2,280 m³/s;
- Dam of HPP Koman requires additional spillway capacities of some 3,000 m³/s;
- KESH must update the existing Operation Rules for the integrated management of Drini river cascade.

RÉSUMÉ

Ce rapport fournit une description de l'évaluation de la sécurité des structures des grands barrages de la cascade de la rivière Drini en Albanie, y compris la surveillance et la gestion actuelles des barrages et des réservoirs, les efforts visant à améliorer les opérations et les mesures prévues pour l'avenir afin d'accroître le potentiel énergétique et la sécurité des barrages.

La hauteur et les types de barrages, les conditions de fonctionnement, les volumes d'eau des réservoirs créés par les barrages, la multiplicité des finalités de leur exploitation, les capacités de puissance installées et la dynamique

d'exploitation des centrales hydroélectriques font de cette cascade fluviale une cascade unique en Europe.

La conception de cette cascade a commencé il y a 60 ans. Jusqu'à présent, 9 grands barrages ont été construits (les barrages de la centrale hydroélectrique de Fierza sont les plus grands barrages d'Albanie) et 8 centrales hydroélectriques d'une capacité totale de 1520 MW et d'une production d'énergie moyenne de 5 000 GWh par an. KESH exploite trois centrales hydroélectriques dans la cascade de la rivière Drin, qui produit environ 70 % de l'électricité du pays.

Le barrage HPP Fierza qui est le premier barrage dans la partie supérieure de cette cascade, est le plus haut barrage d'Albanie. Il s'agit d'un barrage en enrochement avec un noyau d'argile, mesurant 166,5 m de hauteur et 380 m de longueur à la crête. Le réservoir créé par ce barrage est le plus grand réservoir d'Albanie avec un volume maximal prévu de 2,7 milliards de m³. Sur le côté gauche du barrage se trouvent toutes les installations de la centrale hydroélectrique, tandis que sur le côté droit se trouvent les systèmes de déversoir d'eau d'une capacité totale de 2670 m³/s.

Le barrage de HPP Koman est un barrage en enrochement à parement amont en béton d'une hauteur de 115,5 m et d'une capacité de décharge maximale réelle de 3 600 m³/s.

Drini River Cascade est un modèle d'exploitation de réservoir et de routage des crues, qui a été spécialement conçu pour la réalisation d'études de routage et de fonctionnement des réservoirs dans cette cascade. Sur la base de la modélisation hydrologique du bassin de la rivière Drin et de l'application des règles d'exploitation existantes de la KESH (elles ont été approuvées en 1988) pour les trois centrales hydroélectriques, des études de tracé des crues et d'exploitation du réservoir ont été réalisées. La base de données existante sur les précipitations a été étendue pour la période d'exploitation de 1980 à 2015. Une analyse approfondie a été effectuée pour des événements pluvieux de différentes durées. En tenant compte des PMP de différentes durées, de l'analyse de la température et de la couverture neigeuse, les PMF des événements de 1 à 7 jours ont été générés au moyen du modèle de précipitations-ruissellement PANTA RHEI.

Les résultats montrent que, afin de rendre la cascade de la rivière Drin sûre pour l'événement d'une CMP :

- Le barrage de la centrale hydroélectrique de Fierza nécessite des capacités d'évacuation supplémentaires d'environ 2 280 m³/s ;
- Le barrage de la centrale hydroélectrique de Koman nécessite des capacités d'évacuation supplémentaires d'environ 3 000 m³/s ;
- La KESH doit mettre à jour les règles de fonctionnement existantes pour la gestion intégrée de la cascade de la rivière Drini.

1. INTRODUCTION

Climate change will lead to increased flood and drought risks in the Mediterranean region, particularly in the Western Balkans. The adaptation to climate change is presently inadequate, especially in terms of flood and drought risks and risk management.

This report provides a description on the reassessment for the discharge capacities and safety of structures in large dams of Drini river cascade in Albania including the current monitoring and management of the dams and reservoirs, efforts to improve operations, and measures planned for the future to increase energy potential and dams safety.

The height and types of dams, conditions of operation, the water volumes of reservoirs created by dams, the multiply purpose of their operation, the installed power capacities and the dynamic of exploitation of Hydro power plants make the Drini river cascade to be unique cascade in Europe.

The design of this cascade started 60 years ago. Till now, there are constructed 7 large dams in Albania (Dam of HPP Fierza is the biggest dams in Albania) and 6 HPPs with current total power capacity of 1450 MW and average energy production of 5 000 GWH per year. KESH operates three hydropower plants in the Drin River cascade which produces approximately 70% of the electricity of the country.

From the beginning of the study on the exploitation of the hydro power potential of the Drin River, the idea was accepted that the Drin River should be exploited by creating large reservoirs. For the creation of these reservoirs, it was required to design and build very high dams with a height of 60-170 m. In 1964 in the Europe were built only 10 dams with a height of over 160 m.

Relying on the achievements of science and technology in the world for the construction of large dams as well as the professionalism, determination and belief in the technical-scientific values of Albanian designers and engineers it became possible to successfully solve all the problems that arose during the design and construction of these dams and the creation of the largest cascade in our country. During the study of the exploitation scheme of the Drin River, the solution of various problems related to the geological conditions of the area, the type of dam, construction materials, the time of their construction were taken into account.

2. GENERAL INFORMATION ON DAMS OF DRINI RIVER CASCADE

Currently, on the Drin River are built 7 large dams (4 dams of HPP Vau i Dejes with height of 12-60 m, Dam of HPP Fierza with a height of 166.5 m, Dam of HPP

Koman with a height of 115.5 m and Dam of HPP Okshtuni with height 65 m) and is in the design phase dam and HEPP Skavica.

Also, In the downstream part of this river is constructed the hydro-technical complex of HPP Ashta and Spathara.They use the water of HPP Vau I Dejes.

The Exploitation scheme of Drini river in Albania is given in the fig.No.1 below

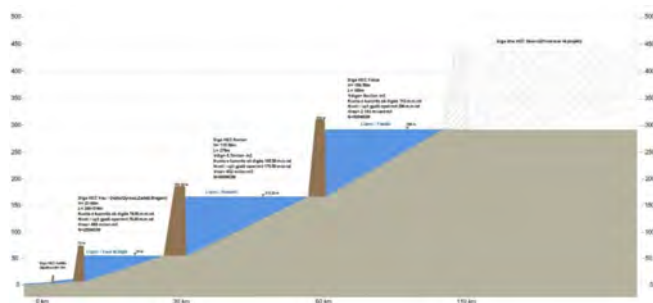


Fig. 1
Hydro- power Exploitation Scheme of Drini River

Dam of HPP Fierza that is the first dam in upper part of this cascade, it is the highest dam in Albania. It is a rock-fill dam with a clay core (RFDC), measuring 166.5 m in height and 380 m in length at the crest. The reservoir created by this dam is the biggest reservoir in Albania with water designed maximum volume of 2.7 billion m³ and current maximum volume of 2.3 billion m³. Two main branches of Drini river discharge their inflow in this reservoir. On the left side of the dam are all the facilities for the hydro power plant, while on the right side are the water spillway systems with a total capacity of 2670 m³/s.



Fig. 2
Dam of HPP Fierza

Dam of HPP Koman that is the second dam in middle part of this cascade, it is a concreted faced rock-fill dam (CFRD), measuring 166.5 m in height and 380 m in length at the crest. The reservoir created by this dam is designed with water maximum volume of 500 million m³. 12 rivers and streams of Drini basin discharge their flow from Albanian Alps to this reservoir. On the left side of the dam are all the works of the Hydro-power plant as well as a spillway tunnel of the water discharge system and on its right side there is a water spillway tunnel. The total maximum capacity of them is 3 600 m³/sec



Fig. 3
Dam of HPP Koman

The main dams of the hydro-technical complex of **HPP Vau i Dejes** consists of:

- **Qyrsaq Dam** with a height of 54 m and a length of the dam crest of 514 m. This dam consists of 2 parts where the first part is a rock-fill dam with clay core and the second part is a concrete dam with gravity. In the concrete dam are also the intake system and the spillway system with a total capacity of 3900 m³/s.
- **Zadeja Dam** with a height of 60 m, length of the dam crest of 387 m. This dam is of the type of rock-fill dam with clay cores. On the left side of this dam is built the discharge system consisting of 2 spillway gates and discharge tunnel with a length of 322 m and height of 11 m. The current discharge capacity of this tunnel is about 2000 m³/s.
- **Rragam dam** with a height of 21 m and a length of the dam crest of 240 m.
- **Gjocaj Dam** with a height of 11.2 m and a length of of dam crest of 295 m. In this dam there is an intake system with a capacity of about 8 m³/s for the irrigation purpose



Fig. 4
Qyrsaqi Dam of HPP Vau i Dejës

3. HYDROLOGICAL ANALYSIS AND MODEL OF DRINI RIVER.

Drini river cascade is part of Drini - Buna Basin. The Drin – Buna basin is a large river basin located in the Western Balkans with international importance as it is shared by the countries Albania, Montenegro, Macedonia and Kosovo. Its catchment covers approximately $20,380 \text{ km}^2$ based on most actual calculations by the consultant. Headquarters of the main river system Drin are the Black Drin (Drini i Zi) which drains the western part of Macedonia (catchment $3,320 \text{ km}^2$) and the White Drin (Drini i Bardhë) which rises in Kosovo (catchment $4,650 \text{ km}^2$).

After crossing the borders to Albania, the two streams merge near the city Kukës at the eastern part of Albania and form the Drin. Further westwards the Drin flows in direction to the Adriatic Sea where it joins the outflow of the Shkodra lake ($377 \text{ km}^2 - 530 \text{ km}^2$) and becomes the Buna river. The water balance of the Shkodra lake, shared by Albania and Montenegro, is highly influenced by the Morača and Zeta rivers which drain the northern mountain range of the sub-basin Montenegro. Upstream of the confluence with the lake outlet, the Drin passes the dam cascade of the three reservoirs: Fierza (73 km^2), Koman (12 km^2) and Vau Dejës (25 km^2) operated by the Albanian power corporation (KESH sh.a). Several tributaries flow directly into the reservoirs.

Among them, the Valbona river draining the central eastern Albanian Alps is the largest one. The outflow of the Vau Dejës reservoir is influenced by a weir at Spathar further downstream.

Because of the complex hydrodynamic interaction between the lake, the rivers Buna/Bojana and Drin and the releases of the Vau Dejës dam, the lower part of the river basin is susceptible to flood events and regional inundations. With regard to the potential of extreme flood flows in the past and flood damage, this area requires special attention for data monitoring and hydrological modeling, in future presumably in combination with hydrodynamic modeling of the surface water levels.

An extensive analysis was performed for rainfall events of different durations. This analysis is done by a Team of LWI in a study funded by GIZ/Germany. Considering PMPs of different durations, temperature and snow cover analysis, PMFs of 1-day to 7-day events were generated by means of the PANTA Rhei rainfall-runoff model.

PANTA Rhei is a hydrological modeling system for the simulation of the rainfall-runoff-process and the water budget at any location within a catchment resp. river basin. The model allows simulations with high spatial and temporal resolutions. The preparation of catchment data is supported by GIS techniques. The model has been developed and is continuously maintained at the Leichtweiss Institute for Hydraulic Engineering and Water Resources (LWI), University of Braunschweig, in collaboration with the Institute for Water Management IfW GmbH, Braunschweig. The model is used for flow forecast, for planning purposes, and – in a more sophisticated version – for research of climate change impact on water resources. Computation time steps can be defined according to the available data and project aims. Often, a time step of 1 hour for flood flow analysis (event-based simulation) and 1 day for the analysis of the water balance (simulation for long-term periods) is selected.

PANTA Rhei is dominated by three model components which reflect the relevant hydrological processes for the transformation of rainfall into runoff. The transformation is divided into (i) the **formation** of runoff, (ii) the **concentration** of runoff, and (iii) the **routing** of flow through the river system

The Panta Rhei structural model now comprises:

- A total catchment size of $AEo = 20,380 \text{ km}^2$
- 2,562 sub-catchments
- 25,200 hydrotops
- 50 gauges or locations to view or generate runoff time series (107 potential locations)
- 13 lakes and reservoirs
- 2 bifurcations to simulate the flow of lake Prespa and lake Ohrid

The quality and reliability of hydrological modeling results depend on a consistent and continuous operating data acquisition network in every country. Regional data exchange and cooperation between the related stakeholders was therefore a key condition to establish an integrated flood early warning system for the whole Drin– Buna basin.

A first analysis and inspection of data quantity and quality with focus on topographic, meteorological and hydrometric data has been accomplished. during

this study. The final outcome of the data collection and the resulting needs for further investigation are summarized in the study. A detailed digital terrain model exists as the base for hydrological modeling. It covers completely the sub-basins located in Albania, Macedonia and Kosovo and includes parts of the Montenegrin sub-basin. Land use data and soil data are only available from internet sources and provide rough information (CLC datasets and IHME1500).

The meteorological data investigation shows a high density of stations although partly location and condition of stations are unclear. Several stations have been renamed and relocated during the time period 1961 – 2013. A number of historical time series data exist for the parameters precipitation and air temperature (daily minimum, daily maximum, daily average) which contain randomly distributed data gaps. Time series data for additional meteorological parameters was rare.

The dam cascade is an important influencing factor and offers a high potential to improve the existing flood risk management. Therefore, a close cooperation between IGEWE and the operator of the Drin Cascade was essential. Operator provided hydrometric data for this study which included hydrographs for daily reservoir inflow, side inflow and spillway outflow from 1991 till 2010. Additional data such as turbine outflow and/or total outflow from each reservoir and storage elevation curves for the three reservoirs was required for calibration purposes and will help to optimize a combined and multi-objective reservoir operation with the help of modeling. In general precipitation data are evaluated as sufficient

A proper hydrological modeling of a catchment requests a credible simulation of the following components of a long-term simulation:

- event based rainfall-runoff events and response time of soil storages
- peak runoff during floods
- travel time of flood waves
- seasonal high flow and low flow
- snow accumulation and melting
- evapotranspiration

The hydrologic modeling system PANTA Rhei was applied. It has proved to gain – in total - reasonable results and a good overall model fitting with respect to the available spatial input data and available time series.

4. FLOOD ROUTING AND RESERVOIR OPERATION

Drini River Cascade is a reservoir operation and flood routing model, which has been specifically tailored for the performance of flood routing and reservoir operation studies in this cascade. Based on the hydrological modeling of the Drin

River Basin and applying the existing KESH operation rules (they are approved at 1988) for the three HPPs, flood routing and reservoir operation studies were carried out. The existing rainfall data base was extended for the operation period from 1980 till 2015. An extensive analysis was performed for rainfall events of different durations. Considering PMPs of different durations, temperature and snow cover analysis, PMFs of 1-day to 7-day events were generated by means of the PANTA RHEI rainfall-runoff model.

Accordingly, the following additional discharge capacities need to be installed.

	Fierza HPP	Komani HPP	Vau I Dejes HPP
Max. Outflow after routing	5 250 m ³ /s at 306.5 masl	7 100 m ³ /s at 175.5 masl	7740 m ³ /s at 77.0 masl
Available discharge capacities	2 970 m ³ /s	4 100 m ³ /s	7740 m ³ /s
Additional discharge capacities required	2 280 m ³ /s	3000 m ³ /s	no additional capacities required

Different options for reducing the required additional spillway capacities at Fierza and Komani were analyzed, including:

- providing additional storage capacity in future upstream Skavica Hydropower Project
- removal of sediment deposits from the reservoirs
- diversion of floods into adjacent catchments
- increase of maximum water level
- lowering of operation water level during flood season; and
- construction of additional spillway.

The studies have shown that a combination of the different measures can reduce the required additional capacity at Fierza and at Komani. Though, taking into account that most of the measures described above are technically, economically and environmentally not feasible, additional spillway capacities are required. Therefore, additional spillways with discharge capacities of 2280 m³/s and 3000 m³/s were engineered for Fierza and Komani.

5. CONCLUSIONS

The results show that, in order to render the Drin River Cascade safe for the event of a PMF:

- Dam of HPP Fierza requires additional spillway capacities of some 2,280 m³/s;
- Dam of HPP Komani requires additional spillway capacities of some 3,000 m³/s;

- Dams of Vau I Dejes are safe
- KESH must update the existing Operation Rules for the integrated management of Drini river cascade.

Given that the Drin River Cascade is safe for PMF by adding additional spillway capacity, the simulations show that the cascade would be safe for a flood event of 1,000 years return period, even in case that the gate of the highest capacity would fail.

The following measures have been assessed as above, but found not to be feasible for technical, economical and ecological reasons:

- reduction of reservoir operation level during the flood season
- restoration of original reservoir storage capacity by means of sediment dredging
- increase of dam height and flood water level
- watershed diversion
- provision of flood retention dams upstream of Fierza

A financial and economic analysis was performed to assess the viability of additional spillway capacity to safely discharge a PMF at the Drin river cascade from the perspective of the economy and from an Investor. In terms of economic viability, it was shown that in case such an event happens, the benefits of the investment significantly outweigh their costs.

Given that safety measures try to prevent exactly such a scenario, an investment decision with respect to safety measures should be based on such considerations. In addition to a static analysis, a cash flow model has been set up to take the probability of the occurrence of the event into account. The results were not favorable towards the investment; however, it must be considered that the value of human life was not taken into account and if the event were to happen, thousands of people would be at risk.

REFERENCES

- [1] Mott MacDonald: A post-disaster comprehensive flood risk assessment & Management study. Final Report – The flood risk management plan for the lower Drini & Buna river basin, July 2012.
- [2] SANXHAKU, M. AND KO, P.: Design Flood Studies for the Drini Hydropower Cascade. Report for KESH, December 2012.
- [3] World Meteorological Organisation (WMO, 2009): Manual on Estimation of Probable Maximum Precipitation (PMP). WMO-No. 1045, 2009

- [4] MEON, G; Pätsch, M: Assessment Study for Gaps and Needs in Establishing a Drin Early Warning System. Final Report for GIZ. Braunschweig, May, 2013.
- [5] GIZ: Flood risk management plan in Shkoder region and Emergency Preparedness Plan, Tirana, 2015
- [6] GIZ: Potential of multi-purpose-use of the hydropower reservoirs of the Drini cascade in Albania, Tirana, 2016
- [7] FICHTNER GmbH, "Study for providing safe flood management of the Drini river cascade, WB project, 2017
- [8] ICOLD Bulletin No.156. "Integrated Flood risk management". 2010
- [9] ICOLD Bulletin No. 170 "Flood Evaluation and Dam Safety", 2015
- [10] ICOLD Bulletin No. 186, "Integrated Optimal Operation of Cascade", 2019
- [11] Albanian Power Corporation (KESH sh.a), "Annual Report for Actual Conditions of dams and reservoir in Drini river cascade and their Monitoring and Dam Safety", Tirana, 2018, 2020, 2022
- [12] ALBCOLD, "Annual Report for Dam Monitoring and Safety in Albania", Tirana, 2018, 2020, 2022.
- [13] ALBCOLD Website, www.albcold.gov.al, english version, Tirana, Albania, 2022

COMMISSION INTERNATIONALE DES
GRANDS BARRAGES

VINGT-HUITIEME CONGRES DES
GRANDS BARRAGES
CHENGDU, MAI 2025

INTELLIGENT TEMPERATURE CONTROL SYSTEM FOR LARGE CONCRETE DAM CONSTRUCTION IN HOT AND HUMID ENVIRONMENTS (*)

Yuxin NIE

Sichuan Energy Internet Research Institute, Tsinghua University, Chengdu

Rui ZHANG

Snohydro Bureau 11 Co., Ltd, Zhengzhou

Zhiyan LIN

*Beijing University of Chemical Technology, College of Mechanical and Electrical
Engineering, Beijing*

Yuanguang LIU & Junjie JIN

Snohydro Bureau 11 Co., Ltd, Zhengzhou

Zichang LI

Sichuan Energy Internet Research Institute, Tsinghua University, Chengdu

CHINA

SUMMARY

Coupled with high heat of cement hydration, massive concrete casting, such as concrete dam building, makes it difficult to control early thermal cracking of concrete, especially for tight schedules and intense construction. To prevent early thermal cracking by controlling concrete temperature, an intelligent temperature control system for concrete water cooling via embedded piping was created based

**Système intelligent de contrôle de la température pour la construction de grands barrages en béton dans des environnements chauds et humides*

on the principles of “small temperature gradient, slow cooling pace, and precise gradient control”. The system's key characteristics include temporal-spatial temperature recording, simultaneous back-calculation of temperature and thermal stress fields, an AI-based cooling water circulation control plan, and rapid strategy updates based on closed-loop data feedback and decision-making. The technique was used to build the concrete dam for Tanzania's Nyerere Hydroelectric Power Station in 2022. During the deployment of the intelligent temperature control system, the maximum temperature, temperature gradient, and thermal field distribution were carefully monitored and managed using intelligent water cooling in accordance with technical standards. As a result, the likelihood of early thermal cracking following concrete casting was greatly reduced. The created intelligent temperature control system offers construction experience for similar construction situations.

RÉSUMÉ

En combinaison avec la chaleur élevée d'hydratation du ciment, la construction de grandes structures en béton, comme la construction de structures en béton armé, rend difficile le contrôle de l'échauffement prématuré du béton, surtout pour les plannings serrés et les constructions intenses. Afin d'éviter les fractures thermiques prématurées en régulant la température, un système de contrôle intelligent de la température interne via des tuyaux intégrés a été mis au point, en se basant sur les principes de “petite gradient de température, de débit de chauffe lent et de contrôle précis de gradient”. Les principales caractéristiques du système comprennent un enregistrement temporel et spatial de la température, la réévaluation simultanée des zones de température et de stress thermique, un plan de contrôle de la circulation de l'eau de refroidissement basé sur l'intelligence artificielle, et les mises à jour rapides de la stratégie basées sur le retour d'expérience et la prise de décision dans le système.

1. INTRODUCTION

Less developed nations continue to see an expansive exploration in hydro-power and water resources. Ensuring the safe and economical development of water resources is contingent upon the quality of construction of large dams [1]. Nowadays, hydroelectric power stations are built with large and/or high concrete dams, subject to fast construction practices and structure soundness. However, under dense construction and complicated environment, temperature stresses may exceed structural stresses, resulting in early thermal cracking, which can cause structural damage, leakage, and/or even dam collapse [2]. To control the

construction quality of concrete casting and curing, temperature control methods for large volumes of concrete are preferable.

Water cooling is a versatile, dependable, and useful temperature control technique [3]. It enables the rapid cooling of water running through embedded pipes to dissipate heat within the concrete. The technology of concrete water cooling via piping for dams was first introduced in the United States for Owyhee and Hoover Dams [4] in the 1930s. In China, numerous projects also implemented piping water cooling, such as Longtan dam [5], Suofengying dam [6], Guanyinyan dam [7], and Lianghekou dam [8]. However, traditional water cooling methods adopt manual monitoring and operation. On-site data and information need to be collected manually, yielding poor accuracy, low efficiency, and human errors [9–12].

Along with the technology booming of internet of things, automation control and artificial intelligence, water cooling technology has been greatly improved. Tan [13] developed a set of intelligent control system applied to the load-bearing platform of Laomian River Bridge of Guizhou Du'an Expressway with principles of hierarchical control in China. By precisely manipulating the interior temperature field to manage the temperature gradient stress and prevent cracking, a set of intelligent control systems were built using the principle of layered control, which substantially increased the space of one-time pouring concrete construction. It can accomplish accurate control of the temperature field inside the concrete to achieve the effect of non-cracking by controlling the temperature gradient stress, greatly expanding the space of one-time pouring concrete construction. Lin and Fan [14–16] proposed a method for determining temperature-controlled cooling water demand for concrete. For the water supply guarantee rate, quantitative evaluation indices were established. A system for intelligent joint control of the water cooling network was developed and applied to the intelligent temperature control of high arch dams, such as the Baihetan and Wudongde arch dams in China. Wang [17] developed a temperature control system for massive concrete casting. It can automatically read and analyze concrete temperature at each temporal-spatial point. This technology was used in the buried section of the West Island of the Deep China Corridor. Other large and medium-sized concrete dams in China also adopted intelligent temperature control measures in the casting process and achieve good application results, such as Dato Gorge Dam [18], Fengmang Reconstruction Dam [19], Huangdeng Dam [20], Ludila Dam [21], etc.

In conclusion, the intelligent temperature control technology for massive concrete has been developed rapidly with digital construction of engineering project. However, the majority of applications of intelligent temperature control technology are found in alpine or hot and dry climates in China. Tanzania's Nyerere Hydroelectric Power Station lies close to the equator, where scorching weather and copious amounts of rainfall present. There were no intelligent temperature control practices in hot and humid climates available for references. For such situations, a novel intelligent temperature control approach was proposed and its successful

implementation served as a reference for projects under similar construction climates and conditions.

2. DIFFICULTIES AND CHALLENGES

- (1) Large volume concrete dam construction involves a number of unique needs, including lengthy construction schedules, heavy workloads, and a high standard of data accuracy. Large volume concrete dam construction involves a number of unique needs, including lengthy construction schedules, heavy workloads, and a high standard of data accuracy. Subjective elements and equipment, with a single control method, extended collecting times, and delayed information return, strongly influence the traditional manual water cooling method. Large-scale concrete projects make it challenging to continue regulating temperature with the artificial approach [22].
- (2) In hot and humid climates, significant variations in daily temperature between the day and night can cause cracking after pouring concrete. As a result, higher demands are placed for temperature control indicators.
- (3) In hot and humid areas, the long duration of the rainy season, the high volume of excess water during flood season and the tight schedule requirements make it challenging to guarantee that projects will be finished on schedule using manual water cooling techniques.

3. INTEGRATED TEMPERATURE CONTROL SYSTEM

This research put forward the temperature control theory of "small gradient, slow cooling, precise control", which can achieve continuous and smooth cooling with phased and continuous optimization, and solve the problems of complex construction environment and high requirements of large volume concrete dam construction. On this basis, a newly intelligent water cooling system for large volume concrete was set up in the construction of large volume concrete dams, by achieving massive temperature sensing acquisition, instantaneous temperature field analysis, accurate dynamic real-time feedback, and intelligent decision-making water cooling.

The system consists of the following parts: integrated intelligent cooling-water control equipment (heat exchanging equipment; auxiliary heat exchange equipment;

data acquisition equipment for dams; control equipment) and integrated software platform for intelligent control. The system framework is presented in Fig. 1.

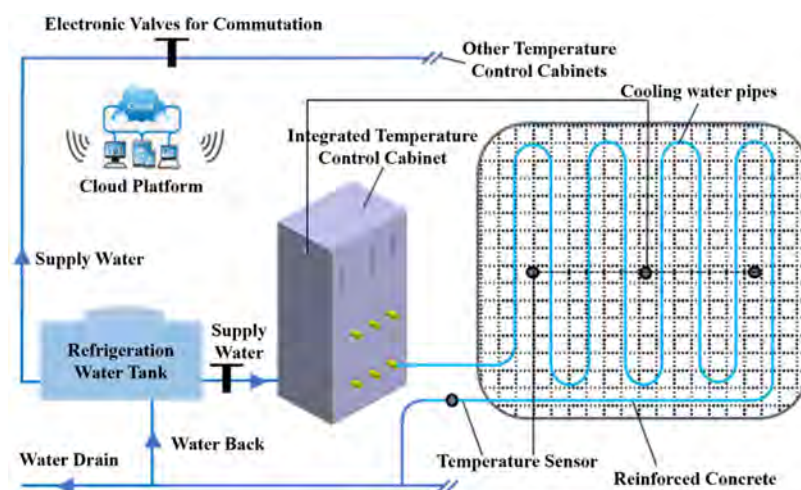


Fig. 1
Intelligent temperature control system

Temperature self-sensing and recording include recording concrete temperature in the silo, aggregate temperature, outlet temperature, inlet temperature, pouring temperature, solar radiation, and temperature gradient on the silo surface by the transducers with pre-embedded, environmental monitoring and non-contact infrared. Integrating historical hydration heat development rules with real-time internal and external concrete temperature data, these data are then combined to create an evolving 3D model of temperature and stress fields in whole space-time for cloud-based analyses. This allows for the determination of transient temperature stress fields and intelligent supply water management strategies. A 3D stress field evolution model is imported into an intelligent decision-making platform for learning and assessment, and determine complete intelligent control strategies, such as adjustments to water inflow temperature, flow rate, direction, and operating duration. The complete intelligent temperature control system for large volume concrete is developed, enabling continuous and smooth cooling and staged continuous feedback optimization of mass concrete, avoiding concrete temperature cracks and reducing the risk of mass concrete cracking. It allows for continuous smooth cooling and staged continuous feedback optimization, reducing cracking risk for large volume concrete.

4. SYSTEM APPLICATION

4.1. PROJECT INFORMATION

The Julius Nyerere Hydroelectric Power Station, located in the south-eastern part of Tanzania, is the largest hydroelectric project in Africa by far. The base of the concrete gravity dam is at EL 56.0 meters, the top at EL 190.0 meters, and the axis of the dam is 1034.0 meters in total length. Its planned installed capacity is 2115 MW and total reservoir is 36.8 billion m³. When completed, Tanzania's installed hydro-power capacity would expand by 270%.

The climate at the dam site consists of an average annual temperature of 27.2°C and an monthly temperature range of 24.3°C to 29.9°C, with a daily variation of 11.5°C, hot and humid all year long. Most rainfall comes in March through May, with an average rainfall of 1,002 mm and annual humidity of 78.3%. The watershed of 184,000 square kilometers yields an average annual flow of 894 m³/s and average annual runoff volume of 28,206 million m³.

4.2. TEMPERATURE FIELD SIMULATION

In order to reduce the temperature gradient during the water piping, supplementary water cooling for EL-74~95m dam area were analyzed and presented as an example. The scenarios discussed are shown in Table 1.

Table 1
List of analyzing scenarios.

CASE	WATER SUPPLY PROGRAMME	WATER SUPPLY AREA
1	No water run-off	EL-74~95m
2	7 days of water supply,21°C	EL-74~95m

At a certain moment when the peak temperature exists in Case 1, the actual temperature field of the dam section of interest obtained from monitoring is shown in Fig. 2a. The simulated temperature field distribution of the dam is shown in Fig.2b. The comparison between the temperature measurement and simulation resu Its is shown in Fig. 3. As can be seen in Fig. 3, slow heat dissipation inside the concrete dam results in a peak of 40.4°C. The 3D modelling results are basically consistent with the actual temperature measurement, verifying the capacity of the model in predicting the history of concrete temperature.

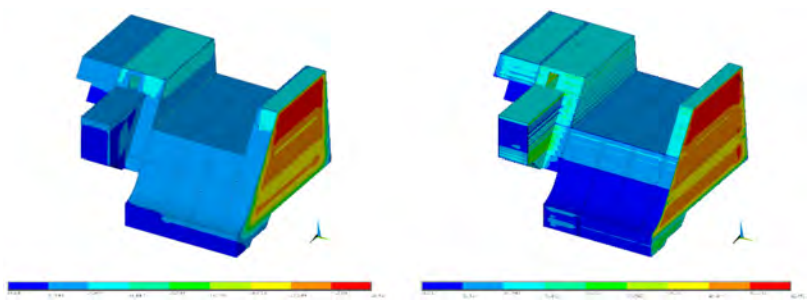


Fig. 2
Temperature distribution of the dam sections in Case 1. (left) Actual temperature cloud image, (right) Simulated temperature cloud image.

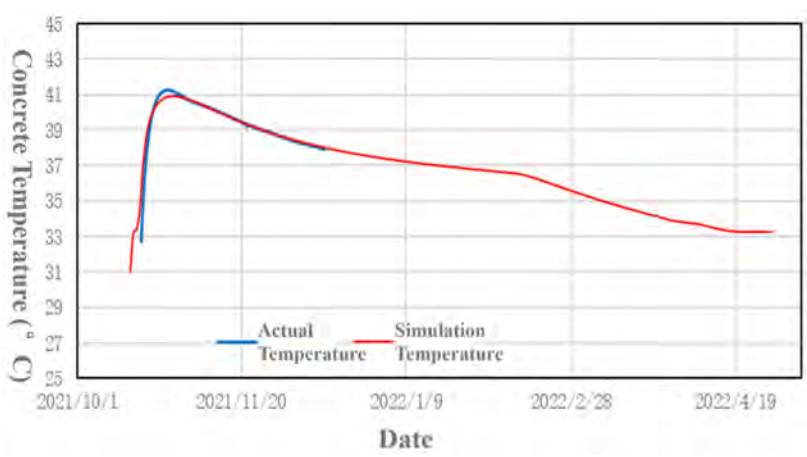


Fig. 3
Comparison of measured and simulation temperatures in dam section R2 (EL93m)

On the overflow area of dam section R2, concrete temperature change curves were created at representative points at elevations of EL 94 m, EL 93 m, and EL 92 m. Fig. 4 presents the temperature history at each representative point. Fig. 5 shows the temperature distribution after water cooling when the peak temperature exists in Case 2.

As can be seen in Fig. 4, the cooling evolution of dam concrete is slow. When the upstream is filled with water, the internal temperature of the concrete is

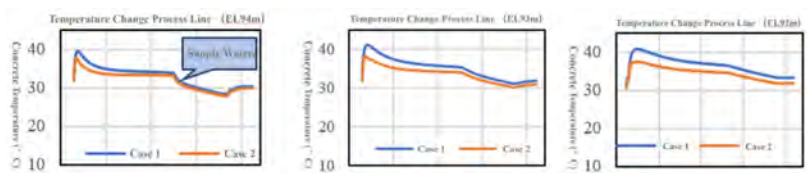


Fig. 4
Concrete temperature history at different elevation. (left) EL 94 m, (middle) EL 93 m, (right) EL 92 m.

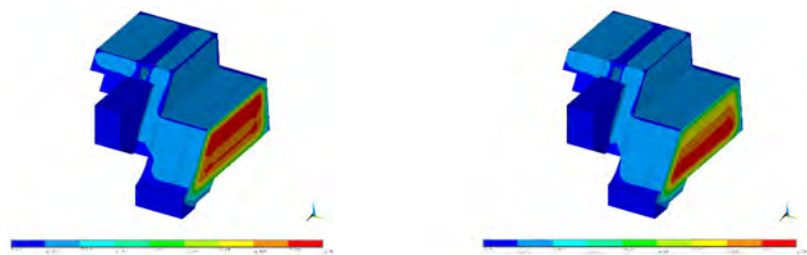


Fig. 5
3D temperature distribution. (left) Case 1, (right) Case 2.

approximately 36.3°C. After overflowing, the dam sections of R1, R2, and R3 are affected by water and the temperature of surface concrete reduces to 27.2°C, yielding a large temperature gradient. As such, the intelligent temperature control system is introduced. After the water cooling treatment is completed, the internal temperature is reduced and the concrete temperature inside and outside tends to be uniform.

4.3. EFFECTIVENESS EVALUATION

The intelligent temperature control system for concrete was implemented for the whole dam construction. The water temperatures and flow rates were determined based on the close monitoring and 3D modelling. According to the actual dam concrete temperature monitoring data, the overall cooling rate distribution is shown in Table 2 and Fig. 6. The average cooling rate controlled by the system was specified to be 0.2 °C/day, and the maximum cooling rate was 0.81°C/day (vs. the design specification of 0.5°C/d or less). The water cooling operation controlled by the system resulted in a compliance rate of 99.93%, ensuring uniform cooling of massive concrete.

Table 2
Stratified Statistics of Cooling Rates

DAILY COOLING RATE	MIN	MAX	COUNTS $\leq 0.5^{\circ}\text{C/D}$	TOTAL COUNTS	AVERAGE	COMPLIANCE RATE
0 $^{\circ}\text{C/day}$	0.81 $^{\circ}\text{C/day}$		797	798	0.02 $^{\circ}\text{C/day}$	99.93%

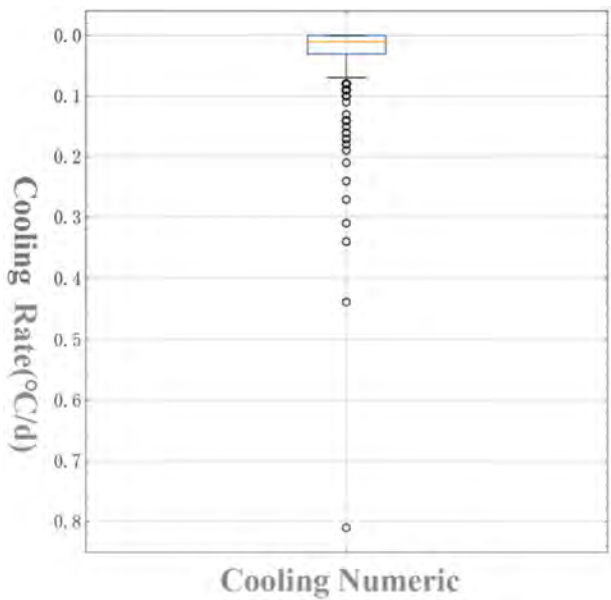


Fig. 6
Statistical graph of cooling rates.

5. CONCLUSIONS

The Julius Nyerere Hydropower Station is located in the equatorial zone, which has hot and humid weather throughout the year and may experience extreme weather. The project is huge in scope and employs continual rising casting. It is difficult to regulate the temperature of massive concrete in such intricate settings. Based on this, a new integrated intelligent temperature control system is provided, and the temperature distribution of concrete under water cooling via piping and water heat exchange feedback was investigated using the aforementioned intelligent temperature control system. The main conclusions are as follows:

An intelligent temperature control system is proposed to enable the sensing, collection, analysis, and feedback control of temperature data in large-scale concrete water-cooling projects. The system includes a heat exchanger, a heat exchange auxiliary device, a dam data gathering device, a control device, and a software platform.

The temperature distribution of dam sections cooled with water via piping was simulated and analysed. After water cooling, concrete's interior and external temperatures tend to merge and be consistent. The intelligent water flow system is capable of properly controlling the temperature of enormous volumes of concrete.

The temperature progression of concrete under stringent constraints was investigated. The results reveal that water cooling via pipes improves the internal heat exchange of concrete and lowers the peak temperature. The temperature rise and fall in various operating bins are essentially identical, and the temperature of output water via pipes is largely steady. Intelligent temperature cooling control of concrete provides good control adaptability. By providing homogeneity in the total thermal properties of dam concrete hydration, the risk of cracking is decreased.

The system was implemented at the Nyerere Dam. The data collected during the operation of the intelligent temperature management system totaled billions, and the daily cooling rate compliance was 99.93%. Compared to traditional operations, personnel for water cooling was decreased by more than 80%, enhancing temperature control quality and efficiency. Reduced likelihood of concrete cracking increased the dam's potential service life. It also gives valuable experience and references for temperature control in similar large-scale concrete projects in hot and humid climates.

ACKNOWLEDGMENTS

The authors are grateful for the financial support from the Sinohydro Tanzania Julius Nyerere Hydropower Station Construction Key Technology Research Scientific and Technological Achievements Consulting Services (Nos. SHC-JNHPP-JSW-01-18012022), the Consulting Services for the Research of Key Technologies and Scientific and Technological Achievements in the Construction of the Lower Kaifuxia Hydropower Station (Nos. SH-KGL-SUB-2021003).

REFERENCES

- [1] YANG JK. Discussion on the main factors affecting the quality control of water conservancy project construction. *Building Materials Development Orientation*, vol. 20, pp. 84–86, 2022.
- [2] WANG XG., YANG RUNLAI., CHEN ZHIJUN. Development and application of intelligent temperature control system for mass concrete. *Water Transport Engineering*, vol. 01 pp. 118–121+143, 2020.
- [3] MYERS T., FOWKES N., BALLIM Y. Modelling the cooling of concrete by piped water. *Journal of Engineering Mechanics*, vol. pp. 135 1375–1383, 2009.
- [4] WALEWSKI J., SADATSAFAVI H. Megaproject Success: Hoover Dam Construction and Pre-Construction Management Ingenuity. *Hoover Dam Anniversary, History Symposium*, 2010.
- [5] LI GAOFENG., LIU SB., ZHAO YC. Temperature-controlled anti-cracking measures for crushed concrete in Longtan Hydropower Station dam. *Sichuan Hydropower*, vol. 29, pp. 225–229+276, 2010.
- [6] HUANG HOUNONG., QIAO HONG. Construction of crushed concrete at Suofengying hydropower station dam. *China Water Resources*, vol. 21, pp. 41–43, 2007.
- [7] ZHANG LEI., LI XIAOQUN., ZHANG HONG. Research on the effect of temperature control of concrete during high and low temperature periods in Guanyinyan Dam during high temperature season. *Hydropower generation*, vol. 43, pp. 35–37+47, 2017.
- [8] WANG JUAN., WANG ZHENHONG., YANG NING. Research on temperature-controlled anti-cracking scheme of concrete spillway spillway in two river mouths. *Hydropower generation*, vol. 46, pp. 48–52+58, 2020.
- [9] ZHAO HONG., JIANG ZHIJIE., ZHOU ZHIHUA. Temperature and crack control of mass concrete in Xiaolangdi project. *Construction Science*, vol. 04, pp. 50–52, 2000.
- [10] ZHANG YX. Simulation and inverse analysis of temperature stress in mass concrete. *Dalian University of Technology*, 2003.
- [11] JI FENGWEI. Internal temperature control of concrete in the dam of Three Gorges III project. *Yunnan Hydropowe*, vol. 05, pp. 33–36, 2006.

- [12] LIU SHICHENG., WU QINGYU. Temperature control and anti-cracking technology of concrete in high arch dam of the Blockze River Hydropower Station. *Yunnan Hydropower Generation*, vol. 25, pp. 5–8, 2009.
- [13] TAN WENPENG., WANG RONGXING., ZHAO WEI. Intelligent temperature control system and method for mass concrete based on temperature difference control. *Highway*, vol. 65, pp. 211–215, 2020.
- [14] LIN PENG., NING ZEYU., LI MING. Prototype test study on intelligent joint control of water cooling pipe network of extra-high arch dam. *Journal of Water Resources*, vol. 5, pp. 819–828, 2021.
- [15] TAN YAO-SHENG., FAN QI-XIANG., WANG ZHI-LIN. Intelligent construction technology and application practice of Baihetan extra-high arch dam. *Journal of Tsinghua University (Natural Science Edition)*, vol. 61, pp. 694–704, 2021.
- [16] NING ZEYU., LIN PENG., PENG HAOYANG. Moving average analysis method and application of real-time concrete temperature data. *Journal of Tsinghua University (Natural Science Edition)*, vol. 61 pp. 681–687, 2021.
- [17] WANG XG., YANG RUNLAI., CHEN ZHIJUN. Development and application of intelligent temperature control system for mass concrete. *Water Transport Engineering*, vol. 01, pp. 118–121+143, 2020.
- [18] WANG FUQIANG. Research on temperature control standards and measures for concrete in Daitengxia lock. *Northeast Water Conservancy and Hydropower*, vol. 39, pp. 27–29, 2021.
- [19] TIAN ZHENG., YAO BAOYONG., LI QI. Application of intelligent temperature control system for mass concrete in reconstruction project of Fengman hydropower station. *Water conservancy construction and management*, vol. 38, pp. 57–60+77, 2018.
- [20] YANG MEI., PING YOUHONG., XIE MIN. Research and practice of concrete temperature control of Huangdeng Dam. *Proceedings of the 2019 Annual Conference of the Chinese Society of Dam Engineering*, 2019.
- [21] YANG JING'AN., HUANG YANYAN., GUO HAOYANG., Research and application of temperature control technology for highly crushed concrete gravity dam in dry and hot area. *Northwest Hydropower*, vol. S1, pp. 54–59, 2020.
- [22] LIU XIAODONG., REN YONGPING., ZHU JING., WEN ZEKUN. Influence of intelligent temperature control system on mass concrete construction. *Concrete*, vol. 06, pp. 179–184, 2022.

COMMISSION INTERNATIONALE DES
GRANDS BARRAGES

VINGT-HUITIEME CONGRES DES
GRANDS BARRAGES
CHENGDU, Mai 2025

**EFFECTS OF SPATIAL AND TEMPORAL VARIATION CHARACTERISTICS OF
EXTREME PRECIPITATION ON DAM SAFETY IN MAJOR RIVER BASINS IN
CHINA IN RECENT 20 YEARS (*)**

Ning ZHOU, Fang WANG, Li HONGEN & Zhu ZHANG
*State Key Laboratory of Hydrology-Water Resources and Hydraulic Engineering,
Nanjing Hydraulic Research Institute, Nanjing*

CHINA

SUMMARY

The purpose of this study is to analyze the distribution characteristics of extreme precipitation and the concentration of precipitation in different river basins in China, and to explore its potential impact on the safe operation of reservoirs and dams. Based on the daily precipitation data of meteorological stations in China from 2000 to 2020, 10 extreme precipitation indexes in the basin were calculated, and the variation characteristics of precipitation concentration and precipitation concentration period in the past 20 years were analyzed. It was found that the reason why dam breaks in Songliaohe River Basin, Huaihe River Basin, Yangtze River Basin and Southeast River Basin did not decrease during 2010 to 2020 may be related to the variation characteristics of extreme rainfall in the basin. From the analysis of climate change trend of extreme precipitation index, both the total precipitation amount and extreme precipitation characteristics in Songliao River Basin show a significant growth trend, and the Yellow River Basin, Yangtze River Basin and southeast river basins show a significant growth trend. From the climate change trend of Rx5day, it is concluded that the persistent heavy precipitation events in

**Effets de la variation spatiale et temporelle des précipitations extrêmes sur la sûreté des barrages dans les principaux bassins fluviaux de Chine au cours des 20 dernières années*

China's river basins have increased year by year in recent years; From the precipitation concentration and precipitation concentration period in the basin, the precipitation concentration in the Songliaohe River Basin is becoming more and more concentrated, while the precipitation in the Southeast River Basin is becoming more and more average. The precipitation concentration period in the northern basin of China is delayed, while the precipitation concentration period in the Yellow River basin, Southeast River Basin and Pearl River basin is advanced. Through the analysis of extreme precipitation and precipitation concentration in different river basins, it provides the direction and possibility of early warning and prediction for the safe operation of reservoirs and dams.

RÉSUMÉ

Le but de cette étude est d'analyser les caractéristiques de distribution des précipitations extrêmes et la concentration de précipitations dans différents bassins fluviaux en Chine, et d'explorer son impact potentiel sur le fonctionnement sûr des réservoirs et des barrages. Sur la base des données de précipitations quotidiennes des stations météorologiques chinoises de 2000 à 2020, 10 indicateurs de précipitations extrêmes dans le bassin ont été calculés et les caractéristiques de changement de la concentration de précipitations et de la période de concentration de précipitations au cours des 20 dernières années ont été analysées. Il a été constaté que la raison pour laquelle les barrages dans le bassin de la rivière Songliaohe, le bassin de la rivière Huaihe, le bassin de la rivière Yangtze et le bassin de la rivière sud-est n'ont pas diminué entre 2010 et 2020 peut être liée aux caractéristiques de changement des précipitations extrêmes dans le bassin. De l'analyse de la tendance du changement climatique de l'indice de précipitations extrêmes, on peut voir que la quantité totale de précipitations et les caractéristiques de précipitations extrêmes du bassin de la rivière Songliao ont montré une tendance de croissance significative, et le bassin de la rivière Jaune, le bassin de la rivière Yangtze et le bassin de la rivière sud-est ont montré une tendance de croissance significative. À partir de la tendance du changement climatique de Rx5day, il est conclu que les précipitations fortes persistantes dans les bassins fluviaux chinois ont augmenté d'année en année ces dernières années; À en juger par la concentration de précipitations et la période de concentration de précipitations dans le bassin, la concentration de précipitations dans le bassin de la rivière Songliaohe devient de plus en plus forte, tandis que les précipitations dans le bassin du sud-est deviennent de plus en plus moyennes. La période de concentration des précipitations dans le bassin nord de la Chine est retardée, tandis que la période de concentration des précipitations dans le bassin de la rivière Jaune, le bassin du sud-est et le bassin de la rivière Zhujiang est avancée. Grâce à l'analyse des précipitations extrêmes et de la concentration de précipitations dans différents bassins fluviaux, il fournit des directions et des possibilités d'alerte précoce et de prévision pour le fonctionnement sûr des barrages des réservoirs.

1. INTRODUCTION

In the context of global warming, global and regional water cycles have intensified, thus increasing the frequency and intensity of extreme precipitation events [1]. With the increasing frequency and intensity of extreme weather events, the guarantee of safe operation of reservoirs and dams in China is facing severe challenges. At present, China has made some progress in the research on the impact of climate change on reservoir dam safety [2-3], but the quantitative analysis and systematic research on extreme weather events and water conservancy project safety are still insufficient [4]. In recent years, different degrees of rainstorm events have occurred in different regions of China. For example, since 2010, there have been many rainstorms in Beijing. Among them, the strongest rainstorm since 1951 occurred on July 20, 2012 [5-6], and the rare rainstorm in history occurred again on July 20, 2016. On July 21, 2021, a heavy rainstorm occurred in central and northern Henan. The highest hourly rainfall in Zhengzhou, located at the center of the rainstorm, reached 201.9 mm, the highest hourly rainfall in mainland China's history. It is found that the frequency and intensity of heavy precipitation and extreme heavy precipitation events can be observed in most areas of China gradually increases, showing the characteristics of light rain decreasing and heavy rain increasing. There are significant regional differences in the changes of extreme precipitation in China. Most extreme precipitation indexes show an increasing trend in northwest, southeast and middle and lower reaches of the Yangtze River in China, while they show a decreasing trend in North China, Northeast China and Southwest China [7-9]. Extreme precipitation events, floods, hydrological droughts and other disasters are directly threatening the safe operation of reservoirs and dams in China. Understanding the changes in the frequency, intensity and duration of extreme precipitation events is of great significance to national disaster prevention and mitigation and the formulation of defense policies to adapt to climate change conditions.

There are significant regional differences in extreme precipitation changes in China, especially in different river basins. Current studies are mostly based on different methods and different precipitation indexes, and there are also differences in related research time periods. Clarifying the temporal and spatial variation characteristics of extreme precipitation in different river basins, the characteristics of precipitation concentration and precipitation concentration periods in different river basins can provide scientific reference for understanding drought and flood disasters related to extreme precipitation, and can also provide theoretical support for my country's reservoirs and dams to cope with extreme climate changes and provide short-term forecasts.

Therefore, this paper focuses on the characteristics of extreme precipitation in different river basins under climate change, its precipitation concentration and concentration period, so as to put forward the management priorities of reservoirs and dams in different river basins in the future, provide a basis for decision makers to formulate policies, and at the same time improve disaster prevention and mitigation capabilities and adaptation to climate change are of great significance.

2. STUDY AREA, DATA AND METHOD

2.1. STUDY AREA AND DATA

The data used includes daily precipitation during the period 2000-2020 at 627 stations throughout China from the National Meteorological Information Center (NMIC), CMA. These daily data have been uniformly adjusted by removing the non-homogeneity caused by station relocation and instrument replacement. We calculated 10 indices defined by ETCCDI in Table 1. We carried out the characteristic analysis of extreme precipitation in China from 2000-2020. The dam failure data is based on the dam basic database of the Dam Safety Management Center of the Ministry of Water Resources.

China consists of nine large river basins: the Songliaohe River basin, the Haihe River basin, the Huaihe River basin, the Yellow River basin, the Yangtze River basin, the Pearl River basin, the Southeast River basins, the Southwest River basins and the Northwest Inland River basins, as shown in Fig. 1.

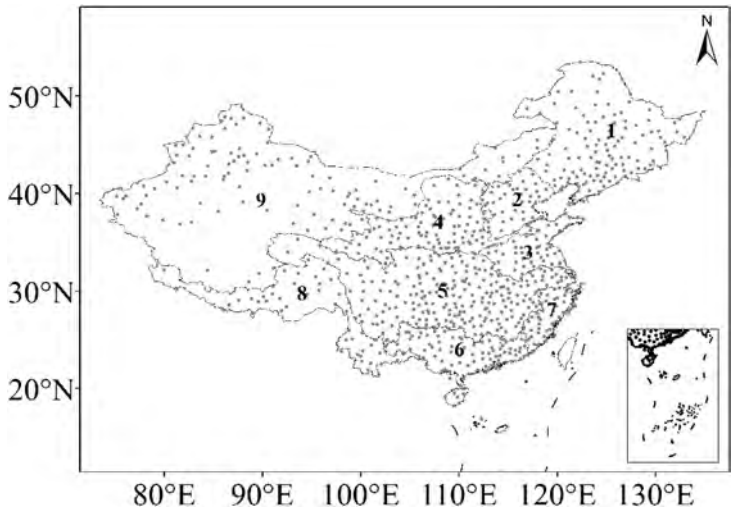


Fig. 1

Nine large river basins in China. (Numbers denote the nine river basins: 1, the Songliaohe River basin; 2, the Haihe River basin; 3, the Huaihe River basin; 4, the Yellow River basin; 5, the Yangtze River basin; 6, the Pearl River basin; 7, the Southeast River basins; 8, the Southwest River basins; 9, the Northwest Inland River basins.)

2.2. PRECIPITATION CONCENTRATION DEGREE AND PRECIPITATION CONCENTRATION

The calculation method of precipitation concentration degree and concentration period used in the study is to use the vector principle to define the parameters of time distribution characteristics, which can be used to quantitatively describe precipitation concentration degree and concentration period. The calculation formula is as follows:

$$PCD_i = \frac{\sqrt{R_{xi}^2 + R_{yi}^2}}{R_i} \quad (1)$$

$$PCP_i = \arctan(R_{xi}/R_{yi}) + 180^\circ \quad (2)$$

$$R_{xi} = \sum_{j=1}^{36} r_{ij} \times \sin \theta_j \quad (3)$$

$$R_{yi} = \sum_{j=1}^{36} r_{ij} \times \cos \theta_j \quad (4)$$

where PCD_i and PCP_i represent the precipitation concentration degree and precipitation concentration period in the i year respectively; i represents the year, j represents the ten-day order ($j = 1, 2, 3, \dots, 36$), and R_i represents the total precipitation (mm) of a meteorological station in the i year; r_{ij} is the precipitation (mm) in the j ten-day of the i year; θ_j is the azimuth angle corresponding to each ten days in the study period of a certain meteorological station, that is, assuming that the azimuth angle of a year is 360° , the total of a year is 36 ten-day, and ten-day is equivalent to 10° , then $\theta_j = j * (360^\circ / 36)$. PCD reflects the concentration degree of total precipitation in each ten-day in the study period. The closer its value is to 1, the more concentrated precipitation in a certain ten days in that year; If the value is closer to 0, it means that the distribution of precipitation in each ten-day of the year is more average; PCP indicates which ten of the year the sum of precipitation in ten-day is concentrated in. Therefore, using precipitation concentration degree and concentration period to study the temporal and spatial distribution pattern of precipitation concentration can indicate the precipitation concentration degree of each ten-day in the study period and which ten-day after precipitation synthesis concentration appears. See the literature for specific calculation methods and principles [10].

2.3. EXTREME PRECIPITATION INDEX

Characteristics of extreme climate events were used to describe their frequency, intensity, and duration. In this paper, 10 precipitation indices defined by ETCCDI were analyzed. The definitions of the 10 indices are shown in Table 1.

Table 1
Definition of extreme precipitation indices defined by ETCCDI

INDICE	NAME	DEFINITION	UNIT
PRCPTOT	Total precipitation in wet days	Annual total precipitation from days >1 mm	mm
SDII	Simple daily intensity index	The ratio of annual total precipitation to the number of wet days (≥ 1 mm)	mm/d
Rx1day	Max 1-day precipitation amount	Annual maximum 1-day precipitation	mm
Rx5day	Max 5-day precipitation amount	Annual maximum consecutive 5-day precipitation	mm
R95p	Very wet days	Annual total precipitation from days >95th percentile	mm
R99p	Extremely wet days	Annual total precipitation from days >99th percentile	mm
R10mm	Heavy precipitation days	Annual count when precipitation ≥ 10 mm	d
R20mm	Very heavy precipitation days	Annual count when precipitation ≥ 20 mm	d
CWD	Consecutive wet days	Maximum number of consecutive days when precipitation ≥ 1 mm	d
CDD	Consecutive dry days	Maximum number of consecutive days when precipitation <1 mm	d

3. TEMPORAL AND SPATIAL DISTRIBUTIONS OF DAM FAILURES IN DIFFERENT BASIN

According to the statistical results of dam failure data, the distribution of dam failure events in different basin is different in each year. It can be seen from Table 2 that before 1980, China was in a high incidence stage of dam failure; dam failure events in China showed a significant downward trend from 1980 to 1999, and further decreased significantly after 2000. This characteristic is mainly due to the continuous promulgation and improvement of relevant laws and regulations on reservoir safety management in recent years, and the continuous standardization of dam design, construction, safety monitoring, maintenance and other systems and mechanisms [11].

From the perspective of the nine major river basins, there was a significant increase in dam failure incidents from 1970 to 1979. Comparing the distribution of dam failure events in various river basins, the Yellow River, Yangtze River and Pearl River basins are the river basins with a larger proportion of dam failure events. During the peak period of dam failure, 390 dam failure events occurred in the Yellow River Basin and 775 dam failure events occurred in the Yangtze River Basin, 198 dam failure events occurred in the Pearl River Basin; The main reason for the peak period of dam break is the catastrophic flood caused by extreme precipitation, which threatens the safety of reservoir dams. From Table 2, it is not difficult to find that as

dam safety management continues to improve, the occurrence of dam failure events in nine river basins is gradually decreasing. However, the Songliaohe River Basin, Huaihe River Basin, Yangtze River Basin and Southeast River Basin in 2010-2021 are not less than those in 2000-2009. Whether this will be related to the frequent occurrence of extreme weather in recent years, and whether the distribution characteristics of extreme precipitation in different river basins in China have changed, these require further analysis of the characteristics of extreme precipitation in different river basins.

Table 2
Temporal and spatial distributions of dam failures in nine large river basins of China

YEAR PERIOD	SONGLIAOHE RIVER BASIN	HAIHE RIVER BASIN	HUAIHE RIVER BASIN	YELLOW RIVER BASIN	YANGTZE RIVER BASIN	PEARL RIVER BASIN	SOUTHEAST RIVER BASIN	SOUTHWEST RIVER BASIN	NORTHWEST RIVER BASIN
1954-1959	11	20	4	22	54	46	17	7	12
1960-1969	49	129	41	99	236	55	52	18	43
1970-1979	138	102	197	390	775	198	79	32	88
1980-1989	22	3	6	25	167	29	14	6	24
1990-1999	46	0	5	23	86	50	5	15	17
2000-2009	3	0	0	5	16	19	1	3	8
2010-2021	3	0	1	3	21	7	1	2	6

4. RESULT AND DISCUSSION

4.1. EXTREME CLIMATE DATA CHARACTERS

This section mainly calculates the climate change rate of each indices in nine major river basins from 2000 to 2020 through 10 extreme precipitation indices, analyzes the change trend of different extreme precipitation indices in different river basins, and then puts forward constructive suggestions on the safety management of reservoirs and dams in different river basins in China.

According to the analysis of climate change rate of annual total precipitation, except Huaihe River Basin and the Southwest River Basin, which showed a decreasing trend (Table 3), other river basins showed an increasing trend, and the Southeast River Basin showed the largest change rate, which was 85.78 mm/10a. Secondly, the growth rate of Songliaohe River Basin and Yangtze River Basin is relatively high, both exceeding 70mm/10a. According to the analysis of the change

trend of precipitation intensity and daily maximum precipitation, the climate tendency rate of Songliaohe River Basin is the highest in both precipitation intensity and daily maximum precipitation, which are 0.75 mm/d/10a and 4.2 mm/10a respectively, while Huaihe River Basin and the Southwest River Basins still show a downward trend. From the variation trend of maximum 5-day precipitation, it is found that all nine major river basins show climate growth characteristics, which indicates that China as a whole shows a trend of increasing year by year in continuous precipitation events, and Pearl River Basin and the Southeast river basins all exceed 100mm/10a. According to the analysis of climate change rate of heavy precipitation and extremely heavy precipitation, the maximum change rate is 48.4 mm/10a and 15.83 mm/10a in Songliaohe River Basin, respectively. The climate change rate of heavy precipitation in Haihe River Basins, Yellow River Basins, Yangtze River Basins and the Southeast River Basin all exceed 20mm/10a, which the climate change rate of extremely heavy precipitation in Haihe River Basin and Yangtze River Basin exceeds 5mm/10a; The trend of extreme heavy rain days, heavy rain days and maximum continuous wet days is not obvious, but the maximum continuous dry days shows a downward trend in all river basins except southwest river basins.

Table 3
Climate propensity rate for 10 precipitation indices defined by ETCCDI in nine large river basins of China during 2000-2020(Unit)

INDICES	SONGLIAOHE RIVER BASIN	HAIHE RIVER BASIN	HUAIHE RIVER BASIN	YELLOW RIVER BASIN	YANGTZE RIVER BASIN	PEARL RIVER BASIN	SOUTHEAST RIVER BASIN	SOUTHWEST RIVER BASIN	NORTHWEST RIVER BASIN
PRCPTOT (mm/10a)	73.72	35.38	-8.09	49.42	71.22	66.89	85.78	-38.12	10.70
SDII (mm/ d/10a)	0.75	0.60	-0.11	0.47	0.26	0.11	0.15	-0.03	0.24
Rxday (mm/10a)	4.20	1.78	-0.76	2.83	1.32	0.60	0.70	-0.18	1.90
Rx5day (mm/10a)	68.90	64.37	82.53	54.64	91.44	118.82	111.08	64.41	22.86
R95p (mm/ 10a)	48.40	27.73	-7.50	29.81	25.65	19.42	20.43	-7.97	9.00
R99p (mm/ 10a)	15.83	7.56	-2.85	10.16	6.76	3.66	3.87	-1.29	4.50
R10mm (d/ 10a)	2.35	1.37	0.09	1.71	2.24	1.96	2.77	-1.30	0.48
R20mm (d/ 10a)	1.48	0.88	-0.07	0.80	1.18	1.12	1.51	-0.29	0.19
CWD (d/ 10a)	0.16	0.06	-0.30	0.04	0.23	0.07	0.47	-0.19	-0.04
CDD (d/ 10a)	-1.43	-0.63	-1.04	-1.17	-0.20	-0.08	-1.18	2.93	-3.79

4.2. CHARACTERISTICS OF PRECIPITATION CONCENTRATION DEGREE AND
PRECIPITATION CONCENTRATION PERIOD

From the spatial distribution of precipitation concentration degree in 2000-2009 (Figure 2a), 2010-2020 (Figure 2b) and 2000-2020 (Figure 2d), it can be seen from the spatial distribution of precipitation concentration that precipitation concentration shows obvious differences in different river basins, and there are obvious north-south differences. The precipitation concentration increases step by step from the Southeast River Basin to the Songliaohe River basin, which indicates that the precipitation from the southeast basin to the north basin of China tends to occur more and more in a year. Among them, the precipitation concentration degree in Songliaohe River Basin, Haihe River Basin and Yellow River Basin is relatively highest, while that in Huaihe River Basin, western Yangtze River Basin and Pearl River Basin is relatively high, while that in eastern Yangtze River and Southeast River Basins is relatively small. The distribution characteristics of the above precipitation concentration degree have similar spatial distribution patterns in 2000-2009 and 2010-2020 and the whole study period.

In order to compare whether there is a significant change in precipitation concentration degree in China around 2010, the average precipitation concentration degree in 2010-2020 is subtracted from the average precipitation concentration degree in 2000-2009, and the river basin with significant changes in precipitation concentration degree in the two periods is obtained. From Figure 2c, it can be seen that the areas with increasing precipitation concentration degree in China are mainly concentrated in Haihe River Basin, Yangtze River Basin and Southeast River Basin, while the western Yellow River Basin, Pearl River Basin and Southern Songliaohe River Basin are the areas with relatively decreased precipitation concentration.

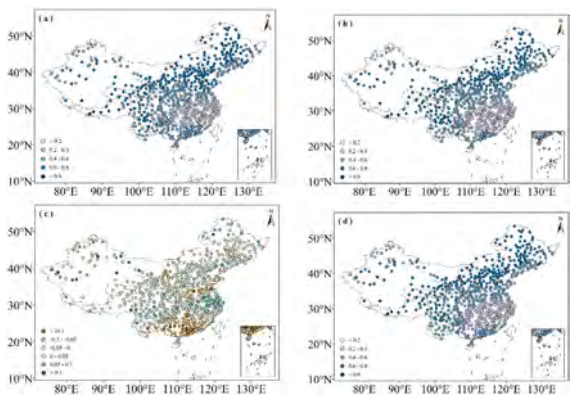


Fig. 2

Spatial distribution characteristics of average precipitation concentration degree (a) during 2000-2009 (b) during 2010-2020 (c) Significant Changes between 2010-2020 and 2000-2009 (d) during 2000-2020

From the spatial distribution of precipitation concentration period, it is basically similar to the distribution characteristics of precipitation concentration degree, mainly showing that precipitation concentration in Songliaohe River Basin, Haihe River Basin, western Yangtze River Basin and Huaihe River Basin occurs in July, Yellow River Basin occurs in August, Southeast River Basin and Pearl River Basin occur in June, eastern Yangtze River Basin shows precipitation concentration period in May, Northwest River Basin and Southwest River basin have no significant characteristics. The distribution characteristics of the above precipitation concentration periods have similar spatial distribution patterns in 2000-2009 and 2010-2020 and the whole study period. Considering the analysis of the significant change characteristics of precipitation concentration period around 2010, it can be seen from Figure 3c that the Yellow River Basin, Southeast River Basins and Pearl River Basin show an obvious advance of concentration period, which is about 10 days in advance. However, some stations in Haihe River Basin, Yangtze River Basin and Songliaohe River Basin have the characteristics of delayed precipitation concentration period, which is about 10-20 days later.

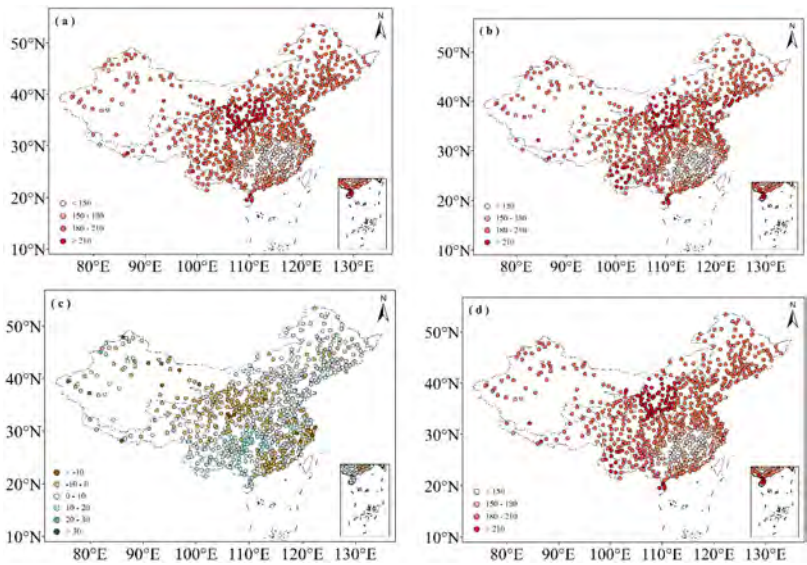


Fig. 3

Spatial distribution characteristics of average precipitation concentration period (a) during 2000-2009 (b) during 2010-2020 (c) Significant Changes between 2010-2020 and 2000-2009 (d) during 2000-2020

5. CONCLUSION

Based on the historical dam failure data, the distribution characteristics of dam failure at different stages in different river basins are analyzed. With the gradual improvement of reservoir dam management in China, the number of dam failure in each river basin is gradually decreasing. However, from 2010 to 2020, the number of dam breaks in Songliaohe River Basin, Huaihe River Basin, Yangtze River Basin and Southeast River Basins has not decreased. Based on the daily precipitation data of 672 stations from 2000 to 2020, this paper calculates the climate change rates of 10 extreme precipitation indices in nine major river basins in China. For PRCPTOT, SDII and Rx1day indices, except Huaihe River Basin and Southwest River Basins, which show a decreasing trend, other river basins show an increasing trend; The climate change rate of extreme precipitation index in Songliaohe River Basin, Yellow River Basin, Yangtze River Basin and Southeast River Basins is relatively high. We should focus on the safety of reservoirs and dams in several river basins, and carry out early warning and prevention in time. In addition, according to Rx5day index, it is found that the climate change rates of nine river basins are all positive, which indicates that the continuous precipitation events in China are tending to increase. After calculating the precipitation concentration degree and concentration period in different river basins from 2000 to 2009 and 2010 to 2020, it is found that the precipitation concentration in Songliaohe River Basin, Yellow River Basin and Haihe River Basin is more concentrated from 2010 to 2020, while the rainfall concentration in southeast river basins and Pearl River Basin shows an average trend, so extremely heavy precipitation may be more difficult to predict. The precipitation concentration period of Yellow River Basin, Southeast River Basin and Pearl River Basin gradually tends to be earlier, about 10 days, while the precipitation concentration period of Haihe River Basin, Yangtze River Basin and Songliaohe River Basin is delayed, about 10-20 days. This provides some theoretical support for the safety management of reservoirs and dams in different river basins during flood season.

ACKNOWLEDGMENTS

The authors are grateful for the financial support from the National Key R&D Program of China (No.2022YFC3005403) and Fundamental Research Funds for the Central Research Institute (No. Y724008 and Y723007).

REFERENCES

- [1] HUANG S Z, DU M, LI P, *ET AL.* Investigation of the abrupt changes in precipitation concentration and the driving forces under the changing environment. *Advances in Water Science*, vol. 30, no. 4, pp. 496–506, 2019.
- [2] QIN P C, LIU M, XIA Z H, *ET AL.* Progress in Assessing the Impacts of Climate Change on China's Water Resources and Major Water Conservancy Projects. *Advances in Meteorological Science and Technology*, vol. 12, no. 6, pp. 7–15, 2022.
- [3] BAN X, SHI C W, GUO H, *ET AL.* Effects of climate change and water conservancy projects on hydrological regime downstream of Danjiangkou Dam. *Advances in Science and Technology of Water Resources*, vol. 40, no. 4, pp. 1–7, 2020.
- [4] ZHANG J Y, XIANG Y. Analysis on the impact of climate change on the water conservancy project safety (in Chinese). *Sci Sin Tech*, vol. 48, pp. 1031–1039, 2018.
- [5] Gan L, Guo W L, Deng C J. Comparative analysis of two torrential rain processes in Beijing. *Journal of Arid Meteorology*, vol. 35, pp. 239–249, 2017.
- [6] Comparison of short duration heavy rainfall environmental conditions during two extreme torrential rainfall events over Beijing area. *Torrential Rain and Disasters*, vol. 40, pp. 27–36, 2021.
- [7] Wu W B, You Q L, Wang D. Characteristics of extreme precipitation in China based on homogenized precipitation data. *Journal of Natural Resources*, vol. 31, pp. 1015–1026, 2016.
- [8] Zhou B T, Xu Y, Wu J, *ET AL.* Changes in temperature and precipitation extreme indices over China: Analysis of a high resolution grid dataset. *Int. J. Climatol.*, vol. 36, pp. 1051–1066, 2016.
- [9] Wang Y J, Zhou B T, Qin D H, *ET AL.* Changes in mean and extreme temperature and precipitation over the arid region of northwestern China: Observation and projection. *Adv. Atmos. Sci.*, vol. 34, pp. 289–305, 2017.
- [10] Zhang L, Qian Y. A Study on the feature of precipitation concentration and its relation to flood-producing in the Yangtze River Valley of China. *Chinese Journal of Geophysics*, vol. 47, no. 4, pp. 622–630, 2004.
- [11] SUN Jinhua. Achievements of reservoir dam safety management in China and challenges. *China Water Resources*, vol. 20, pp. 1–6, 2018.

COMMISSION INTERNATIONALE DES
GRANDS BARRAGES

VINGT-HUITIEME CONGRES DES
GRANDS BARRAGES
CHENGDU, MAI 2025

A HIGH-PRECISION THREE-DIMENSIONAL DAM-BREACH MODEL CONSIDERING BREACH EVOLUTION MECHANISMS (*)

Shengyao MEI & Xu JIANJUN
PowerChina Huadong Engineering Corporation Limited, Hangzhou

CHINA

SUMMARY

With the intensification of global climate change, extreme flood events occur more frequently. Once a flood exceeds the standard and overtops the dam crest, it can easily lead to the overtopping failure of earth-rockfill dams, posing a significant threat not only to economic losses but also to the safety of lives and property downstream. Therefore, accurately predicting the evolution process of earth-rockfill dam overtopping failures under extreme flood conditions is of great significance for enhancing emergency prevention and control capabilities of dams and reducing potential losses. However, existing dam breach models are mostly designed for homogeneous dams and have low simulation accuracy, failing to meet practical application needs. To address this, this paper proposes a three-dimensional high-precision numerical simulation method based on Reynolds-Averaged Navier-Stokes equations to simulate the turbulent flow characteristics of dam breach flows. By incorporating wide-graded dam material erosion equations and breach slope instability criteria, the method constructs breach shape evolution equations, achieving detailed simulation of overtopping failures under complex terrain conditions. The accuracy and rationality of this detailed numerical simulation method are validated through typical moving-bed flume model tests.

**Modèle tridimensionnel précis de brèche de rupture de barrage prenant en compte les mécanismes d'évolution de la brèche*

RÉSUMÉ

Avec l'intensification des changements climatiques mondiaux et la fréquence accrue des événements de crues extrêmes, lorsque les inondations dépassent le sommet du barrage, il est très facile que les digues de terre et de pierres soient submergées et rompent, entraînant non seulement de graves pertes économiques, mais aussi une menace majeure pour la sécurité des vies et des biens des populations situées en aval. Par conséquent, il est important de prévoir avec précision l'évolution des catastrophes de rupture des digues de terre et de pierres sous l'effet des inondations extrêmes afin d'améliorer la capacité de prévention et de contrôle d'urgence des barrages et de réduire les pertes potentielles. La plupart des modèles de rupture de barrage existants sont conçus pour les digues homogènes et leur précision de simulation est faible, ce qui ne permet pas de répondre aux besoins pratiques. Pour cela, ce rapport propose une méthode numérique de simulation raffinée en trois dimensions de la rupture de barrage basée sur les équations de Navier-Stokes moyennées de Reynolds, afin de simuler les caractéristiques du mouvement turbulent du courant lors de la rupture de barrage. En outre, en se fondant sur les équations d'érosion des matériaux de barrage à granulométrie large et sur les méthodes de discrimination de l'instabilité des talus de rupture, nous avons construit l'équation d'évolution de la forme de la brèche, réalisant ainsi une simulation détaillée en trois dimensions du processus de rupture de barrage par submersion dans des conditions de relief complexe. La précision et la rationalité de cette méthode de simulation numérique raffinée ont été vérifiées par des expériences sur un modèle de canal à fond mobile.

1. INTRODUCTION

With the intensification of global climate change, extreme flood events have become more frequent, posing significant challenges to the operational safety of earth-rockfill dams. Once floods exceed the dam crest, overtopping failure is highly likely, and the massive release of water within a short period poses serious threats to the lives and properties of residents downstream. For instance, in 2018, the dam breach of the Sheyuegou Reservoir in Xinjiang, China, resulted in 20 fatalities; and in 2023, two reservoirs in Libya failed consecutively due to a hurricane, causing the deaths of over 20,000 people [1]. Given the severity of the consequences of dam failures, how to predict the breach process scientifically and efficiently is a critical technological challenge in emergency response.

Dam-breach models are typically categorized into three types: empirical models, simplified physically-based breach models, and detailed physically-based

numerical models [2]. From a physical perspective, the dam breach process is a complex coupling of non-steady, non-uniform flow, and transport of broad-graded dam material, with distinct three-dimensional characteristics. Empirical models generally rely on statistical analysis of collected breach data, using regression analysis or machine learning methods to propose empirical formulas for predicting breach characteristics, but they do not typically reflect the underlying breach mechanisms and lack the precision required for emergency situations [3]. Therefore, some researchers have developed simplified breach models based on dam breach mechanism, significantly improving breach prediction accuracy. However, these models introduce many empirical assumptions regarding hydrodynamics and breach development, and do not simulate the movement of high-velocity sediment-laden flows [4]. Furthermore, early detailed numerical simulation methods were often based on assumptions of static pressure distribution and did not consider the three-dimensional dam breach process under complex terrain conditions. They also could not represent the erosion of broad-graded dam materials under high-velocity flows or the complex flow patterns associated with breaches. Additionally, erosion by breach flows can cause scouring of the breach bottom, and the evolution of the breach shape can influence the hydraulic characteristics of the breach flow. These interactions need to be considered in the numerical simulations [5].

In this paper, we develop a high-precision three-dimensional numerical simulation method that couples a three-dimensional hydrodynamic model, turbulence equations, and a broad-graded dam material transport model. This aims to capture the turbulent characteristics of breach flows, and the erosion characteristics of broad-graded dam materials, thereby better simulating the three-dimensional breach process. Typical benchmark experimental cases under moving-bed conditions are selected to validate the applicability of the mathematical model and analyze the accuracy and reasonableness of the computational results.

2. HIGH-PRECISION DAM BREACH NUMERICAL MODEL

2.1. GOVERNMENT EQUATIONS

This study assumes that both the fluid and the dam material are incompressible fluids with constant properties. After Reynolds averaging, the continuity equation of the incompressible Navier-Stokes equations can be referenced in Mei et al. [5].

During the dam breach process, the sediment movement modes can be converted between bedload and suspended load [6]. Variations in sediment

concentration in the flow discharge can result in variations in flow density and viscosity coefficient, thereby affecting the subsequent erosion, as shown in Fig. 1.

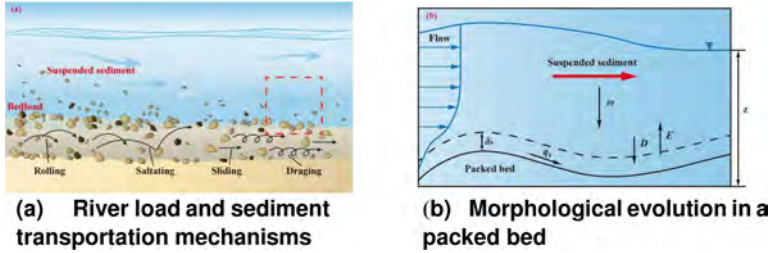


Fig. 1

Schematic diagram of dam material erosion process

In this study, dam material particles are idealized as spherical shapes, and the erosion characteristics of different components of dam materials are considered. The upward entrainment velocity E can be used to calculate the conversion of bedload to suspended load.

$$E = \alpha n_s d^{0.3} (\theta - \theta_{cr})^{1.5} [gd(\rho_s - \rho_w)/\rho_w]^{0.5} \quad (1)$$

where α is the entrainment coefficient for different components of the dam material, n_s is the normal vector filling the breach bottom, d is the dimensionless particle diameter, θ is the dimensionless Shields number, θ_{cr} is the critical shear stress.

The downward deposition velocity D of the dam material refers to the transfer process of particles settling from suspension to bedload due to their own weight:

$$D = \omega C_s \quad (2)$$

Considering the broad gradation characteristics of the dam material, Meyer-Peter and Müller's empirical formula is selected to represent the bedload sediment transport rate per unit width:

$$q_b = K(\theta - \theta_{cr})^{1.5} [gd(\rho_s - \rho_w)/\rho_w]^{0.5} \quad (3)$$

According to the dam breach mechanism, the evolution of the breach shape is updated through strong interaction between the hydrodynamic conditions and the breach boundaries. The transport of dam material along the flow direction can be calculated through mass conservation equations for the bed material, suspended

load, and bedload to determine the elevation of the breach bottom:

$$\phi_s \partial z_b / \partial t = (\partial q_b / \partial x + D - E) \quad (4)$$

2.2. NUMERICAL SCHEME

This study employs the finite volume method for the discrete solution of the numerical model, maintaining computational stability with the dynamic time step. The Pressure-Implicit with the Splitting of Operators (PISO) algorithm is used for the implicit solution of pressure, coupling the time-advanced velocity in the continuity equation with the time-advanced pressure in the momentum equation. Additionally, a fully decoupled detailed breach numerical simulation method based on a three-dimensional structured staggered grid is established in this paper, solving for changes in hydrodynamics, dam material transport, and breach morphology evolution.

3. MODEL VALIDATION

To verify the characteristics of the high-precision three-dimensional dam breach numerical model, this section selects typical flume test cases under moving-bed conditions for inverse calculation.

3.1. SUDDEN ENLARGEMENT OPEN CHANNEL BREACH TEST

This flume test case was completed by the University of Leuven under moving-bed conditions [7]. Eight ultrasonic water level gauges (P1~P8) were positioned downstream in the flume to measure the variation of water level over time during the breach process. The specific dimensions of the instruments and coordinate information for the measurement points are shown in Fig. 2. At the same time, nine cross-sections (cs1~cs9) were measured every 0.05 meters in the range of 1.1~1.5 meters from gate to determine the bed surface changes.

Fig. 3 shows the calculated results of flow depth at various times. It can be observed that the breach flow forms a triangular vortex in the sudden enlargement region of the flume. Due to the reflection from the flume side walls, oblique flow directions are formed. Starting from $t=9s$, a vortex-shaped flow depth can be clearly observed at the corner, indicating significant scouring of sediment at the bottom.

Water levels are calculated for six typical measurement points (P1, P2, P3, P5, P6, and P7) and compared with the experimental measurements (as shown in Fig. 4). The calculated values match well with the measured values, with peak arrival times being largely consistent, indicating the model can effectively compute the hydrodynamic characteristics of breach flows under moving-bed conditions.

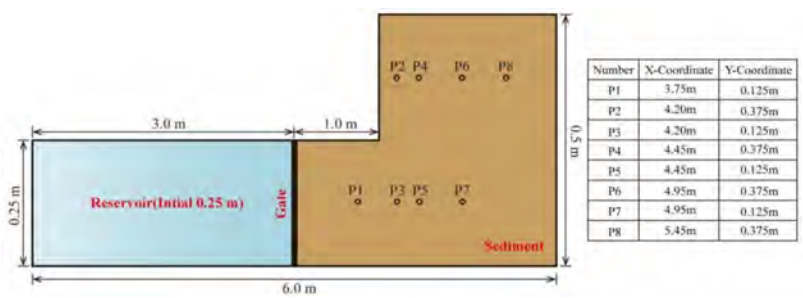


Fig. 2
Schematic diagram of sudden expansion open channel dam-break test and coordinate information of water level gauge measuring points

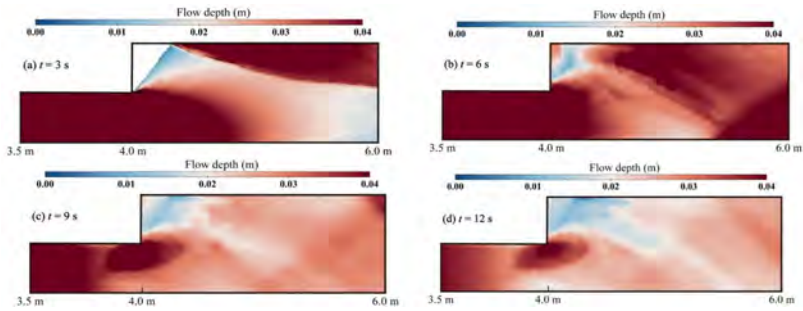


Fig. 3
Calculated flow depth at various times

3.2. CASE 2: DOUBLE-SIDED EXPANSION BREACH TEST

This benchmark test case is a dam breach test with double-sided expansion under moving-bed conditions conducted at the University of Leuven [8]. It primarily involves rapid transient flows and sediment transport in moving-bed breach flows.

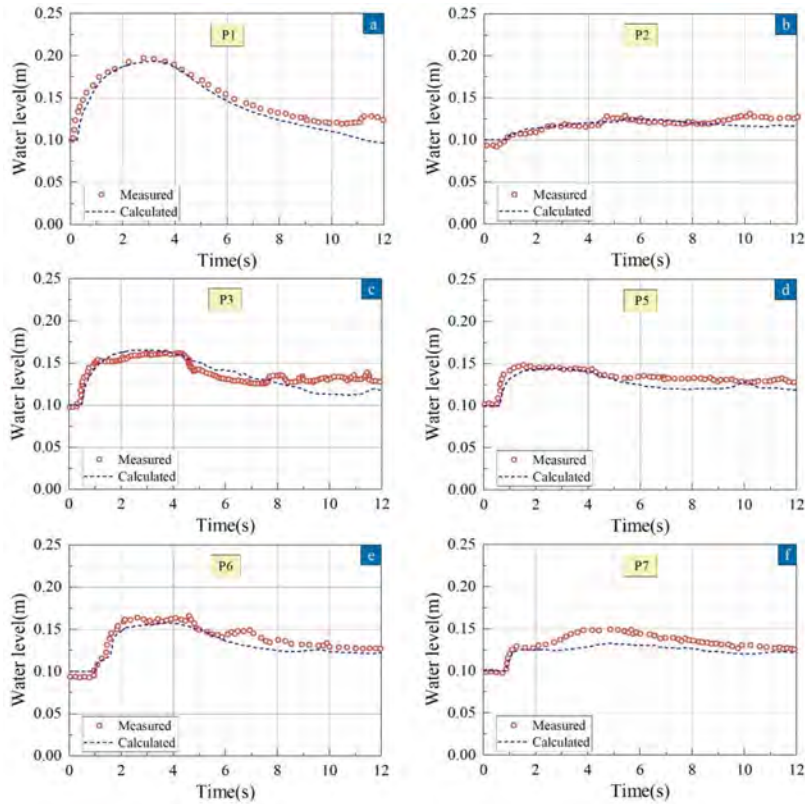


Fig. 4

Comparison of the measured and calculated water level at each monitoring point

Four pairs of water level measurement points were symmetrically arranged in the downstream section of the flume to monitor the variation of water level over time, and the bed elevation changes were measured along three longitudinal profiles. The specific dimensions of the instruments and coordinate information for the measurement points are shown in Fig. 5.

Fig. 6 shows the simulated bed elevation at various times, from which we can observe the scoured pit downstream of the gate and the ring-shaped deposition distributed along the sides of the downstream flume. Additionally, the overall change in the downstream bed exhibits good symmetry, which can be attributed to the symmetrical experimental design. The scoured pits that occur are mainly due to the

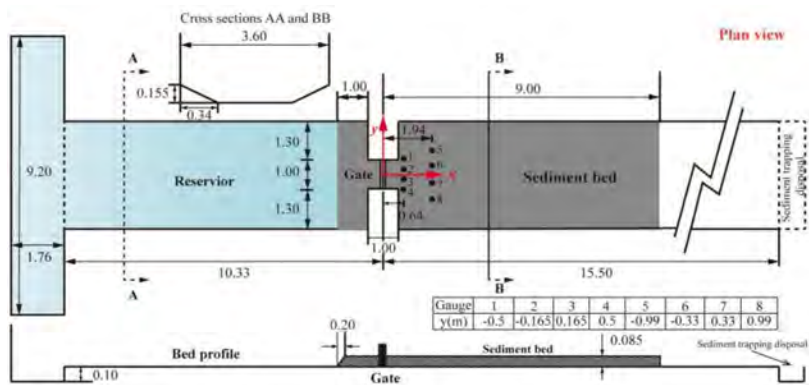


Fig. 5
Schematic diagram of double-sided widening dam-break test

impact of high-velocity breach flows at the double-sided expansion location in the early stages, while the ring-shaped deposition can be attributed to the dissipation of energy from the scouring of bed sediments, causing the downstream flows to gradually slow down.

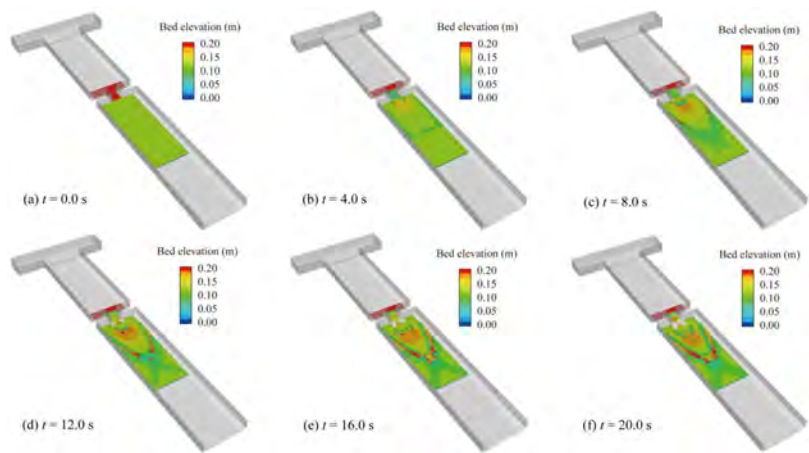


Fig. 6
Simulated bed elevation at different times

Fig. 7 further illustrates the comparison between the calculated and measured bed elevations along three longitudinal profiles ($y = 0.2 \text{ m}$, $y = 0.7 \text{ m}$, $y = 1.45 \text{ m}$), with the initial bed elevation marked for reference. The aforementioned patterns of sediment erosion and deposition can be clearly observed. Sediment erosion occurs near the gate ($x < 2.0 \text{ m}$), while sediment deposition occurs further downstream. Near $x = 2.0 \sim 4.0 \text{ m}$, the model overestimates the scouring zone for all three profiles, and there is a larger deviation close to the wall at $x = 0.0 \sim 2.0 \text{ m}$ for the $y = 1.45 \text{ m}$ profile, which may be due to the adhesion effects near the wall. Additionally, the model's predictions for the maximum scour depth or maximum deposition thickness along the three longitudinal profiles show some discrepancies with the two sets of measurements. However, considering the inherent errors in the experimental measurements, the computational results generally reflect the trends in changes in bed elevation.

Fig. 8 shows the time-varying curves of water level measurements and calculations for the four pairs of water level gauges. Due to the completely symmetrical experimental design, the distribution of water level gauges is also symmetrical. As a result, the water level curves for the four pairs of measurement points are essentially identical, and the trends of the water level calculation values and the measured values are generally consistent, though there are still some deviations. The water levels at measurement points 1~4 exhibit pronounced oscillatory behavior, possibly due to the rapid changes in bed elevation near the gate. There is a certain deviation at measurement points 5~8, where the simulation values are lower than the measured values, which may be due to errors caused by computational stability. Overall, the numerical model can reasonably calculate the measured water levels at the four pairs of measurement points.

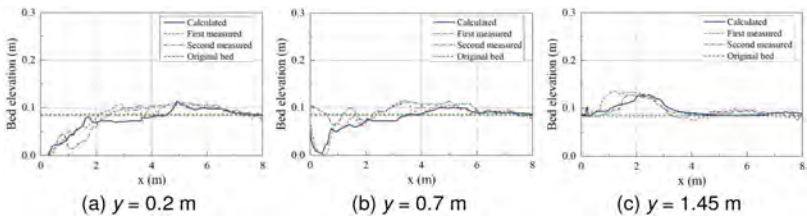


Fig. 7
Comparison of the calculated and measured variations of the bed elevations along three longitudinal profiles

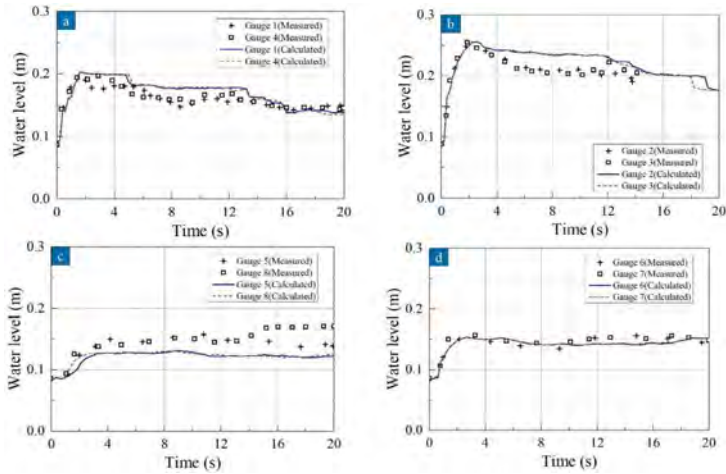


Fig. 8

Comparison of the calculated and measured variations of the water levels at the four pair of gauges

4. CONCLUSIONS

This study developed a high-precision three-dimensional dam breach numerical simulation method that considers the breach evolution mechanisms. The Volume of Fluid method was utilized to track the free surface, and the Reynolds-averaged Navier-Stokes equations were solved, coupled with the broad-graded dam material erosion equations. A finite volume method with an alternating iterative solution strategy was adopted to numerically implement the detailed simulation of the three-dimensional breach process. Typical test cases were selected to validate the accuracy and reasonableness of the model. The results indicate that the high-precision dam breach numerical simulation method yields good agreement between the calculated and measured values of water level and bed elevation at different measurement points, demonstrating its rationality and accuracy in simulating the motion characteristics of breach flows and the transport process of dam materials.

REFERENCES

- [1] YU S., ZHANG Q., CHEN Z. Y., HAO J. W., WANG L., LI P., ZHONG Q. M. Study of the Sheyuegou dam breach - Experience with the post-failure investigation and back analysis[J]. *Engineering Failure Analysis*, vol. 125, pp. 105441, 2021.

- [2] ZHONG Q. M., WANG L., CHEN S. S., CHEN Z. Y., SHAN Y. B., ZHANG Q., REN Q., MEI S. Y., JIANG J. D., HU L., LIU J. X. Breaches of embankment and landslide dams - State of the art review. *Earth-Science Reviews*, vol. 216, pp. 103597, 2021.
- [3] XU Y., ZHANG L. M. Breaching parameters for earth and rockfill dams. *Journal of Geotechnical and Geoenvironmental Engineering*, vol. 135, pp. 1957–1969, 2009.
- [4] WU W. M. Simplified physically based model of earthen embankment breaching. *Journal of Hydraulic Engineering*, vol. 139, pp. 837–851, 2013.
- [5] MEI S. Y., CHEN S. S., ZHONG Q. M., SHAN Y. B. Detailed numerical modeling for breach hydrograph and morphology evolution during landslide dam breaching. *Landslides*, vol. 19, pp. 2925–2949, 2022.
- [6] GUAN M. F., WRIGHT N., SLEIGH P. 2D process-based morphodynamic model for flooding by noncohesive dyke breach. *Journal of Hydraulic Engineering*, vol. 140. pp. 04014022, 2014.
- [7] GOUTIERE L., SOARES-FRAZAO S., ZECH Y. Dam-break flow on mobile bed in abruptly widening channel: experimental data. *Journal of Hydraulic Research*, vol. 49, pp. 367–371, 2011.
- [8] SOARES-FRAZAO S., CANELAS R., CAO Z. Dam-break flows over mobile beds: experiments and benchmark tests for numerical models. *Journal of Hydraulic Research*, vol. 50, pp. 364–375, 2012.

COMMISSION INTERNATIONALE DES
GRANDS BARRAGES

VINGT-HUITIEME CONGRES DES
GRANDS BARRAGES
CHENGDU, MAI 2025

DISASTER ASSESSMENT OF THE LANDSLIDE SURGE CAUSED BY THE DEFORMATION OF THE UPSTREAM RESERVOIR BANK OF THE DAM (*)

Yuelin SUN, Shifa XIA, Jiahong ZHANG & Ping SUN
*Key Laboratory of Construction and Safety of Hydraulic Engineering of Ministry of
Water Resources, China Institute of Water Resources and Hydropower Research,
Beijing*

CHINA

SUMMARY

At a reservoir in Northwest China, obvious tensile cracks appeared at the boundary of two deformed bodies on the right bank near the dam. The results of INSAR analyses showed that the two deformed bodies, BX1 and BX2, were still in the stage of slow creep. The deformation damage mechanism and possible destabilization mode of the two deformed bodies were studied. At the same time, the landslide surges and their propagation process when the deformed bodies are destabilized were analysed. And their effects on the structural safety of the dam and the downstream of the dam were evaluated. The results show that the stability of the deformed bodies after reservoir impoundment is low and they are basically in the critical state. If the two deformed bodies slide to the reservoir at the same time, the surges will cause the overtopping failure of the dam and the maximum average depth of the overtopping is 2.75m. When using calculation model method to calculate the surge pressure, the stresses of the dam body and stability safety factor of dam shoulder under the static and dynamic conditions can basically meet the requirements of the specification. Under normal water level conditions, after the landslide surge, the maximum water level at the downstream 400m away from the dam site is less than the design and check tail water level. So the elevation of the

*Évaluation de l'onde provoqué par un glissement de terrain à l'amont d'un barrage

tail water platform can meet the flood control requirements. Therefore, when the two deformed bodies on the right bank upstream of the dam are destabilized, the surge caused by the landslide will not affect the overall safety of the dam.

RÉSUMÉ

Ce rapport considère deux zones déformables sur la rive droite du réservoir en amont d'un barrage comme principaux objets de recherche, et étudie le mécanisme de dommage par déformation et les modes de déstabilisation possibles de ces zones à partir des conditions géologiques. Il étudie les poussées de glissement de terrain et leur processus de propagation lorsque les zones déformables sont déstabilisées, ainsi que leurs effets sur la sécurité structurelle du barrage et de l'aval du barrage. Les résultats de l'étude montrent que la stabilité de la zone après la mise en eau du réservoir est faible et fondamentalement dans l'état critique. En tenant compte des poussées de glissement de terrain par analyse numérique, lorsque deux zones sont considérées comme glissant en même temps, les glissements causent le débordement du barrage, et la hauteur moyenne maximale du débordement est de 2,75 m. Par une méthode de modélisation informatique, les contraintes dans le barrage et l'appui, dans les conditions statiques et dynamiques, répondent fondamentalement aux exigences de la spécification. La stabilité répond fondamentalement aux exigences du cahier des charges. Dans des conditions normales de niveau d'eau après le barrage anti-glissement de terrain, le niveau d'eau maximal à 400 m en aval est inférieur au niveau d'eau de conception. L'élévation de la plate-forme amont peut répondre aux exigences de contrôle des inondations. Par conséquent, lorsque les deux corps déformés sur la rive droite en amont du barrage sont déstabilisés, la poussée générée par le glissement de terrain n'affectera pas la sécurité globale du barrage.

1. INTRODUCTION

There are three deformed bodies on the right bank of a reservoir in Northwest China, of which the two bodies, BX1 and BX2, are closer to the dam site, about 1,800m to 3,200m upstream the dam. The reservoir started to release water one month after the water level reached the normal water level, and the water level dropped for 23m in 10 days. The reservoir experienced another water level drop of 13m in 3 days on April in the following year. According to the interpretation of the satellite photos of the deformed bodies, comparing the satellite photo before reservoir impoundment with that after the two water level drops, it can be seen that obvious tensile cracks appeared at the boundary of the deformed bodies BX1 and BX2. The results of INSAR analyses show that after two reservoir water level drops, the average sedimentation rate of the deformed body BX1 is in the range of 2.85mm/d to 0.14mm/d,

and that of the deformed body BX1 is in the range of 0.07mm/d to 0.21mm/d, which indicates that the deformed bodies BX1 and BX2 are still in the stage of slow creep.

Considering that the deformed bodies BX1 and BX2 are very close to the dam and are still in the stage of slow deformation, once the sliding occurs, the surge waves generated by the landslide bodies may cross the dam, which will have a direct impact on the normal operation of the ancillary hydraulic structures, and in serious cases, even may cause the dam break, thus resulting in disastrous consequences. In the paper, the two deformed bodies BX1 and BX2 were taken as the main research objects, and the deformation and damage mechanism of the deformed bodies and the possible destabilization modes were studied according to the geological conditions of the deformed bodies. And the landslide surges generated by the destabilization of the deformed bodies and its propagation process were analyzed from the perspective of quantitative analysis to evaluate the impacts of surges on the safety of the dam.

2. ANALYSIS OF DEFORMATION DAMAGE MECHANISM

2.1. ANALYSIS OF DESTABILIZATION MODE

As shown in Figure 1, deformed body BX1 is located at the right bank of the reservoir 1,800m~2,400m upstream of the dam. The slope degree of its natural slope is $35^{\circ}\sim 40^{\circ}$, locally steeply standing, with a total volume of about $6,300,000\text{m}^3$. Deformed body BX2 is located at the right bank 2,600m~3,200m upstream of the dam. The slope degree of its natural slope is $32^{\circ}\sim 40^{\circ}$, with an average thickness of 31.6m, and a total volume of about $2,150,000\text{m}^3$.

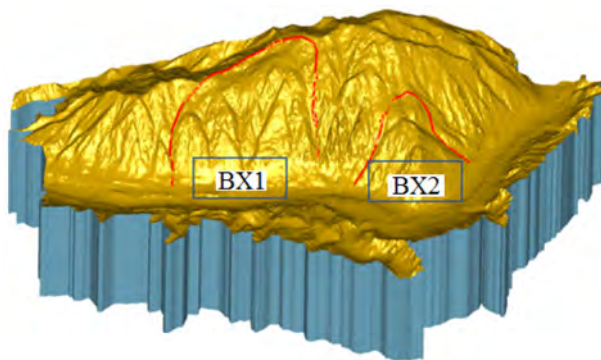


Fig. 1
3D topographic fitting diagram of the deformed bodies BX1 and BX2

The preliminary analysis of the destabilization mode of the two deformed bodies was carried out by using stereographic projection method. The average attitude of the free face of the deformed body BXI is $62^{\circ}/40^{\circ}$, and the corresponding destabilization mode is shown in Fig. 2. The average attitude of the free face of the deformed body BX2 is $56^{\circ}/43^{\circ}$, and the corresponding destabilization mode is shown in Fig. 3. It can be seen from the figure that the possible destabilization mode existing in the deformed body BXI is the planar sliding failure with the fault f01 and the pole of the gneissose structure in the sliding zone. The possible destabilization mode of the deformed body BX2 is the planar sliding failure with the pole of the gneissose structure in the sliding zone.

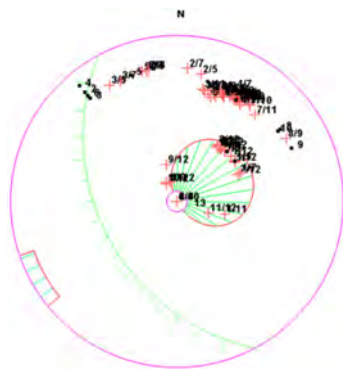


Fig. 2
Destabilization model of the deformed body BX1

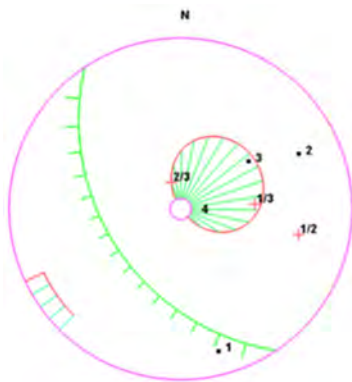


Fig. 3
Destabilization model of the deformed body BX2

2.2. STABILITY ANALYSIS OF THE DEFORMED BODIES

Two profiles were selected as typical calculation profiles for the deformed body BX1 and one profile as a typical calculation profile for the deformed body BX2. The planar position of the three profiles is shown in Fig. 4. Two typical calculation profiles of BX1 are shown in Fig. 5 and Fig. 6.

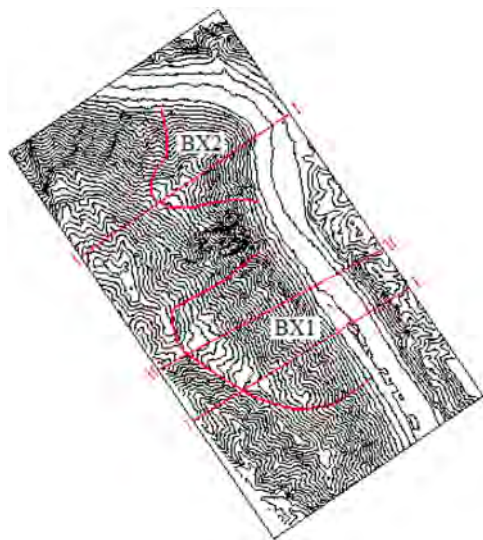


Fig. 4
Planar position of three typical calculation profiles of the two deformed bodies

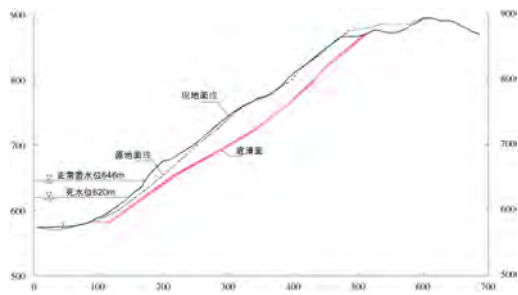


Fig. 5
Geological profile of profile I-I of BX1

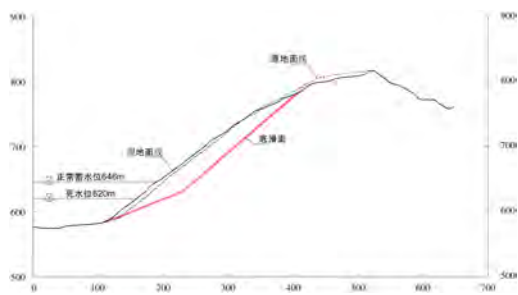


Fig. 6
Geological profile of profile II-II of BX2

The results of the stability analyses of typical profiles of the deformed bodies BX1 and BX2 under different working conditions are shown in Table 1. It can be seen from the table that when the reservoir is impounded to the normal water storage level, the stability safety coefficients of the two deformed bodies are in the range of 0.91~1.06. When considering the impact of sudden drop of water level, the safety coefficients are in the range of 0.86~1.02. And the safety coefficients are in the range of 0.84~0.98 when considering the effect of earthquake. The calculation results show that the stability of the deformed bodies after reservoir impoundment is low and they are basically in the critical destabilization state.

Table 1
Results of stability analyses of the deformed body BX1

CALCULATION PROFILE		NORMAL STORAGE LEVEL	CONSIDERING THE IMPACT OF RAINFALL	CONSIDER THE IMPACT OF SUDDEN DROP OF WATER LEVELS	CONSIDERATION THE IMPACT OF EARTHQUAKE
BX1	I-I	1.06(A)	0.99(A-w)	1.02(A-d)	0.98(A-q)
	II-II	1.00(B)	0.94(B-w)	0.93(B-d)	0.92(B-q)
BX2	I-I	0.91(C)	0.87(C-w)	0.86(C-d)	0.84(C-q)

3. LANDSLIDE SURGE PREDICTION AND ANALYSIS

According to the results of previous analyses, the deformed bodies BX1 and BX2 are both in the critical destabilization state. Once there is a special load, especially under the influence of the earthquake, the deformed bodies may form landslide bodies in the reservoir. A series of secondary disasters will be triggered

by the falling of the landslide bodies with high speed into the reservoir. The most serious consequence is the huge surge caused by the falling of the landslide bodies, which will directly affect the operation of the hydraulic buildings downstream and result in immeasurable disaster. Therefore, it is necessary to estimate the surge height of the landslides after water storage, and to predict its harm degree.

3.1. SURGE PREDICTION AND ANALYSIS METHODS

At present, the research methods on landslide surge mainly include empirical formula method, physical model test method and numerical simulation method. The calculation results obtained by the empirical formula method are relatively rough, and are only applicable to the relatively simple situation [1]-[3]. The model test method costs higher. And it is more difficult to satisfy all the similarity relations in the test [4]-[5]. The numerical simulation method is an important tool for the analysis of landslide surge, which can comprehensively analyze the whole process of the landslide surge. At present, according to the different coupling calculation way of landslide and water, the numerical simulation method can be roughly divided into two categories, namely, the simplified landslide surge model and the fully coupled landslide surge model. Among them, the fully coupled numerical simulation of landslide surge can completely consider the movement of the landslide body, the interaction between the landslide bodies and the water, and the whole process of surge. And in most of current simulations, DEM (Discrete Element) and CFD (Computational Fluid Dynamics) or SPH (Smooth Plasma Hydrodynamics) are coupled to calculate the landslide surge [6]-[8].

3.2. 3D NUMERICAL MODEL AND PARAMETERS

According to the cloud data of 3D terrain point acquired on site, a 3D geometric model including the landslide bed and the landslide surface terrain was established as shown in Figure 7. The model includes the river course of about 7,000m long from 1,000m downstream of the dam body to 2,600,000m upstream of the deformed body BX2. The model was meshed to 637,096 elements with a grid length of 5m.

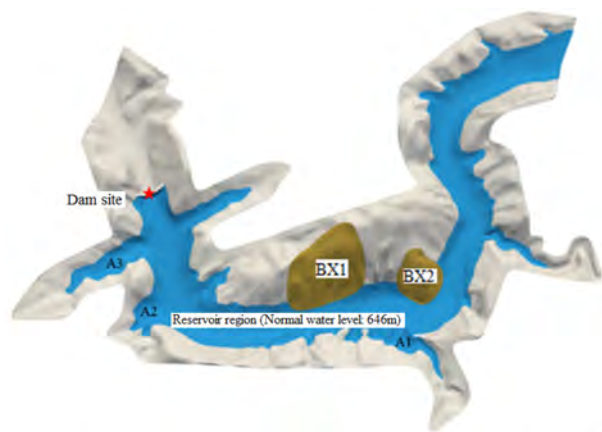


Fig. 7
3D model of the landslide and reservoir

According to the site investigation report, the mechanical properties parameters of the landslide bodies were selected. According to the depth-averaged model in the 2-D shallow water equation, the landslide bodies sliding behavior was simplified to the flow behavior of the mixed medium containing the solid phase and the fluid phase. And the characteristics of the landslide bodies were described by giving the volume fraction to the solid phase and the material parameters to the two phases in the mixed medium. In the model, the density of the solid phase of the mixed medium in the landslide is 2700.00 kg/m^3 . The density of the fluid phase is 1000 kg/m^3 . And the viscosity of the fluid phase is $0.01 \text{ Pa}\cdot\text{s}$. The values of other calculation parameters are shown in Table 2.

Table 2
Material parameter values for landslide surge model

PARAMETER	VALUES
Manning's roughness factor n	0.025
Fluid phase viscosity coefficient μ (Pa·s)	0.01
Fluid phase density ρ_f (kg/m^3)	1000
Solid phase density ρ_s (kg/m^3)	2700
Initial friction angle of landslide bed φ_1 ($^\circ$)	30
Internal friction angle of the landslide φ_2 ($^\circ$)	35
Initial solid volume fraction m_0	0.75
Critical state solid volume fraction m_{crit}	0.72
Characteristic particle size of landslide (m)	0.1

3.3. RESULTS AND ANALYSIS OF LANDSLIDE SURGE CALCULATION

The calculation results of the whole process of landslides and surge propagation in the most hazardous condition when landslides occurring simultaneously of the deformed bodies BX1 and BX2 are shown in Fig. 8.

In the initial stage, considering the most dangerous situation, two landslides slid at the same time, as shown in Fig. 8(a) at the 10th second. The two landslides impacted the reservoir water and generate surges. At this time, the landslides and surge motion are the same with that when calculating two landslides separately.

In Fig. 8(b) at the 15th second, the deformed body BX1 continued to slide and the deformed body BX2 had completed stacking. The surge waves generated by the two deformed bodies began to overlap and propagate to the opposite bank upstream and downstream. Then the slope climbing process of the surge began.

In the climbing stage, as shown in Fig. 8(c) at the 30th second, the surge wave climbed on the opposite bank reaching the highest level. And the surge wave continued to propagate upstream and downstream. At this time, the deformed body BX1 stopped sliding and its stacking and energy exchange with the reservoir water were completed.

In the surge propagation stage, as shown in Fig. 8(d) at the 65th second, after the superposition of the surge wave at the entrance of the A1 valley, the surge wave entered the A1 valley area and inundation occurs. At the same time, the surge wave propagated towards the dam site to the connection region of the areas of A2 and A3. The process of the surge propagation is relatively fast.

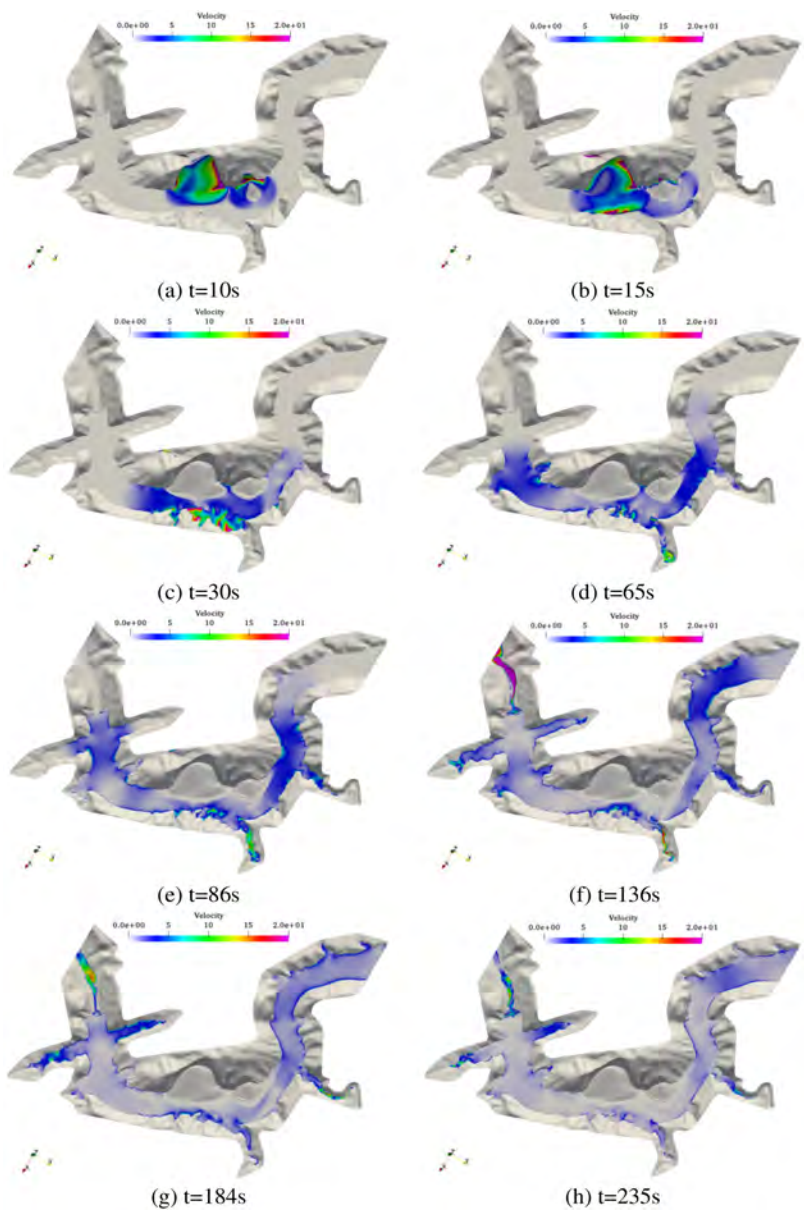


Fig. 8
Overall process of landslides and surges caused by simultaneous sliding of deformed bodies BX1 and BX2

In the overtopping stage, as shown in Fig. 8(e)~(h) at the 86th second, the surge wave arrived at the dam site and the overtopping began to occur. The overtopping process lasted for about 50s from the moment the first wave reaching the dam site and ended at the 136th second. Affected by the topography of the A2 and A3 areas near the dam site, the surge wave fell back after the process of climbing in the valley of the A2 and A3 areas and the second surge wave began to take form in the main river course. The second wave arrived at the dam site at about 184th second and another overtopping occurred which ended at about 235th second with a duration of about 51s.

In order to make further evaluation of the process of overtopping, a time-history curve of the overtopping water depth was plotted, as shown in Fig. 9. It shows that the first overtopping started at around 86th second, and the overtopping water depth peaked at the 98th second. The maximum water depth at P1 (right bank), P2 (middle) and P3 (left bank) is 2.77m, 2.98m and 2.52m separately with the average overtopping water depth of 2.75m. The second overtopping started at about 184th second, and the water depth of overtopping reached the peak at the 200th second. The maximum water depth at above three positions is 1.25m, 1.49m and 1.35m separately. The average overtopping water depth is 1.35m.

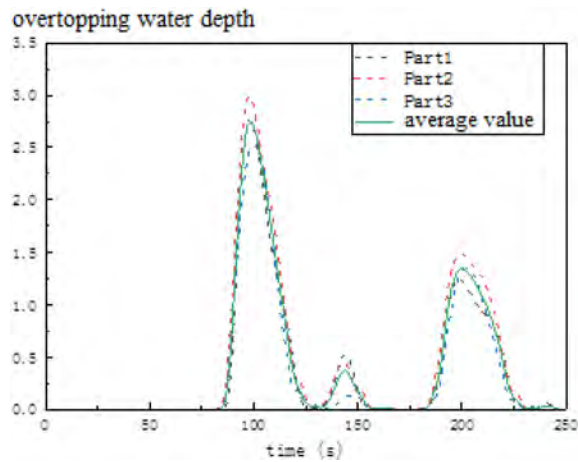


Fig. 9
Time-history curve of overtopping water depth caused by simultaneous sliding of deformed bodies BX1 and BX2

4. ANALYSIS OF DAM SAFETY UNDER LANDSLIDE SURGES

According to the results of the 3D numerical simulation analysis of the surge wave, when the deformed bodies BX1 and BX2 slide at the same time, the surge wave running up to the dam will exceed the top of the dam resulting in the over-topping of the dam. It is necessary to consider the surge pressure and calculate the stress and the safety factor of the dam body under the action of surge waves, and to evaluate the impact of surge waves on the safety of the dam.

4.1. CALCULATION METHOD OF SURGE PRESSURE

Surging waves acting on the dam body will generate a large surge pressure, which will have a certain impact on the stability and safety of the dam. The calculation method of wave pressure defined in the Standard for load on hydraulic structures (GB/T 51394-2020) is mainly applied to the action of wind waves, which is not suitable for the calculation of landslide surge pressure. According to some research on model investigation about the surge pressure[9], as to erect water retaining structure, the surge pressure below static water level is approximately vertically distributed with the peak value of about 1.77~1.89 times the water head of the wave height. Thus the conservative calculation model of the surge pressure can be adopted that the surge climb height in front of the dam is calculated by multiplying the height of surge by 1.9 times, which is taken as the vertical surge pressure below the static water level in front of the dam. And the surge pressure above the static water level is directly calculated according to the hydrostatic pressure distribution law.

4.2. EVALUATION CRITERIA OF DAM STRESS AND STABILITY

The structure grade of the concrete arch dam of this project is 2 according to the Design specification for concrete Arch dams (SL282-2018). The safety factor of allowable compressive stress under special load combinations in non-seismic conditions is 3.5 and the allowable compressive stress will be 7.14MPa. The main tensile stress of the dam body should not be greater than the allowable tensile stress of concrete that is 2.0MPa for special load combinations in non-seismic conditions. The safety factor of the grade 2 arch dam should be not less than 2.75 under special load combination in non-seismic condition.

According to the Design specification for concrete Arch dams (SL282-2018), under seismic condition the allowable compressive stress of the concrete is equal to the dynamic compressive ultimate strength divided by the safety factor and the

allowable tensile stress of the concrete is equal to the dynamic tensile ultimate strength divided by the safety factor. Accordingly, the allowable compressive stress and allowable tensile stress of the dam concrete under seismic condition calculated by the dynamic method in this project are 16.23MPa and 3.01MPa. And the safety factor of the abutment calculated by the shear formula should not be less than 1.2.

4.3. STRESS AND STABILITY ANALYSIS OF DAM UNDER SURGE ACTION

According to the structural calculation results at the design stage, the control load combination of the dam stress calculation contains the hydrostatic pressure of normal storage level and the temperature load under temperature drop condition. This time the surge pressure with the overtopping depth of 2.75m was added to the load combination. And both non-seismic and seismic conditions were considered. Because the surge pressure is a special load, the above two calculation conditions are special load combinations. The stress distribution of the dam under the action of surge pressure is show in Fig. 10 and Fig. 11, in which the dam stresses were the equivalent ones according to the specification requirement.

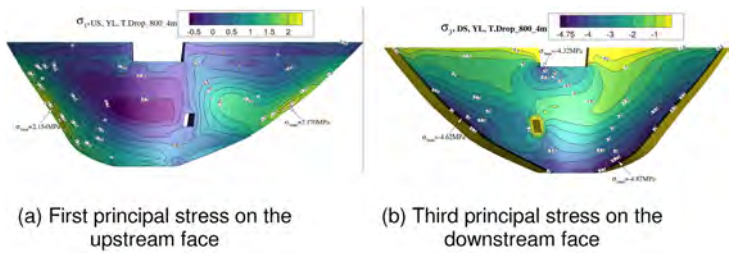


Fig. 10
Distribution of principal equivalent stresses of the dam in static condition (MPa)

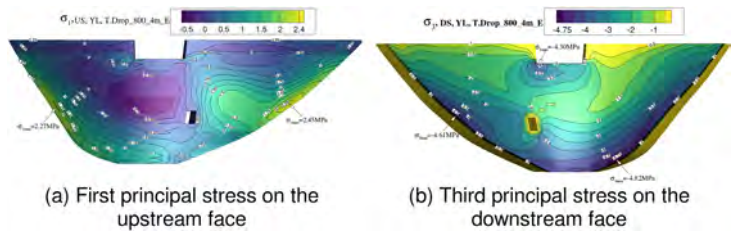


Fig. 11
Distribution of principal equivalent stresses of the dam in dynamic condition (MPa)

From the figure, it can be seen that: (1) Under non-seismic condition, the maximum equivalent value of the third principal stress of the dam after is 4.87MPa, which is smaller than the allowable compressive stress of 7.14MPa and can meet the requirement. The maximum equivalent value of the first principal stress of the dam body is 2.17MPa, which is slightly larger than the allowable tensile stress 2.0MPa. But the range where the tensile stress exceeds the allowable value is very small with the size of about 1m~2m. So the stress of overall dam can meet the specification requirements basically; (2) Under the seismic condition, the maximum equivalent values of the first and the third principal stresses of the dam body are 2.45MPa and 4.82MPa, which are smaller than the allowable tensile stress of 3.01MPa and the allowable compressive stress of 16.23MPa. And they can meet the specification requirements.

According to the analysis results of the stability of the abutment at the design stage and the geological condition revealed after excavation, the typical sliding mode was selected to carry out the analysis of the stability of the abutment. The gently dipping faults on the left bank was picked as the bottom sliding surface, the steeply dipping joints along the river was picked as the side sliding surface, and the transverse fissure at the downstream was picked as the critical surfaces. According to the 3D finite element-rigid body limit equilibrium method, the safety factor of the left abutment considering the surge pressure are 2.78 and 2.45 under the non-seismic and seismic conditions respectively, which are larger than the allowable values e specification and can meet the requirements.

4.4. ANALYSIS OF SURGE IMPACTS DOWNSTREAM OF DAMS

The time curve of water depth and water level at the place 400m downstream of the dam site was drawn as shown in Fig.12 from the calculation results in section 3.3. It can be seen from the figure that under normal water level, the maximum water depth is 4.17m 400m downstream the dam site when the overtopping occurred by the sliding surge of the deformed bodies BX1 and BX2. Adding the water depth to the normal tail water level of 571m, the water level downstream will be 574.17m.

The tail water level is 575.17m when considering the design flood frequency $P=1\%$, the return period of the 100 years. And the tail water level is 575.80 when considering the check flood frequency $P=1\%$, the return period of the 200 years. So when the deformed body BX1 and BX2 slid at the same time and formed the surge waves and overtopping of the dam, the downstream water level will be less than the design and check tail water level. The tail level meets the flood control requirements.

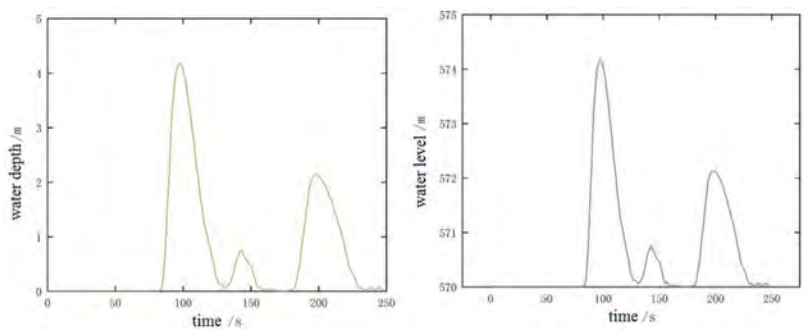


Fig. 12
Depth/level-time variation curve at the place 400 m downstream of the dam

5. CONCLUSIONS

Through the analysis of the deformation instability of the deformed bodies upstream the reservoir, the study of the landslide surge and propagation process caused by the deformed bodies, as well as the analysis of the impact of the surge on the dam structure, the following conclusions can be drawn: (1) The deformed bodies BX1 and BX2 at the right bank of the reservoir are still in the developmental stage of deformation and sedimentation. And the stability of the deformed bodies is basically in the critical state after the reservoir impoundment; (2) Under the condition of normal water level, the maximum average overtopping depth would be 2.75m if the landslide surge occurred by the sliding of the deformed bodies BX1. BX2 at the same time; (3) Under the working conditions in the paper, the dam body stress can basically meet the specification requirements and the safety factor of the abutment can meet the specification. Under the non-seismic condition, only the tensile stress at a very small range of the dam exceeds the standard value of 2.17MPa slightly which will not affect the overall structural safety of the dam; (4) When the landslide surge and overtopping occurred under the normal water level condition, the maximum water level would be 574.17m 400m downstream of the dam, which is less than the design and check tail water level. So the tail level of the platform can meet the requirements of flood control.

ACKNOWLEDGEMENTS

The authors are grateful for the financial support from IWHR Research & Development Support Program (SM0145C012024).

REFERENCES

- [1] WANG Y., YIN K. L., LIU Y. L., ET AL. Model test speed model of fording landslide taking into account water resistance. *Journal of Engineering Geology*, vol. 20, pp. 903–908, 2012.
- [2] SCHEIDEGGER A. E. On the prediction of the reach and velocity of catastrophic landslides. *Rock Mechanics*, vol. 5, pp. 231–236, 1973.
- [3] YIN K. L., DU J., WANG Y. Analysis of surge triggered by Dayantang landslide in Shuibuya reservoir of Qingjiang River. *Rock and Soil Mechanics*, vol. 29, pp. 3266–3270, 2008.
- [4] YIN K. L., LIU Y. L., WANG Y., ET AL. Physical model experiments of landslide-Induced surge in Three Gorges Reservoir. *Earth Science: Journal of China University of Geosciences*, vol. 5, pp. 1067–1074, 2012.
- [5] HUANG B. L., WANG SH. CH., CHEN X. T., ET AL. Prototype physical similarity experimental study of impulsive wave generated by cataclastic rockmass failure. *Chinese Journal of Rock Mechanics and Engineering*, vol. 2, pp. 1417–1425, 2013.
- [6] ZHAO J. D., SHAN T. Coupled CFD-DEM simulation of fluid-particle interaction in geomechanics. *Powder Technology*, vol. 239, pp. 248–258, 2013.
- [7] XU W. J. Fluid-solid coupling method of landslide tsunamis and its application. *Chinese Journal of Rock Mechanics and Engineering*, vol. 39, pp. 1420–1433, 2020.
- [8] TAN H., XU Q., CHEN SH. H., ET AL. Numerical modeling of surge caused by granular deformable landslide based on a coupled DEM-SPH model. *Rock and Soil Mechanics*, vol. 41, pp. 1–11, 2020.
- [9] HUANG J. L., FU B., HUANG ZH. M., ET AL. Discussion on calculation model of landslide surge pressure load on the front of upright dam. *Journal of Hydroelectric engineering*, vol. 32, pp. 135–140, 2013.

COMMISSION INTERNATIONALE DES
GRANDS BARRAGES

VINGT-HUITIEME CONGRES DES
GRANDS BARRAGES
CHENGDU, MAI 2025

ANALYSIS OF THE IMPACT OF EXTREME EVENTS ON DAM DISASTER UNDER CLIMATE CHANGE (*)

Jingchun LEI, Kunming LU & Gaofeng ZHANG
Northwest Engineering Corporation Limited, Xian

CHINA

SUMMARY

Reservoir dams are crucial infrastructure for ensuring water security, and the risk of disasters caused by reservoir dams should be effectively controlled. Therefore, the design, construction, management, and operation scheduling of hydraulic dams must fully consider the impact of climate change and seek effective response measures to ensure the safety and stability of reservoir dams. To correctly understand the impact of extreme weather events under climate change on dam safety, this study sequentially analyzes the characteristics of extreme heavy rain floods, extreme temperatures, and strong typhoons on reservoir dams, and proposes mitigation measures. The results indicate that climate change will have a significant impact on the design, construction, and operation management of reservoir dams and that the impact of climate change on the safety of reservoir dams is characterized by suddenness, uncertainty, and severe consequences. It may evolve into emergencies that pose a serious threat to public safety, potentially resulting in significant loss of life, economic losses, and serious social and environmental hazards, and therefore should be taken seriously to effectively minimize losses. Finally, a chain disaster model for reservoir dams is proposed, aiming to provide a reference for dam risk management and disaster reduction.

**Analyse de l'impact des événements extrêmes sur les risques associés aux barrages dans le cadre du changement climatique*

RÉSUMÉ

Les barrages-réservoirs sont des infrastructures cruciales pour garantir la sécurité de l'eau, et le risque de catastrophes causées par les barrages-réservoirs doit être efficacement contrôlé. La conception, la construction, la gestion et la planification des opérations des barrages hydrauliques doivent donc pleinement prendre en compte l'impact du changement climatique. Il faut rechercher des réponses efficaces pour garantir la sécurité et la stabilité des barrages-réservoirs. Pour comprendre correctement l'impact des événements météorologiques extrêmes sous l'effet du changement climatique sur la sécurité des barrages, cette étude analyse successivement les caractéristiques des inondations extrêmes dues à de fortes pluies, des températures extrêmes et des typhons puissants sur les barrages-réservoirs, et propose des mesures d'atténuation. Les résultats indiquent que le changement climatique aura un impact significatif sur la conception, la construction et la gestion des barrages-réservoirs et que l'impact du changement climatique sur la sécurité des barrages-réservoirs se caractérise par son caractère soudain, son incertitude et ses conséquences graves. Cela peut évoluer en une urgence menaçant la sécurité publique, entraînant potentiellement des pertes en vies humaines, des pertes économiques et des dommages sociaux et environnementaux graves, et devrait donc être pris au sérieux pour minimiser efficacement les pertes. Enfin, un modèle en cascade de catastrophes pour les barrages-réservoirs est proposé dans le but de fournir des références pour la gestion des risques et la réduction des catastrophes induites par les barrages.

1. INTRODUCTION

The essence of dam projects is to eliminate disasters and promote benefits, effectively regulate river water volume, and have functions such as flood control, power generation, water supply, irrigation, and navigation. They are an inevitable choice to ensure the safety of local people's lives and property and safeguard social and economic development. However, reservoirs and dams are mostly distributed in deep mountains and valleys with complex geological conditions and active geological activities. They are subject to special topographical and geological conditions, complex operation and maintenance, and other factors, posing varying degrees of hidden dangers. In the event of extreme events, dams are at risk of collapse or instability, at which time dam projects transform from disaster-bearing bodies into disaster-causing bodies, causing casualties and economic and property losses downstream of the dam, triggering severe disasters.

Climate change is one of the major challenges facing human development. Under the influence of climate change, extreme natural disasters such as extreme rainstorms, giant earthquakes, and extreme droughts have occurred frequently in recent decades, resulting in an increasing frequency of global reservoir dam

collapses and breaches. From 2000 to 2009, more than 200 dam failures of varying degrees occurred globally, causing enormous disaster losses. In 1975, affected by Typhoon Nina, extreme rainstorm events occurred in many parts of China, causing the collapse of two large reservoir dams (Banqiao Dam and Shimantan Dam) and dozens of small and medium-sized reservoirs in Zhumadian, Henan Province, China. This incident resulted in the deaths of more than 26,000 people and the flooding of about 12,000 square kilometers of land [1]. In 2020, the Edenville Dam in Midland County, Michigan, USA, breached, causing the evacuation of more than 10,000 residents and severe damage to downstream infrastructure. The main causes of the dam breach were extreme rainfall and floods, as well as decades of inadequate dam maintenance and supervision [2]. In addition, extreme temperatures pose risks of causing damage to reservoirs and dams, leading to accidents. In a continuous extreme low-temperature environment, the maximum frost heave of the upstream slope of the Zhangjiazuitou Reservoir Dam in Xiji County, Ningxia, was about 23 cm, and the dam slope was damaged due to frost heave caused by freeze-thaw cycles [3]. These events indicate that dams are subject to varying degrees of damage under extreme events and pose a risk of causing disasters in severe cases.

The identification and prevention of disaster risks associated with dams have become a practical issue that must be faced in global dam construction and management. In response to the diverse characteristics of reservoir disasters, numerous scholars have analyzed and studied the disaster-causing factors of dams. Extensive research has shown that dam disasters are caused by various reasons, including leakage, piping, overtopping, landslides, subsidence, and earthquakes. The International Commission on Large Dams (ICOLD) found that 45% of dam collapses are caused by overtopping due to floods [4]. Xing Linsheng reviewed and analyzed 21 hydropower dam accidents in China from 1961 to 1998, proposing that design errors, hidden dangers in construction, and operational management errors can all affect dam safety [5]. Berhane et al. analyzed the causes of excessive leakage in 54 dams in Ethiopia and found that the primary cause of leakage was excessive permeability of rock formations [6]. Based on statistical analysis of the causes of seepage failure in numerous earth-rockfill dams, Jiang Shuhai et al. derived factors influencing seepage deformation in earth-rockfill dams from the uncertainty of seepage risk, including the acting water head, rainfall, soil physical and mechanical indicators, soil layer distribution and structural dimensions of the dam foundation and dam body, and construction quality [7]. In addition, there have been fruitful research results on dam disaster-causing factors such as dam landslides and cracks. Studies have shown that the main causes of dam landslides and cracks include uneven settlement caused by stress, excessive hoop tensile stress, and seismic activities [8–10].

Currently, many scholars' analyses of dam disaster-causing factors mainly focus on dam design, construction, and operation management, while research on the impact of extreme events on dam disasters is relatively weak. However, in the context of climate change, assessing dam disaster analysis under extreme events is crucial, especially in the current era of frequent human activities. Based on this, this paper focuses on analyzing dam disaster-causing factors from the perspective of disaster-causing

characteristics of extreme events and proposes disaster mitigation and prevention measures to provide references for dam risk management and disaster reduction.

2. DISASTER IMPACT ANALYSIS OF DAMS

2.1. ANALYSIS OF DAM DISASTER UNDER THE INFLUENCE OF EXTREME RAINSTORM AND FLOOD

2.1.1. *Analysis of disaster-causing characteristics*

The main manifestations of dam disasters under the influence of extreme rainstorm floods are dam breach and burst. Continuous heavy rainfalls are often the external inducements for dam breaches. Rainstorms can rapidly increase the runoff in the river basin where the dam is located, leading to a surge in flow velocity. This can result in the formation of a flood peak with a certain discharge within a short period, causing the water level of the reservoir dam to soar and overflow the dam crest. In severe cases, this can damage the dam body, causing breaches, and ultimately leading to dam failure. Additionally, when floodwaters overflow the dam crest, the eroding action of the overflowing water on the downstream slope of the dam body can cause instability and result in dam breaches. Frequent extreme floods can exert excessive and frequent impacts on the reservoir dam, severely reducing the stability and load-bearing capacity of its foundation, posing a serious threat to the safety and stability of the dam.

The adverse effects of secondary disasters caused by extreme rainstorms on dams cannot be overlooked. Extreme rainstorms can also lead to soil erosion around the dam, affecting its foundation stability. Water infiltration can increase the internal seepage pressure of the dam, potentially causing structural damage to the dam material, thereby affecting the overall stability of the dam. The increase in the intensity and frequency of extreme precipitation can trigger a range of geological disasters such as landslides, swells, mudslides, and collapses, causing severe damage to roads, tunnels, and bridges in the dam complex area, impacting the safety of reservoir dam projects, and even resulting in significant disasters such as casualties.

2.1.2. *Disaster mitigation measures*

To mitigate dam breaches and overflows caused by extreme rainstorm floods, it is advisable to appropriately enhance the safety protection level of dams and improve the risk tolerance of dispatching principles. Emphasis should be placed on flood forecasting, and necessary hydrological measurement and reporting, as well as engineering safety monitoring facilities, should be installed and embedded in a targeted manner based on the characteristics of reservoir dam projects and potential disaster-causing factors and failure modes. Additionally, the safety monitoring and

inspection system should be strictly enforced to promptly detect accident signs and strengthen the reporting system, thereby gaining the best opportunity for emergency rescue and evacuation. The society should be educated about the risks associated with reservoir dams, and basic knowledge of dam risks and risk prevention and control should be disseminated to reservoir managers and populations at risk in flood-inundated areas through appropriate means to enhance their risk awareness.

To mitigate the temporal and spatial expansion of secondary and derivative disasters directly induced by extreme rainstorm floods on dams, appropriate protective measures should be implemented within the impact area of the reservoir dam, particularly on the slopes of the upstream reservoir area and in special terrain prone to geological disasters. Monitoring of the vulnerable sliding sections of the reservoir dam should be strengthened, and relevant soil and sand fixation measures such as vegetation-covered slopes should be implemented to enhance slope stability. To address the adverse effects of intense rainfall infiltration on dams, monitoring of the upstream and downstream water levels of the dam and the seepage pressure within the dam body should be strengthened. Regular analysis and research of monitoring results should be conducted to assess the operating status of the dam, and reasonable measures should be formulated based on the assessment results.

2.2. ANALYSIS OF DAM DISASTER UNDER THE INFLUENCE OF EXTREME TEMPERATURE

2.2.1. *Analysis of disaster-causing characteristics*

1. Extreme low temperature

During the construction of reservoir dams in plateau mountainous areas under extreme low temperatures (winter), the concrete structure is highly susceptible to freezing due to prolonged exposure to low temperatures in the early stages. After concrete is frozen, its mechanical strength and impermeability are significantly reduced, often posing a direct threat to the safety of reservoir dams in plateau mountainous areas. From the internal perspective of the dam, the free water added during the mixing of concrete undergoes volume expansion under prolonged low-temperature conditions, leading to severe damage to the internal structure of the concrete. Furthermore, repeated cycles of freezing and thawing can result in the proliferation of cracks within the concrete, which can interconnect, significantly reducing the structural strength of the concrete and ultimately leading to permanent damage. This may ultimately trigger tragic casualties.

Externally, the dam's exposure to extreme low temperatures for extended periods can cause damage due to the static ice pressure generated by the expansion of ice layers. When ice layers freeze together with the slope

protection, rising water levels in the reservoir can cause the slope protection plates to be lifted, rotated, or loosened, damaging the protection. Additionally, under prolonged extreme low-temperature conditions, ice pressure can damage gates and water intakes. When ice layers freeze firmly to gates, the expansion pressure generated during temperature rises can cause damage. Fluctuations in water levels can also exert upward or downward forces, impacting and damaging both gates and gate piers [11].

2. Extreme high temperature

Extreme high temperatures can significantly impact the deformation properties and strength of construction materials used in reservoir dams in plateau mountainous areas, with continuously rising temperatures gradually reducing the elastic modulus and strength of these materials. Research indicates that when the atmospheric temperature exceeds 43°C, the surface temperature of the concrete structure of the reservoir dam can rise above 80°C [12]. In a prolonged high-temperature environment, the moisture content within the concrete structure significantly decreases, resulting in a notable reduction in the original bond strength between the mortar and aggregates in the concrete. This leads to a significant decline in various properties of the concrete structure of reservoir dams in plateau mountainous areas, such as deformation capacity and compressive strength.

From an external perspective, for dams protected with turf slopes, continuous extreme high temperatures and drought can cause the grass to die, losing its slope protection function and exposing the soil of the dam body. In the event of heavy rainfall, this can lead to erosion of the dam slope, creating rain gullies and damaging the slope structure. Furthermore, continuous extreme high temperatures can cause the reservoir water level to drop, exposing the upstream dam slope to the air. If the dam originally had termite issues, termite tunnels may form in the frequently fluctuating water level areas of the upstream dam slope. When the water level rises, this could create new potential seepage pathways. When the reservoir dam operates continuously under extreme high temperatures and low water levels, a sudden rise in water level may increase cracks in the concrete face slab, causing compression deformation of the peripheral and vertical joints around the slab, leading to localized damage to the concrete and potentially accelerating the aging and failure of waterstop materials.

2.2.2. *Disaster mitigation measures*

1. Extreme low temperature

In extreme low-temperature environments, dam construction primarily focuses on adopting a series of comprehensive temperature control measures aimed at enhancing the early-age tensile strength of concrete and reducing the later-stage internal and external temperature differences within the

concrete. This is achieved by heating aggregates, mixing concrete with hot water, increasing the production and pouring temperatures of concrete, and adopting heating methods for concrete curing to enhance its early-age tensile strength and crack resistance. Additionally, measures such as temporary and permanent insulation of concrete, as well as the judicious selection of pouring timings for constrained concrete zones, are implemented to mitigate temperature differences and tensile stresses between the inner and outer layers, as well as between the upper and lower layers of the concrete.

During dam operations under continuous low-temperature conditions, permanent antifreeze and insulation protection measures should be implemented. This includes applying a thick layer of polyurethane rigid foam insulation material to the upstream and downstream concrete surfaces of the dam to mitigate the adverse effects of low temperatures. Furthermore, to ensure the integrity of the dam's face slabs and waterstops under continuous low-temperature conditions, de-icing measures should be taken for critical areas such as these. These measures should be tailored to the specific conditions of the reservoir dam and may include methods such as manual ice breaking, ice breaking using machinery or vessels, and jet aeration for ice melting.

2. Extreme high temperature

To mitigate the impacts of extreme heat events on dams, a series of risk management and disaster prevention and mitigation measures need to be implemented. In terms of dam construction, high-temperature retarder and high-efficiency water-reducing agents should be employed to reduce the early hydration heat of cement and delay the setting time of concrete. Low-brittleness and low-heat cement can be used for dam construction, and before concrete mixing, appropriate measures should be taken to lower the temperatures of sand, gravel, and cement, thereby reducing the temperature of the concrete. During the placement of concrete layers, spray cooling should be adopted to prevent concrete from losing moisture, turning white, and hardening, achieving the effects of cooling and insulation.

In terms of dam operation and management, for dams with turf slope protection, continuous high temperatures can easily lead to the withering of slope grasses, losing their protective function. Thus, maintenance work for dam turf slope protection during high-temperature periods should be strengthened. When the reservoir water level drops due to continuous high temperatures, exposing the upstream dam slope to the air, if the dam has existing termite hazards, termite tunnels may form in the frequently fluctuating water level areas of the upstream dam slope. In the event of a rising water level, this could create new potential seepage pathways. Therefore, timely organization and implementation of termite control measures are essential. Routine inspections and checks of reservoir dams under high-temperature conditions should be intensified to prevent the increased risk of concrete face slab cracks caused by continuous high-temperature and low-water-level operations, coupled with sudden

water level rises. Simultaneously, attention should be paid to observing abnormal deformations of ancillary structures such as dam crest access bridges and hoist rooms due to high temperatures, as well as cracking issues in dam concrete caused by excessive temperature stresses exceeding the designed temperature rise.

2.3. ANALYSIS OF DAM DISASTER UNDER THE INFLUENCE OF STRONG TYPHOON

2.3.1. *Analysis of disaster-causing characteristics*

Severe typhoons are characterized by their suddenness, wide range of impact, and high disaster-causing intensity. Their disaster-causing factors for dams mainly manifest as the storm floods induced by typhoons, fluctuations in reservoir water levels caused by typhoons, and the adverse effects of wind load on dams. The disaster-causing characteristics of storm floods triggered by typhoons on dams are similar to those of extreme storm floods mentioned earlier. In addition, the precipitation from typhoon-induced storms typically has a shorter total duration and covers a smaller area, resulting in flood hydrographs that are often more peaked and slenderer compared to those of rainstorms in the same watershed. The peak discharge of floods formed by typhoon-induced storms is significantly greater than that of non-typhoon floods, making the impact of typhoon-induced storms on dams more pronounced. In terms of the disaster-causing characteristics of dams caused by typhoons themselves, the enormous wave surge impact force generated by typhoons can easily cause structural fatigue damage to dams, potentially leading to cracks, leaks, landslides, and other issues. However, the impact of wind load on dams is relatively small and is unlikely to affect the dam body significantly [13].

2.3.2. *Disaster mitigation measures*

In response to the potential disaster-causing factors of dams under severe typhoon conditions, a scientific reservoir dam dispatch approach should be adopted. During rainfall intervals and flood recession periods, the water level should be lowered below the flood control level to prevent flood overflow. Continuous inspections should be conducted to identify and address potential safety hazards in reservoirs, such as dam leaks and cracks caused by typhoons. Furthermore, during typhoon events, intensified round-the-clock patrols of dams should be carried out to ensure that warnings can be issued promptly in case of emergencies, and corresponding emergency response measures can be taken for reservoir dams.

3. COMPREHENSIVE DISASTER MODE ANALYSIS

As mentioned above, there are several main disaster-causing factors for dams, but more often than not, these factors do not occur independently but rather

in combination, where one disaster factor leading to dam disasters may be caused by one or more other factors. Therefore, it is necessary to analyze the chain relationship between the disaster-causing factors of dams.

The disaster chain can be divided into serial disaster chains and concurrent disaster chains. A serial disaster chain refers to a series of disasters triggered by one disaster, while a concurrent disaster chain refers to a series of disasters occurring simultaneously. In most cases, the disaster chain of dam disasters under extreme events is mostly concurrent. The disaster chain of dam disasters under typical extreme events is shown in Fig. 1.

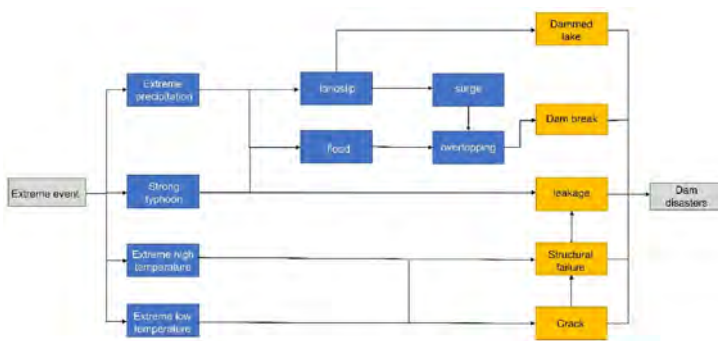


Fig. 1
The disaster chain caused by dams under typical extreme events

The chain reaction of disaster-causing factors in reservoir dams forms different disaster chains of reservoir dams. The main disaster chains can be briefly classified into the following patterns:

- A: Extreme precipitation → landslip → Dammed lake;
- B: Extreme precipitation → landslip → surge → overtopping → dam break;
- C: Extreme precipitation → flood → overtopping → dam break;
- D: Strong typhoon → landslip → Dammed lake;
- E: Strong typhoon → landslip → surge → overtopping → dam break;
- F: Strong typhoon → flood → overtopping → dam break;
- G: Extreme high temperature → structural failure → leakage
- H: Extreme high temperature → crack → structural failure → leakage
- I: Extreme low temperature → structural failure → leakage
- J: Extreme low temperature → crack → structural failure → leakage

Under the changing environment, multiple extreme climate disasters often coexist, causing disaster chains to intertwine and form a disaster network for dam

disasters. To accurately and thoroughly analyze the distribution characteristics of dam disaster-causing factors and the interconnections between them, it is necessary to conduct targeted research on the comprehensive environment within the dam's watershed, including topographical and geomorphological features, the water system layout of the watershed where the dam is located, and the frequency of extreme events. Combining this with the characteristics of the reservoir dam itself, including the condition of hydraulic structures and operational management, a comprehensive assessment can be made to gain an overall understanding of dam disaster-causing factors, disaster chains, and disaster networks. This will enable timely dam warning responses and the adoption of measures to mitigate or avoid dam disasters.

4. CONCLUSIONS

extreme temperatures, and severe typhoons, this study analyzes the potential disaster-causing impact mechanisms of these extreme climate events on reservoir dams from the perspectives of dam breaches and leaks. It explores disaster-causing factors and discusses measures to avoid or mitigate the impacts of disasters. Finally, based on the disaster-causing factors of various extreme climate events, a chain disaster mode for reservoir dams is further proposed to provide references for disaster prevention and mitigation of reservoir dams.

Influenced by global climate change, extreme weather events have increased, posing new challenges to the safe production of reservoir dams. Against this backdrop, research on the safety impacts of reservoir dams under extreme events should be strengthened to provide scientific technical support for the safety of reservoir dam engineering.

ACKNOWLEDGMENTS

The authors are grateful for the financial support provided by the Major Science and Technology Project (No. XBY-ZDKJ-2022-5) of Northwest Engineering Corporation Limited.

REFERENCES

- [1] XU Y, ZHANG L, JIA J S. Lessons from Catastrophic Dam Failures in August 1975 in Zhumadian, China. *In: GeoCongress 2008 Geosustainability Geohazard Mitig.*, no. August, pp. 162–169, 2008.

- [2] WANG T, LI Z, GE W, *ET AL.* Risk consequence assessment of dam breach in cascade reservoirs considering risk transmission and superposition[J]. *Energy*, 2023, 265:126315.
- [3] LI Z, LIU X, SUN Y, *ET AL.* Numerical simulation of frost heaving damage of earth-rock dam berms in cold regions with thermo-hydro-mechanical coupling [J]. *Cold Regions Science and Technology*, 2024, 223.
- [4] RAJABZADEH V, HEKMATZADEH A, SHOURIJEH P T, *ET AL.* Introducing a probabilistic framework to measure dam overtopping risk for dams benefiting from dual spillways, *Reliability Engineering & System Safety*, Volume 231, 2023, 109030.
- [5] XING L. Accident analysis and safety countermeasures of hydropower DAMS in China [J] *DAMS and safety*, 2000, 14(1):26–32.
- [6] BERHANE G, MARTENS K, FARRAH N A, *ET AL.* Water leakage investigation of micro-dam reservoirs in Mesozoic sedimentary sequences in Northern Ethiopia[J]. *Journal of African Earth Sciences*, 2013, 79(MAR.):98–110.
- [7] JIANG S H, FAN Z W. Quantitative assessment method of seepage risk of levee [J]. *Journal of hydraulic engineering*, 2005, 36(8):7.
- [8] ZHANG H, JING Y, CHEN J, *ET AL.* Characteristics and causes of crest cracking on a high core-wall rockfill dam: A case study[J]. *Engineering Geology*, 2022(297-):297.
- [9] A D Z, A K M, A C T, *ET AL.* Study on crack formation and propagation in the galleries of the Dagangshan high arch dam in Southwest China based on microseismic monitoring and numerical simulation[J]. *International Journal of Rock Mechanics and Mining Sciences*, 2019, 115:157–172.
- [10] GAO X F, JI M L, LI Q B, *ET AL.* Prediction of fracture failure and fracture parameters for dam gallery concrete specimens of arbitrary size and age via boundary effect model and fracture extreme theory, *Theoretical and Applied Fracture Mechanics*, Volume 131, 2024, 104376.
- [11] LEI R. Safety evaluation of earth-rock dam under extreme flood and low temperature conditions [D]. *Changsha University of Science and Technology*, 2010.
- [12] YANG J. Analysis on the influence of extreme climate on the safety of reservoir DAMS in plateau mountainous areas [J]. *value engineering*, 2017, 36 (26):3.
- [13] CHU K M, MA F H, SHEN Z Z, *ET AL.* Typhoon effect calculation method for DAMS based on load-unloading response ratio theory [J]. *South-to-north Water Transfer and Water Science and Technology*, 2013, 11(3):5.

COMMISSION INTERNATIONALE DES
GRANDS BARRAGES

VINGT-HUITIEME CONGRES DES
GRANDS BARRAGES
CHENGDU, MAI 2025

**ZONED EMBANKMENT DAM BREACHING DUE TO OVERTOPPING:
ESTIMATING OUTFLOW HYDROGRAPHS THROUGH LABORATORY
EXPERIMENTS AND PARAMETRIC NUMERICAL MODELING (*)**

Matthew HALSO

*Doctoral Researcher, ETH Zurich, Laboratory of Hydraulics, Hydrology and
Glaciology (VAW)*

David F. VETSCH

*Group Head & Lecturer, ETH Zurich, Laboratory of Hydraulics, Hydrology and
Glaciology (VAW)*

Frederic M. EVERS

*Senior Researcher & Lecturer, ETH Zurich, Laboratory of Hydraulics, Hydrology and
Glaciology (VAW)*

Robert M. BOES

*Professor & Director, ETH Zurich, Laboratory of Hydraulics, Hydrology and
Glaciology (VAW)*

SWITZERLAND

SUMMARY

In this contribution, the failure of zoned embankment dams due to overtopping is assessed with laboratory experiments and parametric numerical modeling. A series of 10 laboratory experiments were performed, in which model zoned embankment dams that contained two or three material zones were breached by an

**Rupture d'un barrage en remblai zoné par débordement : estimation des hydrogrammes d'écoulement par des essais en laboratoire et une modélisation numérique paramétrique*

overtopping flood. Based on findings from the laboratory experiments, a method for parametric numerical simulation of zoned embankment dam breaching due to overtopping was developed. That method was then applied to simulation of breaching of a model dam.

The laboratory experiments showed that the failure process for zoned embankment dams began with the development and growth of a breach channel due to erosion by the overtopping flow. The breach channel formed through the granular zones (shell and filter), and existed in two segments: (1) through the dam crest (above the core zone) and (2) through the downstream portion of the dam (downstream of the core zone). The breach channel did not grow through the core zone, which resisted erosion by the overtopping flow. Instead, the core remained intact as the breach channel grew above and downstream of it. As the breach channel grew, the core became increasingly unsupported due to the lack of downstream supporting material. Eventually, the core could not remain stable against the forces from upstream water and sediment pressure. The core cracked and split due to tensile stress from bending, broke near the lateral breach channel extents due to cantilever rotation, and then large pieces detached, creating a large breach in the core.

Based on the results of the laboratory experiments, the method for parametric numerical modeling of zoned embankment dam breaching due to overtopping was developed. The method simulates development of the breach channel through the crest and through the downstream dam portion. The section through the dam crest is simulated using the parametric numerical model for homogeneous embankment dam breaching of Macchione (2008). The downstream section is simulated based on the growth of the first segment, as well as on remaining erosive capacity of the overtopping flow. The core is simulated through a static structure analysis, by comparison of the destabilization from upstream water and sediment pressure to the stability of the core itself. Core failure is simulated when (1) the maximum tensile stress due to bending is greater than the core ultimate tensile strength (resulting in cracking and splitting), and (2) the momentum load acting on the core is greater than the momentum resistance of the core (resulting in cantilever rotation).

The parametric method was applied to simulation of the breaching of a model zoned embankment dam. Breach growth was simulated through the model dam crest and through the downstream portion of the model dam. Compared to the experimental breaching of the same model dam, breach channel growth – as depicted by the rate of core exposure – was successfully reproduced. The timing of core failure was also accurately simulated, and the rapid increase in breach discharge immediately after core failure was estimated. The parametric method reasonably represents the main processes that drive failure of a zoned embankment dam due to overtopping.

RÉSUMÉ

Dans cette contribution, la rupture des barrages en remblai zonés due au débordement est évaluée à l'aide d'essais en laboratoire et d'une modélisation numérique paramétrique. Une série de 10 essais de laboratoire ont été réalisées, dans lesquelles des modèles de barrages en remblai zoné contenant deux ou trois zones de matériaux ont été rompus par un débordement. Sur la base des résultats des essais de laboratoire, une méthode de simulation numérique paramétrique de la rupture de barrages en remblai zonés due à un débordement a été mise au point. Cette méthode a ensuite été appliquée à la simulation de la rupture d'un barrage modèle.

Les essais en laboratoire ont montré que le processus de rupture des barrages en remblai zoné commençait par le développement et la croissance d'un canal de brèche dû à l'érosion par l'écoulement de débordement. Le canal de rupture s'est formé à travers les zones granulaires (coquille et filtre) et a existé en deux sections: (1) à travers la crête du barrage (au-dessus du noyau centrale) et (2) à travers la partie aval du barrage (en aval du noyau). Le chenal de la brèche ne s'est pas développé à travers la zone centrale, qui a résisté à l'érosion par l'écoulement de débordement. Au contraire, le noyau est resté intact tandis que le chenal de la brèche se développait au-dessus et en aval de lui. Au fur et à mesure que le chenal de la brèche s'est développé, le noyau est devenu de plus en plus instable en raison de l'absence de matériau de soutien en aval. Finalement, le noyau n'a pas pu rester stable face aux forces exercées par la pression de l'eau et des sédiments en amont. La carotte s'est fissurée et divisée sous l'effet des contraintes de traction dues à la flexion, et s'est rompue et puis détachée près des extrémités latérales du chenal de la brèche sous l'effet de la rotation en porte-à-faux.

Sur la base des résultats des essais en laboratoire, la méthode de modélisation numérique paramétrique de la rupture d'un barrage en remblai zoné due à un débordement a été développée. La méthode simule le développement du canal de la brèche à travers la crête et à travers la partie aval du barrage. La section à travers la crête du barrage est simulée en utilisant le modèle numérique paramétrique pour la rupture de barrage en remblai homogène de Macchione (2008). La section aval est simulée sur la base de la croissance de la première section, ainsi que de la capacité érosive restante de l'écoulement de débordement. Le noyau est simulé par une analyse statique de la structure, en comparant la déstabilisation due à la pression de l'eau et des sédiments en amont à la stabilité du noyau lui-même. La rupture du noyau est simulée lorsque (1) la contrainte de traction maximale due à la flexion est supérieure à la résistance à la traction ultime du noyau (ce qui entraîne des fissures et des éclatements), et (2) la charge de moment agissant sur le noyau est supérieure à la résistance au moment du noyau (ce qui entraîne une rotation en porte-à-faux).

La méthode paramétrique a été appliquée à la simulation de la rupture d'un modèle de barrage en remblai zoné. La croissance de la brèche a été simulée à travers la crête du barrage modèle et à travers la partie aval du barrage modèle. Par rapport à la rupture expérimentale du même modèle de barrage, la croissance du canal de la brèche - telle qu'elle est décrite par le taux d'exposition du noyau - a été reproduite avec succès. Le moment de la rupture du noyau a également été simulé avec précision, et l'augmentation rapide du débit de la brèche immédiatement après la rupture du noyau a été estimée. La méthode paramétrique représente raisonnablement les principaux processus qui conduisent à la rupture d'un barrage en remblai zoné suite à un débordement.

1. INTRODUCTION

The failure of a dam can produce a floodwave that has disastrous consequences to downstream settlements, infrastructure, and environment. Zoned embankment dams, which are made of earthen or rockfill material and contain a relatively impermeable cohesive mineral core, can fail by breaching due to overtopping. Numerous zoned embankment dams have failed due to overtopping in recent years, including the Elbilad and Bu Mansour Dams in Libya in 2023. These dam failures created a catastrophic flood wave that devastated the city of Derna, with casualties and displaced people numbering in the tens of thousands.

The failure of zoned earthen embankment dams that contain a central vertical core zone has been studied with only a small number of experimental investigations, including those of Bornschein (2014) and Sadeghi et al. (2020). Those studies showed that non-cohesive zones (such as shell and filter zones) fail due to progressive erosion by the overtopping flow, while the central core zone remains intact before eventually breaking due to lack of support against water and sediment pressure from upstream. Similar processes have also been observed in experimental investigations with zoned embankment dams that contain rockfill shells (Franca, 2002; Vaskinn et al., 2004; Morris et al., 2007) and central or upstream face diaphragm wall elements (Simmler, 1982; Rüdissler, 2017), as well as in experiments for design of fuse plug spillways (Pugh, 1985; Fletcher & Gilbert, 1992; Schmocker et al., 2013). But to determine the effects of shell and filter zone erosion on core stability and the mechanisms that control core failure, additional experimental investigations are needed.

With better understanding of the zoned embankment dam failure process, methods for simulation of zoned dam breaching due to overtopping can be developed. Some methods are currently available, such as the parametric models of Wu (2013) and Zhong et al. (2018), but these methods do not encompass all core failure mechanisms. Parametric models that include additional failure modes are

necessary for proper consideration of uncertainty in failure processes and timing. Parametric models that output an estimate of the breach discharge hydrograph can be used to assess the consequences of failure from a specific dam, by simulating the downstream propagation of the resulting flood wave with a hydrodynamic model.

This study investigates the failure of zoned earthen embankment dams that contain a central vertical mineral core, through a series of laboratory experiments. The processes controlling failure of each material zone were determined from the experiments. Based on these findings, a new method for parametric numerical modeling was developed. This new method is designed for the overtopping-induced failure of zoned embankment dams that contain a central vertical mineral core. The method was assessed by simulation of one of the laboratory experiments.

2. EXPERIMENTAL INVESTIGATION OF ZONED EMBANKMENT DAM FAILURE

The failure of zoned embankment dams was studied with a series of laboratory experiments. The laboratory experiments were designed based on a 20 m tall synthetic prototype-scale zoned embankment dam. Experiments were conducted using model dams that were downscaled versions of the synthetic prototype dam, with heights of 0.5 m. Each model dam contained a relatively impermeable central vertical core zone made from cohesive mineral material, and a supporting shell zone made from non-cohesive sand and gravel. Some model dams also contained a sand filter zone along the downstream side of the core zone. For each experiment, the model dam was breached by a flood that overtopped a low spot along the dam crest, leading to formation of a spatial embankment breach.

2.1. SYNTHETIC PROTOTYPE ZONED EMBANKMENT DAM

The synthetic prototype zoned embankment dam was designed to represent typical zoned earthen embankment dams in Switzerland. Three zoned earthen embankment dams in eastern Switzerland were used as the basis for the synthetic prototype zoned dam: Jonenbach Dam in Affoltern-am-Albis (height of 19.35 m), Aabachweiher Dam in Horgen (height of 14.5 m), and Hühnermatt Dam near Einsiedeln (height of 15 m). All three dams contain an earthen shell and a central vertical mineral core (Ingenieurbüro Kälin, 1986; Hochstrasser et al., 2008; Lombardi AG, 2008). Jonenbach Dam and Hühnermatt Dam also contain a sand filter zone located along the downstream side of the core (Hochstrasser et al., 2008; Lombardi AG, 2008). A particular focus was given to Jonenbach Dam, a cross section of which is shown in Figure 1.

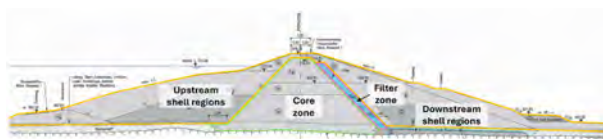


Fig. 1

Cross section of Jonenbach Dam. Adapted from Hochstrasser et al. (2008) and Halso (2024).

Coupe transversale du barrage de Jonenbach. Adapté de Hochstrasser et al. (2008) et Halso (2024).

For the synthetic prototype zoned embankment dam, a height of 20 m was selected (similar to that of Jonenbach Dam). It uses a trapezoidal profile with upstream and downstream face slopes of 2:1 [horizontal:vertical], with a streamwise crest length of 6 m and a streamwise base length of 86 m. The synthetic prototype zoned dam contains three zones: an earthen shell, a central vertical mineral core, and a filter along the downstream side of the core. The shell zone was made of 59% gravel and 41% coarser material including cobbles and boulders (mean grain size of 56 mm). The shell encompassed the majority of the dam volume. The core zone was made of 5% clay, 37% silt, 50% sand, and 8% gravel (mean grain size of 0.11 mm). The core was 18 m tall, with a base length of 20 m and a crest length of 8 m. The filter zone was made of 15% sand and 85% gravel (mean grain size of 5.0 mm). The filter was also 18 m tall, with a base length of 3.0 m and a crest length of 1.5 m. Additional details regarding zoning, materials, and dimensioning of the synthetic prototype zoned dam are given in Halso et al. (2023a) and Halso (2024).

2.2. MODEL ZONED EMBANKMENT DAMS

Model dams had trapezoidal profiles with face slopes of 2:1, and contained two or three zones. Dams that contained two zones had a central vertical mineral core and an earthen shell. Dams that contained three zones also included core and shell zones, as well as a filter along the downstream side of the core. Model dams were downscaled versions of the synthetic prototype dam, with heights of 0.5 m and with scaling according to Froude similarity. Most linear dimensions could be scaled according to the scale factor between model and prototype, which was $\lambda = 20/0.5 = 40$. Heights of the core and filter zones, streamwise lengths of the dam, and streamwise lengths of the filter zone were scaled based on these scale factors, and were therefore 40 times smaller than the corresponding prototype dimensions.

The streamwise lengths of the core zone (i.e. core thickness) in the model dams were scaled differently than the other linear dimensions of the dam. The core zone scaling was related to the expected failure process of the core, which was described by previous experimental investigations to be cantilever rotation due to the forces from

upstream water and sediment pressure. To scale the stability of the core against cantilever rotation, the streamwise length of the core had to be $\lambda^{1.5}$ times smaller than in prototype ($\lambda^{1.5} = 40^{1.5} = 256$). This made the model cores substantially thinner relative to other dimensions of the model dams. Additional details about the scaling process for the core zone are given in Halso et al. (2023b) and Halso (2024).

The sediment used to construct the model core zone was the same mixture of earthen materials as in the prototype core zone. But for the shell and filter zones, the sediment size was scaled. Sediment size was not scaled directly based on λ like most dimensions of the dam, but was instead scaled in relation to transport of the sediment by the overtopping flow. Scaling was based on the process of sediment deposition, to achieve similarity of sediment settling velocity. This resulted in a slight increase in shell and filter sediment size in comparison to scaling directly by λ . For model dams, the shell was a sand (61%) and gravel (39%) mixture (mean grain size of 1.78 mm), and the filter was exclusively sand (mean grain size of 0.36 mm). Additional details about the scaling process for the shell and filter sediments are given in Halso et al. (2023b) and Halso (2024).

2.3. EXPERIMENTATION

Experiments were carried out in a hydraulic flume at the Laboratory of Hydraulics, Hydrology and Glaciology (VAW) at ETH Zurich. Model dams were constructed that spanned the entire flume width, forming a reservoir behind them in the upstream portion of the flume. A pilot channel was cut through the middle of each model dam crest, with invert elevation at 90% of the model dam height (0.45 m). Experiments were conducted by filling the reservoir to 95% of the model dam height (0.475 m). The water level was held constant at this elevation for the entire experiment. Water flowed through the pilot channel, and began to erode the material of the dam. The erosion eventually led to the formation of a breach. The breach expanded until the sidewalls of the flume began to have an impact on the morphodynamic and hydrodynamic processes, at which point the experiments were ended.

3. FAILURE OF ZONED EMBANKMENT DAMS DUE TO OVERTOPPING

The experimental investigation showed that sustained overtopping of a zoned embankment dam can ultimately result in formation of a breach. The breach allows for uncontrolled release of impounded water, resulting in a rapid increase in discharge that can create a large flood wave. The experiments showed a unique failure process for each zone of the embankment dam. The breach process from an experimental zoned embankment dam failure due to overtopping is shown in Figure 2, in which the failure of each zone can be observed. The failure process of each zone is described in the following sections.

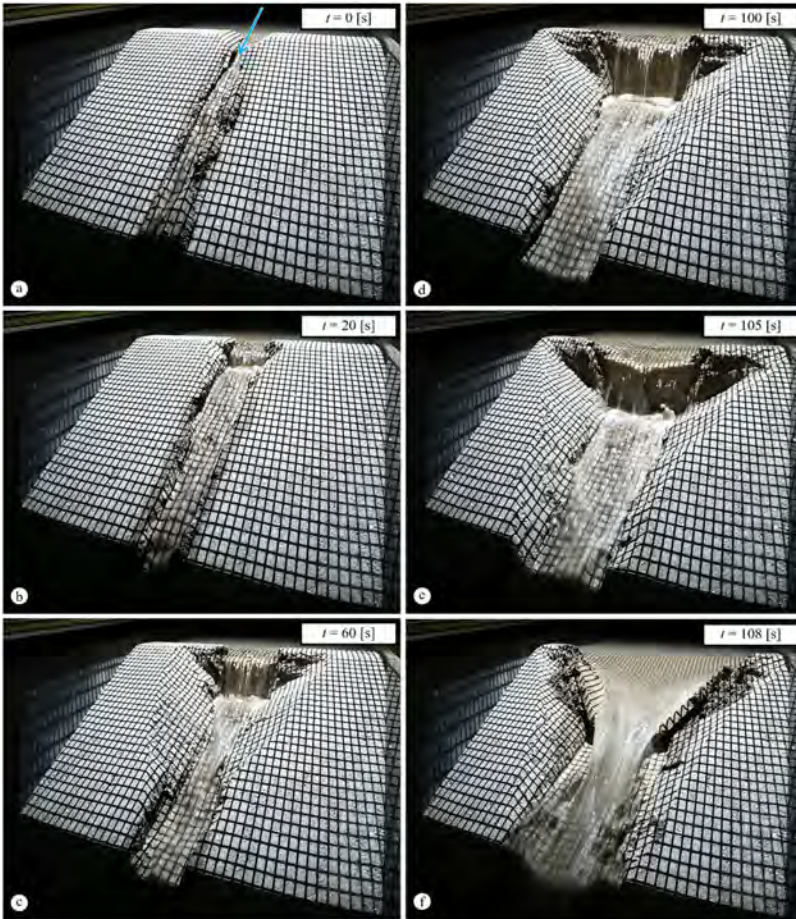


Fig. 2

Experimental zoned embankment dam failure due to overtopping. Adapted from Halso (2024).

*Rupture d'un barrage en remblai zoné expérimental en raison d'un débordement.
Adapté de Halso (2024).*

3.1. FAILURE OF SHELL ZONE

Failure of the zoned embankment dams began in the shell zone. The overtopping water passed through the pilot channel and flowed along the downstream

face of the dam. As it flowed through the pilot channel and along the downstream face, shell zone material was eroded. The erosion created a small channel through the shell zone (Figure 2a). At the dam crest, the erosion caused the channel to widen enough to eventually engulf the pilot channel, but the breach channel only deepened to the crest of the core zone. Downstream of the dam crest, the breach channel deepened due to continuous erosion by the overtopping flow, and initially maintained a rectangular shape (Figure 2b). As the channel deepened, the channel sidewalls became too tall and steep for the shell material to remain stable. Sections of the sidewalls began to experience mass slope failures, in which sidewall material slid into the breach channel and was carried away by the overtopping flow. These mass slope failures caused the top of the breach channel to widen, and the channel cross section transitioned into a trapezoidal shape (Figure 2c). The breach channel in this region deepened well beyond the elevation of the core crest. The breach channel effectively had two sections: at the dam crest (above the core), and in the downstream dam region (downstream of the core). The bottom of the breach channel in these two sections had similar widths.

3.2. FAILURE OF FILTER ZONE

The overtopping flow also eroded material from the filter zone, allowing the breach channel to grow through the filter zone. The channel sidewalls became tall and steep (Figure 2c), and like in the shell zone, the filter zone experienced mass slope failures that widened the breach. But the filter material was more stable against slope failures than the shell material, and thus the rate of breach channel top width widening was slower and the side slopes after each failure were steeper. The breach channel cross section transitioned into a trapezoidal shape, but with steeper side slopes than in the shell zone (Figure 2d).

3.3. FAILURE OF CORE ZONE

Unlike the shell and filter zone materials, which were progressively eroded by the overtopping flow, the core zone material was not substantially eroded. As the breach channel expanded through the shell and filter zones, the core was unaffected. The core acted as a single cohesive structure, that stayed intact while the breach channel grew around it. But one purpose of the shell zone is to provide structural support to the core, and as the breach channel downstream of the core grew, the core became increasingly unsupported against the forces from water pressure and sediment pressure. These forces pushed on the core from upstream, and with reduced support from downstream material, the core began to move in the downstream direction. The core deformation was fastest at the center of the breach channel, where it was least supported, and slowest outside of the breach channel,

where its support was unchanged. This differential movement caused the core to bend. A vertical crack formed in the middle of the core, and the core eventually split along the crack into two separate parts (Figure 2e). Each part then broke near the lateral extents of the breach channel, and large pieces of core detached, forming a large breach (Figure 2f).

4. PARAMETRIC NUMERICAL MODELING OF ZONED DAM FAILURE

Based on findings and observations from the experimental investigation, a method for parametric numerical modeling of zoned embankment dam failure has been developed. The method is designed for the overtopping-induced failure of a dam that contains a central vertical cohesive mineral core zone, surrounded by granular shell and filter zones. The method represents the failure process with three distinct sections:

- Section A: the breach channel through the dam crest (above the core, i.e. shell zone).
- Section B: the breach channel through the downstream portion of the dam (downstream of the core, i.e. filter and shell zones).
- Section C: the core zone.

The sections are shown in Figure 3. The methods for simulation of each section are described in the following sections. Additional details about the methods, detailed equations, and force and moment diagrams are given in Halso et al. (2024) and Halso (2024).

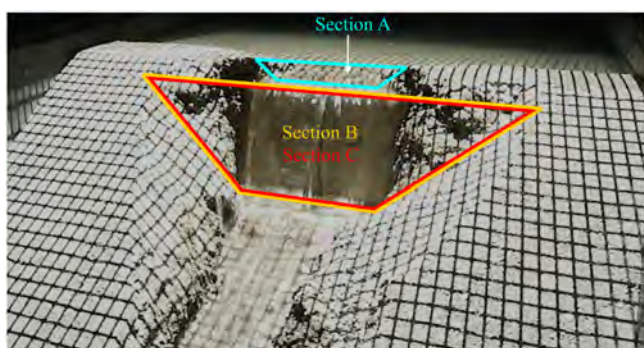


Fig. 3

Sections for simulation of zoned embankment dam failure using parametric numerical model. Adapted from Halso et al. (2024) and Halso (2024).
Sections pour la simulation de la rupture d'un barrage en remblai zoné à l'aide d'un modèle numérique paramétrique. Adapté de Halso et al. (2024) et Halso (2024).

4.1. SIMULATION OF BREACH CHANNEL THROUGH THE DAM CREST (SECTION A)

Section A (above the core zone) can encompass multiple zones of erodible granular material (including a shell zone and a filter zone). The breach channel through the dam crest is simulated using the method for homogeneous embankment dam breaching of Macchione (2008). The breach channel begins with a triangular shape (Figure 4a) that can represent an initial low or weak point along the dam crest (or in the case of the laboratory experiments, the pilot channel). If the reservoir water level is above the bottom of the breach channel, water flows through the channel and begins to erode the channel. The channel maintains a triangular shape as it deepens, until the bottom of the channel reaches the elevation of the core crest (Figure 4b). The rate of erosion depends on a calibration parameter referred to as the *characteristic velocity*. This parameter, which dictates the breach growth rate, is related to the size of the dam and material type of the embankment (Macchione, 2008; Knüsel, 2023).

Once the breach channel bottom reaches the top of the core, the channel can no longer deepen, and the channel transitions to a trapezoidal shape. Further erosion by the overtopping flow causes the breach channel to widen as a trapezoid (Figure 4c). But the erosive force acting on the bottom of the trapezoidal breach channel is considered to act on the top of the core zone, which is negligibly eroded compared to the shell and filter zone erosion. Therefore, that erosive force is not considered to affect the breach growth. The breach channel widening is driven only by the erosive force acting on the sides of the breach channel. Breach discharge is simulated based on the flow through this breach channel using the method of Macchione (2008), by assuming critical flow conditions and using weir discharge equations.

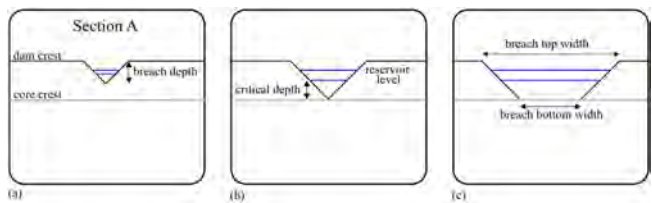


Fig. 4

Schematic representation of Section A breach channel with (a) initial triangular breach channel, (b) maximum extents of triangular breach channel due to presence of core, and (c) trapezoidal breach channel. Adapted from Halso et al. (2024) and Halso (2024).

Représentation schématique de la brèche de la section A avec (a) canal de brèche triangulaire initial, (b) extensions maximales du canal de brèche triangulaire en raison de la présence du noyau, et (c) canal de brèche trapézoïdal. Adapté de Halso et al. (2024) et Halso (2024).

4.2. SIMULATION OF DOWNSTREAM BREACH CHANNEL (SECTION B)

Section B can also encompass multiple zones of erodible granular material. The breach channel downstream of the core is simulated based on the breach channel through the dam crest. When the Section A breach channel is a triangle, the Section B breach channel is assumed to have the same size and shape as the Section A breach channel (Figure 5a). When the Section A breach channel transitions to a trapezoidal shape, the Section B breach channel does as well (Figure 5b). From that point, the widening of the Section B breach channel is simulated by setting the bottom width of the trapezoidal breach channel equal to that of Section A. The same channel side slopes are used as well. The selection of the *characteristic velocity* parameter thus also dictates the breach growth rate in Section B.

Deepening of the breach channel is simulated based on the remaining erosive potential of the overtopping flow. Since the bottom of the Section B breach channel is in the shell and filter zones, the erosive capacity of that flow can be applied to breach growth, unlike in Section A. The total transport capacity of the overtopping flow in Section B is calculated, and the amount not consumed by widening of the breach channel is then applied to deepening of the channel. The trapezoidal Section B breach channel maintains a similar bottom width and side slopes as in Section A, but can have a larger depth (Figure 5c).

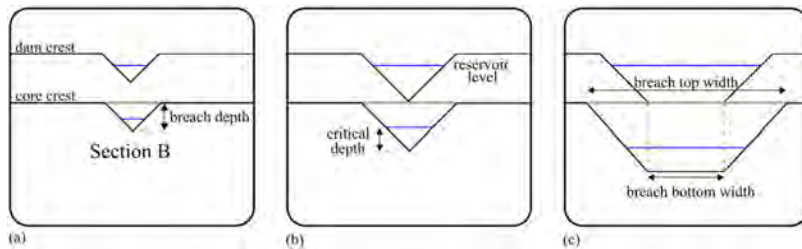


Fig. 5

Schematic representation of Section B breach channel with (a) initial triangular breach channel, (b) maximum extent of triangular breach channel, and (c) trapezoidal breach channel. Adapted from Halso et al. (2024) and Halso (2024).
 Représentation schématique de la brèche du canal de la section B avec (a) canal de brèche triangulaire initial, (b) extensions maximales du canal de brèche triangulaire, et (c) canal de brèche trapézoïdal. Adapté de Halso et al. (2024) et Halso (2024).

4.3. SIMULATION OF CORE FAILURE (SECTION C)

The stability of the core zone is simulated based on two processes: (1) cracking and separation of the core into two separate parts due to core bending around a virtual vertical axis, and (2) breaking and detachment of the separated parts. These processes are driven by the upstream distributed forces from water pressure and sediment pressure.

Bending of the core occurs when sufficient downstream shell and filter material has been eroded to allow the core to be pushed downstream by the forces from water pressure and sediment pressure. The unsupported core region is based on the size of the Section B breach channel in either triangular (Figure 6a) or trapezoidal form (Figure 6b). The extents of the unsupported core region are referred to as the *core exposure*. The *core exposure depth* h_E is the depth of the Section B breach channel. The *core exposure width* b_E is the width of the Section B breach channel at a depth of $2h_E/3$ below the core crest, which is the depth at which the upstream forces are considered to act.

As the Section B breach channel grows, the bending of the core increases. The bending causes a bending moment within the core, which increases as the core becomes more bent. The bending moment causes a tensile stress within the core. The maximum tensile stress is calculated based on the maximum bending moment (which acts at the transverse center of the core), as well as the core thickness and shape. When the maximum tensile stress $\sigma_{t,max}$ becomes greater than the ultimate tensile strength $\sigma_{t,u}$ of the core (an inherent material parameter of the core zone), cracking and splitting of the core at the center is simulated (depicted by red vertical line in Figure 6b). The ultimate tensile strength of the core may be unknown for a given dam, and it can be related to core compaction, water content, cohesion, and other factors. In this parametric modeling method, ultimate tensile strength may be used as a calibration parameter for simulation of core failure (Halso, 2024).

After the core has cracked and split, the core is assumed to be two individual parts, separated in the center. Each core part is acted on by the upstream forces from water pressure and soil pressure, which act together as a distributed force. As the Section B breach channel grows, the length of the distributed forces grows, and thus the net force increases. Considering each core part as a cantilever beam, the cantilever arm increases as the Section B breach channel grows. This increases the cantilever momentum load, which is based on the magnitude of distributed forces times the cantilever arm length. When the momentum load M_L becomes greater than the momentum resistance M_R of the core (which is based on the core tensile strength, as well as the core thickness and shape), detachment of the core pieces at the lateral extents of the Section B breach channel is simulated (Figure 6c). A large breach has thus formed, and a rapid increase in breach discharge is calculated.

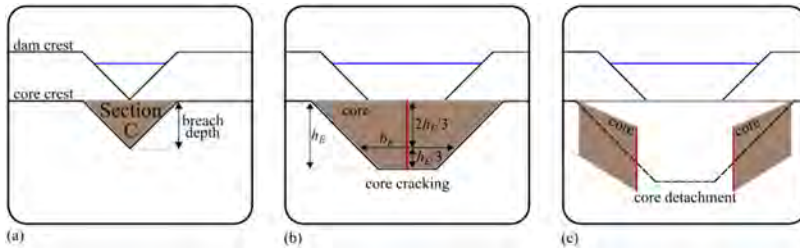


Fig. 6

Schematic representation of simulated core stability (Section C) with (a) exposure of core while downstream breach channel is triangular, (b) exposure of core while downstream breach channel is trapezoidal and core cracking/splitting due to bending, and (c) core breaking/detachment due to cantilever rotation. Adapted from Halso et al. (2024) and Halso (2024).

Représentation schématique de la stabilité simulée du noyau (Section C) avec (a) exposition du noyau tandis que le canal de brèche en aval est triangulaire, (b) exposition du noyau tandis que le canal de brèche en aval est trapézoïdal et fissuration/déformation du noyau en raison de la flexion, et (c) rupture/détachement du noyau en raison de la rotation en porte-à-faux. Adapté de Halso et al. (2024) et Halso (2024).

5. APPLICATION OF PARAMETRIC METHOD

The method for parametric numerical modeling is assessed by simulation of a laboratory experiment that used a 0.5 m tall model dam containing a shell zone and a core zone. The geometry of the model dam was applied, with a trapezoidal embankment with slopes of 2:1, streamwise crest length of 0.15 m, and streamwise base length of 2.15 m. The geometry of the model core was also applied, with a core height of 0.45 m, streamwise crest length of 0.032 m, and streamwise base length of 0.079 m. The initial triangular breach channel in Section A was set equal to the pilot channel.

The model dam was simulated by applying a constant reservoir water level of 0.475 m, which was maintained for the entirety of the simulation. The simulation began with overtopping water flowing through the breach channels. The breach discharge Q_b was calculated as the overtopping water flowing through the breach channels, and breach channel growth was calculated based on the erosion due to the overtopping flow. The *characteristic velocity* calibration parameter was calibrated to best match the rate of increasing core exposure (b_E and h_E), and the ultimate tensile strength calibration parameter was calibrated to match the timing of core failure. After core failure due to both bending ($\sigma_{t,max} > \sigma_{t,u}$) and cantilever rotation ($M_L > M_R$) was simulated, a final breach discharge $Q_{b,f}$ was calculated as an estimate of flow through the newly enlarged breach. After the calculation of $Q_{b,f}$, the simulation was ended.

Figure 7 shows the results of the simulation compared to results of the laboratory experiment. Figures 7a and 7b show that application of the parametric method to breaching of the model dam could successfully simulate the temporal growth of core exposure. Figure 7c shows that the breach discharge prior to core failure ($t < 64$ s), was similarly low to that of the laboratory experiment. Figure 8 shows the core stability against both bending and cantilever rotation. The first core failure process (cracking due to bending) occurs at $t = 63$ s. The second process (cantilever rotation) would already have been possible beginning at $t = 39$ s, but because cracking had not yet occurred and the core was thus not acting as a cantilever, cantilever rotation could not occur until $t = 63$ s (immediately following cracking). Core failure was thus simulated at $t = 63$ s, whereas core failure occurred in the laboratory experiment at $t = 64$ s. The model therefore was successfully calibrated to simulate the timing of core failure. After core failure, the breach discharge increased rapidly in the laboratory experiment, but at a rate of increase that is slower than that represented by the simulation of $Q_{b,f}$.

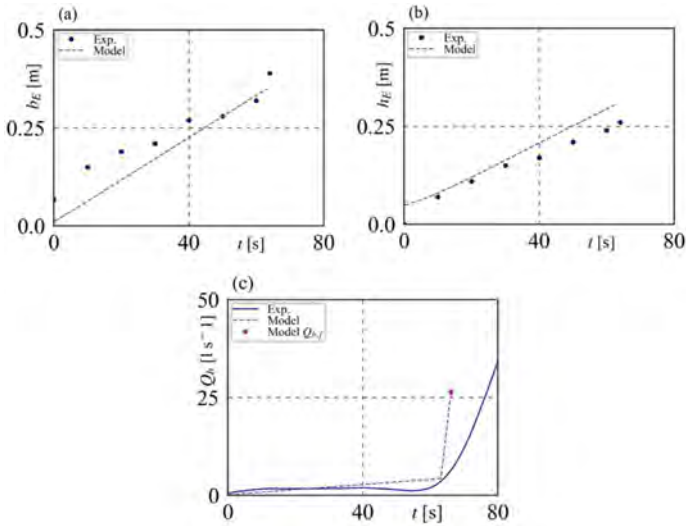


Fig. 7

Results from simulation of 0.5 m tall model zoned embankment dam (*Model*) compared to laboratory experiment (*Exp.*), with (a) core exposure width b_E , (b) core exposure depth h_E , and (c) breach discharge Q_b including estimate of final breach discharge $Q_{b,f}$. Adapted from Halsø (2024).

Résultats de la simulation d'un modèle de barrage en remblai zoné de 0,5 m de hauteur (Modèle) comparés à l'expérience en laboratoire (Exp.), avec (a) la largeur d'exposition du noyau b_E , (b) la profondeur d'exposition du noyau h_E , et (c) le débit de la brèche Q_b , incluant une estimation du débit final de la brèche $Q_{b,f}$. Adapté de Halsø (2024).

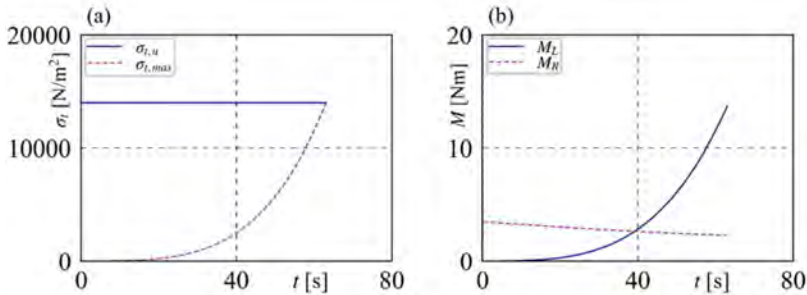


Fig. 8

Results from simulation of core stability in 0.5 m tall model zoned embankment dam, with (a) stability from ultimate tensile strength $\sigma_{t,u}$ against maximum tensile stress $\sigma_{t,max}$ due to bending, and (b) stability from momentum resistance M_R against cantilever rotation due to momentum load M_L . Adapted from Halso (2024).

Résultats de la simulation de la stabilité du noyau d'un barrage en remblai zonné de 0,5 m de haut, avec (a) stabilité de la résistance ultime à la traction $\sigma_{t,u}$ contre la contrainte de traction maximale $\sigma_{t,max}$ due à la flexion, et (b) stabilité de la résistance au moment M_R contre la rotation du porte-à-faux due à la charge du moment M_L .

Adapté de Halso (2024).

6. CONCLUSIONS

This study used laboratory breach experiments to assess the failure of zoned embankment dams due to overtopping. These experiments provide crucial knowledge regarding the failure process of each zone, the rate of breach channel growth, and the mechanisms controlling core failure. Based on these findings, a parametric method for zoned embankment dam failure was developed. The parametric model to simulate breaching of a model dam was successfully calibrated in terms of simulating the growth of the breach channel and the timing of core failure. This method can be a useful tool for dam engineers and practitioners for assessing the risk associated with a specific zoned embankment dam. The method is planned for implementation in BASEbreach, a framework for estimation of breach outflow hydrographs due to failure of embankment dams (Vetsch et al., 2023).

REFERENCES

- [1] BORNSCHIEIN, A. (2014). Breschenentwicklung bei Dämmen mit Dichtungen [Breach development for dams with seals]. *Wasserbauliche Mitteilungen* 50: 303–312, IWD, TU Dresden, Germany (in German).

- [2] FLETCHER, B.P., & GILBERT, P.A. (1992). Center Hill Fuseplug Spillway, Caney Fork River, Tennessee: Hydraulic Model Investigation. Report 92-15, U.S. Army Engineer Waterways Experiment Station.
- [3] FRANCA, M.J.A., A. B. (2002). Experimental tests on rockfill dam breaching process. *IAHR-Int. Symp. on Hydraulic and Hydrological Aspects of Reliability and Safety Assessment of Hydraulic Structures*, St. Petersburg, Russia, 29–31.
- [4] HALSO, M.C. (2024). Spatial breaching of homogeneous and zoned embankment dams. *Doctoral Thesis and VAW Mitteilung 277* (R. Boes, ed.), VAW, ETH Zurich, Switzerland.
- [5] HALSO, M.C., EVERS, F.M., VETSCH, D.F., & BOES, R.M. (2023a). Experimental investigation of the overtopping failure of a zoned embankment dam. *Proc. 12th ICOLD European Club Symposium*, (R. Boes, P. Droz, and L. Raphaël, ed.), Interlaken, Switzerland, September 5-8, 2023, 768-777.
- [6] HALSO, M.C., EVERS, F.M., VETSCH, D.F., & BOES, R.M. (2023b). Material Scaling for Laboratory Experiments of Zoned Dam Breaching due to Overtopping. *Proc. 40th IAHR World Congress*, (H. Habersack, M. Tritthart, and L. Waldenberger, ed.), Vienna, Austria, August 21-25, 2023, 2513-2522.
- [7] HALSO, M.C., VETSCH, D.F., EVERS, F.M., & BOES, R.M. (2024). A simplified method for simulation of the overtopping failure of zoned earthen dams and dikes. *Proc. 12th International Symposium on Fluvial Hydraulics*, Liverpool, UK, September 2-6, 2024.
- [8] HOCHSTRASSER, H., AEMMER, M., & SORGENFREI, A. (2008). Hochwasserrückhaltebecken am Jonenbach, Affoltern am Albis ('Flood retention basin on the Jonenbach River, Affoltern am Albis'). *Wasser Energie Luft*(4), 281–288 (in German).
- [9] INGENIEURBÜRO KÄLIN. (1986). Sicherheitsüberprüfung Stauanlage Aabach ('Safety Inspection Aabachweiher Dam'). Report (in German).
- [10] KNÜSEL, C.L. (2023). Overtopping Dam Breach: Computational Modeling and Laboratory Experiments. *Master Thesis*, VAW, ETH Zurich, Switzerland.
- [11] LOMBARDI AG. (2008). Staudamm Hühnermatt- Erhöhung der Hochwassersicherheit. Report (in German).
- [12] MACCHIONE, F. (2008). Model for predicting floods due to earthen dam breaching. I: Formulation and evaluation. *Journal of Hydraulic Engineering*, 134(12), 1688–1696.

- [13] MORRIS, M.W., HASSAN, M.A.A.M., & VASKINN, K.A. (2007). Breach formation: Field test and laboratory experiments. *Journal of Hydraulic Research*, 45(sup1), 9–17.
- [14] PUGH, C.A. (1985). Hydraulic model studies of fuse plug embankments. Report REC-ERC-85-7, Bureau of Reclamation, US Department of the Interior, Denver.
- [15] RÜDISSE, B. (2017). Einfluss der Kornverteilung des Schüttmaterials und einer Oberflächendichtung auf die Breschenentwicklung und die Abflusskurve beim Versagen eines Schüttdammes durch Überströmen ('Effect of Shell Grain-Size Distribution and the Facing Element on Breach-Processing and Discharge Curve by Embankment Dam Failure due to Overtopping'). *Doctoral Thesis* Technical University of Vienna, Vienna, Austria (in German).
- [16] SADEGHI, S., HAKIMZADEH, H., & AMINI, A.B. (2020). Experimental Investigation into Outflow Hydrographs of Nonhomogeneous Earth Dam Breaching due to Overtopping. *Journal of Hydraulic Engineering*, 146(1), 04019049.
- [17] SCHMOCKER, L., HÖCK, E., MAYOR, P.A., & WEITBRECHT, V. (2013). Hydraulic Model Study of the Fuse Plug Spillway at Hagneck Canal, Switzerland. *Journal of Hydraulic Engineering*, 139(8), 894–904.
- [18] SIMMLER, H., & L. SAMET. (1982). Dam failure from overtopping studied on a hydraulic model. *14th Int. Congress on Large Dams*, Rio de Janeiro, Brazil, V1, 427.
- [19] VASKINN, K.A., LØVOLL, A., HÖEG, K., MORRIS, M., HANSON, G., & HASSAN, M. (2004). Physical modeling of breach formation: Large scale field tests. *Association of State Dam Safety Officials*, Phoenix, USA, 1-16.
- [20] VETSCH, D.F., HALSO, M.C., SEIDELMANN, L., & BOES, R.M. (2023). Software tool for progressive dam breach outflow estimation. *Proc. 12th ICOLD European Club Symposium*, (R. Boes, P. Droz, and L. Raphaël, ed.), Interlaken, Switzerland, September 5-8, 2023, 981-988.
- [21] WU, W. (2013). Simplified Physically Based Model of Earthen Embankment Breaching. *Journal of Hydraulic Engineering*, 139(8), 837–851.
- [22] ZHONG, Q., CHEN, S., & DENG, Z. (2018). A simplified physically-based model for core dam overtopping breach. *Engineering Failure Analysis*, 90, 141–155.

COMMISSION INTERNATIONALE DES
GRANDS BARRAGES

VINGT-HUITIEME CONGRES DES
GRANDS BARRAGES
CHENGDU, MAI 2025

**NEW PROGRESS OF CEMENTED MATERIAL DAMS TO MEET THE
REQUIREMENTS ON DAM SAFETY TO RESIST OVERTOPPING IN CHINA (*)**

Jinsheng JIA

State Key Laboratory of Simulation and Regulation of Water Cycle in River Basin,

²China Institute of Water Resources and Hydropower Research, Beijing

Cuiying ZHENG & Aili LI

China Institute of Water Resources and Hydropower Research, Beijing

CHINA

SUMMARY

Embankment dam failures occur almost every year since the frequency and intensity of extreme weather events have increased significantly due to climate change. New requirements, including innovation in technology, are proposed. Cemented material dam (CMD), cementing local material to build a dam, is an innovated technology and has a great application potential because of its high resistance to overtopping floods, high adaptation to different geological conditions, low cost, and small disturbance to the environment. This paper mainly expounds on the Structural Performance Optimization Design Theory of CMD and its applications. A downstream protection structure for a embankment dam is proposed. The lab test indicated that after overtopping for 44 hours at the maximum flow velocity of 5m/s, the protected dam is safe. The experimental result indicates that this reinforcement method is an effective way to enhance the capacity of resisting overtopping failure for small and medium dams.

**Nouveaux progrès des barrages en matériaux cimentés pour répondre aux exigences pour la sûreté des barrages en cas de surverse en Chine*

RÉSUMÉ

Les ruptures de barrages en remblai se produisent presque chaque année depuis que la fréquence et l'intensité des événements météorologiques extrêmes ont considérablement augmenté en raison du changement climatique. De nouvelles exigences, y compris l'innovation technologique, sont proposées. Le barrage en matériaux cimentés (CMD), qui cimente des matériaux locaux pour construire un barrage, est une technologie innovante. Cette technologie a un grand potentiel d'application en raison de la grande résistance aux débordements, de sa grande adaptation aux différentes conditions géologiques, de son faible coût et de sa faible perturbation de l'environnement. Ce rapport expose principalement la théorie de la conception de l'optimisation des performances structurelles des CMD et ses applications. Un ouvrage de protection en aval pour un barrage en remblai est proposé. Le test en laboratoire a indiqué qu'après un débordement pendant 44 heures à la vitesse d'écoulement maximale de 5 m/s, le barrage protégé est sûr. Le résultat expérimental indique que cette méthode de renforcement est un moyen efficace d'améliorer la capacité de résistance à la rupture par débordement sur la crête pour les petits et moyens barrages.

1. INTRODUCTION

The embankment dam has the advantages of using local materials, simple structure, easy construction, and high adaptability to the foundation, which is the oldest and most widely used type of dam. By the end of 2023, there were more than 97, 000 dams in China, of which the embankment dams account for over 90%. The embankment dam have a low ability to resist overtopping floods and will collapse rapidly once dam failure, which will have a critical impact to downstream area. In recent years, embankment dam failures occur every year in the world since the frequency and intensity of extreme weather events have increased significantly. In 2021, Yong'an embankment dam (14.5m high) failed due to overtopping, causing the failure of Xinfu earth dam (10.6m high, storage capacity of 38hm³). The Chinese government has put forward the requirements on improving the ability of reservoir dams, especially embankment dams, to resist overtopping.

According to statistics of dam failure by ICOLD, more than 80% of embankment dam failures are caused by overtopping and internal erosion (Fig. 1). Soil particles of embankment are easily washed away under the action of infiltration or overtopping flow, which leads to the instability. If cementitious materials are added to local materials to cement soil particles and form a new material between embankment materials and concrete, it would have certain resistance to overtopping and internal erosion and increase the safety of a dam built with local material.

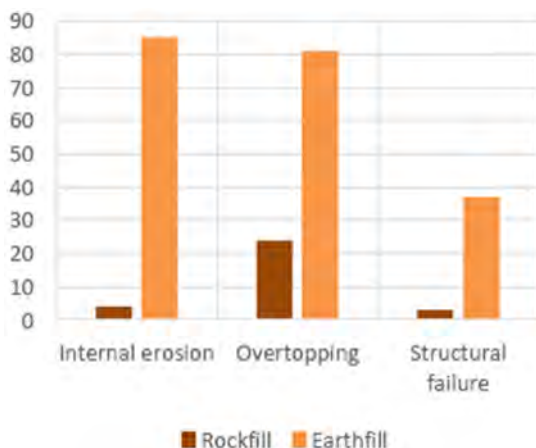


Fig. 1
Failure Mode of Embankment Dams

Based on years of practices of hardfill dams proposed by Londe and Lino[1][2][3], trapezoidal Cemented sand and gravels (CSG) dams in Japan[4], Cemented sand, gravels and rocks (CSGR) dams and Rockfill Concrete (RFC) dams in China, Jia proposed a new type of dam, Cemented Material Dam (CMD) in 2009 and subsequently published a paper on the topic in 2012[5][6]. The International Committee on Large Dams (ICOLD) formed a technical committee dedicated to CMD in 2013[7]. CMD is a new dam type besides the embankment dam and the concrete dam, which is built with cemented local materials and based on a new concept of optimizing the structural performance of dams [8]. Cement, fly ash and other additives are used to cement soil, sand, rock, and other local materials together to form dam materials with certain strengths and shear resistance. According to the particle diameter of raw materials, CMD can be divided into cemented soil dam (CSD), Cemented sand, gravels and rocks dam (CSGRD, the maximum diameter of the aggregates is 150 mm. For cofferdams the largest diameter is 300 mm), and CRD (Cemented rock dam, the maximum diameter of aggregate is over 300 mm).

Design of CMD follows two principles. One is to optimize the dam structure to make better use of local materials and the second is to select proper materials for different parts of the dam to realize better performance of structures. In this way, balanced safety redundancy can be achieved and strength redundancy can be avoided for CMD. Now, at more than 100 projects all over the world, among which 40 projects in China, CMDs have shown significant advantages in terms of high resistance against overtopping, high adaptability to geological terrain and low requirements for raw materials and construction, use of environmental waste, benefits for the environmental protection, high construction efficiency.

Based on previous studies, this paper illustrates the optimizing structural function design for CMD and introduces the new practices. A new reinforcement structure for the existing embankment dams is proposed, and experimental research is carried out to validate the capacity of the method.

2. STRUCTURE PERFORMANCE OPTIMIZATION DESIGN THEORY [8]

Overtopping occurs more frequently at small dams. Considering the unacceptable consequences of dam failure, it is not only the safety under the design load cases that needs to be considered, but also the intrinsic safety even under unusual loading cases, such as overtopping.

The traditional structural optimization of a dam can be stated as follows:

$$\begin{array}{ll} \text{Find:} & X = \{x_1, x_2, \dots, x_n\}^T \\ \text{Minimize:} & V(X) \\ \text{Subject to:} & H_i(X) \geq 0, i = 1, 2, \dots, n \\ & G_j(X) \geq 0, j = 1, 2, \dots, k \end{array}$$

where X , V and H_i , G_j , are design variables, the objective function and the constraints, respectively. Generally, in the structural optimization of dams, the volume of the dam body is considered as an objective function.

When dam is lower than 50m, the stress level is very low, especially in internal region of a dam body, and the stability safety margin is very large. The shape of a dam is usually determined according to construction or operation requirements, which may not be the minimum volume obtained according to the optimization. While when dam height reaches 200m or 300m, water load acting on the dam increases significantly, 4 or 9 times compared with that of a 100-meter-high dam which may lead to different destroy mode, such as hydraulic fracture, but the materials used are not much different from those used for a dam with height of 100m. When dam shape is determined according to optimization, safety margin is much lower for a high dam than a lower dam. In addition, the constraints are given under design conditions, which means that a dam adapted the optimized shape will be safe under design load cases. Structural optimization method for dam design is needed to be improved to achieve better performance, as well as technically feasible and economically reasonable, for a dam under different load cases, including both designed working conditions and off-design working conditions, such as overtopping.

Based on the above conclusions, structural performance optimization design was proposed. The minimum volume of dam body as well as dam safety within a

certain range during its life span need to be taken as the objective functions. More constrains, based on new computing models and design criteria, taking into account of overtopping, hydraulic fracture factor, ageing of materials, long-term behavior of dam structures and etc., need to be included. In addition, by adjusting material and structure of different zones, uniform distribution of safety degree of all region in dam body can be achieved so that to keep the dam structure performance in optimum state all along its life span. That will also solve the problem that for a dam according to traditional optimization theory, strength of material for most region of a dam is more affluent than required while safety factor of some regions is insufficient. The function optimization is stated as follows

$$\begin{array}{ll}
 \text{Find:} & X = \{x_1, x_2, \dots, x_n\}^T \\
 \text{Keep:} & F_{\text{safety}}(X, t) \in \{K_L, K_R\} \text{ and Minimize } V(X) \\
 \text{Subject to:} & H_{\text{con}_i}(X, t) \geq 0, i = 1, 2, \dots, n \\
 & H_{\text{con}_j}(X, t) \geq 0, j = 1, 2, \dots, m \\
 & G_l(X, t) \geq 0, l = 1, 2, \dots, k
 \end{array}$$

where X is design variables, F (dam safety) and V (volume of dam body) are the objective functions, in which F changes over time and is expected to be within a certain range during the life span, and H and G are constraints, in which new constraints are added to include new factors and effects of changes in material properties and structures.

The design method of CMD is based on the structural performance optimization theory. Appropriate materials are used to meet the requirement of different structural parts of the dam, leading to the reduction of serious strength redundancy of concrete in most part of a concrete gravity dam. The shape design of a CMD is based on the optimization of dam structure to make better use of local materials and selection of proper materials for different parts of the dam to realize better performance of structures. A symmetrical or trapezoidal dam shape is not always necessary. Materials with good performance, such as enriched CSGR or concrete, may be used as protection layer for a CMD. Through the above, materials inside a CMD body is normally kept dry and in compression for all loading cases, including earthquake and overtopping cases.

3. APPLICATION PROGRESS OF CMD

3.1. CMD PROJECTS IN CHINA

CMD is environmental and economic friendly with high safety and reliability. It has been promoted by the Ministry of Water Resources, P. R. China and the technical guidelines have been issued by the Ministry. At present, there are more than

40 projects applied in China and it has a great application potential. The typical applications in China are listed in Table 1.

Table 1
Cemented Material dams in China

S/ N	PROJECT NAME	PROVINCES	DAM HEIGHT (M)	DAM CREST LENGTH (M)	SLOPE RATIO		DAM BODY VOLUME (10,000 M ³)	YEAR OF COMPLETION
					UPSTREAM	DOWNSTREAM		
1	Shunjiangyan	Sichuan	11.6	360	Vertical	1:0.7	1.7	2016
2	Shoukoubu	Shanxi	61.4	366	1:0.6	1:0.6	44.0	2020
3	Liangganshan	Guizhou	20.3	150	1:0.3	1:0.5	1.8	2018
4	Jinjigou	Sichuan	33	72	1:0.35	1:0.75	2.7	2019
5	Qianwei Dyke	Sichuan	14.1	2775	1:0.6	1:0.6	38.0	2019
6	Xijiang	Guizhou	48.5	198.5	1:0.6	1:0.6	17.0	2021
7	Lengshuihe	Sichuan	39.5	110	1:0.3	1:0.75	5.5	2022
8	Xiying	Fujian	52	395	1:0.4	1:0.7	23.4	Under construction
9	Dongyang	Sichuan	68	135	1:0.4	1:0.7	13.8	Under construction
10	Heibaoshan	Sichuan	54	173	1:0.6	1:0.6	10	Under construction
11	Shanxi	Henan	56	210	1:0.6	1:0.6	23.03	Under construction
12	Tielekt	Xinjiang	88	220	1:0.5	1:0.7	56.4	Under design
13	Mobao Mountain	Sichuan	54	173	1:0.6	1:0.6	10.0	Under design

3.2. CMD IN GUIZHOU

Xijiang project is located in Leishan County, Guizhou Province in the southwest of China, with a total storage capacity of 4.47 million m³. The main purpose of the project is urban water supply, farmland irrigation and flood control. After the completion of Xijiang project, it can supply 1.63 million m³ of urban water and 1.33 million m³ of irrigation water every year, and raise the flood control standard of Xijiang Town. Xijiang CMD has a maximum dam height of 48.5 m, dam axis length of 198.5 m and a dam crest width of 6m. The anti-seepage slab of upstream face is made of 0.4 m thick C20 reinforced concrete, and the thickened rich CSGR is adopted between the slab and the dam body. The downstream face is made of 0.5 m thick rich CSGR.

The aggregate used were excavated in the riverbed of the project site or the base of access road, as shown in Fig. 2. According to strength tests, the materials

were divided into Material A, Material B and Material C. The compressive strength above 15MPa (below the weakly weathered top) is Material A, the compressive strength between 5 and 10MPa (the middle and upper part of strongly weathered) is Material C, and the compressive strength of rock between 10 and 15MPa (the lower part of strongly weathered) is Material B.

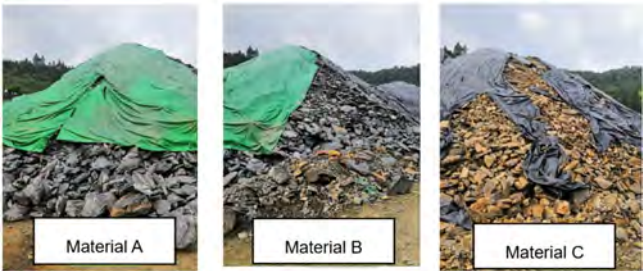


Fig. 2
Excavated rock from Xijiang Dam Site

To make full use of excavated materials, the mix ratio test and rolling test were carried out. The recommended mix ratio scheme is shown in Table 2, and the CSGR material with strength C₁₈₀8 is configured. Considering the rolling quality and safety, Material A was used as aggregate of lower part of the dam. Material C was used in the upper part of the dam, 5 meters from the dam top. On-site construction was carried out by the construction technology of XG626H single steel wheel vibration rolling, and high frequency rolling was adopted, with static rolling 2 times + vibration rolling 8 times. When the paving time exceeded the allowable paving time, cushion mortar was added before paving with the mortar thickness of 10~15mm. When the allowable time of cushion paving was exceeded and formed a cold joint, the layer was required to be flushed by high-pressure water, and then 10~15mm thick cushion mortar should be laid.

Table 2

MIX RATIO NO.	QUANTITY OF MATERIAL USED (KG/M ³)							
	WATER	CEMENT	FLY ASH	MATERIAL A1	MATERIAL A2	MATERIAL B1	MATERIAL C2	SAND A2
1	120	60	60	1561	0	0	0	669
2	115	65	65	0	713	0	1025	398
3	115	60	60	0	0	1516	0	673

Remarks: Material A1 is excavated material A of access road, Material A2 is excavated material A of foundation pit excavation, Material B1 is excavated material B of access road, Material C2 is excavated material C of foundation pit excavation, and Sand A2 is machine-made sand of Foundation Pit Excavation Material A.

The Xijiang CMD Project, built with weathered aggregate, greatly reduced environmental affects and saving project investment. Meantime, it further broadened the application scope of construction materials of CMD, achieving a breakthrough in the application of weathered materials in CMD. During the construction, the dam body went through a flood over dam on June 23, 2024. As shown in Fig. 3, the flood overtopping the dam lasted 48 hours, and the highest water head was 2m. The dam body was safe under the flood over dam, showing a good overall performance. After cleaning the surface, the construction resumed quickly, fully embodying the capacity of the CMD to resist the scouring of flood over dam.



Fig. 3
Xijiang dam under overflow and after overflow during construction

4. A NEW REINFORCEMENT METHOD FOR EMBANKMENT DAMS WITH
CMD MATERIALS TO RES OVERTOPPING FAILURE

4.1. THE SCHEME PROPOSED

On the basis of the characteristic that CMD has the ability to resist overtopping, a new reinforcement structure for existing embankment dams with CMD materials to improve the capacity of resisting overtopping failure is proposed. The dam crest and downstream surface of the embankment dam are reinforced with cemented materials to improve the resistance of overtopping for dam crest and downstream surface. For this reason, the overtopping model test was carried out in the laboratory, and the schematic diagram of the model is shown in Fig. 4. The overtopping model experimental sets are shown in Fig. 5.

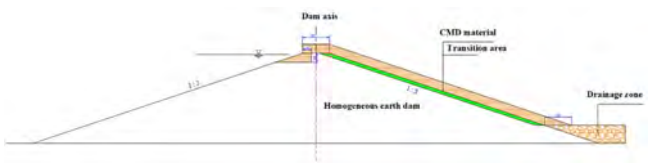


Fig. 4
The downstream protection structure

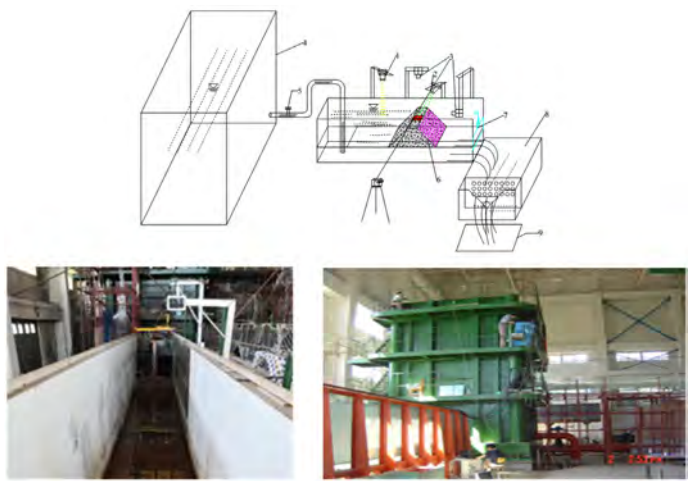


Fig. 5
The overtopping model test facilities

4.2. OVERTOPPING MODEL EXPERIMENT

The homogeneous embankment dam model is built with cohesive soil in the test tank. The model has a height of 1 m and crest width of 30 cm. The slope ratio of downstream and upstream is 1:3. The dam crest and downstream surface lay 20 cm thick CSGR material after sprinkling cement slurry. The average particle size D_{50} of the CSGR material is 20 mm and the maximum particle size is 40 mm. In order to ensure the compaction of filling, the electro-mechanical tamping method is used for layered filling construction, and every 15 cm is one layer. Cemented soil and gravel is set within 20cm of the downstream bottom as the drainage area. The mix ratio of the CSGR Material is shown in Table 3.

Table 3

SAND RATE	WATER-BINDER RATIO	WATER (KG)	CEMENT (KG)	FLY ASH (KG)	SAND (KG)	GRAVEL (KG)
31%	1	120	60	60	670	1490

The homogeneous embankment dam model and the model with reinforcement method are shown in Fig. 6 and Fig. 7, respectively.



Fig. 6
The homogeneous earth dam model



Fig. 7
The test model reinforced with downstream protection

In the test, the inflow flow was increased step by step, from $0.0125 \text{ m}^3/\text{s}$ to $0.25 \text{ m}^3/\text{s}$, and behavior of the model at the downstream dam surface was monitored when overtopping. During the test, the flow velocity at different positions on the downstream surface was measured for different flow rates. When the flow

rate was 0.25 m/s, the maximum flow velocity on the downstream surface was 4.734 m/s.

The test shows the downstream dam slope occurs local denudation after overtopping for 4 hours. The earliest denudation damage occurs at the construction layer, and there are insufficient compaction degree or weak layer due to factors such as formwork overlap and intermittent construction. The denudation area gradually increases with the extension of overtopping time. The cumulative overtopping time is 50 hours, and the maximum erosion depth of the downstream dam surface is 4.5 cm. It is intact for the overall results, without obvious seepage and structural damage caused by long-term overflow erosion.



Fig. 8
The erosion of downstream surface under overtopping

After 50 hours of overtopping, the state of downstream and upstream faces of the dam model is shown in Fig. 9. It can be seen from the figure that there is no obvious damage on the upstream and downstream surfaces.

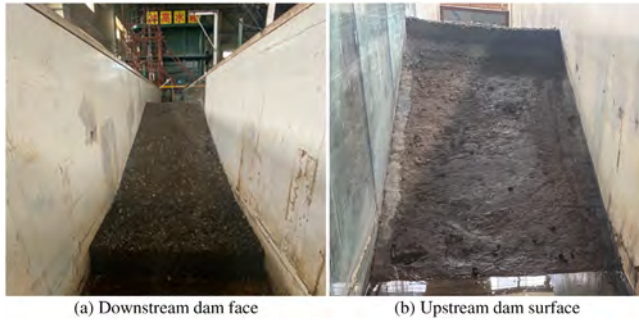


Fig. 9
The status of test model after overtopping for 50h

After the overtopping test is completed, the cemented material reinforcement layer is dismantled, and the bonding between the embankment dam and the cemented material reinforcement layer is observed. The cement slurry is closely combined with the compacted cemented material and the soil body, shown in Fig. 10. The test shows that the reinforcement method for embankment dams with CMD materials has good capacity of resisting overtopping, which provides a solution for improving the flood control capacity of many small and medium-sized reservoirs.



Fig. 10
The bonding between the embankment dam and reinforcement layer

5. CONCLUSIONS

As a new dam type, CMD will surely get more attention with the continuous improvement of dam construction theory and technology. CMD is proposed and developed based on the requirements of practice, but it still needs to be continuously explored, including material and structure behavior evolution, real-time construction control of and safety assessment, and innovated on the basis of practice.

REFERENCES

- [1] RAPHAEL, J.M. The Optimun Gravity Dam [A]. Rapid Construction of Concrete Dams [C], ASCE, 1970:221-224.
- [2] RAPHAEL J M. *The Soil Cement Dam [M]*. University of California Berkeley, U S.A. June, 1976.
- [3] LONDE P, LINO M. Faced symmetrical hardfill dam: a new concept for RCC [J]. *International Water Power & Dam Construction*, 1992, 44 (2):19–24.
- [4] NAKAMURA A. Properties and construction of CSG (1- Dam materials <Special feature>) [in Japanese]. *Civil Engineering Research Institute*, 1994, 36 (10): 40–45.
- [5] JIA J, LINO M, JIN F, *ET AL*. The Cemented Material Dam: A New, Environmentally Friendly Type of Dam[J]. *Engineering*, 2016, 2(004):490–497.
- [6] JIA, J.; ZHENG, G.; MA, F. Studies on cemented material dam and its application in China. In Proceedings of the 6th International Symposium on Roller Compacted Concrete (RCC) Dams, Zaragoza, Spain, 23–25 October 2012.
- [7] WU Y, JIA J, ZHENG C, *ET AL*. A New Method for Constructing the Protection and Seepage Control Layer for CSGR Dam and Its Application[J]. 2024.
- [8] JINSHENG J, CUIYING Z, SHUGUANG L, *ET AL*. Optimizing structural function design and new practices of cemented material dams in China[J]. *International journal on hydropower & dams*, 2020(1):27.

COMMISSION INTERNATIONALE DES
GRANDS BARRAGES

VINGT-HUITIEME CONGRES DES
GRANDS BARRAGES
CHENGDU, MAI 2025

MACHINE LEARNING METHOD BASED DAM BREACH FLOOD SIMULATION (*)

Hongqiu HE

*Department of Geotechnical Engineering, Nanjing Hydraulic Research Institute,
Nanjing*

Qiming ZHONG

*Department of Geotechnical Engineering, Nanjing Hydraulic Research Institute,
Nanjing
National Key Laboratory of Water Disaster Prevention, Nanjing
Key Laboratory of Reservoir and Dam Safety of the Ministry of Water Resources,
Nanjing*

Xueming WU & Kai CHENG

PowerChina Kunming Engineering Corporation Limited, Kunming

Xudong CHEN & Xiaokang CHEN

*Department of Geotechnical Engineering, Nanjing Hydraulic Research
Institute, Nanjing*

CHINA

SUMMARY

In recent years, the frequency of extreme weather events has significantly increased the risk of catastrophic floods caused by dam breaches. In this context, the timeliness and accuracy of flood evolution simulations are crucial for developing effective emergency response measures. However, due to the high uncertainty of

**Méthode d'apprentissage automatique basée sur la simulation de l'onde de rupture d'un barrage*

inflow conditions, existing quantitative analysis methods struggle to meet the demands of real-time flood simulation. To address this issue, this study employs the deterministic methods to simulate the dam breach hydrographs and flood inundation situations based on possible inflow boundaries, and then uses a machine learning method to train on the dam breach flood simulation data of different inflow conditions. When an actual dam breach occurs, the model can quickly utilize the trained data to make predictions and provide real-time information on dam breach flood evolution. Take the Sheyuegou dam breach case in Xinjiang Uygur Autonomous Region in China as the representative to verify the machine learning method. The simulation area is 76.02 km^2 , and the sizes of high- and low-resolution grids are $30 \text{ m} \times 30 \text{ m}$ and $100 \text{ m} \times 100 \text{ m}$, respectively. The comparison shows that the proposed machine learning method performs better than the traditional quantitative analysis method, offering 11 times greater computational efficiency, and achieving the coefficient of determination of 0.95 for the accuracy of maximum water depth in the inundation area compared with the high-resolution model. It is worth mentioning that, the run time of machine learning method is the summation run time of code and low-resolution model, which is more efficient for large simulation area. These findings have significant implications for dam breach flood risk analysis and emergency response.

RÉSUMÉ

Ces dernières années, la fréquence des phénomènes météorologiques extrêmes a considérablement augmenté le risque d'inondations catastrophiques causées par des ruptures de barrages. Dans ce contexte, la rapidité et la précision des simulations de l'évolution des inondations sont cruciales pour élaborer des mesures d'urgence efficaces. Cependant, en raison de la grande incertitude des conditions d'écoulement, les méthodes d'analyse quantitative existantes ont du mal à répondre aux exigences de la simulation d'inondation en temps réel. Pour résoudre ce problème, cette étude utilise les méthodes déterministes pour simuler les hydrogrammes de rupture de barrage et les situations d'inondation basées sur les limites d'afflux possibles, puis utilise une méthode d'apprentissage automatique pour s'entraîner sur les données de simulation d'inondation de rupture de barrage dans différentes conditions d'afflux. Lorsqu'une rupture de barrage se produit, le modèle peut rapidement utiliser les données d'entraînement pour faire des prévisions et fournir des informations en temps réel sur l'évolution de l'inondation. Le cas de la rupture du barrage de Sheyuegou dans la région autonome du Xinjiang Uygur en Chine est représentatif pour vérifier la méthode d'apprentissage automatique. La zone de simulation est de $76,02 \text{ km}^2$, et les tailles des maillages haute et basse résolution sont respectivement de $30 \text{ m} \times 30 \text{ m}$ et de $100 \text{ m} \times 100 \text{ m}$. La comparaison montre que la méthode d'apprentissage automatique proposée est plus performante que la méthode d'analyse quantitative traditionnelle, offrant une efficacité de calcul 11 fois supérieure et atteignant un coefficient de détermination de 0,95 pour la précision de la profondeur d'eau maximale dans la zone d'inondation par rapport au

modèle à haute résolution. Le temps d'exécution de la méthode d'apprentissage automatique correspond à la somme du temps d'exécution du code et du modèle à faible résolution, ce qui est plus efficace pour les grandes zones de simulation. Ces résultats ont des implications significatives pour l'analyse des risques d'inondation liés aux ruptures de barrage et pour les interventions d'urgence.

1. INTRODUCTION

Global warming has led to an increased frequency of extreme rainfall and flood disasters, thereby heightening the risk of natural catastrophes such as dam failures[1]. The numerical simulation of dam-break floods, as a core technology in constructing 'rehearsal' processes for reservoirs, provides critical decision support for emergency flood evacuation management. Traditionally, flood inundation simulations rely on high-resolution two-dimensional hydraulic models to simulate the physical processes of flood events. Widely applied mature models include the HEC-RAS model developed by the U.S. Army Corps of Engineers and the MIKE 21 model by the Danish Hydraulic Institute. These commercial software models focus on data visualization and graphic simulation effects, with their computational foundation primarily based on the two-dimensional Navier-Stokes equations, which describe the movement of water in various directions. However, a major challenge facing current flood models is the high computational cost, particularly in time-sensitive dam-break flood models, where there is a critical demand for rapid response. Although researchers are actively working to improve the computational efficiency of these models, accurate flood modeling at high resolutions remains costly.

With the advancement of data-driven machine learning technologies, many researchers have started applying these methods to predict natural disasters like floods and to evaluate the contributing factors to these catastrophes[2,3]. Compared to traditional models, these data-driven approaches significantly enhance the simulation and prediction capabilities for natural disasters. Gaussian Processes (GP) serve as one example of such machine learning methods. They infer unknown data by analyzing known data and form a stochastic process where we consider each data point a random variable. When we assume that each data point within the process adheres to a Gaussian distribution, we define the process as a GP. However, GP models face computational challenges with large-scale datasets because they require inverting large covariance matrices. In modeling flood inundation events, which may involve thousands of time steps in time series data, using Sparse Gaussian Process (SGP) models to approximate a complete GP has emerged as an effective strategy. This method introduces multiple inducing variables to reduce the computational demands of the model, thereby enhancing the efficiency of processing large datasets.

This study employs machine learning methods to simplify the output simulation of two-dimensional hydraulic flood models. By operating only low-resolution

models, the method reduces the required computational resources and model run-time, thereby lowering computational costs. Additionally, it uses SGP models to correct for the reduced accuracy in resolution modeling results. Based on case study data from Sheyuegou dam breach case in Xinjiang Uygur Autonomous Region in China, this research utilized simulation results from the HEC-RAS model for training on a large dataset. Using the trained machine learning model, the study simulated and evaluated the accuracy of flood disaster scenarios in the study area under conditions not included in the training set.

2. METHODS

The overall concept of the machine learning model is to utilize information obtained from both low-resolution and high-resolution model simulations to quickly produce accurate inundation estimates, thereby avoiding the computational burden of running hydrodynamic models for each new set of boundary conditions. The workflow for training and prediction is illustrated in Fig. 1. By constructing grids of different spatial resolutions in the study area, simulations of the flood progression process under various dam-break scenarios are carried out to establish a dataset of flood inundation at different spatial resolutions. The simulation data undergo Empirical Orthogonal Function (EOF) analysis, simplifying the spatiotemporal data into Empirical Coefficients (ECs) time functions. Subsequently, low-resolution ECs are used as inputs and high-resolution result ECs as outputs to train the SGP model. After completing the model training, this model can be directly applied to new conditions (beyond the original training set range), and directional EOF analysis is used to transform the results of the machine learning model into high-resolution model outputs, thus completing the entire model conversion process from low to high precision without the need to run the high-resolution model.

The SGP model is implemented in Python utilizing the GPflow package[4]. This approach advantageously employs GPU computing to optimize the model and thus significantly reduce computational times. To accommodate the use of inducing points, the formula has been appropriately adjusted, see Equation 1[5]:

$$SGP(x) \sim \mathcal{N}(y|k_{x'}K_M^{-1}\bar{y}, K_{xx} - k_{x'}K_M^{-1}k_x + \sigma_n^2I) \quad [1]$$

where k_x is $k(x, \bar{x})$, K_M is $k(\bar{x}, \bar{x})$, and K_{xx} is $k(x, x')$, σ_n^2I noise variance multiplied by the identity matrix. The variables y and x are the observation and input points, respectively, where y and x are the inducing points for the observations and input points. The observation inducing points (y) can be removed via integration by assuming a prior distribution following the full GP, which is reasonable as y is expected to follow $y[6]$. Consequently, inducing points only need to be found for the input points.

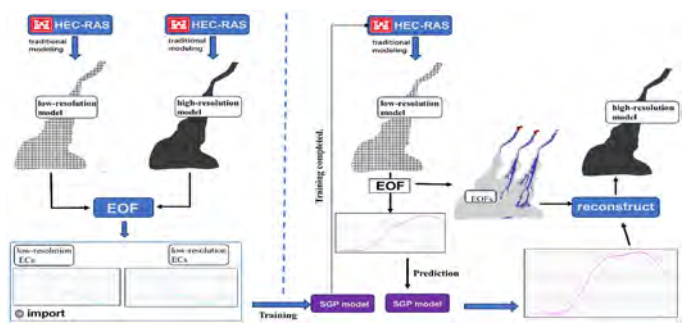


Fig. 1
Machine Learning Model Application Flowchart

A novel approach has been developed, utilizing a single SGP model to predict each effective mode of high-resolution ECs. Each SGP model assimilates all low-resolution EC import to forecast a corresponding high-resolution EC export (Fig. 2). Compared to the traditional method of computing each grid point within a high-resolution model, this approach significantly reduces the computational cost required.

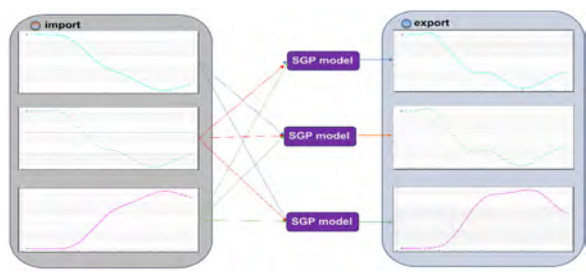


Fig. 2
Schematic diagram of the conversion process using Sparse Gaussian Models

3. CASE STUDY

3.1. SITE DESCRIPTION AND MODELLING DOMAIN

To evaluate the effectiveness of the machine learning model, the Sheyuegou dam breach case was selected for the study. Located on the southern slopes of the Harlik Mountains, the reservoir has a maximum capacity of 6.78 million m³. On July 31, the Sheyuegou watershed experienced heavy rainfall, with the peak inflow to the

reservoir during the flooding process recorded at 1848 m³/s, as determined by an on-site flood mark investigation^[7]. According to the design report of the Sheyuegou reservoir^[8], this flow rate significantly exceeded the design standard for a flood with a 300-year recurrence (peak inflow of 537 m³/s). Indeed, the highest inflow recorded surpassed the 10000-year flood recurrence rate of 1062.9 m³/s. This substantial deviation from the design standards led to the reservoir overtopping and ultimately to dam failure. The disaster resulted in 20 fatalities and 8 missing persons, with over 8,700 houses damaged, along with some farmland, roads, railways, and electrical and communication infrastructure.

3.2. TRAINING DATA

HEC-RAS was employed to simulate the dam breach at Sheyuegou Reservoir, thereby generating a training set. Zhao et al. used the Flash Flood Module Simulation System (FFMS) to simulate the runoff process from the July 31 rainstorm in the Sheyuegou catchment^[9]. Based on this, the inflow hydrograph was resized to create synthetic condition events, which serve as the basis for the boundary conditions of the training model. It is important to note that the original curve was not used for training.

A structured grid methodology was employed, where the high-resolution model was partitioned into 85,730 cells with a grid dimension of 30 × 30 m. This model was operated with a fixed temporal resolution of 30 seconds. In contrast, the grid size for the low-resolution model was expanded to 100 × 100 m, which reduced the number of computational cells to 8,040. This amount represents merely one-tenth of the computational cells in the high-resolution model, as depicted in Fig. 3. To evaluate the differences in computational outcomes between the high and low-resolution models, this study primarily adjusted the quantity of computational grids. The boundary conditions and computation time steps were maintained consistently, with no further optimizations applied to the models.

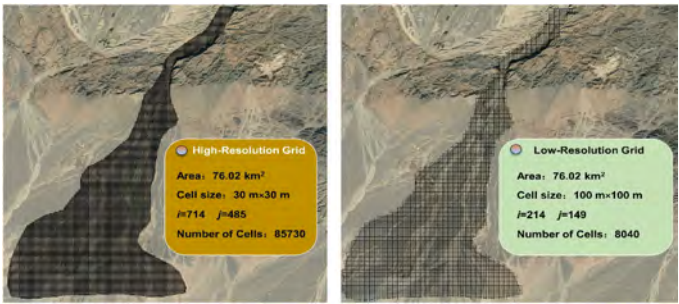


Fig. 3
Comparison Chart of Grid Information between Low-Resolution and High-Resolution Models

3.3. MACHINE LEARNING MODEL RESULTS ANALYSIS

3.3.1. Water depth

Water depth is a commonly used metric for assessing flood risk, as it directly impacts the extent of damage to buildings and other infrastructure, while also posing threats to residents' safety. The capability of machine learning models to predict water depth is evaluated using a coefficient of determination, as shown in Equation 2:

$$R^2 = \frac{\left[\sum_{j=1}^n (H_s - H_{avs})(H_m - H_{avm}) \right]^2}{\sum_{i=1}^n (H_s - H_{avs})^2 \sum_{i=1}^n (H_m - H_{avm})^2} \quad [2]$$

where n is the number of observations; H_s is the water depth predicted by the machine learning model or low-resolution model; H_m is the water depth predicted by the high-resolution model; H_{avs} is the average predicted water depth by the machine learning model or low-resolution model; H_{avm} is the average predicted water depth by the high-resolution model.

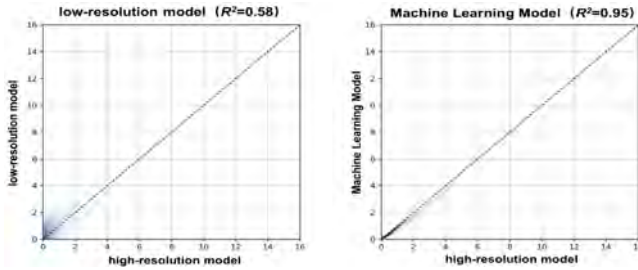


Fig. 4

Comparison Chart of Water Depth Accuracy between Low-Resolution and Machine Learning Models.

Fig. 4 illustrates the comparative results of water depth predictions between low-resolution models and machine learning models. The simulation data reveal that the R^2 for the low-resolution model, which utilizes a coarser grid resolution and is uncalibrated, is significantly higher than that of the machine learning model. This is in line with expectations. The low-resolution model, due to its lack of calibration and coarser resolution, yields a lower fit ($R^2 = 0.58$). In contrast, the machine learning model achieves an R^2 of 0.95, underscoring the efficacy of machine learning techniques in reducing prediction errors.

3.3.2. Model reorganization

wUsing directional EOF analysis, the simulation results are reorganized, with the dataset being decomposed into a series of modes and their corresponding time series. Each mode is associated with a specific variance value, which indicates the proportion of the total variance explained by that mode. Modes with higher numerical values are more significant as they account for a larger proportion of data variation. The mathematical formula is as follows:

$$\text{ExplainedVariance}(\%) = \left(\frac{\lambda_i}{\sum_{j=1}^n \lambda_j} \right) \times 100\% \tag{3}$$

where λ_i represents the eigenvalue of the i -th mode, signifying the variance attributed to that mode; the denominator, $\sum_{j=1}^n \lambda_j$ totals the eigenvalues of all modes, thus representing the dataset's overall variance.

The outcomes of the reorganization, depicted in Fig. 5, reveal a high degree of similarity between the flood models derived from machine learning methods and

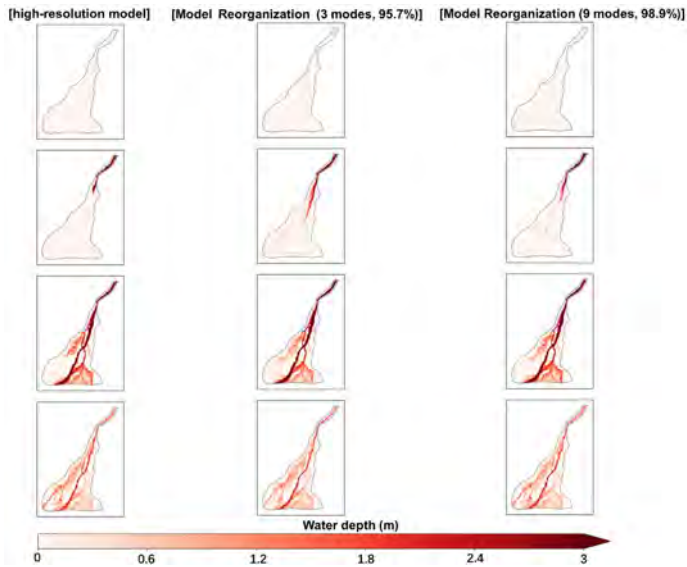


Fig. 5
Machine Learning Model Reorganization Results Chart

those from high-resolution models, particularly in terms of the consistency in predicting the timing of flood peaks. The simulations indicate that the machine learning model explains 95.7% of the variance when restructured using three principal modes, and 98.9% when using nine principal modes. These findings underscore the capability of the machine learning model to effectively simulate the flood process and its accuracy in forecasting critical temporal milestones in flood development.

3.3.3. Computational efficiency

The modeling for this study was performed on a civilian computer with the following specifications: an Intel Core i9 13980HX processor and an NVIDIA GeForce RTX 4060 graphics card. Fig. 6 summarizes the computational time and accuracy comparisons across different methods. The total computation time for the machine learning model used in the Sheyuegou dam breach simulation was 90 seconds (31 seconds for running the low-resolution model and 59 seconds for the code execution process), whereas the high-resolution model took 1003 seconds to simulate the same conditions. Compared to the high-resolution model, the machine learning approach saved approximately 91% of the computational time. The simulation results of the high-resolution model are considered as the observational benchmark ($R^2 = 1$). In terms of simulation accuracy, the low-resolution model and the machine learning model achieved fit values of 0.58 and 0.95, respectively. This indicates that the machine learning model improved prediction accuracy by approximately 81% relative to the low-resolution model, highlighting the machine learning approach's ability to maintain high simulation precision while significantly enhancing computational efficiency.

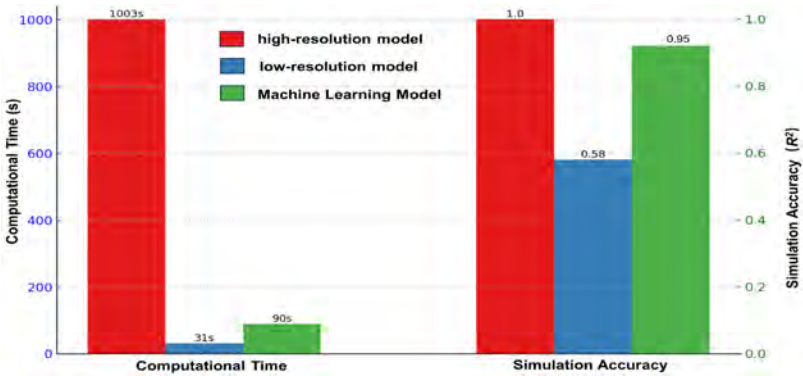


Fig. 6
Comparison Chart of Accuracy and Runtime between Low-Resolution and Machine Learning Models.

4. CONCLUSIONS

The purpose of this study is to examine the practicality of machine learning models in real-world cases. When training the SGP model, the training data included potential dam breach scenarios. After training, a coarse but fast low-resolution model was established to convert the results using machine learning. The results show that even using an uncalibrated low-resolution model can produce simulation results with accuracy comparable to high-resolution models. The coefficient of determination for the accuracy of maximum water depth in the inundation area reached 0.95 compared to the high-resolution model. Additionally, the computational efficiency improved by 11 times. It is worth mentioning that the run time of the machine learning method is the summation of the run time of the code and the low-resolution model, which is more efficient for large simulation areas.

Although machine learning models excel in improving computational time and accuracy, the simulation process of completing a machine learning model is quite cumbersome. Generating an appropriate training dataset requires building numerous high-resolution models to train the machine learning model. Therefore, at this stage, this method is mainly applicable to preventive measures or projects with a longer time span that can generate training data, thereby achieving ideal computational efficiency benefits after training.

ACKNOWLEDGMENTS

The authors greatly acknowledge the financial support from the National Natural Science Foundation of China (Grant No. U22A20602), the Fundamental Research Funds for Central Public Research Institutes (Grant No. Y324006), and the Key Science and Technology Project of PowerChina (Grant No. DJ-ZDXM-2019-45).

REFERENCES

- [1] MUSTAFA D. Gendering flood early warning systems: the case of Pakistan. *Environmental Hazards*, vol. 14, pp.312–328, 2015.
- [2] DONNELLY J., ABOLFATHI S., PEARSON J. Gaussian process emulation of spatio-temporal outputs of a 2D inland flood model. *Water research*, vol. 225, pp. 119100, 2022.

- [3] FRAEHR N., WANG Q.J., WU W. Development of a Fast and Accurate Hybrid Model for Floodplain Inundation Simulations. *Water Resources Research*, vol. 59, pp. 1–22, 2023.
- [4] MATTHEWS A.G.D.G., MARK V.D.W., NICKSON T. GPflow: A Gaussian Process Library using TensorFlow. *Journal of Machine Learning Research*, vol.18, pp. 1–6, 2016.
- [5] FRAEHR N., WANG Q.J., WU W. Upskilling Low-Fidelity Hydrodynamic Models of Flood Inundation Through Spatial Analysis and Gaussian Process Learning. *Water Resources Research*, vol. 58, pp. 1–21, 2022.
- [6] SNELSON E., GHAHRAMANI Z. Sparse Gaussian Process Using Pseudo-inputs. *Advances in neural information processing systems*, vol. 18, pp. 1257–1264, 2006.
- [7] Hami District Institute of Water Resources and Hydropower of Survey and Design Research (HDIWHSDR), *Preliminary design report of Sheyuegou reservoir project in Hami City*, Report, 2007.
- [8] WANG M. X., ZHANG T. X., YU X. J., ZHANG L. C., ZHANG X., Estimation and application of water-collecting amount during an extreme heavy rainfall induced flash flooding in Hami City on July 31 2018. *Arid and Geography*, vol. 18, pp. 939–945, 2020.
- [9] ZHAO X, T., LIU C. J., WANG W. C., GU B. J., YANG K., ZHANG M., MA J. M. Dam break flood simulation of Sheyuegou reservoir and analysis of dam break reasons. *China Rural Water and Hydropower*, vol. 5, pp. 171–177, 2022.



Taylor & Francis

Taylor & Francis Group

<http://taylorandfrancis.com>

GENERAL REPORT ON QUESTION 110

RAPPORT GÉNÉRAL SUR LA QUESTION 110



Taylor & Francis

Taylor & Francis Group

<http://taylorandfrancis.com>

COMMISSION INTERNATIONALE DES
GRANDS BARRAGES

VINGT-HUITIEME CONGRES DES
GRANDS BARRAGES
CHENGDU, MAI 2025

QUESTION 110

SAFETY OF DAMS AND LEVEES FACING



EXTREME HYDROLOGICAL EVENTS

Enrique CIFRES

Doctor in Water Resources, MsC Civil Engineer

Honorary Vice-President of ICOLD

Independent advisor on dams and water resources

SPAIN

GENERAL REPORTER

TABLE OF CONTENTS

1.	Q110 – SUBTOPICS	492
2.	BY WAY OF INTRODUCTION	492
3.	ICOLD CONTRIBUTION	495
4.	RELATED ICOLD'S BULLETINS	496
4.1.	B131 Role of dams in flood mitigation	496
4.2.	B156 Integrated flood risk management	497
4.3.	B170 flood estimation and dam safety	497
4.4.	B197 Dam breach flood consequence assessment	498
4.5.	B203 Best practices for achieving reliability of flood discharge gates	498
4.6.	B204 flood risk assessment	498
5.	Hydrological safety*	499
5.1.	Standards and regulations and national current approaches	499
5.1.1.	Risk assessment at national scale in Spain	500
5.1.2.	French management	501
5.1.3.	Japanese recent cases	501
5.1.4.	Spatial and temporal extreme precipitation in China	501
5.1.5.	Extreme events on dam disaster in China under climate change	502
5.2.	Re-evaluation of extreme floods	502
5.3.	Design event-based precipitation-runoff modeling	504
5.4.	New current trend	505
5.5.	PMF	505
5.6.	Australian enveloping curves	506
5.7.	An innovative methodology (France)	506
5.8.	Necessity of more data	507
5.9.	Data series extension: Paleofloods	507
5.10.	Regional flood frequency analysis	508
5.11.	Synthetic generation	508
5.12.	Conceptual models with physical basis	509
5.13.	Stochastic transposition	510
5.14.	Climate change impact	514
5.15.	Uncertainty	516
6.	Acting facing extremes	516
6.1.	Spillways	517
6.1.1.	Drin river basin	517

6.1.2.	Regajo dam	518
6.1.3.	Structural review in France	519
6.1.4.	Tragedy in Italy	519
6.2.	Labyrinths - PKW Spillways	520
6.2.1.	Southafrican cases	520
6.2.2.	French and vietnamese cases	521
6.2.3.	A singular swedish project	522
6.3.	Overtopping	522
6.3.1.	Chinese contribution to CMD	523
6.4.	Energy dissipation	524
6.4.1.	Kariba dam	524
6.5.	Routing floods and peak attenuation	525
6.6.	Temperature	525
6.7.	Landslides	526
6.8.	Dam management	527
6.8.1.	Advances in dam break and wave propagation models	528
7.	Non-structural measures	530
7.1.	Early warning and emergencies	530
7.2.	Hydrological alert	531
7.3.	Hydraulic alert	531
8.	Levees	532
8.1.	Hazard creeping	532
8.2.	Levees (R12)	533
9.	Concluding remarks	534
9.1.	Our challenges	535
9.2.	World declaration on dam safety, 2019: risk zero does not exist	536
9.3.	World declaration 2024	536
9.4.	Final words	536
	REFERENCES	537
	Papers Q110	537
	Other references	540
	ICOLD bulletins and institutional documents	541

1. QUESTION 110 – SUBTOPICS

- Assessment of extreme events (e.g., flood, droughts*, typhoons/hurricanes, glacial lake outburst floods) in the context of climate change, accounting for uncertainty
- Assessment for the safety of structures for extreme floods; management options (e.g., increasing dam height, spillway capacity, reservoir operation)
- Flood forecasting, hydraulic management of multiple projects within river systems
- Reassessment of the flood data and mitigation e.g., fuse devices, overflow resistance, controlled breach formation, warning and evacuation, crisis and emergency management

2. BY WAY OF INTRODUCTION

"I had never seen this" is an expression that is repeated when an extreme event happens, and it is logical, because it is "extraordinary", it is outside the expected and the conceivable, really outside.

Recently it has been the most repeated phrase in my city, Valencia, after the truly extraordinary floods we have suffered. This work has been prepared under the emotional shock of a terrible storm that has taken the lives of more than two hundred neighbors and the enormous impact on the lives and economies of hundreds of thousands of fellow citizens.

I dedicate this report to them and, together with my condolences, I pledge to work hard for the safety of all people, everywhere, who may be subject to hydrological hazards.

A year earlier, also in the Mediterranean, the inhabitants of Derna, in Libya, suffered from storm Daniel, an extraordinary event that produced even worse consequences, due to the rupture of the Dernah and Abu Mansur dams paradoxically built to protect them.

**Although the first subtopic includes droughts, this problem is deeply addressed in this same Chengdu Congress, in Q108 on "adaptation to CC" and is the reason why none of the papers included in this Q110 is directly focused on droughts, even though they are also the consequence of hydrological extremes.*

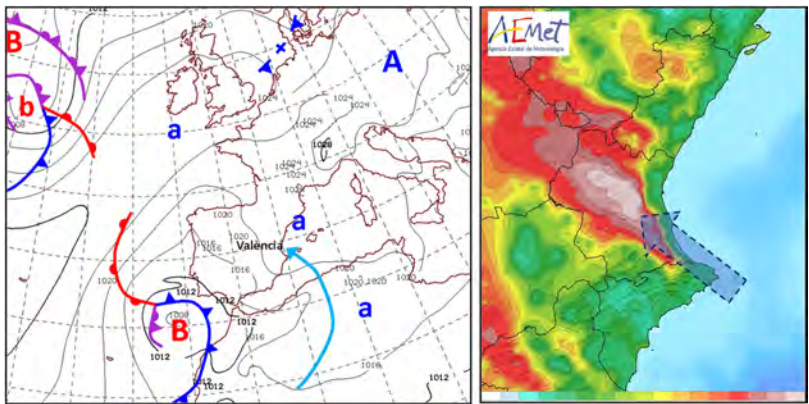


Fig. 1
An atmospheric river flowing along main valley orientation. October 29, 2024

A cold air pool over the Iberian Peninsula, with a low-pressure storm, blocked to the west of the Strait of Gibraltar by high pressure over central Europe that retains it static for two days, a warm Mediterranean Sea that saturates a reheated air on its way through the Sahara: a dangerous cocktail for Valencia.

We know that when something truly extraordinary happens, it is the combination of multiple factors that together make up a terrible scenario and this idea must inspire the analysis, prevention and understanding of extreme phenomena.



Fig. 2
Disaster in Valencia metropolitan area. 2024.

Simulations of the flood wave of Poyo Creek suggested an estimation of peak discharge of around 3,000 m³/s, significantly exceeding the capacity of the town's drainage channel, which could handle a maximum of around 800 m³/s.

Similarly, the Dernah Wadi basin, although relatively small, suffered from the terrible combination of factors with which Storm Daniel generated its fatal discharge.



Fig. 3
Daniel storm creating an atmospheric river along Derna basin.[†]



Fig. 4
Derna disaster. No words needed.

[†]Picture taken from CRISIS GROUP / MAXBOX / OSM

Simulations of the second flood wave that was caused by the collapse of Abu Mansour dam suggest an estimation of discharge of around 7,000 m³/s, significantly exceeding the capacity of the city's drainage channel, which could handle a maximum of around 1,000 m³/s.

Everything points to the fact that the design followed the current standards at the time.

It is worth wondering whether the magnitude of this phenomenon could be foreseen a priori. The answer requires a premise that underlies hydraulic engineering projects: when we select a return period for design, are we aware that more severe episodes cannot be ruled out?

Still an additional question: if the basin has never experienced an episode of a certain magnitude, or similar, should that possibility be ruled out?

Both questions put on the table the classic methodologies of dam design and safety and the need for their revision.

On the other hand, if we admit that global warming is and will continue to exacerbate hydrological extremes in many regions of the planet, historical records lose prominence in favor of new approaches that can incorporate concepts for estimating extreme events that dams, both existing and new, will have to face.

From the experience of the Valencia disaster, and listening to public opinion, relatively good news emerge: society is aware that flood defense works mitigate damage, but do not eliminate it completely, and associated non-structural measures have to be implemented to manage emergencies associated with residual risks once structural measures such as flood control dams canalizations, levees, drains, etc. have been carried out.

In this report, it will be possible to appreciate the border between the enormous contribution of dams and levees to mitigate flood damage and the residual risk, imposed on the territory, associated with their potential breakage. That is the challenge.

3. ICOLD CONTRIBUTION

ICOLD is working on this great challenge for safety that means hydrological extremes, exacerbated by climate change, population growth in prone zones, greater social, health and economic demands, etc. in a changing world. The permanent review of criteria, information, technological knowledge, and regulation requires continuity in the work with the necessary innovation to accommodate

existing dams, future designs and their management, as well as the protection levees under which millions of people live worldwide.

Twenty-eight papers have been received from twelve countries, covering almost all the promoted subtopics of this broad question.

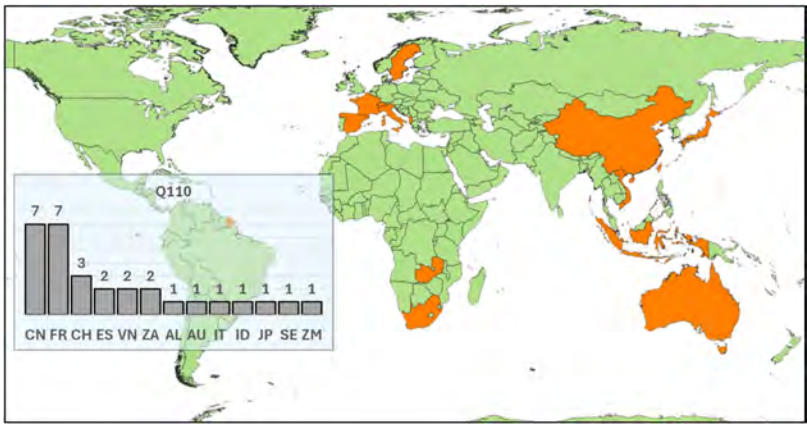


Fig. 5

Contribution to Q110: Papers from China, France, Switzerland, Spain, Vietnam, South Africa, Albania, Australia, Indonesia, Italy, Japan, Sweden and Zambia.

In addition to the multiple contributions in the previous ICOLD congresses, in existence for almost one hundred years, we can highlight some of the technical bulletins published where this issue of extreme hydrology and its influence on dams and levees is deepened.

4. RELATED ICOLD'S BULLETINS

4.1. B131 ROLE OF DAMS IN FLOOD MITIGATION

ICOLD resumed its position with this bulletin in which the foundations of the modern conception of IFM[‡] are laid. Floods, as one of the major types of natural

[‡]Integrated Flood Management

hazards, were responsible for 30% of all economic damage, and for 20% of the fatalities caused by these.

That committee was born simultaneously to the release of the United Nations implemented the International Strategy for Disaster Reduction (ISDR), whose main purpose was “building disaster resilient communities by promoting increased awareness of the importance of disaster reduction as an integral component of sustainable development, with the goal of reducing human, social, economic and environmental losses due to natural hazards” (Berga 2006).

Dams can play a major role in flood mitigation, but as one tool to be taken into account within the framework of Integrated Flood Management (IFM) but recalling that the perception and presumption of total security should be avoided.

4.2. B156 INTEGRATED FLOOD RISK MANAGEMENT

"Integrated Flood Risk Management" is a relatively common approach that has been implemented in recent decades in some countries. Its application in some transboundary basins is underway with the support of international organizations. It is one of the difficult non-structural measures to be actually implemented.

Its approach, subject of bulletin 156, seeks effective and accepted protection systems, but its implementation is more complex than the traditional purely technocratic approach, as it requires the cooperation of all stakeholders. The difficulties lie in the resistance of some parties to give up current privileges.

4.3. B170 FLOOD ESTIMATION AND DAM SAFETY

Four bulletins dealing with floods and dams had been published before this one: Selection of design flood – Currents methods (#82, 1992), Dams and Floods – Guidelines and Cases Histories (2003), Role of Dams in Flood Mitigation (2006) and Integrated Flood Management (2014).

Integrating flood management in reservoir operation, along with other considerations related to climate change and real case experiences are addressed in this publication. Besides a summarized vade mecum of “classical” hydrological methods, an approach to cope with the uncertainties of extreme floods are discussed.

Finally, the applied criteria throughout the world for selecting the design and extreme flood, are compiled.

Some other bulletins are in the pipe ready to be published as:

4.4. B197 DAM BREACH FLOOD CONSEQUENCE ASSESSMENT

The ICOLD Dam Safety Committee works to guide dam safety managers on the principles, contemporary applications and methods used for the analysis and evaluation of the consequences of dam failures, necessary for risk assessments, potential damage estimation and emergency planning. The risk of dam failure combines the estimation of probabilities and the evaluation of potential consequences, including the possible loss of life, the latter factor being the main target of this Bulletin 197, about to be released.

4.5. B203 BEST PRACTICES FOR ACHIEVING RELIABILITY OF FLOOD DISCHARGE GATES

Efficient flood management depends on the reliable operation of the hydro-mechanical equipment of gated spillways. These, inactive for long periods, are crucial in emergency situations to avoid consequences that could be catastrophic.

The publication reviews practices in different regions of the world by comparing advantages and disadvantages of mechanical or hydraulic actuating mechanisms. It also warns of the growing risk of cyberattacks on gates operated by IoT with recommendations to strengthen the security of their control.

4.6. B204 FLOOD RISK ASSESSMENT

This forthcoming bulletin discusses structural measures for flood mitigation, such as levees, reservoirs, drainage systems, and non-structural measures such as reservoir operation, including joint management of reservoir clusters, floodplain zoning, and flood insurance, among others, prediction and warning systems, and real-time risk management. This bulletin emphasizes the need for a comprehensive approach to assessing and managing flood risk, combining predictive modeling, strategic planning, and real-time operational response.

Some of the ideas mentioned in these documents are addressed in the papers received by some countries, insisting on them, confirming or even going deeper with real case studies that are worth reading. Throughout this general report, the reference of the paper in which the idea on which the argument is made will be indicated in parentheses.

The first half of this general report addresses ways to improve the knowledge of hydrological extremes, in particular large floods, as well as those induced by potential breaking, while the second half presents the most efficient actions for mitigation and adaptation of dams to these needs.

5. HYDROLOGICAL SAFETY

Global warming has intensified hydrological cycles, increasing the frequency and intensity of extreme rainfall. This phenomenon represents a critical challenge to the safe operation of dams around the world. These trends pose considerable risks to water infrastructure and underline the need for quantitative and systematic analysis of their impact (R22).

5.1. STANDARDS AND REGULATIONS AND NATIONAL CURRENT APPROACHES

Although it was common practice in the past to design dams without a regulatory framework in almost all countries, with criteria and methodologies developed locally by the responsible engineers based on methodologies taken from current scientific doctrine, the government authorities of many countries established regulations and standards, inspired by criteria derived from the experience shared by the national committees that make up ICOLD in addition to other sources of interest.

In some countries, such as France (R14), regulations and techniques to improve dam safety are already evolving, facing the challenges associated with compliance to climate change before 2030 or 2035 depending on the category of the reservoir.

Periodic reassessment of risk, including hydrological safety, a practice in the process of wide consolidation, leads to the early identification of possible deficiencies, in some dams, in terms of the spillway capacity to face extreme risks. Not all countries still have sufficient regulation that establishes periodic hydrological review or the task of incorporating the impact of climate change

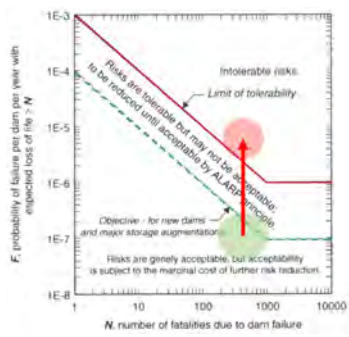


Fig. 6
Periodic reassessment of risk vs acceptability

While it is very common for regulations to enact design criteria based on different return periods depending on the category based on potential damage, extreme or safety floods are also defined, such as those that exhaust the structural safety margin. Extraordinary floods with return periods of up to 10,000 years and PMF in other cases are used for these checks. The SaRRA (R14) methodology allows for the identification of vulnerabilities and prioritization of interventions.

Facing these truly extraordinary risks justifies a great deal of reflection on the methodologies to be used for the estimation of events, the possibilities of a progressive adaptation to greater reservoir evacuation requirements, the way to implement resilience measures in the potentially affected areas with structural and non-structural actions, and the investments necessary to achieve safety levels in line with the socially acceptable level of risk. There is a great deal of work to be done and the support of good, realistic regulations with viable roadmaps are still challenges for the society and decision-making bodies to which the dam community must provide ideas and solutions.

Higher dam safety standards are demanded by society due to uncertainty in the frequency and intensity of floods in climate change conditions, land use changes and larger population exposure downstream. These require enhanced design of new dams increased dam quality through artificial intelligent construction, and continuous efforts to upgrade dam resilience operation both for existing and new dams.

Chengdu ICOLD Declaration on the Role of Dams for Energy Transition and Adaptation to Climate Change, 2025.

5.1.1. *Risk assessment at national scale in Spain*

The Spanish Ministry of *Ecological Transition* has launched a comprehensive management system to assess dam safety across the country (R01) and report to prioritize investments and anticipate the changing risks posed by climate change and identify those dams with potential long-term risks.

By strategically prioritizing investments based on these assessments, Spain can strengthen the resilience of its infrastructure to extreme weather events.

The system is being implemented in several phases, starting with the development of a qualitative and semi-quantitative risk analysis methodology for the 310 state-owned dams. The first phase focuses on 175 dams in four watersheds.

This system represents an important national effort to try to protect Spain's water resources and mitigate the risks posed by climate change, ensuring the

country's long-term sustainability and resilience. The lack of regulatory support does not allow its automatic application to decision-making. On the other hand, there is evidence of a huge investment needed to update to new and more modern hydrological safety standards.

5.1.2. *French Management*

More directly focused on hydrological risk, to safely and efficiently manage basins with dams in France in the context of climate change, EDF (R10) focuses on the management of hydrological risk, both in the short term (forecasts) and in the long term (extreme floods) through innovative tools such as Schadex-sd (hydrological scenarios), Shydonhy (synthetic hydrographs), Melxor (hydraulic propagation), Automat (flood zones) and Fregate (consequences). It is a comprehensive approach that combines hydrological simulation and hydraulic modelling to improve dam management.

Operational flood management, based on the aforementioned tools (R10), allows for the coordination of actions between operators and decision makers, especially in emergency situations, such as those proposed in the Ain river basin. In addition, they facilitate coordination between the actors involved, promoting more effective and safer management of watersheds.

The continuous improvement of reservoir safety in France (R14) reflects a commitment to efficient risk management. The case studies illustrate how modern regulations, and innovative solutions make it possible to address complex challenges, ensuring safety against extreme flooding in the context of climate change.

5.1.3. *Japanese recent cases*

The evolution of flood discharge design standards in Japan (R09) is analyzed, highlighting that many dams built under past regulations are not equipped to handle current and future hydrological challenges.

Three case studies are presented: Hiranabe, Horoka, and Hetoishi dams in Japan (R09), each facing specific issues such as landslide-generated waves, extreme sedimentation, or floods exceeding design standards. These cases underscore the need for tailored safety measures. This insightful paper will be referenced again in the body of this report.

5.1.4. *Spatial and temporal extreme precipitation in China*

The impact of the spatial and temporal variation of extreme precipitation on dam safety in large river basins in China (2000-2020) is analyzed (R22). Since 2010,

episodes of torrential rains have affected different regions of the country, with the events of 2012 and 2021 in Beijing and Henan, respectively, being examples of the increasing incidence of extreme storms.

Between 1954 and 2021, the frequency of dam failures showed a decreasing trend, especially after 1980, due to the implementation of safety regulations. However, there was a stabilization or increase in incidents, possibly related to an increase in extreme rainfall (R22).

An overall increase in total precipitation has been observed in most basins, except for Huaihe and southwestern rivers, where a decrease was observed. The maximum rainfall in 5 consecutive days also suffered a positive trend in all basins, highlighting Perla and the southeast, showing an increase in prolonged and extreme precipitation events (R22).

Although extreme rainfall has increased in most basins, with marked trends in Songliao, Yangtze and southeast, the number of dam failures in these basins has not increased significantly, perhaps related to projects that are increasingly resilient and adapted to climatological changes while warning systems are being prioritized and in high-risk regions (R22).

5.1.5. *Extreme events on dam disaster in China under climate change*

The main causes of disasters such as seepage, flood overloads, landslides, and design and construction errors have been identified as recurrent causes linked to extreme hydrological events (R25). Rapid accumulation of water in reservoirs can exceed safety levels, causing seepage, downstream slope erosion, and catastrophic ruptures.

Other weather extremes (R25), different from floods, such as very low temperatures, which can induce freezing, can cause cracks in the concrete, weakening the structure. Ice pressure on the surface of the reservoir can also affect components such as gates. In turn, high temperatures decrease the strength of the concrete, favoring the formation of cracks and structural failures. Prolonged drought exposes slopes to erosion and infiltration problems that need to be addressed from the outset. Typhoons also generate intense waves and discharge peaks that can exceed critical levels in dams.

5.2. RE-EVALUATION OF EXTREME FLOODS

As a result of the periodic safety review, the hydrology of extremes must be reviewed, especially when there are indications of insufficient evacuation capacity.

The implementation of new, more demanding regulations or the awareness of increased risk of extremes is also assumed in the NAPs[§], according to the nomenclature of the United Nations.

What are we facing?

- Effective estimation of flood quantiles for really large return periods
- Strongly conditioned by the lack of reliable data associated with extreme floods,
- High uncertainty in estimating the upper tail of the distribution function
- Lack of adequate methodologies, or at least little penetration of new practices in engineering
- Feasibility of the practical application basically oriented to the dimensioning of spillways for large dams

The main problem is the use of extrapolation from known, often very short, hydrological behavior to very extreme events, which are the ones we need to know. In addition, climate change nullifies the stationarity hypothesis that would require a thesis that extrapolation is a valid mechanism.

Classical extrapolation methodologies

- Maximum rainfall data in **24 hours**
- **Adjustment** of a distribution function (Gumbel, SQRT-max, L-Person...) obtaining the quantiles of maximum precipitation in 24 hours, (T = 25, 50, 100 and 500 – 10000 years) **Extrapolation** of doubtful reliability
- **Interpolation** to obtain areal rainfall and application of an **areal** reducing factor
- Allocation of average rainfall in each of the **sub-basins**.
- Artificial hyetographs based on conservative **envelope IDF curves** of the temporal distribution that generate a bias in the estimation of the final probabilities.
- Modelling of the response of the basin through the transformation precipitation-net rainfall-runoff.

Most of the time there is a glaring lack of flow data, non-existent or located in other sections of the river network, etc. with series of just a few decades, with a lack of data or precision in extraordinary flows, if they have been recorded, etc.

In the case of rainfall data, the length of the series is usually longer, still spanning only a few decades and rarely more than a century and with little spatial density. Even so, most of the time it is the only truthful source and that is why the reproduction of the rain-runoff cycle is inevitably resorted to determine events.

[§]National Adaptation Plan

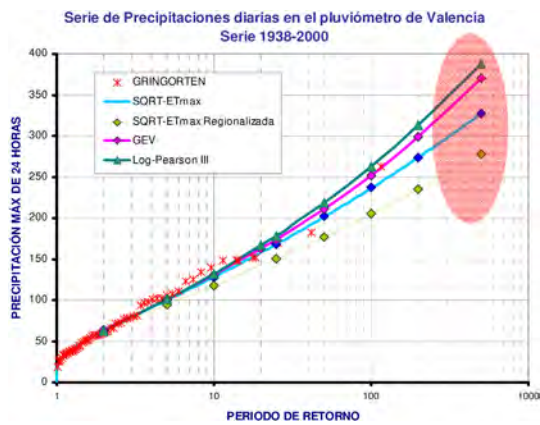


Fig. 7
Uncertainties with classical extrapolation

But within flood events, at least two populations must be distinguished: ordinary and extraordinary floods. If the genesis of both groups is not the same and all events do not belong to a set with the same intrinsic properties, they do not translate into the same statistical properties and two different statistical populations would have to be considered. Be the case of a rainy cold front and a typhoon. They do not have to be analyzed in the same statistical set. If there is little data in a basin and we reduce the events to a smaller number, the difficulty in characterization increases.

That is why methods such as the PMP (WMO, 1986), the Regional Maximum Flood (FMR) (R18) and others that will be referred to in this report, look for data in other neighboring basins, with certain meteorological similarities that facilitate their use on a larger scale of application.

Other attempts propose to identify probabilistic behaviors with double-trend functions, but, if the number of data covers a few decades, it will remain illusory to extrapolate directly to tens of centuries.

5.3. DESIGN EVENT-BASED PRECIPITATION-RUNOFF MODELING

The precipitation-runoff transformation allows us to work with rainfall series, usually with longer data periods, to infer the flood distribution functions.

Precipitation, including its temporal distribution and previous rainfall, is usually the stochastic variable, leaving as descriptive parameters of the transformation the losses through interception and infiltration, the hydrographic characteristics of the basin and its drainage network.

5.4. NEW CURRENT TREND

Nowadays, in many countries, regulation distinguishes the requirement of a design flood, with a return period of around 1,000 years, depending on the risk category, and a much longer return period for the safety flood or the PMF.

The evaluation of the return periods that correspond to the characteristic flows of existing dams, in operation, leads to important challenges:

- Uncertainty in the estimates based on classical methods, the most widespread. In small basins and without direct measurement of tributaries or rainfall, it is more difficult.
- Evaluation of Uncertainty The classic approach to assessing uncertainty in the determination of statistical variables, such as the probability of hydrological extremes, is the Monte Carlo analysis.
- Need to generate probable values of derived variables such as levels, damages, etc., which are variables without recorded values and that may be different despite being a consequence of equiprobable events.
- Impacts of climate change: Increase in the frequency and intensity of extreme events without consensual and easily applied methodologies.
- Limitations of traditional methods: Methodology based on statistics or hydrological models may underestimate extreme conditions.

These are the challenges that are addressed in the following sections of this report.

5.5. PMF

The probable maximum flood (PMF) represents the largest flood event that is reasonably expected to occur. This is especially applied in prey with potential extreme consequences, where conventional statistical methods do not meet the risk criteria or because the country's regulation requires it.

Traditional methods for estimating PMF include statistical analyses of flood data and precipitation-based simulation models. Flood enveloping curves, derived from the analysis of historical maximums, are valuable tools in this context, although their applicability is usually limited to low-latitude regions with high moisture availability.

Climate change conditions can also make hypotheses on which previous estimates of the PMP have been carried out in the past; obsolete.

5.6. AUSTRALIAN ENVELOPING CURVES

Regionalization of flood enveloping curves for preliminary estimates of the probable maximum flood (PMF) for specific flows may be necessary for areas with a lack of data.

Atmospheric reanalysis to explore how maximum precipitable water variability can explain regional differences in extreme floods is now a necessity. An empirical equation was developed based on the relationship between the Francou-Rodier coefficient (k) and the maximum precipitable water, conservatively adjusting the curves to include the largest floods recorded. This approach was tested with a catalog of historical events.

Envelope curves (R08) were generated based on different levels of maximum precipitable water, suitable for various geographical areas, being compatible with detailed studies in the USA, China, Europe and South Africa, showing coherence with recorded severe events. Under changing weather conditions, revision should be necessary in certain regions.

These curves are valuable for feasibility studies and validation of rainfall-based estimates, especially in regions outside the tropics where global curves may underestimate flooding.

Future research should consider other hydrometeorological factors, such as atmospheric rivers, cyclones with long distances, etc. that bring moisture in extreme events. Although the study assumes stationarity in the data, it is necessary to incorporate adjustments for climate changes.

R08 proposes a robust methodology for deriving preliminary estimates of PMFs at the global level. Regionalized enveloping curves make it possible to overcome the limitations of traditional global curves, especially in non-tropical areas. Although these curves are not intended to replace local studies, they do provide a solid basis in the absence of detailed data.

5.7. AN INNOVATIVE METHODOLOGY (FRANCE)

An innovative Methodology for Assessing Extreme Hydrological Events in the Context of Climate Change (R13) is presented by France.

Flood safety assessment in dam design faces significant challenges due to global warming. Traditional methodologies, based on historical rainfall and flow data, are inadequate due to their dependence on a stationary climate (R13).

The Clausius-Clapeyron relationship can give an orientation to this effect:

$$\frac{dp}{dT} = \frac{L}{T\Delta v}$$

where dp/dT is the slope of the curve, L is the latent heat or enthalpy of the phase change and Δv is the variation of specific volume.

This equation gives us a clue about a theoretical 7% increase in the intensity of extreme precipitation for every 1°C increase in atmospheric temperature, although it lacks robust correlation in local applications and shows inconsistent results in specific regions, such as Europe and the tropics (R13).

5.8. NECESSITY OF MORE DATA

The most widespread methodology among the hydrological engineering sector, for the estimation of extreme flood flows, frequently suffers from the scarcity of extreme data to correctly deduce its frequency laws, on all the values of high recurrence period. This generally results in undervaluation or overvaluation of flows due to the small sample size.

- (i) Longer Series: Paleo-Hydrology
- (ii) More geographical space: stochastic transposition

5.9. DATA SERIES EXTENSION: PALEOFLOODS

One temptation to extend the length of data series is paleohydrology.

Paleohydrology can deal with ancient flood events that occurred before systematic measurements existed. Based on geomorphological and stratigraphic records, granulometry of can be tried to evaluate episodes in a very long period of the Holocene. The variability of the natural climate in this last geological period (as the Little Ice Age during XV-XVIII centuries) makes it difficult to incorporate this technique in practice if certain corrections are not made that are not easy to apply.

Periods without floods are also usually useful clues, as long as they were free of distortions of information, such as periods in which certain walls of war defense also defended the cities from floods and therefore did not leave traces easy to interpret.

5.10. REGIONAL FLOOD FREQUENCY ANALYSIS

The estimation of floods for large return periods is strongly conditioned by the lack of reliable data associated with extreme floods, producing large uncertainty in the upper tail estimation of the cumulative distribution function.

In hydrology, obtaining sufficient data at a single site to reliably determine the frequency of rare events through frequency analysis is often challenging. This issue is particularly pronounced for extremely rare events, which are critical for dam safety risk assessments.

To address this limitation, an alternative approach involves substituting time for space to estimate extreme floods. This method leverages hydrological data from multiple locations within a region to overcome the scarcity of long-term records at any individual site. By pooling spatial data from various sites, the approach compensates for the lack of temporal data, providing a more robust basis for estimating the frequency and magnitude of extreme hydrological events. This spatial substitution enhances the reliability of flood frequency analysis, especially for rare and high-impact events.

Three approaches have been considered in the past for regional flood frequency analysis: (1) the average parameter approach, (2) the index flood method, and (3) the specific frequency approach.

5.11. SYNTHETIC GENERATION

The generation of synthetic data, whether in the form of multiple series or continuous simulation, is based on Monte Carlo generation of long and detailed sequences of hydrometeorological variables, including precipitation, air temperature, and wind speed and direction. It is necessary to represent the spatial differences through the catchment basin, it is necessary to generate hydrometeorological variables for several sites simultaneously respecting the correlation and parameters of general coherence at the basin scale. Hydrological response models must transform hydrometeorological series into runoff. Including the effect of reservoirs, for which it is necessary to introduce operating rules that are often linked to the event.

To address these challenges, the EXAR project has been developed using an approach based on continuous hydrometeorological simulations (R05) and subsequently extended to the entire Swiss territory through the EXCH project. They are based on a continuous hydrological simulation, to estimate events with return periods from 1,000 to more than 10,000 years in order to comply with the current national regulation in Switzerland (WRFA) where a return flood of 1,000 years is prescribed as design flood and a value increased by 50% or the PMF prescribed as safety flood.

It is the lack of data in small alpine basins and the uncertainty arising from climate change that forces a new approach based on continuous simulations, developed in the EXAR and ESXCH (extended) projects combining climate and hydrological models to generate realistic series of extreme events. Variables such as peak flow, volume and duration of floods, and previous conditions to consider the influence of factors such as snow melting and soil saturation are also included.

The EXAR project on the Aare River (17,700 km²) was extended to more than 225 dams under federal supervision, in the EXCH project to provide tools to assess risks in small basins. Before its adoption in the regulations, it is necessary to identify the limitations in basins without calibration.

It is not fully demonstrated that the probability functions used for the generation of synthetic series are representative of the tails for really extraordinary events that could be due to phenomena not adequately represented in the stochastic probability functions adopted for the generation of series, even if these are very long.

5.12. CONCEPTUAL MODELS WITH PHYSICAL BASIS

To avoid the lack of sufficient empirical data, it is necessary to know the physical processes that justify them. That is the field of conceptual hydrological models.

The physical processes known and formulated through conceptual models make it possible to take advantage of records of events that occurred in other areas through transposition, or consideration of the conditions under which they would have occurred in another location. Under stationary weather conditions it is possible to carry out this transposition. It is more difficult to do so if the climate change scenario applies.

“Transposition” is the alteration of the descriptive parameters of a storm so that it can be relocated in time and space for use as potential precipitation data in a location other than the one where it occurred.

In the PMP estimation methodology (WMO), its descriptor variables are corrected based on the different distance to the moisture source, the orographic effect of the interposed barrier and even a temporal transposition to other conditions of expected maximum humidity.

Some tests as GSST** provide a more robust analysis of the transposability of model parameters between catchments (R13). Surgen metodologías (R13) para soslayar estas dificultades como la de combinar la generación estocástica de datos climáticos para proveer datos de entrada para modelos hidrológicos usando proyecciones climáticas y el uso de modelos múltiples. Los resultados de modelos calibrados dinámicamente pueden reflejar mejor las condiciones climáticas futuras. La aplicación a la cuenca del Río Madeira (Brasil) muestra que es posible mejorar proyecciones más robustas de caudales extremos bajo escenarios de cambio climático.

5.13. STOCHASTIC TRANSPOSITION

Another option is to carry out a stochastic transposition. "Stochastic transposition" which would be the generalization of transposition, as defined in the PMP methodology, but with variables that are not maximized but probabilistically treated. In a stochastic approach, then, hydrological models are fed by random variables known from their probabilistic point of view. Event generation procedures for the Monte Carlo method must follow the functions of probability distributions, including cross-dependencies, if there are any when there is non-zero covariance. The use of the stochastic approach with precipitation information from a transposition area allows the estimation of magnitude-frequency curves of peak flows, hydrograph volumes, maximum reservoir levels, or other event-defining parameters.

Storm transposition is a viable alternative to effectively use information, external to the basin under analysis, allowing a substantial improvement in the reliability in the estimation of these quantiles of high recurrence in F(Q) distribution so that a greater number of truly extreme events are available and that they provide knowledge to that special subset of storms whose pattern is different from ordinary storms.

Only in the particular case of a totally homogeneous transposition zone where the storms preserve their properties, is this transposition automatic and allows the extension of the spatial integral without further precautions. Storm transposition principles were introduced in the early 60's and widely developed by Fofoula (1989) and Fontaine (1989), who tried to improve previous difficulties for real application in Harriman Dam. At that time heavy difficulties made advances for real applications were really slowed down.

**Generalized split-sample test

However, the need to extend the area to find truly extraordinary phenomena recorded does not always preserve this homogeneity, mainly due to the orographic effects that characterize both territories. A reduced but extraordinary set of selected events constitutes the sample of raw data which needs to be adequately transposed to a reference to be then analyzed under a complex framework to define parametric definition of isolated probabilistic models of frequency, AMC (Antecedent Moisture Condition), temporal and areal patterns, orientation or precipitation depth.

But decades later, substantial improvement of quantiles estimation was obtained, after a general methodological framework based on such principles, which incorporate the required meteorological and topographical factors conditioning the process. Thanks to these improvements the feasibility for practical application of such methodology effectively oriented towards the optimal dimensioning of large dams was proved, becoming one promising technique. This promising methodology has been developed based on principles of the stochastic transposition of storms using the depth of maximum precipitable water in the atmosphere around a given area as the key concept to be considered despite the limitations derived from the orographic effects.

This drawback was demolished (Cifres, 2016) through the concept of the orographic ellipse and the central gradient, which allowed the most conditioning meteorological and orographic factors to be incorporated in a systematic and physically based way. In this way, the feasibility in practice of this methodology was demonstrated, specifically aimed at improving the methods for the dimensioning of hydraulic infrastructures for flood defense and hydrological risk assessment. The study area is the arc of the Gulf of Valencia (Spain). For extreme storms, by means of a physically based development, it is feasible to make the orographic conditioning factor independent in the transposition procedure, in the vicinity of any geographical point.

First of all, it must be stated that for very high return periods, only really severe storms can describe statistically the phenomena and characterization of them cannot be inferred from ordinary or medium events. Transposition area must be defined as capable of providing a number of really extreme events but also homogeneous enough to allow storms to be transposed to a common reference.

Once selected events surpassing threshold of severity criteria have been identified, storm transposition must be carried out in order to create a statistically homogeneous database. Following the principles of PMP transposition (WMO 1986), some improvements were introduced into a water content atmospheric balance, considering not only saturated water profile, wind profile, dew point for humidity source, orography but also elevation of cold interface and precipitation in previous zones.

Separated probability distribution functions of mentioned defining factors must be assessed, making it possible to derive and quantify hypothetic precipitation amounts and distribution under various meteorological conditions or possible geographical places, different from those that historically existed when the extreme

event occurred. This must be done covering the range of their variations in the transposition area creating the result database as a synthetic history of rare events. Total number of parameters must be carefully reduced to gain parsimony and robustness.

The procedure allows extending the actual sample available after the historical records, and therefore, estimating more consistently the upper tail of the extreme value distribution of flood peaks by means of a numerical integration of created result database. Theoretical approach needs meteorological and orographic models to be able to transform events from a large enough zone. These models were conceived by taking into account orography when re-evaluating storms from different locations.

Orography has an influence on the behavior of air masses movement and thus storm shape and orientation could follow its conditions. The complex problem of the topographical influence in the space-time structural properties of extreme precipitation events, is tackled in an original framework seeking a new reduction of stochastic parameters.

We can introduce the concept of central gradient (Cifres, 2007), linked to the depth of maximum precipitable water in the atmosphere, and its variation in the different directions around a given geographical point. Such concept makes it possible to isolate in practice the influence of the topography in the transposition procedure, representing a key aspect gaining robustness to the process. The proposed definition of Central gradient will be “ $\Delta W/d$ ” as difference in water content per unit of distance.

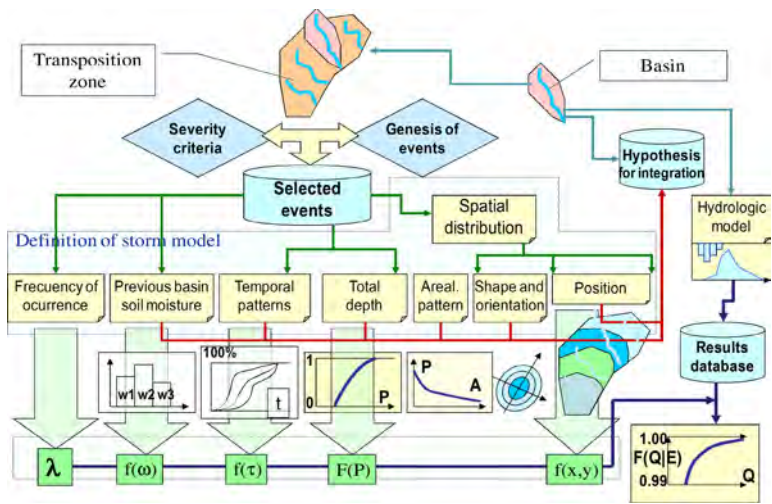


Fig. 8
Flow chart for Stochastic and Orographic Transposition

The technique has been successfully applied when reviewing hydrological safety of Algar dam in Valencia where rainfall depths over 1000 mm in 48 hours have been registered.

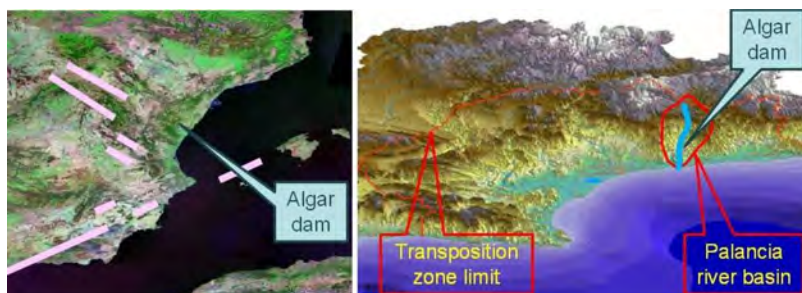


Fig. 9
Transposition zone for Palancia basin (Algar dam case)

These extreme precipitation events used to take place during October-November, and result from the combination of several factors:

- High temperatures in the Mediterranean Sea
- A low-pressure air mass blocked by a high pressure one located in central Europe, forcing warm winds from Sahara, which transport large amounts of humidity, to face Spanish coastal ridges.
- Orographic conditions forcing ascending of the air masses
- Very cold air pool in higher layers of the atmosphere

Extreme storms result from the simultaneous combination of all these factors, even if each of them is moderate or not so extreme. The final location of the storm in a small catchment can result in a really extreme event, never seen there before.

Only one extreme event has actually occurred in the basin, but the evaluation of the flood probability distribution function in that location has been obtained by integration over the entire transposition region, taking advantage of highest 33 events^{††} in the entire transposition zone. Nevertheless, this event selection implies that below 25 years return period floods cannot be reliably assessed, since only really extreme events are described by this probability function.

^{††}Identified by means of a threshold criterium taking into account also meteorological genesis

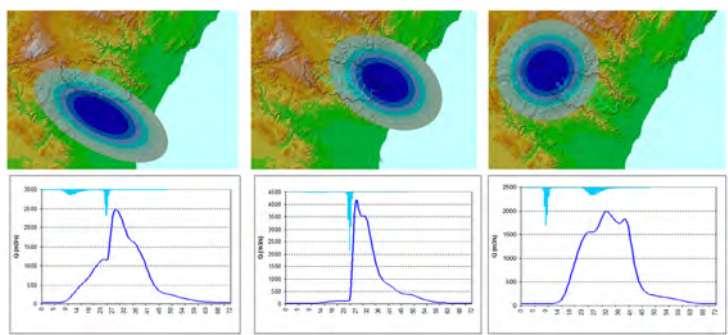


Fig. 10
Different simulations varying position, time pattern and depth

Due to the ability of the methodology assessing very high return period floods and similarities in the procedures between proposed and PMF approaches, PMF probability can be assessed in some way.

5.14. CLIMATE CHANGE IMPACT

A sensitivity analysis just modifying dew point in humidity source helps us understand possible changes in probability by means of adopted meteorological model that governs storm depths. A simple exercise rising dew point by +3°C carried out shows how sea temperature endangers potential meteorological conditions to produce heavy storms due to the higher potential for evaporation and humidity transportation.

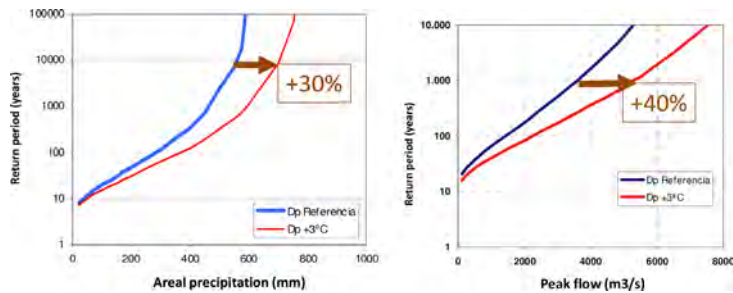


Fig. 11
Impact of Climate change on flood probabilities due to dew point increase

As a result of this experiment, a rise of only 3 °C in seawater temperature, keeping the same values for the same set of the rest of the parameters, means near 40% rise of peak flow increment for extreme floods.

So, feasibility carrying out stochastic and orographic transposition for practical purposes is proven. Physically based models can reduce stochastic component, giving to the overall model more parsimony. We can take practical advantages from detailed studies about winds, temperatures and orography if we promote multi-disciplinary teams including meteorologists to define conceptual models able to facilitate transposition from larger areas.

Stochastic transposition, as well as PMP approaches, consider physical limits and thus tend to lower values than extrapolation for very high return periods where the last ones are totally rejectable. Nevertheless, an underestimation in design range can also be found. Designers and regulators must be aware that a review of assumptions and methodologies could lead to a less safe assessment than they thought.

The physical and meteorological factors used allow for expanding in practice the relevant information contained in the extreme precipitation historical records, which in turn provides the basis for a more robust and reliable estimate of extreme flood probabilities, when compared to the more limited methods based on the classical statistical inference from a reduced sample.

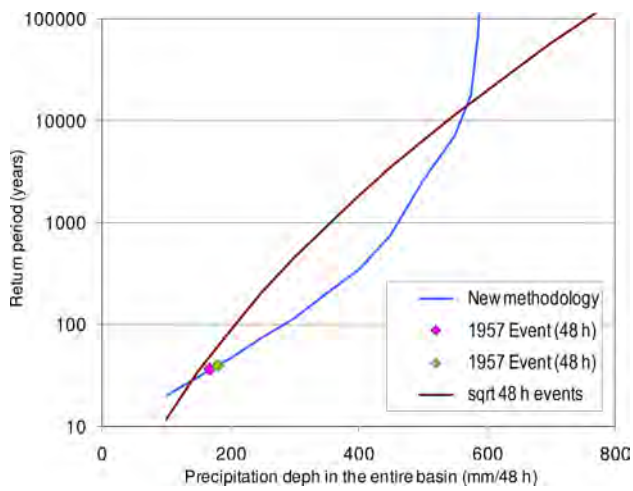


Fig. 12
Comparison between classical and proposed methodology results

5.15. UNCERTAINTY

The floods calculated for use in design, review, reassessment, or risk analysis processes should be associated with their level of uncertainty, especially when they are to be incorporated into safety related decision-making.

The sources of uncertainty are so numerous in hydrology that the indefinite decomposition of reality into smaller and smaller elements, which would be made possible by formidably efficient calculation techniques, does not necessarily bring a convincing improvement to the final quality of a study.

The possibility of detailed analysis of the reliability of the data, the credibility of each of the steps or elements of the calculation methodology used, etc. is not, when multiplying the parameters, a strategy always recommended for the final determination of uncertainty, as a substitute for solid expert advice.

Predictive uncertainty in flood prediction is defined as the probability function of occurrence of a future value of a variable (such as water level, peak flow or hydrograph volume) rather than a mere scalar value.

There is a conceptual difference between the "model uncertainty" commonly used for verification and predictive uncertainty, which is used when forecasting the future and where it must be related to the initial data.

There are currently available processors of uncertainty operational flood prediction systems (Todini 2009) that can be continuous (Hydrological Uncertainty Processor, Bayesian Model Average, Conditional Model Processor, etc.) or binary (Logistic Regression, Bayesian Binary Multivariate Processor, etc.). The incorporation of predictive uncertainty in the decision-making process is a must for improving the current tendency to omit the most widespread practice.

6. ACTING FACING EXTREMES

Aware of the magnitude and probability of truly extraordinary events to be faced, inaction is not acceptable. The list of initiatives to be taken to mitigate the risk may be structural or non-structural in nature.

Among the structural actions, it is necessary to consider the construction of dams that create lamination reservoirs, considering the joint action in the basin with other infrastructures, the review and adaptation of the dams to new load scenarios,

change of maximum expected levels, modification or expansion of spillways or establishment of complementary spillways, emergency or fuses, and also channeling in river sections, levees, drainage systems, etc.

Among the non-structural ones, the adoption of optimal operating rules, including the establishment of safeguards, seasonal emptying and preventive reservoir releases, risk mapping, early warning systems, implementation of emergency plans, improvement of resilience in downstream prone areas, land management, education of civil society and its better involvement in the preparation of plans and also the promotion of better governance for extreme events, through institutional reinforcement.

The widespread practice in dam safety, with periodic reviews that include climate change, will allow the detection of changes in risk that lead to the application of actions leading to the recovery of tolerable risk levels.

A large part of these structural and non-structural actions is described in the papers presented to this Congress under this Q110, as they are designed to deal with extreme hydrological phenomena.

6.1. SPILLWAYS

A certain investment effort is already being made to improve the flood evacuation system, many of them in modification of spillways, considering:

1. Updating of spillways capacity or addition of complementary spillways.
2. Increase in the maximum permitted water level by means of structural reinforcement.
3. Rehabilitation of hydromechanical equipment and improvement of operation during floods.

6.1.1. *Drin river basin*

The re-evaluation of the hydrological safety of dams at the basin scale requires a comprehensive approach, as is the case of the Drini River (R20) in Albania, where the safety of seven large dams and six hydroelectric power plants (HPPs) that generate approximately 70% of the country's electricity is analyzed. The evaluation promoted improved operation and planned measures to increase the energy capacity and safety of the dams, including the upgrade of flood evacuation capabilities.

The system uses the PANTA Rhei model^{††} (see Archfield, 2015) to simulate rainfall and melting events, as well as the water balance of the system under the influence of factors such as climate change, land use, population growth and how societies influence the hydrological cycle and vice versa. The analysis of precipitation events, generating probable maximum flows (PMF) and evaluating the response of the system to extreme events identified the need to increase the discharge capacities of the Fierza (additional 2,080 m³/s) and Koman (additional 3,000 m³/s) dams to safely manage the PMFs and update the operating patterns in the basin.

The Drini River system, as is foreseeable in other basins where a comprehensive reanalysis is carried out, will require significant investments to increase its discharge capacity and ensure safety against extreme events. This puts the valuation of human life as the main risk factor on the table in economic evaluation.

6.1.2. *Regajo dam*

Sometimes it is the implementation of new rules or regulations that requires the revision of the hydrology that was used for the dimensioning of the spillway of a dam. This is, for example, the case of Spain (R04), where a new regulation has been enacted^{§§}, where for concrete dams the adoption of design and extreme floods with return periods of 1000 and 5000 years is required. In Spain, this type of dam predominates in the more than 1200 large dams in operation.

This is the case of the Regajo dam (R4), located in Castellón (Spain), built in 1962 and designed for irrigation. To upgrade the evacuation capacity of 437 m³/s with which it was designed for a return period of 500 years, a new spillway has been designed to go to 1800 m³/s for a return period of 1000 years in accordance with a new regulation and a new official hydrology.

A new complementary spillway, of 132 meters, is to be combined with a reduction of one meter in the maximum exploitation level, the elevation by one meter of the crest of the dam and the replacement of the gates of the existing spillway.

The flow poured by the new spillway over the abutment must dissipate energy in a stilling pool and then into a channel that redirects the water to the foot of the dam. Sometimes, the return and dissipation of energy is one of the main challenges when trying to upgrade the evacuation capacity of large flows as in the case cited.

^{††}International Union of Geodetic and Geophysical Sciences (IUGG)

^{§§}Spanish Technical Safety Standards 2021, NTS

6.1.3. *Structural review in France*

The modification of spillways to increase evacuation capacity often entails structural revision if the normal or extraordinary levels of operation are modified, and it is necessary to ensure that the new operation remains within the safety margins required by the regulation, and without reducing the existing ones, except in exceptional cases of availability of large margins previously available.

Some examples in France illustrate this, such as the La Ravière reservoir (R14) through the construction of an additional PKW spillway, increasing the maximum permitted water level by 50 cm after a detailed structural analysis. Likewise, the La Laye Reservoir (R14), through the construction of a lateral surface spillway with a 30 m long labyrinth spillway and an increase in the maximum water level and elevation of the impermeable core of the reservoir and the Pinet Reservoir (R14) where the modification of the existing gates and optimization of the profiles of the piers of the bridge were carried out, along with a structural analysis to identify margins of stability and adjust the design criteria.

6.1.4. *Tragedy in Italy*

The tragedy of Molare (R16) and the collapse of the secondary dam (1935) due to a storm of great intensity that caused and more than 100 deaths in the city of Ovada in the valley of the Orba River (Genoa, Italy).

The total capacity of the spillways was insufficient compared to the estimated peak flow of the event (2000-2500 m³/s). The automatic siphons and side spillway were unable to evacuate effectively due to poor designs and debris obstruction.

Although the rains of August 13, 1935, were intense (370 mm in 10 hours), their return period was estimated at 200-300 years, less exceptional than previously thought. Still, existing systems were unable to handle peak flows, contributing to the overfilling and collapse of the saddle dam.

Events in 2019 showed similar magnitudes in terms of rainfall volume and flows, reinforcing the idea that the tragedy could have been avoided with more robust designs. That tragedy highlights the risks of inadequate designs and the importance of hydrological-hydraulic planning. Among the main lessons learned, we underline the need to consider events with return periods of up to 1000 years in dam design.

The Molare disaster was caused by failures in the design of evacuation structures and in the assessment of local geological conditions. Numerical simulations have shown that the 1935 event was not exceptional and that, with appropriate preventive measures, such as more efficient discharge systems, the collapse could

have been avoided. This analysis underscores the importance of resilient designs in the face of extreme events, especially in the context of climate change.

6.2. LABYRINTHS - PKW SPILLWAYS^{***}

PKW spillways, as an efficient solution in the management of flows in dams, have gained popularity in recent decades thanks to their compact design and increased discharge capacity, characteristics that make them ideal to face challenges related to the need to increase evacuation capacity without reducing the volume of operation of the reservoir and without increasing the levels (R07) of existing structures.

These structures represent innovative solutions engineered to efficiently discharge floodwaters, overcoming the geometric constraints of traditional labyrinth weirs. By enabling the management of large flow volumes, they significantly reduce the risk of overflow and structural failure. These designs are particularly advantageous for both new dam constructions and upgrading existing dam projects, including the reform of current spillways or the addition of complementary ones. Their compact and efficient design makes them ideal for sites with limited space, offering a practical and effective approach to enhancing flood management and dam safety.

6.2.1. *South African cases*

The revision of the evacuation capacity may be the result of other modifications, such as the raising of dams, to both increase storage capacity and safety against floods (R17) where an extensive collection of discharge options is proposed by means of conventional gates, rubber dams, labyrinth structures, etc.

This is also the case of Tzaneen dam (R18) located in Limpopo, South Africa, designed in 1977, and which now seeks to increase its storage capacity and guarantee security against extreme events.

The increase in the height of the dam, and the lowering of the spillway threshold and the installation of a hybrid labyrinth structure (R18) or others (R17) are compatible to update the flow for extreme events such as those established in the South African regulation based on the concept of Regional Maximum Flooding (FMR).^{†††}

^{***} *Piano Key Weirs*

^{†††} *Regulations Regarding Safety of Dams South African Gvnmt 2012*

Greater demands on energy dissipation make it necessary to reform the still basin, which may involve changing dimensions, reinforcing and anchoring the protection slabs (R18).

6.2.2. *French and Vietnamese cases*

The case of the La Ravière dam (France, R2) is presented by EDF⁺⁺⁺. It is a buttress-type gravity dam with a height of 40 meters with a discharge capacity of 1000 m³/s. Subsequent reports, with new hydrological calculations, established the need to increase the capacity to 1720 m³/s, for which it was decided to complement the gate system with a PKW on the left bank.

The installed PKW is 4.22 m high, has an overall width of 25.82 m and a development length of 176.6 m. Its additional discharge capacity is 300 m³/s, which increases the safety of the dam by 30%. This spillway operates autonomously, significantly reducing the risks associated with mechanical or human failure.

The same paper refers to the case of the Van Phong Dam, Vietnam (R2) located 70 km from Quy Nhon, dedicated to the irrigation. The configuration of its flood evacuation system is mixed, combining an asymmetrical PKW on the sides, with a conventional spillway of 10 radial gates in the central part. This design allows the reservoir level to be maximized without causing an increase in upstream levels. The PKW is capable of handling floods of 1000 years of return period with peaks of 15,350 m³/s.

The combined use of PKW and gates ensures efficient management of the reservoir level and a high level of evacuation in extreme situations, with an economic advantage, although with the requirement to pay attention to the change in downstream dynamics, in addition to requiring special care in the conditions of reflow of flows to the downstream river under adequate energy conditions.

In both cases studied, PKWs have proven to be a cost-effective and efficient option. At La Ravière, PKW significantly increased its unloading capacity without requiring major structural modifications. At Van Phong, the combination of PKW and radial gates optimized the design to meet the project's hydraulic and economic needs.

These examples highlight how the use of advanced technologies and hybrid design approaches can address current and future challenges in water resource management.

Optimization of piano spillways (PKWs) has been carried out in other two Vietnamese projects (R07) to improve flood discharge capacity and downstream

⁺⁺⁺Electricité de France

hydraulic conditions. The projects: Da Si and Cao Ngoi improve hydraulic efficiency by demonstrating better discharge performance with trapezoidal and curved designs, even concluding that the curved PKW increased discharge efficiency by 9-15%.

6.2.3. *A singular swedish project*

The Lillflyforsen reservoir (R03), in central Sweden, was built in 1965 as part of a hydroelectric scheme. The gravity dam is 30 meters high accompanied by an embankment dam of lower height. Over the years, the reservoir has presented two main problems: structural deterioration in the earthfall dam and insufficient capacity of the spillway to handle extreme flows during floods.

To address these shortcomings and comply with **current safety regulations**, an innovative solution is proposed: the construction of a piano spillway (PKW) downstream of the existing dam that will be the first of its kind to be built in Sweden. This design not only significantly increases the discharge capacity but also represents a more cost-effective alternative compared to the complete rehabilitation of the dam from loose materials and the spillway gates.

The final design of the PKW was based on tests on physical scale models, allowing defining the geometry, discharge capacity and energy dissipation to be optimized.

Energy dissipation is a key aspect in PKW designs to mitigate erosion in the impact zone on the bedrock. Horizontal steps at the PKW exits and an aeration system were also designed.

The design and operation of the PKW must also address challenges associated with the Nordic climate. These include the formation of ice that imposes loads in winter on the hydraulic structures, as well as floating trees, especially during floods. Sometimes floating barriers are installed, many times of dubious effectiveness in large floods.

6.3. OVERTOPPING

While gravity concrete dams (PG) are vulnerable to floods due to the effect of instability that could produce excessive over-elevation compared to the design dam, it is the overflow that threatens the embankment dams. This overflow, which can also be caused by landslides in the reservoir, seismic waves or even by sudden settlement induced by seismic action, is more frequent due to extreme hydrological phenomena. Reducing this vulnerability has been a challenge and the subject of research in recent decades.

Faced with this scenario, the degree of resilience of the slopes of fill dams in the face of moderate spills has been studied. ICOLD has addressed the issue at various conferences (Stavanger 2015) and work continues on the determination of the breakage threshold according to the specific flow, height or energy, type of material, etc. as does the Working Group on *Overflowing and Overtopping Erosion of the ICOLD European Club* together with other initiatives such as the Seminar on Dam Protections Against Overtopping (April 2025 in Stillwater, USA) to expand knowledge of the risks and possibilities of prevention of associated damage. The current trend is to propose solutions that manage to avoid or reduce damage to acceptable levels in the event of a crest spill in both dams and dikes (Moran et al, 2023). Among them are fusible spillways, emergency spillways or slope protection in the body of the dam.

The prediction of the effects of a dam failure depends, in addition to the expected inflow hydrograph, on two hydraulic factors: how the rupture occurs, and which hydrograph occurs, and on the propagation of the downstream outflow hydrograph, with the corresponding overflow "in prone zones"

Not only new hydraulic structures have been proposed to address excess flow, by the contributing authors to this congress.

Overtopping in fill dams, as the main cause of dam failure, can be faced by means of solutions of cemented materials suitable for resisting the flow over the crest and downstream slope. In the world, most dams are of the loose material type, more adaptable to all types of foundations, but with less capacity to resist overflow.

The resistance of dams and levees slopes to external erosion during overflows varies widely depending on the type of soil, its water content, density and granulometry (R15). Tests such as the jet erosion test (JET), in which the erosion depth is measured as a function of time, are proposed for its determination. It can be performed both in the laboratory and on site.

Another option is the overflow test, such as the one carried out in the CNR-CESAME laboratory within the OVERCOME (R15) project, using models of dikes built with sand and gravel from the Rhône River. This consists of maintaining a constant flow over the dike until the four successive phases are observed: filling of the reservoir, surface erosion, erosion at the head and formation of a breach.

Significant differences between treated and untreated soils, the former being more resistant where the influence of moisture content and density on the speed and magnitude of erosion can be verified.

6.3.1. *Chinese contribution to CMD*

Increasing the resilience of these dams to the overtopping risk can be achieved through the cemented material dam (CMD) technique, an innovative technology that

combines local materials with cementing agents. China is leading this new technology (R27) through research and subsequent implementation in real cases with the use of local materials, such as soil, gravel and rock, mixed with cement, fly ash and other additives to form a cohesive matrix with improved shear strength.

Depending on the size of the aggregates, the CMDs are usually referred to as Cemented Soil Dams (CSD): They use fine particles such as soil and sand, Gravel, Sand and Cemented Rock Dams (CSGRD): They use aggregates with diameters of up to 150 mm or even Cemented Rock Dams (CRD).

The IWHR authors present the study under extreme conditions such as overflows for moderately high dams where hydraulic loads are already very significant. They present cases in China, where more than 40 MDCs have already been implemented. The example of the Xijiang Project (Guizhou) with a height of 48.5 m that resisted an overflow of 48 hours with a water level of 2 m, demonstrating high resistance to erosion or the Shoukoubu Project (Shanxi) with a height of 61.4 m where it has been possible to reduce the cost significantly through the CMD technique are of great interest as a consolidation of the applicability of this technique. Also, for existing dams, downstream slope reinforcement using CMD can mean improved overflow resistance and erosion mitigation capacity.

CMDs represent a significant advance and offer in many cases an adaptable and robust solution to improve the resilience of hydraulic infrastructures in the face of extreme conditions.

6.4. ENERGY DISSIPATION

Whatever the type of evacuated flow increase solution, it is essential to review the energy dissipation system for an up-to-date flow. Sometimes it is necessary to create a dissipating pool (R2), adapt the existing one (R18). PKWs installed in dams require effective energy dissipation techniques to prevent erosion downstream (R07) in labyrinths.

6.4.1. *Kariba dam*

Sometimes the problem of reintegrating flows into the river in safe and stable conditions does not only correspond to extreme floods, but also to the persistence in the dissipation of energy for years. This is the case of the Kariba dam, on the Zambezi River, which suffered erosion problems due to continuous discharges from its spillway. This process created an impact shaft 80 meters deep, with a corresponding risk to the stability of the dam. The corrective actions taken are described in paper R06. The interesting description of the actions to recover safety, by means of excavation, slab, injections, etc.

The evaluation of the erodibility of the bedrock where the flows evacuated at the dam toe are restored can be estimated with the *Fatigue Method* based on the Paris-Erdogan Law (1963) which is used in rock mechanics to predict the growth of cracks under cyclic loads. This law describes how a crack grows with the number of load cycles, based on the amplitude range of the stress intensity factor.

The evaluation of geomechanical parameters such as rock mass strength and block size in dam weirs where the determination of erosion risks in hydraulic projects is necessary can be based on Annandale's (1995) rational method:

An important lesson learned is that evacuation is not always the critical point in the face of extreme hydrological phenomena, but that the return to the river of evacuated flows, often revised upwards, may require actions in the restitution zone to improve the resilience of the project.

6.5. ROUTING FLOODS AND PEAK ATTENUATION

It is important to analyze the role of the reservoir, with increased evacuation capacity, in contributing to the lamination of floods, reduction of peaks or delay in the time of arrival at critical points downstream. The surprise effect, in the face of a higher slope of the hydrograph (more abrupt growth of the flow) must be implemented in the warning systems and emergency plans, studying the vulnerability of the downstream population.

Hybrid solutions with gate-controlled spillways (R2) that mobilize larger reservoir volumes in the rolling process, mitigate the problem if good operating standards are implemented. On the other hand, the desire to lose the minimum or no volume of reservoir with labyrinthine systems goes hand in hand with the reduction of the capacity to attenuate flood peaks, which is not always acceptable.

6.6. TEMPERATURE

Apart from hydrological extremes, there have been some contributions dealing with other climatic extremes, such as thermal extremes

Other climatic extremes such as thermal extremes, heat waves and extreme cold, could have an influence on the behavior and safety of the dams. EDF presents the case (R11) of arch dams, highly sensitive to thermal loads, a methodology based on increased thermal loads following the guidelines of the French committee of large dams (CFBR).

The characterization of increased thermal loads is addressed (R11) using the thermal temporary seasonal hydrostatic model (HSTT) to quantify the effect of seasonal temperatures and average daily deviations. This model includes

irreversible effect, reversible hydrostatic effect and thermal effect to estimate radial displacements due to extreme temperatures, and with the application of Gumbel law to evaluate the probability of occurrence of critical events. 15 dams were studied during the 2022 heatwave in France, confirming the good behavior of the dams studied, highlighting the reversibility of the observed phenomena.

Although not an extreme hydrological phenomenon, early thermal cracking, caused by the heat of hydration of cement after construction, can compromise structural integrity, cause leaks and even the collapse of dams. Traditionally, temperature control techniques, such as water cooling through embedded circuits, have been applied manually, resulting in moderate efficiency.

The development of intelligent control systems, which incorporate Internet of Things (IoT) technologies, artificial intelligence and real-time feedback platforms, with the support of 3D thermal models, offers an advanced solution, an intelligent temperature control system applied in the construction of the Julius Nyerere hydroelectric dam in Tanzania (R21), highlighting its ability to meet the challenges of hot and humid climates and massive concrete construction.

The intelligent temperature control system proved to be an effective solution for managing hydration heat in massive concrete projects through real-time adaptive control, structural risk reduction, and resource optimization. With global warming, it could be a more common requirement.

Other climate concerns on dams are mentioned by Indonesia (R19). Reservoir operation patterns significantly impact the material integrity of aging embankment dams (≥ 50 years old), particularly those built with residual soil. Changes in water levels and rainfall accelerate material degradation, posing risks to dam safety.

The need for continuous monitoring and assessment, especially in tropical regions where environmental factors intensify deterioration is highlighted. By integrating geotechnical and hydrological evaluations, it provides a framework for improving the management and safety of aging dams. This concern is not only focused on extreme weather conditions or floods, but also on the conditions that the climate imposes on dams in both tropical conditions from the point of view of climate and geological conditions given the types of soils available

6.7. LANDSLIDES

Other closely related extraordinary phenomena, such as waves caused by slope landslides, extraordinary sedimentation dragging or debris flows in addition to the flood flows themselves that exceed design capabilities, require innovative approaches to dam management and safety.

Since the accident of the Vajont dam in 1963, the threat of landslides that can generate dynamic waves in reservoirs has been the subject of follow-up study, improvement in calculation mechanisms and monitoring techniques (ICOLD Bull 124).

Following accumulated rainfall exceeding 1,000 mm, a landslide upstream of the Hiranabe Dam in Japan (R09) was triggered, causing more than 300,000 m³ of debris flow into the reservoir, and the ensuing wave caused an overflow that reached about 2 m above the crest of the dam, and the overflow lasted for a dozen seconds. Despite the overflow, there was no significant anomaly in the dam body, and power generation resumed two months after the recovery of the flood spillway gate control equipment.

Cases are reported in China (R24), where significant tensile cracks are identified due to rapid drops in the reservoir water level. Through satellite radar interferometry (INSAR) analysis, it was determined that both bodies remain in a slow deformation stage, with critical structural stability after the reservoir is filled. From the stability analyses, considering normal operating conditions, rainfall, sudden drops in the water level and seismic effects, safety coefficients oscillate close to the unit are evaluated. The main slip modes include planar faults related to underlying geological structures, such as faults and gneissic fractures.

Two- or three-dimensional numerical models allow the complete process of the landslides and waves generated to be simulated. The resulting waves are highly dependent on the kinematic parameters of the entry of material into the body of water, resulting in waves of great amplitude in some cases (Kofoed, Cifres & Kronborg, 2002). These waves propagate rapidly upstream and downstream depending on the depth of the lake.

In the reported case (R24) the dam was breached, causing it to overflow in two phases: the first in less than two minutes with a maximum average depth of 2.75 m and a second less than three minutes, affecting downstream of the dam, without causing flooding.

It may be necessary to assess the impact of waves on the dam structure by stress analysis under static and dynamic conditions (R24). The reported cases showed acceptable conditions with tensile stresses slightly above the limit that were very localized without compromising overall stability in both static and dynamic regimes.

6.8. DAM MANAGEMENT

The need for proactive (R09) and integrated approaches to dam management should be highlighted. Incorporating specific measures for flow and sedimentation,

supported by numerical analysis and adaptive planning, is crucial to improve resilience to extreme hydrological events.

The implementation of integrated strategies that combine structural and operational measures, developing remote operating systems and security devices in the event of extreme events is recommended. Continuous monitoring must be followed by a correct communication of the risks identified, so that they can be incorporated into the emergency mechanisms.

6.8.1. *Advances in dam break and wave propagation models*

The hydrograph of the outflow of a reservoir due to the rupture of an embankment dam is usually estimated by hypotheses about the characteristics of the rupture breach based on the geometric evolution of the breach, which assumes that the breach progressively increases in size over a given time until it reaches its final shape. Parameters such as the maximum width of the breach, which depends on the characteristics of the material and hydraulic conditions and the height of the breach, which is generally adopted up to the level of the channel at the base of the dam. Also, the time of formation of the breach: It defines how quickly the breakout develops. It can depend on the strength of the material and the volume of water stored.

Prior to the formulation of more developed models, definitions of the gap based on empirical data were used, such as the MacDonald and Langridge-Monopolis (1984) equations, which allow inferring the size and time of formation of the gap, or those of Singh and Snorrason (1984), which related the peak flow to the dimensions of the reservoir and the geometry of the dam. Later, Froehlich's equations (1995) proposed the relationship of the width and time of formation of the breach with the volume stored in the reservoir and the height of water above the breach. They are models that are quick to apply, but they lack the precision to provide reliability in the event of a real emergency. An improvement, by means of simplified physical models are still dependent on simplifications or empirical hypotheses.

Subsequently, commercial software explicitly simulates using numerical hydrodynamic models, taking into account the progressive erosion of the dam material as a function of the hydraulic gradient and the properties of the materials, including the feedback between the increase in flow and the widening of the gap.

These relationships are the subject of experimental research in laboratories (R26) carried out with scale models and parametric numerical simulations. These investigations highlight the erosion processes and failure dynamics in each area of the dam: protective layer, filter and central core. The relationship with different parts in zoned dams with heterogeneous section with materials of different behavior, such

as shells, filters or cores, is of interest. The R26 paper justifies a high correlation in failure progression between scale experiments and numerical simulations shown.

Detailed three-dimensional numerical models allow for a more accurate representation of the hydraulic and mechanical processes involved, although they are complex to implement. This is the case of the proposed high-precision model (R23) that combines hydrodynamic equations, turbulence and transport of dam materials.

The contrast with experiments (R23), such as those carried out at the University of Leuven, has made it possible to accurately replicate the triangular vortices and erosion patterns at the bottom of the channel, confirming its ability to simulate complex flow dynamics or even bidirectional gaps.

By combining sediment transport equations and instability criteria, it is able to address challenges in predicting dam failure of heterogeneous materials under overflow conditions and demonstrates its applicability in complex cases.

The need for proactive (R09) and integrated approaches to dam management should be highlighted. Incorporating specific measures for flow and sedimentation, supported by numerical analysis and adaptive planning, is crucial to improve resilience to extreme hydrological events.

The implementation of integrated strategies that combine structural and operational measures, developing remote operating systems and security devices in the event of extreme events is recommended. Continuous monitoring must be followed by a correct communication of the risks identified, so that they can be incorporated into the emergency mechanisms.

The hydrograph of the outflow of a reservoir due to the rupture of a dam of loose materials is usually estimated by hypotheses about the characteristics of the rupture breach based on the geometric evolution of the breach, which assumes that the breach progressively increases in size over a given time until it reaches its final shape. Parameters such as the maximum width of the breach, which depends on the characteristics of the material and the hydraulic conditions and the height of the gap, which is generally adopted up to the level of the channel at the base of the dam. Also, the time of formation of the breach: It defines how quickly the breakout develops. It can depend on the strength of the material and the volume of water stored.

Before the development of more advanced models, breach definitions were based on empirical data, such as the MacDonald and Langridge-Monopolis Equations (1984), which estimated the size and formation time of a breach, or the Singh and Snorrason Equations (1984), which correlated peak discharge with reservoir dimensions and dam geometry. Later, Froehlich's Equations (1995) introduced a relationship between breach width, formation time, reservoir storage volume, and the water height above the breach.

While these models are quick to apply, they lack the precision required to ensure reliability in real emergency scenarios. Even subsequent improvements, through simplified physical models, still rely on empirical assumptions or simplifications, limiting their accuracy and reliability in complex situations.

Subsequently, commercial software explicitly simulates using numerical hydrodynamic models, taking into account the progressive erosion of the dam material as a function of the hydraulic gradient and the properties of the materials, including the feedback between the increase in flow and the widening of the gap.

These relationships are the subject of experimental research in laboratories (R26) carried out with scale models and parametric numerical simulations. These investigations highlight the erosion processes and failure dynamics in each area of the dam: protective layer, filter and central core. The relationship with different parts in zoned dams with heterogeneous section with materials of different behavior, such as shells, filters or cores, is of interest. The R26 paper justifies a high correlation in failure progression between scale experiments and numerical simulations shown.

Detailed three-dimensional numerical models allow for a more accurate representation of the hydraulic and mechanical processes involved, although they are complex to implement. This is the case of the proposed high-precision model (R23) that combines hydrodynamic equations, turbulence and transport of dam materials.

The contrast with experiments (R23), such as those carried out at the University of Leuven, has made it possible to accurately replicate the triangular vortices and erosion patterns at the bottom of the channel, confirming its ability to simulate complex flow dynamics or even bidirectional gaps

By combining sediment transport equations and instability criteria, it is able to address challenges in predicting dam failure of heterogeneous materials under overflow conditions and demonstrates its applicability in complex cases.

7. NON-STRUCTURAL MEASURES

7.1. EARLY WARNING AND EMERGENCIES

Implementing hydrological monitoring and dam safety systems, improving weather forecasting capabilities, and educating local communities about risks are essential tasks to increase the resilience of the population subjected to potential flooding.

In an overview review (R25) of the case of China, mitigation measures are outlined, including improving hydrological forecasts, safety monitoring systems, and strengthening the structures themselves. In addition, it is recognized that the education of communities is mandatory to reduce potential impacts.

Early warning is, without a doubt, one of the most effective tools for reducing the risk of human victims. These real-time early warnings must activate actions that depend on the expected consequences and that must be supported by information on potential flooding in the territory.

The mapping of flood risk, due to large reservoir discharges or even dam breaks, usually corresponds to scenarios predefined by previously calculated theoretical hydrographs. However, when an emergency plan has to be activated in the event of a singular event, these plans are usually adjusted, and an updated cartography is desirable for the specific characteristics of the event or the prediction of its evolution to respond to emergencies.

Traditional methods based on high-resolution hydrodynamic models have high computational times, which makes it difficult to apply them in some situations that require rapid responses.

7.2. HYDROLOGICAL ALERT

“Improving concerted pre-release from dams with more sophisticated use of weather forecasting, revision of design discharge, and effective sediment control for sustainable maintenance of dams are some of the imminent challenges we need to work hard to resolve”. (Tetsuya SUMI, 2025)

The Ministry of Land, Infrastructure, Transport and Tourism (MLIT) manages 109 trunk rivers in Japan. In 2019, MLIT formalized an increase in the amount of rainfall by 10 to 15% in flood control planning to cope with the effects of climate change in the future. In 2020, the Governmental so established a general rule to change, as far as it is effective, the operation rules of reservoirs to allow for pre-release from dams before the arrival of heavy rains by utilizing weather forecasts. In 2021, “Basin-wide Concerted Measures for Flood Risk Reduction Acts,” which consists of amendments of nine affiliated acts, was enacted to tackle the increased rainfall due to climate change.

7.3. HYDRAULIC ALERT

In practice, the hydrological forecast must feed the hydraulic alert, which places the real effect on the territory in the form of flooded areas, depths, arrival times, etc.

Traditional methods of numerical resolution of the two-dimensional Navier-Stokes equations, such as HEC-RAS, SOBEK, MIKE 21, etc. are widely used to model floods using two-dimensional Navier-Stokes equations. However, these models are computationally intensive and require long times to produce high-resolution results. In contrast, machine learning-based models, such as SGPs, can learn from pre-existing data and make quick predictions under new conditions.

To address this problem, the use of machine learning methods (R28), as an alternative to improve the efficiency and accuracy of rapid flood simulations. Reduce computational costs without compromising the accuracy of results.

The case of the Sheyuegou dam (Xinjiang, China) is shown, relevant because the flood resulting from the rupture caused significant human and material losses and where the effectiveness of the proposed method has been tested.

The methodology is based on the creation of historical and synthetic 2D simulations with conventional hydraulic models, the subsequent application of empirical orthogonal functions (EOF^{§§§}) simplifying the variables. Based on this, SGP models are trained^{***} to predict detailed data based on other low-resolution data and their subsequent validation. This achieves more accuracy than with an RH hydraulic model, with 90% savings in calculation time. The ability to generate results with high accuracy and shorter calculation time represents a significant advance in emergency management.

8. LEVEES

8.1. HAZARD CREEPING

The term "hazard creeping" refers to the gradual accumulation of factors that incrementally increase the risk of disasters, such as floods. This concept includes processes that, although not sudden, exacerbate exposure or vulnerability over time. Examples of these processes include uncontrolled urbanization, degradation of natural ecosystems (such as mangroves or wetlands), and climate change, which intensifies rainfall and raises sea levels. This phenomenon may remain unnoticed until a catastrophic event occurs. Addressing it requires long-term planning, proactive mitigation measures, and continuous monitoring to mitigate its cumulative impacts effectively.

^{§§§} Empirical orthogonal functions

^{***} Sparse Gaussian Process

“There were two types of levees: ***Those that had been overtopped*** by floodwaters, and ***those that were going to be***” (William Hammond Hall, California State Engineer 1880)



Fig. 13
Land management by levees usually forgetting its own history

8.2. LEVEES (R12)

The vulnerability of the Rhône Delta system has been particularly revealed in the face of extreme events such as the flood of December 2003 (R12). The answer was the "Rhône Plan", a comprehensive €450 million program with an innovative approach by prioritizing risk management and controlled acceptance of overflows.

The current levees were conceived in the nineteenth century as "unsinkable". Since then, many breaches have been recorded, mainly caused by internal erosion due to animal burrows and structural deficiencies. The risk of failure depends significantly on flow rates going from 50% for a flow rate of 9,500 m³/s to almost 100% with a flow rate of 10,500 m³/s.

After the 2003 flood, recognizing the need for a different approach, the "Rhône Plan" introduced the following key principles:

1. Avoid the transfer of risks from one area to another by increasing the height of the levees.
2. Accept controlled overflows in more extreme floods
3. Prevent the formation of breaches for exceptional floods (return period of 1,000 years)

This involved reinforcing the levee system to resist overflows and creating structures to manage the drainage of protected areas.

The design included solutions to speed up the drainage of overflowing water, such as modernizing pumping stations and installing siphons to improve flow in

embedded canals. This significantly reduced flooding time in protected areas, increasing the acceptability of the project.

New levees and structures were also built to ensure hydraulic transparency, including viaducts in transversal transport infrastructures.

Among the achievements is the tripled protection of people from 100-year floods, reduction of expected damage, along with greater resilience, since the current infrastructure withstands extreme flood scenarios, with improved drainage systems that minimize the impact of floods.

The experience in the Rhône Delta, with an innovative and resilient model against extreme floods, makes it worthy of being exported. By prioritizing risk management and citizen participation, it has not only improved the security of infrastructure but has also strengthened the capacity for social response to risk.

9. CONCLUDING REMARKS

Reservoirs play a crucial role in flood mitigation, but their operation must be optimized to minimize risks both upstream and downstream. Effective flood risk management demands a **comprehensive approach** (Huang et al.) that integrates risk assessment methods, infrastructure planning, and real-time operations.

The growing complexity of flood management, driven by climate change and human activities, necessitates dynamic and adaptive strategies. In this context, the involvement of experts and the use of advanced data visualization tools are essential for making informed and effective decisions during extreme events.

Among the structural measures, it is essential to consider the construction of dams to create flood attenuation reservoirs, taking into account their coordinated operation within the basin alongside other infrastructure. This includes the assessment and adaptation of existing dams to new load scenarios, adjustments to expected maximum water levels, modification or expansion of spillways, or the implementation of supplementary, emergency, or fuse spillways. Additionally, river channelization, levees, drainage systems, and similar interventions should be considered.

Among the non-structural measures, the adoption of optimal operational rules is crucial. This includes the establishment of buffer storage, seasonal drawdowns, and preventive releases, as well as risk mapping, early warning systems, and the implementation of emergency response plans. Furthermore, enhancing resilience through improved land management downstream, fostering public education, and promoting civil society involvement in planning processes are key. Strengthening

governance frameworks for extreme events through institutional reinforcement also plays a fundamental role.

9.1. OUR CHALLENGES

Many challenges remain open in the light of the insights gathered on this critical issue for the future, demanding immediate attention and sustained efforts from this moment onward.

- Modernize extreme hydrological methodologies through multidisciplinary, especially geologists and meteorologists.
- In hydrology, work on volumes, not only with flows, for the establishment of freeboards or protected land.
- Assume that the review of hydrology entails the acceptance, in many cases, of the existence of residual risks.
- Establish margins in the design of hydraulic structures, based on the uncertainty principle.
- Update studies with consideration of global changes.
- Claim for providing investments to face the essential continuity of the safe operation of more than sixty thousand large dams worldwide.
- Accompany with non-structural measures, such as RTWS (real-time warning systems) and Emergency Action Plans.
- Learning from hazard creeping cases for future land management. Involving cutting-cross strategies to manage flood risk mapping.
- Review regulations incorporating the risk acceptable by society.
- Implement design and maintenance strategies that increase the resilience of these structures.
- Train communities and operators in the management of risks associated with dam failures, promoting transparent citizen participation processes, as a guarantee of success.
- Using the latest technologies, including AI, to assess the risk and to optimize dam operation,
- and more.

Finally, we end this report by recovering some statements by ICOLD in which the content of this report has been inspired:

Remembering the motto coined in the ICOLD European Club Manifesto on Dams and Reservoirs: “Let’s stop thinking about working for society and work with society” (Mazza, 2019^{†††})

^{†††}As exposed in *Otawa*

9.2. WORLD DECLARATION ON DAM SAFETY, 2019: RISK ZERO DOES NOT EXIST

With almost a century of commitment to dam safety, and knowing that **the zero risk does not exist**, ICOLD recognizes in its World Declaration that is necessary to capture & analyze response to events, such as large floods, earthquakes, etc. since **natural hazard change with time, thus risks should be regularly reviewed and updated**. Such hazards as floods are external threats, for which risks are accepted based on known science and likelihood of occurrence. So emergency plans should be developed with the objective of avoiding loss of life and reducing damage to property, infrastructure and the environment resulting from a dam failure. Periodic review, updates and practice of the emergency plan should be mandatory as well as education and public awareness about dams and levees.

The role of regulatory authorities is paramount for safety. Developing norms, standards and safeguards is a key factor to proper dam safety surveillance.

9.3. WORLD DECLARATION 2024

Storage reservoirs help mitigate flood risks and reduce the frequency of inundations. Uncertainty about climate-induced flood events demands enhanced dam safety. Assessment of existing dams and their adaptation where required is high priority (Chengdu ICOLD Declaration on the Role of Dams for Energy Transition and Adaptation to Climate Change, 2025.)

9.4. FINAL WORDS

As a result of the wide spectrum of ideas, some confirming previous experiences of the dam community, others innovative, taken from other fields of technology, we find a common denominator: there is a lot of work to be done in all fields, implementing structural and non-structural measures involving other actors. These tasks, in order to keep in irreplaceable service the more than sixty thousand large dams that provide welfare to the mankind, contribute to the safety of people at risk of flooding, and mitigate the potential consequences of residual risk, aggravated by global warming, requires an enormous economic effort that society must make without excuses under committed programs that ensure its financing. Let's not wait for one catastrophe after another to intermittently recover that social mandate.

"We must be prudent. It is not enough to count on only the most likely circumstance, if the worst happens and it's really extremely dangerous for us, we have

to prepare for that. Remote contingencies, if they're serious enough, we have to be prepared for." (Carl Sagan, 1990, lecture dealing with climate change)

REFERENCES

Papers Q110

- [1] Q110 - R1 ADAPTATION OF 310 DAMS IN SPAIN TO EXTREME EVENTS AND CLIMATE CHANGE THROUGH RISK ASSESSMENT. JUAN CARLOS DE CEA AZAÑEDO ET AL. Spain.
- [2] Q110 – R2 PKW SPILLWAYS: AN INNOVATIVE, SAFE AND ECONOMIC SOLUTION FROM RUN-OF-RIVER DAMS IN PLAINS TO LARGE DAMS IN MOUNTAINS SUITABLE FOR CLIMATE CHANGE CHALLENGES. MICHEL. HO TA KHANH ET AL. Vietnam and France
- [3] Q110 – R3 DAM UPGRADE WITH PIANO KEY WEIR FOR DISCHARGE OF EXTREME FLOODS. JAMES YANG ET AL. Sweden
- [4] Q110 – R4 DESIGN OF THE NEW SPILLWAY FOR REGAJO DAM. ENRIQUE CAMPOS ET AL. Spain
- [5] Q110 – R5 NEW APPROACH TO ESTIMATE EXTREME FLOODS FOR SWISS DAMS BY MEANS OF CONTINUOUS HYDROMETEOROLOGICAL SIMULATIONS. ALEXANDRE JEAN PACHOUD ET AL. Switzerland
- [6] Q110 – R6 KARIBA DAM PLUNGE POOL RESHAPING WORKS FOR THE SAFETY OF STRUCTURES FOR EXTREME FLOODS. L. TARDIEUX ET AL. Switzerland and Zambia
- [7] Q110 – R7 PIANO KEY WEIR GEOMETRIES ADJUSTMENT FOR DOWNSTREAM HYDRAULIC REGIME: LESSONS LEARNED FROM CASE STUDIES IN VIETNAM. LE VAN NGHI ET AL. Vietnam.
- [8] Q110 – R8 REGIONALISATION OF FLOOD ENVELOPE CURVES TO DERIVE PRELIMINARY ESTIMATES OF PROBABLE MAXIMUM FLOODS. PETER HILL ET AL. Australia

- [9] Q110 – R9 CASE STUDY AND ANALYSIS OF SURGE WAVE AND EXCESSIVE FLOOD IN HYDROPOWER DAMS. CHIHAYA ONDA ET AL. Japan

- [10] Q110 – R10 GESTION DES CRUES SUR LES GRANDS BASSINS VERSANTS - PRISE EN COMPTE DE LA COMPLEXITÉ HYDROLOGIQUE ET HYDRAULIQUE (*FLOOD MANAGEMENT IN LARGE WATERSHEDS - CONSIDERATION OF HYDROLOGICAL AND HYDRAULIC COMPLEXITY*). JULIEN VERMEULEN ET AL. France

- [11] Q110 – R11 CHARACTERIZATION AND FEEDBACK ON THE BEHAVIOR OF ARCH DAMS SUBJECTED TO HEATWAVES AND EXTREME COLD. LOUIS SUCHIER ET AL. France

- [12] Q110 – R12 BUILDING A RESILIENT SYSTEM AGAINST FLOOD IN THE RHÔNE DELTA. THIBAUT MALLET ET AL. France

- [13] Q110 – R13 A NOVEL METHODOLOGY FOR ASSESSING EXTREME HYDROLOGICAL EVENTS IN THE CONTEXT OF CLIMATE CHANGE. NICOLAS AVISSE. France

- [14] Q110 – R14 IMPROVEMENT OF THE SAFETY OF THE FRENCH DAMS AGAINST FLOODS. GAËTAN DAUTOIS, MATHIEU ROY ET AL. France

- [15] Q110 – R15 TWO EROSION TESTS TO QUANTIFY RESISTANCE TO EROSION DURING OVERFLOW: THE JET EROSION TEST AND THE OVERFLOW TEST. PATRICK PINETTES ET AL. France

- [16] Q110 – R16 MOLARE TRAGEDY: THE SECONDARY DAM COLLAPSE INDUCED BY A HEAVY RAINFALL EVENT, ANDREA ABBATE. Italy..

- [17] Q110 – R17 CASE STUDY – A DAM RAISING OPTIONS STUDY FOR A DAM IN SOUTHERN AFRICA. . CHENCEN ZHANG *ET AL* , South Africa.

- [18] Q110 – R18 CHALLENGES EXPERIENCES WITH UPGRADING A COMPOSITE DAM IN SOUTH AFRICA - TZANEEN DAM RAISING. HENRY-JOHN WRIGHT, South Africa

- [19] Q110 – R19 THE EFFECT OF RESERVOIR OPERATION PATTERNS ON THE MATERIAL CHARACTERISTICS OF OLD DAMS AND THEIR IMPACT ON DAM SAFETY. MUHAMMAD RIZA ET AL. Indonesia

- [20] Q110 – R20 ASSESSMENT OF THE DISCHARGE CAPACITIES AND SAFETY OF MAIN STRUCTURES IN LARGE DAMS OF DRINI RIVER CASCADE. MR. ARJAN JOVANI ET AL. Albania

- [21] Q110 – R21 INTELLIGENT TEMPERATURE CONTROL SYSTEM FOR LARGE CONCRETE DAM CONSTRUCTION IN HOT AND HUMID ENVIRONMENTS. YUXIN NIE ET AL. China.

- [22] Q110 – R22 EFFECTS OF SPATIAL AND TEMPORAL VARIATION CHARACTERISTICS OF EXTREME PRECIPITATION ON DAM SAFETY IN MAJOR RIVER BASINS IN CHINA IN RECENT 20 YEARS. NING ZHOU ET AL. China

- [23] Q110 – R23 A HIGH-PRECISION THREE-DIMENSIONAL DAM BREACH MODEL CONSIDERING BREACH EVOLUTION MECHANISMS. SHENGYAO MEI ET AL. China

- [24] Q110 – R24 DISASTER ASSESSMENT OF THE LANDSLIDE SURGE CAUSED BY THE DEFORMATION OF THE UPSTREAM RESERVOIR BANK OF THE DAM. YUELIN SUN ET AL. China

- [25] Q110 – R25 ANALYSIS OF THE IMPACT OF EXTREME EVENTS ON DAM DISASTER UNDER CLIMATE CHANGE. JINGCHUN LEI ET AL. China

- [26] Q110 – R26 ZONED EMBANKMENT DAM BREACHING DUE TO OVERTOPPING: ESTIMATING OUTFLOW HYDROGRAPHS THROUGH LABORATORY EXPERIMENTS AND PARAMETRIC NUMERICAL MODELING. MATTHEW HALSO ET AL. Switzerland

- [27] Q110 – R27 NEW PROGRESS OF CEMENTED MATERIAL DAMS TO MEET THE REQUIREMENTS ON DAM SAFETY TO RESIST OVERTOPPING IN CHINA. JINSHENG JIA ET AL. China

- [28] Q110 – R28 MACHINE LEARNING METHOD BASED DAM BREACH FLOOD SIMULATION. HONGQIU HE ET AL. China.

Other references

- [29] PARIS & ERDOGAN A CRITICAL ANALYSIS OF CRACK PROPAGATION LAWS. *Journal of Basic Engineering*, 85(4), 528–534. 1963.
- [30] WMO⁺⁺⁺ MANUAL FOR ESTIMATION OF PROBABLE MAXIMUM PRECIPITATION. OPERATIONAL HYDROLOGY-REPORT NO.1. WMO-NO.332. GENEVE. 1986
- [31] ANNANDALE, G ERODIBILITY. *Journal of Hydraulic Research*, 33(4), 471–494. 1995
- [32] BAKER V PALEOFLOOD HYDROLOGY AND EXTRAORDINARY FLOOD EVENTS. *Journal of Hydrology*, 96, pp.79–99. 1987
- [33] FOUFOULA-G A PROBABILISTIC STORM TRANSPOSITION APPROACH FOR ESTIMATING EXCEEDANCE PROBABILITIES OF EXTREME PRECIPITATION DEPTHS. *Water Resources Research*. Vol. 25 No. 5. 1989
- [34] FONTAINE *ET AL* ESTIMATING PROBABILITIES OF EXTREME RAINFALLS. *Journal of Hydraulic Engineering, ASCE*, 115 (11), pp. 1562–1575. 1989
- [35] KOFOED *ET AL* MODELLING OF LANDSLIDE-GENERATED WAVES, 2001. DHI Water & Environment. Scientific Publications Scientific Publications 2001
- [36] CIFRES, E OROGRAPHIC AND STOCHASTIC STORM TRANSPOSITION FOR ESTIMATION OF LARGE RETURN PERIOD FLOODS. EGU Vienna, April 2007.
- [37] TODINI, E PREDICTIVE UNCERTAINTY IN HYDROLOGICAL FORECASTING. U. Bologna HEPEX – COST731 workshop program –15–18 June 2009.

⁺⁺⁺*World Meteorological Organization*

- [38] JESSICA LUDY^{§§§§} FLOOD RISK PERCEPTION ON LANDS PROTECTED BY LEVEES. WORLD WATER FORUM, MARSEILLE, 2012.
- [39] ARCHFIELD *ET AL* ACCELERATING ADVANCES IN CONTINENTAL DOMAIN HYDROLOGIC MODELING. *Water Resources Research*, 51(12), pp.10078–10091, 2015
- [40] CIFRES, E NEW METHODOLOGY FOR A ROBUST ESTIMATION OF LARGE RETURN PERIOD FLOODS FOR DESIGN OF LARGE DAM SPILLWAYS, ICOLD, Johannesburg 2016.
- [41] CIFRES, E DAM HYDROLOGICAL SAFETY, A PENDING CHALLENGE. Cippoletti (Argentina) CAP, 2022.
- [42] AR6 IPCC_AR6_SYR_LONGERREPORT.PDF, 2023
- [43] MORAN, R *ET AL* QUASI-PROTOTYPE SIZE TESTING OF WEDGE-SHAPED BLOCK FOR ARMORING EMBANKMENT DAMS AND LEVEES. *Water*, 15(4), 662. MDPI. 2023
- [44] JCOLD JAPAN INCORPORATES CLIMATE CHANGE EFFECTS INTO RIVER AND DAM PLANNING. <https://niftp.mlit.go.jp/ksj/gml/datalist/KsjTmplt-W01.html>. 2025.

ICOLD Bulletins and Institutional documents

The main related ICOLD bulletins, in some way related with the main topic, are:

- [45] BERGA & TC A ROLE OF DAMS IN FLOOD MITIGATION. TC DAMS & FLOODS BULLETIN 131, 2006
- [46] GUILLON ET TC RESERVOIR LANDSLIDES: INVESTIGATION AND MANAGEMENT. GUIDELINES AND CASE HISTORIES. ICOLD BULLETIN 124, 2000.

^{§§§§}University of California, Berkeley

- [47] GUILLAUD&TC S INTEGRATED FLOOD RISK MANAGEMENT. TC DAMS & FLOODS BULLETIN 156, 2014

- [48] MAZZA ET AL. MANIFESTO Dams & Reservoirs. European Club of ICOLD. November 2016

- [49] JOOS& TC S FLOOD ESTIMATION AND DAM SAFETY, ICOLD COMMITTEE ON FLOODS EVALUATION AND DAM SAFETY, BULLETIN 170, 2018,

- [50] ROGERS, M &SC WORLD DECLARATION ON DAM SAFETY, ICOLD BOARD, OPORTO, 2019.

- [51] XU & TC H DAM BREACH FLOOD CONSEQUENCE ASSESSMENT, FINAL DRAFT VERSION FOR COMMENTS, BULLETIN 197, 2022

- [52] WESTERMANN TC V BEST PRACTICES FOR ACHIEVING RELIABILITY OF FLOOD DISCHARGE GATES. COMMITTEE ON HYDROMECHANICAL EQUIPMENT. BULLETIN 203. TO BE PUBLISHED SOON

- [53] HUANG & TC S FLOOD RISK ASSESSMENT. ICOLD COMMITTEE ON FLOODS EVALUATION AND DAM SAFETY. BULLETIN 204, TO BE PUBLISHED SOON

- [54] SHARMA-CIFRES & SC CHENGDU ICOLD DECLARATION ON THE ROLE OF DAMS FOR ENERGY TRANSITION AND ADAPTATION TO CLIMATE CHANGE, 2025, SPECIAL COMMITTEE ZA1, 2024.

COMMISSION INTERNATIONALE DES
GRANDS BARRAGES

VINGT-HUITIEME CONGRES DES
GRANDS BARRAGES
CHENGDU, MAI 2025

"1,7,1,0,105PT,105PT,0,0>QUESTION 110

LA SÉCURITÉ DES BARRAGES ET DES DIGUES FACE AUX



ÉVÉNEMENTS HYDROLOGIQUES EXTRÊMES

Enrique CIFRES

Docteur en ressources hydriques, ingénieur civil (MsC)

Vice-président honoraire de la CIGB

Conseiller indépendant sur les barrages et les ressources en eau

RAPPORTEUR GÉNÉRAL

TABLE DES MATIERES

1.	QUESTION 110 - SOUS-THÈMES	546
2.	EN GUISE D'INTRODUCTION.	546
3.	CONTRIBUTION DE LA CIGB.	549
4.	BULLETINS CONNEXES DE LA CIGB	550
4.1.	B131 rôle des barrages dans l'atténuation des crues - synthèse.	550
4.2.	B156 gestion intégrée du risque crue	551
4.3.	B170 évaluation des crues et sécurité des barrages	551
4.4.	B197 évaluation des conséquences de la rupture des barrages sur les inondations.	552
4.5.	B203 meilleures pratiques pour assurer la fiabilité des vannes d'évacuation des crues	552
4.6.	B204 évaluation du risque crues	552
5.	SÉCURITÉ HYDROLOGIQUE*	553
5.1.	Normes et règlements et approches nationales actuelles	553
5.1.1.	Évaluation des risques à l'échelle nationale en espagne	555
5.1.2.	Gestion opérationnelle en france.	556
5.1.3.	Cas récents au japon	556
5.1.4.	Précipitations extrêmes spatiales et temporelles en chine dans le contexte du changement climatique	556
5.1.5.	Les événements extrêmes et la catastrophe des barrages en chine dans le contexte du changement climatique.	557
5.2.	Réévaluations des crues extrêmes	558
5.3.	Conception d'un modèle de précipitations et de ruissellement basé sur les événements.	560
5.4.	Nouvelle tendance actuelle	560
5.5.	PMF.	561
5.6.	Courbes enveloppantes australiennes	561
5.7.	Une méthodologie innovante (france)	562
5.8.	Nécessité d'un plus grand nombre de données.	563
5.9.	Extension de la série de données : paléo-inondations.	563
5.10.	Analyse de la fréquence des inondations au niveau régional	563
5.11.	Génération synthétique	564
5.12.	Modèles conceptuels avec base physique.	565
5.13.	Transposition stochastique.	566
5.14.	Impact du changement climatique	571
5.15.	Incertitude	572

6.	Agir face aux extrêmes	573
6.1.	Évacuateurs de crues	574
6.1.1.	Bassin de la rivière drin	574
6.1.2.	Barrage de regajo	575
6.1.3.	Révision structurelle en france	576
6.1.4.	Tragédie en italie	576
6.2.	Labyrinthes – déversoirs en pkw	577
6.2.1.	Cas sud-africains	577
6.2.2.	Cas français et vietnamien	578
6.2.3.	Un projet suédois singulier	579
6.3.	Débordement	580
6.3.1.	Contribution chinoise aux barrages en matériaux cimentés	581
6.4.	Dissipation d'énergie	582
6.4.1.	Barrage de Kariba	582
6.5.	Laminage des crues et atténuation de la crête	583
6.6.	Température	583
6.7.	Glissement de terrain	584
6.8.	Gestion des barrages	586
6.8.1.	Progrès dans les modèles de rupture de barrage et de propagation des vagues	586
7.	Mesures non-structurelles	589
7.1.	Alerte précoce et situation d'urgence	589
7.1.1.	Alerte hydrologique	590
7.1.2.	Alerte hydraulique	590
8.	Digues	591
8.1.	Aggravation du risque	591
8.2.	Digues (R12)	592
9.	Remarques finales	593
9.1.	Nos défis	593
9.2.	Déclaration mondiale sur la sécurité des barrages – 2019 – Le risque zéro n'existe pas	594
9.3.	Déclaration mondiale 2024	595
9.4.	Derniers mots	595
	RÉFÉRENCES	596
	Documents Q110	596
	Autres références	599
	Bulletins et documents institutionnels de la CIGB	600

1. QUESTION 110 - SOUS-THÈMES

1. Évaluation des événements extrêmes (par exemple, inondations, sécheresses*, typhons/ouragans, inondations par débordement de lacs glaciaires) dans le contexte du changement climatique, en tenant compte de l'incertitude.
2. Évaluation de la sécurité des structures en cas d'inondations extrêmes ; options de gestion (par exemple, augmentation de la hauteur du barrage, de la capacité du déversoir, de l'exploitation du réservoir)
3. Prévision des crues, gestion hydraulique de projets multiples au sein de systèmes fluviaux
4. Réévaluation des données relatives aux inondations et des mesures d'atténuation (par exemple, dispositifs fusibles, résistance aux débordements, formation de brèches contrôlées, alerte et évacuation, gestion des crises et des urgences)

2. EN GUISE D'INTRODUCTION

“Je n'avais jamais vu ça” est une expression que l'on répète lorsqu'un événement extrême se produit, et c'est logique, car il est “extraordinaire”, il est en dehors de l'attendu et du concevable, vraiment en dehors.

Récemment, c'est la phrase la plus répétée dans ma ville, Valence, après les inondations vraiment extraordinaires que nous avons subies. Ce travail a été préparé sous le choc émotionnel d'une terrible tempête qui a coûté la vie à plus de deux cents voisins et qui a eu un impact énorme sur la vie et l'économie de centaines de milliers de concitoyens.

Je leur dédie ce rapport et, tout en leur présentant mes condoléances, je m'engage à travailler dur pour la sécurité de toutes les personnes, où qu'elles soient, qui peuvent être soumises à des risques hydrologiques.

Un an plus tôt, toujours en Méditerranée, les habitants de Derna, en Libye, ont souffert de la tempête Daniel, un événement extraordinaire qui a entraîné des conséquences encore plus graves, en raison de la rupture des barrages Derna et Abu Mansur, paradoxalement construits pour les protéger.

**Bien que le premier sous-thème comprenne les sécheresses, ce problème est traité en profondeur dans ce même congrès de Chengdu, dans la Q108 sur “l'adaptation au CC” et c'est la raison pour laquelle aucun des documents inclus dans cette Q110 n'est directement axé sur les sécheresses, bien qu'elles soient également la conséquence d'extrêmes hydrologiques.*

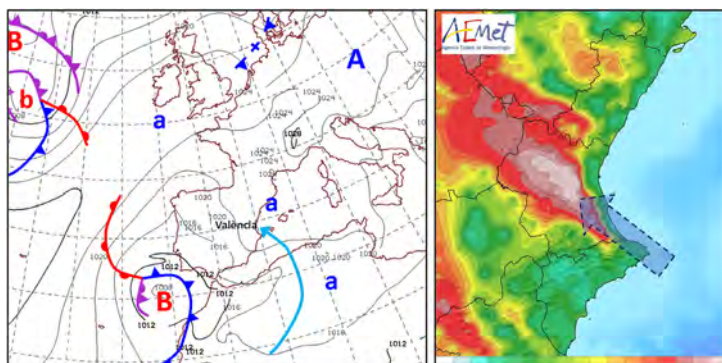


Fig. 1

Une rivière atmosphérique s'écoulant le long de l'orientation de la vallée principale.
29 octobre 2024

Un bassin d'air froid sur la péninsule ibérique, avec une tempête dépressionnaire, bloquée à l'ouest du détroit de Gibraltar par une haute pression sur l'Europe centrale qui la maintient statique pendant deux jours, une mer Méditerranée chaude qui sature un air réchauffé sur son chemin à travers le Sahara : un cocktail dangereux pour Valence.

Nous savons que lorsque quelque chose de vraiment extraordinaire se produit, c'est la combinaison de multiples facteurs qui forment un scénario terrible et cette idée doit inspirer l'analyse, la prévention et la compréhension des phénomènes extrêmes.



Fig. 2

Catastrophe dans l'agglomération de Valence. 2024.

Les simulations de l'onde de crue du ruisseau Poyo ont permis d'estimer le débit de pointe à environ 3 000 m³/s, ce qui dépasse largement la capacité du canal de drainage de la ville, qui ne peut traiter qu'un maximum d'environ 800 m³/s.

De même, le bassin du Wadi Derna, bien que relativement petit, a souffert de la terrible combinaison de facteurs avec laquelle la tempête Daniel a produit sa décharge fatale.



Fig. 3

La tempête Daniel crée une rivière atmosphérique le long du bassin de Derna.[†]



Fig. 4

[†]Photo extraite de CRISIS GROUP / MAXBOX / OSM

La catastrophe de Derna. Il n'y a pas de mots pour le dire. Les simulations de la deuxième vague d'inondation provoquée par l'effondrement du barrage d'Abu Mansour suggèrent une estimation du débit d'environ 7 000 m³/s, dépassant largement la capacité du canal de drainage de la ville, qui ne pouvait supporter qu'un maximum d'environ 1 000 m³/s.

Tout indique que la conception a suivi les normes en vigueur à l'époque.

Il convient de se demander si l'ampleur de ce phénomène est prévisible a priori. La réponse passe par un postulat qui sous-tend les projets d'ingénierie hydraulique : lorsque nous choisissons une période de retour pour la conception, sommes-nous conscients que des épisodes plus sévères ne peuvent être exclus ?

Autre question : si le bassin n'a jamais connu d'épisode d'une certaine ampleur ou similaire, faut-il exclure cette possibilité ?

Ces deux questions mettent sur la table les méthodologies classiques de conception et de sécurité des barrages et la nécessité de les réviser.

D'autre part, si nous admettons que le réchauffement climatique est et continuera d'exacerber les extrêmes hydrologiques dans de nombreuses régions de la planète, les données historiques perdent de leur importance au profit de nouvelles approches qui peuvent intégrer des concepts permettant d'estimer les événements extrêmes auxquels les barrages, existants et nouveaux, devront faire face.

L'expérience de la catastrophe de Valence et l'écoute de l'opinion publique font apparaître des nouvelles relativement bonnes : la société est consciente que les travaux de défense contre les inondations atténuent les dommages, mais ne les éliminent pas complètement, et que des mesures non structurelles associées doivent être mises en œuvre pour gérer les urgences liées aux risques résiduels une fois que les mesures structurelles telles que les barrages de contrôle des inondations, les canalisations, les digues, les drains, etc. ont été mises en œuvre.

Dans ce rapport, il sera possible d'apprécier la frontière entre l'énorme contribution des barrages à l'atténuation des dommages causés par les inondations et le risque résiduel, imposé au territoire, associé à leur rupture potentielle. Tel est le défi.

3. CONTRIBUTION DE LA CIGB

La CIGB travaille sur ce grand défi pour la sécurité qui signifie des extrêmes hydrologiques, exacerbés par le changement climatique, la croissance de la population dans les zones exposées, des demandes sociales, sanitaires et économiques

plus importantes, etc. dans un monde en mutation. La révision permanente des critères, des informations, des connaissances technologiques et de la réglementation exige une continuité dans le travail avec l'innovation nécessaire pour tenir compte des barrages existants, des conceptions futures et de leur gestion, ainsi que des digues de protection sous lesquelles vivent des millions de personnes dans le monde.

Vingt-huit articles ont été reçus de douze pays, couvrant presque tous les sous-thèmes promus de cette vaste question.

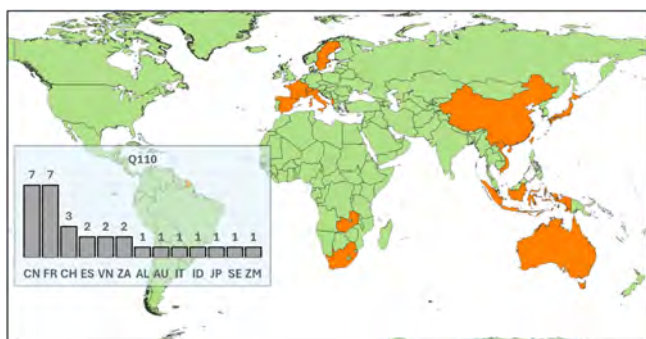


Fig. 5

Contribution à Q110 : documents de la Chine, de la France, de la Suisse, de l'Espagne, du Vietnam, de l'Afrique du Sud, de l'Albanie, de l'Australie, de l'Indonésie, de l'Italie, du Japon, de la Suède et de la Zambie.

Outre les multiples contributions aux congrès précédents de la CIGB depuis près de cent ans d'existence, nous pouvons mettre en évidence certains des bulletins techniques publiés où la question de l'hydrologie extrême et de son influence sur les barrages et les digues est approfondie.

4. BULLETINS CONNEXES DE LA CIGB

4.1. B131 RÔLE DES BARRAGES DANS L'ATTÉNUATION DES CRUES - SYNTHÈSE

La CIGB a repris sa position avec ce bulletin qui pose les bases de la conception moderne de l'OIF[‡]. Les inondations, l'un des principaux types de

[‡]Gestion intégrée des inondations

catastrophes naturelles, sont responsables de 30 % de tous les dommages économiques et de 20 % des décès causés par ces catastrophes naturelles.

Ce comité est né simultanément à la publication de la Stratégie internationale pour la prévention des catastrophes (SIPC) mise en œuvre par les Nations Unies, dont l'objectif principal était de "construire des communautés résilientes aux catastrophes en promouvant une prise de conscience accrue de l'importance de la prévention des catastrophes en tant que composante intégrale du développement durable, dans le but de réduire les pertes humaines, sociales, économiques et environnementales dues aux aléas naturels" (Berga 2006).

Les barrages peuvent jouer un rôle important dans l'atténuation des inondations, mais en tant qu'outil à prendre en compte dans le cadre de la gestion intégrée des inondations (GII), tout en rappelant qu'il convient d'éviter la perception et la présomption d'une sécurité totale.

4.2. B156 GESTION INTEGREE DU RISQUE CRUE

La "gestion intégrée des risques d'inondation" est une approche relativement courante qui a été mise en œuvre au cours des dernières décennies dans certains pays. Son application dans certains bassins transfrontaliers est en cours avec le soutien d'organisations internationales. Il s'agit de l'une des mesures non structurelles les plus difficiles à mettre en œuvre.

Son approche, objet du bulletin 156, vise des systèmes de protection efficaces et acceptés, mais sa mise en œuvre est plus complexe que l'approche traditionnelle purement technocratique, car elle nécessite la coopération de toutes les parties prenantes. Les difficultés résident dans la résistance de certaines parties à renoncer à des privilèges.

4.3. B170 EVALUATION DES CRUES ET SECURITE DES BARRAGES

Quatre bulletins traitant des inondations et des barrages ont été publiés avant celui-ci : Sélection de la crue de référence - Méthodes actuelles (#82, 1992), Barrages et inondations - Lignes directrices et études de cas (2003), Rôle des barrages dans l'atténuation des inondations (2006) et Gestion intégrée des inondations (2014).

Cette publication traite de l'intégration de la gestion des inondations dans l'exploitation des réservoirs, ainsi que d'autres considérations liées au changement climatique et à des expériences concrètes. En outre, un vade-mecum résumé des

méthodes hydrologiques "classiques" et une approche pour faire face aux incertitudes des inondations extrêmes sont discutés.

Enfin, les critères appliqués dans le monde entier pour sélectionner la crue de référence et la crue extrême sont compilés.

D'autres bulletins sont en cours d'élaboration et prêts à être publiés :

4.4. B197 ÉVALUATION DES CONSÉQUENCES DE LA RUPTURE DES BARRAGES SUR LES INONDATIONS

Le Comité de sécurité des barrages de la CIGB s'efforce de guider les responsables de la sécurité des barrages sur les principes, les applications contemporaines et les méthodes utilisées pour l'analyse et l'évaluation des conséquences des ruptures de barrages, nécessaires à l'évaluation des risques, à l'estimation des dommages potentiels et à la planification des mesures d'urgence. Le risque de rupture de barrage combine l'estimation des probabilités et l'évaluation des conséquences potentielles, y compris la perte éventuelle de vies humaines, ce dernier facteur étant le principal objectif de ce Bulletin 197 déjà rédigé et sur le point d'être publié.

4.5. B203 MEILLEURES PRATIQUES POUR ASSURER LA FIABILITÉ DES VANNES D'ÉVACUATION DES CRUES

Une gestion efficace des inondations dépend du fonctionnement fiable de l'équipement hydromécanique des déversoirs à vannes. Ceux-ci, inactifs pendant de longues périodes, sont essentiels dans les situations d'urgence pour éviter des conséquences qui pourraient être catastrophiques.

La publication passe en revue les pratiques dans différentes régions du monde en comparant les avantages et les inconvénients des mécanismes d'actionnement mécaniques ou hydrauliques. Elle met également en garde contre le risque croissant de cyberattaques sur les portails gérés par l'IdO et propose des recommandations pour renforcer la sécurité de leur contrôle.

4.6. B204 ÉVALUATION DU RISQUE CRUES

Ce prochain bulletin traite des mesures structurelles d'atténuation des inondations, telles que les digues, les réservoirs, les systèmes de drainage, et des

mesures non structurelles telles que l'exploitation des réservoirs, y compris la gestion conjointe des groupes de réservoirs, le zonage des plaines inondables et l'assurance contre les inondations, entre autres, les systèmes de prévision et d'alerte, et la gestion des risques en temps réel. Ce document souligne la nécessité d'une approche globale de l'évaluation et de la gestion des risques d'inondation, combinant la modélisation prédictive, la planification stratégique et la réponse opérationnelle en temps réel.

Certaines des idées mentionnées dans ces documents sont abordées dans les documents reçus de certains pays, qui insistent sur ces idées, les confirment ou les approfondissent à l'aide d'études de cas réels qui valent la peine d'être lues. Tout au long de ce rapport général, la référence du document dans lequel l'idée sur laquelle porte l'argument est indiquée entre parenthèses.

La première moitié de ce rapport général traite de la manière d'essayer d'améliorer la connaissance des extrêmes hydrologiques, en particulier les grandes inondations, ainsi que celles induites par des ruptures potentielles, tandis que la seconde moitié présente les actions d'atténuation et d'adaptation des barrages à ces besoins.

5. SECURITE HYDROLOGIQUE

Le réchauffement climatique a intensifié les cycles hydrologiques, augmentant la fréquence et l'intensité des précipitations extrêmes. Ce phénomène représente un défi majeur pour l'exploitation sûre des barrages dans le monde entier. Ces tendances posent des risques considérables pour les infrastructures hydrauliques et soulignent la nécessité d'une analyse quantitative et systématique de leur impact (R22).

5.1. NORMES ET REGLEMENTS ET APPROCHES NATIONALES ACTUELLES

Bien qu'il ait été courant dans le passé de concevoir des barrages sans cadre réglementaire dans presque tous les pays, avec des critères et des méthodologies développés localement par les ingénieurs responsables sur la base de méthodologies tirées de la doctrine scientifique actuelle, les autorités gouvernementales de nombreux pays ont établi des réglementations et des normes, inspirées par des critères dérivés de l'expérience partagée par les comités nationaux qui composent la CIGB, en plus d'autres sources d'intérêt.

Dans certains pays, comme la France (R14), les réglementations et les techniques visant à améliorer la sécurité des barrages évoluent déjà et font face aux

défis associés au changement climatique pour une mise en conformité avant 2030 ou 2035 selon la catégorie du réservoir.

La réévaluation périodique des risques, y compris la sécurité hydrologique, une pratique en cours de consolidation, conduit à l'identification précoce des déficiences possibles en termes de capacité de déversement dans certains barages pour faire face à des risques extrêmes. Tous les pays ne disposent pas encore d'une réglementation suffisante établissant un examen hydrologique périodique ou la tâche d'incorporer l'impact du changement climatique.

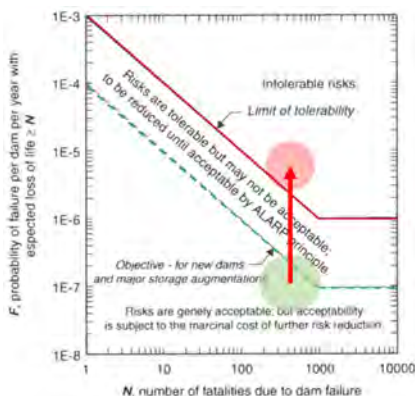


Fig. 6

Réévaluation périodique du risque par rapport à l'acceptabilité

Bien qu'il soit très courant que les réglementations édictent des critères de conception basés sur différentes périodes de retour en fonction de la catégorie basée sur les dommages potentiels, des inondations extrêmes ou de sécurité sont également définies, telles que celles qui épuisent la marge de sécurité structurelle. Les inondations extraordinaires avec des périodes de retour allant jusqu'à 10 000 ans et PMF dans d'autres cas sont utilisées pour ces vérifications. La méthodologie SaRRR (R14) permet d'identifier les vulnérabilités et de hiérarchiser les interventions.

Faire face à ces risques vraiment extraordinaires justifie une grande réflexion sur les méthodologies à utiliser pour l'estimation des événements, les possibilités d'une adaptation progressive à des exigences d'évacuation plus importantes, la manière de mettre en œuvre des mesures de résilience dans les zones potentiellement affectées avec des actions structurelles et non structurelles, et les investissements nécessaires pour atteindre des niveaux de sécurité en ligne avec le

niveau de risque socialement acceptable. Il y a beaucoup de travail à faire et le soutien de bonnes réglementations réalistes avec des feuilles de route viables sont encore des défis de la société auxquels la communauté des barrages doit apporter des idées et des solutions.

La société exige des *normes de sécurité plus élevées les barrages* en raison de l'incertitude liée à la fréquence et à l'intensité des inondations dans les conditions du changement climatique, des changements dans l'utilisation des terres et de l'exposition d'une plus grande population en aval. Cela nécessite une meilleure conception des nouveaux barrages, une qualité accrue des barrages grâce à une construction intelligente artificielle, et des efforts continus pour améliorer les opérations de résilience des barrages existants et nouveaux.

Déclaration de la CIGB de Chengdu sur le rôle des barrages dans la transition énergétique et l'adaptation au changement climatique, 2025.

5.1.1. *Évaluation des risques à l'échelle nationale en Espagne*

Le ministère espagnol de *la transition écologique* a lancé un système de gestion complet pour évaluer la sécurité des barrages dans tout le pays (R01) et établir des rapports afin de hiérarchiser les investissements, d'anticiper l'évolution des risques posés par le changement climatique et d'identifier les barrages présentant des risques potentiels à long terme.

En hiérarchisant stratégiquement les investissements sur la base de ces évaluations, l'Espagne peut renforcer la résilience de ses infrastructures face aux phénomènes météorologiques extrêmes.

Le système est mis en œuvre en plusieurs phases, en commençant par l'élaboration d'une méthodologie d'analyse des risques qualitative et semi-quantitative pour les 310 barrages appartenant à l'État. La première phase se concentre sur 175 barrages dans quatre bassins versants.

Ce système représente un effort national important pour tenter de protéger les ressources en eau de l'Espagne et d'atténuer les risques posés par le changement climatique, en assurant la durabilité et la résilience à long terme du pays. Le manque de soutien réglementaire ne permet pas son application automatique dans la prise de décision. D'autre part, il existe des preuves de l'énorme investissement nécessaire pour mettre à jour les normes de sécurité hydrologique nouvelles et plus modernes.

5.1.2. *Gestion opérationnelle en France*

Plus directement axé sur le risque hydrologique, pour gérer de manière sûre et efficace les bassins avec des barrages en France dans le contexte du changement climatique, EDF (R10) se concentre sur la gestion du risque hydrologique, à la fois à court terme (prévisions) et à long terme (inondations extrêmes) grâce à des outils innovants tels que Schadex-sd (scénarios hydrologiques), Shydonhy (hydrogrammes synthétiques), Melxor (propagation hydraulique), Automat (zones inondables) et Fregate (conséquences). Il s'agit d'une approche globale qui combine la simulation hydrologique et la modélisation hydraulique pour améliorer la gestion des barrages.

La gestion opérationnelle des inondations, basée sur les outils mentionnés ci-dessus (R10), permet de coordonner les actions entre les opérateurs et les optimisateurs, en particulier dans les situations d'urgence, telles que celles proposées dans le bassin de la rivière Ain. De plus, ils facilitent la coordination entre les acteurs impliqués, favorisant une gestion plus efficace et plus sûre des bassins versants.

L'amélioration continue de la sécurité des réservoirs en France (R14) reflète un engagement en faveur d'une gestion efficace des risques. Les études de cas illustrent comment les réglementations modernes et les solutions innovantes permettent de relever des défis complexes, en garantissant la sécurité contre les inondations extrêmes dans le contexte du changement climatique.

5.1.3. *Cas récents au Japon*

L'évolution des normes de conception des débits de crue au Japon (R09) est analysée, soulignant que de nombreux barrages construits selon les anciennes réglementations ne sont pas équipés pour faire face aux défis hydrologiques actuels et futurs.

Trois études de cas sont présentées : les barrages de Hiranabe, Horoka et Hetoishi au Japon (R09), chacun étant confronté à des problèmes spécifiques tels que des vagues générées par des glissements de terrain, une sédimentation extrême ou des inondations dépassant les normes de conception. Ces cas soulignent la nécessité de mesures de sécurité adaptées. Ce document perspicace sera à nouveau référencé dans le corps de ce rapport.

5.1.4. *Précipitations extrêmes spatiales et temporelles en Chine*

L'impact de la variation spatiale et temporelle des précipitations extrêmes sur la sécurité des barrages dans les grands bassins fluviaux en Chine (2000-2020) est analysé (R22). Depuis 2010, des épisodes de pluies torrentielles ont affecté différentes régions du pays, les événements de 2012 et 2021 à Beijing et Henan,

respectivement, étant des exemples de l'incidence croissante des tempêtes extrêmes.

Entre 1954 et 2021, la fréquence des ruptures de barrages a montré une tendance à la baisse, surtout après 1980, en raison de la mise en œuvre de règles de sécurité. Cependant, il y a eu une stabilisation ou une augmentation des incidents, probablement liée à une augmentation des précipitations extrêmes (R22).

Une augmentation globale des précipitations totales a été observée dans la plupart des bassins, à l'exception des rivières Huaihe et du sud-ouest, où une diminution a été observée. Les précipitations maximales sur 5 jours consécutifs ont également subi une tendance positive dans tous les bassins, mettant en évidence Perla et le sud-est, soulignant une augmentation des événements de précipitations prolongées et extrêmes (R22).

Bien que les précipitations extrêmes aient augmenté dans la plupart des bassins, avec des tendances marquées dans le Songliao, le Yangtze et le sud-est, le nombre de ruptures de barrages dans ces bassins n'a pas augmenté de manière significative, ce qui est peut-être lié à des projets qui sont de plus en plus résilients et adaptés aux changements climatiques, tandis que les systèmes d'alerte sont prioritaires et dans les régions à haut risque (R22).

5.1.5. *Les événements extrêmes et la catastrophe des barrages en Chine dans le contexte du changement climatique*

Les principales causes de catastrophes telles que les infiltrations, les surcharges dues aux inondations, les glissements de terrain et les erreurs de conception et de construction ont été identifiées comme des causes récurrentes liées à des événements hydrologiques extrêmes (R25). L'accumulation rapide d'eau dans les réservoirs peut dépasser les niveaux de sécurité, provoquant des infiltrations, l'érosion des pentes en aval et des ruptures catastrophiques.

D'autres conditions météorologiques extrêmes (R25), différentes des inondations, telles que des températures très basses, qui peuvent provoquer le gel, peuvent causer des fissures dans le béton, affaiblissant ainsi la structure. La pression de la glace sur la surface du réservoir peut également affecter des éléments tels que les vannes. À leur tour, les températures élevées diminuent la résistance du béton, favorisant la formation de fissures et de défaillances structurelles. Une sécheresse prolongée expose les pentes à des problèmes d'érosion et d'infiltration qui doivent être traités dès le départ. Les typhons génèrent également des vagues intenses et des pics de débit qui peuvent dépasser les niveaux critiques des barrages.

5.2. REEVALUATION DES INONDATIONS EXTREMES

Dans le cadre de l'examen périodique de la sécurité, l'hydrologie des extrêmes doit être réexaminée, en particulier lorsqu'il y a des indications d'une capacité d'évacuation insuffisante. La mise en œuvre de nouvelles réglementations plus exigeantes ou la prise de conscience d'un risque accru d'extrêmes est également prévue dans les PAN[§], selon la nomenclature des Nations unies.

À quoi sommes-nous confrontés ?

- Estimation efficace des quantiles d'inondation pour des périodes de retour vraiment importantes
- Fortement conditionné par le manque de données fiables associées aux inondations extrêmes,
- Forte incertitude dans l'estimation de la queue supérieure de la fonction de distribution
- Absence de méthodologies adéquates ou, du moins, faible pénétration des nouvelles pratiques en matière d'ingénierie
- Faisabilité de l'application pratique essentiellement orientée vers le dimensionnement des évacuateurs de crues pour les grands barrages

Le principal problème est l'utilisation de l'extrapolation à partir d'un comportement hydrologique connu, souvent très court, vers des événements très extrêmes, qui sont ceux que nous avons besoin de connaître. En outre, le changement climatique annule l'hypothèse de stationnarité qui nécessiterait une thèse selon laquelle l'extrapolation est un mécanisme valide.

Méthodes d'extrapolation classiques

- Données sur les précipitations maximales en **24**
- **Ajustement** d'une fonction de distribution (Gumbel, SQRT-max, L-Person...) obtenant les quantiles des précipitations maximales en 24 heures, (T=25, 50, 100 et 500 - 10000 ans) **Extrapolation** de la fiabilité douteuse
- **Interpolation** pour obtenir des précipitations surfaciques et application d'un facteur de réduction **surfacique**
- Répartition des précipitations moyennes dans chacun des **sous-bassins**.
- Les hyétogrammes artificiels basés sur des **courbes IDF enveloppes** conservatrices de la distribution temporelle qui génèrent un biais dans l'estimation des probabilités finales.
- Modélisation de la réponse du bassin par la transformation précipitation-net pluie-débit.

[§]Plan national d'adaptation

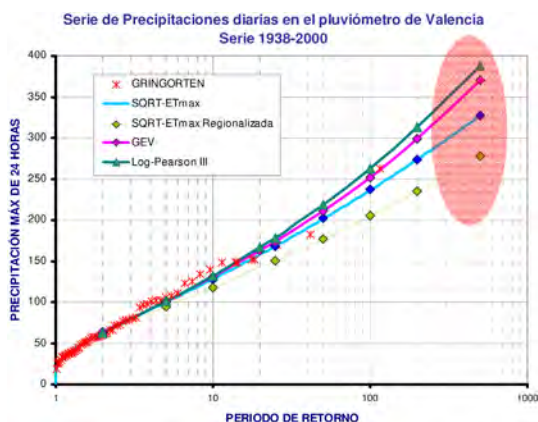


Fig. 7

Incertitudes liées à l'extrapolation classique

La plupart du temps, il y a un manque flagrant de données sur les débits, inexistantes ou situées dans d'autres sections du réseau fluvial, etc. avec des séries de quelques décennies seulement, avec un manque de données ou de précision sur les débits extraordinaires, s'ils ont été enregistrés, etc.

Dans le cas des données pluviométriques, la longueur de la série est généralement plus longue, mais aussi des décennies et rarement plus d'un siècle et avec une faible densité spatiale. Néanmoins, la plupart du temps, il s'agit de la seule source véridique et c'est pourquoi on a inévitablement recours à la reproduction du cycle pluie-ruissellement pour déterminer les événements.

Mais au sein des événements d'inondation, il faut distinguer au moins deux populations : les inondations ordinaires et les inondations extraordinaires. Si la genèse des deux groupes n'est pas la même et que tous les événements n'appartiennent pas à un ensemble ayant les mêmes propriétés intrinsèques, celles-ci ne se traduisent pas par les mêmes propriétés statistiques et il faudrait considérer deux populations statistiques différentes. Prenons le cas d'un front froid pluvieux et d'un typhon. Ils ne doivent pas être analysés dans le même ensemble statistique. Si l'on dispose de peu de données dans un bassin et que l'on réduit le nombre d'événements, la difficulté de caractérisation augmente.

C'est pourquoi des méthodes telles que le PMP (OMM, 1986), le Regional Maximum Flood (FMR) (R18, Afrique du Sud) et d'autres auxquelles il sera fait référence dans ce rapport, recherchent des données dans d'autres bassins voisins, présentant certaines similitudes météorologiques qui facilitent leur utilisation à une plus grande échelle d'application.

D'autres tentatives proposent d'identifier des comportements probabilistes avec des fonctions à double tendance, mais, si le nombre de données couvre quelques décennies, il restera illusoire d'extrapoler directement à des dizaines de siècles.

5.3. CONCEPTION D'UNE MODÉLISATION ÉVÉNEMENTIELLE DES PRÉCIPITATIONS ET DU RUISSELLEMENT

La transformation précipitation-débit nous permet de travailler avec des séries de précipitations, généralement avec des périodes de données plus longues, pour déduire les fonctions de distribution des inondations.

Les précipitations, y compris leur distribution temporelle et les pluies antérieures, sont généralement la variable stochastique, laissant comme paramètres descriptifs de la transformation les pertes par interception et infiltration, les caractéristiques hydrographiques du bassin et son réseau de drainage.

5.4. NOUVELLE TENDANCE ACTUELLE

Aujourd'hui, dans de nombreux pays, la réglementation distingue l'exigence d'une crue de référence, avec une période de retour d'environ 1 000 ans, en fonction de la catégorie de risque, et une crue de sécurité avec une période de retour beaucoup plus longue ou le PMF.

L'évaluation des périodes de retour correspondant aux débits caractéristiques des barrages existants, en cours d'exploitation, pose d'importants problèmes :

- Incertitude dans les estimations basées sur les méthodes classiques, les plus répandues. Dans les petits bassins et sans mesure directe des affluents ou des précipitations, elle est plus difficile.
- Évaluation de l'incertitude L'approche classique pour évaluer l'incertitude dans la détermination des variables statistiques, telles que la probabilité des extrêmes hydrologiques, est l'analyse de Monte Carlo.
- Nécessité de générer des valeurs probables de variables dérivées telles que les niveaux, les dommages, etc., qui sont des variables sans valeurs enregistrées et qui peuvent être différentes bien qu'elles soient la conséquence d'événements équiprobables.
- Impacts du changement climatique : Augmentation de la fréquence et de l'intensité des événements extrêmes sans méthodologies consensuelles et facilement applicables.

- Limites des méthodes traditionnelles : Les méthodes basées sur des statistiques ou des modèles hydrologiques peuvent sous-estimer les conditions extrêmes.

Ce sont ces défis qui sont abordés dans les sections suivantes de ce rapport.

5.5. PMF

La crue maximale probable (CMP ou PMF) représente l'événement de crue le plus important dont on peut raisonnablement s'attendre à ce qu'il se produise. Cette méthode est particulièrement utilisée pour les inondations aux conséquences potentiellement extrêmes, lorsque les méthodes statistiques conventionnelles ne répondent pas aux critères de risque ou parce que la réglementation du pays l'exige.

Les méthodes traditionnelles d'estimation de la PMF comprennent des analyses statistiques des données d'inondation et des modèles de simulation basés sur les précipitations. Les courbes d'enveloppement des crues, dérivées de l'analyse des maximums historiques, sont des outils précieux dans ce contexte, bien que leur applicabilité soit généralement limitée aux régions de basse latitude à forte disponibilité d'humidité.

Les conditions du changement climatique peuvent également rendre obsolètes les hypothèses sur lesquelles les estimations précédentes du PMP ont été réalisées.

5.6. COURBES ENVELOPPANTES AUSTRALIENNES

La régionalisation des courbes d'enveloppement des crues pour les estimations préliminaires des débits spécifiques de la crue maximale probable (CMP) peut être nécessaire pour des zones spécifiques dépourvues de données.

La réanalyse atmosphérique pour explorer comment la variabilité de l'eau maximale précipitable peut expliquer les différences régionales dans les inondations extrêmes est maintenant une nécessité. Une équation empirique a été développée sur la base de la relation entre le coefficient de Francou-Rodier (k) et le maximum d'eau précipitable, en ajustant de manière conservatrice les courbes pour inclure les plus grandes inondations enregistrées. Cette approche a été testée à l'aide d'un catalogue d'événements historiques.

Des courbes enveloppes (R08) ont été générées sur la base de différents niveaux d'eau précipitable maximale, adaptées à diverses zones géographiques,

étant compatibles avec des études détaillées menées aux États-Unis, en Chine, en Europe et en Afrique du Sud, et montrant une cohérence avec les événements graves enregistrés. Dans des conditions météorologiques changeantes, une révision devrait être nécessaire dans certaines régions.

Ces courbes sont précieuses pour les études de faisabilité et la validation des estimations basées sur les précipitations, en particulier dans les régions en dehors des tropiques où les courbes globales peuvent sous-estimer les inondations.

Les recherches futures devraient prendre en compte d'autres facteurs hydrométéorologiques, tels que les rivières atmosphériques, les cyclones sur de longues distances, etc. qui apportent de l'humidité lors d'événements extrêmes. Bien que l'étude suppose la stationnarité des données, il est nécessaire d'incorporer des ajustements pour les changements climatiques.

R08 propose une méthodologie robuste pour obtenir des estimations préliminaires des PMF au niveau mondial. Les courbes enveloppantes régionalisées permettent de surmonter les limites des courbes globales traditionnelles, en particulier dans les zones non tropicales. Bien que ces courbes ne soient pas destinées à remplacer les études locales, elles constituent une base solide en l'absence de données détaillées.

5.7. UNE METHODOLOGIE INNOVANTE (FRANCE)

Une méthodologie innovante pour l'évaluation des événements hydrologiques extrêmes dans le contexte du changement climatique (R13) est présentée par la France.

L'évaluation de la sécurité des inondations dans la conception des barrages est confrontée à des défis importants en raison du réchauffement climatique. Les méthodologies traditionnelles, basées sur des données historiques de précipitations et de débit, sont inadéquates car elles dépendent d'un climat stationnaire (R13).

La relation Clausius-Clapeyron peut donner une orientation à cet effet :

$$\frac{dp}{dT} = \frac{L}{T\Delta v}$$

où dp/dT est la pente de la courbe, L est la chaleur latente ou l'enthalpie du changement de phase et Δv est la variation du volume spécifique.

Cette équation nous donne un indice sur une augmentation théorique de 7% de l'intensité des précipitations extrêmes pour chaque augmentation de 1°C de la

température atmosphérique, bien qu'elle manque de corrélation robuste dans les applications locales et montre des résultats incohérents dans des régions spécifiques, telles que l'Europe et les tropiques (R13).

5.8. NECESSITE D'UN PLUS GRAND NOMBRE DE DONNEES

La méthodologie la plus répandue dans le secteur de l'ingénierie hydrologique, pour l'estimation des débits de crue extrêmes, souffre souvent du manque de données extrêmes pour déduire correctement ses lois de fréquence, sur toutes les valeurs de la période de récurrence élevée. Il en résulte généralement une sous-évaluation ou une surévaluation des débits en raison de la petite taille de l'échantillon.

- (i) Série plus longue : Paléo-hydrologie
- (ii) Plus d'espace géographique : transposition stochastique

5.9. EXTENSION DE LA SERIE DE DONNEES : PALEO-INONDATIONS

La paléohydrologie est l'une des tentations d'allonger la durée des séries de données.

La paléohydrologie peut traiter des inondations anciennes qui se sont produites avant l'existence de mesures systématiques. Sur la base des enregistrements géomorphologiques et stratigraphiques, la granulométrie peut être utilisée pour évaluer les épisodes sur une très longue période de l'Holocène. La variabilité du climat naturel au cours de cette dernière période géologique (comme le petit âge glaciaire au cours des XVe-XVIIIe siècles) rend difficile l'intégration de cette technique dans la pratique si l'on ne procède pas à certaines corrections qui ne sont pas faciles à appliquer.

Les périodes sans inondations sont aussi généralement des indices utiles, à condition qu'elles soient exemptes de distorsions de l'information, comme les périodes où certains murs de défense de guerre défendaient aussi les villes contre les inondations et ne laissaient donc pas de traces faciles à interpréter.

5.10. ANALYSE REGIONALE DE LA FREQUENCE DES INONDATIONS

L'estimation des inondations pour des périodes de retour importantes est fortement conditionnée par le manque de données fiables associées aux

inondations extrêmes, produisant une grande incertitude dans l'estimation de la queue supérieure de la fonction de distribution cumulative.

En hydrologie, il est souvent difficile d'obtenir suffisamment de données sur un seul site pour déterminer de manière fiable la fréquence d'événements rares par le biais d'une analyse de fréquence. Ce problème est particulièrement prononcé pour les événements extrêmement rares, qui sont essentiels pour l'évaluation des risques liés à la sécurité des barrages.

Pour remédier à cette limitation, une approche alternative consiste à substituer le temps à l'espace pour estimer les inondations extrêmes. Cette méthode s'appuie sur des données hydrologiques provenant de plusieurs sites d'une même région pour pallier la rareté des enregistrements à long terme sur un site donné. En mettant en commun des données spatiales provenant de différents sites, l'approche compense le manque de données temporelles et fournit une base plus solide pour l'estimation de la fréquence et de l'ampleur des événements hydrologiques extrêmes. Cette substitution spatiale améliore la fiabilité de l'analyse de la fréquence des inondations, en particulier pour les événements rares et à fort impact.

Trois approches ont été envisagées dans le passé pour l'analyse de la fréquence des inondations régionales : (1) l'approche du paramètre moyen, (2) la méthode de l'inondation indexée et (3) l'approche de la fréquence spécifique.

5.11. GENERATION SYNTHETIQUE

La génération de données synthétiques, que ce soit sous forme de séries multiples ou de simulation continue, est basée sur la génération Monte Carlo de séquences longues et détaillées de variables hydrométéorologiques, notamment les précipitations, la température de l'air, la vitesse et la direction du vent. Il est nécessaire de représenter les différences spatiales à travers le bassin versant, il est nécessaire de générer des variables hydrométéorologiques pour plusieurs sites simultanément en respectant la corrélation et les paramètres de cohérence générale à l'échelle du bassin. Les modèles de réponse hydrologique doivent transformer les séries hydrométéorologiques en écoulement. Y compris l'effet des réservoirs, pour lesquels il est nécessaire d'introduire des règles de fonctionnement qui sont souvent liées à l'événement.

Pour relever ces défis, le projet EXAR a été développé en utilisant une approche basée sur des simulations hydrométéorologiques continues (R05), puis étendu à l'ensemble du territoire suisse dans le cadre du projet EXCH. Ils sont basés sur une simulation hydrologique continue, pour estimer les événements avec des périodes de retour de 1 000 à plus de 10 000 ans afin de se conformer à la

réglementation nationale actuelle en Suisse (WRFA) où une crue de retour de 1 000 ans est prescrite et, pour la sécurité, une valeur augmentée de 50% ou le PMF.

C'est le manque de données dans les petits bassins alpins et l'incertitude liée au changement climatique qui imposent une nouvelle approche basée sur des simulations continues, développée dans les projets EXAR et ESXCH (étendu) combinant des modèles climatiques et hydrologiques pour générer des séries réalistes d'événements extrêmes. Inclure des variables telles que le pic de caudale, le volume et la durée des crues et les associer aux conditions préalables pour tenir compte de l'influence de facteurs tels que le déshuilage et la saturation du sol.

Le projet EXAR sur l'Aar (17 700 km²) a été étendu à plus de 225 barrages sous supervision fédérale, dans le cadre du projet EXCH qui fournira des outils pour évaluer les risques dans les petits bassins. Avant son adoption dans la réglementation, il est nécessaire d'identifier les limites dans les bassins sans calibrage.

Il n'est pas entièrement démontré que les fonctions de probabilité utilisées pour la génération de séries synthétiques sont représentatives des queues d'événements réellement extraordinaires qui pourraient être dus à des phénomènes qui ne sont pas représentés de manière adéquate dans les fonctions de probabilité stochastiques adoptées pour la génération de séries, même si celles-ci sont très longues.

5.12. MODELES CONCEPTUELS AVEC BASE PHYSIQUE

Pour pallier l'absence de données empiriques suffisantes, il est nécessaire de connaître les processus physiques qui les justifient. C'est le domaine des modèles hydrologiques conceptuels.

Les processus physiques connus et formulés à l'aide de modèles conceptuels permettent d'exploiter les enregistrements d'événements survenus dans d'autres régions en les transposant ou en examinant les conditions dans lesquelles ils se seraient produits à un autre endroit. Dans des conditions météorologiques stationnaires, il est possible d'effectuer cette transposition. Il est plus difficile de le faire si le scénario de changement climatique change.

La "transposition" est la modification des paramètres descriptifs d'une tempête de manière qu'elle puisse être déplacée dans le temps et l'espace pour être utilisée comme données potentielles de précipitations dans un lieu autre que celui où elle s'est produite.

Dans la méthodologie d'estimation du PMP (OMM), ses variables descriptives sont corrigées en fonction de la distance à la source d'humidité, de l'effet

orographique de la barrière interposée et même d'une transposition temporelle à d'autres conditions d'humidité maximale attendue.

Certains tests comme GSST** fournissent une analyse plus robuste de la transposabilité des paramètres du modèle entre les bassins versants (R13). Il existe des méthodologies (R13) pour surmonter ces difficultés, comme celle qui consiste à combiner la génération stochastique de données climatiques pour fournir des données d'entrée à des modèles hydrologiques utilisant des prévisions climatiques et l'utilisation de modèles multiples. Les résultats des modèles calibrés de manière dynamique peuvent mieux refléter les conditions climatiques futures. L'application à la région du fleuve Madère (Brésil) montre qu'il est possible d'améliorer les prévisions des caudales extrêmes en fonction des scénarios de changement climatique.

5.13. TRANSPOSITION STOCHASTIQUE

Une autre option consiste à effectuer une transposition stochastique. La "transposition stochastique" serait la généralisation de la transposition, telle que définie dans la méthodologie PMP, mais avec des variables qui ne sont pas maximisées mais traitées de manière probabiliste. Dans une approche stochastique, les modèles hydrologiques sont donc alimentés par des variables aléatoires connues de leur point de vue probabiliste. Les procédures de génération d'événements pour la méthode de Monte Carlo doivent suivre les fonctions des distributions de probabilité, y compris les dépendances croisées, s'il y en a lorsqu'il y a une covariance non nulle. L'utilisation de l'approche stochastique avec des informations sur les précipitations d'une zone de transposition permet d'estimer les courbes de fréquence des débits de pointe, les volumes des hydrogrammes, les niveaux maximaux des réservoirs ou d'autres paramètres définissant les événements.

La transposition des tempêtes est une alternative viable pour utiliser efficacement les informations externes au bassin analysé, permettant une amélioration substantielle de la fiabilité dans l'estimation de ces quantiles de forte récurrence dans la distribution $F(Q)$, de sorte qu'un plus grand nombre d'événements vraiment extrêmes sont disponibles et qu'ils fournissent des connaissances à ce sous-ensemble spécial de tempêtes dont le schéma est différent des tempêtes ordinaires.

Ce n'est que dans le cas particulier d'une zone de transposition totalement homogène où les tempêtes conservent leurs propriétés que cette transposition est automatique et permet l'extension de l'intégrale spatiale sans autres précautions. Les principes de transposition des tempêtes ont été introduits au début des années

** Test généralisé de l'échantillon fractionné

60 et largement développés par Foufoula (1989) et Fontaine (1989), qui ont essayé d'améliorer les difficultés antérieures pour une application réelle au barrage de Harriman. A cette époque, les difficultés importantes qui ont fait progresser les applications réelles ont été vraiment ralenties.

Cependant, la nécessité d'étendre la zone pour trouver des phénomènes vraiment extraordinaires enregistrés ne préserve pas toujours cette homogénéité, principalement en raison des effets orographiques qui caractérisent les deux territoires. Ces événements sélectionnés constituent l'échantillon de données brutes qui doivent être transposées de manière adéquate dans une référence pour être ensuite analysées dans un cadre complexe afin de définir les paramètres de modèles probabilistes isolés de fréquence, d'AMC (Antecedent Moisture Condition), de modèles temporels et spatiaux, d'orientation ou d'épaisseur des précipitations.

Mais des décennies plus tard, une amélioration substantielle de l'estimation des quantiles a été obtenue, après la mise en place d'un cadre méthodologique général basé sur ces principes, qui incorpore les facteurs météorologiques et topographiques requis conditionnant le processus. Grâce à ces améliorations, la faisabilité de l'application pratique d'une telle méthodologie orientée efficacement vers le dimensionnement optimal des grands barrages a été prouvée, devenant ainsi une technique prometteuse. Cette méthodologie prometteuse a été développée sur la base des principes de la transposition stochastique des tempêtes en utilisant la profondeur de l'eau précipitable maximale dans l'atmosphère autour d'une zone donnée comme concept clé à prendre en compte malgré les limitations dérivées des effets orographiques.

Cet inconvénient a été supprimé (Cifres, 2016) grâce au concept de l'ellipse orographique et du gradient central, qui a permis d'incorporer les facteurs météorologiques et orographiques les plus déterminants d'une manière systématique et basée sur la physique. De cette manière, la faisabilité pratique de cette méthodologie a été démontrée, visant spécifiquement à améliorer les méthodes de dimensionnement des infrastructures hydrauliques pour la défense contre les inondations et l'évaluation des risques hydrologiques. La zone d'étude est l'arc du golfe de Valence (Espagne). Pour les tempêtes extrêmes, grâce à un développement basé sur la physique, il est possible de rendre le facteur de conditionnement orographique indépendant dans la procédure de transposition, à proximité de n'importe quel point géographique.

Tout d'abord, il faut préciser que pour les périodes de retour très élevées, seules les tempêtes vraiment violentes peuvent décrire statistiquement les phénomènes et leur caractérisation ne peut pas être déduite d'événements ordinaires ou moyens. La zone de transposition doit être définie comme capable de fournir un certain nombre d'événements vraiment extrêmes, mais aussi suffisamment homogène pour permettre la transposition des tempêtes vers une référence commune.

Une fois que les événements sélectionnés dépassant le seuil des critères de gravité ont été identifiés, la transposition des tempêtes doit être effectuée afin de créer une base de données statistiquement homogène. En suivant les principes de la transposition PMP (OMM 1989), certaines améliorations ont été introduites dans un bilan atmosphérique du contenu en eau, en considérant non seulement le profil de l'eau saturée, le profil du vent, le point de rosée pour la source d'humidité, l'orographie, mais aussi l'élévation de l'interface froide et les précipitations dans les zones précédentes.

Les fonctions de distribution de probabilité séparées des facteurs de définition mentionnés doivent être évaluées, ce qui permet de dériver et de quantifier les quantités et la distribution hypothétiques des précipitations dans diverses conditions météorologiques ou dans des lieux géographiques possibles, différents de ceux qui ont réellement existé historiquement lorsque l'événement extrême s'est produit. Cela doit être fait en couvrant la plage de variation de ces paramètres dans la zone de transposition, en créant la base de données résultante comme un historique synthétique d'événements rares. Le nombre total de paramètres doit être soigneusement réduit pour gagner en parcimonie et en robustesse.

La procédure permet d'étendre l'échantillon réel disponible après les enregistrements historiques et, par conséquent, d'estimer de manière plus cohérente la queue supérieure de la distribution des valeurs extrêmes des pics d'inondation au moyen d'une intégration numérique de la base de données de résultats créée. L'approche théorique nécessite des modèles météorologiques et orographiques pour pouvoir transformer les événements d'une zone suffisamment large. Ces modèles ont été conçus en tenant compte de l'orographie lors de la réévaluation des tempêtes provenant de différents endroits.

L'orographie a une influence sur le comportement du mouvement des masses d'air et, par conséquent, la forme et l'orientation des tempêtes pourraient suivre ses conditions. Le problème complexe de l'influence topographique sur les propriétés structurelles spatio-temporelles des précipitations extrêmes est abordé dans un cadre original cherchant une nouvelle réduction des paramètres stochastiques.

Nous pouvons introduire le concept de gradient central (Cifres, 2007), lié à la profondeur du maximum d'eau précipitable dans l'atmosphère, et sa variation dans les différentes directions autour d'un point géographique donné. Ce concept permet d'isoler en pratique l'influence de la topographie dans la procédure de transposition, ce qui représente un aspect essentiel de la robustesse du processus. La définition proposée du gradient central sera " $\Delta W/d$ " comme différence de teneur en eau par unité de distance.

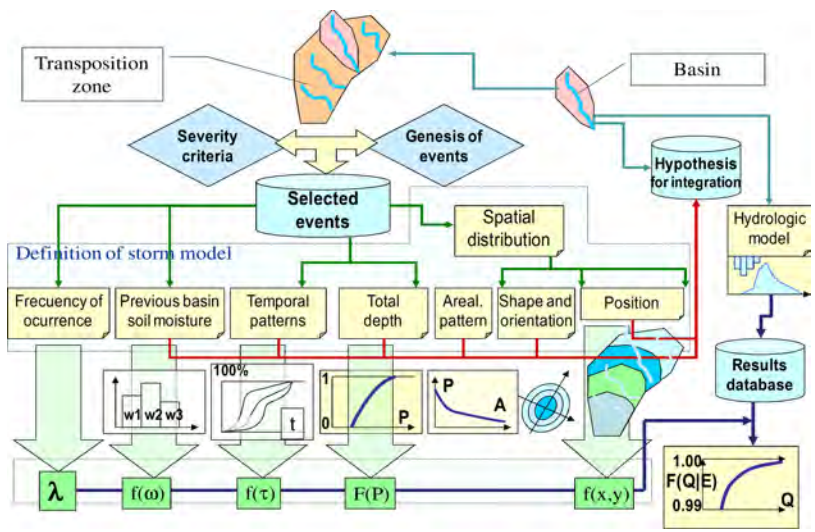


Fig. 8
Organigramme pour la transposition stochastique et orographique

La technique a été appliquée avec succès lors de l'examen de la sécurité hydrologique du barrage d'Algar à Valence, où des précipitations de plus de 1000 mm en 48 heures ont été enregistrées.

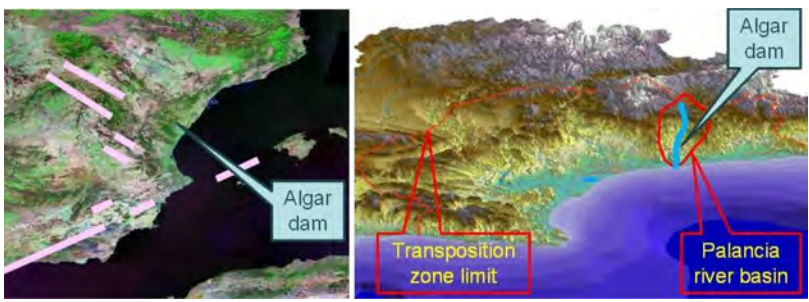


Fig. 9
Zone de transposition pour le bassin de Palancia (cas du barrage d'Algar)

Ces précipitations extrêmes se produisent généralement en octobre-novembre et résultent de la combinaison de plusieurs facteurs :

- Températures élevées dans la mer Méditerranée
- Une masse d'air de basse pression bloquée par un anticyclone situé en Europe centrale, forçant les vents chauds du Sahara, qui transportent de grandes quantités d'humidité, à affronter les crêtes côtières espagnoles.
- Conditions orographiques forçant l'ascension des masses d'air
- Réserve d'air très froid dans les couches supérieures de l'atmosphère

Les tempêtes extrêmes résultent de la combinaison simultanée de tous ces facteurs, même si chacun d'entre eux est modéré ou peu extrême. La localisation finale de la tempête dans un petit bassin versant peut donner lieu à un événement vraiment extrême, jamais vu à cet endroit auparavant.

Seul un événement extrême s'est effectivement produit dans le bassin, mais l'évaluation de la fonction de distribution de la probabilité d'inondation dans le bassin a été obtenue par intégration sur l'ensemble de la région de transposition et en tirant parti de ces 33 événements^{††}. Néanmoins, cette sélection d'événements implique qu'en dessous d'une période de retour de 25 ans, les inondations ne peuvent pas être évaluées de manière fiable, puisque seuls les événements vraiment extrêmes sont décrits par cette fonction de probabilité.

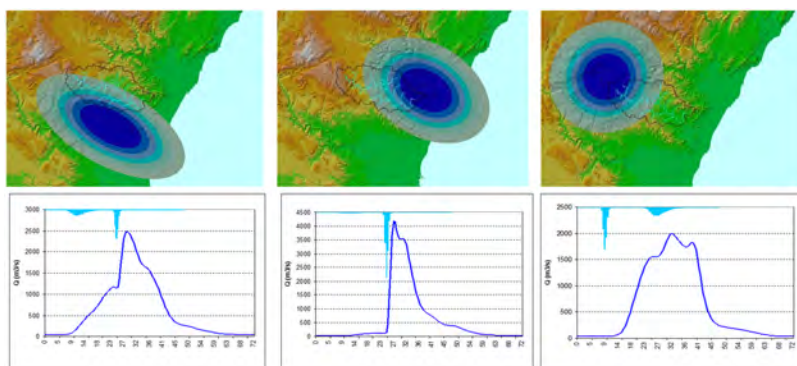


Fig. 10

Différentes simulations variant en fonction de la position, du temps et de la profondeur

En raison de la capacité de la méthodologie à évaluer les inondations à période de retour très élevée et des similitudes dans les procédures entre les

^{††}Identifié au moyen d'un critère de seuil prenant également en compte la genèse météorologique

approches proposées et PMF, la probabilité PMF peut être évaluée d'une certaine manière.

5.14. IMPACT DU CHANGEMENT CLIMATIQUE

Une analyse de sensibilité en modifiant simplement le point de rosée dans la source d'humidité nous aide à comprendre les changements possibles dans la probabilité au moyen du modèle météorologique adopté qui régit les profondeurs des tempêtes. Un simple exercice d'augmentation du point de rosée de +3 °C réalisé montre comment la température de la mer met en danger les conditions météorologiques potentielles pour produire de fortes tempêtes en raison du potentiel plus élevé d'évaporation et de transport de l'humidité.

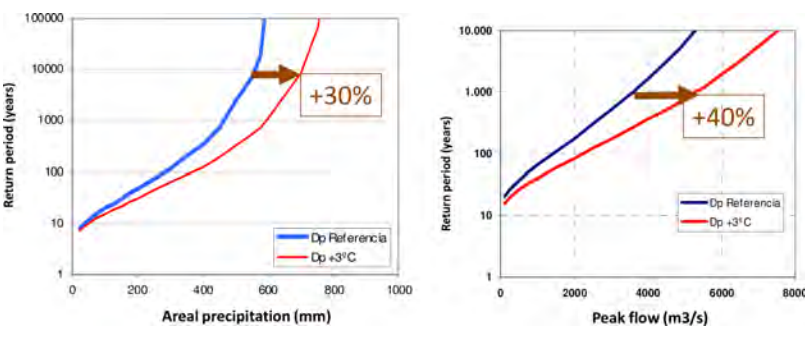


Fig. 11
Impact du changement climatique sur les probabilités d'inondation dues à l'augmentation du point de rosée

Le résultat de cette expérience est que seulement 3 °C dans la température de l'eau de mer, pour le même reste de paramètres, signifie près de 40% de l'augmentation du débit de pointe pour les inondations extrêmes.

La faisabilité de la transposition stochastique et orographique à des fins pratiques est donc prouvée. Les modèles basés sur la physique peuvent réduire la composante stochastique, ce qui confère au modèle global une plus grande parcimonie. Nous pouvons tirer des avantages pratiques d'études détaillées sur les vents, les températures et l'orographie si nous encourageons des équipes multidisciplinaires comprenant des météorologues à définir des modèles conceptuels capables de faciliter la transposition à partir de zones plus vastes.

La transposition stochastique, ainsi que les approches PMP, tiennent compte des limites physiques et tendent donc à des valeurs plus faibles que l'extrapolation pour les périodes de retour très élevées, où les dernières sont totalement rejetées. Néanmoins, une sous-estimation de la plage de conception peut également être constatée. Les concepteurs et les régulateurs doivent être conscients qu'un examen des hypothèses et des méthodologies peut conduire à une évaluation moins sûre qu'ils ne le pensaient.

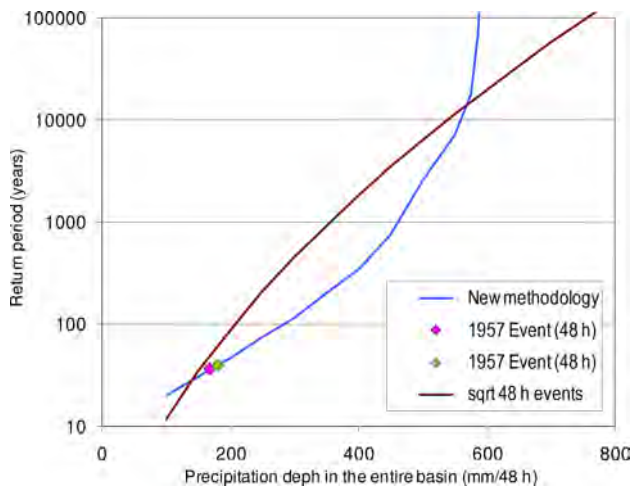


Fig. 12
Comparaison entre les résultats de la méthode classique et ceux de la méthode proposée

Les préoccupations physiques et météorologiques utilisées permettent d'étendre en pratique les informations pertinentes contenues dans les enregistrements historiques des précipitations extrêmes, ce qui fournit à son tour une base pour des estimations plus robustes et plus fiables des probabilités d'inondations extrêmes, par rapport aux méthodes plus limitées basées sur l'inférence statistique classique à partir d'un échantillon réduit.

5.15. INCERTITUDE

Les inondations calculées pour être utilisées dans les processus de conception, d'examen, de réévaluation ou d'analyse des risques doivent être associées à

leur niveau d'incertitude, en particulier lorsqu'elles doivent être intégrées dans la prise de décision en matière de sécurité.

Les sources d'incertitude sont si nombreuses en hydrologie que la décomposition indéfinie de la réalité en éléments de plus en plus petits, qui serait rendue possible par des techniques de calcul formidablement performantes, n'apporte pas nécessairement une amélioration convaincante de la qualité finale d'une étude.

La possibilité d'une analyse détaillée de la fiabilité des données, de la crédibilité de chacune des étapes ou des éléments de la méthodologie de calcul utilisée, etc. n'est pas, lors de la multiplication des paramètres, une stratégie toujours recommandée pour la détermination finale de l'incertitude, en remplacement d'un avis d'expert solide.

L'incertitude prédictive dans la prévision des inondations est définie comme la fonction de probabilité d'occurrence d'une valeur future d'une variable (telle que le niveau d'eau, le débit de pointe ou le volume de l'hydrogramme) plutôt qu'une simple valeur scalaire.

Il existe une différence conceptuelle entre l'"incertitude du modèle" couramment utilisée pour la vérification et l'incertitude prédictive, qui est utilisée pour prévoir l'avenir et qui doit être liée aux données initiales.

Il existe actuellement des processeurs d'incertitude pour les systèmes opérationnels de prévision des inondations (Todini 2009) qui peuvent être continus (Hydrological Uncertainty Processor, Bayesian Model Average, Conditional Model Processor, etc.) ou binaires (Logistic Regression, Bayesian Binary Multivariate Processor, etc.) L'incorporation de l'incertitude prédictive dans le processus de prise de décision est une tâche à améliorer pour sa mise en œuvre en améliorant la tendance actuelle à omettre la pratique la plus répandue.

6. AGIR FACE AUX EXTREMES

Conscients de l'ampleur et de la probabilité d'événements véritablement extraordinaires, l'inaction n'est pas acceptable. La liste des initiatives à prendre pour atténuer le risque peut être de nature structurelle ou non structurelle.

Parmi les actions structurelles, il est nécessaire d'envisager la construction de barrages qui créent des réservoirs de laminage, compte tenu de l'action conjointe dans le bassin avec d'autres infrastructures, la révision et l'adaptation des barrages à de nouveaux scénarios de charge, le changement des niveaux maximaux attendus, la modification ou l'expansion des déversoirs ou l'établissement de déversoirs

complémentaires, d'urgence ou de fusibles, ainsi que la canalisation dans les sections de la rivière, les levées, les systèmes de drainage, etc.

Parmi les mesures non structurelles, l'adoption de règles d'exploitation optimales, y compris la mise en place de mesures de sauvegarde, la vidange saisonnière et les lâchers préventifs de réservoirs, la cartographie des risques, les systèmes d'alerte précoce, la mise en œuvre de plans d'urgence, l'amélioration de la résilience dans les zones exposées en aval, la gestion des terres, l'éducation de la société civile et sa meilleure participation à la préparation des plans, ainsi que la promotion d'une meilleure gouvernance pour les événements extrêmes, par le biais d'un renforcement institutionnel.

La pratique généralisée en matière de sécurité des barrages, avec des examens périodiques qui incluent le changement climatique, permettra de détecter les changements de risque qui conduisent à l'application de mesures permettant de retrouver des niveaux de risque tolérables.

Une grande partie de ces actions structurelles et non structurelles sont décrites dans les documents présentés à ce congrès dans le cadre de cette Q110, car elles sont conçues pour faire face à des phénomènes hydrologiques extrêmes.

6.1. ÉVACUATEURS DE CRUES

Un certain effort d'investissement est déjà fait pour améliorer le système d'évacuation des crues, notamment par la modification des déversoirs :

1. Mise à jour de la capacité des déversoirs ou ajout de déversoirs complémentaires.
2. Augmentation du niveau d'eau maximal autorisé au moyen d'un renforcement structurel.
3. Remise en état des équipements hydromécaniques et amélioration du fonctionnement pendant les inondations.

6.1.1. *Bassin de la rivière Drin*

La réévaluation de la sécurité hydrologique des barrages à l'échelle du bassin nécessite une approche globale, comme dans le cas de la rivière Drini (R20) en Albanie, où la sécurité de sept grands barrages et de six centrales hydroélectriques (HPP) qui génèrent environ 70 % de l'électricité du pays a été analysée. L'évaluation a encouragé l'amélioration du fonctionnement et des mesures planifiées pour augmenter la capacité énergétique et la sécurité des barrages, y compris l'amélioration des capacités d'évacuation en cas d'inondation.

Le système utilise le modèle PANTA Rhe^{††} (voir Archfield, 2015) pour simuler les précipitations et les événements de fonte, ainsi que le bilan hydrique du système sous l'influence de facteurs tels que le changement climatique, l'utilisation des terres, la croissance démographique et la façon dont les sociétés influencent le cycle hydrologique et vice versa. L'analyse des précipitations, la génération de débits maximums probables (PMF) et l'évaluation de la réponse du système aux événements extrêmes ont permis d'identifier la nécessité d'augmenter les capacités de décharge des barrages de Fierza (2 080 m³/s supplémentaires) et de Koman (3 000 m³/s supplémentaires) pour gérer en toute sécurité les PMF et mettre à jour les schémas d'exploitation dans le bassin.

Le système fluvial du Drini, comme cela est prévisible dans d'autres bassins où une réanalyse complète est effectuée, nécessitera des investissements importants pour augmenter sa capacité d'évacuation et assurer la sécurité contre les événements extrêmes. L'évaluation de la vie humaine en tant que principal facteur de risque doit donc être prise en compte dans l'évaluation économique.

6.1.2. *Barrage de regajo*

Parfois, c'est la mise en œuvre de nouvelles règles ou réglementations qui nécessite la révision de l'hydrologie utilisée pour le dimensionnement de l'évacuateur de crues d'un barrage. C'est, par exemple, le cas de l'Espagne (R4), où une nouvelle réglementation a été promulguée^{§§}, qui exige, pour les barrages en béton, l'adoption de crues de conception et de crues extrêmes avec des périodes de retour de 1 000 et 5 000 ans. En Espagne, ce type de barrage prédomine dans les plus de 1200 grands barrages en service.

C'est le cas du barrage de Regajo (R4), situé à Castellón (Espagne), construit en 1962 et destiné à l'irrigation. Pour améliorer la capacité d'évacuation de 437 m³/s avec laquelle il a été conçu pour une période de retour de 500 ans, un nouveau déversoir a été conçu pour atteindre 1800 m³/s pour une période de retour de 1000 ans, conformément à une nouvelle réglementation et à une nouvelle hydrologie officielle.

Un nouveau déversoir complémentaire, de 132 mètres, doit être combiné avec une réduction d'un mètre du niveau maximal d'exploitation, l'élévation d'un mètre de plus au sommet du barrage et le remplacement des vannes du déversoir existant.

Le débit déversé par le nouveau déversoir sur la culée doit dissiper l'énergie dans un bassin de tranquillisation, puis dans un canal qui redirige l'eau vers le pied du barrage. Parfois, le retour et la dissipation de l'énergie constituent l'un des

^{††}Union internationale des sciences géodésiques et géophysiques (UGGI)

^{§§}Normes techniques de sécurité espagnoles 2021, NTS

principaux défis du site lorsqu'il s'agit de mettre à jour la capacité d'évacuation de grands débits, comme dans le cas cité.

6.1.3. *Révision structurelle en France*

La modification des déversoirs pour augmenter la capacité d'évacuation entraîne souvent une révision structurelle si les niveaux d'exploitation normaux ou extraordinaires sont modifiés, et il est nécessaire de s'assurer que la nouvelle exploitation reste dans les marges de sécurité exigées par la réglementation, et sans réduire les marges existantes, sauf dans des cas exceptionnels de disponibilité de grandes marges précédemment disponibles.

Certains exemples en France illustrent cette situation, comme le réservoir de La Raviège (R14), grâce à la construction d'un déversoir PKW supplémentaire, augmentant le niveau d'eau maximal autorisé de 50 cm après une analyse structurelle détaillée. De même, le réservoir de La Laye (R14), grâce à la construction d'un déversoir latéral de surface avec un déversoir en labyrinthe de 30 m de long et une augmentation du niveau d'eau maximal et de l'élévation du noyau imperméable du réservoir, et le réservoir de Pinet (R14) où la modification des vannes existantes et l'optimisation des profils des piliers du pont ont été réalisées, ainsi qu'une analyse structurelle pour identifier les marges de stabilité et ajuster les critères de conception.

6.1.4. *Tragédie en Italie*

La tragédie de Molare (R16) et l'effondrement du barrage secondaire (1935) à la suite d'une tempête de grande intensité qui a causé plus de 100 morts dans la ville d'Ovada dans la vallée de la rivière Orba (Gênes, Italie).

La capacité totale des déversoirs était insuffisante par rapport au débit de pointe estimé lors de l'événement (2000-2500 m³/s). Les siphons automatiques et le déversoir latéral n'ont pas pu évacuer efficacement en raison d'une mauvaise conception et de l'obstruction par des débris.

Bien que les pluies du 13 août 1935 aient été intenses (370 mm en 10 heures), leur période de retour a été estimée à 200-300 ans, ce qui est moins exceptionnel que ce que l'on pensait auparavant. Néanmoins, les systèmes existants n'ont pas été en mesure de gérer les débits de pointe, ce qui a contribué au débordement et à l'effondrement du barrage de la selle.

Les événements de 2019 ont montré des amplitudes similaires en termes de volume de pluie et de débit, ce qui renforce l'idée que la tragédie aurait pu être évitée grâce à des conceptions plus robustes. Cette tragédie met en évidence les risques liés à des conceptions inadéquates et l'importance de la planification

hydrologique et hydraulique. Parmi les principaux enseignements tirés, nous soulignons la nécessité de prendre en compte, dans la conception des barrages, des événements dont la période de retour peut atteindre 1 000 ans.

La catastrophe de Molare a été causée par des défaillances dans la conception des structures d'évacuation et dans l'évaluation des conditions géologiques locales. Des simulations numériques sur le site ont montré que l'événement de 1935 n'était pas exceptionnel et qu'avec des mesures préventives appropriées, telles que des systèmes d'évacuation plus efficaces, l'effondrement aurait pu être évité. Cette analyse souligne l'importance des conceptions résilientes face aux événements extrêmes, en particulier dans un contexte de changement climatique.

6.2. Labyrinthes - Déversoirs PKW^{***}

Les déversoirs PKW, en tant que solution efficace pour la gestion des flux dans les barrages, ont gagné en popularité au cours des dernières décennies grâce à leur conception compacte et à leur capacité de décharge accrue, des caractéristiques qui les rendent idéaux pour relever les défis liés à la nécessité d'augmenter la capacité d'évacuation sans réduire le volume de fonctionnement du réservoir sans augmenter les niveaux (à partir de R07).

Ces structures représentent des solutions innovantes conçues pour évacuer efficacement les eaux de crue, en surmontant les contraintes géométriques des déversoirs labyrinthiques traditionnels. En permettant la gestion de volumes d'écoulement importants, ils réduisent considérablement le risque de débordement et de défaillance structurelle. Ces conceptions sont particulièrement avantageuses pour la construction de nouveaux barrages et l'amélioration des projets de barrages existants, y compris la réforme des déversoirs actuels ou l'ajout de déversoirs complémentaires. Leur conception compacte et efficace les rend idéales pour les sites où l'espace est limité, offrant une approche pratique et efficace pour améliorer la gestion des inondations et la sécurité des barrages.

6.2.1. Cas sud-africains

La révision de la capacité d'évacuation peut être le résultat d'autres modifications, telles que le rehaussement des barrages, pour augmenter à la fois la capacité de stockage et la sécurité contre les inondations (R17) où une vaste gamme d'options de décharge est proposée au moyen de vannes conventionnelles, de barrages en caoutchouc, de structures en labyrinthe, etc.

^{***} Déversoirs à touches de piano

C'est également le cas du barrage de Tzaneen (R18) situé dans le Limpopo, en Afrique du Sud, conçu en 1977, et qui cherche aujourd'hui à augmenter sa capacité de stockage et à garantir la sécurité contre les événements extrêmes.

L'augmentation de la hauteur du barrage, l'abaissement du seuil du déversoir et l'installation d'une structure hybride en labyrinthe (R18) ou autre (R17) sont compatibles avec la mise à jour du débit pour des événements extrêmes tels que ceux établis dans la réglementation sud-africaine basée sur le concept de Regional Maximum Flooding (FMR).^{†††}

Les exigences accrues en matière de dissipation de l'énergie imposent de réformer le bassin de tranquillisation, ce qui peut impliquer de modifier les dimensions, de renforcer et d'ancrer les dalles de protection (R18).

6.2.2. *Cas français et vietnamien*

Le cas du barrage de La Ravière (France, R2) est présenté par EDF^{†††}. Il s'agit d'un barrage-poids à contreforts d'une hauteur de 40 mètres et d'une capacité d'évacuation de 1000 m³/s. Des rapports ultérieurs, avec de nouveaux calculs hydrologiques, ont établi la nécessité d'augmenter la capacité à 1720 m³/s, pour laquelle il a été décidé de compléter le système de vannes avec un PKW sur la rive gauche.

Le PKW installé a une hauteur de 4,22 m, une largeur totale de 25,82 m et une longueur de développement de 176,6 m. Sa capacité de décharge supplémentaire est de 300 m³/s, ce qui augmente la sécurité du barrage de 30 %. Cet évacuateur de crues fonctionne de manière autonome, ce qui réduit considérablement les risques liés à une défaillance mécanique ou humaine.

Le même article se réfère au cas du barrage de Van Phong, Vietnam (R2) situé à 70 km de Quy Nhon, dédié à l'irrigation. La configuration de son système d'évacuation des crues est mixte, combinant un PKW asymétrique sur les côtés, avec un déversoir conventionnel de 10 vannes radiales dans la partie centrale. Cette conception permet de maximiser le niveau du réservoir sans provoquer d'augmentation des niveaux en amont. Le PKW est capable de gérer des inondations d'une période de retour de 1000 ans avec des pointes de 15 350 m³/s.

L'utilisation combinée des PKW et des vannes assure une gestion efficace du niveau du réservoir et un niveau élevé d'évacuation dans les situations extrêmes, avec un avantage économique, bien qu'il faille prêter attention au changement de la dynamique en aval, en plus de nécessiter une attention particulière dans les

^{†††}Réglementations relatives à la sécurité des barrages Gouvernement sud-africain 2012

^{†††}Electricité de France

conditions de reflux des flux vers la rivière en aval dans des conditions énergétiques adéquates.

Dans les deux cas étudiés, les PKW se sont révélés être une option rentable et efficace. À la Raviège, les PKW ont considérablement augmenté la capacité de déchargement sans nécessiter de modifications structurelles majeures. À Van Phong, la combinaison d'un PKW et de vannes radiales a permis d'optimiser la conception pour répondre aux besoins hydrauliques et économiques du projet.

Ces exemples montrent comment l'utilisation de technologies avancées et d'approches de conception hybrides peut permettre de relever les défis actuels et futurs en matière de gestion des ressources en eau.

L'optimisation des déversoirs à piano (PKW) a été réalisée dans le cadre de deux autres projets vietnamiens (R07) afin d'améliorer la capacité d'évacuation des crues et les conditions hydrauliques en aval. Les projets Da Si et Cao Ngoi améliorent l'efficacité hydraulique en démontrant une meilleure performance de décharge avec des conceptions trapézoïdales et incurvées, concluant même que le PKW incurvé a augmenté l'efficacité de décharge de 9-15%.

6.2.3. *Un projet suédois singulier*

Le réservoir de Lillflyforsen (R03), dans le centre de la Suède, a été construit en 1965 dans le cadre d'un projet hydroélectrique. Le barrage-poids a une hauteur de 30 mètres et est accompagné d'un barrage en remblai d'une hauteur inférieure. Au fil des ans, le réservoir a présenté deux problèmes principaux : la détérioration structurelle du barrage en terre et la capacité insuffisante de l'évacuateur de crues pour gérer les débits extrêmes pendant les inondations.

Pour remédier à ces lacunes et se conformer aux **règles de sécurité en vigueur**, une solution innovante est proposée : la construction d'un déversoir à piano (PKW) en aval du barrage existant, qui sera le premier de ce type à être construit en Suède. Cette conception permet non seulement d'augmenter considérablement la capacité d'évacuation, mais représente également une alternative plus rentable que la réhabilitation complète du barrage à partir des matériaux détachés et des vannes de l'évacuateur de crues.

La conception finale du PKW s'est appuyée sur des essais réalisés sur des modèles physiques à l'échelle, ce qui a permis d'optimiser la géométrie, la capacité de décharge et la dissipation d'énergie.

La dissipation de l'énergie est un aspect essentiel de la conception des PKW afin d'atténuer l'érosion dans la zone d'impact sur le substratum rocheux. Des marches horizontales à la sortie des PKW et un système d'aération ont également été conçus.

La conception et l'exploitation du PKW doivent également relever les défis liés au climat nordique. Il s'agit notamment de la formation de glace qui, en hiver, impose des charges aux structures hydrauliques, ainsi que des arbres flottants, en particulier lors des inondations. Des barrières flottantes sont parfois installées, mais leur efficacité est souvent douteuse lors de grandes inondations.

6.3. DÉBORDEMENT

Alors que les barrages-poids en béton (PG) sont vulnérables aux inondations en raison de l'effet de l'instabilité qui pourrait produire une surélévation excessive par rapport au barrage de conception, c'est le débordement qui menace les barrages en remblai. Ce débordement, qui peut également être causé par des glissements de terrain dans le réservoir, des ondes sismiques ou même par un tassement soudain induit par l'action sismique, est plus fréquent en raison de phénomènes hydrologiques extrêmes. La réduction de cette vulnérabilité a été un défi et un sujet de recherche au cours des dernières décennies.

Face à ce scénario, le degré de résilience des pentes des barrages de remblai face à des déversements modérés a été étudié. La CIGB a abordé la question lors de diverses conférences (Stavanger 2015) et les travaux se poursuivent pour déterminer le seuil de rupture en fonction du débit spécifique, de la hauteur ou de l'énergie, du type de matériau, etc., comme le fait le groupe de travail sur les *débordements et l'érosion par débordement* du Club européen de la CIGB, ainsi que d'autres initiatives telles que le séminaire sur les protections des barrages contre les débordements (avril 2025 à Stillwater, États-Unis), afin d'élargir les connaissances sur les risques et les possibilités de prévention des dommages qui y sont associés. La tendance actuelle est de proposer des solutions qui parviennent à éviter ou à réduire les dommages à des niveaux acceptables en cas de déversement en crête, tant pour les barrages que pour les digues (Moran et al, 2023). Parmi ces solutions, on peut citer les déversoirs fusibles, les déversoirs d'urgence ou les protections de pente dans le corps du barrage.

La prévision des effets d'une rupture de barrage dépend, en plus de l'hydrogramme d'entrée prévu, de deux facteurs hydrauliques : la façon dont la rupture se produit et quel hydrogramme se produit, et la propagation de l'hydrogramme de sortie en aval, avec le débordement correspondant "dans les zones prédéfinies"

Non seulement de nouveaux ouvrages hydrauliques ont été proposés pour remédier à l'excès de débit, par les auteurs qui ont contribué à ce congrès.

Le débordement des barrages en remblai, principale cause de défaillance des barrages, peut être évité grâce à des solutions de matériaux cimentés capables de résister à l'écoulement sur la crête et la pente en aval. Dans le monde, la plupart des

barrages sont constitués de matériaux meubles, qui s'adaptent mieux à tous les types de fondations, mais dont la capacité à résister aux débordements est moindre.

La résistance des talus des barrages et des levées à l'érosion externe lors des débordements varie fortement en fonction du type de sol, de sa teneur en eau, de sa densité et de sa granulométrie (R15). Des tests tels que le test d'érosion par jet (JET), dans lequel la profondeur d'érosion est mesurée en fonction du temps, sont proposés pour déterminer cette résistance. Il peut être réalisé à la fois en laboratoire et sur le terrain.

Une autre option est le test de surverse, tel que celui réalisé au laboratoire CNR-CESAME dans le cadre du projet OVERCOME (R15), à l'aide de modèles de digues construites avec des sables et graviers du Rhône. Il consiste à maintenir un débit constant sur la digue jusqu'à l'observation des quatre phases successives : remplissage du réservoir, érosion de surface, érosion en tête et formation d'une brèche.

Différences significatives entre les sols traités et non traités, les premiers étant plus résistants où l'influence de la teneur en eau et de la densité sur la vitesse et l'ampleur de l'érosion peut être vérifiée.

6.3.1. *Contribution chinoise à la CMD*

L'amélioration de la résistance de ces barrages à ce risque peut être obtenue grâce à la technique des barrages en matériaux cimentés (CMD), une technologie innovante qui associe des matériaux locaux à des agents de cimentation. La Chine est à la pointe de cette nouvelle technologie (R27) grâce à la recherche et à la mise en œuvre ultérieure dans des cas réels avec l'utilisation de matériaux locaux, tels que le sol, le gravier et la roche, mélangés à du ciment, des cendres volantes et d'autres additifs pour former une matrice cohésive avec une résistance au cisaillement améliorée.

En fonction de la taille des agrégats, les barrages CMD sont généralement appelés barrages en terre cimentée (CSD) : Ils utilisent des particules fines telles que la terre et le sable, les barrages de gravier, de sable et de roche cimentée (CSGRD) : Ils utilisent des agrégats d'un diamètre allant jusqu'à 150 mm ou même des barrages en roche cimentée (CRD).

Les auteurs de l'IWHR présentent l'étude dans des conditions extrêmes telles que des débordements pour des barrages de hauteur modérée où les charges hydrauliques sont déjà très importantes. Ils présentent des cas en Chine, où plus de 40 CDM ont déjà été mis en œuvre. L'exemple du projet Xijiang (Guizhou) d'une hauteur de 48,5 m qui a résisté à un débordement de 48 heures avec un niveau d'eau de 2 m, démontrant une grande résistance à l'érosion ou le projet Shoukoubu (Shanxi) d'une hauteur de 61,4 m où il a été possible de réduire le coût de manière

significative grâce à la technique CMD sont d'un grand intérêt pour consolider l'applicabilité de cette technique. De même, pour les barrages existants, le renforcement des pentes en aval à l'aide de la technique CMD peut améliorer la résistance au débordement et la capacité d'atténuation de l'érosion.

Les CMD représentent une avancée significative et offrent dans de nombreux cas une solution adaptable et robuste pour améliorer la résilience des infrastructures hydrauliques face à des conditions extrêmes.

6.4. DISSIPATION D'ÉNERGIE

Quel que soit le type de solution d'augmentation de débit sous vide, il est indispensable de revoir le système de dissipation d'énergie pour une mise à jour du débit. Il est parfois nécessaire de créer un bassin de dissipation (R2), d'adapter le bassin existant (R18). Les PKW installés dans les barrages nécessitent des techniques de dissipation d'énergie efficaces pour éviter l'érosion en aval (R07) dans les labyrinthes.

6.4.1. *Barrage de Kariba*

Parfois, le problème de la réintégration des flux dans le fleuve dans des conditions sûres et stables ne correspond pas seulement à des inondations extrêmes, mais aussi à la persistance de la dissipation d'énergie pendant des années. C'est le cas du barrage de Kariba, sur le fleuve Zambèze, qui a connu des problèmes d'érosion en raison des déversements continus de son déversoir. Ce processus a créé une zone d'impact de 80 mètres de profondeur, avec un risque correspondant pour la stabilité du barrage. Les mesures correctives prises sont décrites dans le document R06. La description intéressante des actions visant à rétablir la sécurité, au moyen d'excavations, de dalles, d'injections, etc.

L'évaluation de l'érodabilité du substratum rocheux où sont restitués les écoulements évacués au pied du barrage peut être estimée avec la *méthode de fatigue* basée sur la loi de Paris-Erdogan (1963) qui est utilisée en mécanique des roches pour prédire la croissance des fissures sous des charges cycliques. Cette loi décrit la croissance d'une fissure en fonction du nombre de cycles de charge, sur la base de la plage d'amplitude du facteur d'intensité de contrainte.

L'évaluation des paramètres géomécaniques tels que la résistance de la masse rocheuse et la taille des blocs dans les déversoirs de barrage où la détermination des risques d'érosion dans les projets hydrauliques est nécessaire peut être basée sur la méthode rationnelle d'Annandale (1995) :

Un enseignement important est que l'évacuation n'est pas toujours le point critique face à des phénomènes hydrologiques extrêmes, mais que la restitution à la rivière de débits, souvent revus à la hausse, peut nécessiter des actions pour améliorer la résilience du projet dans la zone de restitution.

6.5. LAMINAGE DES CRUES ET ATTÉNUATION DE CRÊTE

Il est important d'analyser le rôle du réservoir, avec une capacité d'évacuation accrue, en contribuant au laminage des crues, à la réduction des pics ou au retardement de l'arrivée aux points critiques en aval. L'effet de surprise, face à une pente plus élevée de l'hydrogramme (croissance plus abrupte du débit) doit être pris en compte dans les systèmes d'alerte et les plans d'urgence, en étudiant la vulnérabilité de la population en aval.

Les solutions hybrides avec déversoirs à vannes (R2) qui mobilisent des volumes de retenue plus importants dans le processus de laminage, atténuent le problème si de bonnes normes d'exploitation sont mises en œuvre. D'un autre côté, le désir de perdre le minimum ou aucun volume de réservoir avec des systèmes labyrinthiques va de pair avec la réduction de la capacité d'atténuer les pics de crue, ce qui n'est pas toujours acceptable.

6.6. TEMPÉRATURE

Outre les extrêmes hydrologiques, d'autres extrêmes climatiques, tels que les extrêmes thermiques, ont fait l'objet de quelques contributions.

D'autres extrêmes climatiques tels que les extrêmes thermiques, les vagues de chaleur et les grands froids, pourraient avoir une influence sur le comportement et la sécurité des barrages. EDF présente le cas (R11) des barrages voûtes, très sensibles aux charges thermiques, une méthodologie basée sur des charges thermiques accrues suivant les directives du comité français des grands barrages (CFBR).

La caractérisation des charges thermiques accrues est abordée (R11) en utilisant le modèle hydrostatique saisonnier temporaire thermique (HSTT) pour quantifier l'effet des températures saisonnières et des écarts quotidiens moyens. Ce modèle inclut l'effet irréversible, l'effet hydrostatique réversible et l'effet thermique pour estimer les déplacements radiaux dus aux températures extrêmes, et avec l'application de la loi de Gumbel pour évaluer la probabilité d'occurrence des événements critiques. 15 barrages ont été étudiés pendant la canicule de 2022 en France, confirmant le bon comportement des barrages étudiés, mettant en évidence la réversibilité des phénomènes observés.

Bien qu'il ne s'agisse pas d'un phénomène hydrologique extrême, la fissuration thermique précoce, causée par la chaleur d'hydratation du ciment après la construction, peut compromettre l'intégrité structurelle, provoquer des fuites et même l'effondrement des barrages. Traditionnellement, les techniques de contrôle de la température, telles que le refroidissement de l'eau par des circuits intégrés, ont été appliquées manuellement, avec une efficacité modérée.

Le développement de systèmes de contrôle intelligents, qui intègrent les technologies de l'Internet des objets (IoT), l'intelligence artificielle et les plateformes de retour d'information en temps réel, avec l'appui de modèles thermiques en 3D, offre une solution avancée, un système de contrôle intelligent de la température appliqué à la construction du barrage hydroélectrique Julius Nyerere en Tanzanie (R21), mettant en évidence sa capacité à relever les défis des climats chauds et humides et de la construction massive en béton.

Le système intelligent de contrôle de la température s'est avéré être une solution efficace pour gérer la chaleur d'hydratation dans les projets de béton massifs grâce à un contrôle adaptatif en temps réel, à la réduction des risques structurels et à l'optimisation des ressources. Avec le réchauffement climatique, il pourrait s'agir d'une exigence plus courante.

L'Indonésie (R19) mentionne d'autres préoccupations climatiques concernant les barrages. Les modes d'exploitation des réservoirs ont un impact significatif sur l'intégrité matérielle des barrages en remblai vieillissants (≥ 50 ans), en particulier ceux construits avec des sols résiduels. Les variations des niveaux d'eau et des précipitations accélèrent la dégradation des matériaux, ce qui présente des risques pour la sécurité des barrages.

La nécessité d'une surveillance et d'une évaluation continues, en particulier dans les régions tropicales où les facteurs environnementaux intensifient la détérioration, est mise en évidence. En intégrant les évaluations géotechniques et hydrologiques, il fournit un cadre pour améliorer la gestion et la sécurité des barrages vieillissants. Cette préoccupation n'est pas seulement axée sur les conditions météorologiques extrêmes ou les inondations, mais aussi sur les conditions que le climat impose aux barrages, tant dans les conditions tropicales du point de vue du climat que des conditions géologiques compte tenu du type de sols disponibles

6.7. GLISSEMENTS DE TERRAIN

D'autres phénomènes extraordinaires étroitement liés, tels que des vagues causées par des glissements de terrain, une sédimentation extraordinaire ou des coulées de débris, en plus des débits de crue eux-mêmes qui dépassent les

capacités de conception, nécessitent des approches innovantes en matière de gestion et de sécurité des barrages.

Depuis l'accident du barrage de Vajont en 1963, la menace de glissements de terrain pouvant générer des ondes dynamiques dans les réservoirs a fait l'objet d'études de suivi, d'amélioration des mécanismes de calcul et des techniques de surveillance (ICOLD Bull 124).

A la suite de précipitations cumulées supérieures à 1 000 mm, un glissement de terrain en amont du barrage d'Hiranabe au Japon (R09) s'est déclenché, provoquant l'écoulement de plus de 300 000 m³ de débris dans le réservoir. La vague qui a suivi a provoqué un débordement qui a atteint environ 2 m au-dessus de la crête du barrage, et le débordement a duré une douzaine de secondes. Malgré le débordement, il n'y a pas eu d'anomalie significative dans le corps du barrage, et la production d'électricité a repris deux mois après la récupération de l'équipement de contrôle des vannes de l'évacuateur de crues.

Des cas ont été signalés en Chine (R24), où des fissures de traction significatives ont été identifiées en raison de baisses rapides du niveau d'eau du réservoir. L'analyse de l'interférométrie radar par satellite (INSAR) a permis de déterminer que les deux corps restent dans une phase de déformation lente, avec une stabilité structurelle critique après le remplissage du réservoir. Les analyses de stabilité, prenant en compte les conditions normales d'exploitation, les précipitations, les baisses soudaines du niveau d'eau et les effets sismiques, ont permis d'évaluer les coefficients de sécurité qui oscillent à proximité de l'unité. Les principaux modes de glissement comprennent des failles planes liées aux structures géologiques sous-jacentes, telles que les failles et les fractures gneissiques.

Les modèles numériques à deux ou trois dimensions permettent de simuler le processus complet des glissements de terrain et des vagues générées. Les vagues qui en résultent dépendent fortement des paramètres cinématiques de l'entrée du matériau dans la masse d'eau, ce qui donne des vagues de grande amplitude dans certains cas (Kofoed, Cifres & Kronborg, 2002). Ces vagues se propagent rapidement vers l'amont et vers l'aval en fonction de la profondeur du lac.

Dans le cas rapporté (R24), le barrage a été atteint, provoquant un débordement en deux phases : la première en moins de deux minutes avec une profondeur moyenne maximale de 2,75 m et la seconde en moins de trois minutes, affectant l'aval du barrage, sans provoquer d'inondation.

Il peut être nécessaire d'évaluer l'impact des vagues sur la structure du barrage par une analyse des contraintes dans des conditions statiques et dynamiques (R24). Les cas rapportés ont montré des conditions de traction acceptables avec des contraintes de traction légèrement supérieures à la limite qui étaient très localisées sans compromettre la stabilité globale dans les régimes statique et dynamique.

6.8. GESTION DES BARRAGES

La nécessité d'approches proactives (R09) et intégrées de la gestion des barrages doit être soulignée. L'incorporation de mesures spécifiques pour le débit et la sédimentation, soutenue par une analyse numérique et une planification adaptative, est cruciale pour améliorer la résilience aux événements hydrologiques extrêmes.

Il est recommandé de mettre en œuvre des stratégies intégrées qui combinent des mesures structurelles et opérationnelles, en développant des systèmes d'exploitation à distance et des dispositifs de sécurité en cas d'événements extrêmes. La surveillance continue doit être suivie d'une communication correcte des risques identifiés, afin qu'ils puissent être intégrés dans les mécanismes d'urgence.

6.8.1. *Progrès dans les modèles de rupture de barrage et de propagation des vagues*

L'hydrogramme du débit sortant d'un réservoir à la suite de la rupture d'un barrage en remblai est généralement estimé à partir d'hypothèses sur les caractéristiques de la brèche de rupture basées sur l'évolution géométrique de la brèche, ce qui suppose que la brèche

La taille de la brèche augmente progressivement au cours d'une période donnée jusqu'à ce qu'elle atteigne sa forme finale. Des paramètres tels que la largeur maximale de la brèche, qui dépend des caractéristiques du matériau et des conditions hydrauliques, et la hauteur de la brèche, qui est généralement adoptée jusqu'au niveau du chenal à la base du barrage. Le temps de formation de la brèche est également pris en compte : il définit la vitesse de développement de la brèche. Il peut dépendre de la résistance du matériau et du volume d'eau stocké.

Avant la formulation de modèles plus développés, des définitions de la brèche basées sur des données empiriques ont été utilisées, telles que les équations de MacDonald et Langridge-Monopolis (1984), qui permettent de déduire la taille et le temps de formation de la brèche, ou celles de Singh et Snorrason (1984), qui relient le débit de pointe aux dimensions du réservoir et à la géométrie du barrage. Plus tard, les équations de Froehlich (1995) ont proposé la relation entre la largeur et le temps de formation de la brèche avec le volume stocké dans le réservoir et la hauteur d'eau au-dessus de la brèche. Il s'agit de modèles rapides à appliquer, mais qui manquent de précision pour être fiables en cas d'urgence réelle. Une amélioration, au moyen de modèles physiques simplifiés, reste tributaire de simplifications ou d'hypothèses empiriques.

Par la suite, les logiciels commerciaux simulent explicitement à l'aide de modèles hydrodynamiques numériques, en tenant compte de l'érosion progressive du matériau du barrage en fonction du gradient hydraulique et des propriétés des

matériaux, y compris la rétroaction entre l'augmentation du débit et l'élargissement de la brèche.

Ces relations font l'objet de recherches expérimentales en laboratoire (R26) menées à l'aide de modèles réduits et de simulations numériques paramétriques. Ces recherches mettent en évidence les processus d'érosion et les dynamiques de rupture dans chaque zone du barrage : couche protectrice, filtre et noyau central. La relation avec les différentes parties dans les barrages zonés à section hétérogène avec des matériaux au comportement différent, tels que les recharges, les filtres ou les noyaux, est intéressante. L'article R26 justifie une corrélation élevée dans la progression des défaillances entre les expériences à l'échelle et les simulations numériques montrées.

Les modèles numériques tridimensionnels détaillés permettent une représentation plus précise des processus hydrauliques et mécaniques impliqués, bien qu'ils soient complexes à mettre en œuvre. C'est le cas du modèle de haute précision proposé (R23) qui combine les équations hydrodynamiques, les turbulences et le transport des matériaux du barrage.

Le contraste avec des expériences (R23), telles que celles menées à l'Université de Louvain, a permis de reproduire avec précision les tourbillons triangulaires et les schémas d'érosion au fond du canal, confirmant ainsi sa capacité à simuler des dynamiques d'écoulement complexes ou même des lacunes bidirectionnelles.

En combinant les équations de transport des sédiments et les critères d'instabilité, il est capable de relever les défis de la prédiction de la rupture des barrages en matériaux hétérogènes dans des conditions de débordement et démontre son applicabilité dans des cas complexes.

La nécessité d'approches proactives (R09) et intégrées de la gestion des barrages doit être soulignée. L'incorporation de mesures spécifiques pour le débit et la sédimentation, soutenue par une analyse numérique et une planification adaptative, est cruciale pour améliorer la résilience aux événements hydrologiques extrêmes.

Il est recommandé de mettre en œuvre des stratégies intégrées qui combinent des mesures structurelles et opérationnelles, en développant des systèmes d'exploitation à distance et des dispositifs de sécurité en cas d'événements extrêmes. La surveillance continue doit être suivie d'une communication correcte des risques identifiés, afin qu'ils puissent être intégrés dans les mécanismes d'urgence.

L'hydrogramme du débit sortant d'un réservoir à la suite de la rupture d'un barrage en matériaux meubles est généralement estimé par des hypothèses sur les caractéristiques de la brèche de rupture basées sur l'évolution géométrique de la brèche, qui suppose que la taille de la brèche augmente progressivement au cours

d'une période donnée jusqu'à ce qu'elle atteigne sa forme finale. Des paramètres tels que la largeur maximale de la brèche, qui dépend des caractéristiques du matériau et des conditions hydrauliques, et la hauteur de la brèche, qui est généralement adoptée jusqu'au niveau du canal à la base du barrage. Le temps de formation de la brèche est également pris en compte : Il définit la vitesse de développement de la brèche. Il peut dépendre de la résistance du matériau et du volume d'eau stocké.

Avant le développement de modèles plus avancés, les définitions des brèches étaient basées sur des données empiriques, telles que les équations de MacDonald et Langridge-Monopolis (1984), qui estimaient la taille et le temps de formation d'une brèche, ou les équations de Singh et Snorrason (1984), qui mettaient en corrélation le débit de pointe avec les dimensions du réservoir et la géométrie du barrage. Plus tard, les équations de Froehlich (1995) ont introduit une relation entre la largeur de la brèche, le temps de formation, le volume de stockage du réservoir et la hauteur d'eau au-dessus de la brèche.

Bien que ces modèles soient rapides à appliquer, ils n'ont pas la précision nécessaire pour garantir leur fiabilité dans des scénarios d'urgence réels. Même les améliorations ultérieures, grâce à des modèles physiques simplifiés, reposent toujours sur des hypothèses empiriques ou des simplifications, ce qui limite leur précision et leur fiabilité dans des situations complexes.

Par la suite, les logiciels commerciaux simulent explicitement à l'aide de modèles hydrodynamiques numériques, en tenant compte de l'érosion progressive du matériau du barrage en fonction du gradient hydraulique et des propriétés des matériaux, y compris la rétroaction entre l'augmentation du débit et l'élargissement de la brèche.

Ces relations font l'objet de recherches expérimentales en laboratoire (R26) menées à l'aide de modèles réduits et de simulations numériques paramétriques. Ces recherches mettent en évidence les processus d'érosion et les dynamiques de rupture dans chaque zone du barrage : couche protectrice, filtre et noyau central. La relation avec les différentes parties dans les barrages zonés à section hétérogène avec des matériaux de comportement différent, tels que les recharges, les filtres ou les noyaux, est intéressante. Le document R26 justifie une corrélation élevée dans la progression de la rupture entre les expériences à l'échelle et les simulations numériques montrées.

Les modèles numériques tridimensionnels détaillés permettent une représentation plus précise des processus hydrauliques et mécaniques impliqués, bien qu'ils soient complexes à mettre en œuvre. C'est le cas du modèle de haute précision proposé (R23) qui combine les équations hydrodynamiques, les turbulences et le transport des matériaux du barrage.

Le contraste avec des expériences (R23), telles que celles menées à l'Université de Louvain, a permis de reproduire avec précision les tourbillons triangulaires et les schémas d'érosion au fond du canal, confirmant ainsi sa capacité à simuler des dynamiques d'écoulement complexes ou même des lacunes bidirectionnelles.

En combinant les équations de transport des sédiments et les critères d'instabilité, il est capable de relever les défis de la prédiction de la rupture des barrages en matériaux hétérogènes dans des conditions de débordement et démontre son applicabilité dans des cas complexes.

7. MESURES NON STRUCTURELLES

7.1. ALERTE PRÉCOCE ET SITUATIONS D'URGENCE

La mise en œuvre de systèmes de surveillance hydrologique et de sécurité des barrages, l'amélioration des capacités de prévision météorologique et la sensibilisation des communautés locales aux risques sont des tâches essentielles pour accroître la résilience de la population soumise à des inondations potentielles.

Dans une revue générale (R25) du cas de la Chine, des mesures d'atténuation sont décrites, notamment l'amélioration des prévisions hydrologiques, des systèmes de surveillance de la sécurité et le renforcement des structures elles-mêmes. En outre, il est reconnu que l'éducation des communautés est obligatoire pour réduire les impacts potentiels.

L'alerte précoce est, sans aucun doute, l'un des outils les plus efficaces pour réduire le risque de victimes humaines. Ces alertes précoces en temps réel doivent déclencher des actions qui dépendent des conséquences attendues et qui doivent être soutenues par des informations sur les inondations potentielles sur le territoire.

La cartographie des risques d'inondation, dus à des décharges de grands réservoirs ou même à des ruptures de barrage, correspond généralement à des scénarios prédéfinis par des hydrogrammes théoriques calculés au préalable. Cependant, lorsqu'un plan d'urgence doit être activé en cas d'événement singulier, ces plans sont généralement ajustés, et une cartographie actualisée est souhaitable pour les caractéristiques spécifiques de l'événement ou la prédiction de son évolution pour répondre aux urgences.

Les méthodes traditionnelles basées sur des modèles hydrodynamiques à haute résolution ont des temps de calcul élevés, ce qui les rend difficiles à appliquer dans certaines situations qui nécessitent des réponses rapides.

7.1.1. *Alerte hydrologique*

"L'amélioration de la pré-libération concertée des barrages avec une utilisation plus sophistiquée des prévisions météorologiques, la révision de la décharge de conception et le contrôle efficace des sédiments pour l'entretien durable des barrages sont quelques-uns des défis imminents que nous devons nous efforcer de résoudre". (Tetsuya SUMI, 2025)

Le ministère du territoire, des infrastructures, des transports et du tourisme (MLIT) gère 109 grands fleuves au Japon. En 2019, le MLIT a officialisé une augmentation du volume des précipitations de 10 à 15 % dans la planification de la lutte contre les inondations afin de faire face aux effets du changement climatique à l'avenir. En 2020, le gouvernement a établi une règle générale pour modifier, dans la mesure où elles sont efficaces, les règles d'exploitation des réservoirs afin de permettre une libération anticipée des barrages avant l'arrivée de fortes pluies en utilisant les prévisions météorologiques. En 2021, les "Basin-wide Concerted Measures for Flood Risk Reduction Acts", qui consistent en des amendements de neuf lois affiliées, ont été promulguées pour faire face à l'augmentation des précipitations due au changement climatique.

7.1.2. *Alerte hydraulique*

En pratique, la prévision hydrologique doit alimenter l'alerte hydraulique, qui traduit l'effet réel sur le territoire sous forme de zones inondées, de profondeurs, de temps d'arrivée, etc.

Les méthodes traditionnelles de résolution numérique des équations de Navier-Stokes bidimensionnelles, telles que HEC-RAS, SOBEK, MIKE 21, etc. sont largement utilisées pour modéliser les inondations à l'aide des équations de Navier-Stokes bidimensionnelles. Cependant, ces modèles sont très gourmands en ressources informatiques et nécessitent beaucoup de temps pour produire des résultats à haute résolution. En revanche, les modèles basés sur l'apprentissage automatique, tels que les SGP, peuvent apprendre à partir de données préexistantes et faire des prédictions rapides dans de nouvelles conditions.

Pour résoudre ce problème, l'utilisation de méthodes d'apprentissage automatique (R28), comme alternative pour améliorer l'efficacité et la précision des simulations rapides d'inondation. Réduire les coûts de calcul sans compromettre la précision des résultats.

Le cas du barrage de Sheyuegou (Xinjiang, Chine) est présenté, car l'inondation résultant de la rupture a causé d'importantes pertes humaines et matérielles et l'efficacité de la méthode proposée a été testée.

La méthodologie est basée sur la création de simulations historiques et synthétiques en 2D avec des modèles hydrauliques conventionnels, l'application

ultérieure de fonctions orthogonales empiriques (EOF^{§§§}) simplifiant les variables. Sur cette base, les modèles SGP sont entraînés^{***} pour prédire des données détaillées basées sur d'autres données à faible résolution et leur validation ultérieure. On obtient ainsi une plus grande précision qu'avec un modèle hydraulique RH, avec un gain de temps de calcul de 90 %. La capacité à générer des résultats avec une grande précision et un temps de calcul plus court représente une avancée significative dans la gestion des urgences.

8. DIGUES

8.1. AGGRAVATION DU RISQUE

L'expression "danger rampant" fait référence à l'accumulation progressive de facteurs qui augmentent le risque de catastrophes, telles que les inondations. Ce concept inclut des processus qui, sans être soudains, exacerbent l'exposition ou la vulnérabilité au fil du temps. L'urbanisation incontrôlée, la dégradation des écosystèmes naturels (tels que les mangroves ou les zones humides) et le changement climatique, qui intensifie les précipitations et élève le niveau des mers, sont des exemples de ces processus. Ce phénomène peut passer inaperçu jusqu'à ce qu'un événement catastrophique se produise. Pour y remédier, il faut une planification à long terme, des mesures d'atténuation proactives et une surveillance continue afin d'atténuer efficacement ses effets cumulatifs.

"Il y avait deux types de digues : ***Celles qui avaient été débordées*** par les eaux de crue et ***celles qui allaient l'être***" (William Hammond Hall, ingénieur de l'État de Californie, 1880)



Fig. 13

L'aménagement du territoire par les digues oublie généralement sa propre histoire

^{§§§}Fonctions orthogonales empiriques

^{***}Processus gaussien clairsemé

8.2. DIGUES (R12)

La vulnérabilité du système a été particulièrement révélée lors d'événements extrêmes tels que l'inondation de décembre 2003 (R12). La réponse a été le "Plan Rhône", un programme global de 450 millions d'euros avec une approche innovante en donnant la priorité à la gestion des risques et à l'acceptation contrôlée des débordements.

Les digues actuelles ont été conçues au XIXe siècle comme étant "insubmersibles". Depuis, de nombreuses brèches ont été enregistrées, principalement causées par l'érosion interne due aux terriers d'animaux et aux déficiences structurelles. Le risque de rupture varie considérablement en fonction du débit, passant de 50 % pour un débit de 9 500 m³/s à près de 100 % pour un débit de 10 500 m³/s.

Après l'inondation de 2003, reconnaissant la nécessité d'une approche différente, le "Plan Rhône" a introduit les principes clés suivants :

1. Éviter le transfert des risques d'une zone à l'autre en augmentant la hauteur des digues.
2. Accepter des débordements contrôlés en cas d'inondations plus extrêmes
3. Prévenir la formation de brèches pour les inondations exceptionnelles (période de retour de 1 000 ans)

Il s'agissait de renforcer le système de digues pour résister aux débordements et de créer des structures pour gérer le drainage des zones protégées.

La conception comprenait des solutions pour accélérer le drainage des eaux de débordement, telles que la modernisation des stations de pompage et l'installation de siphons pour améliorer le débit dans les canaux encastrés. Cela a permis de réduire considérablement le temps d'inondation dans les zones protégées, augmentant ainsi l'acceptabilité du projet.

De nouvelles digues et structures ont également été construites pour assurer la transparence hydraulique, y compris des viaducs dans les infrastructures de transport transversales.

Parmi les réalisations, on peut citer le triplement de la protection des personnes contre les inondations centennales, la réduction des dommages attendus, ainsi qu'une plus grande résilience, puisque l'infrastructure actuelle résiste à des scénarios d'inondation extrêmes, avec des systèmes de drainage améliorés qui minimisent l'impact des inondations.

L'expérience du delta du Rhône, avec un modèle innovant et résilient face aux inondations extrêmes, mérite d'être exportée. En donnant la priorité à la gestion des risques et à la participation des citoyens, elle a non seulement

amélioré la sécurité des infrastructures, mais aussi renforcé la capacité de réponse sociale aux risques.

9. REMARQUES FINALES

Les réservoirs jouent un rôle crucial dans l'atténuation des inondations, mais leur fonctionnement doit être optimisé pour minimiser les risques en amont et en aval. Une gestion efficace des risques d'inondation exige une **approche globale** (Huang et al.) qui intègre les méthodes d'évaluation des risques, la planification des infrastructures et les opérations en temps réel.

La complexité croissante de la gestion des inondations, due au changement climatique et aux activités humaines, nécessite des stratégies dynamiques et adaptatives. Dans ce contexte, l'implication d'experts et l'utilisation d'outils de visualisation de données avancés sont essentielles pour prendre des décisions informées et efficaces lors d'événements extrêmes.

Parmi les mesures structurelles, il est essentiel d'envisager la construction de barrages pour créer des réservoirs d'atténuation des crues, en tenant compte de leur fonctionnement coordonné dans le bassin avec d'autres infrastructures. Cela comprend l'évaluation et l'adaptation des barrages existants aux nouveaux scénarios de charge, l'ajustement des niveaux d'eau maximum prévus, la modification ou l'expansion des déversoirs, ou la mise en œuvre de déversoirs supplémentaires, d'urgence ou de fusibles. En outre, la canalisation des rivières, les digues, les systèmes de drainage et autres interventions similaires doivent être envisagés.

Parmi les mesures non structurelles, l'adoption de règles opérationnelles optimales est cruciale. Il s'agit notamment de la mise en place d'un stockage tampon, de prélèvements saisonniers et de lâchers préventifs, ainsi que de la cartographie des risques, de systèmes d'alerte précoce et de la mise en œuvre de plans d'intervention en cas d'urgence. En outre, il est essentiel de renforcer la résilience en améliorant la gestion des terres en aval, en favorisant l'éducation du public et en encourageant l'implication de la société civile dans les processus de planification. Le renforcement des cadres de gouvernance pour les événements extrêmes par le biais d'un renforcement institutionnel joue également un rôle fondamental.

9.1. NOS DEFIS

De nombreux défis restent à relever à la lumière des informations recueillies sur cette question cruciale pour l'avenir, qui requièrent une attention immédiate et des efforts soutenus à partir d'aujourd'hui.

- Moderniser les méthodes d'hydrologie extrême en faisant appel à la pluridisciplinarité, en particulier aux géologues et aux météorologues.
- En hydrologie, il faut travailler sur les volumes, et pas seulement sur les débits, pour l'établissement de zones franches ou de terres protégées.
- Supposons que l'examen de l'hydrologie implique l'acceptation, dans de nombreux cas, de l'existence de risques résiduels.
- Établir des marges dans la conception des structures hydrauliques, sur la base du principe d'incertitude.
- Mettre à jour les études en tenant compte des changements mondiaux.
- Demande d'investissements pour faire face à la continuité indispensable du fonctionnement de plus de soixante mille grands barrages dans le monde.
- Accompagner de mesures non structurelles, telles que RTWS et PADE
- Tirer les leçons des cas de réputation des risques pour la gestion future des terres. Impliquer des stratégies transversales pour gérer la cartographie des risques d'inondation.
- Réviser les réglementations en y intégrant le risque acceptable par la société.
- Mettre en œuvre des stratégies de conception et d'entretien qui augmentent la résilience de ces structures.
- Former les communautés et les opérateurs à la gestion des risques associés aux ruptures de barrages, en promouvant des processus de participation citoyenne transparents, comme garantie de succès.
- Utiliser les dernières technologies, y compris l'IA, pour entretenir les barrages
- Et plus encore ...

Enfin, nous terminons ce rapport en reprenant quelques déclarations de la CIGB qui ont inspiré le contenu de ce rapport :

Rappelons la devise du Manifeste du Club européen de la CIGB sur les barrages et les réservoirs : "Cessons de penser à travailler pour la société et travaillons avec la société" (Mazza, 2019).^{††††}

9.2. DÉCLARATION MONDIALE SUR LA SÉCURITÉ DES BARRAGES, 2019 : LE RISQUE ZÉRO N'EXISTE PAS

Avec près d'un siècle d'engagement en faveur de la sécurité des barrages, et sachant que **le risque zéro n'existe pas**, la CIGB reconnaît dans sa Déclaration mondiale qu'il est nécessaire d'enregistrer et d'analyser les réponses aux événements, tels que les grandes inondations, les tremblements de terre, etc. Ces risques, comme les inondations, sont des menaces externes, pour lesquelles les risques sont acceptés sur la base des connaissances scientifiques et de la probabilité d'occurrence. Les plans d'urgence doivent donc être élaborés dans le

^{††††} *Tel qu'exposé à Ottawa*

but d'éviter les pertes en vies humaines et de réduire les dommages causés aux biens, aux infrastructures et à l'environnement par la rupture d'un barrage. ... l'examen périodique, la mise à jour et la mise en pratique du plan d'urgence devraient être obligatoires, de même que l'éducation et la sensibilisation du public aux barrages et aux digues.

Le rôle des autorités réglementaires est primordial pour la sécurité.

L'élaboration de normes, de standards et de mesures de protection est un facteur clé pour une surveillance adéquate de la sécurité des barrages.

9.3. DÉCLARATION MONDIALE 2024

Les réservoirs de stockage contribuent à atténuer les risques d'inondation et à en réduire la fréquence. L'incertitude liée aux inondations provoquées par le climat exige un renforcement de la sécurité des barrages. L'évaluation des barrages existants et leur adaptation, le cas échéant, sont hautement prioritaires (Déclaration de la CIGB de Chengdu sur le rôle des barrages dans la transition énergétique et l'adaptation au changement climatique, 2025).

9.4. DERNIERS MOTS

Le large éventail d'idées, certaines confirmant des expériences antérieures de la communauté des barrages, d'autres innovantes, issues d'autres domaines technologiques, nous permet de trouver un dénominateur commun : il y a beaucoup de travail à faire dans tous les domaines, en mettant en œuvre des mesures structurelles et non structurelles impliquant d'autres acteurs. Ces tâches, afin de maintenir en service irremplaçable les plus de soixante mille grands barrages qui assurent le bien-être de l'humanité, contribuent à la sécurité des personnes exposées au risque d'inondation et atténuent les conséquences potentielles du risque résiduel, aggravé par le réchauffement climatique, exigent un énorme effort économique que la société doit consentir sans excuses dans le cadre de programmes engagés qui en assurent le financement. N'attendons pas que les catastrophes se succèdent pour récupérer par intermittence ce mandat social.

"Nous devons être prudents. Il ne suffit pas de compter sur les circonstances les plus probables ; si le pire se produit et que la situation est vraiment extrêmement dangereuse pour nous, nous devons nous y préparer. Les éventualités lointaines, si elles sont suffisamment sérieuses, nous devons être préparées". (Carl Sagan, 1990, conférence sur le changement climatique)

RÉFÉRENCES

Documents Q110

- [1] Q110 - R1 ADAPTATION OF 310 DAMS IN SPAIN TO EXTREME EVENTS AND CLIMATE CHANGE THROUGH RISK ASSESSMENT. JUAN CARLOS DE CEA AZAÑEDO *ET AL.* Spain.
- [2] Q110 – R2 PKW SPILLWAYS: AN INNOVATIVE, SAFE AND ECONOMIC SOLUTION FROM RUN-OF-RIVER DAMS IN PLAINS TO LARGE DAMS IN MOUNTAINS SUITABLE FOR CLIMATE CHANGE CHALLENGES. MICHEL. HO TA KHANH *ET AL.* Vietnam and France.
- [3] Q110 – R3 DAM UPGRADE WITH PIANO KEY WEIR FOR DISCHARGE OF EXTREME FLOODS. JAMES YANG *ET AL.* Sweden
- [4] Q110 – R4 DESIGN OF THE NEW SPILLWAY FOR REGAJO DAM. ENRIQUE CAMPOS *ET AL.* Spain
- [5] Q110 – R5 NEW APPROACH TO ESTIMATE EXTREME FLOODS FOR SWISS DAMS BY MEANS OF CONTINUOUS HYDROMETEOROLOGICAL SIMULATIONS. ALEXANDRE JEAN PACHOUD *ET AL.* Switzerland
- [6] Q110 – R6 KARIBA DAM PLUNGE POOL RESHAPING WORKS FOR THE SAFETY OF STRUCTURES FOR EXTREME FLOODS. L. TARDIEUX *ET AL.* Switzerland and Zambia
- [7] Q110 – R7 PIANO KEY WEIR GEOMETRIES ADJUSTMENT FOR DOWNSTREAM HYDRAULIC REGIME: LESSONS LEARNED FROM CASE STUDIES IN VIETNAM. LE VAN NGHI *ET AL.* Vietnam.
- [8] Q110 – R8 REGIONALISATION OF FLOOD ENVELOPE CURVES TO DERIVE PRELIMINARY ESTIMATES OF PROBABLE MAXIMUM FLOODS. PETER HILL *ET AL.* Australia
- [9] Q110 – R9 CASE STUDY AND ANALYSIS OF SURGE WAVE AND EXCESSIVE FLOOD IN HYDROPOWER DAMS. CHIHAYA ONDA *ET AL.* Japan

- [10] Q110 – R10 GESTION DES CRUES SUR LES GRANDS BASSINS VERSANTS - PRISE EN COMPTE DE LA COMPLEXITÉ HYDROLOGIQUE ET HYDRAULIQUE. JULIEN VERMEULEN *ET AL.* France
- [11] Q110 – R11 CHARACTERIZATION AND FEEDBACK ON THE BEHAVIOR OF ARCH DAMS SUBJECTED TO HEATWAVES AND EXTREME COLD. LOUIS SUCHIER *ET AL.* France
- [12] Q110 – R12 BUILDING A RESILIENT SYSTEM AGAINST FLOOD IN THE RHÔNE DELTA. THIBAUT MALLET *ET AL.* France
- [13] Q110 – R13 A NOVEL METHODOLOGY FOR ASSESSING EXTREME HYDROLOGICAL EVENTS IN THE CONTEXT OF CLIMATE CHANGE. NICOLAS AVISSE. France
- [14] Q110 – R14 IMPROVEMENT OF THE SAFETY OF THE FRENCH DAMS AGAINST FLOODS. GAËTAN DAUTOIS, MATHIEU ROY *ET AL.* France
- [15] Q110 – R15 TWO EROSION TESTS TO QUANTIFY RESISTANCE TO EROSION DURING OVERFLOW: THE JET EROSION TEST AND THE OVERFLOW TEST. PATRICK PINETTES *ET AL.* France
- [16] Q110 – R16 MOLARE TRAGEDY: THE SECONDARY DAM COLLAPSE INDUCED BY A HEAVY RAINFALL EVENT, ANDREA ABBATE. Italy.
- [17] Q110 – R17 CASE STUDY – A DAM RAISING OPTIONS STUDY FOR A DAM IN SOUTHERN AFRICA. CHENCEN ZHANG *ET AL.*, South Africa.
- [18] Q110 – R18 CHALLENGES EXPERIENCES WITH UPGRADING A COMPOSITE DAM IN SOUTH AFRICA - TZANEEN DAM RAISING. HENRY-JOHN WRIGHT, South Africa.
- [19] Q110 – R19 THE EFFECT OF RESERVOIR OPERATION PATTERNS ON THE MATERIAL CHARACTERISTICS OF OLD DAMS AND THEIR IMPACT ON DAM SAFETY. MUHAMMAD RIZA *ET AL.* Indonesia

- [20] Q110 – R20 ASSESSMENT OF THE DISCHARGE CAPACITIES AND SAFETY OF MAIN STRUCTURES IN LARGE DAMS OF DRINI RIVER CASCADE. MR. ARJAN JOVANI *ET AL.* Albania

- [21] Q110 – R21 INTELLIGENT TEMPERATURE CONTROL SYSTEM FOR LARGE CONCRETE DAM CONSTRUCTION IN HOT AND HUMID ENVIRONMENTS. YUXIN NIE *ET AL.* China.

- [22] Q110 – R22 EFFECTS OF SPATIAL AND TEMPORAL VARIATION CHARACTERISTICS OF EXTREME PRECIPITATION ON DAM SAFETY IN MAJOR RIVER BASINS IN CHINA IN RECENT 20 YEARS. NING ZHOU *ET AL.* China

- [23] Q110 – R23 A HIGH-PRECISION THREE-DIMENSIONAL DAM BREACH MODEL CONSIDERING BREACH EVOLUTION MECHANISMS. SHENGYAO MEI *ET AL.* China

- [24] Q110 – R24 DISASTER ASSESSMENT OF THE LANDSLIDE SURGE CAUSED BY THE DEFORMATION OF THE UPSTREAM RESERVOIR BANK OF THE DAM. YUELIN SUN *ET AL.* China

- [25] Q110 – R25 ANALYSIS OF THE IMPACT OF EXTREME EVENTS ON DAM DISASTER UNDER CLIMATE CHANGE. JINGCHUN LEI *ET AL.* China

- [26] Q110 – R26 ZONED EMBANKMENT DAM BREACHING DUE TO OVERTOPPING: ESTIMATING OUTFLOW HYDROGRAPHS THROUGH LABORATORY EXPERIMENTS AND PARAMETRIC NUMERICAL MODELING. MATTHEW HALSO *ET AL.* Switzerland

- [27] Q110 – R27 NEW PROGRESS OF CEMENTED MATERIAL DAMS TO MEET THE REQUIREMENTS ON DAM SAFETY TO RESIST OVERTOPPING IN CHINA. JINSHENG JIA *ET AL.* China

- [28] Q110 – R28 MACHINE LEARNING METHOD BASED DAM BREACH FLOOD SIMULATION. HONGQIU HE *ET AL.* China.

Autres références :

- [29] PROPAGATION LAWS. Journal of Basic Engineering, 85(4), 528–534. 1963.
- [30] WMO⁺⁺⁺ MANUAL FOR ESTIMATION OF PROBABLE MAXIMUM PRECIPITATION. Operational Hydrology-Report No.1. WMO-No.332. Geneve. 1986
- [31] ANNANDALE, G ERODIBILITY. Journal of Hydraulic Research, 33(4), 471–494. 1995
- [32] BAKER V PALEOFLOOD HYDROLOGY AND EXTRAORDINARY FLOOD EVENTS. Journal of Hydrology, 96, pp.79–99. 1987
- [33] FOUFOULA-G A PROBABILISTIC STORM TRANSPOSITION APPROACH FOR ESTIMATING EXCEEDANCE PROBABILITIES OF EXTREME PRECIPITATION DEPTHS. Water Resources Research. Vol. 25 No. 5. 1989
- [34] FONTAINE *ET AL* ESTIMATING PROBABILITIES OF EXTREME RAINFALLS. Journal of Hydraulic Engineering, ASCE, 115(11), pp. 1562–1575. 1989
- [35] KOFOED *ET AL* MODELLING OF LANDSLIDE-GENERATED WAVES, 2001. DHI Water & Environment. Scientific Publications Scientific Publications 2001
- [36] CIFRES, E OROGRAPHIC AND STOCHASTIC STORM TRANSPOSITION FOR ESTIMATION OF LARGE RETURN PERIOD FLOODS. EGU Vienna, April 2007.
- [37] TODINI, E PREDICTIVE UNCERTAINTY IN HYDROLOGICAL FORECASTING. U. Bologna HEPEX – COST731 workshop program –15–18 June 2009.
- [38] JESSICA LUDY^{\$\$\$\$} FLOOD RISK PERCEPTION ON LANDS PROTECTED BY LEVEES. WORLD WATER FORUM, MARSEILLE, 2012.

⁺⁺⁺Organisation météorologique mondiale

^{\$\$\$\$}University of California, Berkeley

- [39] ARCHFIELD *ET AL* ACCELERATING ADVANCES IN CONTINENTAL DOMAIN HYDROLOGIC MODELING. *Water Resources Research*, 51(12), pp.10078–10091, 2015
- [40] CIFRES, E NEW METHODOLOGY FOR A ROBUST ESTIMATION OF LARGE RETURN PERIOD FLOODS FOR DESIGN OF LARGE DAM SPILLWAYS, ICOLD, Johannesburg 2016.
- [41] CIFRES, E DAM HYDROLOGICAL SAFETY, A PENDING CHALLENGE. Cippoletti (Argentina) CAP, 2022.
- [42] AR6 IPCC_AR6_SYR_LONGERREPORT.PDF, 2023
- [43] MORAN, R *ET AL* QUASI-PROTOTYPE SIZE TESTING OF WEDGE-SHAPED BLOCK FOR ARMORING EMBANKMENT DAMS AND LEVEES. *Water*, 15(4), 662. MDPI. 2023

Bulletins et documents institutionnels de la CIGB

Les principaux bulletins de la CIGB, liés d'une manière ou d'une autre au thème principal, sont les suivants :

- [44] JCOLD JAPAN INCORPORATES CLIMATE CHANGE EFFECTS INTO RIVER AND DAM PLANNING. <https://nlfpt.mlit.go.jp/ksj/gml/datalist/KsjTmplt-W01.html>. 2025.
- [45] BERGA & TC A ROLE OF DAMS IN FLOOD MITIGATION. TC DAMS & FLOODS BULLETIN 131, 2006
- [46] GUILLON ET TC RESERVOIR LANDSLIDES: INVESTIGATION AND MANAGEMENT. GUIDELINES AND CASE HISTORIES. ICOLD BULLETIN 124, 2000.
- [47] GUILLAUD&TC S INTEGRATED FLOOD RISK MANAGEMENT. TC DAMS & FLOODS BULLETIN 156,2014

- [48] MAZZA *ET AL.* MANIFESTO Dams & Reservoirs. European Club of ICOLD. November 2016

- [49] JOOS& TC S FLOOD ESTIMATION AND DAM SAFETY, ICOLD COMMITTEE ON FLOODS EVALUATION AND DAM SAFETY, BULLETIN 170,2018,

- [50] ROGERS, M &SC WORLD DECLARATION ON DAM SAFETY, ICOLD BOARD, OPORTO, 2019.

- [51] XU & TC H DAM BREACH FLOOD CONSEQUENCE ASSESSMENT, FINAL DRAFT VERSION FOR COMMENTS, BULLETIN 197, 2022

- [52] WESTERMANN TC V BEST PRACTICES FOR ACHIEVING RELIABILITY OF FLOOD DISCHARGE GATES. COMMITTEE ON HYDROMECHANICAL EQUIPMENT. BULLETIN 203. TO BE PUBLISHED SOON

- [53] HUANG & TC S FLOOD RISK ASSESSMENT. ICOLD COMMITTEE ON FLOODS EVALUATION AND DAM SAFETY. BULLETIN 204, TO BE PUBLISHED SOON

- [54] SHARMA-CIFRES & SC CHENGDU ICOLD DECLARATION ON THE ROLE OF DAMS FOR ENERGY TRANSITION AND ADAPTATION TO CLIMATE CHANGE, 2025, SPECIAL COMMITTEE ZA1, 2024.



Taylor & Francis

Taylor & Francis Group

<http://taylorandfrancis.com>